
REMOTE SENSING OF FOREST ENVIRONMENTS: CONCEPTS AND CASE STUDIES

REMOTE SENSING OF FOREST ENVIRONMENTS

Concepts and Case Studies

Edited by

Michael A. Wulder¹ and Steven E. Franklin²

¹ Canadian Forest Service (Pacific Forestry Centre), Natural Resources Canada, Victoria, British Columbia, V8Z 1M5, Canada

² Department of Geography, University of Calgary, Calgary, Alberta, T2N 1N4, Canada



Springer Science+Business Media, LLC

Library of Congress Cataloging-in-Publication

Remote sensing of forest environments : concepts and case studies / edited by Michael A.

Wulder and Steven E. Franklin.

p. cm.

Includes index.

ISBN 978-1-4613-5014-9 ISBN 978-1-4615-0306-4 (eBook)

DOI 10.1007/978-1-4615-0306-4

1. Forests and forestry—Remote sensing. 2. Forests and

forestry—Remote sensing—Case

studies. I. Wulder, Michael A. II. Franklin, Steven E.

SD387.R4R46 2003

634.9'0287—dc21

Copyright © 2003 Springer Science+Business Media New York

Originally published by Kluwer Academic Publisher in 2003

Softcover reprint of the hardcover 1st edition 2003

All rights reserved. No part of this publication may be reproduced, stored in a retrieval system or transmitted in any form or by any means, electronic, mechanical, photo-copying, microfilming, recording, or otherwise, without the prior written permission of the publisher, with the exception of any material supplied specifically for the purpose of being entered and executed on a computer system, for exclusive use by the purchaser of the work.

Permissions for books published in the USA: permissions@wkap.com

Permissions for books published in Europe: permissions@wkap.com

Printed on acid-free paper.

Dedication

This book is dedicated to:

Karen, Hank, and Cleo
—MW

Jean and Eric
—SEF

Contents

Dedication	v
Editor Profiles	xi
Preface	xiii
Acknowledgements	xv
<i>Section 1: Data collection and pre-processing</i>	1
1. Remote sensing of forest environments, Introduction. The transition from theory to information MICHAEL A. WULDER and STEVEN E. FRANKLIN	3
2. Selection of remotely sensed data MICHAEL A. LEFSKY and WARREN B. COHEN	13
3. The roles of aerial photographs in forestry remote sensing image analysis RONALD J. HALL	47
4. Indirect measurement of forest canopy structure from <i>in situ</i> optical sensors RICHARD A. FOURNIER, DANIEL MAILLY, JEAN-MICHEL N. WALTER, and KAMEL SOUDANI	77

5. Accuracy assessment of maps of forest condition: Statistical design and methodological considerations RAYMOND L. CZAPLEWSKI	115
<i>Section 2: Common methods for data processing and information generation</i>	141
6. Geometric correction of remotely sensed images THIERRY TOUTIN	143
7. Radiometric image processing DEREK R. PEDDLE, PHILIPPE M. TEILLET, and MICHAEL A. WULDER	181
8. Per-pixel analysis of forest structure: Vegetation indices, spectral mixture analysis and canopy reflectance modeling GREGORY P. ASNER, JEFFREY A. HICKE, and DAVID B. LOBELL	209
9. Extracting individual tree information: A survey of techniques for high spatial resolution imagery DARIUS S. CULVENOR	255
10. Rationale and conceptual framework for classification approaches to assess forest resources and properties JANET FRANKLIN, STUART R. PHINN, CURTIS E. WOODCOCK, and JOHN ROGAN	279
11. Remote sensing of forests over time: Change types, methods, and opportunities PENG GONG and BING XU	301
<i>Section 3: Case studies illustrating methods and applications for remote sensing of forests</i>	335
12. National scale forest information extraction from coarse resolution satellite data, Part 1. Data processing and mapping land cover types JOSEF CIHLAR, RASIM LATIFOVIC, JEAN BEAUBIEN, ALEXANDER TRISHCHENKO, JING CHEN, and GUNAR FEDOSEJEVS	337

13. National scale forest information extraction from coarse resolution satellite data, Part 2. Forest biophysical parameters and carbon JOSEF CIHLAR, RICHARD FERNANDES, ROBERT FRASER, JING CHEN, WENJUN CHEN, RASIM LATIFOVIC, JANE LIU, and ZHANQING LI	359
14. Regional forest land cover characterisation using medium spatial resolution satellite data CHENGQUAN HUANG, COLLIN HOMER, and LIMIN YANG	389
15. Modeling forest productivity using data acquired through remote sensing NICHOLAS C. COOPS and JOSEPH D. WHITE	411
16. Experiences in field data collection: In support of land use and land cover change classification in boreal and tropical environments G. ARTURO SÁNCHEZ-AZOFÉIFA, MARK KACHMAR, MARGARET KALÁCSKA, and STEPHEN HAMILTON	433
17. Estimation of foliar chemistry of western hemlock using hyperspectral data K. OLAF NIEMANN and DAVID G. GOODENOUGH	447
18. Using georeferenced large-scale aerial videography as a surrogate for ground validation data DANA SLAYMAKER	469
19. Tree and canopy height estimation with scanning lidar BENOÎT ST-ONGE, PAUL TREITZ, and MICHAEL A. WULDER	489
20. Remote sensing of forest environments, Conclusions. Challenges and opportunities STEVEN E. FRANKLIN and MICHAEL A. WULDER	511
Index	515

Editor Profiles

Michael A. Wulder (BSc Calgary, MES PhD Waterloo) is a research scientist with the Canadian Forest Service of Natural Resources Canada, located at the Pacific Forestry Centre in Victoria, British Columbia. Dr. Wulder leads a research and applications program on '*Forest Geomatics*', that is focused on the use of spatial data to estimate forest inventory and structural attributes. To meet these objectives, spatial data collected from a range of remote sensing instruments, forest inventory data, and other sources are utilized. Dr. Wulder plays an active role in support of national programs (such as the National Forest Inventory and carbon accounting initiatives) and on international panels. Current support from the Canadian Space Agency is enabling leadership of a land-cover mapping program for the forested area of Canada with Landsat ETM+ data. Other complete, or on-going research projects, include biomass estimation, change detection applications, spatial statistical description of forest structure, and lidar remote sensing of forest inventory attributes.

Steven E. Franklin (Dipl. For. Lakehead, BES MA PhD Waterloo) is a professor of geography with the University of Calgary, in Calgary, Alberta. Dr Franklin was a Natural Sciences and Engineering Research Council (NSERC) Postdoctoral Fellow at Memorial University of Newfoundland, and has had visiting appointments at Oregon State University and the University of California-Santa Barbara. His research program '*Remote sensing of biophysical properties and environmental change*' is supported by grants from NSERC and Natural Resources Canada, and is located in the Earth Systems Modelling Laboratory of the University of Calgary. He has published on environmental management issues and remote sensing methods

in Canada, the United States, and South America; his contributions have focused on forest defoliation and inventory monitoring, as well as image analysis and digital terrain modelling applications. Recently, he began applying geospatial tools to biodiversity issues, including caribou habitat mapping, grizzly bear management in Alberta, and forest fragmentation and structure quantification over large areas and long time periods.

Thus, this book provides a series of case studies that exemplify the ways in which remotely sensed data are used in the field, in the decision-making process, and in the scientific study of forests. In selecting this material we have attempted to balance the presentation of results from different types of forests, the widely-available and deployed sensors, the different image and GIS processing approaches, and the implications for management or science. We feel that practitioners and students alike will find the materials collected here enlightening and useful.

Acknowledgements

The editors are grateful for the support and advice in preparing this book from colleagues at the University of Calgary and the Canadian Forest Service of Natural Resources Canada. We are particularly indebted to the many authors for their diligent efforts in assisting us to identify and complete the necessary material to provide a comprehensive and extensive view of the concepts and case studies that have come to constitute the complex enterprise of remote sensing of forests. The contribution this book may make is largely due to their commitment to quality and the necessary timelines for submission and revision of material. We thank the reviewers of individual chapters and, in particular, Dr. E. R. Hunt, Jr. of the USDA Hydrological Modelling Lab, Gordon Fraser of the University of Victoria, Dr. Bryan Mercer of Intermap Inc., and Martin Flood for their insightful comments and suggestions. General editorial support and assistance was provided by David Seemann and Steve Glover (Canadian Forest Service) and David Nuell and Kirk Montgomery (University of Calgary). Steve Pridgeon is also thanked for expert editorial support. We appreciate the help we received from Lance Wobus, Susan Lagerstrom-Fife, Sharon Palleschi, and Deborah Doherty of Kluwer Academic Publishers. Their efforts were important in turning the final manuscripts into this book. Research silviculture staff at the Canadian Forest Service are thanked for providing the cover image. Financial support for publication of the colour plates was provided by a grant from the Canadian Forest Service.

September, 2002

*MW – Victoria, British Columbia
SEF – Calgary, Alberta*

SECTION 1: DATA COLLECTION AND PRE-PROCESSING

Chapter 1

REMOTE SENSING OF FOREST ENVIRONMENTS, INTRODUCTION.

The Transition from Theory to Information

Michael A. Wulder¹ and Steven E. Franklin²

¹ Canadian Forest Service (Pacific Forestry Centre), Natural Resources Canada, Victoria, British Columbia, V8Z 1M5, Canada

² Department of Geography, University of Calgary, Calgary, Alberta, T2N 1N4, Canada

1. INTRODUCTION

The remote sensing of forests has reached a developmental stage that allows practitioners to expend the largest proportion of project efforts on information generation, rather than data preparation. The significant progress that has been realised in the remote sensing of forests in recent years is related to the three linked developments of:

- 1) Greater technological sophistication in sensor design and deployment (Technological Advances),
- 2) Explosive growth in information extraction techniques and user-driven tools for analysis of imagery (Data Processing), and
- 3) A parallel improvement in understanding how and why remotely sensed data and methods are important in forestry and forest science (Information Synthesis).

This latter development is, in turn, linked to the growing awareness that understanding forests may be essential for successful human and natural world coexistence. In fact, there are limits to human knowledge and understanding of the natural world that must be addressed if future trends in resource management and exploitation are to continue at anything near their current levels. The combination of these linked developments allows for the development of applications – the use of remotely sensed data to generate specific information requirements (Application Context).

Remote sensing systems are increasingly sensitive to the actual phenomena we wish to observe. A wide range of spectral and spatial resolution options now exist for the user to tailor their information needs with the most appropriate data inputs. Image preparation techniques, such as radiometric and geometric adjustments, previously occupied a significant amount of total time spent on forest characterisation application projects. Data delivery options that allow for the user to request these image analysis enabling procedures to be included, for a price, are increasingly available. Digital data delivery options also allow for a decrease in the amount of time between acquisition and data analysis. Once the data are delivered, image analysis and geographic information systems are increasingly able to process the available data into the actual information desired. Analysis and computing environments now allow for the transformation of data, from a diverse and often multivariate form, to a usable state. Concurrently, developments in the understanding of forests from field-based perspectives are increasingly common. Forest management regimes are also becoming more flexible and able to integrate the advances in forest science to the management frameworks developed. While the technological ability to characterise forests has increased, so has the level of detail and the precision of the information desired. A renewed commitment to understanding forests at different scales, and with a process-based perspective, has helped generate demand for information about forests that may only be collected by remote sensing. And these data can be used best in the context of existing or traditional forest data that can acquire new importance in light of the insights available through remote sensing.

In compiling this book, we have attempted to capture the range of knowledge and activities required to use remotely sensed data to characterise forests. The book is organised with sections on data collection and processing, common methodological approaches, and a sample of applications. In this Chapter we endeavour to introduce the current state-of-the-art regarding the remote sensing of forest environments. The breadth of information regarding the remote sensing of forests will unfortunately result in the omission of pertinent material. In this Chapter we summarise a selection of advances and indicate the role that each of the Chapters included in this book have in the communication of these advances.

2. TECHNOLOGICAL ADVANCES

Greater technological sophistication in sensor design and deployment has led to the launch of a wide selection of sensors providing for data that is specifically suited to an increasing range of applications (Glackin and

Peltzer 1999). High spatial resolution data are an example of what can be accomplished with a new model for the development of remote sensing satellites. The notion of “small sats” was developed to take advantage of existing technologies and allow for a quick turnaround time from idea to launch. Cost savings exist through not having to invent and engineer all required materials. A small satellite bus can be obtained, a sensor built, and a launch arranged, enabling a low cost satellite deployment. While the number of failed launches may have increased, the cost per project has also decreased making a failed launch, while disappointing, less financially catastrophic than previously found. Both commercial and government agencies have used this satellite development approach.

The link between sensors, the data to be collected, and the desired information products, has also been solidified. The Moderate Resolution Imaging Spectroradiometer (MODIS) program (Running et al. 1994) is an example of the development of a sensor and product program to meet global mapping needs. The link between the products and the information required for models at the global scale was also addressed (Friedl et al. 2000). The data collected and the products generated by the MODIS program are also available with no copyright restrictions to the public. Web based data order and delivery results in a short turn-around time, with the data accompanied by the appropriate meta-data. The open data policy of the United States government has also led to favourable data sharing policies currently existing for Landsat Enhanced Thematic Mapper Plus (ETM+) and Advanced Very High Resolution Radiometer (AVHRR) data.

3. DATA PROCESSING

Explosive growth has been demonstrated in data processing options, information extraction techniques, and user-driven tools for analysis of imagery. The analysis of remotely sensed data generally follows from data collection, radiometric and geometric processing, through to image analysis and data integration. Data collection is now possible from a variety of sensors, each characterising the earth’s surface in a differing manner. The suite of tools now available allow for ease in the integration of differing spatial data sets (Millington et al. 2001) over a range of applications. The ability to exploit concurrent advances in spatial analysis and statistics (eg. Wulder and Boots 1998) is also improved, through either, frequent software updates, flexible analysis environments, or new niche software tools. The availability of a range ancillary data sets is exploitable with existing software tools. The ability of users to use the differing data sets is also aided by communication of the issues to be addressed when integrating data from

different sources or scales. The appropriate statistical techniques, such as avoiding the use of spatially autocorrelated or collinear data, are included and described in successful applications projects.

3.1 Data collection and project preparation (Section 1)

In many well-designed research studies employing remotely sensed images, easily 50 % of the effort is expended prior to analysis of the data. The proportion of time collecting and formatting remotely sensed data can increase almost exponentially if the data and application do not match; for example, if an aerial mission were flown with the wrong sensor type, or if an inappropriate spatial resolution was used to collect data. Anecdotal estimates of the time required to collect and prepare geospatial data in typical natural resources applications, such as forest inventory or land cover mapping, range as high as 80 %, leaving only 20 % for data analysis and information product generation. A key decision point that can shape the amount of time spent preparing data rests within an understanding of the data characteristics as Lefsky and Cohen present in Chapter 2; their discussion of the several image resolutions, aspects of quality, and requirements for analysis lead naturally to a sense that the data collection and project preparation steps are not to be undertaken lightly. While selecting the appropriate remotely-sensed data for a given application is important in launching successful applications, another oft-overlooked, yet related aspect of the data collection effort in remote sensing, is the availability and complementary use of aerial photographs. In Chapter 3, Hall provides a synopsis of the many ways in which aerial photography continue to play a critical role in successful remote sensing of forests. To complete the data collection discussion, the role and characteristics of field data are discussed by Fournier et al. (Chapter 4). Their contribution highlights the many possible strategies and data quality issues that arise when incorporating indirect measures of forest structure – so important as forest information needs have grown – yet often only poorly understood relative to the available remotely sensed data. This first section of the book is completed by Czaplewski (Chapter 5) in which issues related to accuracy assessment and validation procedures used in remote sensing map generation are highlighted. Such issues must be addressed early in any remote sensing activity if the resulting products are to be received credibly by the user community.

4. INFORMATION SYNTHESIS

Parallel improvements in the understanding of how and why remotely sensed data and methods are important in forestry and forest science have particularly aided information synthesis developments. Field based techniques for the measurement of phenomena that can be detected through remote sensing are burgeoning; one such application is the measurement of forest structure with *in situ* optical instruments described in this book. The problem is in linking these field based measures with the remotely sensed data (Asner et al., Chapter 8). An understanding of how landscapes are represented in remotely sensed imagery has necessitated field based measurement techniques that are applicable at a variety of scales. Plot based field measures are often difficult to utilise when describing a landscape. Sampling techniques that can provide calibration, or validation, information useful over a range of scales is an area of active research and experimentation. Attributes that are difficult to measure on the ground, or that are based upon complex definitions, will continue to be problematic for remote characterisation. A clear communication between what can be measured on the ground, to what can be generated from remotely sensed data, will result in products that are useful in an applications context. Clear determination of the project purpose and the potential of the source data to address these needs are a hallmark of a successful application.

A potential perception of limitations to the characterisation of forests with remotely sensed data is often due to an ill fit between desired outcomes and available data inputs. For instance, forest inventory polygons that are generated manually from interpretation are difficult to recreate with automated methods. The decision rules applied by the photo interpreter encompass a range of qualitative choices, some of which are not related to what is visibly present, but on what is known to the interpreter (such as disturbance history, ownership, or management regime). As a result, it should not be surprising that methods based upon remotely sensed data will not exactly replicate forest inventory polygons. Where the remote sensing of forests has made the greatest impact, however, is where project purpose and input data potential coincide. For instance, satellite data has provided for the characterisation of forests, and non-forest land cover, at the local to regional to global scales. These global data provide for model inputs and the monitoring of change at unprecedented levels of detail for vast areas; the regional data nest within these larger models to permit analysis over typical forest management-sized areas; and local analyses are accomplished for key areas of interest at the stand and forest ecosystem scales. Significant contributions to the understanding of the Earth system have been afforded through these remote sensing studies; in one recent compilation, Franklin

and Wulder (2002) surveyed land cover mapping projects representing a range of scales but focussing on large areas with changes monitored over long periods of time. This has always been the promise and potential of satellite remote sensing, finally now being realised in what amounts to an eclectic collection of international, national, and regional imaging initiatives and mapping projects.

4.1 Common methods for data processing and information generation (Section 2)

All remote sensing work in forests can be considered in light of a handful of reasonably common steps that comprise the process of converting remotely sensed data to information products: this is the domain of the image processing system. Image processing systems are designed to support and augment users' needs to handle and develop information products from remotely sensed data of all types and descriptions. Considered here are the geometric and radiometric processing issues, the application of information extraction tools, and the design of spatial and temporal analyses that underlay the successful remote sensing application to forests. By necessity, only certain aspects, perhaps considered as exemplars, of these steps are dealt with individually in this section of the book; but the overall theme of the presentations is to emphasize the connections that each step will have to the preceding and following ones. First, Toutin (Chapter 6) reviews geometric image processing with the goal of providing users with an understanding of the current capabilities and future potential; for example, how straightforward are the decisions necessary to bring remotely-sensed data into registration with other data sets? And, how useful are the emerging tools for geometric correction based on rational functions? Peddle et al. (Chapter 7) continue the discussion of dataset preparation with a comprehensive review of radiometric image processing. They highlight atmospheric correction work and show how attention to radiometry can lead to more successful applications of remotely-sensed data. Image analysis methods are increasingly complex but also increasingly available; Asner (Chapter 8) and Culvenor (Chapter 9) show state-of-the-art image information extraction applied to per-pixel analysis of forest structure and individual trees in high spatial detail imagery, respectively. This section concludes with two chapters containing specific insights into the fundamental concepts which have evolved to become the foundation for image classification (Franklin et al., Chapter 10) and image change detection (Gong and Xu, Chapter 11).

5. APPLICATION CONTEXT

An increasing number and range of users currently are seeking information products based on remotely sensed data. There is an expectation that information needs can be met with little new research. For some applications, particularly land cover mapping, the expectations for consistency and accuracy are high. The large and growing value-added community is evidence of the maturity of a range of remote sensing applications. The mainstream usage of imagery to describe forests is tied to the type of application. While turn-key applications for land cover maps are possible, the same expectation is not present for more complex attributes, such as forest productivity based upon models and remotely sensed inputs. While the core of the application for more complex attributes may exist, parameterisation to account for location, forest type, local conditions, etc. need to be integrated.

Remote sensing is widely taught in post-secondary educational institutions in a range of departments. The pool of practitioners available from this range of interest areas enables the generation of well-suited information products.

Currently a danger exists that the methods developed to meet application needs are not sufficiently communicated to users as part of the momentum gaining for more widespread adoption of remote sensing technology. Intellectual property rights often preclude an interest in too thorough a description of methods. Applications may also be based upon incremental adjustments to existing techniques, thereby not warranting a full description in peer reviewed literature. Additionally, peer reviewed communications are not necessarily the place for an in-depth methodological description. A step-by-step accounting of methods is often not the most important aspect of projects described in peer review. As a result, project reports and descriptions are increasingly important. Web based communication of project reports is becoming a primary source of methodological descriptions utilised in applications. Communication of the methods developed and used in an applications context enables an advancement of the approaches taken, and aids in the avoidance or unnecessary duplication of less than successful approaches.

5.1 Case studies illustrating methods and applications for remote sensing of forests (Section 3)

The number of case study applications that could be included in this book was limited, but to illustrate the level of accomplishment in the broad field of remote sensing of forests, we have selected complete presentations at

three scales of interest in forest monitoring: large-area, regional, and local remote sensing. Cihlar et al. demonstrate that remotely sensed data can be used to map a large region for both land cover (Chapter 12) and biophysical parameters (Chapter 13). The pre-processing and analysis stages are documented and used to illustrate the high degree of maturity in the standardised mapping of large (national) areas with coarse spatial resolution (AVHRR) data. Huang et al. (Chapter 14) describe two projects and associated procedures undertaken in the USA with medium spatial resolution (Landsat) data. Remotely sensed data may also be utilised, not only as a source for mapping, but for providing input data to models and as a validation source for a forest productivity model (Coops and White, Chapter 15). Then, Sanchez et al. (Chapter 16) illustrate field data collection in support of land use and land cover mapping applications; one boreal, one tropical. The promise of space-borne high spectral resolution data has encouraged studies to identify new types of forest characteristics that may be possible to monitor routinely. Niemann and Goodenough (Chapter 17) statistically equate ground observed spectral data to processed airborne hyperspectral data.

Land cover mapping is perhaps the most common use of satellite remotely sensed data. A typical situation is an interest in an area that is contained within one image (i.e. Landsat); users typically have the ability to collect ground data in support of such mapping. With the recent decrease in image data costs, and an interest in the characterisation of larger (multiple scene) areas, the ability to collect representative ground data is diminished. Slaymaker (Chapter 18) presents one possible solution: an effective, efficient, yet low-cost use of airborne data. The use of these high spatial resolution data as a means to calibrate and validate more coarse spatial resolution data is an application area likely to become more widespread. Another data-type poised to become more available is airborne lidar (light detection and ranging) data. Lidar data are unique in that they can be used to describe both the ground and canopy elevations of forests at a high spatial resolution. St-Onge et al. (Chapter 19) describe the key issues and methods to allow for the remote estimation of tree heights using lidar data, from points, to surfaces, to heights.

6. CONCLUSION

The maturity of processing and analysis methods combined with readily available data, at low costs, over a range of spatial resolutions and scales, is providing for a democratisation of geospatial information. The producer of the data is no longer the sole voice on the interpretation and information

generation. Non-governmental organisations are increasingly using remotely sensed data as a key source of natural resources information of all kinds. The description of forested landscapes by a range of stakeholders indicates the need for transparency in data inputs and methods applied. Differences in mapped outcomes are not necessarily indicative of different accuracies, but of differing methods. The selection of methods is tightly linked to the purpose of the map. Different mapping purposes will inevitably result in the development of different surfaces. Both surfaces may be correct in meeting the objectives of a particular project, but may appear “wrong” when compared. The transparency required would include the spatial resolution of the data used, the image processing steps applied to the data, the methods used for information development, a description of the characteristics of the mapped categories, validation data characteristics, accuracy assessment techniques applied, etc. The credibility of the products derived from remotely sensed and other spatial data is directly related to the ability of the users to understand the product development. An informed user is poised to make the correct interpretation of the information produced.

With clarity of data requirements, image processing, data analysis, and information extraction non-specialist communities can generate information products to meet their specific needs. The remote sensing community has been successful in developing applications that can be implemented in readily available software environments. Non-specialists can exploit the current watershed in data availability and analysis options to generate the information desired to meet their specific needs. The application realm is also increasingly large, allowing users to address issues from local to global scales.

In many ways, the future of remote sensing of forests is now upon us. The early promise of remote sensing is now being realised, perhaps even beyond what early developers thought possible. We no longer need to speak of the potential of remote sensing but can point to concrete success stories. The success stories may be related to technological advances, increased understanding of contents of image data and processing needs, our ability to generate information from the collected data, and the combination of the aforementioned developments in an applications context. The high state-of-the-art of remote sensing presented in this volume is a tribute to the efforts, diligence, and foresight of previous researchers and practitioners.

REFERENCES

- Franklin, S., & Wulder, M. (2002). Remote sensing methods in medium spatial resolution satellite data land cover classification of large areas. *Progress in Physical Geography*, 26, 173-205.
- Friedl, M., Muchoney, D., McIver, D., Gao, F., Hodges, J., & Strahler, A. (2000). Characterization of North American land cover from NOAA-AVHRR data using the EOS MODIS land cover classification algorithm. *Geophysical Research Letters*, 27, 977-980.
- Glackin, D., & Peltzer, G. (1999). Civil, Commercial, and International Remote Sensing Systems and Geoprocessing. *American Institute of Aeronautics and Astronautics*. Aerospace Press Series.
- Running, S., Justice, C., Salomonson, V., Hall, D., Barker, J., Kaufmann, Y., Strahler, A., Huete, A., Muller, J., Vanderbilt, V., Wan, Z., Teillet, P., & Carnegie, D. (1994). Terrestrial remote sensing science and algorithms planned for EOS/MODIS. *International Journal of Remote Sensing*, 15, 3587-3620.
- Millington, A., Walsh, S., & Osborne, P. (2001). *GIS and Remote Sensing Applications in Biogeography and Ecology*. Kluwer Academic Publishers, Dordrecht.
- Wulder, M., & Boots, B. (1998). Local spatial autocorrelation characteristics of remotely sensed imagery assessed with the Getis statistic. *International Journal of Remote Sensing*, 19, 2223-2231.

Chapter 2

SELECTION OF REMOTELY SENSED DATA

Michael A. Lefsky^{1,*} and Warren B. Cohen²

¹ *Oregon State University, Department of Forest Science, Corvallis, Oregon, 97331, USA*

² *USDA Forest Service, Corvallis, Oregon, 97331, USA*

1. INTRODUCTION

An increasing number of sensors are available for forest ecologists and managers seeking to map attributes of forest canopy cover, forest structure and composition, and their dynamics. This Chapter seeks to put these advances within the context of the needs of forest managers and scientists. To do so, we review the basic physics behind a variety of imagery types, discuss fundamental limitations and trade-offs that apply to all remotely sensed data, review sensor options for several established and emerging technologies, and present our approach for matching imagery and attributes of interest.

2. PARAMETERS OF IMAGE CREATION

The choices involved in the selection of a remote sensing data type are increasingly complicated. Images may be created using active or passive techniques, in optical or microwave wavelengths, and with ranging techniques like LIDAR (light detection and ranging) or IFSAR (interferometric synthetic aperture radar). Nevertheless, the spatial, spectral, radiometric and temporal resolution of the imagery remains key to their utility for the user. Furthermore, trade-offs between these resolutions, the

* Current affiliation: Department of Forest Sciences, Colorado State University, Fort Collins, Colorado, 80523-1470, USA

extent of the imagery, and other sensor particulars are often key elements of designing a remote sensing solution.

2.1 Modes of image formation

While it is tempting to resort to the familiar example of photographs when viewing remotely sensed images, it is important to remember that only conventional optical remote sensing is clearly analogous to photography; the physical processes involved in radar or lidar remote sensing are quite unlike the familiar interaction of light with either the human eye or camera. Radar, in particular, behaves in ways outside the common sense experience of non-specialists. It is therefore important to review the physical bases of each sensor.

2.1.1 Optical images

Optical images have been, and will likely continue to remain for some time, the most frequently used type of remote sensing. In this Chapter, optical denotes that the medium (analog or digital) is sensitive to light in the range of 400 nm (nanometers, i.e., violet), to 2500 nm in the shortwave infrared (Colour Plate 1). From 2500 nm to 14,000 nm is the thermal range of the electromagnetic spectrum, in which most radiation observed by sensors has been emitted from the Earth's surface, not from the Sun. While thermal remote sensing can be very important for certain kinds of natural resource investigations, including geological mapping (Abrams et al. 1984; Mouginis-Mark et al. 1994), estimation of plant-canopy temperatures (Sader 1986; Luvall et al. 1991), and prediction of runoff from snow pack, it is beyond the scope of this discussion, as these are of secondary interest to the forest ecologist and manager. The optical range of wavelengths is important for remote sensing of vegetation because the majority of the Sun's energy is emitted in this range, and plants have become adapted to either absorb (e.g., for photosynthesis) or reflect (e.g., to maintain their heat balance) at various wavelengths (Gates 1952). Although optical images can be created using an independent source of energy, such as a flash lamp, they are normally created passively, using the Sun as a source of energy, and therefore, to adequately understand these images, we will have to start with the quantities and qualities of energy emitted by the Sun.

The bulk of solar radiation at the top of the atmosphere is distributed above 200 nanometers (in the ultraviolet), with peak strength at 500 nm (in the visible), and thereafter declining so that by 2500 nm (in the shortwave infrared) it has roughly one-twentieth of its peak power (Colour Plate 1- top panel). However, the output of the Sun is only the first part of the story,

because the atmosphere is not uniformly transmissive to energy at these wavelengths (Colour Plate 1, top panel). The sharp atmospheric absorption features (e.g., at 940 nm) are due to molecular absorptance by CO_2 and H_2O in the atmosphere, even under clear sky conditions (Schowengerdt 1997). As important as these individual features are, it is the general pattern of decreasing transmittance from 1200nm to 400nm, due to scattering by air molecules themselves, as well as by aerosols and other particulates, that plays a more important role in the atmosphere's effects on optical images.

Beginning at the top of the atmosphere, most solar radiation takes one of three paths to an optical sensor (Schowengerdt 1997). *Unscattered, surface-reflected radiation* passes through the atmosphere without being intercepted, will interact with the surface, and be reflected back to the sensor. *Scattered, surface-reflected skylight* will encounter one or more scattering events in the atmosphere that deflects the light into target pixel, where it will be reflected in the direction of the sensor. *Path radiance* consists of radiation that encounters one or more scattering events in the atmosphere, and is reflected back up in the direction of the sensor, without having reached the surface.

Reflectance is the physical interaction between solar radiation and the Earth's surface that gives rise to the spectral information content of an optical image. Energy is reflected from surfaces in what is often considered to be a spatially uniform (or Lambertian) manner but is in fact a complex pattern that is dependent on illumination and view angle and surface roughness; this pattern is referred to as the bi-directional reflectance distribution function or BRDF (Kimes et al. 1993; Ranson et al. 1994; Asner et al. 1998). More relevant for the applications-oriented user of optical imagery is the spectral variability of reflectance. As shown in Colour Plate 1 (middle panel), plants tend to exhibit a number of common features, including low reflectance in the visible spectral range (especially in the blue and red wavelengths), a steep increase in reflectance around 700 nm (the so-called red-edge) and high reflectance in the near-infrared. While many minerals have sharp spectral features, spectra that are distinct from other minerals, and often occur in isolation over large areas, most species of plants have similar spectra and tend to be mixed at the sub-pixel level with other spectra, such as soil and shadow (Li and Strahler 1992; Cohen et al. 1995). As a consequence, discrimination of physiognomy and species from optical imagery is problematic.

After reflecting off the target, radiation proceeds back through the atmosphere (where once again it may be intercepted by the atmosphere) and then to the sensor, where it is either recorded as an arrangement of differentially exposed halide crystals (as in Hall, Chapter 3), or as a set of digital numbers of a given precision. Both air photos and digital images record energy properties at a point in time for a portion of the Earth's

surface. Using different combinations of film sensitivity and filters, air photos can selectively record certain wavelength ranges of the electromagnetic spectrum. Digital sensors also use filters, but in lieu of using halide crystals in a film emulsion to record the image, they use energy detectors that are similar in concept to voltmeters. Energy incident upon a detector is converted to a digital number, commonly 8-bit, but often 9-, 10-, 12-, or 16-bit. Normally, one detector is dedicated to a single wavelength range, and multiple ranges are sensed using multiple detectors. Whereas photographic film is limited in sensitivity to a narrow range of the electromagnetic spectrum (400-900 nm), digital optical sensors can operate in a much wider range of the spectrum (400-14000 nm, Lillesand and Kiefer (2000)).

At any wavelength the power of the recorded signal is due to the entire series of conditions discussed thus far; the irradiance of the Sun at the top of the atmosphere, the transmittance and scattering by the atmosphere, and the reflectance of the target, all of which vary as a function of wavelength, topography and BRDF effects. Of these, only reflectance and its variation expressed in the BRDF, are properties of the vegetation, and they are the quantities that most remote sensing analyses strive to extract from the at-sensor radiances recorded by either film or digital sensors. The process of deriving reflectance is discussed in detail in Peddle et al. (Chapter 7).

2.1.2 SAR images

Whereas most optical images are collected passively, most microwave images are collected actively, with the device providing the energy illuminating the scene and collecting the backscattered radiation from the target (passive microwave devices, while useful for sea ice detection (Eppler and Farmer 1991), airborne water vapor, and some soil moisture measurements (Chauhan 1997), are again outside the purview of this discussion). Active sensors can operate without concern for the Sun's illumination angle and can even be flown at night. The most common implementation for microwave sensors is synthetic aperture radar or SAR. As in the optical spectrum, varying microwave wavelengths have been established as being particularly useful for different purposes. However, the illumination from microwave sensors generally has a wavelength of 1 mm to 1 m, about two thousand to two million times the wavelength of green light (500 nm). As a consequence, the physical interaction of microwave illumination with forests is very different from that in the optical range. Whereas pigments, leaf structure, and leaf water content reflect optical radiation, and patterns of foliage and shadow allow the prediction of structure; the microwave portion of the spectrum is directly sensitive to the

structure of the forest itself, with each microwave band being preferentially backscattered by objects of approximately the band's wavelength (Ranson and Williams 1992). Radar in the shorter wavelengths (X and C, see Figure 2-1), are sensitive to small twigs and leaves, while long wavelength bands (L and P) are sensitive to boles and branches. Therefore, shorter wavelength bands are most sensitive to the uppermost canopy level, while longer wavelength bands penetrate the upper canopy and provide information on the woody structure and underlying ground surface. An additional feature of microwave sensors is that they can be configured to send and receive signals in a vertical (V) or horizontal (H) direction. Combining these send and

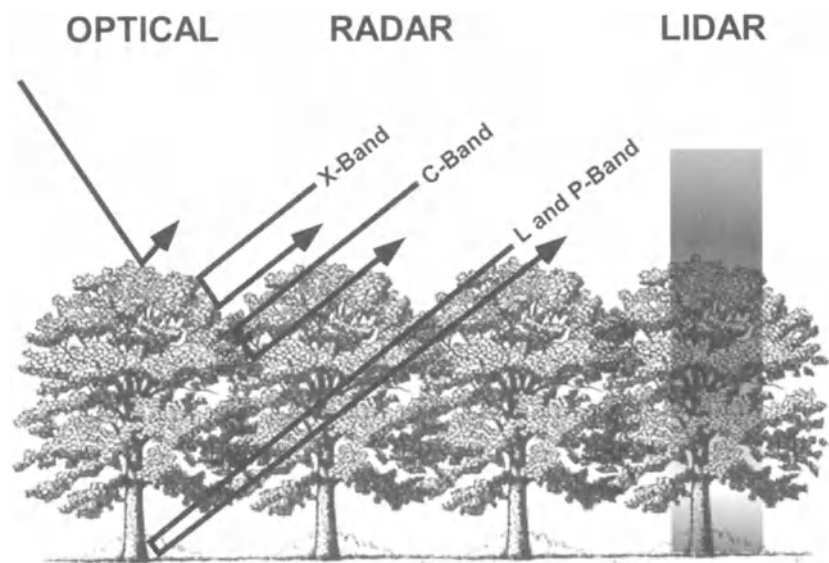


Figure 2-1. Diagram indicating the conceptual differences in the depth to which various sensors will penetrate into the forest canopy, indicating the ability of L- and P-band radar to penetrate leaves and twigs, and only be reflected by larger structures. Lidar is an optical instrument, but due to the ability to track the depth of penetration through open spaces in the canopy, information concerning sub-canopy features can be recorded.

receive options, quadruple polarized sensors can use all four combinations (HH, VV, HV, VH) to accentuate the backscatter from features with particular orientations, such as tree boles in a recent clear cut (Kasischke et al. 1994). One clear advantage that microwave sensors hold over optical remote sensing is the transparency of the atmosphere, and atmospheric aerosols, in the microwave portion of the spectrum. This allows SAR to be used during cloudy or smoke-filled conditions when optical remote sensing would be useless or nearly so. As a consequence, microwave instruments

have been extensively used in the tropics (Luckman 1998) and in the higher latitudes (Kasischke et al. 1994), where cloud free conditions are rare.

In addition to being sensitive to vegetation structure, a surface's inherent reflectivity in the microwave is determined by its dielectric constant, which governs electromagnetic wave propagation. In vegetated areas, the moisture and freeze-thaw state of the ground and canopy surfaces predominantly determines this constant. This phenomenon has been used to map freeze-thaw conditions (Rignot and Way 1994; Rignot et al. 1994; Way et al. 1994), water stress in trees (Way et al. 1991), and, in the absence of appreciable biomass, can measure soil moisture in the upper 10 cm of the soil profile (Dobson et al. 1992; Wang et al. 1994). In addition, the combination of open water and standing vegetation (e.g., in flooded areas with either trees or other vegetation with an upright orientation, such as reeds) results in an extremely high backscatter, making these areas easy to detect. While this dielectric effect can be useful for hydrological and freeze/thaw mapping, this phenomenon can also interfere with the remote sensing of vegetation structure, if moisture conditions are not uniform across the area of interest.

A recent innovation in microwave remote sensing is the technique of Interferometric SAR (IFSAR). IFSAR uses two radar receivers separated in space, and measures the difference in signal phase between the two return signals to estimate the three-dimensional position of the mean scattering elements (Baltzer 2001). In some applications, a single microwave sensor makes the IFSAR measurement by recording two images of the same area from different orientations, sometimes at different times (repeat pass interferometry). The primary use of this technology is topographic mapping, as with the Shuttle Radar Topographic Mission (SRTM, Eineder et al. 2000). In addition to producing topographic information, the strength of the correlation (coherence) between the two IFSAR return signals is affected by the presence of volumetric scattering, such as occurs in vegetation canopies, as first pointed out by Rodriguez and Martin (1992). The estimation of canopy structure parameters from a single interferometric measurement relies on assumptions about the canopy structure, such as the canopy dielectric properties. An alternate approach that has been used successfully is the joint use of lidar and interferometric data to retrieve canopy parameters from the IFSAR data (Rosen et al. 2000; Rodriguez et al. 2002).

2.1.3 Lidar remote sensing

Laser altimetry, or lidar is an alternative remote sensing technology that directly measures the three-dimensional distribution of the plant canopy and sub-canopy topography. The basic measurement made by these devices is the distance between the sensor and a target surface, made by determining

the elapsed time between the emission of a short-duration laser pulse and the arrival of the reflection of that pulse (the return signal) in the sensor's receiver. Dividing this time interval by the speed of light results in a measurement of the round-trip distance traveled, and dividing this distance by two results in the distance between the sensor and the target (Bachman 1979). Key differences among lidar sensors are related to the wavelength, power, pulse duration, size, divergence, and repetition rate of the laser itself; the size and spacing of the laser-illuminated samples on the ground, and the information recorded for each reflected pulse. Lasers for terrestrial applications generally have wavelengths in the range of 900-1064 nm, where vegetation reflectance is high (compared with the visible wavelength (400-700) where absorptance is high and little signal would return from the surfaces). Early lidar sensors were profiling systems; recording observations along a single narrow transect. Later systems operated in a scanning mode, in which the orientation of the laser illumination and receiver field of view was directed from side to side by a rotating mirror, or mirrors, so that as the plane moved forward, the sampled points fell across a wide band or swath. It must be noted that, unlike optical or microwave remote sensing, lidar produces swaths of points, not images. However, these can be used to create gridded coverages that resemble images, after appropriate post-processing.

The intensity or power of the lidar return signal is limited by several factors: the total power of the transmitted pulse, the reflectance of the intercepted surface at the laser's wavelength, the fraction of the laser pulse that is intercepted by a surface, and the fraction of reflected illumination that is scattered in the direction of the sensor. The laser pulse returned after intercepting a morphologically complex surface, such as a vegetation canopy, will be a complex combination of energy returned from surfaces at numerous distances, the distant surfaces represented later in the reflected signal (Harding et al. 2001). The type of information collected from this return signal distinguishes two broad categories of sensors. *Discrete-return* lidar devices measure either one (single-return systems) or a small number (multiple-return systems) of heights by identifying, in the return signal, major peaks that represent discrete objects in the path of the laser illumination. The distance corresponding to the time elapsed before the leading edges of the peak(s), and often the power of each peak, are typical values recorded by this type of system (Wehr and Lohr 1999; St. Onge et al., Chapter 19). *Waveform-recording* devices record the time-varying intensity of the returned energy from each laser pulse, providing a record of the height distribution of the surfaces intercepted by the laser pulse (Harding et al. 2001; Lefsky et al. 2002). Both discrete-return and waveform recording sensors are typically used in combination with instruments for locating the return signals in three dimensions.

2.2 General characteristics of imagery

There are four general concepts that apply, with slight modifications, to sensors in all three of the modes of image formation we have discussed (i.e., optical, microwave, and lidar). These are: spatial resolution and extent, spectral resolution, radiometric resolution, and temporal resolution and extent.

2.2.1 Spatial resolution and extent

Spatial resolution, commonly referred to as “pixel size” in digital images, is a key element of both digital and air photo remote sensing. Air photos have an inherent spatial scale that is a function of camera focal length and aircraft flying height. Although photo scale can be thought of as related to the unit area of the Earth's surface that can be resolved, resolution of air photos is also a function of the film's halide crystal grain size (or film speed). Digital sensors also have inherent spatial properties, but rather than referring to scale, the term spatial resolution or pixel size is most commonly used. Digital image spatial resolution refers to the size of the individual physical sample unit on the ground that is sensed by a given detector at any instant in time. For example, a resolution of 10 m means a single digital cell contains integrated spectral information from a nominal 10 m x 10 m unit of the Earth's surface. In practice, the design of a sensor can allow the energy that is recorded for a single pixel to come from beyond that pixel's nominal boundary, but this is rarely an issue in applications.

The spatial resolution of lidar data cannot be summarized in a single pixel size as can be done for optical and microwave images. For these latter images types, data is usually collected such that the instantaneous field of view (IFOV; the area over which each pixel integrates) approximates the spacing between adjacent pixels. For airborne discrete-return lidar, measurements are usually made in a Z-shaped or sinusoidal path as the platform moves forward. The IFOV of an individual measurement is determined by the divergence of the (initially narrow) laser beam, and the altitude above ground level of the platform. The lidar IFOV for forested areas is usually less than a meter, while the spacing between measurements is generally a meter or more, therefore the coverage of the scene is not spatially comprehensive. However, these spot measurements of height can be processed to a gridded image of the maximum height surface (Digital Surface Model), minimum height surface (Digital Terrain Model), or an image of canopy height above the terrain. Waveform recording lidar uses large footprints that are contiguous, and the concept of spatial resolution applies as it would for conventional optical sensors. However, these sensors

add a vertical component to spatial resolution, as their measurements are made using vertical bins of specified depth within each pixel (Harding et al. 2001).

Users of remote sensing data have developed a common frame of reference for efficient and effective communication, starting with the taxonomic structure for remote sensing models developed by Strahler et al. (1986). This taxonomy distinguishes between a ground scene and an image of that scene, the continuous versus discrete nature of a scene, image spatial resolution and scene object resolution, and deterministic and empirical models of a scene. Concepts associated with scale and spatial resolution in relation to image processing models are further developed by Woodcock and Strahler (1987). This paper is required reading for anyone faced with a choice of image data and processing schemes for a specific set of mapping objectives. What Woodcock and Strahler (1987) demonstrate is that the spatial structure of a scene in combination with the type of information desired from associated imagery, tend to limit the choice of appropriate image processing models for classification (e.g. spectral classifiers, spatial classifiers, mixture models, and texture models). Together, these two seminal papers provide a foundation from which to build a solid understanding of the spatial aspects of remote sensing.

2.2.2 Spectral and radiometric resolution

Spectral resolution is a complex attribute that refers to both the number and spectral width of the bands in a given sensor. Sensors with more bands and narrower spectral widths are spoken of as having higher spectral resolution. The spectral resolution of most current operational remote sensing systems is quite limited. Landsat TM has six spectral bands in the reflective portion of the electromagnetic spectrum and one in the thermal-infrared region. SPOT HRV multispectral imagery consists of only three spectral bands. Hyperspectral data (e.g., instruments with more than 200 narrow spectral bands) is becoming more widely available (Vane and Goetz 1993), but is not yet at the stage where satellite data can be ordered, although this may change in the next few years.

For microwave, spectral resolution refers both to the number of bands available, and because of their ability to increase the utility of the data, the number of polarization combinations that can be used. Terrestrial lidar sensors have, until recently, used only a single spectral band, most often between 900 and 1064 nm. Bathymetric sensors have long used two wavelengths, one to determine the height of the water surface, another to penetrate it. Bathymetric sensors have been used in terrestrial applications (Nilsson 1996), with improved discrimination of the foliage and ground

surfaces. However, there are now emerging plans for several multispectral lidar devices, including NASA's Experimental Advanced Airborne Research Lidar (EAARL, Brock and Wright 2000).

Radiometric resolution is often interpreted as the number of intensity levels that a sensor can use to record a given signal. In an optical sensor this signal is the at-sensor radiance, which is commonly quantized to 8 bits. This gives the sensor 256 grayscale levels to record a given signal. However, many sensors use 10 or 16 bits to record a given signal, yielding 1024 or 65536 levels of gray respectively, thus allowing finer discrimination of the radiance at a particular wavelength.

2.2.3 Temporal resolution and extent

Temporal resolution, often referred to as the "revisit interval", is the time between opportunities to obtain imagery over a given spot. Temporal resolution is a key attribute even when only one image is required, especially when adverse atmospheric conditions are in place during much of the time when one wishes to obtain imagery. The probability of obtaining an image with clear sky conditions in a place like the Pacific Northwest of the U.S. or the Brazilian Amazon is directly related to the number of viewing opportunities, and therefore to temporal resolution. While one image per area of interest is the norm for most studies, the ability to capture phenological changes (Townsend et al 1985; Oetter et al. 2000) and, in passive optical images the changing interaction of the Sun with the geometry of a forest canopy, can lead to substantial improvement in the prediction of forest attributes (Wolter et al. 1995; Lefsky et al. 2001).

Temporal extent is an often-overlooked aspect of sensors. Normally, we look for an optimal sensor in terms of its ability to meet our current needs. However, many forestry applications have, or will develop, a significant historical component. This fact should be considered when designing a remote sensing project. For instance, the MSS is a four-band sensor with an unusual rectangular pixel that is 57 m x 80 m. For most applications, images from the TM sensor have replaced it. However, MSS has one attribute that no other sensor can ever match – it was the first moderate-resolution, multispectral, digital satellite sensor. If you need to map forests in the years between 1972 and 1983, or assemble (in the year 2002) a 30-year record of forest change, you will need to work with MSS, and consider how to compare it to more modern imagery types (Franklin et al., Chapter 10). Similarly, if there is likely to be a continuing demand for work in the study area, the ability to collect similar imagery at a later time should also be considered.

2.3 Sensor tradeoffs

Three sensor tradeoffs need to be discussed before a brief review of commonly used sensors is made. These tradeoffs include the use of a sensor on an airborne or satellite platform, the use of digital or analog image collection and processing, and the tradeoff between the various types of resolution and image extent.

2.3.1 Airborne versus satellite

Trade-offs between airborne and satellite image collection include both practical logistical tradeoffs and fundamental tradeoffs in the kinds and quality of data that are available. At the most practical level, most satellite collections of data are available only on predetermined schedules, and even those with an “on-demand” capability are also limited by their orbits and the demands of other users. In contrast, airborne data collections usually offer a much greater level of flexibility. An airborne system can wait for better weather conditions (although that may be costly), whereas a satellite may not be overhead for weeks – at which time the phenomenon you want to view may be gone. Airborne systems can also sample at any time of the day (and sometimes night) whereas satellites generally pass over a site at the same time each day. Airborne sensors can wait for clouds to clear, or to fly the cloud-free areas of a large area until the project is completed. In addition, many missions are simply flown below the altitude of the clouds that would show up on a satellite image.

An additional set of advantages of airborne data result from the relative ease with which sensors can be fitted in an airborne platform, as opposed to being launched on a satellite. As a consequence a wider, and more technologically advanced, set of sensors is available for airborne platforms. These sensors include systems with higher spectral resolution, and advanced microwave and lidar sensors, many of them “proof-of-concept” devices for what (we hope) will be future satellite systems. Of course, higher spatial resolutions are easier to obtain from airborne platforms, due to their lower altitude.

While airborne sensors have their advantages, it is generally satellite systems that have the most advantages for the scientist or manager interested in understanding, mapping and managing large areas. Landsat TM and ETM+ images, one of the most widely used types of imagery, are each 185 km wide by 185 km long, and are taken at an altitude of 705 km. In the absence of clouds or haze, that entire area will be radiometrically consistent, and can in some cases be analyzed with only a few preprocessing steps. In contrast, images collected from an airborne platform will require radiometric

correction and mosaicking before they can be used. In addition, geometric distortions due to topography are less pronounced in imagery collected at higher altitudes, making the satellite images easier to geo-register.

2.3.2 Digital versus analog

Given the recent emergence of high spatial-resolution digital sensors on both satellite and airborne platforms, and our general eagerness for new technology, it would seem that air photos would gradually be phased out of forest remote sensing. Nevertheless, they retain a number of advantages over digital sensors. Aerial photography is the oldest, most frequently used, and best understood form of remote sensing. The spatial resolution of aerial photographs is variable, but high-resolution aerial photography has the best spatial resolution of all remote sensing techniques. For forestry applications, a moderate resolution photo would have a 1:12000 scale, equivalent to a spatial resolution of about 0.4 m. Higher resolution aerial photography (1:5000), would have a spatial resolution of about 0.16 m, and could be used for mapping of forest regeneration and similar purposes (Pitt et al. 1997). Digital frame cameras or satellite sensors such as IKONOS cannot currently match this level of spatial resolution at the swath widths available with aerial photography.

The advantage of digital images is that they are ready to be used with *image processing* software, allowing a number of automated enhancement and classification procedures to be applied. In contrast, *image interpretation* generally requires an experienced specialist, using manual procedures, to extract forest inventory information, and as a result the interpreted information can be expensive, time-intensive, and may vary from one interpreter to another (Wulder 1998). As a consequence, digital methods have been introduced in an attempt to expedite the photo-interpretation process and make it more consistent. However, interpretation is often still necessary, and in some cases cost-effective, for extracting those forest stand attributes that rely on sophisticated identification of subtle spectral and textural signatures.

2.3.3 Resolution versus extent

We have discussed four types of resolution- spatial, spectral, radiometric and temporal. All else being equal, we might prefer to address our remote sensing problems using images with small pixels, a large number of spectral bands, and with multiple images taken closely in time. However, there is a drawback to such a strategy – we cannot increase any of these resolutions without increasing the quantity of data collected. While processor speed and

storage capacities seem to be increasing without end, our on-going informal survey of remote sensing labs suggests that the volume of data they are processing is increasing as fast or faster than improvement in the technology. Fortunately, the optimal resolution for a given application is hardly ever the maximum available resolution.

2.3.3.1 Spatial resolution

Spatial resolution, as discussed by Strahler et al. (1986), can be best understood in reference to the size of the objects that we want to sense. Imagery whose spatial resolution is coarser than these objects are low, or L-resolution. The radiance of image pixels of this type is a function of multiple objects (including background), and this averaging effect can be useful by reducing high spatial frequency variance. This is useful, for example, in that it creates the kind of stable and representative spectral classes needed for many types of image processing. However, when pixels are much larger than the objects of interest, they will tend to average multiple objects that have different attributes. In contrast, high, or H-resolution, images will contain multiple pixels for each object, which adds to the overall variance of the image. For instance, in an image in which individual trees are represented by multiple pixels, each pixel may be shadowed or sunlit, young foliage or old, or may contain one of a variety of different understorey components. If one is going to map forest as a single class, rules will need to be developed to incorporate all of these cover types into one, and also to separate, for instance, shadow in the forest from shadow on the shoulder of a road (Culvenor, Chapter 9). As a consequence, images with a spatial resolution near the size of the objects of interest are usually preferred (Woodcock and Strahler 1987).

One successful strategy that numerous researchers have pursued is the combination of high and moderate (or moderate and low) spatial resolution data. Cohen et al. (2001) used aerial photography to visually estimate total and coniferous tree cover, and visual crown diameter, for photo-plots over western Oregon, which could be done reliably and did not require expensive fieldwork. They then used regression between this data and Landsat TM spectral indices to create comprehensive coverages of these variables throughout the study area. By using high-resolution data, direct visual interpretation of the imagery was possible, and the resulting estimates could be used to train the lower-resolution data, providing a coverage that would not be as efficiently achieved with aerial photography or TM alone.

2.3.3.2 Spectral resolution

Increasing the number of spectral bands would seem to be an obvious way to improve prediction of forest attributes. Hyperspectral sensors expand

on the capabilities of sensors like Landsat TM by replacing their few broad spectral bands with many narrow spectral bands (Niemann and Goodenough, Chapter 17). The motivation for this modification is the assumption that improved identification of particular spectral features will lead to improved discrimination of cover attributes. This assumption has been supported for the problem of the identification of mineral composition (Van Der Meer 1994), and specific features of canopy chemistry (Martin and Aber 1997; Zagolski et al. 1996), but not yet for remote sensing of forest structural attributes. Lefsky et al. (2001) found that AVIRIS hyperspectral images did poorly with respect to predicting forest structural attributes. This result, while tentative, can be explained by the relatively high level of correlation between the reflectance at closely spaced wavelengths, and the spectral simplicity of most forested scenes.

2.3.4 Temporal resolution

While temporal resolution might seem applicable only to change detection studies, multiple images from the same growing season have increased potential to detect forest structural attributes. For forest structural attributes such as basal area, biomass, and foliage biomass, Lefsky et al. (2001) found substantial increases in predictive power were obtained using a multi-temporal Landsat TM dataset (six images from a single growing season) in comparison to other imaging sensors, including high spatial and high spectral resolution images. The use of this sequence of images allows information on vegetation phenology to be considered (Oetter et al. 2001). It also includes images with both low and high Sun angles, which allows an indirect measure of shadow through the variable shadowing in the canopy, which is closely related to canopy height and canopy height variability (Li and Strahler 1992; Schriever and Congalton 1995).

3. CLASSES OF IMAGERY

The discipline of remote sensing is experiencing an unprecedented period of increase in sensor numbers. However, while academic research may be increasingly concerned with these newer instruments, application work is still focused on those sensors that are established and relatively well understood. Therefore, we will focus only on these most commonly used sensors. Comprehensive reviews of currently available sensors are available in a number of texts (e.g. Kramer 2001).

In principle, any sensor can be used for any problem; for instance, it would be possible to address global land-cover using one-meter

hyperspectral imagery. If there were products that could only be created from such imagery, and if the demand for those products were great enough, then resources for such an effort might be made available. In practice there exists classes of problems that are most efficiently addressed using imagery with certain data characteristics, and we have divided sensors into these classes for the purpose of discussion. However, it must be borne in mind that these classes only reflect dominant usage at this time, and that demand for particular data products may, in the future, reassign or blur the assignment of some sensors. (Figure 2-2).

3.1 Low resolution optical sensors

Although less often used by an individual forest manager or ecologist interested at the regional or smaller scales, these lower resolution devices have numerous advantages for regional, continental and global scale mapping (Cihlar et al., Chapter 12). Many of the existing vegetation data products have been have and continue to be created using this data type, and their potential and limitations should be understood. In addition, numerous techniques used with data of higher spatial resolution were first developed for AVHRR applications, an important piece of context to bear in mind.

3.1.1 Advanced Very High Resolution Radiometer (AVHRR)

Although designed by NOAA as a weather satellite, AVHRR has seen extensive use in wide area land-cover and biophysical mapping at its intrinsic spatial resolution of 1.1 km, and resampled resolutions up to 16 km. Most often the data used in such studies are vegetation indices created from the red and near-infrared bands (Tucker 1996), in fact the vegetation index approach first saw widespread use in the interpretation of AVHRR data. The high temporal resolution of this sensor, which has a repeat interval that can provide two observations per day, has promoted the development of creating cloud-free scenes through taking maximum normalized difference vegetation index (NDVI) in a period (often bi-weekly), and the use of multi-temporal datasets for land-cover classification. Currently, high quality radiometrically corrected dataset are readily available (e.g. the Pathfinder Datasets, including an 8 km resolution product, available globally from 1981-1986). AVHRR data have been used for monitoring vegetation productivity (Tucker et al. 1980), herbaceous biomass (Tucker et al. 1983), and a variety of other ecological phenomena (Loveland 1991; Tucker 1996; Moisen and Edwards 1999).

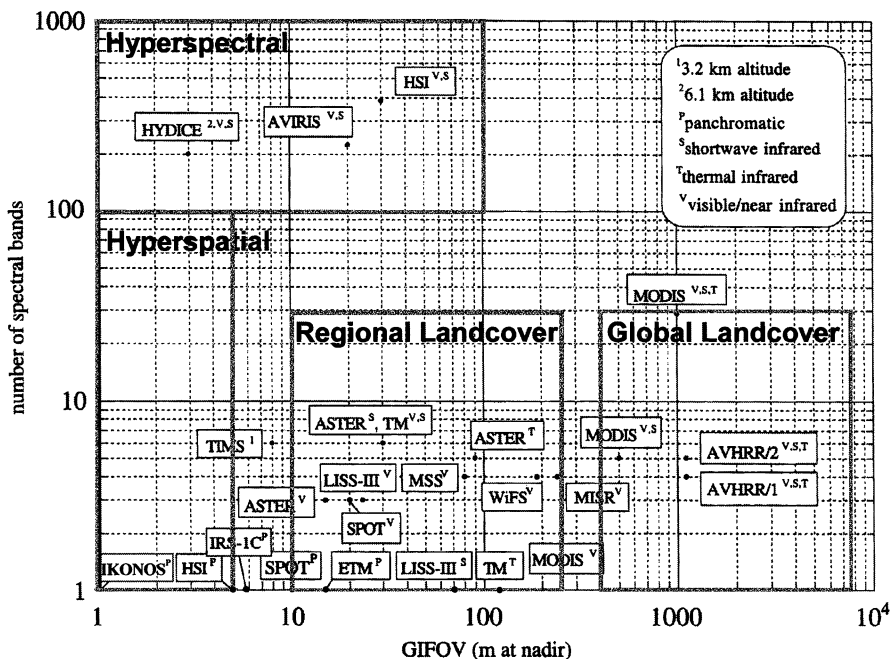


Figure 2-2. Diagram of commonly used sensors, plotted in a space formed by their ground-projected instantaneous field of view (GIFOV, i.e. pixel size) and number of spatial bands.

The boundaries of the four sensors types used in the text are indicated. Adapted from Schowengerdt (1997) with permission.

One technique of direct interest to forest ecologists and managers is the method of combining two different classes of imagery, in this case, AVHRR and Landsat TM, to map an attribute of interest. In these studies (Iverson et al. 1989; Zhu and Evans 1992), a subset of TM images for the study area were classified into timberland or non-timberland and then the fraction of each of the 30 m TM pixels within each AVHRR pixel was calculated. Regressions were then performed between the TM estimate of percent timberland and indices derived from the AVHRR image to provide wide area coverage of forest cover. Starting with Townsend et al. (1985), classification of NDVI trajectories for the growing season (calculated using AVHRR) have also been used extensively for land cover classification (Loveland 1991).

3.1.2 Moderate resolution Imaging Spectrometer (MODIS)

Partially in response to the utility of devices like AVHRR, MODIS was designed as a low to moderate resolution sensor to address question concerning land surface processes, atmospheric water vapor, clouds and aerosol monitoring, ocean color, phytoplankton and biogeochemistry, and temperatures of the surface and clouds (Masuoka et al. 1998; Justice et al. 1998). In contrast to AVHRR, which has two bands of interest for vegetation mapping, MODIS has at least 7 (Colour Plate 1) suitable for vegetation studies. Whereas AVHRR had a resolution of 1.1 km, MODIS data has variable spatial resolution in each band, including 250 m resolution bands in the red and near-infrared, 500 m bands for blue, green, and middle infrared, and 1000 m in the visible and near infrared. MODIS, the instrument, is currently flying on the Terra spacecraft; a second satellite, Aqua (EOS PM) was launched in the spring of 2002, with the same model of MODIS sensor (among others) on board. The temporal resolution of MODIS data is currently 1-2 days, when Aqua is operation, the interval will be half that.

A unique feature of the MODIS program is the time and effort spent of algorithm development for the sensor. In addition to the raw data typically provided from a sensor, the MODIS datasets include radiometrically corrected reflectance (Colour Plate 2A & B), vegetation indices, leaf area index (Colour Plate 2C), land cover and land cover change, and even a model based estimate of NPP (Running et al. 1994). While these products will require extensive validation (Cohen and Justice 1999), and may not be relevant for some individual's purposes, many researchers will find them useful as, at least, inputs for intermediate steps in the creation of data products.

3.2 Moderate resolution optical satellites

For all the variety in sensors available to the remote sensing analyst today, the majority of digital image processing for terrestrial projects is still being done with this class of instruments, and with one of two families of sensors: Landsat TM and SPOT. In our opinion, this reflects the general utility of these devices, rather than the timidity of the remote sensing community. Each strikes a balance between spatial, spectral and temporal resolution that has met the needs of land managers and scientists for (in the case of Landsat) the last three decades.

3.2.1 Multispectral Scanner (MSS), Thematic Mapper (TM), and Enhanced Thematic Mapper Plus (ETM+)

Launched in July of 1972, Landsat 1 carried two instruments, the Return Beam Vidicon (eliminated after the launch of Landsat 3 in 1978) and the Multispectral Scanner, (eliminated after the launch of Landsat 5 in 1984). Few people today use the Return Beam Vidicon data, so we will focus on MSS. MSS had four principal bands: green, red and two bands in the near-infrared. A fifth band in the thermal was added for Landsat 3, then subsequently removed. The pixel size of MSS is source of some confusion: the IFOV of the pixels is 79.5 m (81.5 m in Landsat 4 and 82.5 m in Landsat 5), but the pixel size in the cross-track direction is over-sampled to 56.5 m. While MSS has been distributed with the 56.5 x 79.5 m pixel size, it is also routinely resampled to a 60 x 60 m pixel size for distribution. MSS data has relatively low radiometric resolution, 7 bits for the first three bands (green, red, and the first near-infrared) and 6 bits for the second near-infrared band. Although MSS is no longer part of the Landsat complement of sensors, it is still in use for historic and change-detection studies (Cohen et al. 1996).

TM was first included on Landsat 4, launched in 1982. It contains seven bands (Colour Plate 1) including red, green, blue, near-infrared, two mid-infrared and a thermal band. Pixel size is 28.5 meters in all bands except the thermal (120m). The sensor design allows each pixel to be observed for a longer period than in the MSS, which allows smaller pixel size and 8-bit resolution. Improvements in ETM+, launched on Landsat 7 in 1999, include the addition of a 15 m panchromatic band, and improved spatial resolution (60 M) on the thermal band. Early Landsat satellites (1-3) had a revisit interval of 18 days; later satellites had orbits with a revisit interval of 16 days. MSS, TM and ETM+ all have an image size of 185 km x 185 km. Colour Plate 2D presents a single tasseled cap transformed TM image from the H.J. Andrews Experimental forest on the western slope of the Cascade range in Oregon. Colour Plate 2E shows the first three principal components from a 6-image stack of tasseled cap images for the same area, as described in Lefsky et al. (2001).

3.2.2 Système Pour d'Observation de la Terre (SPOT)

The French SPOT system was first launched in 1986, and a total of four satellites with three different sensors have been launched. The earliest device, the HRV, is similar to Landsat MSS in spectral resolution, consisting of green, red, and near-infrared bands. It has a narrower swath (60 km vs. MSS 185 km), but higher spatial resolution (20 m vs. MSS 56 x 79 m). It can also work in a panchromatic mode to achieve 10 x 10 m resolution – a

significant achievement in 1984. SPOT 4 carries an updated HRVIR instrument that adds a mid-infrared band to allow some of the TM capabilities dependent on that spectral range, such as the tasseled cap wetness index.

3.3 High spatial resolution sensors

Although there are many sources of high spatial resolution (hyperspatial) imagery, we will focus on the two digital technologies: digital frame cameras and high-resolution satellites. Aerial photography has already been discussed in section 2.3.2.

Digital frame cameras replace the film in a conventional camera with a solid-state array of imaging elements. Because of similarity of the two systems, much of what is known about aerial photographs can be directly applied to DFC's. The use of DFC's allows real time viewing of results, eliminates film processing and printing charges, and the errors associated with scanning conventional photographs or transparencies. Unlike similar line-imager devices, each pixel in the DFC image is acquired simultaneously, which simplifies geo-rectification. Current sensor arrays (as in the ADAR 5000/5500) result in narrower swath widths than conventional aerial photographs, and are generally flown with a spatial resolution of about 1 m, but can be flown at higher resolutions at the expense of even narrower swath width. With projected improvements in the sensor arrays, it has been estimated that the data from DFC's will replace conventional aerial photographs for many applications (Pitt et al. 1997). Colour Plate 2F shows data from the ADAR 5500 from the H.J. Andrews Experimental Forest. Colour Plate 2G shows the area within the yellow box in Colour Plate 2F.

High-resolution satellites, such as the IKONOS system, have recently become available for commercial use. The IKONOS system, launched in September 1999, offers images with high spatial resolution (1m panchromatic, 4 m multispectral [R, G, B, NIR] – See Colour Plate 1) that are geo-rectified to one of two levels of precision. The IKONOS system can, for an additional fee, be “special-tasked” to an area to acquire images within a seven-day period. A sensor with even higher spatial resolution, Quickbird, was launched in October 2001, with 0.61 m resolution in the panchromatic, and 2.44 m resolution for multispectral [R, G, B, NIR] images.

Aerial photography and digital frame cameras are airborne sensors which will allow for the most flexibility in planning deployments; however selection of an airborne sensor will demand that some time be devoted to plan and coordinate contracting for collection of images. Of the two airborne sensors, aerial photographs have superior spatial resolution, and can be analyzed without being scanned and geo-rectified, which may save time in

analysis. If it will be necessary to directly manipulate the image data, digital frame cameras have the advantage of providing a digital product, without the errors associated with the scanning process. However, it should be noted that data collected from unrectified aerial photographs is often successfully incorporated into a GIS framework through simple visual comparison of features on the photos to existing rectified images, and subsequent on-screen digitization. The chief advantage of using data from high-resolution satellites is that they are available “off the shelf”, and will require minimal planning. However, as with 1m DFC imagery, their spatial resolution is still relatively coarse for some analyses typically done with aerial photography (Pitt et al. 1997; Culvenor, Chapter 9).

3.4 Hyperspectral sensors

The sensors discussed so far are multispectral – wherein they record a small number of spectral bands that represent relatively wide spectral ranges. Multispectral sensors are one strategy for obtaining spectral data. To efficiently record most variation, they break the spectra into a few bands where there are significant differences between the spectra of a wide range of materials. The process inevitably results in compromises, as a good band interval for one application may not suit another. As technology improved and more data could be recorded, hyperspectral sensors were developed. These sensors record many (often more than 200 as in AVIRIS – See Colour Plate 1) narrow bands, and avoid the errors introduced by low spectral resolution (Niemann and Goodenough, Chapter 17). Although these sensors have been in the commercial market, and satellite systems are being worked on, they are more costly and more difficult to obtain than satellite images or *hyperspatial* images. The spectral resolution of one of these sensors is impossible to capture in the three bands available in the print medium, Colour Plate 2H and 4J present the first (1-3) and second (4-6) set of three principal components of an AVIRIS image collected at the H.J. Andrews Experimental Forest. Richards and Jia (1999) detail the features of six popular airborne hyperspectral sensors.

3.5 SAR sensors

There are currently three operational satellite SAR systems, the European ERS-1 and ERS-2, and the Canadian Radarsat. The ERS satellites, launched in 1991 and 1995, operate in the C band with a single (VV) polarization, and cover a 100 km wide swath with 30 m pixels. Although the ERS satellites were primarily designed for oceanographic applications, these also have seen wide use on land. Radarsat is the more versatile of these satellites, with one

standard and six non-standard modes, all with a C band, HH polarization signal. Incidence angles can range from 19 to 49 degrees, and swath widths from 50 to 500 km. Cross-track (or range) resolution is 27 m while along-track (azimuth) resolution varies from 19-24 m. Either satellite can be used for interferometry, with some limitations (Baltzer 2001).

There are also a number of airborne radar systems that have potential for use in remote sensing of forests. TOPSAR, developed by NASA's Jet Propulsion Laboratory (JPL), was designed as a topographic mapping sensor by radar interferometry, and can collect multi-polarization data in the L, P and C bands. As mentioned before, the coherence between the two interferometric return signals has been used to estimate vegetation height (Rodriguez and Martin 1992). Typical swath width is 10 km. GEOSAR, developed by JPL, the California Department of Conservation, and Calgis, Inc, is another device designed for interferometric mapping of topography, that could also provide multi-polarization data in the X and P bands, over a 20 km wide swath (Hensley et al. 1999).

3.6 Lidar sensors

Discrete-return lidar has become a growth area for both specialized remote sensing suppliers, as well as larger surveying and photogrammetry firms (Flood and Gutelis 1997). The primary customers of these firms are municipalities, developers and natural resource managers seeking a relatively low cost alternative to traditional surveying to provide high resolution topographic maps and digital terrain models (DTM), or companies looking for rapid methods to survey utility right-of-ways. While these firms are making lidar remote sensing more available, their systems are designed and operated with the needs of their primary customers in mind. Therefore, a careful consideration of the sensor configuration and post-processing techniques must be made with project goals in mind. Numerous different discrete-return systems are available; for a detailed technical review of these sensors, see Wehr and Lohr (1999). A directory of sensors and lidar remote sensing firms can be found in Baltsavias (1999).

4. MATCHING IMAGERY WITH APPLICATIONS

When thinking about the attributes of the forest that we want to remotely sense, it becomes clear that there are several broad classes of attributes that share related mechanisms of, and limitations on, their remote estimation. For instance, the mechanisms involved in the remote sensing of canopy cover, absorbed photosynthetically active radiation (F_{APAR}), and leaf area index

(LAI) are going to be similar, although the formal definition of these attributes, and their estimation in the field, can be quite different. For the purposes of this discussion, we have defined classes of attributes related to: canopy cover, stand structure, stand composition, and disturbance. Each class is defined by the commonality among the attributes themselves, by the aspect of canopy structure that they are related to, and by the way that aspect of canopy structure modifies the quantity and quality of electromagnetic radiation.

4.1 Attributes related to canopy cover

These attributes, which include foliage or canopy cover, F_{APAR} , and leaf area index, have the clearest link with the aspects of the physical organization of the canopy that remote sensing can most easily measure. In conventional optical imagery, such as aerial photos, Landsat ETM+, or SPOT HRV, reflected energy from the canopy and background surfaces mix in a roughly linear fashion, so that if there is 50% canopy cover, then 50% of the signal returned to the sensor will be from foliage, and 50% from the other cover components, such as bare soil, rock, and ground vegetation. Increasing canopy cover will be indicated by decreased reflectance in the visible (especially red) wavelengths (darker tones on aerial photography), due to the high absorptance of foliage in this spectral range. At the same time, foliage is highly reflective in the near-infrared, so that increasing foliage does not affect brightness in this region as much.

Numerous indices ((Normalized Difference Vegetation Index (Tucker 1979), Tasseled Cap Greenness (Crist and Cicone 1983), Simple Ratio (Spanner et al. 1994)) exploit the continuous spectral difference to distinguish between high and low canopy cover (Asner et al., Chapter 8). Any one of these indices can do a reasonable job of predicting a variable like canopy cover or F_{APAR} . One variable that is more difficult to predict, and which has received a lot of attention from the remote sensing community, is LAI. LAI can be considered as the number of layers of leaves that occur above a single point on the forest floor (for details, see Fournier et al., Chapter 4). In forests, LAI can be expected to vary from 0 to 10 and occasionally even higher. Although LAI is a desirable variable for biogeochemical models, the relationship between it and cover is asymptotic; with each additional layer of leaves the amount of additional cover becomes smaller, so that after a leaf area index of 4-6, the additional layers of leaves have little effect on cover. Because changes in reflectance are being driven mostly by the change in cover, the relationship between reflectance (and reflectance derived indices) and LAI is also asymptotic (Sader et al. 1990; Spanner et al. 1990; Chen and Cihlar 1996).

Microwave sensors have also been evaluated for the estimation of cover and LAI, despite their problems with moisture on the leaf surfaces leading to variations in the dielectric constant (Sader 1987). In addition, the horizontal orientation of leaves has been a problem in estimation of LAI in deciduous canopies. However, in needle-leaf coniferous canopies, SAR systems have been able to assess LAI up to values of 4 (Franklin et al. 1994, Ulaby and Dobson 1993).

Estimates of canopy cover have been made using both discrete-return and waveform-sampling lidar sensors. These estimates are made using the fraction of the lidar measurements considered to have been returned from the ground surface (Nelson et al. 1984; Ritchie et al. 1992, 1995, 1996; Means et al. 1999) where the measurements are the number of discrete returns, or the integrated power of a waveform. In most cases, a scaling factor (implicit or explicit) is needed to correct for the relative reflectance of ground and canopy surfaces at the wavelength of the laser (Harding et al. 2001). In these measurements, the definition of the ground surface is a critical aspect of cover determination. If the number or power of the measurements assigned to the ground return are overestimated (i.e., the elevation of the ground surface is overestimated) cover will be underestimated, and vice versa. Lefsky et al. (1999b) reported on a novel technique to estimate LAI in temperate coniferous forests, using measurements of canopy volume from a waveform recording lidar. However, this result has yet to be examined in other ecosystems.

4.2 Attributes related to canopy height

The next group of variables are related to the mean and variability of canopy height. These include tree volume, aboveground biomass, basal area, mean diameter-at-breast-height (DBH), stem density and stand age. Again, the formal definition of these attributes, and their estimation in the field, are quite variable. One variable, age, does not seem to belong at all. However, since age itself cannot be directly sensed, it is most often predicted from variables that are related to height and its variability.

Change in these attributes during the early stages of stand development can be estimated using the same cover-related spectral patterns described above, during the period in which change in vegetation cover is rising with vegetation biomass. However, with the exception of very low productivity stands, canopy closure occurs early on in most stands, while height and other attributes continue to change. Trees continue to grow in height for much of their individual lifetimes without dramatic spectral changes at the leaf level. However the spatial organization of the forest does change, as the size of the average dominant or co-dominant crown increases. Furthermore, the

development of patch-scale dynamics, as the initial cohort of trees dies and younger trees take their place, means that the canopy's structure keeps changing long after the oldest trees die. This increasing variability is a sign of older stands in many forest types and can be seen in optical imagery as the presence of increasing shadow.

Accurate estimation of height-related variables is one of the most difficult tasks in the remote sensing of forests, especially in moderate to high biomass forests. Passive optical and active microwave sensors can predict these variable well in the first stages of stand development, but at moderate and high levels of biomass or volume they have poor discrimination or none at all. In a summary of research on SAR systems, Waring et al. (1995) stated that single-band systems with a single polarity had a detection limit of 150 Mg ha⁻¹ for biomass and that even a combination of bands and polarizations would reach their limit at 250 Mg ha⁻¹. Similar results pertain for optical remote sensing (Sader et al. 1989; Hyppa et al. 1998; Lefsky et al. 2001). Nevertheless, for monitoring the first stages of forest development, managed stands with a short rotation age, or forests with naturally low biomass, microwave and optical systems can be effective. In some conifer forests (in particular Douglas-Fir / western hemlock) the observable aspects of canopy structure continue to change throughout stand development, and prediction of height, and its relative variables (such as aboveground biomass and in some cases, age) are more successful. These aspects of canopy structure can include trees of large stature, deep shadow, snags and dead wood in the canopy, and extensive colonization of the canopy by lichens.

It is becoming widely accepted that lidar sensors have a capacity for measuring height related attributes, including volume and aboveground biomass, to a greater degree than any other sensor type. Studies involving both discrete-return and waveform-record sensors have had success measuring height (Nelson et al. 1988), volume (Maclean and Krabill 1986), biomass (Lefsky et al. 1999a; Lefsky et al. 1999b; Drake et al. 2002), and basal area (Lefsky et al. 1999a, 1999b). These studies have involved deciduous (Lefsky et al. 1999a; Drake et al. 2002), coniferous (Nelson et al. 1988; Nilsson 1996; Naesset 1997; Lefsky et al. 1999b) and mixed (Maclean and Krabill 1986) stands in boreal (Naesset 1997; Nilsson 1996), temperate (Maclean and Krabill 1986; Nelson et al. 1988; Lefsky et al. 1999a, 1999b) and tropical sites (Nelson et al. 1997; Drake et al. 2002). While lidar currently remains one of the more expensive remote sensing datasets to obtain, the increasing use of this technology for land surveying may bring down costs. In addition, analyses pairing lidar with either optical (Hudak et al. 2002) or interferometric SAR (Rodriguez et al. 2002) may result in a lower cost alternative to comprehensive lidar coverage.

4.3 Composition attributes

Attributes related to composition are the most difficult set of attributes to summarize, due to the diversity of attributes themselves and the variety of spectral or other features used to predict them. Compositional attributes include physiognomy, phenological types (deciduous vs. evergreen), species level composition, and a variety of cover type classifications. Composition can be related to the spectral qualities of the vegetation itself, vegetation cover and its pattern, and even the spectral qualities of the background that the vegetation partially obscures. This presents an inherently complicated picture, however in many forested landscapes the tasseled cap transformation can simplify the spectral qualities of a scene, by contrasting the vegetation against soil, shadow and other scene components. Although the coefficients of the tasseled cap were derived from examination of multiple MSS (Kauth and Thomas 1976), and later TM (Crist and Cicone 1983), scenes, an empirical analysis of images from forested scenes usually produces three bands that are similar to it. Therefore, it is justifiable to use this ordering of the spectral variance of a scene as a tool to understand composition.

Within the context of western Oregon, Cohen et al. (2001) found that brightness (essentially the average of the six non-thermal TM bands) is associated with soil and litter cover (soil is commonly brighter), varying proportions of vegetation cover (high cover is darker), and with the distinction between conifer and deciduous cover (conifer is darker). Greenness (the contrast between visible and infrared bands) is associated with changes in vegetation cover (similar to NDVI) and with the proportion of conifer versus hardwood. Wetness, which is a contrast between the visible and near-infrared channels and the mid-infrared bands, is associated with increasing age and crown size in conifer stands, with lower wetness in more developed stands. In western Oregon, these three simple transformed bands have been shown to explain much of the variation in vegetation cover, conifer cover, conifer crown diameter and age (Cohen et al. 2001).

Any sensor that approximates the selection of bands that Landsat offers (e.g., the HRVIR sensor on SPOT 4) should be able to duplicate these results. However, sensors that do not include the middle-infrared band may not be able to adequately represent the wetness component of the tasseled cap, which may set a lower bound on the number and kind of bands that a sensor for forestry applications should have. Setting an upper bound on the spectral information that is needed for such a sensor is more difficult. Hyperspectral sensors have been advanced as one way to get better composition information, and some results support this (Gong and Yu 1997; Martin et al. 1998). However, as pointed out earlier, most plants have very

similar spectral responses, and sunlit foliage (from which the spectra will be most clear) occurs in mixture with other components of a canopy image: shadow, shadowed foliage, and background. Therefore it is unclear whether the hyperspectral approach will yield widespread advances in predicting forest composition.

4.4 Change / disturbance monitoring

Change detection involves the comparison of images from a given location at two or more points in time. One can simply compare summaries of classifications for a given area at different points in time, or can conduct a spatially explicit analysis involving direct comparisons on a pixel-by-pixel basis (Gong and Xu, Chapter 11). In the latter, and more usual case, accurate spatial registration of two or more images is required.

Optical images are the dominant type of remote sensing for change detection, and have proven to be useful for the detection of both dramatic (stand replacement disturbances, Hall et al. 1989; Cohen et al. 2001) and subtle disturbances (insect, low intensity fire, thinning (Franklin et al. 1995; Jakubauskas et al. 1990; Franklin et al. 2000). Image processing approaches developed for optical images have also been applied to SAR images (Banner and Ahern 1995), despite difficulties with the high variability in backscatter due to moisture and seasonality (Cihlar et al. 1992), and the dependence of backscatter on topography and incidence angles (Drieman 1994; Edwards and Rioux 1995). However, the development of interferometric SAR systems, especially those on space borne platforms may soon begin to supplement optical images as a source of data for change detection. The coherence measurement appears to be more stable (Baltzer 2001) than backscatter as variable for change detection analysis. No work on change detection from lidar has yet been published, but numerous groups are looking at doing change detection in height over relatively short time increments (3-10) years. It is believed that such data may provide an estimate of net primary productivity or mean annual increment of volume.

5. CONCLUSION – SELECTING A SOURCE OF IMAGERY

Selecting a source of imagery can be a complicated process, but the first priority must be to select a data source that has a record, preferably in the peer reviewed literature, of being able to predict the attributes you are interested in, and the resolution of the dependent variables you will need.

Resolution in this case refers to the number of levels you need, from a binary presence/absence (as in forest/non-forest determinations) to continuous estimates of a variable like age or aboveground biomass. Increasing resolution in the dependent variable requires a higher level of correlation between the imagery and the dependent variable. For example, accurately distinguishing, with a given confidence, three classes of an attribute requires a lower level of correlation between the attribute and the data source than does distinguishing ten classes or estimating that attribute continuously.

We have reviewed four classes of forest attributes and their ability to be predicted from various imagery types. Variables related to canopy cover will, in the absence of overwhelming cloud cover problems, usually be predicted from optical imagery; the option of using microwave data in this instance will require more complex processing, but is capable of making some of the same measurements, particularly in coniferous canopies. Optical sensors of any spatial resolution are appropriate for cover-like measurements, and hyperspectral data may offer some benefits by being able to use only those narrow spectral regions with the highest contrast, but multispectral data should do an adequate job.

Stand structure can be successfully estimated from optical and microwave sensors, up to relatively low levels of plant biomass. Therefore, if one's study area is predominately low biomass forest, or you only need a few classes of structure, they can be useful. If detailed estimates of forest structure are required in a high biomass study area, lidar will provide the best results. However, for study areas greater than a few tens of km^2 lidar, it is currently too expensive ($\sim\text{US\$ 500 / km}^2$) for many studies.

For general land and forest cover classification, the same caveat used above still holds; unless you have overwhelming cloud cover problems you will probably want to use optical remote sensing. Again, data of many spatial resolutions can be used for these applications, and there is also a good case for hyperspectral data for these applications. One caveat for *hyperspatial* data that bears repeating is that, if individual trees fall in multiple pixels, each pixel may be in one of several classes (shadow or sunlit, young foliage or old), requiring a detailed analysis to retrieve common land-use classes.

For change detection, hyperspectral data does not offer any obvious improvements over multispectral data – the types of change commonly being mapped are related to differences in canopy cover, which is well within a multispectral sensor's ability to describe. High spatial resolution data could have some interesting applications for change detection – but precisely matching images from two dates becomes more difficult as pixel sizes decrease. Low spatial resolution devices will almost always contain changed and unchanged area in a large pixels, although the MODIS device will

produce a 250 m change detection product for global monitoring of land cover change hotspots. The 250 m resolution probably represents an upper limit for accurate change detection and, for most studies, one of the moderate resolution optical sensors would be preferable.

Finally, we believe that our review of sensors for forestry applications strongly suggests that the “best” sensor is often more than one sensor. Whether the combination is high-resolution and lower-resolution (as in Cohen et al. 2001; or Zhu and Evans 1992), multi- and hyper-spectral (Ranchin and Wald 2000), or conventional optical and lidar (Hudak et al. 2002), the motivation is the same – combining the strengths of two or more sensors to create a solution that is tailored for the application being considered. Recognizing the individual strengths and weaknesses of each type of sensor is the first step towards applications that properly use them.

REFERENCES

- Abrams, M. J., Kahle, A. B., Palluconi, F. D., & Schieldge, J. P. (1984). Geologic mapping using thermal images. *Remote Sensing of Environment*, 16, 13-33.
- Asner, G. P., Braswell, B. H. Schimel, D. S., & Wessman, C. (1998). Ecological research needs from multiangle remote sensing data. *Remote Sensing of Environment*, 63, 155-165.
- Bachman, C. G. (1979). *Laser Radar Systems and Techniques*. Artech House, MA.
- Baltsavias, E. P. (1999). Airborne laser scanning: existing systems and firms and other resources. *ISPRS Journal of Photogrammetry & Remote Sensing*, 54, 164-198.
- Baltzer, H. (2001) Forest mapping and monitoring with interferometric synthetic aperture radar (InSAR). *Progress in Physical Geography*, 25, 159-177.
- Banner, A. V., & Aherne, F. J. (1995). Incidence angle effects on the interpretability of forest clearcuts using airborne C-HH SAR imagery. *Canadian Journal of Remote Sensing*, 21, 64-66.
- Brock, J. C., & Wright, C. W. (2000). Preliminary results from a NASA Experimental Advanced Airborne Research LIDAR (EAARL) survey of Pacific Reef in Biscayne National Park, Florida. *Proc. 9th International Coral Reef Symposium*, 233. USGS Center For Coastal Geology, Florida.
- Chauhan, N. S. (1997). Soil Moisture Estimation Under a Vegetation Cover: Combined Active Passive Microwave Remote Sensing Approach. *International Journal of Remote Sensing*, 18, 1079-1097.
- Chen, J. M., & Cihlar, J. (1996). Retrieving leaf area index of boreal conifer forests using Landsat TM images. *Remote Sensing of Environment*, 55, 153-162.
- Cihlar, J., Pultz, T. J., & Gray, A. L. (1992). Change detection with synthetic aperture radar. *International Journal of Remote Sensing*, 13, 401-414.
- Cohen, W., Harmon, M., Wallin, D., & Fiorella, M. (1996). Two decades of carbon flux from forests of the Pacific Northwest. *Bioscience*, 46, 836-844.
- Cohen, W., Spies, T. A., & Fiorella, M. (1995). Estimating the age and structure of forests in a multi-ownership landscape of western Oregon, U.S.A. *International Journal of Remote Sensing*, 16, 721-746.

- Cohen, W., & Justice, C. (1999). Validating MODIS terrestrial ecology products: linking in situ and satellite measurements. *Remote Sensing of Environment*, 70, 1-3.
- Cohen, W., Maiersperger, T. K., Spies, T. T. A., & Oetter, D. R. (2001). Modeling Forest Cover Attributes as Continuous Variables in a Regional Context with Thematic Mapper Data. *International Journal of Remote Sensing*, 22, 2279-2310.
- Crist, E. P., & Cicone, R. C. (1983). Investigations of thematic mapper data dimensionality and features using field spectrometer data. *Proc. Seventeenth Int. Symp. Remote Sensing of Environment*, 3. Environ. Res. Inst. Michigan, Ann Arbor MI, 9-13 May.
- Dobson, M. C., Pierce, L., Sarabandi, K., Ulaby, F. T., & Sharik, T. (1992). Preliminary analysis of ERS-SAR for forest ecosystem studies. *IEEE Transactions on Geoscience and Remote Sensing*, 30, 412-415.
- Drake, J. B., Dubayah, R. O., Clark, D. B., Knox, R. G., Blair, J. B., Hofton, M. A., Chazdon, R. L., Weishampel, J. F., & Prince, S. (2001). Estimation of Tropical Forest Structural Characteristics using Large-footprint Lidar. *Remote Sensing of Environment*, 79, 305-319.
- Drieman, J. A. (1994). Forest cover typing and clearcut mapping in Newfoundland with C-band SAR. *Canadian Journal of Remote Sensing*, 20, 11-16.
- Edwards, G., & Rioux, S. (1995). A detailed assessment of relative displacement error in cutover boundaries derived from airborne C-band SAR. *Canadian Journal of Remote Sensing*, 21, 185-197.
- Eineder, M., Bamler, R., Adam, N., Suchandt, S., & Breit, H. (2000). Analysis of SRTM Interferometric X-Band Data: First Results. *Proceedings of the International Geoscience and Remote Sensing Symposium 2000*, 6, 2593-2595. Honolulu, Hawaii.
- Eppler, D. T., & Farmer, L. D. (1991). Texture analysis of radiometric signatures of new sea ice forming in Arctic lands. *IEEE Transactions on Geoscience and Remote Sensing*, 29, 233-241.
- Flood, M., & Gutelis, B. (1997). Commercial implications of topographic terrain mapping using scanning airborne laser radar. *Photogrammetric Engineering and Remote Sensing*, 63, 327-366.
- Franklin, S. E., Lavigne, M. B., Wilson, B. A., & Hunt, E. R. (1994). Empirical relations between balsam fir (*Abies balsamea*) forest stand conditions and ERS-1 SAR data in western Newfoundland. *Canadian Journal of Remote Sensing*, 20, 124-130.
- Franklin, S. E., Bowers, W. W., & Ghitter, G. (1995). Discrimination of adelgid-damage on single balsam fir trees with aerial remote sensing data. *International Journal of Remote Sensing*, 16, 2779-2794.
- Franklin, S. E., Moskal, L. M., Lavigne, M. B., & Pugh, K. (2000). Interpretation and classification of partially harvested forest stands in the Fundy Model Forest using multitemporal Landsat TM. *Canadian Journal of Remote Sensing*, 26, 318-333.
- Gates, D. M., & Tantraporn W. (1952). The reflectivity of deciduous trees and herbaceous plants in the infrared to 25 microns. *Science*, 115, 613-616.
- Gong, P., Pu, R., & Yu, B. (1997). Conifer species recognition: an exploratory analysis of in situ hyperspectral data. *Remote Sensing of Environment*, 62, 189-200.
- Hall, R. J., Kruger, A. R., Scheffer, J., Titus, S. J., & Moore, W. C. (1989). A statistical evaluation of Landsat TM and MSS for mapping forest cutovers. *Forest Chronicle*, 65, 441-449.
- Harding, D. J., Lefsky, M. A., & Parker, G. G. (2001). Lidar altimeter measurements of canopy structure: methods and validation for closed-canopy broadleaf forest. *Remote Sensing of the Environment*, 76, 283-297.

- Hensley, S., Chapin, E., & Bartman, R. K. (1999). Baseline Calibration Of The Geosar Interferometric Mapping Instrument. *Presented at the Committee on Earth Observing Satellites*. Toulouse, France. October 1999.
- Hudak, A. T., Lefsky, M. A., Cohen, W. B., & Berterretche, M. (2002). Integration of lidar and Landsat ETM+ data for estimating and mapping forest canopy height. *Remote Sensing of Environment*, 82, 398-417.
- Hypsa, J., Huuppa, H., Inkinen, M., & Engdahl, M. (1998). Verification of the potential of various remote sensing data sources for forest inventory. *Proceedings of IEEE Geosciences and Remote Sensing Society*, 1812-1814. July 6-10, 1998, Seattle Washington. IEEE, Piscataway, NJ.
- Iverson, L. R., Cook, E. A., & Graham, R. L. (1989). A technique for extrapolating and validating forest cover across large regions: Calibrating AVHRR data with TM data. *International Journal of Remote Sensing*, 10, 1805-1812.
- Jakubauskas, M. E., Lulla, K. P., & Mausel, P. W. (1990). Assessment of vegetation change in a fire-altered forest landscape. *Photogrammetric Engineering and Remote Sensing*, 56, 371-377.
- Justice, C., Vermote, E., Townshend, J., DeFries, R., Roy, D., Hall, D., Salomonson, V., Privette, J., Riggs, G., Strahler, A., Lucht, W., Myneni, R., Knyazikhin, Y., Running, S., Nemani, R., Wan, Z., Huete, A., van Leeuwen, W., Wolfe, R., Giglio, L., Muller, J.-P., Lewis, P., & Barnsley, M. (1998). The Moderate Resolution Imaging Spectroradiometer (MODIS): land remote sensing for global change research. *IEEE Transactions on Geoscience and Remote Sensing*, 36, 1228-1249.
- Kasischke, E. S., Bourgeau-Chavez, L. L., Christensen, N. L., & Haney, E. (1994). Observations on the sensitivity of ERS-1 SAR image intensity to changes in aboveground biomass in young loblolly pine forests. *International Journal of Remote Sensing*, 15, 3-16.
- Kauth, R. J., & Thomas, G. S. (1976). The tasseled cap--A graphic description of the spectral-temporal development of agricultural crops as seen by Landsat. *Proc. Second Ann. Symp. Machine Processing of Remotely Sensed Data*. Purdue U. Lab. App. Remote Sens., West Lafayette IN, 6 June-2 July.
- Kimes, D. S., Kerber, A. G., & Sellers, P. J. (1993). Spatial averaging errors in creating hemispherical reflectance (albedo) maps from directional reflectance data. *Remote Sensing of Environment*, 45, 85-94.
- Kramer, H. J. (2001). *Observation of the earth and its environment: survey of missions and sensors* (4th ed.). Springer-Verlag, Berlin.
- Lefsky, M. A., Harding, D., Cohen, W. B., & Parker, G. G. (1999a). Surface lidar remote sensing of basal area and biomass in deciduous forests of eastern Maryland, USA. *Remote Sensing of the Environment*, 67, 83-98.
- Lefsky, M. A., Cohen, W. B., Acker, S. A., Spies, T. A., Parker, G. G., & Harding, D. (1999b). Lidar remote sensing of biophysical properties and canopy structure of forest of Douglas-fir and western hemlock. *Remote Sensing of Environment*, 70, 339-361.
- Lefsky, M. A., Cohen, W. B., & Spies, T. A. (2001). An evaluation of alternate remote sensing products for forest inventory, monitoring, and mapping in Douglas-fir forests of western Oregon. *Canadian Journal of Forest Research*, 31, 78-87.
- Lefsky, M. A., Cohen, W. B., Parker, G. G., & Harding, D. J. (2002). Lidar remote sensing for ecosystem studies. *Bioscience*, 52, 19-30.
- Li, X., & Strahler, A. H. (1992). Geometric-optical bidirectional reflectance modeling of the discrete crown vegetation canopy: Effect of crown shape and mutual shadowing. *IEEE Transactions on Geoscience and Remote Sensing*, 30, 276-292.

- Lillesand, T. M., & Kiefer, R. W. (2000). *Remote sensing and image interpretation*. John Wiley and Sons, New York.
- Loveland, T. R., Merchant, J. W., Ohlen, D. O., & Brown, J. F. (1991). Development of a land-cover characteristics database for the conterminous U.S. *Photogrammetric Engineering & Remote Sensing*, 57, 1453-1463.
- Luckman, A., Baker, J., Honzak, M., & Lucas, R. (1998). Tropical forest biomass density estimation using JERS-1 SAR: seasonal variation, confidence limits, and application to image mosaics. *Remote Sensing of Environment*, 63, 126-139.
- Luvall, J. C., & Holbo, H. R. (1991). Thermal remote sensing methods in landscape ecology. Turner, M. G., & RGardner, R. H. (Eds.). *Quantitative Methods in Landscape Ecology*, 127-152. Springer-Verlag, New York NY.
- Maclean, G. A., & Krabill, W. B. (1986). Gross-merchantable timber volume estimation using an airborne LIDAR system. *Canadian Journal of Remote Sensing*, 12, 7-18.
- Martin, M., & Aber, J. (1997). High spectral resolution remote sensing of forest canopy lignin, nitrogen, and ecosystem processes. *Ecological Applications*, 7, 431-443.
- Martin, M., Newman, S., Aber, L., & Congalton, R. (1998). Determining forest species composition using high resolution remote sensing data. *Remote Sensing of Environment*, 65, 249-254.
- Masuoka, E., Fleig, A., Wolfe, R., & Patt, F. (1998). Key characteristics of MODIS data products. *IEEE Transactions on Geoscience and Remote Sensing*, 36, 1313-1323.
- Means, J. E., Acker, S. A., Harding, D. J., Blair, J. B., Lefsky, M. A., Cohen, W. B., Harmon, M., & McKee, W. A. (1999). Use of large-footprint scanning airborne lidar to estimate forest stand characteristics in the western Cascades of Oregon. *Remote Sensing of the Environment*, 67, 298-308.
- Moisen, G., & Edwards, T. C., Jr. (1999). Use of generalized linear models and digital data in a forest inventory of northern Utah. *Journal of Agricultural, Biological, and Environmental Statistics*, 4, 372-390.
- Mouginis-Mark, P. J., Garbeil, H., & Flament, P. (1994). Effects of viewing geometry on AVHRR observations of volcanic thermal anomalies. *Remote Sensing of Environment*, 48, 51-60.
- Naesset, E. (1997). Determination of mean tree height of forest stands using airborne laser scanner data. *ISPRS Journal Photogrammetry and Remote Sensing*, 52, 49-56.
- Nelson, R. F., Krabill, W. B., & Maclean, G. A. (1984). Determining forest canopy characteristics using airborne laser data. *Remote Sensing of Environment*, 15, 201-212.
- Nelson, R. F., Krabill, W. B., & Tonelli, J. (1988). Estimating forest biomass and volume using airborne laser data. *Remote Sensing of Environment*, 24, 247-267.
- Nilsson, M. (1996). Estimation of Tree Heights and Stand Volume Using an Airborne Lidar System. *Remote Sensing of Environment*, 56, 1-7.
- Otter, D., Cohen, W., Berterretche, M., Maiersperger, T., & Kennedy, R. (2001). Land cover mapping in an agricultural setting using multiseasonal Thematic Mapper data. *Remote Sensing of Environment*, 76, 139-155.
- Pitt, D. G., Wagner, R. G., Hall, R. J., King, D. J., Leckie, D. G., & Runesson, U. (1997). Use of remote sensing for forest vegetation management: A problem analysis. *Forestry Chronicle*, 73, 459-477.
- Ranchin, T., & Wald, L. (2000). Fusion of high spatial and spectral images: the ARSIS concept and its implementation. *Photogrammetric Engineering & Remote Sensing*, 66, 49-61.

- Ranson, K. J., & Williams, D. L. (1992). Remote sensing technology for forest ecosystem analysis. Shugart, H. H., Leemans, R., & Bonan, G. B. (Eds.). *A Systems Analysis of the Global Boreal Forest*, 267-290. Cambridge U. Press, New York NY.
- Ranson, K. J., Irons, J. R., & Williams, D. L. (1994). Multispectral bidirectional reflectance of northern forest canopies with the advanced solid-state array spectroradiometer (ASAS). *Remote Sensing of Environment*, 47, 276-289.
- Richards, J. A., & Jia, X. (1999). *Remote Sensing Digital Imagery Analysis: An Introduction*. Springer Berlin.
- Rignot, E. J., & Way, J. B. (1994). Monitoring freeze-thaw cycles along north-south Alaskan transects using ERS-1 SAR. *Remote Sensing of Environment*, 49, 131-137.
- Rignot, E. J., Way, J. B., McDonald, K., Viereck, L., Williams, C., Adamas, P., Payne, C., Wood, W., & Shi, J. (1994). Monitoring of environmental conditions in taiga forests using ERS-1 SAR. *Remote Sensing of Environment*, 49, 145-154.
- Ritchie, J. C., Everitt, J. H., Escobar, D. E., Jackson, T. J., & Davis, M. R. (1992). Airborne laser measurements of rangeland canopy cover and distribution. *Journal of Range Management*, 45, 189-193.
- Ritchie, J. C., Humes, K. S., & Weltz, M. A. (1995). Laser altimeter measurements at Walnut Gulch watershed, Arizona. *Journal of Soil and Water Conservation*, 50, 440-442.
- Ritchie, J. C., Menenti, M., & Weltz, M. A. (1996). Measurements of land surface features using an airborne laser altimeter: The HAPEX-Sahel experiment. *International Journal of Remote Sensing*, 17, 3705-3724.
- Rodriguez, E., & Martin, J. M. (1992). Theory and design of interferometric synthetic aperture radars. *IEEE Proceedings-F Radar and Signal Processing*, 139, 147-159.
- Rodriguez, E., Michel, T.R., & Harding, D.J. 2002. Interferometric measurements of canopy height characteristics for coniferous forests, *IEEE Transactions on Geoscience and Remote Sensing*, (In Review)
- Rosen, P.A., Hensley, S., Joughin, I. R., Li, F.K., Madsen, S.N., Rodriguez, E., & Goldstein, R.M. (2000). Synthetic aperture radar interferometry - Invited paper, *Proc. IEEE* 88, 3, 333-382.
- Running, S. W., Justice, C. O., Salmonson, V., Hall, D., Barker, J., Kaufmann, Y. J., Strahler, A. H., Huete, A. R., Muller, J. -P., Vanderbilt, V., Wan, Z. M., Teillet, P., & Carnegie, D. (1994). Terrestrial remote sensing science and algorithms planned for EOS/MODIS. *International Journal of Remote Sensing*, 15, 3587-3620.
- Sader, S. A. (1986). Analysis of effective radiant temperatures in a Pacific Northwest forest using thermal infrared multispectral scanner data. *Remote Sensing of Environment*, 19, 105-115.
- Sader, S.A. (1987). Forest biomass, canopy structure, and species composition relationships with multipolarization L band synthetic aperture radar data. *Photogrammetric Engineering and Remote Sensing*, 53, 193-202.
- Sader, S. S., Waide, R. B., Lawrence, W. T., & Joyce, A. T. (1989). Tropical forest biomass and successional age class relationships to a vegetation index derived from Landsat TM data. *Remote Sensing of Environment*, 28, 143-156.
- Sader, S. A., Stone, T. A., & Joyce, A. T. (1990). Remote sensing of tropical forests: An overview of research and applications using non-photographic sensors. *Photogrammetric Engineering & Remote Sensing*, 56, 1343-1351.
- Schriever, J. R., & Congalton, R. G. (1995). Evaluating seasonal variability as an aid to cover-type mapping from Landsat Thematic Mapper data in the Northeast. *Photogrammetric Engineering & Remote Sensing*, 61, 321-327.

- Schowengerdt, R. A. (1997). *Remote Sensing: Models and methods for image processing*. Academic Press, San Diego, CA.
- Spanner, M. A., Pierce, L. L., Peterson, D. L., & Running, S. W. (1990). Remote sensing of temperate coniferous forest leaf area index: The influence of canopy closure, understory vegetation and background reflectance. *International Journal of Remote Sensing*, 11, 95-111.
- Spanner, M. A., Johnson, L., Miller, J., McCreight, R., Freemantle, J., Runyon, J., & Gong, P. (1994). Remote sensing of seasonal leaf area index across the Oregon transect. *Ecological Applications*, 4, 258-271.
- Strahler, A. H., Woodcock, C. E., & Smith, J. A. (1986). On the nature of models in remote sensing. *Remote Sensing of Environment*, 20, 121-139.
- Townsend, J.R.G., Goff, T. E., & Tucker, C. J. (1985). Multitemporal dimensionality of images of normalized difference vegetation index at continental scales. *IEEE Transactions on Geoscience and Remote Sensing*, 23, 888-895.
- Tucker, C. J. (1979). Red and photographic infrared linear combinations for monitoring vegetation. *Remote Sensing of Environment*, 8, 127-150.
- Tucker, C. J., Holben, B. N., Elgin, J. H., & McMurtrey, J. E. (1980). Relationship of spectral data to grain yield variation. *Photogrammetric Engineering & Remote Sensing*, 46, 657-666.
- Tucker, C. J., Vanpraet, C., Boerwinkel, E., & Gaston, A. (1983). Satellite remote sensing of total dry matter production in the Senegalese Sahel. *Remote Sensing of Environment*, 13, 461-474.
- Tucker, C. J. (1996). History of the use of AVHRR data for land applications. D'Souza, G., Belward, A. S., & Malingeau, J. P. (Eds.). *Advances in the use of NOAA AVHRR data for land applications*, 1-19. ECSC, EEC and EAEC. Brussels and Luxembourg.
- Ulaby F.T., & Dobson, M. C. (1993). Radar response of vegetation: an overview. *Proceedings of the Third Spaceborne Imaging Radar Symposium*, 151-183. Jet Propulsion Lab Publications 93-16.
- Van der Meer, F. (1994). Extraction of mineral absorption features from high-spectral resolution data using non-parametric geostatistical techniques. *International Journal of Remote Sensing*, 15, 2193-2214.
- Vane, G., & Goetz, A. F. (1993). Terrestrial imaging spectrometry: Current status, future trends. *Remote Sensing of Environment*, 44, 117-126.
- Wang, Y., Kasischke, E. S., Melack, J. M., Davis, F. W., & Christensen, N. L. (1994). The effects of changes in loblolly pine biomass and soil moisture on ERS-1 SAR backscatter. *Remote Sensing of Environment*, 49, 25-31.
- Waring, R. H., Way, J., Hunt, E. R., Morrissey, L., Ranson, K. J., Weishampel, J. F., Oren, R., & Franklin, S. E. (1995). Imaging radar for ecosystem studies. *BioScience*, 45, 715-723.
- Way, J., Paris, J., Dobson, M., McDonald, K., Ulaby, F., Weber, J., Ustin, S., Vanderbilt, V., & Kasischke, E. (1991). Diurnal change in trees as observed by optical and microwave sensors: The EOS synergism study. *IEEE Transactions on Geoscience and Remote Sensing*, 29, 807-821.
- Way, J., Rignot, E. J., McDonald, K. C., Oren, R., Kwok, R., Bonan, G., M. Dobson, M. C., L. Viereck, A., & Roth, J. E. (1994). Evaluating the type and state of Alaska taiga forests with imaging radar for use in ecosystem models. *IEEE Transactions on Geoscience and Remote Sensing*, 32, 353-370.
- Wehr, A., & Lohr, U. (1999). Airborne laser scanning-an introduction and overview. *ISPRS Journal of Photogrammetry & Remote Sensing*, 54, 68-82.

- Wolter, P. T., Mladenoff, D. J., Host, G. E., & Crow, T. R. (1995). Improved forest classification in the Lake States using multi-temporal Landsat imagery. *Photogrammetric Engineering & Remote Sensing*, 61, 1129-1143.
- Woodcock, C. E., & Strahler, A. H. (1987). The factor of scale in remote sensing. *Remote Sensing of Environment*, 21, 311-332.
- Wulder, M. (1998). Optical remote-sensing techniques for the assessment of forest inventory and biophysical parameters. *Progress in Physical Geography* 22, 449-476
- Zagolski, F. P., Pinel, V., Romier, J., Alcayde, D., Fontanari, J., Gastellu-Etchegorry, J. P., Giordano, G., Marty, G., Mougin, E., & Joffre, R. (1996). Forest canopy chemistry with high spectral resolution remote sensing. *International Journal of Remote Sensing*, 17, 1107-1128.
- Zhu, Z., & Evans, D. L. (1992). Mapping midsouth forest distributions. *Journal of Forestry*, 90, 27-30.

Chapter 3

THE ROLES OF AERIAL PHOTOGRAPHS IN FORESTRY REMOTE SENSING IMAGE ANALYSIS

Ronald J. Hall

Canadian Forest Service (Northern Forestry Centre), Natural Resources Canada, Edmonton, Alberta, T6H 3S5, Canada

1. INTRODUCTION

Aerial photographs have been and continue to be the most frequently used remote sensing data source in forestry, particularly in natural resource assessment, inventory, and monitoring (Gillis and Leckie 1993; Hall and Fent 1996; Caylor 2000). Their use in operational forestry was anticipated to decrease as technological advances improved in the capabilities of new airborne and satellite sensors. The incentives were obvious. Within a growing digital arena, an increasing array of both geographic information system (GIS) and image processing system capabilities exist to integrate and analyze digital image data. Digital remote sensing systems tend to offer data with higher radiometric and spectral resolution capabilities than their aerial photo counterparts, and it is often in a format ready for analysis without costly scanning as in the case of the photograph. Despite predictions that digital cameras will eliminate the need for aerial photography and film scanner technologies, no such system has yet been able to match their spatial resolution, data storage or hardcopy output capabilities (Hinz and Heier 2000; Gruber and Leberl 2001). For example, a single 230 × 230 mm aerial photograph at a scale of 1:20,000 scanned at a resolution of 10 micrometres would have a pixel size representing 0.20 m on the ground and require about 450 megabytes of storage, an awesome amount of information contained within a single analogue photograph. Thus, there are advantages and disadvantages when comparing digital systems with aerial photography.

Instead of viewing aerial photographic technology as a competitor to digital remote sensing technology, it is more effective to understand the various roles it can play in our quest for efficient and effective analysis and monitoring of our natural resources.

Significant technological advances have and continue to be made in the camera and film components of aerial photography. Specifically, improvements have been made to aerial cameras with 1) forward motion compensation (FMC) to remove image smear, 2) improved lens resolution to at least 90–100 line-pairs/mm, which exceeds that of digital sensors (King 2000), 3) gyro-stabilized mounts to reduce tangential image motion, 4) integrated computer exposure controls for more precise exposure, and 5) integration with Global Positioning System (GPS) receivers for more precise positioning (Newby 1996; Light 2001). Aerial film advances have also occurred in film type, speed, processing, and resolution characteristics (Fent et al. 1995; Eastman Kodak Company 2002). With these camera and film innovations, air photo quality can be enhanced to a greater degree because of the improved controls available to the photo acquisition process (Hall and Fent 1996). Consequently, the potential for information extraction through air photo interpretation is greater, and the potential for a higher quality product exists for digital capture. Without question, aerial photography is a technology in transition from the analogue to digital air photo environments (Light 1996; Caylor 2000).

To understand the various roles aerial photographs may play in the analysis of remote sensing images, a sound knowledge is required of the information needed for the application. Foresters, for example, typically manage landscapes that comprise forest stands, an entity consisting of trees possessing sufficient uniformity in composition, age, arrangement, or condition (Canadian Council of Forest Ministers 2001). The scales of aerial photographs used in Canada often range from 1:10,000 to 1:20,000 (Ahern and Leckie 1987), and stands are often labeled in polygons as small as 2 ha by trained air photo interpreters using attributes such as species, height, and crown closure (Gillis and Leckie 1993; Nesby 1997). In the past, satellite sensors have not been able to provide sufficient information for forest management level inventories. While improvements will emerge with the increasing availability of new, higher resolution satellites such as IKONOS (Space Imaging Inc. 2002), a problem remains in how technologists stratify the landscape for analysis using digital remote sensing methods. The fundamental issue is that high and medium resolution imaging sensors consist of pixels that record the spectral response of objects contained within a cell, whereas stand polygons are interpreted as homogenous objects relative to a given classification system and their size tends to be much

larger than a pixel. A stand polygon 5 ha in size, for example, will be represented by 55 Landsat Thematic Mapper 30 m pixels. Fundamentally these appear as two completely different entities. The objective of this Chapter, however, is to describe how one technology could be supportive of the other, and to illustrate this concept with selected examples from the literature.

Significant improvements to products derived from satellite analysis can be attained if integrated with information from aerial photographs. The question is how? To answer this question, this Chapter is organized into two sections. The first section provides basic concepts about aerial photography, how it is characterized, how it is acquired, how it is processed, and how it is interpreted. This information provides essential knowledge in its intelligent use for supporting remote sensing analysis. The second section describes four roles that aerial photography can serve in undertaking remote sensing analysis including image rectification, image classification from training and validation perspectives, and high resolution image feature extraction (Figure 3-1).

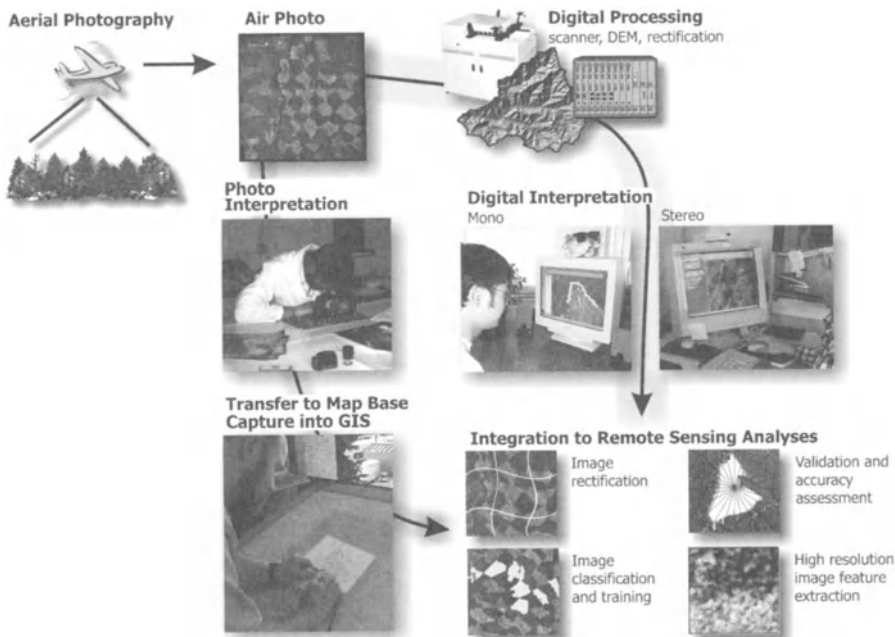


Figure 3-1. Schematic flow chart illustrating the use of air photos in remote sensing image analysis.

2. AERIAL PHOTOGRAPHY: WHAT DO YOU NEED TO KNOW?

2.1 How to characterise

Forest information is captured based on the spatial, tonal and textural properties of the photographic image; how these are resolved has a direct influence on the information captured and how it may be used in analysis of remote sensing images. Resolution is the quality of a remote sensing image acquired by a sensor system. In the remote sensing domain, spatial, spectral and radiometric resolution are the attributes often used in defining image characteristics, but there are some differences in how these terms are used to characterize aerial photos. Spatial resolution in remote sensing refers to the ground area viewed by a detector in the optics of a sensor at any particular moment in time. The higher the spatial resolution, the smaller the object that can be observed. In aerial photography, spatial resolution is described by the resolving power, which is an estimate of the smallest detail that may be visually observable, and combines the spatial resolution properties of the camera lens, film, the effects of image motion, and the contrast of the object. A frequently used approach to estimate resolution for the entire system of lens, film and motion is line pairs/millimeter (Graham and Read 1986). The computation of system line pairs/millimeter can be simplified by assuming image motion is minimal and can be used to compute the nominal total resolution of a system based on model of aerial camera and films of different resolving power using the following equation:

$$\frac{1}{R_T^2} = \frac{1}{R_L^2} + \frac{1}{R_F^2} \quad \text{where} \\ R_T^2 = \text{Total resolution,} \\ R_L^2 = \text{Lens resolution, and} \\ R_F^2 = \text{Film resolution.} \quad (1)$$

The computed values can, in turn, be converted to effective spatial resolution at a given scale. Values were computed at a photo scale of 1:20,000 to illustrate the potential influence of aerial camera, lens and film on the operational resolution element that could be resolved (Table 3-1). We would gain little in the operational forestry domain by scanning below these nominal values.

Table 3-1. Effective spatial resolution of aerial photos for selected aerial cameras, lenses, and films at a scale of 1:20,000.

Aerial camera	Lenses	Ground resolution for lens/film combinations (m) @ 1:20 000				
		24121	A80	2405	2445	2443
Wild RC-10	15 UAG	0.52	0.54	0.64	0.71	0.80
	UAGI	0.43	0.45	0.57	0.64	0.74
	UAGII	0.40	0.41	0.54	0.62	0.72
	30/4NAT	0.40	0.41	0.54	0.62	0.72
Wild RC-10A	15/4UAGA	0.33	0.35	0.49	0.58	0.69
	30/4NATA	0.33	0.35	0.49	0.58	0.69
Wild RC-20	15/4UAG-F	0.30	0.32	0.47	0.56	0.67
	30/4NATA-F	0.33	0.35	0.49	0.58	0.69
Wild RC-30	15/4UAG-S	0.27	0.30	0.46	0.55	0.66
	30/4NAT-S	0.28	0.31	0.46	0.55	0.67
Zeiss RMK	Pleogon A	0.30	0.32	0.47	0.56	0.67
	Topar A	0.30	0.32	0.47	0.56	0.67
Zeiss RMK TOP	PleogonA3	0.26	0.28	0.45	0.54	0.66
	Topar A3	0.31	0.34	0.48	0.57	0.68
Zeiss LMK	Lamegar P1	0.30	0.32	0.47	0.56	0.67
Zeiss LMK-1000	LC 1015C	0.27	0.30	0.46	0.55	0.66
	LC 1030C	0.26	0.28	0.45	0.54	0.66
Zeiss LMK-2000	LC 2015	0.26	0.28	0.45	0.54	0.66
Zeiss LMK-3000	LC 3015	0.25	0.27	0.44	0.54	0.65

¹ 2412, Kodak Panatomic-X 2412; A80, Agfa Aviphot Pan 80 PE-1; 2405, Kodak Double-X 2405; 2445, Kodak Aerocolor Negative 2445; 2443, Kodak Aerochrome Infrared 2443.

Spectral resolution from a remote sensing system refers to the number of wavelength channels and their respective widths that a given sensor is sensitive to. The Landsat 7 satellite for example, has 6 spectral channels that are sensitive to the visible, near infrared and shortwave infrared portions of the spectrum. In aerial photography, spectral sensitivity is used to describe the range of the electromagnetic spectrum that a given film is responsive to, and it varies by film (Hall and Fent 1996; Agfa-Gevaert Group 2002; Eastman Kodak Company 2002) (Table 3-2). The basic film types are black-and-white, black-and-white infrared, colour and colour infrared (Lillesand and Kiefer 1994). Within the black-and-white films, there are subtle spectral differences especially at the red-edge portion of the electromagnetic

Table 3-2. Characteristics of selected aerial films (as of March, 2002).

Emulsion	Film speed ¹	Spectral sensitivity	RMS granularity	Line pairs/mm		Processing conditions
Black-and-White:						
Kodak Tri-X 2403	640	720	40	100	40	885 chemistry, G ² = 1.38
Kodak Double-X 2405	400	720	26	125	50	885 chemistry, G = 1.10
Kodak Plus-X 2402	200	720	20	160	50	885 chemistry, G = 1.80
Kodak Aero LX 2408	64	720	12	250	63	885 chemistry, G = 1.40-1.80
Kodak Panatomic-X 2412	40	720	9	400	125	885 chemistry, G = 1.80
Agfa Aviphot Pan 80	64-100	750	9	202	101	G-74, 42s dev., 30°C
Agfa Aviphot Pan 200	200	750	29	100	50	G74 chemistry, G = 1.50
Kodak Infrared 2424	varies, 400	900	27	125	50	885 chemistry, G = 1.45
Colour Negative:						
Kodak Aerocolor 2444	125	690	10-16	100-125	80	AN-6, C-41, replaces 2445
Kodak Aerocolor HS SO-846	160	690	9	100	63	C-41
Agfa Aviphot Color H100	50 or 100	670	N/A	115	50	C-41
Agfa Aviphot Chrome 200	200	670	12	110	50	E6
Agfa Aviphot Color X100	100 or 160	670	6	140	55	C-41
Agfa Aviphot Color N400	400 or 640	670	8	130	55	C-41
Agfa Aviphot Color N800	800	670	9	110	40	C-41
Colour Diapositive:						
Kodak Aerochrome 2427	32	680	13	100	80	AR-5, replaces 2448
Kodak Aerochrome HS SO-359	125	700	19	80	25	E-6
Kodak Aerochrome IR 1443	40	900	23	100	63	AR-5, AN-6, C-41, replaces 2443

¹ The aerial film speed for panchromatic films will vary with the exposure and processing used to achieve specified average gradients.

² G, Average gradient, the level of contrast given to the film during development

spectrum that are particularly advantageous for haze penetration and for detecting vegetation patterns (Table 3-2). Reference to an aerial film manufacturer's web site is the most effective means of obtaining current technical specifications about aerial films as advancements continue to be made that result in improved or new products. As such, there is latitude in selecting the film most suited to provide the best contrast between the object of interest and its background (Falkner and Morgan 2002). More generally, a film emulsion contains silver halide crystals that are light-sensitive and when exposed, results in the formation of a latent image. The latent image only becomes visible when developed. The average size and shape of the silver halide crystal is an important characteristic of an aerial film, because it has a significant influence on 1) the amount of light required to expose the film and form an image, and 2) the film's graininess, which affects resolution. The photographic process is more complex when considering colour films because it consists of 3 colour sensitive layers (Jensen 2000). When attempting to digitally capture an aerial colour film image, a 3 channel digital image would be generated whereby each channel would represent a colour dye layer and the portion of the electromagnetic spectrum that dye layer was sensitive to. For example, scanning a frame of Kodak Aerocolor III negative film 2444 would result in blue, green and red spectral channels that would represent the 380-510, 440-590, and 540-690 nm wavelengths, respectively. This has implications on how features may be interpreted. Broad species differences may be visible when interpreting a colour image from this film, but subtle changes such as pre-visual detection of spectral responses due to physiological impacts on tree and stand health may or may not be visible. Keeping the objectives in mind continue to be important when attempting to extract features from aerial photographs for use in remote sensing analysis.

Radiometric resolution in the remote sensing arena refers to detector sensitivity to differences in energy recorded by the detector in different wavelengths. Often it is interpreted as the quantization level where a 6-bit sensitivity would provide grey level response to 64 values verses an 8-bit sensitivity which would provide data to 256 grey levels. This is not a direct measure of radiometric resolution (Franklin 2001b) though it does provide a measure of reflectance response recorded at the pixel level. In aerial photography, radiometric resolution is a measure of the quality of the image as recorded by contrast or density on the film. It is a direct response of the spectral sensitivity (spectral dyes) of the film, its exposure (amount of light), and the density of the metallic silver on the film which attenuates the incident light during printing (Graham and Read 1986). The brightness and darkness of objects on a photograph is expressed in its density values and the

contrast is the range in these density values (Agfa-Gevaert, undated). There is a direct relation between the range of densities on film as recorded during exposure and processing that is then captured during scanning to produce the digital image. All panchromatic aerial films can be exposed and processed to different average gradients, the level of contrast given to the film during development. To enhance interpretability, some consideration should be given to select the appropriate average gradient in the case of black-and-white films to ensure sufficient contrast in the objects of interest. The quality of the air photo can influence the degree to which certain features can be interpreted. Past research has reported, for example, that film type and average gradient will influence the accuracy to which forest inventory attributes may be interpreted (Fent et al. 1995). Operational procedures currently being advocated in forest inventory photography are to have the interpreter select the paper or film grade when printing from the negative. Higher contrast papers and diapositive materials can help to enhance the interpretability of the final product, particularly if working with film that has already been exposed and processed. Scanning air photos to create digital images, however, requires a different approach. Of interest is the ability to capture in the digital image both the dynamic range and the maximum levels of grey inherent in the photographic image. An image with less of a contrast will enable the image analyst to use the complete tonal information content of the photographic image for subsequent digital image enhancement. Thus, if the intended purpose of the aerial film is for digital capture for interpretation purposes, particularly for use in a remote sensing analysis, then due attention should be given to the film and how it is exposed, processed and printed.

2.2 How to acquire

Two considerations in the acquisition of aerial photographs are the photogrammetric acquisition parameters relative to their intended use, and the timing of acquisition relative to its influence on object reflectance. A few of the important parameters involved in acquiring aerial photographs include the aerial camera model, camera lens and focal length, photographic scale, film type, global positioning satellite (GPS) positioning, and timing with respect to time of day and time of year. The cost of a particular photographic mission can vary depending on the airborne system used as the more advanced cameras tend to be charged at higher rates. The lowest cost does not necessarily result in the optimal product for interpretation, especially if fine features must be discerned in the support of a remote sensing analysis

whether that be for training or validation. Table 3-3 lists a few of the attributes for selected aerial cameras and lenses from which differences can

Table 3-3. List of selected features for large-format aerial cameras.

Aerial camera	Description of selected camera and lens features
Wild RC-10	No FMC, 1.6 sec. fastest cycling between frames, overlap range 5 – 95% in 5% steps, shutter speed range 1/100s – 1/1000s (same for all Wild Cameras), no annotation capability, no GPS interface, 3 lenses: UAG (f/5.6 – f/16, 8 mm distortion, 40 lp/mm AWAR ³), UAGI (f/5.6 – f/16, 5 mm distortion, 55 lp/mm AWAR), UAGII (f/4.0 – f/22, 4 mm distortion, 55 lp/mm AWAR)
Wild RC-10A	No FMC but can measure, 2 sec fastest cycling between frames, overlap range 0 – 99% in 1% steps, PEM2A exposure control system – shutter priority, annotation with optional unit: 2 rows of 32 digits, GPS interface, improved lenses from RC-10: UAGA (f/4.0 – f/22, 3 mm distortion, 70 lp/mm AWAR)
Wild RC-20	FMC (2 – 64 mm/s), 1.7 sec fastest cycling between frames, overlap range 0 – 99% in 1% steps, PEM exposure system for shutter & aperture control, Electronic Data Interface option, upgradeable to RC-30, annotation 2 rows-32 digits, GPS interface, improved lens UAG-F (f/4.0 – f/22, 2-3 mm distortion, 80 lp/mm AWAR)
Wild RC-30	FMC (2 – 64 mm/s), 1.7 sec fastest cycling between frames, overlap range 0 – 99% in 1% steps, PEM-F exposure control system, ASCOT system includes annotation 2 rows-100 digits, GPS interface, improved lens UAG-S (f/4.0 – f/22, 2 mm distortion, 90 lp/mm AWAR)
Zeiss RMK	FMC (0 – 30 mm/s), 2 sec fastest cycling between frames, overlap range 1 – 99% in 1% steps all Zeiss cameras, EMI-2 (aperture priority exposure) or EMI-3 (aperture/shutter speed exposure), shutter speed range 1/100s – 1/1000s, no annotation, GPS with FMC, Pleogon A lens (f/4.0 – f/11, 2 mm distortion, 80 lp/mm AWAR)
Zeiss RMK Top	FMC (0 – 64 mm/s), 1.5 sec fastest cycling between frames, Intelligent Exposure Control system, shutter speed range 1/50s – 1/1000s, 3 internal filters, annotation 2 rows-48 digits, GPS interface, Pleogon A3 lens (f/4.0 – f/22, 2-3 mm distortion, 99 lp/mm AWAR)
Zeiss LMK	FMC (0 – 64 mm/s), 2 sec fastest cycling between frames, differential brightness automatic exposure control all LMK cameras, shutter speed range 1/30s – 1/500s, no annotation, GPS interface, Lameger lens (f/4.5 – f/11, 3 mm distortion, 80 lp/mm AWAR)
Zeiss LMK-1000	FMC (0 – 33 mm/s), 2 sec fastest cycling between frames, shutter speed range 1/64s – 1/1024s, no annotation, GPS interface, LC 1015C lens (f/4.5 – f/11, 3 mm distortion, 90 lp/mm AWAR)
Zeiss LMK-2000	FMC (0.3 – 64 mm/s), 2 sec fastest cycling between frames, shutter speed range 1/64s – 1/1024s, 90 digit free data - 48 digit camera – 90 digit GPS annotation, GPS interface, LC 2015C lens (f/4 – f/16, 2 mm distortion, 100 lp/mm AWAR)
Zeiss LMK-3000	FMC (0.3 – 64 mm/s), 2 sec fastest cycling between frames, shutter speed range 1/64s – 1/1024s, 90 digit free data - 48 digit camera – 90 digit GPS annotation, GPS interface, LC 3015C lens (f/4 – f/16, 2 mm distortion, 100 lp/mm AWAR)

³ AWAR: Area-Weighted Average Resolution: A measure of overall resolution based on calculating the average resolution for a lens divided into annular zones (Graham and Read 1986).

be observed from one camera model to another. The newer generation aerial cameras possess FMC features and higher resolution camera lenses that alone will significantly improve how fine details are resolved on the resultant photograph that should be considered in project planning. There are numerous books that readers can refer to for the procedures, formulas, and mechanics of project planning for aerial photo acquisition (Graham and Read 1986; Lillesand and Kiefer 1994; Warner et al. 1996; Wolf and Dewitt 2000). It is, perhaps, more important to appreciate the concept of aerial photo planning and its role in governing the final product that would be used in supporting remote sensing image analysis. In terms of advantages, aerial photographs are typically acquired with much higher spatial resolution than data acquired by satellite, and they can be obtained at the critical times needed for interpretation of the objects of interest. In the support of a remote sensing analysis, these attributes are advantageous from both pixel training and validation perspectives.

The scale of the photograph is arguably the most important attribute the user must specify for a given project. Much has been written about scale (Lillesand and Kiefer 1994; Falkner and Morgan 2002) and fundamentally, scale refers to the resolution and area over which objects of interest can be detected, interpreted or mapped (Franklin 2001b). The photo scale should be selected with care as it will determine the area on the ground at the pixel level that can be detected once the photograph has been scanned. Scan resolution is often given in dots per inch (dpi) and the size of a single pixel on the ground can be easily computed by expressing scale as 1 cm = X m and using a simple formula which can then be expanded to create a table of pixel size based on scan resolution (Table 3-4):

$$\text{Pixel size (m)} = \frac{2.54 \times \text{Scale (m)}}{\# \text{ dots (dpi)}} \quad (2)$$

The fundamental unit of analysis in a remote sensing image is the picture element, or pixel. A scanner, by function, converts light transmitted through the photographic image into pixels of fixed size, shape and spacing with variable brightness values (I.S.M. International Systemap Corp. 1999). These brightness values range from black to white, and are typically represented digitally on an 8-bit scale ranging from 0 to 255, respectively. When an aerial photograph is to be scanned, consideration should be given to the camera system's resolving power, the scale of the photograph itself, and the desired pixel size for the intended application (Nelson et al. 2001). Not all scanners are created equal, however, which raises the issue that

factors such as geometric fidelity, dynamic range, colour reproduction and data compression should be considered during digital conversion of the photographic image (Kolbl and Bach 1996). The scan resolution will govern the size of the pixel and the area it represents on the ground, and the grey value assigned to the pixel will be dependent on the objects contained within a given cell (Figure 3-2). A general rule to determine the desired pixel size is to scan to a size no larger than one-quarter to one-fifth of the output size of the object to be resolved. For example, at a map scale of 1:20,000, the effective spatial precision at this scale is 1 mm at map scale that translates to a value of 20 m. To map to this level of precision from a digital image, it should have a pixel size no larger than 4 to 5 m.

Table 3-4. A table of effective ground resolution pixel size based on air photo scale and scan resolution.

Scan resolution		Ground Resolutions (m)			
DPI	micrometres	1:5,000	1:10,000	1:20,000	1:40,000
100	250	1.25	2.50	5.00	10.00
200	125	0.63	1.25	2.50	5.00
300	83	0.42	0.83	1.67	3.33
400	63	0.31	0.63	1.25	2.50
500	50	0.25	0.50	1.00	2.00
600	42	0.21	0.42	0.83	1.67
700	36	0.18	0.36	0.71	1.43
800	31	0.16	0.31	0.63	1.25
900	28	0.14	0.28	0.56	1.11
1000	25	0.12	0.25	0.50	1.00
1100	23	0.11	0.23	0.45	0.91
1200	21	0.10	0.21	0.42	0.83
1300	19	0.10	0.19	0.38	0.77
1400	18	0.09	0.18	0.36	0.71
1500	17	0.08	0.17	0.33	0.67
1600	16	0.08	0.16	0.31	0.63
1700	15	0.07	0.15	0.29	0.59

The time of day and time of year the photos are taken will govern the solar altitude and illumination of the objects within a photograph. The anti-solar hot spot will also affect the quality of the photograph in addition to the tonal and textural renditions typically affected by the time of day a photograph is taken. Reflectance from vegetation changes with phenology during the growing season, and this will have a profound influence on how their features are recorded on aerial film and on digital images as well. In total, the system used to acquire the aerial photographs can greatly influence air photo quality, and this is particularly important as digital capture is

increasingly being undertaken for production of digital orthophotos⁴, to produce images as a backdrop for on-screen image interpretation, and to provide data for use in analysis of remote sensing images.

2.3 How to process

This section is concerned with a brief overview of the aerial film process, and an overview of softcopy photogrammetry as it relates to its supporting role in remote sensing analysis. Following exposure in the aircraft, aerial films will possess the latent image that through processing to either a negative or positive, is converted into a visible, stable and permanent image (Agfa-Gevaert undated; Lillesand and Kiefer 1994). While processing monochrome films is relatively straightforward, there are opportunities to influence the gamma or contrast by varying processing times. Aerial films are processed in developers that contain rollers to move the long rolls of film through the development process. How long a given piece of film is in contact with the developer will govern the density of the processed film. To enhance contrast through changes in film density, monochrome (black and white) films are sometimes developed at slower rates so that any given piece of film will be in contact with the developer for longer periods of time. The processing and printing process is best discussed between the photographer and the user relative to the intended use of the aerial film as opportunities may exist to alter the contrast of the final image. Colour processing is more complex due to stricter adherence to processing chemistry, and the blue, green, and red sensitive emulsion layers that are each devoted to producing varying amounts of yellow, magenta and cyan dye layers, respectively, in proportion to the silver produced by the developer. Some of the newer colour aerial films can now accommodate a broader range of over- or under-exposure including over-processing for saturation enhancement without serious loss of quality (Warner et al. 1996), and this flexibility can be used to enhance contrast before digital capture. Thus, when new aerial photographs are being acquired to support remote sensing analysis, opportunities do exist to enhance the final product that may help to accentuate subtle tones that will be interpreted or digitally processed.

⁴ A digital orthophoto is a photo-quality digital image that shows images of objects in their true orthographic positions. Orthophotos are geometrically equivalent to planimetric maps but maps depict the true orthographic positions of objects as symbols and lines (Wolf and Dewitt 2000).



Figure 3-2. An illustration of the area on the ground represented by each square or pixel that would be created from digital scanning of the photograph. The arrow points to a pixel that would contain three objects: water, shoreline and vegetation. The digital value of this pixel would be an average of the spectral response patterns of the three objects contained within it.

One of the most significant developments in aerial photography has been the evolution of digital photogrammetry. The distinction between digital and conventional photogrammetry is sometimes confused, but for simplicity digital photogrammetry is based on digital (e.g., softcopy) images whereas the conventional approach is based on film (hardcopy) images (I.S.M. International Systemap Corp. 1999). Within this domain, the digital orthophoto offers the most to those interested in its potential roles to support remote sensing analysis. A digital orthophoto is the product of a digital rectification process that incorporates a digital elevation model, photogrammetric rectification process and image resampling of intensity values to form the output image (Michael 1994). In this process, image displacements due to camera orientation and photographic tilt and terrain relief are removed through the solution of collinearity equations, and applied

to each pixel in the input raw image in order to place them in their correct locations in the output image (Wolf and Dewitt 2000). Workstations have now been developed for mono or stereo interpretation that greatly improve the efficiency by which the digital capture of photo interpretation can be made (ref. Digital interpretation, Figure 3-1) (Graham et al. 1997; I.S.M. International Systemap Corp. 1999). The significant impact of these digital (softcopy) systems is that they bring remote sensing and photogrammetric applications together on the same platform with high potential for mutual benefit (Mikhail 1996), particularly in support of mapping and GIS applications (Welch and Jordan 1996). Some of these applications are further explored in section 3.0 of this Chapter.

2.4 How to interpret

The interpretation of aerial photographs in forestry is the process of identifying objects or features and assessing their importance relative to the information being sought. The elements of photo interpretation most often cited in the literature include tone/colour, texture, pattern, size, shape, shadow and location/association (Paine 1981; Lillesand and Kiefer 1994; Jensen 2000). Photo interpretation relies on the convergence of evidence based on deductive and inductive reasoning, and it is a process that integrates knowledge of ecology, soils and biology with local knowledge of field conditions. The interpretation process entails an integration of these domains with a knowledge of the factors that may influence object representation such as scale, air photo quality, vegetation health, and timing of air photo acquisition (Figure 3-3). Many of these attributes also apply to the manual interpretation of digital images. Thus, an ability to synthesize the elements of interpretation are key to extracting information from aerial photographs or digital images.

There is an important philosophical difference in how information is interpreted on an aerial photograph and how it may be used in supporting analysis of digital remote sensing images. Most importantly, interpretation is a subjective process that is based on several integrative elements (Figure 3-3) and as such has been subject to criticism due to the variation in the consistency of interpretation that can occur. To minimize this problem, interpretation keys are often employed, and certification/training programs are often used to build trained and skilled interpreters. In Alberta, Canada, for example, forest interpreters are trained to meet standards set out in the Alberta Vegetation Inventory (Nesby 1997) through a series of certification programs. In digital remote sensing, image classification is most often undertaken on the spectral data, which is analogous to the tone and colour of

objects on the photograph. Recognition of this important difference has led, in part, to the development of the spatial domain with empirical texture and contextual algorithms as a supplement to the dimensionality of data that can be used in image classification.

There are four fundamental ways of incorporating information from aerial photographs into a digital remote sensing analysis (Figure 3-1). First, aerial photographs may be orthorectified and used to identify control points for geometrically rectifying the image. Second, aerial photographs may be interpreted and then digitally captured in a GIS, or used in on-screen delineation of features of interest that could then be imported to the remote sensing database. Third, manual or digitally classified images could be overlaid or integrated with the digital aerial photographic image in a validation or classification accuracy exercise. Fourth, the high quality of aerial photographs now possible is lending itself for investigations to extract features at the individual tree level such as tree crown area and density. The following section will explore these four methods of using aerial photographs in digital remote sensing image analysis.

3. SELECT ROLES OF AIR PHOTOS IN REMOTE SENSING

3.1 Image rectification

Image rectification is the process of rectifying spatial distortions in a digital image to produce a geometrically corrected image that is spatially consistent, similar to a map. Distortions in an image depend on the sensor and imaging geometry, platform (airborne, satellite), topography, and other factors (Lillesand and Kiefer 1994). A procedure typically utilized include n^{th} order polynomials that provide for rotation, translation and scale translations between geographic and pixel coordinates that are satisfactory in areas with moderate or low relief (Richards 1993; Toutin, Chapter 6). In areas with significant topography, geometric distortions can only be rectified with the use of digital elevation models, sensor geometry information and orthorectification procedures. The judicious selection of ground control points (GCPs) are often used in both procedures and the availability of aerial photographs or digital orthophotos can be used in conjunction with digital or hardcopy maps in the geometric rectification of digital airborne or satellite images.

3.1.1 Digital orthophotos for image-image correction

One of the methods available to geometrically correct images is to employ a master-slave image-to-image process whereby GCPs from a spatially corrected image known as a “master”, could be used to correct the pixel position of the uncorrected “slave” image. The fully digital format of the orthophoto makes them useful as base maps that could serve as ground control in remote sensing or GIS systems (Welch and Jordan 1996; Lear 1997). Digital orthophotos have an advantage over maps whether they be in hardcopy or digital format in that objects that may be suitable as GCPs are more readily identified from images than from cartographic symbols as depicted on maps. While visual matching by comparing a digital photographic image with a digital airborne or satellite image can be a tedious process (Abd-Elrahman et al. 2001), its advantage far outweighs conventional reference to hardcopy maps and manual measurement and estimation of map coordinates. This process has been applied to the geometric correction of both digital airborne and satellite data.

Digital orthophotos can be used to detect positional errors in small-format digital aerial photographs. Digital camera images are considered to have excellent image quality but relatively poor positional accuracy despite on-board GPS receiver and attitude and heading measuring devices. Area-based matching techniques were used to relate the digital aerial photograph with United States Geological Survey (USGS) digital orthophoto quadrangles that were used as reference images. Forest, urban and suburban areas were evaluated and the orthophotos were considered a viable, operational data source by which to assess the spatial integrity of the airborne digital camera images.

Airborne multispectral scanner imagery has also been georeferenced with digital orthophotos (Pope and Scarpone 2000). While airborne scanner data is considered to have greater spatial, spectral, and temporal resolution than satellite data, a concern is the geometric distortions in the imagery. A method based on a digital orthophoto and a DEM was developed to define a “virtual landscape” over which a mathematical model of the scanner and its airborne platform could be defined.

Digital orthophotos have been used to derive GCPs in the evaluation of methods to rectify IKONOS Geo satellite imagery (Toutin and Cheng 2000, 2001). IKONOS data is produced at five different product levels each with different levels of positioning accuracy. Because IKONOS does not provide orbital information, users have more difficulty in undertaking geometric corrections themselves. Several methods were evaluated to undertake these corrections and in their study, GCPs were derived from 20 cm digital

orthophotos. A multi-sensor geometric model has been developed (Toutin 1995) that has also been adapted for data from the high resolution IKONOS satellite (Toutin and Cheng 2000). This solution was further evaluated over a larger range of sites that spanned low-to-high relief environments in order to track the propagation of errors during the full geometric correction process including bundle adjustment and orthorectification (Toutin 2001).

Digital orthophotos have also been used to rectify aerial photographs (Jennings and Jarnagin 2000). To rectify historical aerial photographs scanned at 1 m pixel resolution, USGS digital orthophoto quarter quads were used as reference data in an orthoimage-to-image registration process similar to map-to-image correction with second order polynomial transformation algorithms. This process was used to rectify six dates of historical photography and to study changes in impervious surface cover and streamflow as indicators of changes in landscape characteristics.

These studies exemplify the use of digital orthophotos in spatially rectifying a range of digital remote sensing images that range from aerial photographs to satellite. In standard geometric correction procedures with polynomial transforms (Richards 1993; Lillesand and Kiefer 1994), digital orthophotos provide a source of two-dimensional geographic coordinates. If the image is to be orthorectified, then the orthophoto would be the source of GCP collection and the Z-elevation would be derived from a DEM (Toutin 2001).

3.1.2 GPS integration

The collection of GPS data points is most often used for acquiring training or validation data (Zhang et al. 1997; Mickelson et al. 1998; Muller et al. 1998; Thenkabail et al. 2000). It could also be used, however, to collect geographic positions of GCPs in the field that correspond to their pixel representations in the image (Pellegrini et al. 1997; McGregor 1998). The process of determining where to locate a GCP point usually starts with identifying a feature on the image that may be identifiable in the field. While an aerial photograph is not required for this process, its availability may be advantageous when the location of the desired GCP is also co-located on the air photo. Aerial photos are almost always at a larger scale than the digital image being corrected, and locating the desired GCP on the photo based on its identification on the uncorrected image provides a natural navigation aid to facilitate its location in the field. Thus, if available, an aerial photo should be requisite ancillary data that could help ensure the point being collected in the field with GPS is, in fact, the point that was identified on the uncorrected image.

3.2 Digital image processing: Training for image classification and validation

The analysis of a remote sensing image in forestry typically entails a classification process to produce a thematic representation of the landscape that consists of relatively homogeneous classes of interest. The major steps in undertaking a multispectral image classification include definition of the classification scheme, selection of training areas, and classification and accuracy assessment. In undertaking this exercise, the most important requisite is the definition of the classification system that defines the classes to be mapped. These classes must be defined by their ground characteristics, and the assumption that the optical properties of the ground cover is correlated with the attributes of the remote sensing image must be valid (Duggin and Robinove 1990). Within this framework, the classification and mapping of land cover has been one of frequent interest due to its importance for many scientific, resource management and policy purposes (Cihlar 2000; Oetter et al. 2000). In the mapping of land cover and other applications such as change detection and forest attributes, aerial photographs can be used in training for image classification and in the validation components of a remote sensing analysis.

3.2.1 Training for image classification

Image classification procedures are often categorized as supervised or unsupervised (Lillesand and Kiefer 1994). The supervised method involves the creation of training data to define, for example, land cover classes of interest based upon prior knowledge of the study area. The statistical characteristics of the training data are generated, using an algorithm such as the maximum likelihood, and then used to classify the image. Aerial photographs have served as a source of training data from both analogue and digital arenas and its integration with the digital remote sensing image can be accomplished in at least three ways. First, hardcopy photographs may be interpreted, and areas delineated may be used to guide the identification of training areas on the image. Second, photo interpretation may be digitized and represented in a GIS that could then be imported to the digital image for use as training. Third, digital interpretation could be undertaken to outline areas of interest that could be used directly as training areas. Some of the philosophies and assumptions underlying these processes and their relevance for image classification will follow four studies from the literature.

Franklin (2001a) led a study to model forest net primary productivity (NPP) with reduced uncertainty by remote sensing of cover type and leaf

area index. The heart of ecosystem process models are polygons that are assumed homogeneous, and a common source of this information are photo interpreted forest inventory areas that are stored in a GIS polygon format (Gillis and Leckie 1993). Users of this information have to assume that the boundaries are correct, that the classification system used is relevant to the proposed remote sensing analysis, and that variability within the polygon is not important to the operation of the model. Also, while the forest cover classification from photo interpretation may be suited for forest management applications, it may not be an optimal source of information on cover types for modeling. Two methods of collecting training data were evaluated to compare the use of photo interpreted polygons in the GIS versus individual TM pixels selected from within polygons. An average accuracy of 74 % was achieved from the use of GIS polygons in comparison to 91 % accuracy from individual pixels. The accuracy from the use of GIS polygons was consistent with previous work (Wulder 1998), and the lower accuracy was attributed to errors in the GIS polygons. It outlined the problem that polygon information from photo interpretation may not have distinct signatures for training remote sensing classifiers, a problem that has been identified in a study by Ghitter et al. (1995). This is, in part, attributed to the structure and composition of the classification system used for labeling the photo interpreted polygons in the GIS which may be quite different than the classification system to be used to label classes from remote sensing.

Forest inventory polygons in a GIS can be used to stratify the landscape, and areas of interest can be isolated for image processing. In a study to map conifer understorey in the boreal mixedwoods, polygons from a 1:20,000 scale forest inventory were initially used to focus the remote sensing work to only the areas of interest, the deciduous-dominant mixed-wood stands (Hall et al. 2000). Subsequently, 1:10,000 leaf-off colour infrared aerial photographs were photo interpreted to identify areas of nil, light, moderate and heavy understorey, which was calibrated from both field and aerial surveys. This interpretation was digitized and integrated with the original forest inventory polygons to provide information about understorey distributions within overstorey species composition and stand structure for the deciduous-dominant stands. A random sample of pixels within these revised polygons served as training data in a supervised evidential reasoning classifier that resulted in a 71 % classification accuracy. The classification system devised for labeling understorey classes incorporated structure information from the overstorey in recognition of the contributions of both overstorey and understorey to the spectral response recorded at the pixel level.

Aerial photographs have been interpreted to provide estimates of percent cover on 2 ha plots from which a portion were used for training and the remaining used for validation (Oetter et al. 2000). A combination of low-level 35-mm colour photographs, 1:24 000 colour aerial photographs, and ancillary GIS coverages were combined as reference data that were used with a multi-seasonal Landsat TM data set to characterize agricultural and related land cover in the Willamette River Basin of western Oregon. For the forest component, the training plots were used to label unsupervised clusters derived from a 15-band Tasseled Cap data set. An overall accuracy of 74 % was achieved for a 20 class map that consisted of agricultural crops, forest and natural cover types, and urban building densities.

Several reference data sources including digital orthophotos that were interpreted with heads-up digitizing were incorporated into a study to develop a Landsat TM-based forest area estimation technique for use in an annual inventory and change system (Wayman et al. 2001). Forest and non-forest polygons were digitized by US Forest Service employees and County foresters and their expert knowledge was considered the most cost-effective of methods reviewed for data collection. A hybrid classification method was built that used specific rejection criteria and large numbers of reference pixels to reject or label spectral classes. Interpreted orthophotos were recommended as one approach for effective collection of reference data. Similarly, Wirth et al. (1997) delineated the locations of aspen stands on colour aerial photographs that were subsequently located and digitized onto the satellite image for use as supervised training sites.

These studies exemplify the various methods by which photo interpretation could be undertaken in the provision of training data for use in digital analysis of a remote sensing image. There are many possible reasons that contribute to the variable results reported including the photo versus the image classification system used to label spectral clusters, the cognitive nature of photo interpretation (Figure 3-3) versus the predominant use of tone used in spectral classification, and the nature of an interpretative polygon versus the focus on the pixel in digital images. The inherent fuzziness associated with photo interpreted boundaries is also an issue that has been identified as being difficult to verify (Thierry and Lowell 2001). Many of these issues apply when considering the photo interpretation of a forest stand in comparison to the difficulty in its derivation from digital remote sensing. The aerial photograph is a rich source of information that can be instrumental towards the success of a remote sensing classification. The philosophical differences described merely highlight that due care and attention must be exercised in its application to ensure integrating these data sources are both technically correct and appropriate.

3.2.2 Validation of image classification: aerial photographs and accuracy assessment

Aerial photographs, in conjunction with field surveys, are used as a source of ground reference data in the accuracy assessment of thematic maps (Macleod and Congalton 1998). Users should be aware, however, of some considerations that pertain to their use. Accuracy assessments are most often undertaken on a point-for-point basis, and two issues that govern their validity are the selection of the correct class for the reference data and the potential positional errors of the sample points on the photograph (Khorram et al. 2000). These issues raise questions about the accuracy of the interpretations reflected in the map reference labels, and the precision of the points located relative to their true location on the ground (Congalton and Green 1999). Any problems within these two issues can cause the accuracy of the image classification to be underestimated (Congalton 1991).

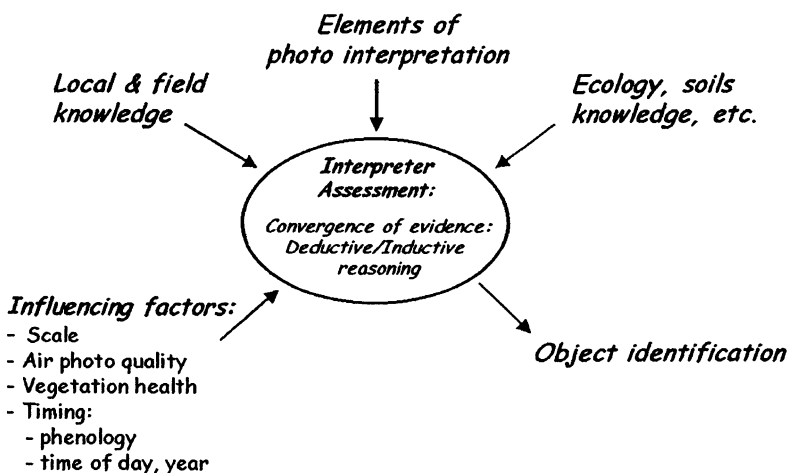


Figure 3-3. Graphical illustration of the photo interpretation process.

Aerial photographs could be interpreted, especially for the validation exercise, or be reflected in the production of inventory maps used to validate remote sensing classifications. In both cases, the air photo interpretation used to create the reference data are often assumed to be correct. Seldom are verification exercises undertaken to assess the accuracy of the interpretation. Biging and Congalton (1991) suggested accuracy assessments with field data would be preferable if the accuracy of the photo interpretation is not sufficiently high. A concern with using field data, however, is that accuracy assessment may not be possible at a single point. Image classification is an

exercise to simplify the input digital image when producing a thematic product. Computing accuracy based on a sample of pixels assumes that the true class values are verifiable at each pixel, but in reality this may not be true (Wang and Howarth 1993). A stand label from photo interpretation or its thematic classification assumes that a polygon is sufficiently homogenous for the class label to be representative of its composition. In the field, stand polygons are seldom homogenous as there are natural micro-type ecological variations within a stand. When validating air photo interpretation from the field, consideration also needs to be given to the number of samples, where they are located, and how are they located for registration with the image (Koukoulas and Blackburn 2001). These concerns can be addressed, in part, by implementing quality control procedures to ensure the air photo interpretation is consistent and properly calibrated, if necessary. Adaptive procedures as refinements could also be considered. Khorram et al. (2000), for example, assessed both primary and alternate interpreted land cover labels in a three-by-three sample point window that was anticipated to provide a more representative estimate of accuracy than point-for-point methods.

Positional errors for reference points can occur from manual location on hardcopy photographs. Even with the digital photogrammetric products now becoming available, small residual errors from digitizing (e.g., control point location), georeferencing (e.g., model residuals, DEM errors) and mosaicking aerial photographs can result in some uncertainty in sample point location (Khorram et al. 2000). Care in procedures and acquiring metadata where available can help to minimize the likelihood or magnitude of potential positional errors.

In studies that have utilized aerial photographs in validation assessment, Hansen et al. (2001) selected a random sample of pixels that were either visited in the field or interpreted on aerial photographs. Up to 50 pixels per class were located which was consistent with recommendations from the literature (Mather 1989) although other methods such as that based on binomial statistics have also been suggested (Richards 1993). The methods implemented enabled reporting of the accuracy of the habitat maps produced from satellite classifications. Franklin et al. (2001) also conducted an accuracy assessment based on independent sample points that were interpreted on digital orthophotos. The photo interpretation was considered to be clear and obvious, and the assessment resulted in identifying poor forest class separability from the spectral response patterns for these classes that were largely contributing to classification error. The use of aerial photographs in validating thematic map classifications can be successful if

considerations are given to how the validation data is derived, what is its positional accuracy, and how it is planned and implemented in the study.

3.3 High resolution feature extraction

Digitized aerial photographs may be more useful than satellite images because of their higher spatial resolution, as this will improve the classification of forest stands and provide estimates of stand characteristics commonly required in forest inventory (Wang et al. 1998). As a result, there has been growing interest in capturing sub-metre resolution (10–100 cm/pixel) data from scanned aerial photographs and airborne sensors that would provide opportunities to study trees at the individual tree crown level (Brantberg 1997; Bolduc et al. 1999; Gougeon and Leckie 2001; Culvenor, Chapter 9). Algorithms and methods have been developed to extract features that represent individual tree characteristics from high spatial resolution images. The ability to digitally delineate individual tree crowns of a forest allows for improved estimation of inventory attributes such as crown closure, stand density, and volume (Wulder 1998). The use of aerial photographs for this application raises the need to carefully consider factors that influence image data quality and its role in resolving the image (i.e., tone, texture, pattern) of tree crowns for different species (Brandtberg 1997).

One of the driving factors for developing applications at the tree crown level is the increasing need for forest inventory information. Forest inventories are based predominately on the photo interpretation of medium-scale aerial photographs that define similar stands of vegetation with respect to species composition, height, crown closure, age and productivity (Gillis and Leckie 1993; Nesby 1997). In addition, precise estimates of stand volume and stem density are being sought for forest inventory, as are information about gap size and gap distribution for biodiversity and wildlife habitat studies. Pressures to ensure forests are being managed sustainably are resulting in these stand attributes being mapped to increasingly finer levels of detail. The degree to which these information needs can be met with conventional photo interpretation, however, is limited.

Extracting tree and stand attributes from high resolution aerial images is one approach that can complement existing inventory data acquisition programs. Algorithms and software programs have been developed to delineate or classify individual tree crowns (Gougeon 1995; Brandtberg 1997; Gougeon and Leckie 2001). Similar approaches were implemented in a test in Alberta to determine the extent species composition, crown closure and stem density could be derived and used to estimate stand volume for softwood, hardwood and mixed-wood species (Gerylo et al. 1998; Hall et al.

1998). To estimate stand volume reliably, species, crown closure and stem density are not sufficient predictors without a measure of tree size. One approach to acquire this information is through spatial integration with a digital forest inventory that typically has the stand height attribute (Gerylo et al. 1998; Bolduc et al. 1999). Scanning LIDAR data for either the individual tree or averaged for the stand is an alternative remotely sensed approach to obtaining height measures (St-Onge et al. Chapter 19; Lim et al. 2002). While research with LIDAR alone has been reported for estimating height, volume, biomass and canopy closure (Nilsson 1996; Means et al. 2000), a more promising approach would be integrating LIDAR data with the stand structural attributes derived from scanned aerial photographs or airborne images. The future will no doubt see a closer blending of these complementary technologies.

4. SUMMARY

In forestry, aerial photographs have long been the remote sensing data of choice. With the increasing opportunities for spectral and spatial data acquisition from airborne and satellite platforms, there has been a perception for some time that these sensors will provide the operational alternatives to the use of aerial photographs (Leckie 1990). More than 10 years later, this alternative has not yet occurred in the operational forestry domain. What was not anticipated, however, were the technological improvements in acquisition technology with innovations to aerial cameras, lenses, films and exposure systems, the increasing role of digitally scanned aerial photographs, and rapid developments in softcopy photogrammetry. Several vendors for example, now offer operational photogrammetric systems that can fully integrate into digital remote sensing or GIS systems. To reiterate, aerial photography is a technology in transition from the analogue to digital domains (Light 1996; Caylor 2000), and it seems likely that digital sensors will eventually become the remote sensing medium of choice.

With the increasing demands for timely, cost-effective information about our forest resources, just how can aerial photography and digital remote sensing be integrated? Deriving an answer to this question requires an understanding of how aerial photography is characterized, acquired, processed and interpreted. These are fundamental concepts, yet many are novel and advanced if we consider their technological implications within the framework of its role in remote sensing image analysis. Regardless, their key role is in data integration from both analogue and digital perspectives (Figure 3-1). How aerial photographs are used in digital image processing

depend on the resolution and scale of the remote sensing image, which in turn, depend on its application. The application of aerial photographs in image rectification, training for classification, and validation represent what can be done today. Its use in high-resolution feature extraction represents what can be done tomorrow. High resolution aerial photographs digitally captured, provides a viable data source that serves the potential to implement a new paradigm in the undertaking of forest inventories based on individual tree detection and its assemblage to what we know as forest stands with attribute labels (Franklin 2001b). Aerial photographs serve multiple roles in the analysis of remote sensing images in forestry, and are anticipated to continue to serve in both analogue and digital domains for some time to come.

ACKNOWLEDGMENTS

Several people contributed to the preparation of this book Chapter. I am grateful to Ms. D. Mucha who provided valuable assistance in the literature search and help in preparing the references. Mr. M. Gartrell created the graphics for Figure 3-1, and Mr. L. Fent provided valuable review comments and contributed material to several of the tables. My previous collaborative research with Mr. Fent provided some of the foundation for this article and is gratefully acknowledged. Drs. S. Franklin and M. Wulder reviewed the book Chapter outline that led to this article. Two anonymous reviewers provided valuable review comments. Finally, the Canadian Forest Service is acknowledged for supporting this endeavor.

REFERENCES

- Abd-Elrahman, A., Pearlstine, L., Dewitt, B. A., & Smith, S. E. (2001). Detection of positional errors in systems utilizing small-format digital aerial imagery and navigation sensors using area-based matching techniques. *Photogrammetric Engineering and Remote Sensing*, 67, 825-831.
- Agfa-Gevaert Group (2002). *Aerial photography*. Agfa-Gevaert Group. Belgium. <<http://www.agfa.com/industry/>>.
- Agfa-Gevaert, N. V.(undated). *Aerial imaging*. B-2640. Martsel, Belgium.
- Ahern, F. J., Leckie, D. G. (1987). Digital remote sensing for forestry: requirements and capabilities, today and tomorrow. *Geocarto International*, 3, 43-52.
- Biging, G. S., & Congalton, R. G. (1991). A comparison of photointerpretation and ground measurements of forest structure. *Proc. ASPRS 56th Annual Convention* (Vol. 3). Baltimore, MD. CD-ROM.

- Bolduc, P., Lowell, K., & Edwards, G. (1999). Automated estimation of localized forest volume from large-scale aerial photographs and ancillary cartographic information in a boreal forest. *International Journal of Remote Sensing*, 20, 3611-3624.
- Brandtberg, T. (1997). Towards structure based classification of tree crowns in high resolution aerial images. *Scandinavian Journal of Forest Research*, 12, 89-96.
- Canadian Council of Forest Ministers (2001). *Sustainable forestry: a reality in Canada*. Natural Resources Canada, Canadian Forest Service, Ottawa Ontario.
- Caylor, J. (2000). Aerial photography in the next decade. *Journal of Forestry*, 98, 17-19.
- Cihlar, J. (2000). Land cover mapping of large areas from satellites: status and research priorities. *International Journal of Remote Sensing*, 21, 1093-1114.
- Congalton, R. G. (1991). A review of assessing the accuracy of remotely sensed data: principles and practices. *Remote Sensing of Environment*, 37, 35-46.
- Congalton, R.G., & Green, K. (1999). *Assessing the Accuracy of Remote Sensed Data: Principles and Practices*. Lewis Publishers, CRC Press Inc., New York, N.Y.
- Duggin, M. J., & Robinove, C. J. (1990). Assumptions implicit in remote sensing data acquisition and analysis. *International Journal of Remote Sensing*, 11, 1669-1694.
- Eastman Kodak Company (2002). *Aerial imaging*. Eastman Kodak Company, Rochester, N.Y. Accessed 1 March 2002. <<http://www.kodak.com/go/aerial>>.
- Falkner, E., & Morgan, D. (2002). *Aerial Mapping* (2nd ed.). Lewis Publishers, CRC Press Inc., New York, N.Y.,
- Fent, L., Hall, R. J., & Nesby, R. K. (1995). Aerial films for forest inventory: optimizing film parameters. *Photogrammetric Engineering and Remote Sensing*, 61, 281-289.
- Franklin, S.E. (2001a). Modeling forest net primary productivity with reduced uncertainty by remote sensing of cover type and leaf area index. Hunsaker, C. T., Goodchild, M. F., Friedl, M. A., & Case, T. J. (Eds.) *Spatial Uncertainty in Ecology Implications for Remote Sensing and GIS Applications*, 284-307. Springer-Verlag, New York, N.Y.
- Franklin, S.E. (2001b). *Remote Sensing for Sustainable Forest Management*. Lewis Publishers, CRS Press Inc., New York, N.Y.
- Franklin, S. E., Stenhouse, G. B., Hansen, M. J., Popplewell, C. C., Dechka, J. A., & Peddle, D. R. (2001). An integrated decision tree approach (IDTA) to mapping land cover using satellite remote sensing in support of grizzly bear habitat analysis in the Alberta Yellowhead Ecosystem. *Canadian Journal of Remote Sensing*, 27, 579-592.
- Gerylo, G., Hall, R. J., Franklin, S. E., Roberts, A., & Milton, E. J. (1998). Hierarchical image classification and extraction of forest species composition and crown closure from airborne multispectral images. *Canadian Journal of Remote Sensing*, 24, 219-232.
- Ghitter, G. S., Hall, R. J., & Franklin, S. E. (1995). Variability of Landsat Thematic Mapper data in boreal deciduous and mixed-wood stands with conifer understory. *International Journal of Remote Sensing*, 16, 1989-3002.
- Gillis, M. D., & Leckie, D. G. (1993). Forest inventory mapping procedures across Canada. *Information Report P1-X-114*. Can. For. Serv., Petawawa Natl. For Inst., Chalk River, Ont.
- Gougeon, F. A. (1995). A crown-following approach to the automatic delineation of individual tree crowns in high spatial resolution aerial images. *Canadian Journal of Remote Sensing*, 21, 274-284.
- Gougeon, F. A., & Leckie, D. G. (2001). Individual tree crown image analysis – a step towards precision forestry. *Proc. First Held International Precision Forestry Symposium*, 43-49. June 17-20, 2001, University of Washington, Seattle, Washington. CD-ROM.

- Graham, L. N., Ellision, K., & Riddell, C. S. 1997. The architecture of a softcopy photogrammetry system. *Photogrammetric Engineering and Remote Sensing*, 63, 1013-1020.
- Graham, R. W., & Read, R. E. (1986). *Manual of Aerial Photography*. Focal Press, London, England.
- Gruber, M., & Leberl, F. (2001). Description and evaluation of the high quality photogrammetric scanner UltraScan 5000. *ISPRS Journal of Photogrammetric Engineering and Remote Sensing*, 55, 313-329.
- Hall, R. J., Gerylo, G. R., & Franklin, S. E. (1998). Estimation of stand volume from high resolution multispectral images. *Proc. 20th Can. Symp. Remote Sensing*, 191-196. May 10-13, 1998, Calgary, Alta.
- Hall, R. J., & Fent, L. (1996). Influence of aerial film spectral sensitivity and texture on interpreting images of forest species composition. *Canadian Journal of Remote Sensing*, 22, 350-359.
- Hall, R. J., Peddle, D. R., & Klita, D. L. (2000). Mapping conifer understory within boreal mixedwoods from Landsat TM satellite imagery and forest inventory information. *The Forestry Chronicle*, 76, 887-902.
- Hansen, M. J., Franklin, S. E., Woudsma, C. G., & Petersen, M. (2001). Caribou habitat mapping and fragmentation analysis using Landsat MSS, TM, and GIS data in the North Columbia Mountains, British Columbia, Canada. *Remote Sensing of Environment*, 77, 50-65.
- Hinz, A., & Heier, H. (2000). The Z/I imaging digital camera system. *Photogrammetric Record*, 16, 929-936.
- I.S.M. International Systemap Corp. (1999). *The fundamentals of digital photogrammetry*. I.S.M. International Systemap Corp., Vancouver, B.C.
- Jennings, D. B., & Jarnagin, S.T. (2000). Impervious surface and streamflow discharge: a historical remote sensing perspective in a northern Virginia subwatershed. *Proc. ASPRS 2000*. Washington, D.C., May 22-26, 2000. CD-ROM.
- Jensen, J. R. (2000). *Remote Sensing of the Environment: An Earth Resource Perspective*. Prentice Hall, Upper Saddle River, New Jersey.
- Khorram, S., Knight, J., Cakcir, H., Yuan, H., Mao Z., & Dai, X. (2000). Improving estimates of the accuracy of thematic maps using aerial photos as the ground reference source. *Proc. ASPRS 2000*. May 22-26, 2000, Washington, D.C., American Society Photogrammetry and Remote Sensing, Bethesda, MD. CD-ROM.
- King, D. J. (2000). Airborne remote sensing in forestry: sensors, analysis and applications. *The Forestry Chronicle*, 76, 859-876.
- Kolbl, O., & Bach, U. (1996). Tone reproduction of photogrammetric scanners. *Photogrammetric Engineering and Remote Sensing*, 62, 687-694.
- Koukoulas, S., & Blackburn, G. S. (2001). Introducing new Indices for accuracy evaluation of classified images representing semi-natural woodland environments. *Photogrammetric Engineering and Remote Sensing*, 67, 499-510.
- Lear, A. C. (1997). Digital orthophotography, mapping with pictures. *IEEE Computer Graphics and Applications*, 17, 12-14.
- Leckie, D. G. (1990). Advances in remote sensing technologies for forest surveys and management. *Canadian Journal of Forest Research*, 20, 464-483.
- Light, D. L. (1996). Film cameras or digital sensors? The challenge ahead for aerial imaging. *Photogrammetric Engineering and Remote Sensing*, 62, 285-291.

- Light, D. (2001). An airborne direct digital imaging system. *Photogrammetric Engineering and Remote Sensing*, 67, 1299-1305.
- Lillesand, T. M., & Kiefer, R. W. (1994). *Remote sensing and image interpretation* (3rd ed.). John Wiley & Sons, Inc., New York, N.Y.
- Lim, K., Treitz, P., Wulder, M., St-Onge, B., & Flood, M. (2002). LiDAR remote sensing of forest structure, *Progress in Physical Geography*, in press.
- Mather, P. (1989). *Computer Processing of Remotely Sensed Images: An Introduction*. Wiley, Chichester, England.
- Macleod, R. D., & Congalton, R. G. (1998). A quantitative comparison of change-detection algorithms for monitoring eelgrass from remotely sensed data. *Photogrammetric Engineering and Remote Sensing*, 64, 207-216.
- McGregor, S. J. (1998). An integrated geographic information system approach for modeling the suitability of conifer habitat in an alpine environment. *Geomorphology*, 21, 265-280.
- Means, J. E., Acker, S. A., Fitt, B. J., Renslow, M., Emerson, L., & Hendrix, C. J. (2000). Predicting forest stand characteristics with airborne scanning Lidar. *Photogrammetric Engineering and Remote Sensing*, 66, 1367-1371.
- Michael, J. (1994). Creating digital orthophotos requires careful consideration of project design elements. *Earth Observation Magazine*, 3, 34-37.
- Mickelson, J. G., Jr., Covco, D. L., & Silandes, J. A. Jr. (1998). Delineating forest canopy species in the northeastern United States using multi-temporal TM imagery. *Photogrammetric Engineering and Remote Sensing*, 64, 891-904.
- Mikhail, E. H. (1996). From the Kelsh to the digital photogrammetric workstation and beyond. *Photogrammetric Engineering and Remote Sensing*, 62, 680.
- Muller, S. V., Walker, D. A., Nelson, F. E., Auerbach, N. A., Bockheim, J. G., Guyer, S., & Sherba, D. (1998). Accuracy Assessment of a land-cover map of the Kuparuk River Basin, Alaska: considerations for remote regions. *Photogrammetric Engineering and Remote Sensing*, 64, 619-628.
- Nelson, T., Wulder, M. A., & Niemann, K. O. (2001). Spatial resolution implications of digitising aerial photography for environmental applications. *The Journal of Imaging Science*, 49, 223-232.
- Nesby, R. (1997). *Alberta Vegetation Inventory Standard Manual Version 2.2*, Alberta Environmental Protection, Edmonton, Alberta.
- Newby, P. R. T. (1996). Digital images in the map revision process. *ISPRS J. Photogrammetry and Remote Sensing*, 51, 188-195.
- Nilsson, M. (1996). Estimation of tree heights and stand volume using an airborne Lidar system. *Remote Sensing of Environment*, 56, 1-7.
- Oetter, D. R., Cohen, W. B., Berterretche, M., Maiersperger, T. K., & Kennedy R. E. (2000). Land cover mapping in an agricultural setting using multiseasonal Thematic Mapper data. *Remote Sensing of Environment*, 75, 139-155.
- Paine, D. P. (1981). *Aerial Photography and Image Interpretation for Resource Management*. John Wiley and Sons, New York, N.Y.
- Pellegrini, P. F., Piazza, E., & Coman, I. (1997). Using Global Positioning Systems to Verify the location of Ground Control Points used in Satellite Remote Sensing. *Proc. GER '97, International Symposium on Geomatics in the Era of Radarsat*, paper 284, Session E-5. May 25-30, 1997, Ottawa, Ont., CD-ROM.
- Pope, P. A., & Scarpone, F. L. (2000). Development of a method to geographically register airborne scanner imagery through parametric modeling with image to image matching.

- Proc. ASPRS 2000.* May 22-26, 2000, Washington, D.C., American Society of Photogrammetry and Remote Sensing, Bethesda, MD. CD-ROM.
- Richards, J. A. (1993). *Remote Sensing Digital Image Analysis: An Introduction* (2nd ed.). Springer-Verlag, New York, N.Y.
- Space Imaging, Inc. (2002). *Satellites constellation IKONOS.* Space Imaging, Inc. Thornton, Co. Accessed 28 February 2002. <<http://www.spaceimaging.com/aboutus/satellites/IKONOS/ikonos.html#stats>>.
- Thenkabail, P. S., Nolte, C., & Lyon J. G. (2000). Remote sensing and GIS modeling for selection of benchmark research area in the inland valley agroecosystems of West and Central Africa. *Photogrammetric Engineering and Remote Sensing*, 66, 755-768.
- Thierry, B., & Lowell, K. (2001). An uncertainty-based method of photointerpretation. *Photogrammetric Engineering and Remote Sensing*, 67, 65-72.
- Toutin, T. (1995). Multisource data fusion with an integrated and unified geometric modeling. *EARSEL Journal Advances in Remote Sensing*, 4, 118-129.
- Toutin, T. (2001). Geometric processing of IKONO GEO images with DEM. *Proc. ISPRS Joint Workshop on High Resolution Mapping*, 264-271. September 19-21, Hanover, Germany. CD-ROM.
- Toutin, T., Cheng, P. (2000). Demystification of IKONOS. *Earth Observation Magazine*, 9, 13-16.
- Toutin, T., & Cheng, P. (2001). DEM with stereo IKONOS: A reality if... *Earth Observation Magazine*, 10, 17-21.
- Wang, G., Poso, S., Waite, M. -L., & Holopainen M. (1998). The use of digitized aerial photographs and local operation for classification of stand development classes. *Silva Fennica*, 32, 215-225.
- Wang M., & Howarth, P. J. (1993). Modelling errors in remote sensing image classification. *Remote Sensing of Environment*, 45, 261-271.
- Warner, W. S., Graham, R. W., & Read, R. E. (1996). Small format aerial photography. *American Society of Photogrammetry and Remote Sensing*. Bethesda, MD.
- Wayman, J. P., Wynne, R. H., Scrivani, J. A., & Reams, G. A. (2001). Landsat TM-based forest areas estimation using iterative guided spectral class rejection. *Photogrammetric Engineering and Remote Sensing*, 67, 1155-1166.
- Welch, R. A., & Jordan, T. R. (1996). Digital orthophoto production in the desktop environment. *GIM Magazine*, 10, 26-27.
- Wirth, T., Maus, P., Powell, J., Lachowski, H., Suzuki, K., McNamara, J., Riordan, P., & Broham, R. (1997). Monitoring aspen decline using remote sensing and GIS. *Proc. GIS '97*, 75-79. Vancouver, B.C.
- Wolf, P. R., & Dewitt, B. A. (2000). *Elements of photogrammetry with applications in GIS* (3rd ed.). McGraw Hill, New York, N.Y.
- Wulder, M. A. (1998). Optical remote sensing techniques for the assessment of forest inventory and biophysical parameters. *Progress in Physical Geography*, 22, 449-476.
- Zhang, X., Li, C., & Yuan, Y. (1997). Application of neural networks to identifying vegetation types from satellite images. *AI Applications*, 11, 99-106.

Chapter 4

INDIRECT MEASUREMENT OF FOREST CANOPY STRUCTURE FROM *IN SITU* OPTICAL SENSORS

Richard A. Fournier¹, Daniel Mailly², Jean-Michel N. Walter³, and Kamel Soudani⁴

¹Centre de Recherches et Applications en Télédétection (CARTEL), Université de Sherbrooke, Quebec, J1K 2R1, Canada

²Division de la recherche forestière, Ministère des Ressources naturelles du Québec, Québec, G1P 3W8, Canada

³Institut de Botanique, Université Louis Pasteur, Strasbourg, 67070, France

⁴Laboratoire d'Ecophysiologie Végétale, Université Paris-Sud XI, 91405, Orsay, France

1. INTRODUCTION

This Chapter covers the major requirements for the estimation of forest canopy structure from *in situ* remote sensing. *In situ* measurements of forest canopy structure provide the basis for remote sensing of forest attributes at all scales. Selection of a measurement strategy requires knowledge of available measurement methods and must address data set availability, constraints in forest applications and scale related considerations. The main objective of this Chapter is to describe methods that estimate parameters related to forest canopy structure. This will be accomplished through: (i) defining and describing the relevant elements of the canopy structure, (ii) providing background information on the theory and practice of *in situ* measurements of canopy structure, together with their limitations, and (iii) suggesting strategies for generalising ground measurements into spatially extended estimations.

This Chapter will describe the architectural elements composing the canopy structure with emphasis on leaf area, in particular the leaf area index (LAI), because of its importance for gas-vegetation exchange. This will be

followed by a theory of LAI measurement, and subsequently by a discussion of methods for measuring *in situ* LAI. The last two sections will deal with the main factors affecting LAI measurement methods and methods of defining adapted measurement strategies through (i) the comparison of measurement methods, (ii) the availability and potential use of relevant data sets, and (iii) scaling issues.

Measurement and mapping of forest canopy structure in operational forest inventories have traditionally relied upon aerial photography interpretation and ground-based sampling (Avery and Burkhart 2002; Hall, Chapter 3). Mapping canopy structure using aerial photographs requires an experienced interpreter and site-specific interpretation keys to visually assess patterns of image texture, tone and colour (Howard 1992; Sayn-Wittgenstein 1960; Zsilinszky 1964). Indirect measurements of the canopy structure using remote sensing methods may be viewed as either a complement to existing inventory data or as an alternative source of information in areas without traditional forest inventory coverage.

Although not yet integrated in operational forest inventory procedures, remote sensing methods may potentially overcome certain limitations of traditional inventory practices. For example, traditional forest inventories are laborious, time-consuming and expensive and may only occur every few years, particularly when management areas are large or remote. Cost-effective remote sensing techniques may therefore be used to offset these high costs when more frequent inventory updates are required; they may also be used to retrieve alternative stand-level forest measurements that support the recent shift towards sustainable forest management (Cohen and Spies 1992; Franklin 2001; Lefsky et al. 2002).

Remotely sensed data have also been successfully used to parameterise coarse-scale ecological models that predict the effects of primary environmental drivers (temperature, precipitation, atmospheric CO₂, solar radiation, etc.) and regional climate change on forest ecosystem function (net primary productivity [NPP]; carbon, nutrient, and water cycling, etc.) (Justice et al. 1998; Running et al. 1989; Lucas and Curran 1999; Aber et al. 2001). Due to this recent and growing demand for forest measurements, as well as the increasing availability of a variety of ground, air and satellite-based sensors, improved methods are rapidly developing for the remote sensing of forest canopy structure at all spatio-temporal scales.

Forest measurements and measurement tools vary according to research and management objectives, forest type, and the temporal and spatial scale of interest. For example, manual ground-based measurements in fixed or variable forest inventory plots provide detailed information on the species composition, size, density and shape of trees as important inputs for growth

and yield models (Avery and Burkhart 2002). Remote sensing techniques have been developed to measure forest canopy structure from two different vantage points and spatial scales. Ground-based (*in situ*) methods use gap-fraction analysis to measure forest canopy structure from beneath the canopy – sensors typically face skyward (Pearcy 1989; Norman and Campbell 1989; Welles 1990; Welles and Norman 1991; Welles and Cohen 1996; Gower et al. 1999). These techniques are sensitive to fine-scale variations in forest canopy structure and therefore optimised for plot-level measurements. Airborne or satellite sensors are used to assess coarser-scale patterns of forest canopy structure from above and thus facilitate forest measurements at the stand and landscape levels (Spies et al. 1994; Hyppä et al. 2000; Danson 2000; Lefsky et al. 2001). The success of above-canopy remote sensing in forestry has been mixed (Holmgren and Thuressen 1998); however, the increasing demand for ecological data and models provides incentive for improving remote sensing products to support current forecasting, monitoring and operational requirements (Fournier et al. 2000). Therefore, emphasis is often placed on forest canopy structure variables that can be scaled from ground plots to regional maps.

In this Chapter, we describe a number of indirect optical techniques that can be used to measure forest canopy variables *in situ* and also discuss the practical aspects of their use for fine- and coarse-scale mapping. The Chapter is organised into three logical sections. First, we identify those attributes of forest canopy structure that are relevant to forest management and ecological modelling. Second, we summarise the background theory, assumptions, and limitations of *in situ* measurements of stand leaf area index (LAI). Lastly, we discuss potential strategies for integrating fine-scale *in situ* measurements of LAI with coarse-scale remotely sensed data collected from airborne and satellite sensors.

Although several reviews exist on semi-direct (Gregoire et al. 1995) and indirect *in situ* measurement methods (Pearcy 1989; Norman and Campbell 1989; Welles 1990; Welles and Norman 1991; Welles and Cohen 1996), our synthesis of this topic includes a detailed summary of the currently available methods, a discussion on the practical aspects, limitations and solutions for *in situ* measurements, and recommendations for integrating indirect measurement with other sources of canopy structure data.

2. VARIABLES ASSOCIATED WITH FOREST CANOPY STRUCTURE

Forest canopy structure is defined differently according to the objectives and spatio-temporal scales adopted. In order to address the data requirements and management objectives in forestry, the vertical and horizontal structures are described, in inventories, by variables meaningful to the management unit. For instance, horizontal structure is described with continuous or categorical variables such as species composition, spatial distribution of trees, stands, crown cover, height class, etc. On the other hand, the vertical structure is often referred to as the social hierarchy of the overstorey composed of, starting from the top of the canopy, dominant, codominant, intermediate and suppressed trees.

For the landscape ecologist, the forest is viewed as a complex mosaic of homogeneous patches, dynamic in both time and space (Whittaker 1975; O'Neill et al. 1986). Regardless of the scale of view adopted, many ecological indices and structural variables such as density, frequency and fragmentation are used (Legendre and Fortin 1986; Li and Reynolds 1995; Gustafson 1998). Landscape representations of the forest mosaic are currently analysed for neighbourhood relationships like dispersion, aggregation, or competition indices (Squires and Klosterman 1981; Wagner and Radosevich 1998).

There are two general ways that forest canopy structure data can be represented: (i) as discrete points (a network of inventory plots) within a continuous forest cover, or (ii) as two-dimensional thematic maps depicting the spatial extent of homogenous units (e.g., forest cover map derived from air photo interpretation). Information from both approaches is useful, but current analysis methods tend to focus on one or the other (Gustafson 1998). Remote sensing methods are well adapted for the integration of these two measurement types, but this topic is beyond the scope of this Chapter.

From the most general perspective, forest canopy structure refers to the architectural and functional elements of a forest canopy. For the sake of simplicity, canopy structure is often equated with the temporal and spatial organisation of the aboveground vegetation components including their position, extent, quantity, type, orientation, shape, and connectivity (Norman and Campbell 1989; Welles 1990; Parker 1995; Oliver and Larson 1996; Spies 1998). Independent variables at the tree- or stand-level, are usually linked by allometric relationships with other dependent variables. For example, stem DBH (diameter at breast height) is often used to predict tree height, volume and biomass (Aldred and Alemdag 1988; Avery and Burkhart 2002). Growth curves and frequency distributions of stand DBH,

height, and age are also used to describe the different stages of stand development (Oliver and Larson 1996).

There are two predominant canopy components, foliage and tree boles. The interest in tree boles is directly linked to wood volume requirements of the forest industry and to current inventory data sets. In contrast, foliage distribution can be linked to the functional aspects of the canopy and can also be included in a quantitative biophysical approach to model canopy processes. Furthermore, foliage distribution, surface area and orientation are characteristics of canopy structure that are most able to adapt to small temporal changes in the forest environment (i.e., responses related to competition for light, moisture and nutrients; natural disturbance and phenology).

Leaf area index (LAI) is a measure of the amount of foliage per unit surface area and is an important input parameter for ecological modelling. Foliage provides the main surface for the exchange of mass, energy and gas between the photosynthetically active vegetation and the atmosphere. The distribution and density of foliage also controls light, thermal and moisture conditions within the canopy (Parker 1995; Chen et al. 1999; Soudani and Bréda 2002). Consequently, LAI is the main driving variable in most forest growth and productivity models based on physiological processes (usually called process-based models). Examples of such models are: FOREST-BGC (Running and Coughan 1988), BIOMASS (McMurtrie and Landsberg 1992), TREGROW (Weinstein et al. 1991), and 3-PG (Landsberg and Waring 1997). LAI is also used to predict the amount of light available in the forest understorey (Welles 1990; Welles and Norman 1991; Rich et al. 1993; Machado and Reich 1999; de Castro 2000).

Finally, an important issue common to most measurements is the ability to rely on a variable that will remain consistent from one scale to another (Enquist and Niklas 2001). LAI has therefore been a convenient and ecologically relevant variable for multi-scale studies that range from leaf to region. Consequently, recent *in situ* and above-canopy remote sensing techniques have focussed on the measurement and use of LAI as a structural variable. We have therefore placed significant emphasis on *in situ* measurements of LAI in the following sections. Although the measurements of other structural variables will be discussed, we will restrict most of our discussion in the remaining sections to LAI theory, measurement techniques, and multi-scale applications.

3. LAI MEASUREMENT THEORY

The cumulative LAI (unitless) of a canopy is calculated as the sum of the vertical projection of the foliage area on a horizontal plane from the ground ($z=0$) to the top of the canopy ($z=h$). LAI depends on the average surface density coefficient of the foliage (u) expressed in m^2/m^3 (Ross 1981):

$$L(z) = \int_{z=0}^h u(z) dz . \quad (1)$$

There are several definitions for LAI and therefore each study must be explicit about the definition used (Barclay 1998). However, the most current definition used is the one-half the total green leaf area (in m^2) per horizontal unit surface area (in m^2) (Lang et al. 1991; Chen and Black 1992; Fassnacht et al. 1994; Stenberg et al. 1994; Chen et al. 1997).

3.1 Effective LAI from gap fraction

LAI can be estimated from indirect light measurement within the canopy by an instrument looking at zenith or towards the sun. Several techniques provide angular information about the amount and distribution of openings in the canopy, often called gap fractions (Norman and Campbell 1989). Mathematical procedures are available to translate the angular distribution of gap fractions into measures of stand LAI. Most procedures assume a random distribution of foliage (Welles and Norman 1991).

Algorithms developed for LAI calculations from hemispherical sensors involve a division of the 2π steradian (180-degree) field of view (FOV) into concentric equiangular annuli (e.g., 9 sections in zenith of $\Delta V_\theta = 10^\circ$ from $\theta = 0^\circ$ to 90°). For imaging systems like hemispherical photos, the gap fraction of each of these annuli is the ratio between the number of pixels in a gap (pixel illuminated by the sky) and the total number of pixels in this angular sector. However for other hemispheric viewing instruments integrating the signal spatially (e.g., LAI-2000 PCA), a series of normalized intensities associated with a zenith annulus are used. The gap fraction, which can also be interpreted as the probability $P(\theta)$ ⁵ of light penetration through the foliage at zenith angle θ . $P(\theta)$ can be expressed mathematically by (Lang et al. 1985; Campbell and Norman 1989; Nobel et al. 1993):

⁵ This probability is often referred to as the light transmission coefficient: $T(\theta)$ or $\tau(\theta)$.

$$P(\theta) = \exp [-G(\theta) \cdot L / \cos(\theta)] \quad (2)$$

where $G(\theta)$ is the projection coefficient of the foliage on a plane (normal) perpendicular to incoming radiation (Nilson 1971; Campbell and Norman 1989) and L is the LAI of the forest canopy including all aboveground structural components (branches, boles, cones, and epiphytes). $G(\theta)$ depends greatly on the angular distribution of the foliage, and determines the light interception by the canopy. Several foliage angle distributions (e.g., planophile, spheric or elliptical) are used to simulate real leaf angle (de Witt 1965; Campbell and Norman 1989). Equation 2, can be rearranged:

$$-\ln(P(\theta)) = K(\theta) \cdot L \quad (3)$$

where the extinction coefficient ($K(\theta) = G(\theta)/\cos(\theta)$) gives the average projected area of the canopy components on a horizontal plane. Particular attention must be brought to the practical consideration of using K with commercial instruments. Light extinction is assumed to be linked to geometric-optic properties of the forest canopy and therefore closely linked to the structure.

The geometric-optic properties of forest canopies have been used extensively in the development of vegetation canopy models for the interpretation of satellite images (Goel 1988; Myneni 1989; Li and Strahler 1992). More specifically, K depends on the incidence angle of the incoming radiation, the orientation of leaves and woody parts and the spectral wavelengths used for the measurements. Leaves do not transmit light equally throughout the visible spectrum. Commercially available light sensors operate at various spectral bands; e.g., 380-490 nm for LAI-2000, around 430 nm for DEMON, 400 to 700 nm (photosynthetically active radiation – PAR) for quantum sensors, and 300-3000 nm for pyranometers. The extinction coefficient measured for a range of spectral values ($\Delta\lambda$) can be written as:

$$K_{\Delta\lambda} = K_{\text{black}} (1 - \tau_{\Delta\lambda}), \quad (4)$$

where K_{black} is the extinction coefficient for opaque leaves and $\tau_{\Delta\lambda}$ is the transmission coefficient of leaves in the spectral band used. The effects of radiation scattering within the canopy is not explicitly treated and therefore imbedded in $\tau_{\Delta\lambda}$ with the direct radiation component. Because $K_{\Delta\lambda}$ is spectrally dependent, great care must be taken while comparing results from different instruments. A detailed theoretical treatment of both the projection

and extinction coefficients is available in Nilson (1971), Ross (1981), Campbell (1986), and Campbell and Norman (1989).

Equation 3 can be integrated by zenith angle to find the LAI using a least mean squares method. The probability P centred at θ_j is estimated using the gap fraction from indirect optical measurements. K can be calculated from the theoretical function with dependence on θ_j and the foliage inclination angle (θ_f) (Campbell and Norman 1989). With P and K known, the LAI can be calculated from of a system of linear equations:

$$-\ln P(\theta_j) = \sum_{f=1}^m K(\theta_j, \theta_f) \cdot L_f \quad (5)$$

where j refers to the midpoint zenith angle for each annulus and f is the inclination angle class of the foliage at zenith angle j . The numerical method used to calculate this series of equations is referred to as an inversion to resolve L . Among those using different inversion methods, the least squares approach is mentioned by Menke (1984) and Lang et al. (1985). Alternatively Campbell (1986), Wang and Jarvis (1988), Campbell and Norman (1989), and Norman and Campbell (1989) reported on the use of an ellipsoidal distribution of the foliage normals. The solution to the equation for m leaf angle classes and for $j = 0$ to n zenith angle annuli gives the L_f values. n must be equal to or higher than m to resolve the linear equations system. When $n > m$ the equation system is overdetermined (i.e., there are more equations than unknown variables). At this point, the linear system can be solved under a scalar constraint in order to avoid negative values of L_f resulting from errors on P_j . The total LAI value is the sum of L_f ($\text{LAI} = \sum L_f$). An example of calculation is provided in Norman and Campbell (1989) along with another iterative method for LAI calculation.

3.2 Foliage clumping

Two important corrections must be applied to LAI measurements from indirect optical methods to compensate for the effects of foliage clumping and the light obstruction from canopy components other than foliage. The first limitation is technical, in which gap fractions measured with hemispherical sensors do not differentiate between the obstructions caused by foliage and other canopy components like branches, boles and reproductive components. In addition, in the case of conifer canopies, optical sensors are insensitive to the surface area of individual needles because they lack the power to resolve elements this small. The second limitation is

theoretical; the indirect methods for LAI calculations are most often based on a random distribution of foliage within a specified canopy volume, an assumption that does not hold true in most forest stands (Chen and Cihlar 1995a; Larsen and Kershaw 1996). Smith et al. (1993) suggested that the gap fraction calculations underestimate LAI by about 38 %, whereas Gower and Norman (1991) found LAI underestimation between 35 and 40 % in four conifer stands. Furthermore, Cutini et al. (1998) found an average underestimation of about 26.5 % compared to the LAI from litter collection. Based on a literature review, Gower et al. (1999) suggested a generalised underestimation of LAI by indirect techniques of about 25 to 30 % in most forest canopies. Clumping of canopy elements is considered the primary source of LAI underestimating by inversion of gap fractions.

Foliage clumping occurs mostly at the shoot level for conifer trees, but may also occur at the branch and crown levels for most forest types (Chen and Black 1991). Therefore, the LAI values calculated with Equation 3 are almost always systematically underestimated unless the foliage is randomly distributed within the canopy volume and the contributions from branches, boles and other plant components are negligible. Nilson (1971) was the first to modify the Poisson model (Equation 2) to take into account the non-randomness of canopy elements:

$$P(\theta_j) = \exp [-G(\theta_j) \cdot \Omega \cdot L_t / \cos(\theta_j)]. \quad (6)$$

Ω is the stand-clumping factor. L_t is the total stand LAI, and the product $(\Omega \cdot L_t)$ is the LAI based on the inversion of the Poisson model. It is suggested that the term 'effective LAI' (L_e) be used for values directly calculated from gap fraction information (Oker-Blom et al. 1991; Chen and Black 1991; Chen et al. 1991; Smith et al. 1993; Chen and Cihlar 1995a and b; Chen et al. 1997) while the true stand LAI can be obtained by introducing a general clumping coefficient:

$$L_e = \Omega \cdot L_t \quad (7)$$

where L_t is the total LAI of the plants including all canopy elements and Ω equals 1 when the foliage distribution is random, and decreases towards zero as leaf clumping increases. For a given LAI, clumped canopies allow more light into the understorey than those with random distributions of canopy elements (Smith 1993).

Optical instruments estimate $P(\theta)$, whereas L_e is calculated from the hemispherical distribution of gap fractions obtained from a wide range of

view angles. In the case of conifer stands, the clumping factor can be further separated in two components:

$$\Omega = \Omega_E / \gamma_E \quad (8)$$

where γ_E refers to the clumping at the shoot level which is related to the needle-to-shoot area ratio (after Fassnack et al. 1994; Chen et al. 1997) or the silhouette total needle area ratio (STAR after Stenberg et al. 1994). Ω_E is the stand-level clumping factor for all scales coarser than the shoot (usually called crown-level clumping – referred to as the element clumping factor by Chen 1996; Chen et al. 1997). In the case of deciduous stands, γ_E is assumed to be equal to 1.

3.2.1 Shoot-level clumping

Several methods exist for estimating the shoot clumping parameter. For example, Gower and Norman (1991) determined the shoot clumping the ratio between the total projected area of the needles within the shoot and the silhouette area of the shoot projected vertically. Values of 1.5, 1.6, 1.49 and 1.6 were calculated for *Pinus resinosa*, *Pinus strobus*, *Larix decidua*, and *Picea abies*, respectively. This technique was developed further by Fassnacht et al. (1994) and Chen (1996) to include a greater number of shoot projections. They suggested calculating the shoot-level clumping in conifers using the needle-to-shoot area ratio:

$$\gamma_E = A_n / A_s, \quad (9)$$

where A_n is half of the total needle area for all the needles of a shoot. A_s is half the total integrated area projected by the shoot calculated (Chen 1996):

$$A_s = \frac{1}{\pi} \cdot \int_0^{2\pi} \int_0^{\pi/2} A_p(\theta, \phi) \cdot \cos \theta \, d\theta d\phi, \quad (10)$$

where ϕ and θ are the azimuth and zenith projection angles in relation with the main axis of the shoot. $A_p(\theta, \phi)$ is the projected area for given angles of θ and ϕ .

A_n can be calculated from the volume displacement method (Beets 1977; Chen et al. 1997; Sellers et al. 1994, Appendix K), where the volume displacement of the shoot without needles is subtracted from the total

volume displaced by the shoot with the needles intact. The equation used varies according to the cross-sectional shape of the needle:

$$A_n = \beta (V \cdot n \cdot l)^{1/2} \quad (11)$$

where V is the volume displaced by the needles only (cm^3 or g), n is the total number of submerged needles, and l is the average length of needles (cm). β is a shape dependent factor that takes values of 2.00 for approximately square shaped needles (*Picea abies*), 2.08 for ellipsoid shaped needles (*Pseudotsuga menziesii*), 1.77 for cylindrical shaped needles (*Pinus cembroides* var. *monophylla*), and 2.05 for hemi-cylindrical shaped needles (*Pinus sylvestris*). It can be mathematically proven that the coefficient in each A_n expression is half of the ratio between the needle's perimeter over the square root of its cross-section area.

The geometric measurements of a statistically significant sample of needles are also another alternative to the volume displacement method (Oker-Blom and Smolander 1988; Johnson 1984). Using this method, A_n is measured as the projected area of needles multiplied by a correction factor dependent on the cross-sectional shape of the needles. Projected area can be determined using commercial instruments (LI-COR, Delta-T or CID planimeters or image analysis software; e.g., WinSEEDLE&NEEDLE by Regent Instruments). Great care must be taken to account for the non-cylindrical aspect of the needle shapes as well as the shape variability. The correction factor is relatively easy to evaluate for needles with simple geometric shapes. For example, the correction factor for cylindrical, hemi-cylindrical or flat (deciduous species) leaves equals π , $1 + \pi/2$ and 2, respectively (Soudani and Bréda 2002). However, needles with complex shapes may require multi-directional projections to evaluate the correction factor. A correction factor of approximately 3 is typically used for most conifer species (Oker-Blom and Smolander 1988).

3.2.2 Stand-level clumping

Stand-level clumping (Ω_E) includes clumping within a stand at all scales greater than the shoot, including within-crown clumping (mutual shading of shoots within branches, branches within whorls, whorls within crowns) and between-crown clumping. Most calculation methods of Ω_E rely on the gap-size distributions derived from optical measurements of sunflecks sampled along transects in the understorey or from the pattern of discrete gaps preserved in hemispherical photos (Kucharik et al. 1999). Until recently, the only way of assigning the crown-level clumping factor required the

comparison between semi-direct *in situ* measurements of LAI and the LAI as calculated using a negative binomial model of gap fraction distribution. For example, Chason et al. (1991) suggested calculating the LAI (L) with a clumping factor (g) from:

$$L = -\ln T(\theta) \cdot g / \{\ln [1 + g G(\theta)] / \cos \theta\}. \quad (12)$$

In theory, Lang and Xiang (1986) suggested leaf area indices derived by a spatial logarithmic averaging of sunbeam fractional transmission. Values of contiguous light openings (T) are averaged as $\ln \bar{T}$ where \bar{T} are localised T values linearly averaged over distances equal to 10 times the specific width of the leaves, assuming randomness at this scale. This procedure is known as the finite-length averaging method and it forms the underlying analytical theory on which the DEMON instrument is based (section 4.2.3). The finite-length averaging method has also recently been adapted for the retrieval of LAI and clumping indices from hemispherical photographs (Gardinen et al. 1999; Soudani et al. 2001; Walter 2002). Another way to improve effective LAI estimates is to calculate an average LAI from local azimuthal L_a values (Walter 2002). The 'logarithmic averaging' and azimuthal averaging of local estimates both constitute 'quasi-random' methods (Planchais and Pontailler 1999).

Neumann et al. (1989) developed a unique method based on the spatial autocorrelation of canopy gaps to retrieve clumping factors directly from hemispherical photographs. The clumping factor was computed from a conditional probability of a light ray passing through the canopy in the same opening separated by a distance Δd . However, the choice of Δd had a strong influence on the computed conditional probability and was theoretically difficult to justify.

Another method uses the TRAC (Tracing Radiation and Architecture of Canopies) instrument based on Chen and Cihlar (1995 a and b) algorithm (section 4.2.4.). As clumped canopies are characterised by large gaps intermingled with small gaps, Chen and Cihlar (1995a) formulated the derivation of the clumping factor as:

$$\Omega_E = (1 + \Delta g) \ln [F_m(0)] / \ln [F_{mr}(0)] \quad (13)$$

where F_m represents the observed gap size distribution extracted from the actual aggregated canopy, F_{mr} is the theoretical gap size distribution in the case of a random canopy where large gaps have been iteratively removed, and Δg is the removed gap fractions: $F_m(0) - F_{mr}(0)$. The TRAC algorithm

has also been implemented in hemispherical photography analysis programs (Walter 2002).

A more recent method based on the segregation coefficient and theory developed by Pielou (1962) has been adapted by Walter et al. (2002) to estimate clumping and LAI indices using hemispherical photographs. This method is based on the sequences of white and black pixels on a hemispherical photograph from which a threshold is applied to separate sky and vegetation classes. The probabilities of encountering a black (foliage) pixel or white (gap) pixel along an arc of equal zenith angle are p and q respectively; where $p+q=1$. Let us note that p and q are the maximum likelihood estimates of p and q ; i.e., $p+q = 1/m_B + 1/m_W$, where m_B and m_W are the mean lengths of sequences of black and white pixels measured in numbers of pixels. For a random dispersion, $p+q$ will equal 1, while values less than 1 represent a clumped dispersion, and values greater than 1 indicate a uniform dispersion of gaps. This algorithm has been implemented in the CIMES image analysis software package developed by Walter (2002).

3.2.3 Plant area index

LAI, by definition, represents one-half of the total leaf area per unit ground surface area and therefore does not include non-photosynthetic components of the canopy. However, indirect optical sensors do not discriminate between foliage, branches and boles, and therefore produce gap fractions that include the shading effects produced by all aboveground components of the forest – trunk, branches, cones, seeds and flowers. Thus, the LAI associated to the foliage (L_{tF}) can be calculated using the formula developed by Chen et al. (1997):

$$L_{tF} = (1-\alpha) \cdot L_e / \Omega = (1-\alpha) \cdot L_e \cdot \gamma_E / \Omega_E \quad (14)$$

where α is the ratio between the projected area of the other material (primarily wood – boles and branches) over the total projected area. The woody-to-total area ratio α can be found from destructive sampling (Chen 1997): $\alpha = W / L_t$, where W is the wood obstruction index (*woody area index*) and L_t is the total LAI from the wood and green foliar material combined (as in Equations 6 and 7). The influence of tree boles has been known to be highly variable from one study to another. For instance, Cutini et al. (1998) and Barclay et al. (2000) found that it contributed significantly in their test sites, whereas Fournier et al. (1996) suggested that branches and boles contributed to LAI increases of less than 5 % in three relatively dense stands of conifers in temperate eastern Canada. Using destructive sampling

data Gower et al. (1997) and Chen et al. (1997) estimated values of α of 0.05, 0.32, and around 0.16 for stands of young jack pine, mature jack pine and mature black spruce respectively. Very few indirect methods are available to assess the effect of wood and other non-foliar components of the canopy on LAI. Kucharik et al. (1997) proposed the use of a two band camera. In view of the limited possibilities to evaluate W and also to its variability in impact, the importance of including this factor must be carefully assessed. Because of the constraints, most studies have ignored this variable.

4. ***IN SITU LAI MEASUREMENT***

4.1 **Semi-direct methods**

Table 4-1 summarises the main *in situ* methods used for LAI measurement in forest canopies and suggested references. Measurements using semi-direct methods imply a partial sampling through physical access (Campbell and Norman 1989; Daughtry 1990; Nobel et al. 1993) of canopy elements in order to determine their characteristics. A method could be assumed direct if all the foliage components were measured. Few studies exist using direct measurement (e.g., Hutchison et al. 1986) because of the colossal field resources required in most forest canopies.

The destructive sampling method primarily consists of falling individual trees and measuring their total foliage. In forestry, foliage area is measured within a subset of representative trees, then extrapolated to the whole population by using regression and allometric relationships. These relationships link foliage area to the basal diameter of the branches, the trunk DBH or other canopy characteristics. For example, relationships have been established between foliar mass of conifers and sapwood area. These methods are based on the pipe model theory originally proposed by Shinozaki et al. 1964.

The leaf litter method is practical in broadleaf forests when an adequate spatio-temporal sampling procedure can be implemented. LAI is obtained by weighting foliage on a dry weight basis and by using predetermined species-specific leaf area-to-dry weight ratios. Leaf litter has the disadvantage of not providing information on LAI profiles. Moreover, LAI estimates based on litter-fall in conifer forests are more troublesome, because autumn litter-fall is dependent on needle age and longevity and on the climatic conditions prevailing during the whole life of trees rather than on just the annual production of new needles (Gholz et al. 1991; Chen et al. 1997).

The point-quadrat method (point-contact sampling or inclined point-quadrat) (Campbell and Norman 1989; Norman and Campbell 1989) was first used by Levy and Madden (1933). It makes use of a small probe, which is run through the canopy to determine LAI at the scale of the plant. Probe insertion is done at predetermined zenith and azimuth angles, and path lengths. The number of times that the probe head comes into contact with an element of the canopy is a function of leaf orientation, density and surface area. The difficulty for the operator is to be near the probe in order to record the contacts without disturbing the foliage (Norman and Campbell 1989; Nobel et al. 1993). Also, this technique is impractical in tall, dense forest canopies (Chen et al. 1997). A system to detect the number of contact points was developed by Caldwell et al. (1986). This technique uses a light source and detector mounted on a probe to record the number of contacts (Norman and Campbell 1989). Another disadvantage of the point-quadrat method is that it is labour intensive and therefore time consuming. Indeed, several probe insertions through the foliage are necessary to obtain the most accurate estimates of LAI (Campbell and Norman 1989). The estimation of LAI using the point-quadrat method is based on hypotheses and equations similar to those described in Welles (1990).

Table 4-1. List of suggested *in situ* LAI measurement methods.

Semi-direct <i>in situ</i> measurement methods	
Allometric methods	
References:	Grier and Waring (1974), Marshall and Waring 1986, Gregoire and al. (1995), Whitford et al. (1995), Gower et al. (1997), Gregoire and Valentine (1997), Turner et al. 2000
Principle:	Statistical sampling of canopy components but focused on trunk, branches, leaves for weight and dimensional measurements. Use of statistical models to derive allometric equations based on branch or trunk diameter, or another canopy measurable component.
Litter fall collection	
References:	Neumann et al. (1989), Burton et al. (1991)
Principle:	LAI is obtained by weighting foliage on a dry weight basis and by using predetermined species-specific leaf area-to-dry weight ratios.
Point-quadrat method (point-contact sampling or inclined point-quadrat)	
References:	Levy and Madden (1933), Warren Wilson and Reeve (1960), Warren Wilson (1963, 1965), Anderson (1966), Cadwell et al. (1983), Dufrêne and Bréda (1995)
Principle:	Use of probe insertion at predetermined zenith and azimuth angles, and path lengths to estimate LAI from number of contacts.
Indirect optical <i>in situ</i> measurement methods	
LAI-2000 Plant Canopy Analyzer (from Li-Cor)	
References:	Welles (1990), Welles and Norman (1991), Chason et al. (1991), Stenberg et al. (1994), Chen et al. (1997).
Principle:	Gap fraction is measured on five rings centered at 7°, 23°, 38°, 53° and 68° zenith angles. The effective LAI is extracted from the matrix inversion of the gap fraction values following Campbell and Norman (1989).
Hemispherical photography	
References:	Anderson (1966), Becker et al. 1989, Rich (1990), Mitchell and Whitmore (1993), Chen et al. (1997), Frazer et al. (1997), Wagner (2001), Walter (2002)
Principle:	A photograph is taken under the forest canopy using a camera with a fish-eye lens pointing at zenith. The resulting image is treated to separate gaps from canopy obstruction.
DEMON (from Decagon)	
References:	Lang et al. (1985), Welles (1990)
Principle:	The sensor is pointed at the sun corolla and takes into account the variations in gap fraction with changing solar zenith angle. LAI is derived by a spatial logarithmic averaging of sun's beam fractional transmission.
TRAC (Tracing Radiation and Architecture of Canopies)	
References:	Chen and Cihlar (1995a and b) Chen (1996), Leblanc et al. (2002).
Principle:	Quantum meters facing up record light intensities while sensors are moved at a constant speed. LAI values and clumping factor are calculated from gap-size distributions.
Downwelling irradiance meters (e.g., pyranometers, quantum meters, solarimeters, radiometers)	
References:	Jordan (1969), Pierce and Running (1988), Houssard and Escarre (1981), Lang and Xiang (1986), Welles (1990), Black et al. (1991)
Principle:	Link the reduction of light transmission within the forest canopy with the extinction coefficient of the Beer-Lambert equation.

4.2 Indirect optical methods

Indirect optical methods rely on both passive (i.e., cameras and solar radiation sensors) and active (i.e., laser range-finders and 3-D imaging lasers) optical sensors to measure the canopy gap fraction (Welles and Cohen 1996). Gap fractions can be measured directly using hemispherical photos or indirectly as the proportion of direct or diffuse light penetrating through the canopy. Nevertheless, both approaches are considered to be indirect, since no direct contact with the canopy is required. Indirect optical techniques also require mathematical models to predict LAI and other structural parameters (leaf inclination angles) from the distribution of canopy gaps (this is known as gap-fraction analysis or gap-fraction inversion; Norman and Campbell 1989). For passive methods, the response of the canopy to solar radiation is measured under suitable conditions and the model is then inverted in order to determine the structural parameters of the forest canopy. All the instruments designed for indirect optical measurement of LAI are used from ground level while looking upwards or towards the sun. There are generally three types of indirect optical measurements of LAI: (i) those that measure diffuse light transmission or record canopy gaps within a hemispherical view (e.g., LAI-2000 Plant Canopy Analyzer (PCA) and hemispherical photography), (ii) those that measure the direct solar irradiance (sunflecks) at known solar angles along a finite transect (e.g., DEMON, Quantum Sensor, and TRAC), and (iii) those that measure the vertical distribution of canopy elements (the optical point-quadrat method).

4.2.1 LAI-2000 PCA

The LAI-2000 PCA from LI-COR was developed to estimate effective LAI using measurements of diffuse solar radiation above and below the forest canopy. The method is based on known empirical relationships between the quantity of leaf area and the penetration of diffuse radiation through the canopy. The instrument uses five silicon detectors arranged in 15-degree concentric rings with mid-point zenith angles at 7°, 23°, 38°, 53° and 68°. The LAI-2000 PCA is generally operated in two-sensor mode, with one instrument placed above the canopy or in a clearing as reference and the other used for below-canopy measurements. The LAI-2000 light sensor is composed of a fish-eye lens with an optical filter that only transmits ultraviolet to blue wavelengths (380-490 nm). LAI estimation is based on the following assumptions: (1) the foliage blocks or absorbs all the light in the spectrum of 490 nm and less, (2) the canopy elements are much smaller than the projected surface area of each concentric ring, and (3) the foliage is

distributed randomly with respect to azimuth. One disadvantage of this method is the need for reference data acquisition, which may require the installation of scaffolding for above-canopy access or finding a significant clearing close to the measurement site. The LAI calculation method employed by the LAI-2000 is identical to the gap-fraction inversion method presented above (section 3.1.2.); however, this instrument uses gap-fractions measured within five concentric rings (0 to 75 degrees). The azimuthal field of view (FOV) is often restricted in discontinuous or patchy canopies to avoid the underestimation of LAI, which can occur when the light transmitted through exceedingly large gaps is averaged with the light from smaller gaps (LI-COR LAI-2000 PCA manual 1992). Furthermore, one or two of the outer zenith rings can also be eliminated to avoid any potential enrichment of the diffuse fraction by reflected light. This enrichment generally causes an underestimation of stand LAI (Leblanc and Chen 2001). Eliminating the last one or two rings from the calculations is also a common practice when one needs to avoid any potential slope effects (Walter and Torquebiau 2000).

4.2.2 Hemispherical canopy photography

Hemispherical canopy photography, one of the oldest optical methods, has benefited from recent advances in digital photography, image analysis and data processing. Hemispherical photographs are taken beneath the canopy using a 180-degree FOV fisheye lens and camera oriented towards the sky, and used to record the size, position and distribution of canopy gaps. This technique offers some advantages over other optical methods: (i) the effects of light reflection, transmission and scattering, which are all responsible for increases in gap size, can be controlled by exposure settings, film type and lens filters, and by choosing an appropriate threshold or colour RGB plane to separate sky from foliage on the digitized image, (ii) the spatial information permanently recorded in photos allows for detailed structural analyses or the modelling of direct and diffuse light transmission within all directions of the hemisphere, (iii) hemispherical photography offers a valuable tool for analysing foliage clumping at the canopy level (Neumann et al. 1989; Gardinen et al. 1999; Walter et al. 2002), (iv) photographs are a precious visual aid for the interpretation of canopy structure and parameter estimates, and finally, (v) hemispherical photography provides a valuable alternative when sky conditions for data acquisition are not adequate for other optical techniques.

In hemispherical photography, special attention must be given to the geometric distortion of the lens and the orientation of the camera. It is also

important to carefully select the proper film type (ISO sensitivity, colour/BW) and exposure settings, methods of film digitization and image analysis tools. All of these considerations have been thoroughly discussed elsewhere (see Table 4-1). With the advent, growing popularity and improving performance of digital cameras, film selection, processing and scanning can be avoided using these fully digital technologies - a great simplification. Reasonably priced, consumer-grade digital cameras are currently a practical solution if the analytical procedure does not depend on extremely high-quality images (Frazer et al. 2001). Rapid technological developments are likely to overcome current limitations thus making digital cameras the future tool for hemispherical photography.

4.2.3 DEMON

The DEMON is an instrument that measures direct solar radiation along a transect beneath a forest canopy using a sensor pointed towards the sun. Light is measured through a very narrow FOV centred on the sun's corona to eliminate as much diffuse radiation as possible. Filters are used to limit the radiation within a spectral window around 430 nm, thus minimising the scattering effect within the foliage. The sensor can be held by an operator or assembled on a system of rails. The DEMON measures the gap fraction of the canopy for various solar positions. Measurements must be carried out several times a day under perfectly clear skies to take into account the variations in gap fraction with changing solar zenith angle. The measurements are made on transects that are avoid interference from understorey vegetation, unless the contribution of all aboveground components of the canopy are of interest. Measurements are taken along linear transects, perpendicular to the view-sun vector, with distances of approximately 300 m long or more, depending on the structural heterogeneity of the stand. For each solar position, the gap fractions are calculated using the ratio of direct radiation taken from below and above the canopy.

4.2.4 TRAC

The TRAC (Tracing Radiation and Architecture of Canopies) is an optical instrument developed by Chen and Cihlar (1995a and b) for measuring the LAI of clumped forest canopies. The instrument consists of three quantum sensors connected to an internal datalogger. Total (transmitted plus diffuse) PAR is measured by two upward-facing sensors, both aligned normally to the zenith. One sensor is fitted with a restricted

view cap to eliminate the measurement of direct sunlight. Measurements of direct PAR transmission are used to extract gap-size distributions, while gap fractions are computed from the transmitted diffuse portion. The downward facing sensor measures ground-reflected PAR, allowing calculations of the fraction of incident PAR (F_{PAR}) absorbed by the canopy. A two-sensor operation mode of the TRAC is also possible (one looking up and the second looking down) where the diffuse downwelling PAR portion is extracted as some quantile of the minimum intensities from total PAR measurements (Leblanc pers. comm.). As with the DEMON, measurement transects should be taken on a line perpendicular to the view-sun vector. Chen and Cihlar (1995a) have developed a new theory and technique to obtain a clumping factor (Ω_E) from gap-size distributions measured with the TRAC (section 3.2.2). This method has the advantage of being applicable in all kinds of plant canopies without the need for any assumptions regarding the random distribution of canopy elements. Clumped canopies are characterised by relatively large gaps mixed with small ones. The probability of encountering large gaps for a 'randomly' distributed canopy can be derived from the distribution of gap sizes.

4.2.5 Optical point-quadrat sampling

MacArthur and Horn (1969) developed a field technique and probability theory based on the principals of vertical point-quadrat method (Warren Wilson 1959 and 1965) that is known today as optical-point quadrat sampling. The optical-point quadrat method was originally used to compute the density of foliage within discrete height intervals (layers) of the canopy from measurements of the vertical distances to the first leaf; however, Aber (1979a) modified this technique further to compute estimates of stand LAI and foliage-height profiles. The method requires the use of a reflex type camera equipped with a reticulated, frosted glass which sets up virtual vertical lines. The method has been updated by using a hand-held laser range finder (Radtko and Bolstad 2001). Comparisons of stand LAI derived from optical-point quadrats with LAI estimates determined through direct sampling all show poor correlations; however, these same studies reveal substantial agreement between foliage-height profiles measured directly and using the optical-point quadrat approach (Aber 1979b; Fukushima et al. 1998; Radtko and Bolstad 2001).

4.2.6 LAI from downwelling radiation

Several LAI evaluation methods use the absorption properties of downwelling solar radiation by forest canopies, regardless of the angular direction. For example, Jordan (1969) found in a tropical forest, a linear relationship between the LAI and a factor formed by the ratio of the transmitted visible and near infrared radiation. The applicability of this method was suggested to be valid only for areas where the structure is relatively homogeneous (Norman and Jarvis 1975a and b) as well as for a near infrared to visible ratio calibrated with direct *in situ* measurement of the LAI (Houssard and Escarre 1981).

Optical light sensors such as the AccuPAR Ceptometer and the LI-COR Line Sensor and quantum sensors mounted on tramways can be used for the determining LAI. These PAR sensors can be placed in the forest understorey to record continuous measurements of global light. By assuming a certain foliage angle distribution for the canopy, light transmission at a given angle allows estimates of LAI (Lang and Xiang 1986; Pierce and Running 1988; Welles 1990; Black et al. 1991).

LAI can also be measured with a simple and inexpensive instrument, the LAIL, described in Cournac et al. (2002). This apparatus measures the light transmitted through the canopy by means of a light dependent resistor (LDR), equipped with an off-the-shelf fisheye lens (spy-hole optics) and connected to an ohmmeter that instantaneously measures the resistance output. The method is based on the extinction of light by the canopy, following Beer-Lambert law. The instrument is calibrated for the sun overhead at noon and thus particularly useful in the tropics. It also allows for instantaneous readings and quick assessment of LAI at high spatial resolution over long transects and large grids.

5. FACTORS AFFECTING *IN SITU* LAI MEASUREMENTS

Although *in situ* LAI estimates are more easily obtained by optical instruments compared to semi-direct methods, the user must bear in mind that many factors may come into play while making the measurements. Factors such as sky conditions, topography, foliage clumping, non-photosynthetic materials, and plant phenology all affect LAI estimates. Special attention should be given to the instrument's operational requirements and to the unique characteristics of each sampling location.

5.1 Measurement conditions

Optical instruments, such as the LAI-2000 PCA and TRAC, were designed to operate under two very different sky conditions. For example, the TRAC and the DEMON require full sunshine, because both instruments record direct radiation transmittance through the canopy, as well as the width and intensity of sunflecks along a linear transect. These instruments are also dependent upon solar elevation and require sampling along several transects and at varying solar positions. Conversely, a uniformly diffuse overcast sky or a clear sky at dawn or dusk, provides suitable conditions for hemispherical photographs and LAI-2000 measurements. These conditions prevent bias caused by direct sunlight and light scattering from bark and foliage. With the use of optical filters, the bias created by blue light scattering from foliage is minimised for the LAI-2000 and the DEMON. The fisheye lenses for hemispherical photographs can be used with or without filters (blue, red); however, skylight filters will often improve the colour quality of photos, particularly if they were taken under clear skies.

5.2 Corrections for slope effects

In complex terrain, slope may be an important factor affecting the estimation of LAI (Frazer et al. 1997; Walter and Torquebiau 2000). Slope adjustments are seldom considered, and are complicated by the fact that optical instruments and their supporting inversion algorithms were not designed with non-flat surfaces in mind. Yet, it can easily be demonstrated that slope significantly affects LAI measurements in two ways: (i) on steep slopes a portion of the optical sensor will look directly into the hill slope – the probability of measuring a gap at large zenith angles in the upslope direction is zero, and (ii) inversion algorithms that average gap fractions through all angles of azimuth ignore the angular variation in path length (distance that a light ray must travel through the canopy) that occurs when optical instruments are held normal to the zenith on sloping surfaces. The first problem can be easily corrected by limiting the number of outer annuli used in the gap-fraction inversion; however, the second problem is more troublesome.

On a slope, path length through a canopy may differ significantly for two opposite points of the hemisphere located at a given zenith angle. For example, along the maximum slope, and for the same zenith angle, the path length is longer upslope and shorter downslope. Under a continuous forest canopy of fixed height on a regular slope, the forest canopy seems dense with small gaps when looking upslope, while the forest appears more open,

with larger gaps downslope. Thus, even for an ideal homogeneous canopy, an azimuthal variation of gap distribution can be observed under a given view angle. In irregular, natural forests, the azimuthal heterogeneity of gap distribution is maximised and the apparent variation in foliage density is exacerbated. In all cases, gap fractions should be adjusted for variable path lengths to all directions of the hemisphere when data are on a site with significant slope. This is not possible for instruments that produce azimuthal averages (e.g., LAI-2000) unless the view is restricted. Therefore, some researchers use a 270-degree view restrictor for measurements parallel to contours to minimise slope effects. Fortunately, spatially explicit imaging methods like hemispherical photographs provide the ability to apply more precise corrective methods. Calculations on the effects of slope on LAI estimation can be found in Frazer et al. (1997), Walter and Torquebiau (2000), and Walter (2002).

5.3 Foliage clumping

The inability to precisely measure foliage clumping is a strong limitation for LAI calculations. Several optical instruments, such as the DEMON and the TRAC and their related analytical methods, were designed to address this problem in order to evaluate Ω_E . However, they both depend on continuous measurement of direct solar irradiance taken at relatively high solar elevation angles while walking with the instrument at a fixed displacement speed. Instrument levelling and movement at a constant speed are difficult to assume in most operational environments.

Alternative techniques to measure Ω_E from gap-size distributions have recently been developed for use in hemispherical canopy photography (Walter et al. 2002). These new methods take advantage of the fine-scale canopy architecture preserved in fisheye photos, and are used to simulate light transmission measurements taken along a curvilinear transect within the hemispherical view of the canopy. Assuming that sufficient spatial resolution is available, neighbouring pixels can be sampled along annuli (from 0 to 360 degrees in azimuth) for any number of fixed zenith angles. The resulting pixel intensity data can be extracted at optimised angles of azimuth and zenith to maintain the requirements for spatial independence and equal distances between sampling points, and are therefore compatible with the current methods for calculating foliage clumping (section 3.2.2.). Since the estimation of crown clumping is such a critical parameter for the calculation of the real LAI, it is expected that further improvement over existing methods will be an active field of research.

5.4 Non-photosynthetic material

The non-photosynthetic component of forest canopies consists mainly of the woody structures, such as branches and boles, both of which support foliage, as well as mosses and vascular epiphytes in temperate and tropical rain forests. Woody surfaces within the forest canopy may intercept varying amounts of solar radiation, depending on their size and density. The amount of canopy shading contributed by branches and boles can be assessed directly, using destructive sampling, or indirectly, using either allometric methods, radiation sensors or hemispherical photos.

Optical methods can be used in defoliated forest stands that have succumbed to disease, insect herbivory or crown fires, and also during leafless periods (after leaf drop) in deciduous broad-leaved forests. Differences in LAI between leaf out and leaf drop are used to infer the contribution of the woody fraction to stand-LAI estimates. Measurements of the woody fraction of canopies have been made, but often without being validated using an alternative method. Generally speaking, the woody fraction within young dense stands and in stands with an open canopy structure could have a significant influence on optical estimates of LAI. In contrast, wood structure has often a limited effect on mature, closed canopies with LAI distributed evenly in the horizontal plane and in a compact vertical upper layer (section 3.2.3.). The relative importance of a clumping factor or non-photosynthetic material is widely variable from one stand to another. It is considered generally that the most important factors are respectively shoot-level clumping, stand-level clumping and non-photosynthetic material. Clumping factors lead to LAI underestimation while wood structures tend to overestimate LAI. Therefore, there are occasions when the last two factors compensate each other to a certain degree.

6. OPERATIONAL STRATEGIES FOR MEASURING FOREST CANOPY STRUCTURE

Developing a strategy to measure forest canopy structure may appear complex, given the wide choice of numerous, commercially available optical instruments. Also, each optical technique and associated sampling strategy has its own unique set of advantages and disadvantages, which complicates the decision process even further. Nevertheless, several comparison studies exist that may help guide the selection process. The following sections discuss some of the more relevant findings from these comparison studies.

6.1 Comparison studies of measurement techniques

Many recent published studies have compared the results from direct, semi-direct and indirect measurements of forest canopy structure (e.g., Kussner and Mosandl 2000; Soudani et al. 2001). These studies demonstrate the practical application and limitations of many of these techniques under a variety of stand conditions. The LAI-2000 was a significant focus of interest in many of the earlier studies (Chason et al. 1991; Chen et al. 1991; Gower and Norman 1991; Deblonde et al. 1994; Fassnacht et al. 1994; Stenberg et al. 1994); however, more recent comparative studies have looked at the utility of digital fisheye photography (Gardingen et al. 1999; Englund et al. 2000; Frazer et al. 2001).

Nevertheless, one should keep in mind the inherent particularities of each method in order not to bias comparisons (section 5). The comparison of optical methods provides important information on practical aspects of sampling, data acquisition and analysis (Deblonde et al. 1994, Martens et al. 1993, Marshall and Waring 1986, Whitford et al. 1995). However, the recent emphasis on foliage clumping and its importance, in most situations, reduces the usefulness of studies that have not directly addressed this factor. One strategy to assess the clumping factor was adopted by Stenberg et al. (1994) where the Ω_e was estimated from the differences of LAI values between a semi-direct method and those calculated from LAI-2000 data (including shoot clumping).

A common strategy for validating real LAI involves the use of a semi-direct measurement method along with an indirect method (Neumann et al. 1989; Fassnacht et al. 1994; Dufrêne and Bréda 1995; Chen et al. 1997; Gower et al. 1999). Unfortunately, the use of semi-direct methods for LAI estimation is often challenging and therefore not always possible. Tropical rain forests are examples of challenging environments (Chason et al. 1991). Thus when available, comparison studies on LAI using optical methods are most useful if they include at least one semi-direct method, as well as evaluating foliage clumping factors, and if possible, the woody area index. Such comparison studies can provide a pool of solutions relevant to LAI measurement problems.

6.2 Forest inventory data

Forest inventories provide relevant information about the composition, structure and productivity of forest stands (Avery and Burkhart 2002). Forest inventory data typically exist in two forms: (i) as descriptive or quantitative attribute data collected from ground surveys (e.g., tree heights, densities,

volumes, species, crown class, etc.), or (ii) as forest cover maps interpreted directly from aerial photographs. Geographic information systems (GIS) are used to link these two forms of data and are invaluable for the management and analysis of forest canopy structure and other ancillary environmental data when land-management areas are large. Other environmental GIS data showing the spatial distribution of streams, lakes and wetlands; slope, aspect and elevation; soils and geomorphology; and other ecologically relevant variables may facilitate identification of unique ecological units and also the potential to spatially extend *in situ* measurements of forest canopy structure.

Structural measurements taken from indirect optical methods are usually limited in spatial extent and in scope. If results from indirect measurements are combined with forest inventory data sets and synthesis maps, a spatial generalisation of the results can be achieved. It is conceivable, for example, to confine the LAI values within known windows of potential values associated with inventory strata. The spatial distribution of species can be taken from the available stand maps or from remote sensing images. Changes in time of the stand structural factors can further be modelled using both the inventory data and the mapped data sets of dependent variables. In turn, LAI is often an input parameter for process-based models at the level of the forest stand, the region and the globe. Consequently, LAI estimates extended in both time and space are required for ecological modelling. Moreover, the upscaling of individual plot measurements and product validation are two serious issues currently facing national and global space-borne monitoring programs (e.g., Justice et al. 1998; Wood et al. 2002). The availability of both inventory and dependent map data sets is critical for the spatial generalisation of a structural parameter and results validation.

6.3 Scale-dependent strategies

A description of forest canopy structure is particularly dependent on temporal and spatial scales. LAI measurements are closely linked with process modelling, and in turn, ecological processes are scale-dependent. Temporal variations relate to stand dynamics, natural and man-made disturbances, and climate change. LAI is not a fixed parameter with time; it varies during the growing season and from year to year in both deciduous and evergreen forests. Seasonal variation in needle dynamics has scarcely been studied in detail, especially as it relates to LAI (e.g., Gholz et al. 1991). In addition to seasonal effects, important differences in specific leaf area and mass have also been measured within and among species; with height in the canopy; and from one year to another. Strategies for measuring temporal dynamics in LAI at different spatio-temporal scales include the

chronosequence approach for stand dynamics (e.g., Bradshaw and Spies 1992; Cohen and Spies 1992; Frazer et al. 2000) or change detection using satellite imagery (e.g., Spies et al. 1994). However, changes in time are inextricably bound with changes in space.

The primary forest entity for spatial scale from fine to coarse gradually shifts from leaf, tree, stand, landscape, ecotone, and biome. Therefore in practice, the strategy for *in situ* data collection of LAI changes with three scales: ground plot, stand, and regional/national. Spatial generalisation of LAI estimation methods usually requires the plot-level data sets either for method development or for validation. Inventory procedures rarely include optical LAI measurement methods. Unless the requirements for LAI measurements in standard inventory change, plot-level values of LAI are primarily available from either allometric methods applied on existing plots, or from special plot data sets of *in situ* optical measurements. Estimates of forest canopy structure at the stand-level represent the first level of generalisation from plot-level data. Stand types and their descriptive structural parameters are stratified into categorical classes for the purpose of deriving stand maps from aerial photographs. The spatial sampling of each stratum from ground plots is based on statistics. A possible strategy to link plot- and stand-level measurements and their related LAI values, involves calculating representative values from inventory data sets for each stratum. Alternatively, a common strategy used with above-canopy remote sensing sensors involves linking LAI values with spectral values or indices. At the stand-level, a spatial generalisation can therefore be developed from two sets of strategies including stratified inventory data sets or spectral relationships.

Regional-level reporting is similar to stand-level reporting in many respects with the exception that it deals with a coarser spatial grid. The selection of representative point values may be taken first from the plot-level to the stand-level, and after to a coarser grid-level. The validation of a coarse grid map with ground plots requires two main constraints: the verification of geometric correspondence, and finding ground plots in quantity and quality that are representative of the spatial extent of the coarse grid. These constraints make the link between the plot-level and the regional-level difficult to achieve. Fortunately, a coarser resolution is usually associated with attribute stratification broader than at the stand-level. Generalising the plot-level values of forest canopy structures to a coarser level for mapping purposes is an important application of *in situ* measurements. Even though this task poses many difficulties, defining strategies for generalising plot-level measurements is a natural continuation of the issues related to *in situ* LAI measurement.

7. CONCLUSIONS

Several conclusions can be drawn from this review. From the theoretical perspective it is suggested that the main forest canopy structure parameters measured from *in situ* optical remote sensing instruments are the LAI, the foliage clumping and the amount of non-photosynthetic material. Optical methods rely on the angular distribution of gap fractions in forest canopies to calculate their structure. Most mathematical techniques to evaluate LAI assume random foliage distribution filled by foliage only. Clearly, this assumption does not hold for most forest canopies. Consequently, the evaluation of foliage clumping and the contribution of non-photosynthetic material must also be done in order to readjust the LAI estimations. Development of methods for both aspects will be an active field of research to address this weakness in current methods.

From an instrumental perspective, no one optical measurement method dominates other methods. The use of LAI-2000 is widespread but other methods like hemispherical photography, DEMON, or TRAC provide more information on the spatial distribution of gaps. When possible, it is recommended to use optical *in situ* methods in combination with semi-direct methods for unbiased validation. Technological advances have resulted in improved sensors, more adapted mathematical evaluation techniques, and better links between measurements at all scales. For instance, 3-D imaging lasers for estimating the distribution of gap fractions are becoming more available. Alternatively, the increased availability of digital cameras combined with advances in desktop computer technology favour the use of hemispherical photographs. Specialised software to analyse hemispherical photographs is now widely accessible and affordable. Even with these improvements, selecting a method remains a difficult choice, as project planners must achieve a delicate balance between suitable measurement methods, accuracy requirements, ecological complexity, sampling strategy, and available resources.

Lastly, from a global monitoring perspective, LAI is the structural parameter that is best suited for multi-scale analysis as an important input parameter for ecological modelling. It can be measured using a wide array of remote sensing methods. Therefore, most satellite earth observation programs have adopted LAI mapping to facilitate ecological modelling. While such measurements are yet to become included in standard inventory procedures, it is foreseeable that new resource management approaches will improve the integration between ecological modelling and forest inventories. More specifically, the importance of bioindicators for sustainable development is pressuring managers to look for better measurements and

prediction tools such as process-based models. These indicators will also include climatic, soil and other variables. The plot-level measurement of forest canopy structure is the primary level from which we can generalise the information. The problem of linking plot-level data with information retrieved at a coarser scales is also a very active research subject in remote sensing and database management. Further use of *in situ* optical measurements in forest canopies relies greatly on the ability to apply data points to other management scales. Thus the spatial generalisation of point-data from ground plots to mapped estimates is a key issue for the remote sensing of forest canopy structure.

ACKNOWLEDGEMENTS

The authors wish to show their appreciation to the members of the ECOLEAP research group of the Canadian Forest Service for supporting the review of remote sensing methods to measure forest structure. Financial support for the international exchanges was provided by the French Embassy in Canada through the France-Canada Scientific Collaboration Programme. Lastly, we are greatly indebted to Gordon Fraser for reviewing our initial manuscript and providing many judicious suggestions.

REFERENCES

- Aber, J., Neilson, R. P., McNulty, S., Lenihan, J.M., Bachelet, D., & Drapek, R. J. (2001). Forest processes and global environmental change: predicting the effects of individual and multiple stressors. *BioScience*, 51, 735-751.
- Aber, J. D. (1979b). Foliage-height profiles and succession in northern hardwood forests, *Ecology*, 60, 18-23.
- Aber, J. D. (1979a). A method for estimating foliage-height profiles in broad leaved forests. *Journal of Ecology*, 67, 35-40.
- Aldred, A. H., & Alemdag, I. S. (1988). Guidelines for forest biomass inventory. *Information Report PI-X-77*. Canadian Forest Service, Petawawa National Forestry Institute. Chalk River, ON,
- Anderson, M. C. (1966). Stand structure and light penetration. II. A theoretical analysis. *Journal of Applied Ecology*, 3, 41-54.
- Avery, T. E., & Burkhardt, H. E. (2002). *Forest Measurements* (5th ed.). McGraw-Hill, New York.
- Barclay, H. J. (1998). Conversion of total leaf area to projected leaf area in lodgepole pine and Douglas-fir. *Tree Physiology*, 18, 185-193.

- Barclay, H. J., Trofymow, J. A., & Leach, R. I. (2000). Assessing bias from boles in calculating leaf area index in immature Douglas-fir with the LI-COR canopy analyzer. *Agricultural and Forest Meteorology*, 100, 255-260.
- Becker, P., Erhart, D. W., & Smith, A. P. (1989). Analysis of forest light environments. I. Computerized estimation of solar radiation from hemispherical canopy photographs. *Agricultural and Forest Meteorology*, 44, 3-4.
- Beets, P. (1977). Determination of the fascicle surface area for *Pinus radiata*. *New-Zealand Journal of Forest Science*, 7, 397-407.
- Black, T. A., Chen, J. M., Lee, X., & Sagar, R. M. (1991). Characteristics of shortwave and longwave irradiances under a Douglas-fir forest stand. *Canadian Journal of Forest Research*, 21, 1020-1028.
- Bradshaw, G. A., & Spies, T. A. (1992). Characterizing canopy gap structure using wavelet analysis. *Journal of Ecology*, 80, 255-260.
- Burton, A. J., Pregitzer, K. S., & Reed, D. D. (1991). Leaf area and foliar biomass relationships in northern hardwood forests located along an 800 km acid deposition gradient. *Forest Science*, 37, 1041-1059.
- Caldwell, M. M., Meister, H. P., Tenhunen, J. D., & Lange, O. L. (1986). Canopy structure, light microclimate and leaf gas exchange of *Quercus coccifera* L. in a Portuguese macchia: measurements in different canopy layers and simulations with a canopy model. *Trees*, 1, 25-41.
- Campbell, G. S. (1986). Extinction coefficients for radiation in plant canopies calculated using an ellipsoidal inclination angle distribution. *Agricultural and Forest Meteorology*, 36, 317-321.
- Campbell, G. S., & Norman, J. M. (1989). The description and measurement of plant canopy structure. Russell G., Marshall, B., & Jarvis, P.G. (Eds.). *Plant canopies: their growth, form, and function*. Cambridge University Press, Cambridge, pp. 1-19.
- Castro, F. de. (2000). Light spectral composition in a tropical forest: measurements and model. *Tree Physiology*, 20, 49-56.
- Chason, J. W., Baldocchi, D. D., & Huston, M. (1991). A comparison of direct and indirect methods for estimating forest canopy leaf area. *Agricultural and Forest Meteorology*, 57, 107-128.
- Chen, J., Saunders, S. C., Crow, T. R., Naiman, R. J., Brososke, K. D., Mroz, G. D., Brookshire, B. L., & Franklin, J. F. (1999). Microclimate in forest ecosystem and landscape ecology. *BioScience*, 49, 288-297.
- Chen, J. M. (1996). Optically-based methods for measuring seasonal variation of leaf area index in boreal conifer stands. *Agricultural and Forest Meteorology*, 80, 135-163.
- Chen, J. M., Rich, P. M., Gower, S. T., Norman, J. M., & Plummer, S. (1997). Leaf area index of boreal forests: theory, techniques, and measurements. *Journal of Geophysical Research*, 104, 29,429-29,443.
- Chen, J. M., & Cihlar, J. (1995a). Plant canopy gap size analysis theory for improving optical measurements of leaf area index. *Applied Optics*, 34, 6211-6222.
- Chen, J. M., & Cihlar, J. (1995b). Quantifying the effect of canopy architecture on optical measurements of leaf area index using two gap size analysis methods. *IEEE Transactions in Geoscience and Remote Sensing*, 33, 777-787.
- Chen, J. M., & Black, T. A. (1992). Foliage area and architecture of plant canopies from sunfleck size distributions. *Agricultural and Forest Meteorology*, 60, 249-266.
- Chen, J. M., & Black, T. A. (1991). Measuring leaf area index of plant canopies with branch architecture. *Agricultural and Forest Meteorology*, 57, 1-12.

- Chen, J. M., Black, T. A., & Adams, R. S. (1991). Evaluation of hemispherical photography for determining plant area index and geometry of a forest stand. *Agricultural and Forest Meteorology*, 56, 129-143.
- Cohen, W. B., & Spies, T. A. (1992). Estimating structural attributes of Douglas-fir/western hemlock forest stands from, Landsat and SPOT imagery. *Remote Sensing of Environment*, 41, 1-17.
- Cournac, L., Dubois, M. A., Chave, J., & Riéra, B. (2002). Fast determination of light availability and leaf area index in tropical forests. *Journal of Tropical Ecology*, 18, 295-302.
- Cutini, A., Matteucci, G., & Scarascia Mugnozza, G. (1998). Estimation of leaf area index with the Li-Cor LAI 2000 in deciduous forests. *Forest Ecology and Management*, 105, 55-65.
- Danson, F. M. (2000). Temperate resources assessment by remote sensing. Meyers, R. A. (Ed.). *Encyclopedia of Analytical Chemistry*, 8814-8827.
- Daughtry, C. S. T. (1990). Direct measurement of canopy structure. *Remote Sensing Reviews*, 5, 45-60.
- Deblonde, G., Penner, M., & Royer, A. (1994). Measuring leaf area index with the Li-Cor LAI-2000 in pine stands. *Ecology*, 75, 1507-1511.
- Dufrêne, E., & Bréda N. (1995). Estimation of deciduous forest leaf area index using direct and indirect methods. *Oecologia*, 104, 156-162.
- Englund, S. R., O'Brien, J. J., & Clark, D. B. (2000). Evaluation of digital and film hemispherical photography and spherical densiometry for measuring forest light environments. *Canadian Journal of Forest Research*, 30, 1999-2005.
- Enquist, B. J., & Niklas, K. J. (2001). Invariant scaling relations across tree-dominated communities. *Nature*, 410, 655-660.
- Fassnacht, K., Gower, S. T., Norman, J. M., & McMurtrie, R. E. (1994). A comparison of optical and direct methods for estimating foliage surface area index in forests. *Agricultural and Forest Meteorology*, 71, 183-207.
- Fournier, R. A., Guindon, L., Bernier, P.Y., Ung, C.-H., & Raulier, F. (2000). Spatial implementation of models in forestry. *Forestry Chronicle*, 76, 929-940.
- Fournier, R. A., Landry, R., August, N. M., Fedosejevs, G., & Gauthier, R. P. (1996). Modelling light obstruction in three conifer forests using hemispherical photography and fine tree architecture. *Agriculture and Forest Meteorology*, 82, 47-72.
- Franklin, S. E. (2001). *Remote sensing for sustainable forest management*. Lewis Publishers, Boca Raton, Fla.
- Frazer, G. W., Fournier, R. A., Hall, R. J., & Trofymow, J. A. (2001). A comparison of digital and film fisheye photography for analysis of forest canopy structure and gap-light transmission. *Agriculture and Forest Meteorology*, 109, 249-255.
- Frazer, G. W., Trofymow, J. A., & Lertzman, K. P. (2000). Canopy openness and leaf area in chronosequences of coastal temperate rainforests. *Canadian Journal of Forest Research*, 30, 239-256.
- Frazer, G. W., Trofymow, J. A., & Lertzman, K. P. (1997). A method for estimating canopy openness, effective leaf area index, and photosynthetically active photon flux density using hemispherical photography and computerized image analysis techniques. *Information Report BC-X-373*, Pacific Forestry Centre, Victoria, BC.
- Fukushima, Y., Hiura, T., & Tanabe, S. (1998). Accuracy of the MacArthur-Horn method for estimating a foliage profile. *Agricultural and Forest Meteorology*, 92, 203-210.

- Gardinen, P. R. van, Jackson, G. E., Hernandez-Daumas, S., Russell, G., & Sharp, L. (1999). Leaf area index estimates obtained for clumped canopies using hemispherical photography. *Agricultural and Forest Meteorology*, 94, 243-257.
- Gholz, H. L., Vogel, S. A., Cropper, W. P., McKlevey, K., Ewel, K. C., Teskey, R. O., & Curran, P. J. (1991). Dynamics of canopy structure and light interception in *Pinus elliottii* stands of north Florida. *Ecological Monographs*, 61, 33-51.
- Goel, N. S. (1988). Models of vegetation canopy reflectance and their use in estimation of biophysical parameters from reflectance data. *Remote Sensing Reviews*, 4, 1-212.
- Gower, S. T., & Norman, J. M. (1991). Rapid estimation of leaf area index in conifer and broad-leaf plantations. *Ecology*, 72, 1896-1900.
- Gower, S. T., Kucharik, C. J., & Norman, J. M. (1999). Direct and indirect estimation of leaf area index, fAPAR, and net primary production of terrestrial ecosystems. *Remote Sensing and Environment*, 70, 29-51.
- Gower, S. T., Vogel, J. G., Stow, T. K., Norman, J. M., Steele, S. J., & Kucharik, C. J. (1997). Carbon distribution and aboveground net primary production in aspen, jack pine, and larch spruce stands in Saskatchewan and Manitoba Canada. *Journal of Geophysical Research*, 104, 29429-29442.
- Gregoire, T. G., & Valentine, H. T. (1996). Sampling methods to estimate stem length and surface area of tropical tree species. *Forest Ecology and Management*, 83, 229-235.
- Gregoire, T. G., Valentine H. T., & Furnival, G. M. (1995). Sampling methods to estimate foliage and other characteristics of individual trees. *Ecology*, 76, 1181-1194.
- Grier, C. C., & Waring, R. H. (1974). Conifer foliage mass related to sapwood area. *Forest Science*, 20, 205-206.
- Gustafson, E. J. (1998). Quantifying landscape spatial pattern: what is the state of the art? *Ecosystems*, 1, 143-156.
- Holmgren, P., & Thuresson, T. (1998). Satellite remote sensing for forestry planning – A review. *Scandinavian Journal of Forest Research*, 13, 90-110.
- Houssard, C., & Escarre, J. (1981). Mesures de la quantité relative de feuillage par strates dans des taillis de chêne pubescent. *Annales des Sciences Forestières*, 38, 449-468.
- Howard, J. A. (1992). *Remote sensing of forest resources: Theory and application*. Chapman and Hall, London.
- Hutchison, B. A., Matt, D.R., McMillen, R. T., Gross, L. J., Tajchman, S. J., & Norman, J.M. 1986. The architecture of a deciduous forest canopy in Eastern Tennessee, USA. *Journal of Ecology*, 74, 635-646.
- Hyypä, J., Hyypä, H., Inkinen, M., Engdahl, M., Linko, S., Zhu, Y-H. (2000). Accuracy comparison of various remote sensing data sources in the retrieval of forest stand attributes. *Forest Ecology and Management*, 128, 109-120.
- Johnson, J. D. (1984). A rapid technique for estimating total surface area of pine needles. *Forest Science*, 30, 913-921.
- Jordan, C. J. (1969). Derivation of leaf area index from quality of light on the forest floor. *Ecology*, 50, 663-666.
- Justice, C., Vermote, E., Townshend, J. R. G., Defries, R., Roy, D. P., Hall, D. K., Salomonson, V. V., Privette, J., Riggs, G., Strahler, A., Lucht, W., Myneni, R., Knjazihhin, Y., Running, S., Nemani, R., Wan, Z., Huete, A., van Leeuwen, W., Wolfe, R., Giglio, L., Muller, J-P., Lewis, P., & Barnsley, M. (1998). The Moderate Resolution Imaging Spectroradiometer (MODIS): Land remote sensing for global change research. *IEEE Transactions on Geoscience and Remote Sensing*, 36, 1228-1249.

- Kucharik, J. C., Norman, J. M., & Gower, S. T. (1999). Characterization of radiation regimes in non-random forest canopies: theory, measurements, and a simplified modeling approach. *Tree physiology*, 19, 695-706.
- Kucharik, C. J., Norman, J. M., & Gower, S. T. (1998). Measurements of branch area and adjusting leaf area index indirect measurements. *Agricultural and Forest Meteorology*, 91, 69-88.
- Kucharik, C. J., Norman, J. M., Murdock, L. M., & Gower S. T. (1997). Characterizing canopy non-randomness with a multiband vegetation imager (MVI). *Journal of Geophysical Research*, 102, 29455-29474.
- Kussner, R., & Mosandl, R. (2000). Comparison of direct and indirect estimation of leaf area index in mature Norway spruce stands of eastern Germany. *Canadian Journal of Forest Research*, 30, 440-447.
- Landsberg, J. J., & Waring, R. H. (1997). A generalised model of forest productivity using simplified concepts of radiation-use efficiency, carbon balance and partitioning. *Forest Ecology and Management*, 95, 209-228.
- Lang, A. R. G., Xiang, X., & Norman, J. M. (1985). Crop structure and the penetration of direct sunlight. *Agricultural and Forest Meteorology*, 35, 83-101.
- Lang, A. R. G., McMurtrie, R. E., Benson, M. L. (1991). Validity of surface area indices of *Pinus radiata* estimated from transmittance of sun's beam. *Agricultural and Forest Meteorology*, 57, 157-170.
- Lang, A. R. G. and Xiang, Y. (1986). Estimation of leaf area index from transmission of direct sunlight in discontinuous canopies. *Agricultural and Forest Meteorology*, 37, 229-243.
- Larsen, D. R. and Kershaw, J. A. J. (1996). Influence of canopy structure assumptions on predictions from Beer's law. A comparison of deterministic and stochastic simulations. *Agricultural and Forest Meteorology*, 81, 61-77.
- Leblanc, S.G., Chen, J.M., & Kwong, M. (2002). Tracing radiation and architecture of canopies. *TRAC Manual Version 2.1*. Natural Resources Canada, Canada Centre for Remote Sensing, Ottawa, Ont.
- Leblanc, S. G., & Chen, J.M. (2001). A practical scheme for correcting multiple scattering effects on optical LAI measurements. *Canadian Journal of Forest Research*, 110, 125-139.
- Legendre, P., & Fortin, M. -J. (1989). Spatial pattern and ecological analysis. *Vegetatio*, 80, 107-138.
- Lefsky, M. A., Cohen, W. B., Parker, G. G., & Harding, D. J. (2002). Lidar remote sensing for ecosystem studies. *BioScience* 52, 19-30.
- Lefsky, M. A., Cohen, W. B., & Spies, T. A. (2001). An evaluation of alternate remote sensing products for forest inventory, monitoring, and mapping of Douglas-fir forests in western Oregon. *Canadian Journal of Forest Research*, 31, 78-87.
- Levy, E. B., & Madden, E. A. (1933). The point method of pasture analysis. *New Zealand Journal of Agriculture*, 46, 267-279.
- Li, H., & Reynolds, J. F. (1995). On definition and quantification of heterogeneity. *Oikos*, 73, 280-284.
- Li, X., & Strahler, A. H. (1992). Geometric-optical bi-directional reflectance modeling of the discrete crown vegetation canopy: effect of crown shape and mutual shadowing. *IEEE Transactions in Geoscience and Remote Sensing*, 30, 276-292.
- Lucas, N. S., & Curran, P. J. (1999). Forest ecosystem simulation modelling: the role of remote sensing. *Progress in Physical Geography*, 23, 391-423.

- MacArthur, R. H., & Horn, H. S. (1969). Foliage profile by vertical measurements. *Ecology*, 50, 802-804.
- Machado, J. L., & Reich, P. B. (1999). Evaluation of several measures of canopy openness as predictors of photosynthetic photon flux density in deeply shaded conifer-dominated forest understorey. *Canadian Journal of Forest Research*, 29, 1438-1444.
- Marshall, J. D., & Waring, R. H. (1986). Comparison of methods of estimating leaf-area index in old-growth Douglas-fir. *Ecology*, 67, 975-979.
- Martens, S. N., Ustin, S. L., & Rousseau, R. A. (1993). Estimation of tree canopy leaf area index by gap fraction analysis. *Forest Ecology and Management*, 61, 91-108.
- McMurtrie, R. E., & Landsberg, J. J. (1992). Using a simulation model to evaluate the effects of water and nutrients on the growth and carbon partitioning of *Pinus radiata*. *Forest Ecology and Management*, 52, 243-260.
- Menke, W. (1984). *Geophysical Data Analysis: Discrete Inverse Theory*. Academic Press, New York.
- Mitchell, P. L., & Whitmore, T. C. (1993). Hemispherical photographs in forest ecology. *OFI Occasional Papers N° 44*. Oxford Forestry Institute, Department of Plant Sciences, University of Oxford.
- Myineni, R. B., Ross, J., & Asrar, G. (1989). A review on the theory of photon transport in leaf canopies, *Agricultural and Forest Meteorology*, 45, 1-153.
- Neumann, H. H., den Hartog, G., & Shaw, R. H. (1989). Leaf area measurements based on hemispheric photographs and leaf-litter collection in a deciduous forest during autumn leaf-fall. *Agricultural and Forest Meteorology*, 45, 325-345.
- Nilson, T. (1971). A theoretical analysis of the frequency of gaps in plant stands. *Agricultural Meteorology*, 8, 25-38.
- Nobel, P. S., Forseth, I. N., & Long, S. P. (1993). Canopy structure and light interception. Hall, D. O., Scurlock, J. M. O., Bolhär-Nordenkampf, H. R., Leegood, R. C., & Long, S. P. (Eds.), *Photosynthesis and production in a changing environment: a field and laboratory manual*, 79-90. Chapman & Hall, London.
- Norman, J. M., & Campbell, G. S. (1989). *Canopy structure*. Pearcy, R. W., Ehleringer, J., Mooney, H. A., & Rundel, P. W. (Eds.). *Plant physiological ecology - field methods and instrumentation*, 301-325. Chapman and Hall, London.
- Norman, J. M., & Jarvis, P. G. (1975a) Photosynthesis in Sitka spruce (*Picea sitchensis* [Bong.] Carr.). III. Measurements of canopy structure and interception of radiation. *Journal of Applied Ecology*, 12, 839-878.
- Norman, J. M., & Jarvis, P. G. (1975b). Photosynthesis in Sitka spruce (*Picea sitchensis* [Bong.] Carr.). V. Radiation penetration theory and a test case. *Journal of Applied Ecology*, 12, 839-877.
- Oker-Blom, P., Lappi, J., Smolander, H. (1991). Radiation regime and photosynthesis of coniferous stands. In Myineni R. B., & Ross J. (Eds.). *Photon-vegetation interactions*, 469-496. Springer-Verlag, Berlin.
- Oker-Blom, P., & Smolander, H. (1988). The ratio of shoot silhouette area to total needle area in scots pine. *Forest Science*, 34, 894-906.
- Oliver, C. D., & Larson, B. C. (1996). *Forest stand dynamics*. John Wiley & Sons, Inc. New York.
- O'Neill, R. V., DeAngelis, D. L., Waide, J. B., & Allen, T. F. H. (1986). *A hierarchical concept of ecosystems*. Princeton University Press, Princeton, New Jersey, USA.
- Parker, G. G. (1995). Structure and microclimate of forest canopies. Lowman, M. D., & Nadkarni, N. M. (Eds.). *Forest canopies*, 73-98. Academic Press, Orlando, Fla.

- Pearcy, R. W. (1989). Radiation and light measurements. Pearcy R. W., Ehleringer J., Mooney H. A., & Rundel P. W. (Eds.), *Plant physiological ecology - field methods and instrumentation*, 95-116. Chapman and Hall, London.
- Pielou, E. C. (1962). Runs of one species with respect to another in transects through plant populations. *Biometrics*, 18, 579-593.
- Pierce, L. L., & Running S. W. (1988). Rapid estimation of coniferous forest leaf area index using a portable integrating radiometer. *Ecology*, 69, 1762-1767.
- Planchais, I., & Pontailler, J.-Y. (1999). Validity of leaf areas and angles estimated in a beech forest from analysis of gap frequencies, using hemispherical photographs and a plant canopy analyzer. *Annals of Forest Sciences*, 56, 1-10.
- Radtke, P. J., & Bolstad, P. V. (2001). Laser point-quadrat sampling for estimating foliage-height profiles in broad-leaved forests. *Canadian Journal of Forest Research*, 31, 410-418.
- Rich, P. M., Clark, D. B., Clak, D. A., & Oberbauer, S. F. (1993). Long-term study of solar radiation regimes in a tropical wet forest using quantum sensors and hemispherical photography. *Agricultural and Forest Meteorology*, 65, 107-127.
- Rich, P. M. (1990). Characterizing plant canopies with hemispherical photographs. *Remote Sensing Review* 5, 13-29.
- Ross, J., (1981). *The radiation regime and architecture of plant stands*. Dr Junk W, The Hague, The Netherlands.
- Running, S. W., Nemani, R. R., Peterson, D. L., Band, L. E., Potts, D. F., Pierce, L. L., & Spanner, M. A. (1989). Mapping regional forest evapotranspiration and photosynthesis by coupling satellite data with ecosystem simulation. *Ecology*, 7, 1090-1101.
- Running, S., & Coughlan, J. (1988). A general model of forest ecosystem processes for regional applications, I. Hydrologic balance, canopy gas exchange, and primary production processes. *Ecological Modelling*, 42, 125-154.
- Sayn-Wittgenstein, L. (1960). Recognition of tree species on air photographs by crown characteristics. *Technical note no. 95*. Forest Research Division, Department of Forestry, Canada.
- Sellers et al. (Eds.). (1994). *BOREAS Experimental Plan* (Vers. 3.0). NASA Goddard Space Flight Center, Greenbelt, Md.
- Shinozaki, K., Yoda, K., Hozimu, K., & Kira, T. (1964). A quantitative analysis of plant form - the pipe model theory. I. Basic analyses. *Japanese Journal of Ecology*, 14, 97-105.
- Smith, N. J., Chen, J. M., & Black, T. A. (1993). Effects of clumping on estimates of stand leaf area using the LI-COR LAI-2000. *Canadian Journal of Forest Research*, 23, 1940-1943.
- Smith, N. J. (1993). Estimating leaf area index and light extinction coefficients in stands of Douglas-fir (*Pseudotsuga menziesii*). *Canadian Journal of Forest Research*, 23, 317-321.
- Soudani, K. and Bréda, N. (2002) *Analyse bibliographique des différentes méthodes de mesures du LAI en forêt, au regard d'objectifs donnés. Précis méthodologiques à l'usage des utilisateurs*, in press. GIP-INRA, France.
- Soudani, K., Trautmann, J., & Walter, J. -M. N. (2001). Comparison of optical methods for estimating canopy openness and leaf area index in broad-leaved forests. *Comptes Rendus de l'Académie des Sciences, Série III, Sciences de la Vie*, 324, 381-392.
- Spies, T. A., Ripple, W. J., & Bradshaw, G. A. (1994). Dynamics of a managed coniferous forest landscape in Oregon. *Ecological Applications*, 4, 555-566.
- Spies, T. A. (1998). Forest stand structure, composition, and function. Kohm, K. A., & Franklin, J. F. (Eds.). *Creating a forestry for the 21st century*, 11-30. Island Press, Washington, D.C.

- Squiers, E. R., & Klosterman, J. E. (1981). Spatial patterning and competition in an aspen-white pine successional system. *American Journal of Botany*, 68, 790-794.
- Stenberg, P. S., Linder, S., Smolander, H., & Flower-Ellis, J. (1994). Performance of the LAI-2000 plant canopy analyzer in estimating leaf area index of some Scots Pine stands. *Tree Physiology*, 14, 981-995.
- Turner, D. P., Acker, S. A., Means, J. E., & Garman, S. L. (2000). Assessing alternative allometric algorithms for estimating leaf area of Douglas-fir trees and stands. *Forest Ecology and Management*, 126, 61-76.
- Wagner, S. (2001). Relative radiance measurements and zenith angle dependent segmentation in hemispherical photography. *Agricultural and Forest Meteorology*, 107, 103-115.
- Wagner, R. G., & Radosevich, S. R. (1998). Neighborhood approach for quantifying interspecific competition in coastal Oregon forests. *Ecological Applications*, 8, 779-794.
- Walter, J. -M. N., Fournier, R. A., Soudani, K., & Meyer E. (2002). Integrating clumping effects in forest canopy structure: an assessment through hemispherical photographs. *Canadian Journal of Remote Sensing*, submitted.
- Walter, J. -M. N., & Torquebiau, E. F. (2000). The computation of forest leaf area index on slope using fish-eye sensors. *Comptes Rendus de l'Académie des Sciences, Série III, Sciences de la Vie*, 323, 801-813.
- Walter, J. -M. N. (2002). *CIMES. A package of programs for the assessment of canopy geometry through hemispherical photographs*. Université Louis Pasteur, Strasbourg, France.
- Wang, Y. P., & Jarvis, P. G. (1988). Mean leaf angles for the ellipsoidal inclination angle distribution. *Agricultural and Forest Meteorology*, 43, 319-321.
- Warren Wilson, J. (1965). Stand structure and light penetration. I. Analysis by point quadrats. *Journal of Applied Ecology*, 2, 383-390.
- Warren Wilson, J. (1963). Estimation of foliage denseness and foliage angle by inclined point quadrats. *Australian Journal of Botany*, 11, 95-105.
- Warren Wilson J., & Reeve, J. E. (1960). Inclined point quadrats. *New Phytologist*, 59, 1-8.
- Warren Wilson, J. (1959). Analysis of the spatial distribution of foliage by two-dimensional point quadrats. *New Phytologist*, 58, 92-101.
- Weinstein, D. A., Beloin, R. M., Yanai, R. D. (1991). Modelling changes in red spruce carbon balance and allocation in response to interacting ozone and nutrient stresses. *Tree Physiology*, 9, 127-146.
- Welles, J. M. (1990). Some indirect methods of estimating canopy structure. *Remote Sensing of Environment*, 5, 31-43.
- Welles, J. M., & Cohen, S. (1996). Canopy structure measurement by gap fraction analysis using commercial instrumentation. *Journal of Experimental Botany*, 47, 1135-1342.
- Welles, J. M., & Norman, J. M. (1991). Instrument for indirect measurement of canopy architecture. *Agronomy Journal*, 83, 818-825.
- Whitford, K. R., Colquhoun, I. J., Lang, A., & Harper, B. M. (1995). Measuring leaf area index in a sparse eucalypt forest: a comparison of estimates from direct measurement, hemispherical photography, sunlight transmittance and allometric regression. *Agricultural and Forest Meteorology*, 74, 237-249.
- Whittaker, R. H. (1975). *Communities and Ecosystems* (2nd ed.). MacMillan, New York.
- Wit, C.T. de (1965). Photosynthesis of Leaf Canopies. *Agric. Res. Report 663*. Institute for Biological & Chemical Research on Field Crops and Herbage, Wageningen.
- Wood, J. E., Gillis, M., Goodenough, D., Hall, R. J., Leckie, D., Luther, J. E., & Wulder, M. A. (2002). Earth Observation for Sustainable Development of Forests: Project Overview.

- Proceedings, International Geoscience and Remote Sensing Symposium (IGARSS '02),*
June 24-28, 2002, Toronto, ON, Canada.
- Zsilinszky, V. G. (1964). The practice of photo interpretation for a forest inventory.
Photogrammetria, XIX no 5. Commission VII, Lisbon.

Chapter 5

ACCURACY ASSESSMENT OF MAPS OF FOREST CONDITION

Statistical Design and Methodological Considerations

Raymond L. Czaplewski

USDA Forest Service, Rocky Mountain Research Station, Fort Collins, Colorado, 80526-1891, USA

1. INTRODUCTION

No thematic map is perfect. Some pixels or polygons are not accurately classified, no matter how well the map is crafted. Therefore, thematic maps need metadata that sufficiently characterize the nature and degree of these imperfections. To decision-makers, an accuracy assessment helps judge the risks of using imperfect geospatial data. To analysts, an accuracy assessment helps describe the reliability of the map for geospatial analyses and modeling, and the distribution of different types of “true” land cover within each mapped category. To producers of thematic maps, an accuracy assessment measures the degree of technical success for alternative algorithms or techniques. To project managers, an accuracy assessment helps determine contract compliance or measure performance of technical staff.

1.1 Random sampling

There are two general methods to obtain reference data for an accuracy assessment: *ad hoc* sampling and probability sampling. Both methods commonly appear in remote sensing projects. However, for the following reasons, only probability sampling is considered in this Chapter.

Ad hoc methods often rely on a sampling plan that selects convenient sites in order to minimize cost of reference data. Experts purposively select sites believed to be representative of the mapped area. This method can

produce an error matrix (e.g., Tables 5-1 to 5-3) at relatively low cost. This matrix accurately describes the results for the sampled sites. However, does that same error matrix provide a useful assessment of classification accuracy for the entire thematic map? The producer of the accuracy assessment would argue that this approach is good enough for practical purposes. In some benign cases, this can be true. But what if a user of the thematic map is skeptical of its accuracy, or what if there are disagreements over performance or contract compliance? Furthermore, convenient sampling sites are often near roads, which are frequently associated with unique landforms, land uses, management histories, and landscape patterns. Are such sites truly representative of the entire map? Are the conditions that cause misclassification errors similar among convenient and inconvenient sampling sites? Other than expert opinion, there is no good way to answer these questions. And what if there is a disagreement among the experts? In pathological situations, some “experts” might intentionally seek atypical sites to discredit the map’s accuracy. It is far easier to discredit the accuracy of a map than prove otherwise with *ad hoc* methods.

The cost savings offered by *ad hoc* methods can also be achieved with probability sampling. The random sample can be constrained to a sub-population that is accessed relatively inexpensively (e.g., all portions of the thematic map that are less than 500 m from a road). Valid inference is limited to this sampled population, but at least the inference is scientifically defensible. The remainder of this Chapter considers only probability sampling methods.

1.2 Objectives

The objective of this Chapter to present simple, statistically valid, and cost-effective statistical methods to estimate a contingency table during an accuracy assessment. Each row of the contingency table represents a category from the thematic map, and each column represents a category from the reference data. In the remote sensing literature, the most familiar contingency table (e.g., Table 5-1) is the “error matrix” or “confusion matrix” (Story and Congalton 1986). However, the contingency table could use different classification systems for the reference data and the map. For example, the reference data could include categories that can only be reliably applied by a field crew, and these data used to characterize the map categories in greater thematic detail. Another type of contingency table uses “fuzzy-set” categories (Gopal and Woodcock 1994), which cross-classifies points based on their thematic categories on the map and categories such as “Correct”, “Acceptable”, “Not right” or “Very wrong” (e.g., Table 5-2). These contingency tables share most of the same statistical issues, and are

considered simultaneously in this Chapter. In addition, this Chapter covers only simple random sampling of points on the thematic map, and one specialized type of stratified random sampling. An informed non-statistician can apply these simple and robust designs with little risk of procedural error.

Table 5-1. Error matrix based on a simple random sample of 100 points from a 1,000,000-ha sample population, which are cross-classified by both the Map Classifier and the Reference Classifier.

Map Classifier	Count of sample points				Mapped area (ha)	
	Reference Classifier			Total	Estimated (100 sampled points)	Exact (all Map Objects in the GIS)
	Forest	Old-growth forest	Non-forest			
Forest	43	1	4	48	480,000	409,346
	2	6	0	8	80,000	41,634
	14	3	27	44	440,000	549,020
Total	59	10	31	100		
Estimated true area (ha)	590,000	100,000	310,000	1,000,000	1,000,000	1,000,000
Estimated overall accuracy: $(43+6+27)/100=76\%$						
Kappa: $[100 \cdot (43+6+27) - (59 \cdot 48 + 10 \cdot 8 + 31 \cdot 44)] / [100^2 - (59 \cdot 48 + 10 \cdot 8 + 31 \cdot 44)] = 0.58$						
Estimated producer's accuracy			Estimated user's accuracy			
Forest	43/59=	73%		43/48=	90%	
Old-growth forest	6/10=	60%		6/8=	75%	
Non-forest	27/31=	87%		27/44=	61%	

1.3 Definitions

“Map Objects” are either pixels or polygons. Map Objects are modeled as internally homogeneous, even though in reality they often include some internal heterogeneity, at least at a fine spatial scale. Therefore, problems associated with “mixed pixels”, or atypical inclusions within a polygon, are not covered in this Chapter. A “Map Classifier” is defined as a process that assigns a Map Object into one, and only one, thematic category, such as water, forest or barren classes, within a user-defined classification system. The Map Classifier might be a supervised or unsupervised algorithm operating on Landsat data, a photo-interpreter using aerial photography for a “wall-to-wall” stand map, or a geospatial model (e.g., wildlife habitat suitability). The Map Classifier is applied to every Map Object in the map.

The Reference Classifier is the process that assigns an infinitesimally small point on the map into its “true” or “correct” category. This category could exactly correspond to the classification system used for the map (e.g., Table 5-1), a user-defined classification system that differs from the system used for the map, or it could be a fuzzy-set category (e.g., Table 5-2). This point on the map is surrounded by a larger pixel or polygon (i.e., a Map Object), which serves as a “support region” for application of a classification protocol. The Reference Classifier might be a ground crew or an interpreter using high-resolution aerial photography. The Reference Classifier is considerably more expensive to apply than the Map Classifier. Therefore, the Reference Classifier can only be applied to a relatively small sample of points (and the Map Objects that form their support regions).

Table 5-2. Simple contingency table in which the Reference Classifier uses fuzzy-set categories to assign different degrees of correctness or error to each sample point.

Map Classifier	Reference Classifier				Row Total
	Correct	Acceptable	Not right	Very wrong	
Forest	43	2	2	1	48
	6	0	1	1	8
	27	10	4	3	44
Column Total		76	11	8	100

Table 5-1 is an example of a simple error matrix, in which a sample of $n=100$ points is cross-classified by both the Map Classifier and the Reference Classifier. In this example, both the Map and Reference Classifiers classified 43 points as forest, while only one point is incorrectly classified as old-growth forest on the map but classified as forest with the reference data. On the other hand, Table 5-2 is a simple example of a fuzzy-set contingency table, where the Reference Classifier uses linguistic values to describe the relative degree of correctness or error to each point. Assume this sample of 100 points came from a statistically valid, simple random sample of points on the map. Then the counts in Tables 5-1 and 5-2 can be directly used to estimate probabilities that any point in the map would be so classified by the Map and Reference Classifiers.

1.4 Accuracy assessment statistics

The following statistics quantitatively describe classification accuracy and other types of metadata for a thematic map.

- Overall accuracy: What is the probability that any point on the map is assigned to exactly the same category by the Map Classifier and the

Reference Classifier? For example, the overall accuracy in Table 5-1 is estimated to be 76 %.

- Fuzzy-set accuracy: What is the probability that any point on the map would be assigned to one or several linguistic categories by the Reference Classifier? For example, the probability that the classification of any point on the map is “Correct” or “Acceptable” is estimated to be $(76 \% + 11 \%) = 87 \%$ from Table 5-2.
- Marginal proportions: What is proportion of the population is classified as Category X ? Using Table 5-1 as an example, 10 % of the thematic map (100,000 ha) is estimated to be truly old-growth forest based on the Reference Classifier. Using that same sample of 100 points, the estimated proportion of the map classified as old-growth forest is 8 % (80,000 ha).
- Kappa coefficient of agreement: Kappa is a scalar statistic that quantifies the agreement between the Reference and Map Classifiers in a multivariate error matrix (Campbell 1996). Values of kappa exceeding 0.6 are considered good (Czaplewski 1994). However, the analytical value of the kappa statistic is questionable (Stehman, 2002), and this Chapter treats kappa as merely a conventional descriptive statistic.
- Conditional probabilities given the Reference Classifier: For any point assigned to Category Y by the Reference Classifier, what is the probability that this same point would be assigned to Category X by the Map Classifier? For example, assume you are standing over a point on the ground that is surrounded by old-growth forest (based on the protocol used by the Reference Classifier for the support region). Table 5-1 estimates that there is a $3/10 = 30 \%$ chance of that same point being classified as non-forest on the map (i.e., an “omission error”). “Producer’s accuracy” is a special case (Story and Congalton 1986). Given that the Reference Classifier assigns the point to category X , what is the probability that the point is correctly assigned to category X by the Map Classifier? Producer’s accuracy is 60 % in this old-growth forest example.
- Conditional probabilities given the Map Classifier: For any point assigned to Category X by the Map Classifier, what is the probability that this same point would be assigned to Category Y by the Reference Classifier? For example, pick any point on the map that is classified as old-growth forest, and then find that same point in the field. Table 5-1 estimates that there is a $(8-6)/8 = 25 \%$ chance of that point being mislabeled as some other map class (i.e., “commission error”). User’s accuracy is a special case of this statistic (Story and Congalton 1986), which is 75 % in this example.

2. FIVE STEPS IN AN ACCURACY ASSESSMENT

Five steps are necessary to produce a successful, yet simple and cost effective, accuracy assessment.

1. Select a probability sample of points for which expensive reference data will be collected to compare with classifications of corresponding points on the map.
2. Define the response design, which is the protocol used to apply the Reference Classifier to the support region for each sample point selected in Step 1. The response design must produce a “true” classification that is acceptable to users of the accuracy assessment.
3. Use correct statistical methods to estimate accuracy assessment statistics with the sample data from Steps 1 and 2.
4. Use diagnostic statistics to detect potential problems in the execution of Steps 1, 2, and 3.
5. Present the results to both the users and producers of the map in an informative and intuitive format.

The value of the accuracy assessment depends on how well each and every step is conducted.

The general subject of sample surveys is well covered in general references, such as Cochran (1977), Särndal et al. (1992), Schreuder et al. (1993), Salant and Dillman (1994), Lloyd (1999), and Lohr (1999). In the context of accuracy assessments in remote sensing studies, Stehman and Czaplewski (1998) and Stehman (2001) discuss the first three steps.

2.1 Selection of the reference sample

The sample design specifies how to select the points at which the reference data are gathered. The “target population” is the area or region represented by the thematic map, while the “sampled population” is the portion of the target population that is chosen for sampling. Ideally, the target and sampled populations are identical, but practical constraints often require selecting a sampled population that is a smaller segment of the target population.

For example, assume the target population is a 4,000,000 ha region covered by the thematic map. To reduce the cost of the accuracy assessment, the probability sample of reference points will be drawn from only those areas within a 500 m “buffer” from any road. A GIS is used to identify all portions of the thematic map within the 500 m buffer. In this example, only 1,000,000 ha of the entire map is within the 500 m buffer. The estimated error matrix will validly estimate classification accuracy for that 1,000,000 ha. Unfortunately, inferences for the remaining 3,000,000 ha of target

population cannot be scientifically supported with data from this accuracy assessment.

2.1.1 Simple random sampling

The most straightforward and robust design is a simple random sample of n points on the map. Tables 5-1 and 5-2 are examples. Every sample point has exactly the same probability of being included in the sample, regardless of the map classification. Therefore, a simple random sample can be drawn before the final thematic map is available.

2.1.2 Stratified random sampling

There are often rare map categories that are especially important to the user. Unfortunately, a simple random sample is expected to allocate only a small number of reference samples to any rare category. However, “stratified random sampling” can be used to allocate a different sampling intensity to each map category based on the importance of that category to the user. Usually, stratification improves statistical precision, even when the sample size is in each stratum is proportional to the prevalence of each stratum (i.e., proportional allocation).

This Chapter defines a “stratum” as all portions of the thematic map that are classified into the same map category on the final thematic map. Rather than select a single random sample from the entire sampled population, a simple random sample is independently drawn within each category after the thematic map is completed. Compared to random sampling, stratified random sampling is slightly more complex; however, it remains a feasible choice for non-statisticians. Other approaches to stratification can be valid, but estimation is more complex, thus requiring the aid of a consulting statistician (Czaplewski 2000).

Table 5-3A is an example of a stratified random sample, in which an equal number of sample points is allocated to each stratum, regardless of the stratum’s prevalence. However, unlike a simple random sample (e.g., Table 5-1), raw counts in a stratified sample cannot be directly used to make unbiased estimates for statistics that are computed from multiple strata (i.e., multiple rows in the error matrix). With stratified random sampling, each cell in Table 5-3A must be converted into an estimated joint probability in order to consider the full suite of assessment statistics. This conversion has been done to produce Table 5-3B. Table 5-8 gives all estimators needed with stratified sampling.

Stratified random sampling has several disadvantages compared to simple random sampling. In order to stratify on the mapped categories, the

final thematic map must be available before reference data are collected. This can be several years after the remotely sensed data were originally acquired. Therefore, some misclassifications will actually be caused by changes in land cover. Furthermore, if changes are made to the thematic map after drawing the stratified random sample, then more complex estimators are needed (e.g., Czaplewski 2000), which are not covered in this Chapter. Alternatively, a simple random sample of reference data can be implemented during the earliest phases of a remote sensing study. The next section recommends use of an expected error matrix during the planning phase to evaluate the expected precision of the accuracy assessment statistics, and this same planning tool can help evaluate the advantages of simple random sampling compared to stratified random sampling.

2.1.3 Sample size

One of the most fundamental questions in any accuracy assessment is “How many points should be sampled?” For a simple random sample, Czaplewski and Catts (1992) found relatively little gain in statistical precision beyond 500 to 1,000 sample points. Congalton (1991) recommends a sample size of 50 for each map category if a stratified random sample is used, and map categories are used to define the strata. Some stratified random samples allocate half of the total sampling intensity to emulate proportional allocation, and the remaining half to improve estimates for rare categories. For example, if n_{i*} is the sample size allocated to mapped stratum i , n is the total sample size, p_{i*} is the proportion of the sampled population mapped as category i , and there are a total of k mapped categories, then $n_{i*} = [p_{i*}(n/2) + (1/k)(n/2)]$.

Figure 5-1 and Tables 5-4 to 5-7 help the practitioner chose sample sizes in more specific applications. Consider a simple random sample of 100 points. If each point is classified into “Correct” or “Incorrect”, then the proportion of correct classifications is equivalent to Overall Accuracy. Assume the expected Overall Accuracy is 75 %; the 90 % confidence interval from Table 5-5 is 67 % to 82 %, meaning there is a 5 % chance that the true Overall Accuracy is less than 67 %, and another 5 % chance that the true Overall Accuracy is greater than 82 %. If the simple random sample were increased to 250 points, then the confidence interval would shrink to approximately 70 % to 80 % (Table 5-5). Likewise, assume old-growth forest is expected to cover 10 % of the sampled population. The 90 % confidence interval from a simple random sample of 100 points would be 6 % to 16 % (Table 5-5), while the confidence interval from 250 points would be 7 % to 14 % (Table 5-5). Only the user and producer of an accuracy

assessment can judge whether the increase in statistical precision is worth the extra cost for reference data.

Table 5-3. Error matrix based on a stratified sample of 100 from the population in Table 5-1

Map Classifier (strata)	Count of points from stratified sample				Mapped area (ha)	
	Reference Classifier				“Estimated”	Exact
	Forest	Old-growth forest	Non-forest	Total		
Map Classifier (strata)	Forest	30	1	3	34	409,346
	Old-growth forest	9	22	2		41,634
	Non-forest	10	2	21		549,020
	Total	49	25	26	100	1,000,000
B Estimates from stratified sample						
Map Classifier	Forest	36.1%	1.2%	3.6%	40.9%	409,346
	Old-growth forest	1.1%	2.8%	0.3%		41,634
	Non-forest	16.7%	3.3%	35.0%		549,020
	Total	53.9%	7.3%	38.9%	100.0%	
Estimated true area (ha)	538,912	73,070	388,018	1,000,000	1,000,000	1,000,000
Estimated overall accuracy: $(36.1+2.8+35.0)/100=73.9\%$						
Estimated producer's accuracy			Estimated user's accuracy			
Forest	36.1/53.9=	67.0%	36.1/40.9=	30/34=	82.2%	
Old-growth forest	2.8/7.3=	38.4%	2.8/4.2=	22/33=	66.7%	
Non-forest	35.0/38.9=	90.0%	35.0/54.9=	21/33=	63.6%	

The prudent practitioner will use the literature and expert judgment to construct an expected error matrix during the planning phase of the accuracy assessment. Then, the expected confidence intervals for alternate sample sizes and sampling designs can be computed with methods that follow in this Chapter. This hypothetical exercise will help anticipate the precision of the accuracy assessment statistics for various funding levels and sample designs.

Table 5-4. Confidence belts for estimated proportions (p) in an error matrix for 95 % confidence coefficient (see Figure 5-1).

p	Limit	95% Confidence limits					
		n=10	20	50	100	250	1000
0%	Upper	30.8	16.8	7.1	3.6	1.5	0.4%
	Lower	0.0	0.0	0.0	0.0	0.0	0.0%
5%	Upper		24.9	15.1	11.3	8.5	6.5%
	Lower		0.1	0.9	1.6	2.7	3.7%
10%	Upper	44.5	31.7	21.8	17.6	14.4	12.0%
	Lower	0.3	1.2	3.3	4.9	6.6	8.2%
15%	Upper		37.9	27.9	23.5	20.0	17.4%
	Lower		3.2	6.5	8.6	10.8	12.8%
20%	Upper	55.6	43.7	33.7	29.2	25.5	22.6%
	Lower	2.5	5.7	10.0	12.7	15.2	17.6%
25%	Upper		49.1	39.3	34.7	30.8	27.8%
	Lower		8.7	13.8	16.9	19.8	22.3%
30%	Upper	65.2	54.3	44.6	40.0	36.1	32.9%
	Lower	6.7	11.9	17.9	21.2	24.4	27.2%
35%	Upper		59.2	49.8	45.2	41.3	38.0%
	Lower		15.4	22.1	25.7	29.1	32.0%
40%	Upper	73.8	63.9	54.8	50.3	46.4	43.1%
	Lower	12.2	19.1	26.4	30.3	33.9	36.9%
45%	Upper		68.5	60.7	55.3	51.4	48.1%
	Lower		23.1	31.8	35.0	38.7	41.9%
50%	Upper	81.3	72.8	64.5	60.2	56.4	53.1%
	Lower	18.7	27.2	35.5	39.8	43.6	46.9%
55%	Upper		76.9	69.1	65.0	61.3	58.1%
	Lower		31.5	40.3	44.7	48.6	51.9%
60%	Upper	87.8	80.9	73.6	69.7	66.1	63.1%
	Lower	26.2	36.1	45.2	49.7	53.6	56.9%
65%	Upper		84.6	77.9	74.3	70.9	68.0%
	Lower		40.8	50.2	54.8	58.7	62.0%
70%	Upper	93.3	88.1	82.1	78.8	75.6	72.8%
	Lower	34.8	45.7	55.4	60.0	63.9	67.1%
75%	Upper		91.3	86.2	83.1	80.2	77.7%
	Lower		50.9	60.7	65.3	69.2	72.2%
80%	Upper	97.5	94.3	90.0	87.3	84.8	82.4%
	Lower	44.4	56.3	66.3	70.8	74.5	77.4%
85%	Upper		96.8	93.5	91.4	89.2	87.2%
	Lower		62.1	72.1	76.5	80.0	82.6%
90%	Upper	99.7	98.8	96.7	95.1	93.4	91.8%
	Lower	55.5	68.3	78.2	82.4	85.6	88.0%
95%	Upper		99.9	99.1	98.4	97.3	96.3%
	Lower		75.1	84.9	88.7	91.5	93.5%
100%	Upper	100	100	100	100	100	100%
	Lower	69.2	83.2	92.9	96.4	98.5	99.6%

Table 5-5. Confidence belts for estimated proportions (p) in an error matrix for 90 % confidence coefficient (see Figure 5-1)..

p	Limit	90% Confidence limits				
		n=10	20	50	100	250
0%	Upper	25.9	13.9	5.8	3.0	1.2
	Lower	0.0	0.0	0.0	0.0	0.0
5%	Upper		21.6	13.4	10.2	7.9
	Lower		0.3	1.2	2.0	3.0
10%	Upper	39.4	28.3	19.9	16.4	13.7
	Lower	0.5	1.8	4.0	5.5	7.0
15%	Upper		34.4	25.9	22.2	19.2
	Lower		4.2	7.5	9.5	11.4
20%	Upper	50.7	40.1	31.6	27.7	24.6
	Lower	3.7	7.1	11.3	13.7	15.9
25%	Upper		45.6	37.0	33.1	29.9
	Lower		10.4	15.3	18.0	20.5
30%	Upper	60.7	50.8	42.4	38.4	35.1
	Lower	8.7	14.0	19.5	22.5	25.2
35%	Upper		55.8	47.6	43.6	40.3
	Lower		17.7	23.8	27.1	30.0
40%	Upper	69.6	60.6	52.6	48.7	45.4
	Lower	15.0	21.7	28.3	31.8	34.8
45%	Upper		65.3	57.5	53.7	50.4
	Lower		25.9	32.9	36.5	39.7
50%	Upper	77.8	69.8	62.4	58.6	55.4
	Lower	22.2	30.2	37.6	41.4	44.6
55%	Upper		74.1	67.1	63.5	60.3
	Lower		34.7	42.5	46.3	49.6
60%	Upper	85.0	78.3	71.7	68.2	65.2
	Lower	30.4	39.4	47.4	51.3	54.6
65%	Upper		82.3	76.2	72.9	70.0
	Lower		44.2	52.4	56.4	59.7
70%	Upper	91.3	86.0	80.5	77.5	74.8
	Lower	39.3	49.2	57.6	61.6	64.9
75%	Upper		89.6	84.7	82.0	79.5
	Lower		54.4	63.0	66.9	70.1
80%	Upper	96.3	92.9	88.7	86.3	84.1
	Lower	49.3	59.9	68.4	72.3	75.4
85%	Upper		95.8	92.5	90.5	88.6
	Lower		65.6	74.1	77.8	80.8
90%	Upper	99.5	98.2	96.0	94.5	93.0
	Lower	60.6	71.7	80.1	83.6	86.3
95%	Upper		99.7	98.8	98.0	97.0
	Lower		78.4	86.6	89.8	92.1
100%	Upper	100	100	100	100	100
	Lower	74.1	86.1	94.2	97.0	98.8

Table 5-6. Confidence belts for estimated proportions (p) in an error matrix for 80 % confidence coefficient (see Figure 5-1)..

p	Limit	80% Confidence limits					
		n=10	20	50	100	250	1000
0%	Upper	20.6	10.9	4.5	2.3	0.9	0.2%
	Lower	0.0	0.0	0.0	0.0	0.0	0.0%
5%	Upper		18.1	11.6	9.1	7.3	6.0%
	Lower		0.5	1.6	2.5	3.3	4.1%
10%	Upper	33.7	24.5	17.8	15.0	12.9	11.3%
	Lower	1.0	2.7	4.9	6.3	7.6	8.8%
15%	Upper		30.4	23.6	20.6	18.3	16.5%
	Lower		5.6	8.8	10.5	12.1	13.6%
20%	Upper	45.0	36.1	29.1	26.1	23.6	21.7%
	Lower	5.5	9.0	12.8	14.9	16.7	18.4%
25%	Upper		41.5	34.5	31.4	28.9	26.8%
	Lower		12.7	17.1	19.4	21.5	23.2%
30%	Upper	55.2	46.7	39.8	36.6	34.0	31.9%
	Lower	11.6	16.6	21.5	24.0	26.2	28.1%
35%	Upper		51.8	45.0	41.8	39.1	37.0%
	Lower		20.7	26.0	28.7	31.0	33.0%
40%	Upper	64.6	56.7	50.1	46.9	44.2	42.0%
	Lower	18.8	24.9	30.6	33.4	35.9	38.0%
45%	Upper		61.5	55.0	51.9	49.2	47.1%
	Lower		29.3	35.3	38.3	40.8	42.9%
50%	Upper	73.3	66.2	59.9	56.9	54.2	52.1%
	Lower	26.7	33.8	40.1	43.1	45.8	47.9%
55%	Upper		70.7	64.7	61.7	59.2	57.1%
	Lower		38.5	45.0	48.1	50.8	52.9%
60%	Upper	81.2	75.1	69.4	66.6	64.1	62.0%
	Lower	35.4	43.3	49.9	53.1	55.8	58.0%
65%	Upper		79.3	74.0	71.3	69.0	67.0%
	Lower		48.2	55.0	58.2	60.9	63.0%
70%	Upper	88.4	83.4	78.5	76.0	73.8	71.9%
	Lower	44.8	53.3	60.2	63.4	66.0	68.1%
75%	Upper		87.3	82.9	80.6	78.5	76.8%
	Lower		58.5	65.5	68.6	71.1	73.2%
80%	Upper	94.5	91.0	87.2	85.1	83.3	81.6%
	Lower	55.0	63.9	70.9	73.9	76.4	78.3%
85%	Upper		94.4	91.2	89.5	87.9	86.4%
	Lower		69.6	76.4	79.4	81.7	83.5%
90%	Upper	99.0	97.3	95.1	93.7	92.4	91.2%
	Lower	66.3	75.5	82.2	85.0	87.1	88.7%
95%	Upper		99.5	98.4	97.5	96.7	95.9%
	Lower		81.9	88.4	90.9	92.7	94.0%
100%	Upper	100	100	100	100	100	100%
	Lower	79.4	89.1	95.5	97.7	99.1	99.8%

Table 5-7. Confidence belts for estimated proportions (p) in an error matrix for 50 % confidence coefficient (see Figure 5-1)..

p	Limit	50% Confidence limits					
		n=10	20	50	100	250	1000
0%	Upper	12.9	6.7	2.7	1.4	0.6	0.1%
	Lower	0.0	0.0	0.0	0.0	0.0	0.0%
5%	Upper		12.9	8.8	7.3	6.3	5.5%
	Lower		1.4	2.7	3.4	4.0	4.5%
10%	Upper	24.7	18.7	14.5	12.8	11.6	10.7%
	Lower	2.8	4.8	6.8	7.8	8.6	9.3%
15%	Upper		24.2	19.9	18.2	16.8	15.8%
	Lower		8.7	11.2	12.4	13.4	14.2%
20%	Upper	35.5	29.6	25.2	23.4	22.0	20.9%
	Lower	9.6	12.8	15.7	17.0	18.2	19.1%
25%	Upper		34.8	30.5	28.6	27.1	26.0%
	Lower		17.1	20.3	21.8	23.0	24.0%
30%	Upper	45.8	40.0	35.6	33.7	32.2	31.0%
	Lower	17.6	21.6	25.0	26.6	27.9	29.0%
35%	Upper		45.1	40.7	38.8	37.3	36.1%
	Lower		26.1	29.7	31.4	32.8	33.9%
40%	Upper	55.5	50.1	45.8	43.9	42.3	41.1%
	Lower	26.1	30.7	34.5	36.3	37.7	38.9%
45%	Upper		55.0	50.8	48.9	47.3	46.1%
	Lower		35.4	39.4	41.2	42.7	43.9%
50%	Upper	64.9	59.8	55.7	53.9	52.3	51.1%
	Lower	35.1	40.2	44.3	46.1	47.7	48.9%
55%	Upper		64.6	60.6	58.8	57.3	56.1%
	Lower		45.0	49.2	51.1	52.7	53.9%
60%	Upper	73.9	69.3	65.5	63.7	62.3	61.1%
	Lower	44.5	49.9	54.2	56.1	57.7	58.9%
65%	Upper		73.9	70.3	68.6	67.2	66.1%
	Lower		54.9	59.3	61.2	62.7	63.9%
70%	Upper	82.4	78.4	75.0	73.4	72.1	71.0%
	Lower	54.2	60.0	64.4	66.3	67.8	69.0%
75%	Upper		82.9	79.7	78.2	77.0	76.0%
	Lower		65.2	69.5	71.4	72.9	74.0%
80%	Upper	90.4	87.2	84.3	83.0	81.8	80.9%
	Lower	64.5	70.4	74.8	76.6	78.0	79.1%
85%	Upper		91.3	88.8	87.6	86.6	85.8%
	Lower		75.8	80.1	81.8	83.2	84.2%
90%	Upper	97.2	95.2	93.2	92.2	91.4	90.7%
	Lower	75.3	81.3	85.5	87.2	88.4	89.3%
95%	Upper		98.6	97.3	96.6	96.0	95.5%
	Lower		87.1	91.2	92.7	93.7	94.5%
100%	Upper	100	100	100	100	100	100%
	Lower	87.1	93.3	97.3	98.6	99.4	99.9%

2.1.4 Independence of reference sample

The sample of reference sites should not include any sites used for training or labeling the Map Classifier. In some sense, the Map Classifier is optimized to agree with a sample of training or labeling sites; therefore, the classification accuracy for that particular sample of sites will likely be greater than the accuracy expected at other sites. If training sites are used for accuracy assessment, then the metadata should indicate that the estimated accuracy is likely an overestimate of the true accuracy. If the training or labeling sites will be a subset of the probability sample of reference sites, then a simple random sub-sampling procedure should be used to separate the sample into two independent groups: reference sites and training sites. This assures that the reference sites remain a reliable probability sample. More complex sub-sampling procedures could produce reliable results, but a consulting statistician should become involved to assure that correct statistical estimators are used.

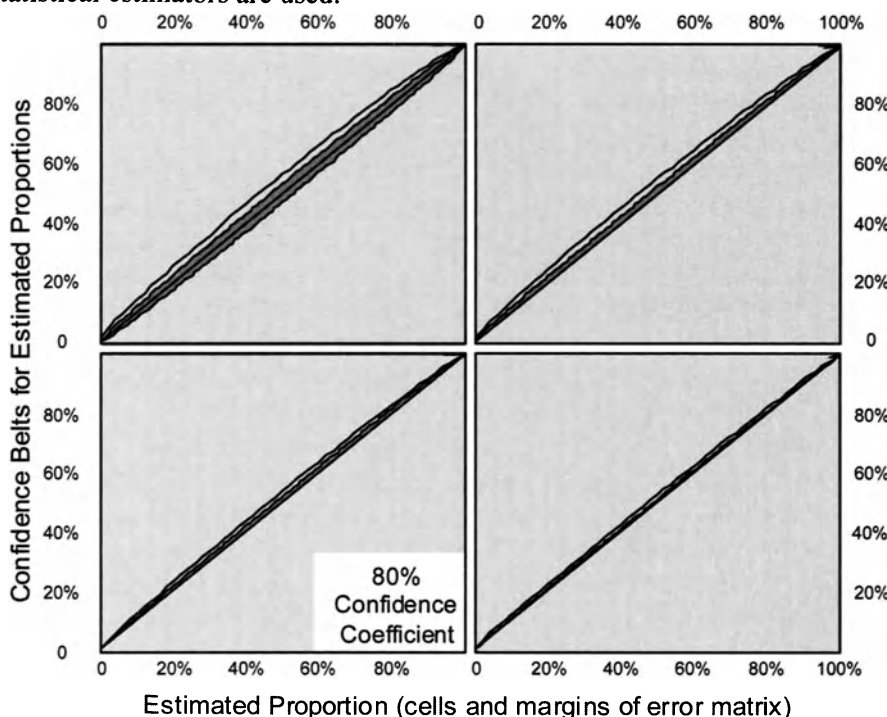


Figure 5-1. Confidence belts for estimated proportions in the cells and margins of an error matrix. The confidence coefficient is the probability that the true (but known) value is within the confidence belt. The effective sample size is denoted as n (see Table 5-8). Use Tables 5-4 to 5-7 to make more precise interpolations.

2.2 Response design

The response design specifies how to determine the reference classification at a given sample point. The first step is to select the “spatial support region” for which the reference classification is made (Stehman and Czaplewski 1998). The support region for a pixel map is discussed first, followed by consideration of a polygon map.

2.2.1 Pixel map

Assume the Map Object is a 30 m pixel. The support region might be a 30 m square area that surrounds the sample point, even though the true “boundaries” of the target pixel on the map are not well known in the field or on an aerial photograph. Or the support area could be a circle with 50 m radius centered on the sample point. Regardless, the objective is to determine, as accurately as possible, the correct reference classification of the target pixel. This is accomplished within a support region that is well defined on the ground or an aerial photograph.

Misregistration of sample points to the thematic map can bias the accuracy assessment statistics. The classification on the map at the intended sample point might be correct, but misregistration causes the reference classification to be compared to a different, nearby pixel, which might not have the same classification on the map. A larger support region can partially compensate for misregistration between the map and the sample point. However, if the support region becomes too large, then the reference classifier may not well represent the true classification of the single map pixel that surrounds the sample point. The support region should be similar to the spatial scale of the Map Object.

Some studies lower the spatial resolution of the map near a sample point so that the sampled pixel will likely have the same map classification as the intended pixel. For example, assume the map consists of unique classifications of individual pixels (i.e., a moving window is not used to spatially filter classifications of adjacent pixels). However, during the accuracy assessment, a 3x3 block of pixels is formed around each sample point used for reference data, and some rule is used to assign a single map category to this block of nine potentially heterogeneous map pixels. This can mitigate affects of registration error, and it is possible to compare a reference classification for the sample point to the classification of this surrounding block of pixels. Regrettably, this process assesses the accuracy of an imaginary thematic map to which the same filtering rule was applied to all

pixels, not the individual-pixel map that was actually produced. The accuracy of the unfiltered map might be similar to the accuracy of the filtered map, but this is speculative. If registration error is significant, then perhaps the entire map should be subjected to the same filtering rule. At least the map being assessed is the same map being delivered.

Boundaries between adjacent forest stands and other types of land cover are often more heterogeneous than interiors of stands. Therefore, the effect of registration error can be greatest near stand edges. Some studies move the sample point away from edges into conditions that are more homogeneous. This can be useful for developing training data in a digital classification. However, this same practice can reduce the scope of the accuracy assessment because some parts of the thematic map are excluded from the target population. Edge conditions can be very prevalent in detailed thematic maps for diverse landscapes. If the producer of the accuracy assessment avoids boundary conditions, such areas should be identified for the entire map with a GIS procedure. The extent and mapped composition of the excluded zone can be tabulated and reported in the assessment documentation, and the user of the assessment can judge the value of an assessment that is limited to interior conditions.

Alternative methods are available to mitigate the effect of registration errors on the quality of the accuracy assessment. In addition to producing the reference classification, the field crew or photo-interpreter can record data that indicate the likelihood of misregistration error:

1. Distance from the sample point to a stand boundary or other edge condition. The frequency of misclassification errors can be compared with the distance from an edge to gain insights into the nature of misregistration and misclassification errors.
2. Classification of stands based on internal heterogeneity relative to the scale of the pixel (e.g., dense and uniform fine-grained canopy, frequent gaps with coarse-grained canopy). If the apparent misclassification error is remarkably higher in heterogeneous stands, then misregistration error might be a significant problem.

2.2.2 Polygon map

Assume a Map Object is a 10 ha forest stand delineated on a thematic map through image segmentation or photo-interpretation. The entire stand is classified into one and only one category on the map.

The support area is the entire polygon that surrounds a sample point. The Reference Classifier is applied to the entire polygon from the map, not a portion of the polygon in the immediate vicinity of the sample point. It is important to use the polygon boundaries on the map when applying the

Reference Classifier, and not use a special polygon delineation procedure that is only applied to each sample point. Otherwise, the analysis will not assess the thematic map being evaluated. Rather, it will assess an imaginary map that would have been produced if the special delineation procedure used for the accuracy assessment were applied to the entire thematic map.

2.2.3 Labeling protocol for reference data

The next part of the Response Design is specification of the labeling protocol for the support region around each sample point. This could be photo-interpretation with higher-resolution imagery, qualitative observations by a field crew, or sub-sampling and physical measurements by a field crew.

The labeling protocol needs to consider the size and configuration of the support region (as discussed above). If the support region is large (e.g., a polygon), then inexpensive methods might be necessary, such as photo interpretation or low-intensity stand examinations. If the support region is small (e.g., 1 ha or smaller), then more expensive classifications using tree measurements might be feasible. The advantage of the latter is more precise and repeatable reference classifications of forest conditions. The value of the accuracy assessment depends upon the credibility of the labeling protocol to the user of the assessment.

The quality of reference data also depends on compatibility of definitions. For example, there are a variety of definitions for forest and old-growth forest, and the response design must use definitions acceptable to users of the assessment. Otherwise, the investment in the accuracy assessment might yield little practical value. However, there can be advantages with a more detailed classification system for the reference data. For example, assume that the reference data separates “shrubby wetlands” from “forested wetlands”, but the map groups both types of wetland into a single category called “wooded wetlands”. The reference data statistically estimate the proportion of wooded wetlands that are actually shrubby and forested woodlands, even though these detailed categories are not separated on the map.

The quality of reference data is often a compromise between the ideal and the feasible. For example, interpretation of aerial photography is an inexpensive alternative to field classifications. Photo-interpretation is acceptable if the resolution of the photography is sufficient relative to the thematic classification system, the photography is available for the entire sampled population, the acquisition dates reasonably coincide with the remotely sensed imagery used to produce the thematic map, and these materials are acceptable to the user of the accuracy assessment

There are often variations among photo-interpreters when classifying the land cover for a reference point. A similar problem occurs with field crews who produce “ocular” classifications that are not based on physical measurements. To partially mitigate this source of uncertainty with the reference data, multiple interpreters can classify the same reference points, and a majority rule engaged to select the classification used in the accuracy assessment. Sample points that have different reference classifications among interpreters can be inspected more closely, and perhaps a different protocol used to determine a more reliable reference classification.

Secondary classifications of the sample point can also provide useful reference data. For example, a sample point in a forest with diverse conditions could be classified by an interpreter (in the field or from an aerial photograph) as a pine stand, but the interpreter could also record that the stand might nearly meet the definition of a mixed pine/hardwood stand. Some assessments consider the map classification to be correct if it agrees with either the primary or secondary reference classification. This approach can be acceptable if well documented and apparent to users of the accuracy assessment. However, it is prudent to publish a complementary assessment, in which only the primary classification is used as reference data. This allows different users to choose the assessment that best meets their standards, and broadens the potential applications of the error matrix, such as calibration of areal estimates for misclassification bias (Czaplewski 1992).

Fuzzy-set classifications (e.g., Gopal and Woodcock 1994) are another type of reference protocol. An interpreter classifies each sample plot into categories such as “Correct”, “Acceptable”, “Not right” or “Very wrong”. An interpreter needs to know the map classification before making the reference classification into a fuzzy set. This could influence the reference interpretation, perhaps leading to biased estimates of classification accuracy.

Metadata should document the quality of the reference data. If multiple interpreters are used to collect reference data, a then a summary of the variability among interpreters provides useful information for quantitative characterization. In addition, interpreters can classify each sample point based on their own confidence in the interpretation, for example: “Confident that the interpretation is correct”, “Uncertain classification”, or “Nearly a guess”. Such information may aid in a detailed analysis of the accuracy assessment data.

2.3 Analysis

The analysis design specifies how to mathematically combine the data collected in Steps 1 and 2 to accurately infer accuracy assessment statistics, which are listed in the beginning of this Chapter, for the sampled population.

Stehman and Czaplewski (1998) provide general guidance and key references. This Chapter only considers the two simple designs that can be reliably analyzed by an informed user: simple random point sampling, and stratified random point sampling based on map categories as strata. Table 5-8 provides the estimators for accuracy assessment statistics and their variances for these two designs.

The analysis must be compatible with the statistical design. Otherwise, estimates can be biased and misleading. For example, consider the stratified random sample described in Table 5-3. If these data were incorrectly analyzed as though they came from a simple random sample, then the biased estimate of producer's accuracy for old-growth would be $22/25=88.0\%$ (Table 5-3A) rather than the unbiased estimate of $2.8/7.3=38.4\%$

Table 5-8. Estimators for simple random sampling and stratified random sampling, where each map category is a stratum.

Sampling estimation symbols, descriptions, and equations	
Symbol	Description
i	Row subscript, which designates the Map Classifier in the error matrix, and stratum i in stratified random sampling
j	Column subscript, which designates the Reference Classifier in the error matrix
n_{ij}	Number of sample points in row i and column j
$n_{i\bullet}$	Total number of sample points in row i
n	Total number of sample points
η_k	"Effective" sample size for estimate k , which is used to approximate the confidence interval with certain estimates
A	Total area of sampled population (known exactly from GIS)
$A_{\bullet j}$	Total area of sampled population in class i had all Map Objects been classified with the Reference Classifier (estimated from accuracy assessment sample)
$A_{i\bullet}$	Total area of sampled population in map class i (known exactly from GIS)
p_{ij}	Proportion of sampled population classified as category i by the Map Classifier and category j by the Reference Classifier
$p_{i\bullet j}$	Proportion of sampled population in which the Map and Reference Classifiers agree (i.e., overall accuracy)
$p_{i\bullet}$	Proportion of sampled population classified as category i by the Map Classifier
$p_{\bullet j}$	Proportion of sampled population classified as category j by the Reference Classifier
$p_{j=Y i=X}$	Proportion of sampled population in reference category class Y given that the map classification is category X . For $X=Y$, $p_{j=Y i=X}$ equals "user's accuracy."
$p_{i=X j=Y}$	Proportion of sampled population in map class X given that the reference classification is category Y . For $X=Y$, $p_{i=X j=Y}$ equals "producer's accuracy."

Sampling estimation symbols, descriptions, and equations	
$\text{var}(p)$	Variance of the estimated proportion p
Simple Random Sample	
$\hat{p}_{ij} = \frac{n_{ij}}{n}$, $\text{var}(\hat{p}_{ij}) = \hat{p}_{ij}(1 - \hat{p}_{ij})/n$	
$\hat{p}_{i\bullet} = \sum_j \frac{n_{ij}}{n}$, $\text{var}(\hat{p}_{i\bullet}) = \frac{\hat{p}_{i\bullet}(1 - \hat{p}_{i\bullet})}{n}$	
$\hat{p}_{\bullet j} = \sum_i \frac{n_{ij}}{n}$, $\text{var}(\hat{p}_{\bullet j}) = \frac{\hat{p}_{\bullet j}(1 - \hat{p}_{\bullet j})}{n}$	
$\hat{p}_{i=j} = \sum_i \frac{n_{ij}}{n}$, $\text{var}(\hat{p}_{i=j}) = \frac{\hat{p}_{i=j}(1 - \hat{p}_{i=j})}{n}$	
$\hat{p}_{j=Y i=X} = \frac{\hat{p}_{ij}}{\hat{p}_{i\bullet}}$, $\text{var}(\hat{p}_{j=Y i=X}) = \frac{(\hat{p}_{i\bullet} - \hat{p}_{ij})\hat{p}_{ij}}{n\hat{p}_{i\bullet}^3}$	
$\hat{p}_{i=X j=Y} = \frac{\hat{p}_{ij}}{\hat{p}_{\bullet j}}$, $\text{var}(\hat{p}_{i=X j=Y}) = \frac{(\hat{p}_{\bullet j} - \hat{p}_{ij})\hat{p}_{ij}}{n\hat{p}_{\bullet j}^3}$	
Stratified random sample (stratum = i)	
$\hat{p}_{ij} = \left(\frac{n_{ij}}{n_{i\bullet}}\right) \hat{p}_{i\bullet}$, $\text{var}(\hat{p}_{ij}) = \frac{\hat{p}_{ij}(\hat{p}_{i\bullet} - \hat{p}_{ij})}{n_{i\bullet}}$	
$p_{i\bullet} = A_{i\bullet}/A$, $\text{var}(p_{i\bullet}) = 0$	
$\hat{p}_{\bullet j} = \sum_i \hat{p}_{ij}$, $\text{var}(\hat{p}_{\bullet j}) = \sum_i \text{var}(\hat{p}_{ij})$	
$\hat{p}_{i=j} = \sum_i \hat{p}_{ii}$, $\text{var}(\hat{p}_{i=j}) = \sum_i \text{var}(\hat{p}_{ii})$	
$\hat{p}_{j=Y i=X} = \frac{\hat{p}_{ij}}{\hat{p}_{i\bullet}}$, $\text{var}(\hat{p}_{j=Y i=X}) = \frac{\hat{p}_{j=Y i=X}(1 - \hat{p}_{j=Y i=X})}{n_{i\bullet}}$	
$\hat{p}_{i=X j=Y} = \frac{\hat{p}_{ij}}{\hat{p}_{\bullet j}}$, $\text{var}(\hat{p}_{i=X j=Y}) = \left(\frac{\hat{p}_{ij}^2}{\hat{p}_{\bullet j}^4}\right) \text{var}(\hat{p}_{\bullet j}) - \left(\frac{2\hat{p}_{ij} - \hat{p}_{\bullet j}}{\hat{p}_{\bullet j}^3}\right) \text{var}(\hat{p}_{ij})$	
Effective sample size for each of the above estimators	
$\eta_e = p_k(1 - p_k)/\text{var}(p_k)$, for $k = \{ij; i=j \text{ or } \bullet; i=X j=Y; j=Y i=X\}$	
Conversion of proportions to areas for each of the above estimators	
$\hat{A}_k = \hat{p}_k A$, $\text{var}(\hat{A}_k) = \text{var}(\hat{p}_k)A^2$, for $k = \{ij; i=j \text{ or } \bullet; i=X j=Y; j=Y i=X\}$	
Cohen's kappa coefficient of agreement	
See Hudson & Ramm (1987), Czaplewski (1994), Campbell (1996), Stehman (1996)	

in Table 5-3B. Likewise, the biased estimate for the true area of old-growth would be $(25/100) \cdot 1000000 = 250,000$ ha from Table 5-3A, whereas the unbiased estimate from Table 5-3B is 73,070 ha. Table 5-8 compares the estimators for accuracy assessment statistics for both sampling designs.

Often overlooked is the effect of random sampling error on estimated accuracy statistics. Any sample estimate includes uncertainty because inference is made for the entire population based on a very small sample of that population. Sometimes this uncertainty can be large. For example, Tables 5-1 and 5-3B provide different estimates for the same sampled population. The extent of old-growth forest in the sampled population that is actually mapped as old-growth (i.e., producer's accuracy) is estimated to be 60.0 % from Table 5-1 and 38.4 % from Table 5-3B. Likewise, the true total area of old-growth forest in the sampled population is estimated at 100,000 ha with Table 5-1 and 73,070 ha with Table 5-3B. All of these are unbiased because estimates from the two different sampling designs would converge on the same true value given a sufficiently large sample size. The differences among estimates are caused by different degrees of random sampling error. The magnitude of sampling error can be objectively estimated from "variance statistics" (Table 5-8) and communicated as confidence intervals Tables 5-4 to 5-8).

2.3.1 Confidence intervals for accuracy assessment statistics

Confidence intervals are important to interpretation of statistics from any probability sample. For example, the 90 % confidence interval for overall accuracy in Table 5-1 is 68 % to 83 % (i.e., there is a 5 % chance that the true accuracy is less than 68 %, and another 5 % chance that the true accuracy is greater than 83 %). If a similar estimate were obtained with a sample size of 20 points, then the 90 % confidence interval would be 54 % to 90 % (Table 5-5). If an overall accuracy of 70 % is required from the sampled portion of the map, then a sample size of 20 points is insufficient to determine success with much confidence. Another example is the estimated area of old-growth forest in Table 5-3B, which is 7 % or 70,000 ha. From Table 5-8, the estimated variance is $\text{var}(p_{*2})=0.000672$, which gives an effective sample size of $\eta_{*2} = 101$ (Table 5-8). The approximate 90 % confidence interval is 3 % to 13 % of the sampled population (interpolated from Table 5-5), which equals 30,000 ha to 130,000 ha. If a similar estimate were made from a stratified random sample of 1000 points, then the 90 % confidence interval would be 6 % to 9 % or 60,000 ha to 90,000 ha. If confidence intervals are ignored, then there is a high risk of misinterpreting the results of an accuracy assessment.

2.3.2 Confidence coefficient

Figure 5-1 and Tables 5-4 to 5-7 give confidence intervals for the 95 %, 90 %, 80 % and 50 % confidence coefficients. The choice of the confidence coefficient depends on the risks of incorrect inference to the user of the thematic map. If the user needs to be relatively certain that the true value is within the confidence interval, then the 95 % level would be a good choice. There is only a 2.5 % chance that the true value is less than the lower bound of the confidence interval, and another 2.5 % chance that the true value exceeds the upper bound of the interval. If more risk is acceptable, then the 50 % level could be used; there would be a 25 % chance that the true value is less than the lower bound of the confidence interval, and another 25 % chance that the true value exceeds the upper bound of the interval. For example, assume a mapped stratum is sampled with 50 points; and assume that the estimate of user's accuracy is 90 % (i.e., 45 of the 50 points are classified as forest with the reference data). The confidence interval at the 95 % level for the estimate of user's accuracy would be 78.2 % to 96.7 % (Table 5-4), while the confidence interval for the same estimate at the 50 % level would be 85.5 % to 93.2 % (Table 5-7).

2.3.3 Computation of confidence intervals

Confidence intervals can be interpolated from Tables 5-4 to 5-7. However, these functions are non-linear, and interpolations can be inaccurate, especially for sample sizes that vary considerably from those in the tables. Alternatively, several confidence interval calculators for proportions (i.e., the binomial distribution) are available on the Internet.

Table 5-8 provides approximate methods to estimate confidence intervals using an "effective sample size" (η_e) with Tables 5-4 to 5-7. This procedure will yield the exact interval, except for any statistic that is a ratio of two estimates (e.g., producer's accuracy). In this latter case, the confidence interval computation requires a Taylor-series approximation for the estimated variance, plus the beta-binomial distribution and specialized software for a numerical solution. In this case, use of an effective sample size with the binomial distribution is a convenient approximation. The effective sample size can be a non-integer, and is rounded to the nearest integer value.

2.3.4 Cells that equal zero and perfect accuracy

Through random sampling error, a cell in the error matrix, usually representing a classification error, can have a value of zero. The true value is

likely small, but greater than zero. Tables 5-4 to 5-7 include confidence intervals that cover such unobserved cross-classifications. For example, in Table 5-1, there were no cases among the $n=100$ sample points in which the map classification is old-growth forest and the reference classification is non-forest. Therefore, the estimated proportion of the map that is classified as old-growth forest and is truly non-forest is 0. However, from Table 5-5, the 90 % confidence interval for this estimate is 0 % to 3 %, or up to 30,000 ha; this means that there is an estimated 10 % chance that the true number of hectares so cross-classified exceeds 30,000 ha. A similar situation arises when all sample points are correctly classified, which is most likely observed with producer's or user's accuracy for rare category. For example, assume that the producer's accuracy is estimated at 100 % with an effective sample size of $\eta_e=10$. From Table 5-5, the approximate 90 % confidence interval would be 74.1 % to 100 %, meaning that there is a 10 % chance that the true producer's accuracy for that category is less than 74.1 %. See Lloyd (1999) for a more detailed summary of these issues.

2.4 Quality assurance

In addition to the usual care required during data collection and management, other steps can help assure the quality of an accuracy assessment. One very useful diagnostic tool is estimation of known values with the sample of reference points and the selected analysis design (i.e., Steps 1 and 3 above). If the sample estimates do not reasonably agree with the known values, then a procedural error is likely. For example, the sampled area of the map labeled as non-forest in Table 5-1 is exactly 549,020 ha, which is determined through a tally of all Map Objects in the GIS or image processing system. The same area estimated from the 100 sample points is 440,000 ha, with a 95 % confidence interval of 341,000 ha to 543,000 ha (interpolated with Table 5-5). This confidence interval does not cover the known true value; there is less than a 5 % chance that the true value (549,020 ha) is outside the bounds of the 95 % confidence interval (i.e., more than 543,000 ha or less than 341,000 ha). In one out of every 20 accuracy assessments, an unfortunate, but valid, random sample of points could cause this degree of apparent discrepancy. However, this discrepancy remains weak evidence for a potential procedural error. For example, the sampled population used to draw the sample might be defined differently than the sampled population used to tally the area statistics in Table 5-1. Displaying the location of all sample points on a map base might reveal geographic areas that were unknowingly omitted from the sampled population. Alternatively, a stratified random sample might have been analyzed as though it was a simple random sample, or the thematic map

might have been modified after the stratified sample was drawn. Whenever possible, diagnostic tests should be conducted before gathering expensive reference data in Step 2 to detect procedural errors in Steps 1 and 3.

In the case of stratified random sampling, the thematic map is used to define strata, and different comparisons must be used to detect discrepancies. For example, the stratified sample of points could be used to estimate the known areas of different soil types, elevation zones, or administrative areas in a GIS database.

2.5 Interpretation of results

The investment in a valid accuracy assessment has little value unless the results are effectively communicated to the user. This Chapter has already presented examples of informative statistics and their interpretations. The producer of an accuracy assessment should provide similar interpretations for their own error matrix. Stacked bar charts can provide a visual display of a large error matrix, and such displays can provide insights. The full error matrix or fuzzy-set contingency table should be published as metadata, thus maximizing options for alternative interpretations.

The terms “Producer’s Accuracy” and “User’s Accuracy” are prevalent in today’s remote sensing literature, but these terms are somewhat misleading. Both types of statistics are important to both the producer of a remotely sensed map and a user of that map. These and other conditional probabilities are more useful statistics than widely recognized. For example, Table 5-1 estimates that only 60 % of the old-growth forest, as defined in Step 2, is labeled as old-growth forest on the map; an estimated 40 % of the old-growth forest truly exists in the sampled population, but it is mislabeled as something else on the map, and its location is unknown on the map. As another example, Table 5-1 estimates that the old-growth forest category on the map is truly composed of 75 % old-growth forest and 25 % other types of forest. Therefore, the conditional probabilities from the error matrix document the composition of each thematic category as metadata.

Marginal proportions are also important metadata. For example, Table 5-3B estimates that the true extent of old-growth forest is 73,070 ha within the sampled population, with a 90 % confidence interval of 33,000 ha to 126,000 ha. However, only 41,634 ha are mapped as old-growth forest, and only 75 % of that mapped area is estimated to be truly old-growth forest in the sampled population. Therefore, analyses with the thematic map will likely underestimate attributes associated with old-growth forest. Both misclassification error and random sampling error cause these differences between the map and estimates of the true exist conditions. Czaplewski (1992) discusses these “discrepancies” in more detail.

3. CONCLUDING REMARKS

There is a large body of remote sensing literature devoted to accuracy assessments. However, this chapter is limited to a few techniques that are simple and robust. The goal is to provide methods that can be applied by professionals who have no training in sample survey statistics. Large mapping projects often use elements that are more complex (e.g., cluster plots, two-phase and two-stage sampling, alternative stratification materials, multiple sampling frames) to reduce costs and improve efficiency (Stehman and Czaplewski 1998; Czaplewski 2000). However, complex designs require consultation with a statistician knowledgeable in sample surveys. Otherwise, there is high risk of using invalid methods that produce unreliable and biased estimates of accuracy assessment statistics. The bias can be large and can lead to unwise decisions.

Too often, the number of sample sites for reference data is inadequate for sufficiently precise estimates of accuracy assessment statistics. For example, assume the true user's accuracy for old-growth forest is 75 %. Unfortunately, this true value is never known in real-world applications, and an imperfect estimate from a sample is typically the best available information. With an effective sample size of 20 reference sites, there is about one chance in four that the estimated accuracy will be less than 65 %, even though the true accuracy is 75 %. However, with a sample of 50 reference sites, there is only about one chance in 10 that the estimated accuracy will be less than 65%. A closely related issue is precision of area estimates. For example, assume old-growth forest truly covers 120,000 ha of a 1,000,000 ha sampled population. With an effective sample size of 20 reference sites, there is about one chance in four that the extent of old-growth forest will be estimated at 50,000 ha or less. However, with a sample of 50 reference sites, the probability of this degree of underestimation decreases to one in 10. This chapter recommends that a hypothetical, although realistic, error matrix be constructed during the early planning phase of the accuracy assessment. If precision of hypothetical assessment statistics appears inadequate, then the number of reference sites should be increased, or the accuracy assessment should be omitted. There is no real value in expending scarce resources on an unreliable assessment.

The best data that can be realistically produced are imperfect estimates of classification accuracies and the true area of different forest conditions, and an imperfect map of where those conditions are located. The goal of image classification and accuracy assessment is to minimize these imperfections, and reduce the risk of mis-informed decisions, within a reasonable budget. This Chapter provides methods that can help achieve this goal.

REFERENCES

- Campbell, J.B. (1996). *Introduction to Remote Sensing* (2nd ed.). Guilford Press, New York.
- Cochran, W. G. (1977). *Sampling Techniques* (3rd ed.). John Wiley & Sons, New York.
- Congalton, R. G. (1991). A review of assessing the accuracy of classifications of remotely sensed data. *Remote Sensing of Environment*, 37, 35-46.
- Czaplewski, R. L. (1992). Misclassification bias in areal estimates. *Photogrammetric Engineering and Remote Sensing*, 58, 189-192.
- Czaplewski, R. L. (1994). Variance approximations for assessments of classification accuracy. *Research Paper RM-316*. Fort Collins, CO: U.S. Department of Agriculture, Forest Service, Rocky Mountain Research Station.
- Czaplewski, R. L., & Catts, G. P. (1992). Calibration of remotely sensed proportion or area estimates for misclassification error. *Remote Sensing of Environment*, 39, 29-43.
- Czaplewski, R. L. (2000). Accuracy assessments and areal estimates using two-phase stratified random sampling, cluster plots, and the multivariate composite estimator. *Quantifying Spatial Uncertainty in Natural Resources: Theory and Applications for GIS and Remote Sensing*, 79-100. Ann Arbor Press, Chelsea, MI.
- Gopal, S., & Woodcock, C. (1994). Theory and methods for accuracy assessment of thematic maps using fuzzy-sets. *Photogrammetric Engineering and Remote Sensing*, 60, 181-188.
- Hudson, W. D., & Ramm, C. W. (1987). Correct formulation of the kappa coefficient of agreement. *Photogrammetric Engineering and Remote Sensing*, 53, 421-422.
- Lloyd, C. J. (1999) *Statistical Analysis of Categorical Data* (3rd ed.). John Wiley & Sons, New York.
- Lohr, S. L. (1999). *Sampling: Design and Analysis*. Brooks/Cole Publishing, Pacific Grove, CA.
- Salant, P., & Dillman, D. A. (1994). *How to conduct your own survey*. John Wiley & Sons, New York.
- Särndal, C. -E., Swensson, B., & Wretman, J. (1992). *Model-assisted survey sampling*. Springer-Verlag, New York.
- Schreuder, H. T., Gregoire, T. G., & Wood, G. (1993). *Sampling methods for multiresource forest inventory*. John Wiley & Sons, New York.
- Stehman, S.V. (1996). Estimating the kappa coefficient and its variance under stratified random sampling, *Photogrammetric Engineering and Remote Sensing*, 62, 401-407.
- Stehman, S.V. (2002). Response to letter by G. Turk on chance correction and map evaluation. *Remote Sensing of Environment*, 82, 4.
- Stehman, S. V., & Czaplewski, R. L. (1998). Design and analysis for thematic map accuracy assessment: fundamental principles. *Remote Sensing of Environment*, 64, 331-344.
- Stehman, S. V. (2001). Statistical rigor and practical utility in thematic map accuracy assessment. *Photogrammetric Engineering and Remote Sensing*, 67, 727-734.
- Story, M., & Congalton, R. G. (1986). Accuracy assessment: a user's perspective. *Photogrammetric Engineering and Remote Sensing*, 52, 397-399.

SECTION 2: COMMON METHODS FOR DATA PROCESSING AND INFORMATION GENERATION

Chapter 6

GEOMETRIC CORRECTION OF REMOTELY SENSED IMAGES

Thierry Toutin

Natural Resources Canada, Canada Centre for Remote Sensing, 588 Booth Street, Ottawa, Ontario, K1A 0Y7, Canada

1. INTRODUCTION

Remotely sensed images usually contain geometric distortions so significant that they cannot be used directly with base map products in a geographic information system (GIS). Consequently, multi-source data integration (raster and vector) for cartographic applications, such as forestry, requires geometric and radiometric processing adapted to the nature and characteristics of the data in order to keep the best information from each image in the composite ortho-rectified image.

The processing of multi-source data can be based on the concept of "terrain-geocoded images", a term originally invented in Canada in defining value-added products (Guertin and Shaw 1981). Photogrammetrists, however, prefer the term "ortho-image", referring to a unit of terrain-geocoded data, in which all distortions, including the relief, are corrected. According to this concept, each raw image must, before integration, be separately converted to an ortho-image so that each component ortho-image of data set can be registered, compared, combined, etc. pixel by pixel within the set and also with cartographic vector data in a GIS.

Although geometric distortions have always been present in remotely sensed images, they have become a more significant problem in recent years. In 1972, the impact of the distortions was quite negligible for the following reasons (Toutin 1996):

- The images, such as Landsat-MSS, were nadir viewing and the resolution was coarse (around 80-100 m);

- The products resulting from the image processing were analogue on paper;
- The interpretation of the final products was performed visually; and
- The fusion and integration of multi-source and multi-format data did not exist.

Today, however, the impact of the distortions is no longer negligible because:

- The images are off-nadir viewing and the resolution is fine (sub-meter level);
- The products resulting from image processing are fully digital;
- The interpretation of the final products is realised on computer;
- The fusion of multi-source images (different platforms and sensors) is in general use; and
- The integration of multi-format data (raster/vector) is a general tendency in geomatics.

Advances in every aspect of remote sensing—the quality of acquired data, data processing, analysis and interpretation—since the 1970s, have made it ever more important to accurately apply corrections to these geometric distortions.

Although the literature is quite abundant, mainly in terms of peer review articles, it is important to update this body of knowledge with the latest developments and research studies from around the world. An exhaustive list of books, journals and papers are given at the end of this Chapter.

This Chapter will address:

- The source of geometric distortions and deformations with different categorisations (section 2);
- The modelling of the distortions with different models and mathematical functions (section 3); and
- The geometric correction method with processing steps and errors (section 4).

Comparisons between the models and mathematical functions, their applicability and their performance on different types of images (frame camera, Visible and Infra-Red (VIR) oscillating or push-broom scanners, Synthetic Aperture Radar (SAR) sensors, high or medium resolution) are also addressed. The errors, together with their propagation from the input data to the final results, are also evaluated through the full processing steps.

2. GEOMETRIC DISTORTIONS AND MODELS

2.1 Distortion sources

Each image acquisition system (Figure 6-1) produces unique geometric distortions in its raw images; consequently the geometry of these images does not correspond to the terrain, nor to end-user maps. The geometric distortions vary considerably with different factors such as the platform (airborne versus satellite), the sensor (low to high resolution) and the total field of view. However, it is possible to make general categorisations of these distortions.

The sources of distortion can be grouped into two broad categories: 'observer' distortions, caused by the acquisition system (platform, imaging sensor and other measuring instruments, such as gyroscope, stellar sensors, etc.), and 'observed' distortions, introduced by atmosphere and the Earth. Deformations related to map projection are also included in the 'observed' distortion category. Terrain and most GIS end-user applications are generally represented and performed respectively in a topographic space, not in the geoid or a referenced ellipsoid, leading to inconsistencies between maps and remotely sensed data. Table 6-1 describes in more detail the sources of distortion for each category and sub-category. Figures 6-1 and 6-2 illustrate the geometry of acquisition and the elliptical orbit approximation of remote sensing satellites around the Earth, respectively.

Table 6-1. Description of error sources for the two categories, "the observer" and "the observed", and the different sub-categories.

Category	Sub-category	Description
The Observer (The Acquisition System)	Platform	Variation of the elliptic movement (Figure 6-2) Variation in platform attitude (low to high frequencies)
	Sensor	Variation in sensor mechanics (scan rate, scanning velocity, etc.) Viewing/look angles
	Measuring instruments	Panoramic effect with field of view Time-variations or drift Clock synchronicity
The Observed	Atmosphere	Refraction and turbulence
	Earth	Curvature, rotation, topographic effect
	Map	Geoid to ellipsoid Ellipsoid to map

Previous studies made a second-level categorisation into low, medium and high frequency distortions (Friedmann et al. 1983), where "frequency" is determined by or compared to the image acquisition time. Examples of low,

medium and high frequency distortions are orbit variations, Earth rotation, and local topographic effects, respectively. The proliferation of acquisition system designs since the 1980s has, however, rendered this classification system obsolete. For example, attitude variation is a high-frequency distortion for Quickbird or airborne push-broom scanner, a medium-frequency distortion for SPOT and Landsat ETM+ and a low-frequency distortion for Landsat MSS.

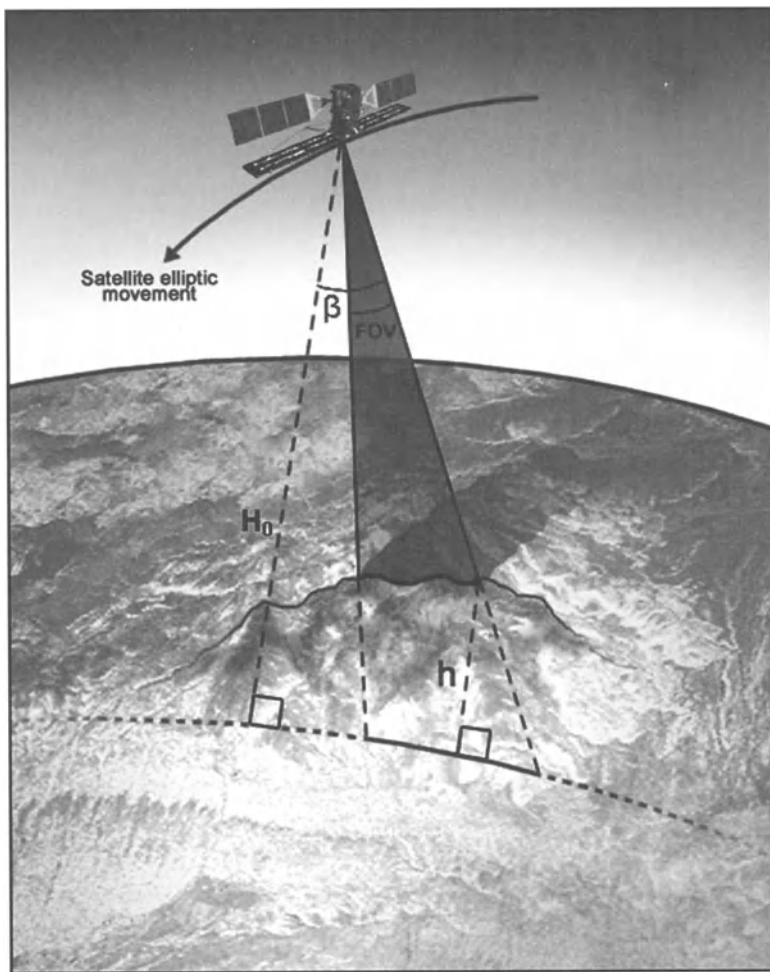


Figure 6-1. Geometry of viewing of a satellite scanner in orbit around the Earth. H_0 is the satellite altitude; h is the terrain elevation; β is the viewing/look angle; and FOV is the field of view.

The geometric distortions of Table 6-1 are predictable or systematic and generally well understood. Some of these distortions, especially those related to the instrumentation, are generally corrected at ground receiving stations or

by image vendors. Others, for example those related to the atmosphere, are not taken into account or corrected because they are specific to each acquisition time and location and information on the atmosphere is rarely available. They also are negligible for low-to-medium resolution images.

The remaining distortions associated with the platform (Figure 6-2) are mainly orbit and Earth related (elliptic movement, Earth gravity, shape and movement) (Escobal 1965; CNES 1980; Light et al. 1980). Depending on the acquisition time and the size of the image, the orbital perturbations may cause a range of distortions. Some effects include:

- Platform altitude variation in combination with sensor focal length, Earth's flatness and terrestrial relief can change the pixel spacing;
- Platform attitude variation (roll, pitch and yaw) can change the orientation and the shape of VIR images; it does not affect SAR image geometry;
- Platform velocity variations can change the line spacing or create line gaps/overlaps.

The remaining sensor-related distortions include:

- Calibration parameter uncertainty such as in the focal length and the instantaneous field of view (IFOV) for VIR sensors or the range gate delay (timing) for SAR sensors;
- Panoramic distortion in combination with the oblique-viewing system, Earth curvature and topographic relief changes the ground pixel sampling along the column.

The remaining Earth-related distortions include (Figure 6-1):

- Rotation, which generates latitude-dependent displacements between image lines;
- Curvature, which for large width image creates variation in the pixel spacing;
- Topographic relief, which generates parallax in the scanner direction.

The remaining deformations associated with the map projection are:

- The approximation of the geoid by a reference ellipsoid;
- The projection of the reference ellipsoid on a tangent plane.

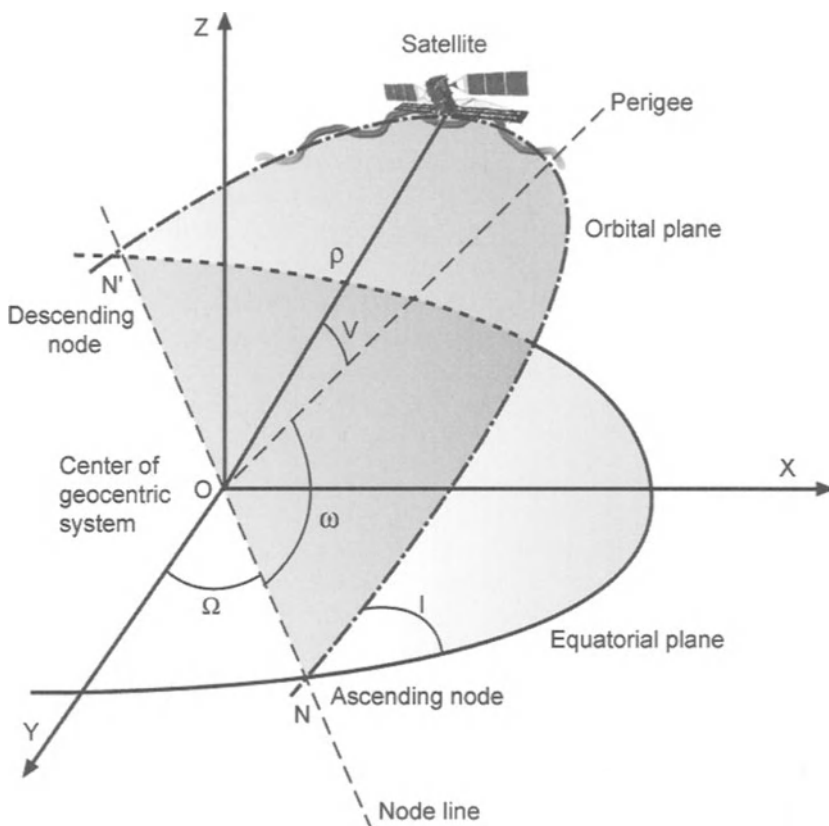


Figure 6-2. Description of a satellite orbit and its approximation by an ellipse. XYZ are the geocentric frame reference system. Different osculatory parameters describe the ellipse and the satellite position: e.g., Ω is the longitude of the ascending node (N); i is the orbit inclination; ω is the argument of the perigee (P); $(\omega + v)$ is the argument of the satellite; ρ is the distance from the Earth centre (O) and the satellite (Toutin 1983).

All of these remaining geometric distortions require models and mathematical functions to perform geometric corrections of imagery: either through 2D/3D non-parametric models (such as 2D/3D polynomial or 3D rational functions) or with rigorous 3D parametric models. With 3D parametric models, geometric correction can be performed step-by-step with a mathematical function for each distortion or simultaneously with a “combined” mathematical function. The first solution is generally applied at the ground receiving station when the image distributors sell value-added products (geo-referenced, map oriented or geocoded), while the end-users generally prefer and use the last solution.

2.2 2D/3D non-parametric models

The 2D/3D non-parametric models, based on different mathematical functions (Table 6-2), can be used when the parameters of the acquisition systems or a rigorous 3D parametric model are not available. Since they do not reflect the source of distortions described previously, these models do not require *a priori* information on any component of the total system (platform, sensor, Earth and map projection).

Table 6-2. Mathematical equations and numbers of unknown terms for the different geometric models. For each geometric model there are two equations. In some conditions, specific terms, such as XY^2 for 2D or XZ , YZ^2 or Z^3 , etc. for 3D, can be dropped of the polynomial functions, when these terms can not be related to any physical element of the image acquisition geometry; it also reduces correlation between terms.

Geometric Models	Mathematical Functions* P_{2D} , P_{3D} & R_{3D}	Number of unknown terms
2D Polynomial	$P_{2D}(XY) = \sum_{i=0}^m \sum_{j=0}^n a_{ij} X^i Y^j$	1 st order: 3 + 3 2 nd order: 6 + 6 3 rd order: 10 + 10
3D Polynomial	$P_{3D}(XYZ) = \sum_{i=0}^m \sum_{j=0}^n \sum_{k=0}^p a_{ijk} X^i Y^j Z^k$	1 st order: 4 + 4 2 nd order: 10 + 10 3 rd order: 20 + 20
3D Rational	$R_{3D}(XYZ) = \frac{\sum_{i=0}^m \sum_{j=0}^n \sum_{k=0}^p a_{ijk} X^i Y^j Z^k}{\sum_{i=0}^m \sum_{j=0}^n \sum_{k=0}^p b_{ijk} X^i Y^j Z^k}$	1 st order: 8 + 8 2 nd order: 20 + 20 3 rd order: 40 + 40

* X, Y, Z are the cartographic co-ordinates; i, j, k are integer increments; m, n and p are integer values, generally comprised between 1 and 3 with m + n + p being the order of the polynomial functions.

2.2.1 2D Polynomial Functions

Since the 2D polynomial functions, with their formulation, have been well known and documented for the last 20 years (Billingsley 1983), only a few characteristics are given. The polynomial functions of the 1st order (6 terms) only allow for correcting a translation in both axes, a rotation, scaling in both axes and an obliquity (Table 6-2). The polynomial functions of the 2nd order (12 terms) allow for correction, in addition to the previous

parameters, torsion and convexity in both axes. The polynomial function of the 3rd order (20 terms) allows for correction of the same distortions as a 2nd order polynomial function with others, which do not necessarily correspond to any physical reality of the image acquisition system. In fact, previous research studies demonstrated that 3rd order polynomial functions introduce errors in the relative pixel positioning in ortho-images (Caloz and Collet 2001) or in geocoding and integration of multi-sensor images (Toutin 1995a).

Since the 2D polynomial functions do not reflect the sources of distortion during image formation and do not correct for terrain relief distortions, they are limited to images with few or small distortions, such as nadir-viewing images, systematically-corrected images and/or small images over flat terrain. Since these functions correct for local distortions at the ground control point (GCP) location they are very sensitive to input errors; hence GCPs have to be numerous and regularly distributed. Consequently, these functions should not be used when precise geometric positioning is required for multi-source / multi-format data integration.

The 2D polynomial functions were used mainly in the 70's and 80's, on images (Billingsley 1983) whose systematic distortions, excluding the relief, had already been corrected for by the image providers. As mentioned in the Introduction, good geometric accuracy was not a key point in the analysis of analogue images. However, while it is now known that 2D polynomial functions are not suitable for accurately correcting remotely sensed images, some users still apply them, apparently without knowing the implications for subsequent processing operations and resulting digital products. Some comparisons of processing and of results based on 2D polynomial and 3D parametric functions will be provided in a later section.

2.2.2 3D Polynomial Functions

The 3D polynomial functions are an extension of the 2D polynomial function by adding Z-terms related to the third dimension of the terrain (Table 6-2). However, apart from relief they are prone to the same problems as other non-parametric functions, i.e. they are applicable to small images, they need numerous regularly distributed, GCPs they correct locally at GCPs, they are very sensitive to errors and they lack robustness and consistency in operational environments. Their use should thus be limited to small or systematically corrected images, where all distortions except the relief have been pre-corrected.

3D polynomial functions have been recently used with the following geo-referenced image data sets: SPOT-HRV (level 1B), Landsat TM (level bulk or geo-referenced) (Palà and Pons 1995) and IKONOS Geo-products

(Hanley and Fraser 2001). Kratky (1989) used 3rd order 3D polynomial functions to approximate a 3D parametric model developed for SPOT raw images in order to reduce the computing time for implementing his solution on-line into a stereo-workstation. One reason was that the real-time computation of his preferred mathematical model was not feasible.

The terms related to terrain elevation in the 3D polynomial function could be reduced to a_iZ for VIR images and to a_iZ and a_jZ^2 for SAR images, whatever the order of the polynomial functions used. The main reason is that there is no physical interrelation in the X and Z or Y and Z directions for most of the sensors used.

2.2.3 3D rational functions

3D rational functions have recently drawn interest from the civilian photogrammetric and remote sensing communities, due to the launch of the civilian high-resolution IKONOS sensor in 1999, and subsequently EROS-A1 and QuickBird-2 sensors in 2000 and 2001, respectively. The major reason for their recent interest is that Space Imaging does not release information on the IKONOS satellite and the sensor. The 3D rational functions can be used in two ways:

1. To approximate an already-solved existing 3D parametric model; and
2. To normally compute the unknowns of all the polynomial functions with GCPs.

The first approach is performed in two steps. A 3D regular grid of the imaged terrain is first defined and the image co-ordinates of the 3D grid ground points are computed using the already-solved existing 3D parametric model. These grid points and their 3D ground and 2D image co-ordinates are then used as GCPs to resolve the 3D rational functions and compute the unknown terms of polynomial functions.

This approach has proven adequate for aerial photographs and satellite images (Tao and Hu 2001a). However, they found that the results are very sensitive to GCP distribution for SPOT images. When the image is too large, the image itself has to be subdivided and separate 3D rational functions are required for each sub-image. It sometimes results in “less user-friendly” processing than a 3D parametric model. Image vendors or government agencies that do not want to deliver satellite/sensor information with the image are the main users of this piecewise approach. They thus provide with the image all the parameters of 3D rational functions. Consequently, the user can directly process the images for generating ortho-images or DEM or even post-process to improve the rational function parameters. However, this approach is considered unsuitable for endusers because it requires knowledge of a 3D parametric model. In this situation, the user can directly

use and apply the 3D parametric model. Furthermore, this approximation of a 3D parametric model will not generally be as precise as the 3D parametric model itself.

The second approach can be performed by the endusers with the same processing method as with polynomial functions. Since there are 40 and 80 parameters for the four 2nd and 3rd order polynomial functions (Table 6-2), a minimum of 20 and 40 GCPs, respectively are required to resolve the 3D rational functions. However, the rational functions, such as the 2D/3D polynomial functions, do not model the physical reality of the image acquisition geometry and are sensitive to input errors. Consequently in an operational environment, many more GCPs will be required to reduce their error propagation.

Rational functions, such as the 2D/3D polynomial functions, mainly correct locally at GCP locations, and the distortions between GCPs are not entirely eliminated. A piecewise approach as described previously should then be used for large images (SPOT, Landsat, IRS), however the number of GCPs will increase proportionally to the number of sub-images, making the method impractical.

In conclusion, the 3D rational functions are certainly the best selection among the non-parametric functions, but only when no 3D parametric solution, such as described below, is available.

2.3 3D parametric functions

3D parametric functions to perform geometric correction differ depending on the sensor, the platform and its image acquisition geometry:

- The instantaneous acquisition systems, such as photogrammetric cameras, Metric Camera (MC) or Large Format Camera (LFC);
- The rotating or oscillating scanning mirrors, such as Landsat-MSS, TM or ETM+;
- The push-broom scanners, such as SPOT-HRV, IRS-1C/D, IKONOS or Quickbird;
- The SAR sensors, such as ERS-1/2, RADARSAT-1/2 or ENVISAT.

It is possible to create an overall model for the development of 3D parametric functions, which will take into account the unique characteristics of each platform and which will fully correct all distortions described previously. The 3D parametric functions should model the distortions of the platform (position, velocity, attitude for VIR sensors), the sensor (viewing angles, panoramic effect), the Earth (ellipsoid and relief) and the cartographic projection. The geometric correction process can address each distortion one by one and step by step or simultaneously. It is better to consider the overall viewing geometry (platform + sensor + Earth + map),

because some of the distortions are correlated and have the same type of impact on the ground. It is theoretically more precise to compute one “combined” parameter only than each component of this “combined” parameter, separately.

Some examples of “combined” parameters include:

- The “orientation” of the image is a combination of the platform heading due to orbital inclination, the yaw of the platform and the convergence of the meridian;
- The “scale factor” in the along-track direction is a combination of the velocity, the altitude and the pitch of the platform, the detection signal time of the sensor and the component of the Earth’s rotation in the along-track direction; the “levelling angle” in the across-track direction is a combination of platform roll, the viewing angle, the orientation of the sensor and the Earth’s curvature.

Considerable research has been carried out to develop robust and rigorous mathematical models describing the acquisition geometry related to different types of image (VIR and SAR) and of platforms (spaceborne and airborne) (Table 6-3). The starting point of these studies is generally the well-known collinearity condition and equations (Wong 1980) for VIR images and the Doppler and range equations for radar images (Curlander 1986) (Table 6-4). It should be noted that the collinearity equations were adapted as radargrammetric equations to process radar images (Leberl 1972; 1990; Konecny et al. 1986) and later as integrated and unified mathematical equations to indiscriminately process VIR or radar images (Toutin 1995b).

Table 6-3. References on research studies for the development of 3D parametric models applied to different platforms and sensors.

Platforms and Sensors	Airborne	Spaceborne
Medium Resolution VIR		Friedmann et al. (1983); Gugan (1987); Guichard (1983); Khizhnichenko (1982); Konecny et al. (1987); Kratky (1989); de Masson d'Autume (1979); Paderes et al. (1989); Salamonowicz (1986); Sawada et al. (1981); Toutin (1983); Westin (1990)
High Resolution VIR	Ebner and Muller (1986); Gibson (1984); Hoffmann and Muller (1988)	Dial and Grodecki (2002); Toutin (2001, 2002b); Toutin and Cheng (2000, 2002); Toutin et al. (2002)
SAR	Derenyi (1970) Gracie et al. (1970); Konecny and Schuhr (1984); La Prade, (1963); Leberl (1972); Rosenfield (1968); Toutin et al. (1992)	Curlander (1982); Guindon and Adair (1992); Leberl (1978); Naraghi et al. (1983); Toutin and Carboneau (1992)

Table 6-4. 3D parametric models with their mathematical equations for VIR and SAR images (Wong 1980; Curlander 1986).

3D Parametric Models	Mathematical Equations	Description of Parameters
VIR Images (Collinearity Equations)	$x = (-f) \frac{[m_{11}(X - X_0) + m_{12}(Y - Y_0) + m_{13}(Z - Z_0)]}{[m_{31}(X - X_0) + m_{32}(Y - Y_0) + m_{33}(Z - Z_0)]}$ $y = (-f) \frac{[m_{21}(X - X_0) + m_{22}(Y - Y_0) + m_{23}(Z - Z_0)]}{[m_{31}(X - X_0) + m_{32}(Y - Y_0) + m_{33}(Z - Z_0)]}$	(x,y) the image co-ordinates; (X,Y,Z) the map co-ordinates; (X ₀ ,Y ₀ ,Z ₀) the projection centre co-ordinates; -f the focal length of the VIR sensor; [m _{ij}] the 9 parameters of the orthogonal 3-rotation matrix
SAR Images (Doppler-range Equations)	$f = \frac{2(\vec{V}_S - \vec{V}_P) \bullet (\vec{S} - \vec{P})}{\lambda \vec{S} - \vec{P} }$ $r = \vec{S} - \vec{P} $	f the Doppler value; r the range distance; \vec{S} and \vec{V}_S the sensor position and velocity; \vec{P} and \vec{V}_P the target-point position and ground velocity; λ the radar wavelength

The collinearity equations are valid for an instantaneous image or scan-line acquisition, such as photogrammetric cameras (LFC, MC) and VIR scanner sensors (SPOT, Landsat), while the Doppler-range equations are valid for a SAR scan-line. However, since the parameters of neighbouring scan-lines of scanners are highly correlated, it is possible to link the exposure centres and rotation angles of the different scan-lines to integrate supplemental information, such as:

- The ephemeris and attitude data using celestial mechanic laws (Figure 6-2) for satellite images; or
- The global positioning system (GPS) and inertial navigation system (INS) data for airborne images.

The integration of the different distortions and the derivation of equations for different sensors are outside the scope of this Chapter. They are described for photogrammetric cameras in Wong (1980), for Landsat data in Salamonowicz (1986) and Shu (1987), for SPOT data in Guichard (1983) and Toutin (1983) and for SAR data in Leberl (1972) or Curlander (1982). For example, the solution for the 3D parametric functions given in Guichard (1983) and Toutin (1983, 1995) starts from the collinearity equations written in the instrument reference system. They have been adapted to suit the geometry of scanner imagery, but also have benefited from theoretical work in celestial mechanics to determine the satellite's osculatory orbit and parameters more accurately than by simply using a "constant ellipse" orbit (Figure 6-2). The collinearity equations were then converted into the cartographic projection system with elementary transformations (rotations

and translations), which are functions of parameters describing the geometric distortions detailed in a previous section, namely:

- Rotation from the sensor reference to the platform reference;
- Translation to the Earth's centre;
- Rotation which takes into account the platform time variation;
- Rotation to align the z-axis with the image centre (M_0) on the ellipsoid;
- Translation to the image centre (M_0);
- Rotation to align the y-axis in the meridian plane;
- Rotation to have xM_0y tangent to the ellipsoid;
- Rotation to align the x-axis in the image scan direction; and
- Rotation-translation into the cartographic projection.

The final results, which link the 3D cartographic co-ordinates to the image co-ordinates, are two equations:

$$P_p + y(1 + \delta\gamma X) - \tau H - H_o \Delta T^* = 0 \quad (1)$$

$$X + \theta \frac{H}{\cos \chi} + \alpha q (Q + \theta X - \frac{H}{\cos \chi}) - Q \Delta R = 0 \quad (2)$$

with:

$$X = (x - ay)(1 + \frac{h}{N_o})by^2 + cxy \quad (3)$$

$$H = h - \frac{x^2}{2N_o} \quad (4)$$

Each parameter has a mathematical parametric formula (Toutin 1983) that represents the physical realities of the full viewing geometry (satellite, sensor, Earth, map projection):

- | | |
|-------|---|
| H | is the altitude of the point corrected for the Earth's curvature; |
| H_o | is the satellite elevation at the image centre line; |
| N_o | is the normal to the ellipsoid; |

α	is a function of the rotation of the Earth;
α	is the instantaneous field-of-view ;
p, q	are the image co-ordinates;
P, Q	are the scale factors in Y and X, respectively;
T and θ	are a function of the levelling angles in Y and X, respectively;
ΔT^* and ΔR	are the non-linear variations in attitude if they exist (ΔT^* : combination of pitch and yaw, ΔR : roll);
x, y and h	are the ground co-ordinates;
$b, c, \chi, \delta y$	are known 2 nd order parameters.

2.4 Comparisons of non-parametric and parametric models

Table 6-5 summarises the main characteristics and comparisons of the 2D/3D non-parametric methods and the 3D parametric methods. The main difference between 2D and 3D models is noted in **bold** type. Some major differences between non-parametric and parametric models which enable the 3D parametric models to be more consistent and robust are noted in *italic* type. The 2D/3D differences are mainly related to the ability of 3D models to integrate the terrain elevation information in the different processing steps:

- By adding the Z- elevation to the GCPs; and
- By adding DEM or a mean elevation in the rectification process.

Furthermore, in order to make a qualitative comparison between non-parametric and parametric models, the two extreme models (2nd-order 2D polynomial and 3D parametric) were applied to a data fusion of panchromatic SPOT-image and two airborne SAR images (C-band and HH-polarisation) (Colour Plate 3). These results are used from a previous research study over Sherbrooke, Quebec with 200-m elevation topography (Toutin 1995a). Colour Plate 3 shows a composite image using IHS transformation (assigning SPOT-PLA to hue and the two other airborne SAR to intensity and saturation). They were rectified with a 3D parametric model using

a DEM (top) and 2D non-parametric model (bottom). The road vector (accuracy of 3-5 m) has also been registered on each sub-image. The radiometric processing operations performed (HIS, LUT, etc.) are exactly the same for both sub-images, only the geometric processing differs.

Table 6-5. Comparison of the different characteristics between 2D/3D non-parametric models and 3D parametric models.

2D/3D Non-Parametric Model	3D Parametric Model
Does not respect the viewing geometry	Respects the viewing geometry
Not related to geometric distortions	<i>Reflects the geometric distortions</i>
Do not use metadata (ephemeris and attitude)	<i>Uses metadata</i> (ephemeris and attitude)
2D models do not use terrain elevation	Uses terrain elevation information
Corrects image locally at GCPs	Corrects the image globally
Does not filter blunders	<i>Filters blunders</i> with the knowledge of the geometry
Individual adjustments of one image	Simultaneous adjustment of more than one image
Image-to-image correction	Image-to-ground correction
Needs many (>20-60) GCPs	Need few (3-8) GCPs
Sensitive to GCPs distribution	Not sensitive to GCPs distribution
Problem of choice for tie points	GCPs choice as a function of each image

The top image is much more homogeneous in its colours, surfaces and variations. As there is greater contrast between the elements, their boundaries are clear and well defined. In the bottom image, the colour variations are greater, giving an impression of texture, and the image seems more blurred. As there is less contrast between the elements, they appear less well defined. Using the vector file from the topographic map, the analysis of certain cartographic elements showed, in the bottom image (letters a to d refer to parts of the image identified in Colour Plate 3), that:

- The linear elements (roads and rivers) are doubled or even disappear (bridge, roads), which corresponds to a relative error of registration;
- The lack of sharpness in this part prevents us from distinguishing the road from the forest and areas of bare soil;
- On surface elements, artefacts are created; there is an inversion between forest (green) and clear-cuts (burgundy);
- The texture and colour variations do not correspond to the real information.

These examples, together with similar ones which can be clearly identified on these sub-images, show that geometric registration errors have generated radiometric merging errors, artefacts and erroneous information in the composite image, which do not correspond to any physical reality.

The road vector file, registered to these sub-images, allows us to check the geometric accuracy. Visual analysis confirms the earlier statistical error

results for the polynomial method (30-50 m), but shows an improvement for the photogrammetric method (10 m), with maximum errors of 20 metres. Checks on other parts of the images illustrate the consistency of the results. These values correspond to the absolute error of registration. Since these tests and comparisons were performed on small sub-images over rolling topography, the differences are likely to be more pronounced on larger images over rougher topography.

The general superiority of 3D parametric modelling over non-parametric modelling is mainly due to the fact that the 3D mathematical functions correspond to the physical reality of the viewing geometry and take into account all the distortions generated in the image formation. It is thus more capable of detecting errors in an operational environment. Since all the parameters have a physical meaning, they are also easy to interpret when bad or erroneous results occur.

Table 6-6. Results (root mean square and maximum errors in metres) computed on Independent Check Points (ICPs) from 3D 1st-order rational model and 3D parametric model adjustment for EROS A1, IKONOS and QuickBird-2 images (Toutin et al. 2002).

High-resolution Image Correction Model	RMS Errors (m)		Maximum Errors (m)	
	X	Y	X	Y
EROS A1				
3D 1 st -order Rational	8.0	13.2	20	23
3D Parametric	3.9	3.5	6.2	6.0
IKONOS				
3D 1 st -order Rational	2.2	5.2	5.1	10.4
3D Parametric	1.3	1.3	3.0	3.0
QuickBird-2				
3D 1 st -order Rational	4.0	2.1	9.5	4.3
3D Parametric	1.4	1.3	2.5	2.8

Previous research studies with medium-resolution images (Salamonowicz 1986; Novak 1992; Toutin 1995a; de Sève et al. 1996), review papers and books (Leberl 1990; Bannari et al. 1995; Calloz and Collet 2001) are all in agreement with these above statements. More recently with high-resolution images, 3D rational models show worse and less consistent results (Toutin et al. 2002) and some inconsistencies in the results were not explained (Davis and Wang 2001). Table 6-6 gives comparisons for the three new high-resolution sensors geometrically processed with 3D rational functions and 3D parametric functions. They are the statistical results (root mean square and maximum errors in metres) computed on Independent Check Points (ICPs) from 3D 1st-order rational model and 3D parametric model adjustment for EROS A1, IKONOS and QuickBird-2 (Toutin et al. 2002). The results on ICPs for the 3D parametric models are always two to three times better than with 3D 1st-order rational models. However, other studies have demonstrated the

feasibility of using 3D non-parametric models with high-resolution images, but only in a well-controlled research environment with just one image acquired over flat terrain (Hanley and Fraser 2001; Tao and Hu 2001b) a scenario rarely, if ever, expected to be encountered by end-users in an operational environment. More research should be thus performed to evaluate the true applicability and limitations of these 3D rational functions for high-resolution images.

The arguments presented in these research studies to support the 3D rational models as a *Universal Sensor Model* include simplified mathematical functions, easier to use, fast computation and universality of its form due to sensor independence (frame camera, scanner) (Madani 1999). However, since no application with SAR or airborne scanner sensors, and very few with medium-to-high resolution VIR sensors, were performed, the case for calling 3D rational models a *Universal Sensor Model* is not very strong. Furthermore, Madani (1999) also addressed their disadvantages:

- Inability to model local distortions (such as with CCD arrays or worse with SAR sensors);
- Limitation in the image size;
- Difficulty in the interpretation of the parameters due to the lack of physical meaning;
- Potential failure to zero denominator; and
- Potential correlation between the terms of polynomial functions.

Furthermore, the arguments of simplified mathematical functions, universality and ease of development and use, can also be applied to extant 3D parametric models. In fact, some 3D parametric models were “mathematically generalised” (Leberl 1972; Masson d’Autumne 1979; Konecny 1986; Toutin 1995b) and they have all these advantages in addition to the general advantages previously mentioned for 3D parametric models.

In these conditions, 3D rational models should mainly be used where no 3D parametric model has been developed. In fact, the parameterisation of models has always been a major issue in scientific research and achievements. When it becomes theoretically and/or practically impossible, statistical methods such as 3D rational models take over.

3. METHODS, PROCESSING AND ERRORS

Whatever the mathematical functions used, the geometric correction method and processing steps are more and less the same. The processing steps are (Figure 6-3):

- Acquisition of image(s) and *pre-processing of metadata*;
- Acquisition of the ground points (control/check/pass) with image co-ordinates and map co-ordinates X, Y, (Z);

- Computation of the unknown parameters of the mathematical functions used for the geometric correction model for one or more images;
- Image(s) rectification with or without DEM.

The main differences in the processing steps between non-parametric and parametric models are in *italic* type and between 2D non-parametric and 3D models are in **bold** type. The metadata are not necessary for non-parametric models because the models do not reflect the geometry of viewing, while the Z-elevation co-ordinates for GCPs and DEM/DSM are of no use for 2D non-parametric models.

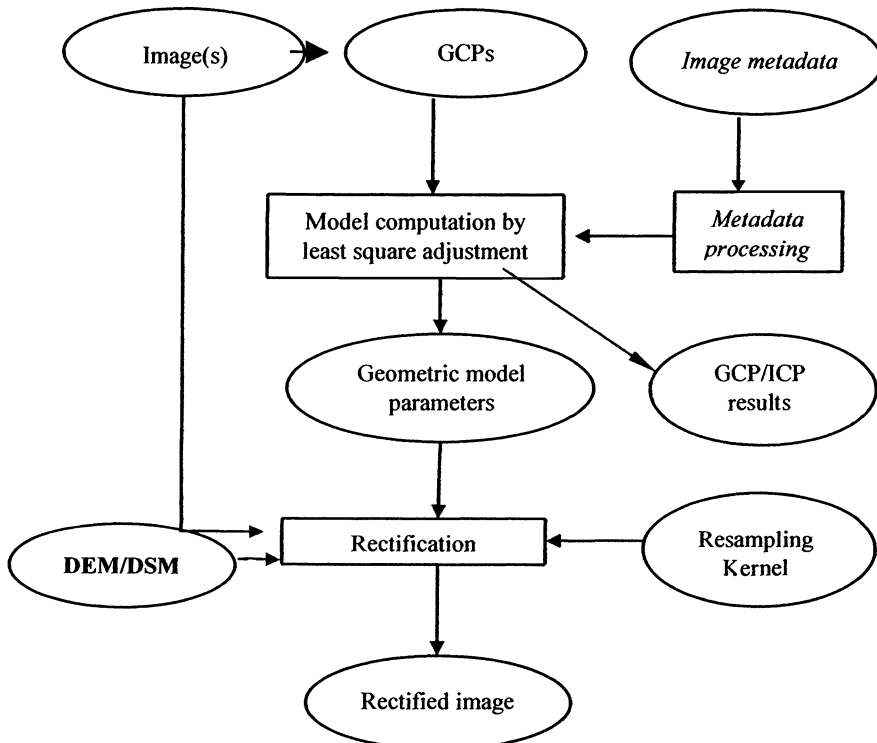


Figure 6-3. Description of the geometric correction method and processing steps. The ellipse symbols are input/output data and the box symbols are processes.

3.1 Acquisition of images and metadata

With VIR images, different types of image data with different levels of pre-processing can be obtained, but different image providers use differing terminology to denote the same type of image data. Standardisation should be better defined, mainly for the convenience of end-users:

- Raw images with only normalisation and calibration of the detectors (e.g. level 1A for SPOT or 1B for QuickBird-2) without any geometric correction are satellite-track oriented. In addition, full metadata related to sensor, satellite (ephemeris and attitude) and image are provided;
- Geo-referenced images (e.g. level 1B for SPOT or 1G for Landsat-ETM+) corrected for systematic distortions due to the sensor, the platform and the Earth rotation and curvature are satellite-track oriented. Generally, few metadata related to sensor and satellite are provided; some metadata are related to the 1B processing; or
- Map-oriented images, also called geocoded images, (e.g. level 2A for SPOT or Cartera Geo for IKONOS) corrected for the same distortions as geo-referenced images are North oriented. Generally, very few metadata related to sensor and satellite are provided; most of the metadata are related to the 2A processing and the ellipsoid/map characteristics.

For the sake of clarity, the easiest terminology defined for SPOT images is used. The raw “level 1A” images are preferred by photogrammetrists because 3D parametric models derived from co-linearity equations are well known and developed and easily used in softcopy workstations. Since different 3D parametric models are widely available for such VIR images, raw 1A-type images should now be favoured by the remote sensing community as well. Specific software to read and pre-process the appropriate metadata (ephemeris, attitude, sensor and image characteristics) has to be developed for each image sensor according to the 3D parametric model used. Using celestial mechanics laws and Lagrange equations (Escobal 1965; CNES 1980; Light et al. 1980), the ephemeris (position and velocity) can be transformed into osculatory orbital parameters (Figure 6-2) (Toutin 1983). Since the Lagrange equations take into account the variation of the Earth’s gravitational potential to link the different positions of the satellite during the image formation, it is more accurate and robust than using a constant ellipse with 2nd-order time-dependent polynomial functions (Guichard 1983; Toutin 1983; Bannari et al. 1995). This statement is more applicable when long images from the same orbit are used with path processing (Toutin 1985; Sakaino et al. 2000) or a block bundle adjustment method (Veillet 1991; Toutin et al. 2001a; Toutin 2002a). 3D parametric models also apply well to high-resolution airborne (Gibson 1984; Ebner and Muller 1986) or spaceborne images, such as QuickBird-2 (Toutin and Cheng 2002) for achieving pixel accuracy or better. Some results were presented using 3D rational functions with raw SPOT images (Tao and Hu 2001a), but not with high-resolution spaceborne or airborne images.

Since they have been systematically corrected and geo-referenced, the “level 1B” images retain only the terrain elevation distortion, in addition to a

rotation-translation related to the map reference system. A 3D 1st-order polynomial model with Z-elevation parameters could thus be efficient, depending on the requested final accuracy. For scanners with across-track viewing capability, only the Z-elevation parameter in the X-equation is useful. The 2nd-order non-parametric models could also be used (Palà and Pons 1995) for correcting some residual errors of the 1B processing. When possible, solutions to overcome the non-parametric model approximation are either to convert the 1B-images back into 1A-images using the metadata and the reverse transformation (Al-Roussan et al. 1997), or to “re-shape and re-size” the 1B-images to the raw imagery format (Valadan Zoej and Petrie 1998). This 1B-geometric modelling can be mathematically combined with a normal 1A 3D parametric model to avoid multiple image re-sampling. Although this mathematical procedure used for 1B images works better than non-parametric models, it is still recommended that raw images with 3D rigorous parametric models (co-linearity equations) be directly used.

The map-oriented images (“level 2A”) also retain the elevation distortion but image lines and columns are not related to sensor-viewing and satellite directions. A 3D 1st-order polynomial model with Z-elevation parameters in both axes can thus be efficient depending on the requested final accuracy. As with level 1B, 2nd-order non-parametric models (polynomial or rational) can be used for correcting some residual errors of the 2A processing, but it is generally no longer possible to convert back the 2A image with the reverse transformation. These 2D/3D non-parametric models were recently applied with IKONOS Geo images to achieve pixel accuracy or better:

- 2D first-order polynomial and rational models (Hanley and Fraser 2001);
- 3D first-order polynomial models (Fraser et al. 2002);
- 3D third-order rational models by Space Imaging using the 1st approach (described in 2.2.3) with coefficients computed from their camera model (Dial and Grodecki 2002);
- 3D 1-order rational models using the 2nd approach (described in 2.2.3) with computation of the model parameters using GCPs (Tao and Hu 2001b).

Although the results, generally achieved in a well-controlled research environment using (sub-)images acquired over flat terrain, are in the order of pixel accuracy or sometimes better due to good quality of cartographic data, no results, to our knowledge, were published with IKONOS images in high relief terrain. Care must be then taken by end-users in the extrapolation of these results to any image acquired over any terrain and processed with any cartographic data.

However, a 3D parametric model has been approximated and successfully developed for IKONOS Geo images using basic metadata

information and celestial mechanics laws, and has been applied to various images acquired over flat-to-rough topography (Toutin and Cheng 2000; Toutin 2002b). Even approximated, this 3D parametric model ("using a global geometry and adjustment") has been proven to be more robust (Toutin et al. 2002) and to achieve more consistent results over the entire image than 3D rational models ("using a local adjustment") (Davis and Wang 2001).

SAR images are standard products in slant or ground range presentations. They are generated digitally during post-processing from the raw signal SAR data (Doppler frequency, time delay). Errors present in the input parameters related to the image geometry model will propagate through to the image data. These include errors in the estimation of slant range and of Doppler frequency and also errors related to the satellite's ephemeris and the ellipsoid. Assuming the presence of some geometric error residuals, the parameters of a 3D parametric model reflect these residuals.

As mentioned previously, the 3D parametric model starts generally either from the traditional Doppler and range equations (Curlander 1982), from the equations of radargrammetry (Leberl 1990), or from generalised equations (Leberl 1972; Toutin 1995b). Due to the large elevation distortions in SAR images, 2D polynomial models cannot be used, even in rolling topography (Toutin 1995a) or to extract planimetric features (de Sève et al. 1996). Furthermore, since different 3D SAR parametric models are largely available, no attempt has been made, to our knowledge, to apply 3D polynomial or rational models to SAR images (spaceborne or airborne).

3.2 Acquisition of GCPs

Whatever the VIR and/or SAR geometric model used, some GCPs have to be acquired to refine the parameters of the mathematical functions with a least-square adjustment process in order to obtain a cartographic standard accuracy. The number of GCPs is a function of different conditions: the method of collection, the sensor type and resolution, the image spacing, the geometric model, the study site, the physical environment, the GCP definition, the map accuracy and the final expected accuracy. Figures 6-4 to 6-6 are GCP examples for different sensors (Landsat-7 ETM+, RADARSAT-SAR fine mode, and IKONOS) in different contexts (flat to mountainous terrain, urban or rural environment). If GCPs are determined *a priori* without any knowledge of the images to be processed 50 % of the points may be rejected (Toutin and Carbonneau 1989). If GCPs are determined *a posteriori* with knowledge of the images to be processed, the reject factor will be smaller (20-30 %). Consequently, all aspects of GCP collection should be considered, not separately, but as a whole, to avoid excessive discrepancies in the accuracy of these different aspects. For example, 1) a GPS survey

should not be used to process Landsat data in a mountainous study site, 2) do not use road intersection and 1: 50,000 topographic maps to process IKONOS images if you expect 1-2 m final accuracy. The weakest aspect of GCP collection, which will of course be different for each study site and image, will thus be the major source of error in the error propagation and overall error budget of the bundle adjustment.

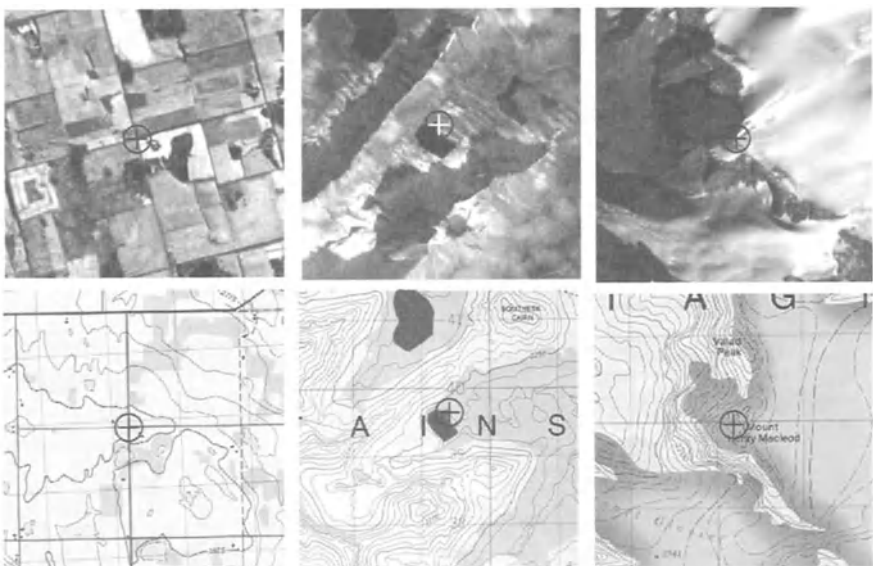


Figure 6-4. Three examples of GCP collection for Landsat-7 ETM+ images with different features and accuracy and their respective location on 1:50,000 topographic map. A road intersection with better than one-pixel accuracy (left); a lake feature with one-to-two pixel accuracy (centre); the top of a mountain with better than two-to-three pixel accuracy (right) and their respective location on 1:20,000 scanned topographic map (Toutin et al. 2001b).

Since non-parametric models do not reflect the geometry of viewing and do not filter errors, many more GCPs than the theoretical minimum are required to reduce the propagation of input errors in the geometric models. When the map and positioning accuracy is in the same order of magnitude as the image resolution, a minimum of twice the theoretical number of GCPs is required: approximately 20, 40 or 80 GCPs should then be acquired for 2nd-order 2D polynomial, 3D polynomial or 3D rational models respectively. The 3rd-order models require more, particularly the rational functions. Furthermore, to ensure robustness and consistency in an operational environment, it is safer to collect even more than twice the theoretical minimum. This restricts the usefulness of such non-parametric models. When more than one image is processed, each image requires its own GCPs

and the geometric models are generally computed separately, which does not set up a relative orientation or link between the images. GCPs should be spread over the full image(s) in planimetry and also in the elevation range for the 3D models. It is also better to have medium-accurate GCPs than no GCP at the tops of mountains, such as with Landsat-7 (Figure 6-4, right). If the image is larger than the study site it is recommended that GCP collection be restricted to the study site area, because the non-parametric models only correct locally.



Figure 6-5. Example of stereo GCP collection on RADARSAT-SAR fine mode stereo-images: a field corner with one-to-two pixel accuracy and its location on 1:20,000 scanned topographic map. RADARSAT Images © Canadian Space Agency 2001.

With 3D parametric models, few GCPs (1 to 6) are required per image. When more than one image is processed a spatio-triangulation method with 3D block-bundle adjustment can be used to process all images together (VIR and SAR). The use of tie points (TPs) enables users to drastically reduce the number of GCPs for the block (Veillet 1991; Sakaino et al. 2000; Toutin et al. 2001a, b; Dial and Grodecki 2002). When the map and positioning accuracy is of the same order of magnitude as the image resolution, twice (or a little less) the theoretical minimum is recommended. When the accuracy is worse, the number should be increased depending on the final expected

accuracy (Savopol et al. 1994). Since more confidence, consistency and robustness can be expected with parametric models (global image processing, filtering input errors) than with non-parametric models, it is not necessary to increase the number of GCPs in operational environments. GCPs should preferably be spread at the border of the image(s) to avoid extrapolation in planimetry; it is also preferable to cover the full elevation range of the terrain (lowest and highest elevations). Unlike non-parametric models, GCPs need not be regularly distributed in the planimetric and elevation ranges. Since parametric models correct globally, GCP collection should be performed across the full image, even if the study site is smaller. This is advantageous, as it will be easier to find GCPs over the entire image rather than just one section, and the GCPs will be more homogeneous.



Figure 6-6. Example of GCP collection on IKONOS image: a sidewalk corner with one-to-two pixel accuracy and its location on digital 1-m pixel ortho-photo. Sidewalks are better defined and more precise than road intersections (Toutin 2002b). IKONOS Images © Space Imaging LLC 2000.

GCP cartographic co-ordinates can be obtained from global positioning system (GPS), air photo surveys, paper or digital maps, ortho-rectified images, chip data base, etc. The cartographic co-ordinates obtained from these sources have drastically different levels of accuracy, from better than 1 m with GPS to 25-50 m with paper maps, certainly the most common GCP source used around the world. With lower accuracy, more GCPs must be used (Savopol et al. 1994). The image co-ordinates are plotted interactively on the screen or automatically using GCP chip database and image correlation tools. When multiple images with overlapping coverage are

processed, the image co-ordinates are obtained simultaneously in “double monoscopy”, because some workstations do not have full stereoscopic capabilities for multi-sensor images. This plotting will then create artificial X- and Y-parallaxes (few pixels) between the images, and the parallax errors will propagate through the bundle adjustment (relative and absolute orientations). The error propagation is larger with SAR images than with VIR images due to a lower plotting accuracy (1-2 pixels versus 1/3-1/2 pixel), and increases with smaller intersection angles, but also with shallower same-side SAR look angles (Toutin 1998, 1999). To avoid these errors, true stereoscopic plotting using human depth perception should be used when possible. This enables a better relative correspondence of the GCP between the images and a better absolute positioning on the ground.

3.3 Geometric model computation by least-square adjustment

When more than one image (VIR or SAR) is processed, a spatio-triangulation process based on a block adjustment can be applied to simultaneously compute all geometric models (Figure 6-3). Colour Plate 4 is an example of a block over the Canadian Rocky Mountains (BC) with 15 Landsat-ETM+ images using three rows and five strips (Toutin et al. 2001b). All model parameters of each image/stripe are determined by a common adjustment, so that the individual models are properly tied in and the entire block is optimally oriented in relation to the GCPs. With the spatio-triangulation process, the same number of GCPs is theoretically needed to adjust a single image, an image strip or a block. However, some tie points (TPs) between the adjacent images have to be used to link the images and/or strips. Elevation of TPs (ETPs) must be added when the intersection geometry of the adjacent images is weak, such as with intersection angles less than 15°-20° (Toutin et al. 2001a, b). There are a number of advantages to the spatio-triangulation process, namely to:

- Reduce the number of GCPs;
- Obtain a better relative accuracy between the images;
- Obtain a more homogeneous and precise mosaic over large areas; and
- Generate homogeneous GCP network for future geometric processing.

Whatever the number of images (spatio-triangulation or single image) and the geometric models (parametric or non-parametric) used, each GCP contributes to two observation equations: an equation in X and an equation in Y. The observation equations are used to establish the error equations for GCPs, TPs, and ETPs. Each group of error equations can be weighted as a function of the accuracy of the image and cartographic data. The normal equations are then derived and resolved with the unknowns computed. In

addition, for the 3D parametric models, conditions or constraints on osculatory orbital or other parameters can be added in the adjustment to take into account the knowledge and the accuracy of the ephemeris or other data, when available. They thus prevent the adjustment from diverging and also filter the input errors.

Since there are always redundant observations to reduce the input error propagation in the geometric models a least-square adjustment is generally used. When the model equations are non-linear, which is the case for 2nd- and higher order non-parametric and parametric models, some means of linearization (series expansions or Taylor's series) must be used. A set of approximate values for the unknown parameters in the equations must be thus initialised:

- To zero for the non-parametric models, because they do not reflect the image acquisition geometry; or
- From the osculatory orbital and sensor parameters of each image for the 3D parametric models.

More information on least-squares methods applied to geomatics data can be obtained in Mikhail (1976) and Wong (1980). The results of this processing step are:

- The parameter values for the geometric model used for each image;
- The residuals in X and Y directions (and Z if more than one image is processed) for each GCP and their root mean square (RMS) residuals;
- The errors and bias in X and Y directions (and Z if more than one image is processed) for each Independent Check Point (ICPs) if any, and their RMS errors; and
- The computed cartographic co-ordinates for each point, including ETPs and TPs.

When more GCPs than the minimum theoretically required are used, the GCP residuals reflect the modelling accuracy, while the ICP errors reflect the final accuracy. As mentioned previously, this final accuracy is mainly dependent on the geometric model and the number of GCPs used versus their cartographic and image co-ordinates.

When no ICP is available, RMS residuals can be carefully used as an approximation of the final accuracy, but only when using 3D parametric models. However, the fact that RMS residuals can be small with 2D/3D non-parametric models does not mean necessarily a good accuracy because these models correct locally at GCPs and the least-square adjustment minimises residuals at GCPs. Errors are still present between GCPs. On the other hand, with the use of overabundant GCPs with 3D parametric models, the input data errors (plotting and/or map) do not propagate through the parametric models but are mainly reflected in the GCP residuals due to a global adjustment. Consequently, it is thus "normal and safe" with 3D parametric

models to obtain RMS residuals in the same order of magnitude as the GCP accuracy, but the model by itself will be more precise. In contrast to polynomial methods, which are sensitive to GCP number and spatial distribution (including their elevation), the 3D parametric models are not affected by these factors because they precisely retain the complete viewing geometry, given that there is no extrapolation in planimetry and also in elevation.

3.4 Image rectification

The last step of the geometric processing is the image rectification (Figure 6-3). To rectify the original image into a map image, there are two processing operations:

- A geometric operation to compute the cell co-ordinates in the original image for each map image cell; and
- A radiometric operation to compute the intensity value or digital number (DN) of the map image cell as a function of the intensity values of original image cells that surround the previously-computed position of the map image cell.

3.4.1 Geometric operation

The geometric operation requires the two equations of the geometric model with the previously-computed unknowns, and sometimes elevation information. In fact, since 3D parametric models take into account the elevation distortion, a DEM is needed to create more precise ortho-images. The rectification should then be called an ortho-rectification. If no DEM is available, different altitude levels can be input for different parts of the image (a kind of “rough” DEM) to minimise this elevation distortion. It is then important to have a quantitative evaluation of the DEM impact on the ortho-rectification process, both in term of elevation accuracy for the positioning accuracy and grid spacing for the level of details. This last aspect is more important with high-resolution images because a poor grid spacing when compared to the image spacing could generate artifacts for linear features (wiggly roads or edges). Figures 6-7 and 6-8 give the relationship between the DEM accuracy (including interpolation), the viewing/look angles and the resulting positioning error on SAR and VIR ortho-images, respectively. These curves were mathematically computed with the elevation distortion parameters of a 3D parametric model (Toutin 1995b). However, they could be also used as an approximation for other 3D parametric models and for the 3D non-parametric models. One of the advantages of these curves is that they can be used to find any third parameter when the two

others are known. It can be useful not only for quantitative evaluation of the ortho-rectification, but to forecast the appropriate input data, DEM or the viewing/look angles, depending of the objectives of the project.

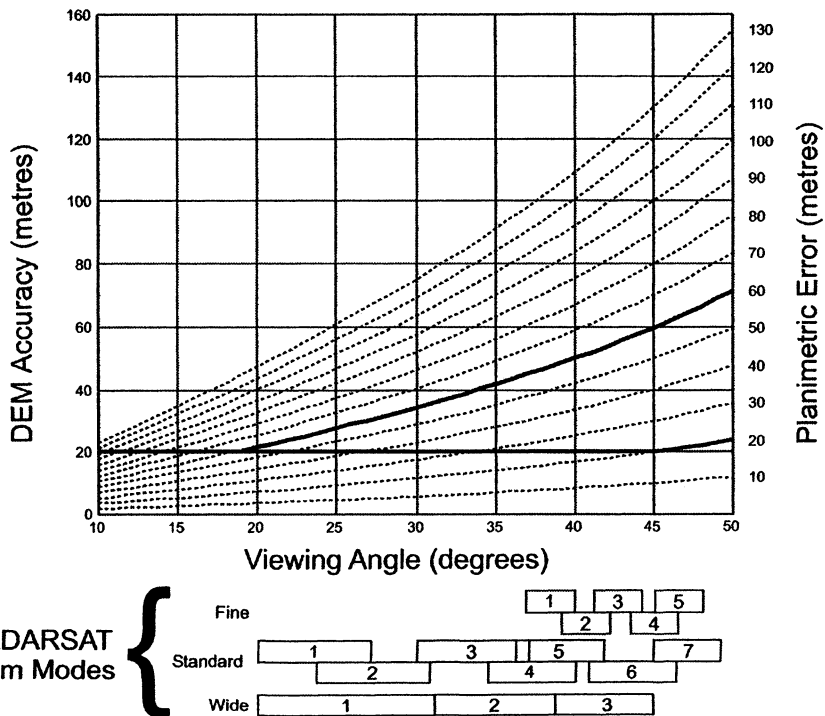


Figure 6-7. Relationship between the DEM accuracy (in metres), the look angle (in degrees) of the SAR image, and the resulting positioning error (in metres) generated on the SAR ortho-image. The different boxes at the bottom represent the range of look angles for each RADARSAT beam mode (Toutin 1998).

For example (Figure 6-7), with a SAR image acquired with a viewing angle of 10° and with a 45-m DEM accuracy, the error generated on the ortho-image is 9 m. Inversely, if a 4-m final positioning accuracy for the ortho-image is required with a 10-m DEM accuracy, the SAR image should be acquired with a viewing angle less than 20°. The same error evaluation can be applied to VIR data using the curves of Figure 6-8. As another example, if positioning errors of 60 m and 20 m on standard-1 (S1) and fine-5 (F5) ortho-images, respectively, are required, 20-m elevation error, which includes the DEM accuracy and the interpolation into the DEM, is thus sufficient. For high-resolution images (spaceborne or airborne), the surface heights (buildings, forest, hedges) should be either included in the DTM to generate a digital surface model (DSM) or taken into account in the overall elevation error. In addition, an inappropriate DEM in terms of grid spacing

can generate artifacts with high-resolution images acquired with large viewing angles over high relief areas (Zhang et al. 2001).

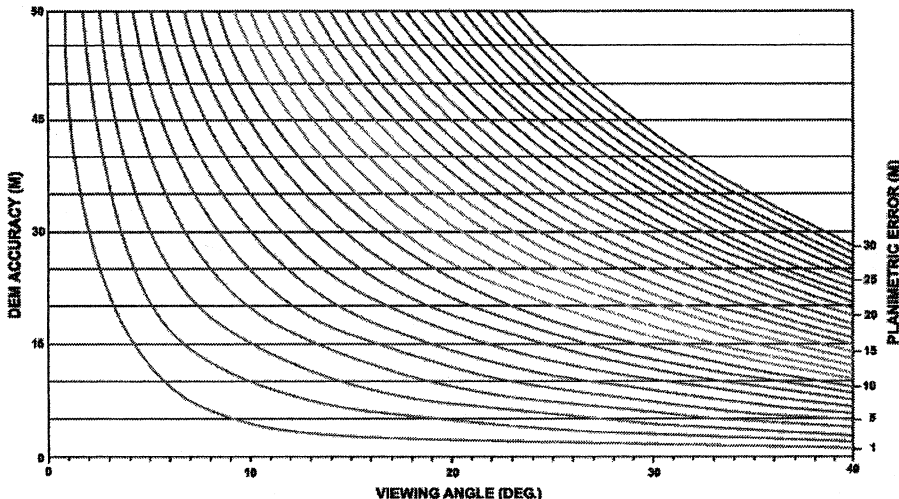


Figure 6-8. Relationship between the DEM accuracy (in metres), the viewing angle (in degrees) of the VIR image, and the resulting positioning error (in metres) generated on the ortho-image (Toutin 1995b).

Finally, for any map co-ordinates (X, Y) with the Z-elevation extracted from a DEM when 3D models are used, the original image co-ordinates (column and line) are computed from the two resolved equations of the model. However, the computed image co-ordinates of the map image co-ordinates will not directly overlay in the original image; in other words, the column and line computed values will rarely, if ever, be integer values.

3.4.2 Radiometric operation

Since the computed co-ordinate values in the original image are not integers, one must compute the DN to be assigned to the map image cell. In order to compute the DN to be assigned to the map image cell, the radiometric operation uses a re-sampling kernel applied to original image cells. This is either the DN of the closest cell (called nearest neighbour re-sampling) or a specific interpolation or de-convolution algorithm using the DNs of surrounding cells.

In the first case, the radiometry of the original image and the image spectral signatures are not altered, but the visual quality of the image is degraded. In addition to the visual degradation, a geometric error of up to half pixel is also introduced. This can cause a disjointed appearance in the

map image. If these visual and geometric degradations are acceptable for the end-user, it can be an advantageous solution.

In the second case, different interpolation or de-convolution algorithms (bilinear interpolation or sinusoidal function) can be applied. The bilinear interpolation takes into account the four cells surrounding the cell. The final DN is then either computed from two successive linear interpolations in line and column using DNs of the two surrounding cells in each direction or in one linear interpolation using DNs of the four surrounding cells. The DNs are weighted as a function of the cell distance from the computed coordinate values. Due to the weighting function this interpolation creates a smoothing in the final map image.

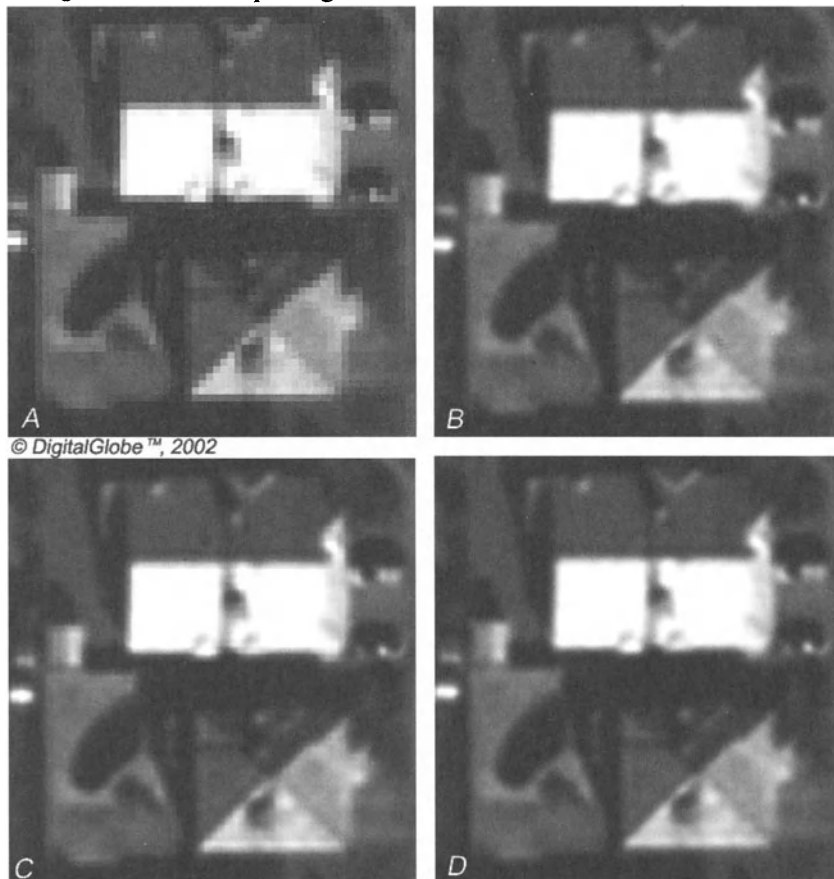


Figure 6-9. Examples of applications of geometric resampling kernels used in the rectification process with a Quickbird image. The sub-images are 350 by 350 pixels with 0.10-m spacing.

Letters A, B, C and D refer to different geometric resampling kernels (nearest neighbour, bilinear, cubic convolution, $\sin(x)/x$ with 16x16 window), respectively. Quickbird Image © Digital Globe 2002.

The theoretically ideal de-convolution function is the $\sin(x)/x$ function. As this $\sin(x)/x$ function has an infinite domain it cannot be exactly computed. Instead, it can be represented by piecewise cubic function, such as the well-known cubic convolution. The cubic convolution then computes 3rd-order polynomial functions using a 4x4-cell window. DNs are first computed successively in the four-column and -line direction, and the final DN is an arithmetical mean of these DNs. This cubic convolution does not smooth, but enhances and generates some contrast in the map image (Kalman 1985).

Due to recent computer advances, the $\sin(x)/x$ function can now be directly applied as a de-convolution function with different window sizes (generally 8 by 8 or 16 by 16). The computation time with a 16 by 16 cell window can be 40 to 80 times more than the computation time for nearest neighbour re-sampling. The final image is sharper with more details on features.

All these interpolation or de-convolution functions can be applied to VIR or SAR images. However, they are geometric re-sampling kernels, not very well adapted to SAR images. For these, it is better to use statistical functions based on the characteristics of the radar, such as existing adaptive filters, using local statistics (Lee 1980; Lopes et al. 1993; Touzi 1999). Combining the filtering with the re-sampling also avoids multiple radiometric processing and transformation, which greatly degrades the image content and its interpretation (Toutin 1995b).

Since interpolation or de-convolution functions transform the DNs and then alter the radiometry of the original image, problems may be encountered in subsequent spectral signature or pattern recognition analysis. Consequently, any process based on the image radiometry should be performed before using interpolation or de-convolution algorithms.

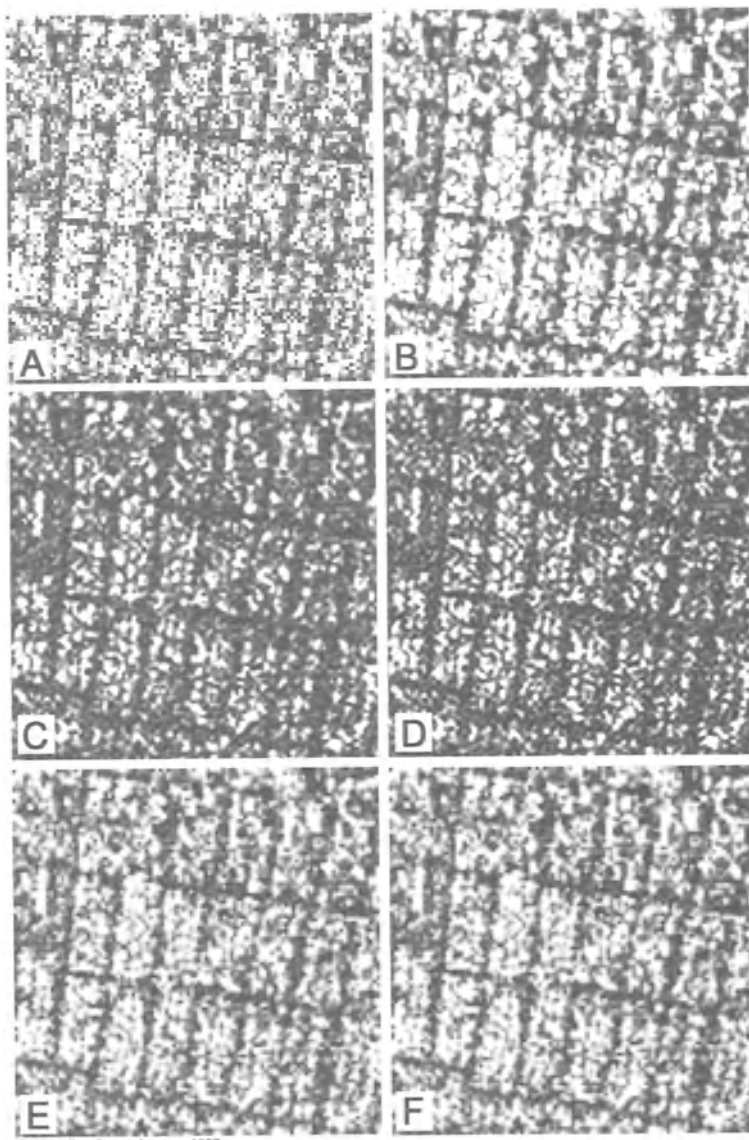


Figure 6-10. Examples of applications of geometric resampling kernels used in the rectification process with RADARSAT-SAR fine mode (F5) image. The sub-images are 600 by 600 pixels with 1.00-m spacing. Letters A, B, C and D refer to different geometric resampling kernels (nearest neighbour, bilinear, cubic convolution, $\sin(x)/x$ with 16x16 window), respectively and Letters E and F refer to statistical SAR filters (Enhanced Lee and Gamma), respectively. RADARSAT Images © Canadian Space Agency 2001.

Figures 6-9 and 6-10 are examples of the application of different re-sampling kernels with Quickbird high-resolution VIR image and RADARSAT-SAR fine mode (F5) image, respectively. Sub-images (200 by 200 pixels) were resampled with a factor of six to better illustrate the variations of the re-sampling kernels: the Quickbird and RADARSAT resampled image pixels are then 0.10 m and 1.10 m, respectively. Letters A, B, C and D refer to different geometric re-sampling kernels (nearest neighbour, bilinear, cubic convolution, $\sin(x)/x$ with 16x16 window), respectively and Letters E and F refer to statistical SAR filters (Enhanced Lee and Gamma), respectively. For both VIR and SAR images, the nearest neighbour re-sampling kernel (A) generates "blocky" images with rectangular-edge features, while the bilinear re-sampling kernel (B) generates fuzzy images with an "out-of-focus" feeling. The best results are obtained with the sinusoidal re-sampling kernels (C & D): even if there are few differences the true sinusoidal function generates sharper features. For example, on the Quickbird image (Figure 6-9), the two cars in the front of the houses are better defined in D: the windshield and rear window can be perceived on the car underneath while only the windshield is visible on the other car. It helps to differentiate between a sedan and a station wagon! For the SAR image (Figure 6-10), the two filters (E & F) give even better image appearance than the sinusoidal re-sampling, due to the fact that the SAR speckle is filtered at the same time.

4. CONCLUDING REMARKS

Since the launch of the first civilian remote sensing satellite 30 years ago, the requirements for the geometric processing of remotely sensed images have changed drastically. Furthermore, the integration of multi-format data in a digital world requires the highest accuracy possible so as to perform the ortho-rectification of multi-sensor images. While different mathematical functions and solutions can be used, non-parametric solutions are acceptable for low-resolution images, while parametric solutions are more appropriate for medium and high-resolution images. Even if 3D non-parametric solutions (mainly with 3D rational functions) have some advantages and can perform well in research environments, 3D parametric solutions have been proven to be more precise and robust and to achieve more consistent results in operational environments than 3D rational solutions. Consequently, they should be the primary choice whenever available. In fact, the mathematical parameterisation of physical models has always been a major issue in scientific research and achievements. When it becomes theoretically and/or practically

impossible, however, statistical methods such as 3D rational models can be used.

REFERENCES

- Al-Roussan, N., Cheng, P., Petrie, G., Toutin Th., & Valadan Zoej, M. J. (1997). Automated DEM extraction and ortho-image generation from SPOT level-1B imagery. *Photogrammetric Engineering and Remote Sensing*, 63, 965-974.
- Bannari, A., Morin, D., Bénié, G. B., & Bonn, F. J. (1995). A Theoretical Review of Different Mathematical Models of Geometric Corrections Applied to Remote Sensing Images. *Remote Sensing Reviews*, 13, 27-47.
- Billingsley, F. C. (1983). Data Processing and Reprocessing. *Manual of Remote Sensing*, 1, 719-722, (2nd ed.). Editor-in-chief Colwell, R. N., Falls Church, Virginia, U.S.A., Sheridan Press.
- Caloz, R., & Collet, C. (2001). Précis de télédétection, Volume 3 : Traitements numériques d'images de télédétection, 76-105, Chapitre 5. Presse de l'Université du Québec, Ste Foy, Québec, Canada.
- Centre National d'Études Spatiales (CNES), (1980). *Le mouvement du véhicule spatial en orbite*, Toulouse, France: CNES.
- Cheng, Ph., & Toutin, Th. (1998). Unlocking the potential for IRS-1C data. *Earth Observation Magazine*, 7, 24-26.
- Curlander, J. C., (1982). Location of Spaceborne SAR Imagery. *IEEE Transaction of Geoscience and Remote Sensing*, GE-22, 106-112.
- Davies C. H., & Wang, X. (2001). Planimetric accuracy of IKONOS 1-m panchromatic image products. *Proceedings of the 2001 ASPRS Annual Conference*, 23 - 27 April, St. Louis, Missouri, (ASPRS, Bethesda, Maryland), unpaginated CD-ROM.
- Derenyi, E. E., (1970). An Exploratory Investigation into the Relative Orientation of Continuous Strip Imagery. *Research Report No. 8*, University of New Brunswick, Canada.
- de Sève, D., Toutin, Th., & Desjardins, R. (1996). Evaluation de deux méthodes de corrections géométriques d'images Landsat-TM et ERS-1 RAS dans une étude de linéaments géologiques. *International Journal of Remote Sensing*, 17, 131-142.
- Dial, G., & Grodecki, J. (2002). Block adjustment with rational polynomial camera models. *Proceedings of the ACSM- ASPRS Annual Conference/XXII FIG International Congress*, Washington D.C., USA, April 19-26, (ASPRS, USA), CD-ROM.
- Ebner, H., & Muller, F. (1986). Processing of Digital Three Line Imagery Using a Generalized Model for Combined Point Determination. *International Archives of Photogrammetry and Remote Sensing*, 26, 212-222.
- Escobal, P. R. (1965). *Methods of orbit determination*. Malabar, USA. Krieger Publishing Company.
- Friedmann, D. E., Friedel, J. P., Magnusses, K. L., Kwok, K., & Richardson, S. (1983). Multiple Scene Precision Rectification of Spaceborne Imagery with Few Control Points. *Photogrammetric Engineering and Remote Sensing*, 49, 1657-1667.
- Gibson, J. (1984). Processing Stereo Imagery from Line Imagers. *Proceedings of 9th Canadian Symposium on Remote Sensing*, 471-488. Canada.
- Gracie, G., Bricker, J. W., Brewer, R. K., & Johnson, R. A. (1970). Stereo Radar Analysis. *U.S. Engineer Topographic Laboratory, Report No. FTR-1339-1*, Ft. Belvoir, VA, U.S.A.

- Guertin, F., & Shaw, E. (1981). Definition and potential of geocoded satellite imagery products. *Proceedings of the 7th Canadian Symposium on Remote Sensing*, 384-394, held in Winnipeg, Canada, September 8-11, Manitoba Remote Sensing Centre, Canada.
- Gugan, D. J. (1987). Practical aspects of topographic mapping from SPOT imagery. *Photogrammetric Record*, 12, 349-355.
- Guichard, H. (1983) Etude théorique de la précision dans l'exploitation cartographique d'un satellite à défilement : application à SPOT. *Société Française de Photogrammétrie et de Télédétection*, 90, 15-26.
- Guindon, B., & Adair, M. (1992). Analytic Formulation of Spaceborne SAR Image Geocoding and Value-Added Products Generation Procedures Using Digital Elevation Data. *Canadian Journal of Remote Sensing*, 18, 2-12.
- Hanley, H. B., & Fraser, C. S. (2001). Geopositioning accuracy of IKONOS imagery: Indications from two dimensional transformations. *Photogrammetric Record*, 17, 317-329.
- Hoffmann, O., & Muller, F. (1988). Combined Point Determination Using Digital Data of three line Scanner Systems. *International Archives of Photogrammetry and Remote Sensing*, 27 (B11), III / 567 - III / 577.
- Kalman, L. S., (1985). Comparison of Cubic-convolution Interpolation and Least-squares Restoration for Resampling Landsat-MSS Imagery. *Proceedings of the 51st Annual ASP-ASCM Convention: "Theodolite to Satellite"*, 546-556, Washington D.C., USA .
- Khizhnichenko, V. I, (1982). Co-ordinates transformation when geometrically correcting Earth space scanner images. (in Russian) *Earth Exploration From Space*, 5, 96-103.
- Konecny, G., & Schuhr, W. (1984). Practical Results of Geometric SAR-580, Image Evaluation. *International Archives for Photogrammetry and Remote Sensing*, 25 (A3).
- Konecny, G., Kruck, E., & Lohmann, P. (1986). Ein universeller Ansatz für die geometrische Auswertung von CCD-Zeilenaufnahmen. *Bildmessung und Luftbildwesen*, 54, 139-146.
- Konecny, G., Lohmann, P., Engel, H., & Kruck, E. (1987). Evaluation of SPOT Imagery on Analytical Instruments. *Photogrammetric Engineering and Remote Sensing*, 53, 1223-1230.
- Kratky, W. (1987). Rigorous Stereophotogrammetric Treatment of SPOT Images. *Comptes-rendus du Colloque International sur SPOT-1 : utilisation des images, bilans, résultats*, 1281-1288. Paris, France.
- Kratky, W. (1989). On-line aspects of stereophotogrammetric processing of SPOT images. *Photogrammetric Engineering and Remote Sensing*, 55, 311-316.
- La Prade, G. L. (1963). An Analytical and Experimental Study of Stereo for Radar. *Photogrammetric Engineering*, 29, 294-300.
- Leberl, F.W. (1972). On Model Formation with Remote Sensing Imagery. *Österreichisches Zeitschrift für Vermessungswesen*, 2, 43-61.
- Leberl, F. W. (1978). Satellite radargrammetric. *Deutsche Geodactische Kommission*, Munich, Germany, Serie C, 239.
- Leberl, F. W. (1990). *Radargrammetric image processing*. Artech House, Norwood, USA.
- Lee, J. S. (1980), Digital Image enhancement and noise filtering by use of local statistics. *IEEE Transactions on Pattern Analysis and Machine Intelligence*, 2, 165-168.
- Light, D. L., Brown, D., Colvocoresses, A., Doyle, F., Davies, M., Ellasal, A., Junkins, J., Manent, J., McKenney, A., Undrejka, R., & Wood, G. (1980). Satellite Photogrammetry. *Manual of Photogrammetry*, 883-977 (4th ed.). Chapitre XVII, Editor in chief Slama, C. C. ASP Publishers, Falls Church, USA.

- Lopes, A., Nezry, E., Touzi, R., & Laur, H., (1993). Structure Detection and Statistical Adaptive Speckle Filtering in SAR Images. *International Journal of Remote Sensing*, 14, 1735-1758.
- Madani, M. (1999). Real-Time Sensor-Independent Positioning by Rational Functions. *Proceedings of ISPRS Workshop on Direct Versus Indirect Methods of Sensor Orientation*, 64-75. Barcelona, Spain, November 25-26.
- Masson d'Autume, G. de (1979). Le traitement géométrique des images de télédétection. *Bulletin de la Société Française de Photogrammétrie et de Télédétection*, 73-74, 5-16.
- Mikhail, E. M. (1976). *Observations and Least Squares*. Harper & Row Publishers, New York USA.
- Naraghi, M., Stromberg, W., & Daily, M. (1983). Geometric Rectification of Radar Imagery using Digital Elevation Models. *Photogrammetric Engineering and Remote Sensing*, 49, 195-159.
- Paderes, F. C., Mikhail, E. M., & Fagerman, J.A. (1989). Batch and On-line Evaluation of Stereo SPOT Imagery. *Proceedings of the ASPRS - ACSM Convention*, 3, 31-40. Baltimore, MD, U.S.A.
- Palà, V., & Pons, X. (1995) Incorporation of Relief in Polynomial-Based Geometric Corrections. *Photogrammetric Engineering & Remote Sensing*, 61, 935-944.
- Rosenfield, G. H. (1968). Stereo Radar Techniques. *Photogrammetric Engineering*, 34, 586-594.
- Sakaino, S., Suzuki, H., Cheng, P., & Toutin, Th. (2000). Updating maps of Kazakhstan using stitched SPOT images, *Earth Observation Magazine*, 9, 11-13.
- Salomonowicz, P.H. (1986). Satellite Orientation and Position for Geometric Correction of Scanner Imagery. *Photogrammetric Engineering and Remote Sensing*, 52, 491-499.
- Savopol, F., Leclerc, A., Toutin, Th., & Carboneau, Y. (1994). La correction géométrique d'images satellitaires pour la Base nationale de données topographiques. *Geomatica*, 48, 193-207.
- Sawada, N., Kikode, M., Shinoda, H., Asada, H., Iwanaga, M., Watanabe, S., & Mori, K. (1981). An Analytic Correction Method for Satellite MSS Geometric Distortion. *Photogrammetric Engineering and Remote Sensing*, 47, 1195-1203.
- Shu, N. (1987). Restitution géométrique des images spatiales par la méthode de l'équation de colinéarité. *Bulletin de la Société Française de Photogrammétrie et de Télédétection*, 105, 27-40.
- Tao, V., & Hu, Y. (2001a). A Comprehensive Study of the Rational Function Model for Photogrammetric Processing, *Photogrammetric Engineering and Remote Sensing*, 67, 1347-1357.
- Tao, V. & Hu, Y. (2001b). 3-D Reconstruction Algorithms with the Rational Function Model and their Applications for IKONOS Stereo Imagery. *Proceedings of ISPRS Joint Workshop "High Resolution Mapping from Space"*, 253-263. Hannover, Germany, September 19-21, CD-ROM.
- Toutin, Th. (1983). Analyse mathématique des possibilités cartographiques du satellite SPOT. *Mémoire du diplôme d'Etudes Approfondies*, 1-74. Ecole Nationale des Sciences Géodésiques Saint-Mandé, France.
- Toutin, Th. (1985). Analyse mathématique des possibilités cartographiques de système SPOT. *Thèse de Docteur-Ingénieur*, École Nationale des Sciences Géodésiques, St-Mandé, France, IGN.
- Toutin, Th. (1995a). Intégration de données multi-sources : comparaison de méthodes géométriques et radiométriques. *International Journal of Remote Sensing*, 16, 2795-2811.

- Toutin, Th. (1995b). Multi-source Data Integration with an Integrated and Unified Geometric Modelling. *EARSeL Journal Advances in Remote Sensing*, 4, 118-129.
- Toutin, Th. (1996). La correction géométrique rigoureuse : un mal nécessaire pour la santé de vos résultats. *Journal canadien de télédétection*, 22, 184-189.
- Toutin, Th. (1998). Evaluation de la précision géométrique des images de RADARSAT. *Journal canadien de télédétection*, 24, 80-88.
- Toutin, Th. (1999). Error tracking of radargrammetric DEM from RADARSAT images. *IEEE Transactions on Geoscience and Remote Sensing*, 37, 2227-2238.
- Toutin, Th. (2001). Geometric processing of IKONOS Geo images with DEM. *Proceedings of ISPRS Joint Workshop "High Resolution Mapping from Space"*, 264-271. Hannover, Germany, September 19-21, CD-ROM.
- Toutin, Th. (2002a). Block adjustment of IKONOS Images. *International Journal of Remote Sensing*, 23, in press.
- Toutin, Th. (2002b). Error tracking in IKONOS geometric processing using a 3D parametric modeling. *Photogrammetric Engineering and Remote Sensing*, 68, in press.
- Toutin, Th. & Carboneau, Y. (1989). La multi-stéréoscopie pour les corrections d'images SPOT-HRV, *Canadian Journal of Remote Sensing*, 15, 110-119.
- Toutin, Th., & Carboneau, Y. (1992). MOS and SEASAT Image Geometric Corrections. *IEEE Transactions on Geoscience and Remote Sensing*, 30, 603-609.
- Toutin, Th., Carboneau, Y., & St. Laurent, L. (1992). An Integrated Method to Rectify Airborne Radar Imagery using DEM. *Photogrammetric Engineering and Remote Sensing*, 58, 417-422.
- Toutin, Th., & Cheng, P. (2000). Demystification of IKONOS. *Earth Observation Magazine*, 9, 17-21.
- Toutin, Th., Carboneau, Y., & Chénier, R. (2001). Ajustement de bloc d'images : Exemples avec SPOT, Landsat-7 et IKONOS. *Comptes-rendus du 23^{ème} Symposium canadien sur la télédétection*, 35-39. Ste-Foy, Québec, Canada, 21-24 août.
- Toutin, Th., Carboneau, Y., & Chénier, R. (2001). Block adjustment of Landsat7 ETM+ images. *Proceedings of ISPRS Joint Workshop "High Resolution Mapping from Space"*, 281-290. Hannover, Germany, September 19-21, CD-ROM.
- Toutin, Th., Chénier, T., & Carboneau, Y. (2002). 3D Models for High Resolution Images: Examples with QuickBird, IKONOS and EROS. *Proceedings of Joint International Symposium on Geospatial Theory, Processing and Applications (ISPRS, IGU, CIG)*. Ottawa, Ontario, Canada, July 8-12, 2002, CD-ROM.
- Toutin, Th., & Cheng, P. (2002). QuickBird: A Milestone to High Resolution Mapping. *Earth Observation Magazine*, 11, 14-18.
- Touzi, R. (1999). Speckle filtering of stationary and nonstationary scene signals in SAR imagery. *Proceedings IGARSS'99*, 1-3. Hamburg, Germany.
- Valadan Zoej, M.J., & Petrie, G. (1998). Mathematical modelling and accuracy testing of SPOT Level-1B stereo-pairs. *Photogrammetric Record*, 16, 67-82.
- Veillet, I. (1991). Triangulation spatiale de blocs d'images SPOT. *Thèse de Doctorat*, Observatoire de Paris, Paris, France.
- Westin, T. (1990). Precision Rectification of SPOT Imagery. *Photogrammetric Engineering and Remote Sensing*, 56, 247-253.
- Wong, K. W. (1980). Basic Mathematics of Photogrammetry. *Manual of Photogrammetry 37-101 (4th ed.)*, Chapter II, Editor, Slama, C. C. ASP Publishers, Falls Church, USA.
- Zhang Y., Tao, V., & Mercer, B. (2001). Assessment of the influences of satellite viewing angle, Earth curvature, relief height, geographical location and DEM characteristics on planimetric displacement of high-resolution satellite imagery. *Proceedings of the ASPRS*

Annual Conference, St Louis, Missouri, USA, April 23-27, (ASPRS, USA), CD-ROM (unpaginated).

Chapter 7

RADIOMETRIC IMAGE PROCESSING

Derek R. Peddle¹, Philippe M. Teillet², and Michael A. Wulder³

¹ *Department of Geography, University of Lethbridge, Lethbridge, Alberta, T1K 3M5, Canada*

² *Canada Centre for Remote Sensing, Natural Resources Canada, Ottawa, Ontario, K1A 0Y7, Canada*

³ *Canadian Forest Service (Pacific Forestry Centre), Natural Resources Canada, Victoria, British Columbia, V8Z 1M5, Canada*

1. INTRODUCTION

Based on a rich tradition of remote sensing in forest applications using aerial photography, the emergence of digital imagery from airborne and satellite platforms has created new frontiers for the remote sensing of forests. Today, a wide array of sophisticated sensors offer data at spatial, spectral, radiometric and temporal resolutions that approach or surpass aerial photography, with capabilities also available for imaging at synoptic regional, continental and planetary scales. As a result of these technical advances, together with improved forest practices and increased environmental concerns, the expectations of information derived from forest remote sensing has risen dramatically in applications ranging from baseline forest inventory and management, ecosystem health, forest fire and disease, to the broader contexts of sustainable resource development, national and international policy, and environmental and global change. Over time, the emphasis on quantitative data processing and analysis has increased such that, today, a significant proportion of users rely on accurate, high-quality data to obtain detailed surface cover, biophysical and structural information about forested areas of the Earth at particular locations and at specific times. This information may be of economic, social, strategic, political, or environmental value but, without it, the significant effort and cost to put Earth sensing capabilities in place is difficult to justify (MacDonald 1997).

The original, or “raw” data acquired by a remote sensor contain intrinsic, extrinsic, systematic, and non-systematic errors inherent to the process of signal acquisition and the complex Earth system being sensed including the intervening atmosphere. These data in raw form are unsuitable for most forest information applications and therefore a variety of procedures are required to improve or correct these data to a form suitable for the demanding information retrieval stages that follow. These procedures form the domain of “radiometric image processing” and include (as major sections of this Chapter): (1) sensor radiometric calibration, (2) surface reflectance retrieval based on atmospheric corrections, (3) image normalization for larger area or multi-temporal analyses to provide radiometric consistency across multiple scenes, and (4) specialised corrections for surface terrain induced variations. The linkages amongst these topics for satellite imagery are illustrated in Figure 7-1, which shows the necessary procedures prior to the information extraction phase, which are dealt with elsewhere in this book. For the purposes of this Chapter, radiometric image processing is formally considered to be the radiometric treatment of remotely sensed image data between acquisition and analysis. The data acquisition may consist of satellite data reception and recording by a ground station and / or completion of an airborne data acquisition mission. Without going into details because of space limitations, this Chapter outlines the key aspects of radiometric image processing, which is intended to make remote sensing data ready for analysis from the radiometric perspective. Emphasis is placed on digital image data of forests acquired in the solar reflective part of the electromagnetic spectrum, with a working framework consisting of the individual properties and the geometry of the sun-sensor-surface system.

2. SENSOR RADIOMETRIC CALIBRATION

2.1 Introduction

An imaging sensor system converts the radiant energy that reaches it into data that capture that energy’s intensity, spectral character and, in some cases, phase and polarization. The data are subsequently processed in various ways to yield Level 0 or Level 1 products for users. As denoted in Figure 7-1, by convention, raw image data and calibrated radiances at the top of the atmosphere (TOA) are referred to as Level 0 and Level 1 data. For quantitative analysis and to use the best quality data for forest applications, Level 2 data consisting of radiometrically calibrated and geolocated physical variables such as surface reflectance, emittance, temperature, etc. are preferred or required. Unfortunately, few remote sensing data product

generation systems offer Level 2 products and users must instead undertake this step themselves using in-house or commercial image analysis software systems, or through a suitable value-added company. Overall, there are many factors and functions that affect the radiometry of Earth observation data. Some of these factors are addressed by the sensor builders, sensor operators, and/or data processing organizations, whereas others are left to the user.

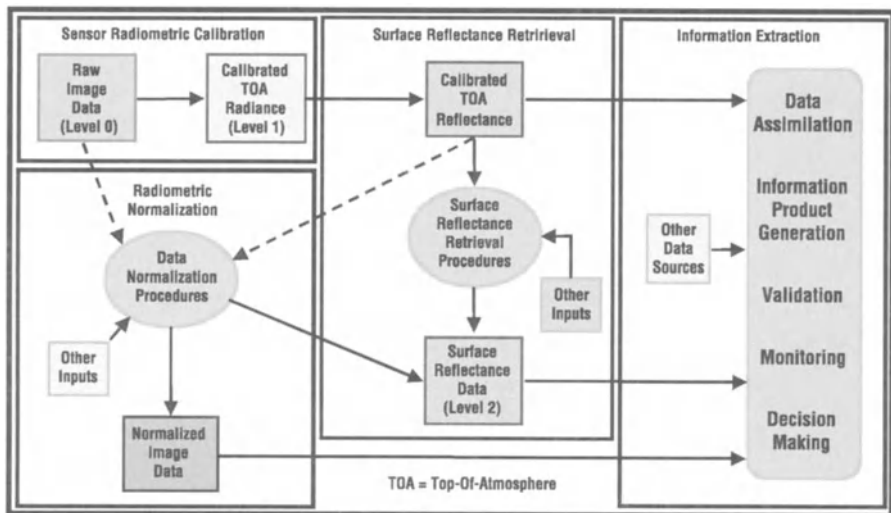


Figure 7-1. Satellite data consistency in terms of radiometric scale for information extraction.

In forest applications, surface reflectance is the geophysical variable of particular interest in the solar reflective part of the electromagnetic spectrum. Overstorey and understorey vegetation, soils, water bodies, and other surface features, which together make up “land cover”, often have differences in their reflectance characteristics that help to distinguish them, at least as one aspect of the detection, identification and characterization process. More subtle differences in the reflectance spectra can sometimes be used to distinguish specific forest species of interest, estimate biophysical and structural parameters, or to identify vegetation stress conditions.

The surface spectral reflectance, ρ_{surf} , can be defined as the ratio of the upward radiance, L , from the target (as measured just above the target) divided by the downward irradiance, E , that illuminates the target:

$$\rho_{surf}(\lambda) = \frac{\pi L(\lambda)}{E(\lambda)} \quad (1)$$

where λ indicates that these quantities are wavelength-dependent. Radiance describes the flux of energy impinging on a given area from a specified direction. Conventional units for radiance are watts per square metre per steradian ($\text{Wm}^{-2}\text{sr}^{-1}$), although some data suppliers use different units. Irradiance describes the flux of energy impinging on a given area from all directions and is measured in watts per square metre (Wm^{-2}). There are numerous specialized definitions of reflectance (Slater 1980; Schott 1997), but the definition given in equation (1) is simple and widely accepted by Earth observation specialists and will be used here.

Because most sensors acquire data in spectral bandpasses and not at single wavelengths, it is customary to express radiances and irradiances normalized with respect to the spectral band, i.e., per unit wavelength, usually per micrometer (hence, the units are $\text{Wm}^{-2}\text{sr}^{-1}\mu\text{m}^{-1}$ and $\text{Wm}^{-2}\mu\text{m}^{-1}$, respectively). Thus, for remote sensing imagery in a given spectral band, the goal is to determine the band-average surface reflectance:

$$\rho_{\text{surf}}(\bar{\lambda}) = \frac{\pi L(\bar{\lambda})}{E(\bar{\lambda})} \quad (2)$$

where the symbol $\bar{\lambda}$ is used to indicate that these variables have been wavelength-averaged for a given spectral band.

2.2 Defining calibration

The international Committee on Earth Observation Satellites (CEOS) Working Group on Calibration and Validation defines “calibration” as the process of quantitatively defining the system response to known, controlled signal inputs (CEOS 1995), as set in the context of “*calibration/validation*” which refers to: “... *the entire suite of processing algorithms used to convert raw data into accurate and useful geophysical quantities on the surface of the Earth that are verified to be self-consistent*” Teillet (1997). To derive calibrated data from an optical satellite remote sensing system requires knowing the relationship between quantized data, Q , recorded on the ground from data output by the satellite sensor (raw, Level-0 data, in units of digital counts) and the TOA at-satellite radiance input to the sensor (calibrated, Level 1 data).

Rather than computing radiance directly, image data production systems typically transform raw data, Q , to calibrated data, Q_{cal} . It is then up to the user to use the calibration coefficients supplied with the data product to transform calibrated digital counts, Q_{cal} , to TOA radiance, L^* , where the asterisk indicates a TOA quantity. Thus, both the production system and the

user require information about the sensor's radiometric calibration. This remains one of the most challenging aspects of the production and quantitative use of satellite imagery.

2.2.1 Dynamic range

The range of quantized levels and radiances that any given sensor system's performance can encompass is known as the dynamic range. The dynamic range in counts will be determined primarily by the data representation scheme that is chosen. For Landsat and many other optical sensors, Q is recorded as an eight-bit integer, such that it can take on any integer value from 0 to 255. If greater precision is needed, higher-order (e.g. 10-bit or 12-bit) or floating-point representations can be used. Once the data representation scheme is established, it is necessary to specify the range and scaling parameters that will actually be used to represent intensities. The dynamic range in radiance units is set by the sensor design and calibration teams. For sensor systems with linear response, it is specified in terms of the minimum radiance, L_{\min} , which corresponds to a digital level of $Q_{\text{cal}, \min}$, and the maximum radiance, L_{\max} , which corresponds to a digital level of $Q_{\text{cal}, \max}$ (Markham and Barker 1987). The dynamic range must be set to cover the full range of radiance ("brightness") of objects to be imaged. The four parameters, $Q_{\text{cal}, \min}$, $Q_{\text{cal}, \max}$, L_{\min} , and L_{\max} , establish a known relationship between calibrated data, Q_{cal} , and radiance at the sensor, L^* .

2.2.2 Relative calibration for destriping

Digital data from optical sensors can have various cosmetic defects such as striping or coherent noise patterns (Helder et al. 1996; Singh 1985; Poros and Peterson 1985). Image data production systems generally have algorithms to reduce or eliminate these effects. In most cases, the destriping correction is based on scene statistics, i.e., the assumption that, over an entire image, each detector in a given spectral band is exposed to the same radiance distribution on average. Thus, the gains and biases of the individual detectors can be fine-tuned to minimize striping. Although this relative calibration yields data that are not calibrated on an absolute radiometric scale, they can be used in cases where the user is only interested in a single scene for further analysis and there is to be no comparison with other scenes and no retrieval of surface reflectances.

2.3 Converting digital counts to at-sensor radiance

The radiometric calibration equation is,

$$L^* = \frac{1}{G} [Q_{cal} - Q_o] \quad (3)$$

The gain and bias calibration parameters G and Q_o are specified in terms of the spectral radiances corresponding to $Q_{cal, \min}$ and $Q_{cal, \max}$, i.e., $L_{\min} = L^*$ when $Q_{cal} = Q_{cal, \min}$ and $L_{\max} = L^*$ when $Q_{cal} = Q_{cal, \max}$. Then it can be shown that:

$$G = \frac{Q_{cal, \max} - Q_{cal, \min}}{L_{\max} - L_{\min}} \quad (\text{units are counts per unit radiance}) \quad (4)$$

and

$$Q_o = -(Q_{cal, \max} - Q_{cal, \min}) \frac{L_{\min}}{L_{\max} - L_{\min}} \quad (\text{units are counts}). \quad (5)$$

If a particular project involves the intercomparison of scenes from multiple sensors, it is necessary to transform to radiance units before they can be compared. If a particular project involves the intercomparison of several scenes from a single sensor, the data can be used in the form of calibrated counts, Q_{cal} . In the latter case, it is not necessary to transform to radiance units.

2.3.1 Establishing sensor radiometric calibration coefficients

Approaches to sensor radiometric calibration and cross-calibration between sensors have been well-documented (Dingirard and Slater 1999) and new methodologies continue to evolve (Teillet et al. 2001a,b). Briefly, temporal radiometric consistency for a given sensor and between different sensors starts with calibration of the individual sensors, including the development of a stable sensor, detailed pre-launch characterization, and on-orbit calibration. Post-launch radiometric calibrations can be based on reference to onboard standards, solar and/or lunar illumination, and ground-based test sites. Cross-calibration between sensors can be based on prelaunch measurements in the laboratory using common sources or transfer radiometers at the same or different times. For those missions operating during the same time periods, post-launch cross-calibration can make use of near-simultaneous imaging of common targets on the surface of the Earth or Moon or mutual reference to pseudo-invariant features or data from a third sensor.

In the case of Landsat-7, for example, the Enhanced Thematic Mapper Plus (ETM+) sensor was calibrated repeatedly before launch by observing

well-calibrated spectral radiance standards in a laboratory. The Landsat-7 sensor system includes three independent post-launch calibration devices onboard. The radiometric calibration data from these onboard calibration systems, as well as data from ground-look calibration (often called vicarious calibration (Thome 2001)), are reviewed periodically by a team of specialists. The best-available parameters for the calibration transformation are made available with each product and on the Internet in a Calibration Parameter File (CPF), which is updated quarterly⁶.

2.4 Converting at-sensor radiance to at-sensor reflectance

The TOA or at-sensor reflectance, ρ^* , can be defined as a function of the radiance observed by the sensor at the satellite as follows:

$$\rho^*(\bar{\lambda}) = \frac{\pi d_s^2 L^*(\bar{\lambda})}{E_0(\bar{\lambda}) \cos(\theta_z)} \quad (6)$$

where the symbol $\bar{\lambda}$ is used to indicate that these variables are wavelength-averaged for each spectral band and the asterisk indicates TOA values. E_0 is the exo-atmospheric solar irradiance, θ_z is the solar zenith angle (SZA: 90°-sun elevation), and d_s is the Earth-Sun distance in Astronomical Units. The use of TOA reflectance as opposed to radiance corrects for at least some of the sources of variation that affect satellite data and makes possible a greater degree of automation than would be possible otherwise. In particular, using top-of-atmosphere reflectance removes variations in solar illumination caused by cyclical changes in the Earth-sun distance and in SZA, as well as differences in irradiance due to differences in spectral bands from sensor to sensor.

3. SURFACE REFLECTANCE RETRIEVAL

3.1 Introduction

Scattering and absorption due to gas molecules and aerosols in the atmosphere modify surface reflectance information propagated through the atmosphere to the satellite sensor. Given that the optical properties of the Earth's atmosphere are not uniform spatially or temporally, image

⁶ http://ltpwww.gsfc.nasa.gov/IAS/handbook/handbook_htmls/chapter9/chapter9.html

corrections for these effects in the solar-reflective spectral bands are needed to put satellite data on the same radiometric scale for investigations intended to monitor terrestrial surfaces over time and space. The various approaches to atmospheric correction are well documented in the literature (e.g., Schott 1997) and several atmospheric radiative transfer codes are routinely available in modern image analysis systems. Current solutions typically involve the use of a radiative transfer code or pre-computed look-up table results to save computation time. Although there is presently no widely-accepted standard as to which atmospheric correction code should be used, MODTRAN-4 (Anderson et al. 2000) is recommended based on our experience. However, of greater importance is the fact that most of the predominantly used codes tend to disagree significantly only for very large aerosol optical depths and large off-nadir geometries ($>60^\circ$). Therefore, the proper use of a given atmospheric code should be of greater concern than which code to use, although the choice of code is an important factor in the correction of high spectral resolution data (Staenz et al. 1994). Monochromatic computations should not be used (Teillet 1989) while bandpass calculations based on relative spectral response profiles with 0.0025 micrometer spacing or better are recommended.

The key to operational atmospheric correction for surface reflectance retrieval (Figure 7-2) is timely and ready access to information on atmospheric variables such as aerosol optical depth (AOD, the degree to which atmospheric aerosols prevent light from passing through the atmosphere) and water vapour content (WVC). Although the computational tools are available, the user is still left with the problem of obtaining the necessary atmospheric parameters for input to the image correction. The main possibilities in this respect are as follows.

1. Measure the required parameters in the field at the same time as image acquisition.
2. Query an on-line source of radiosonde and/or sunphotometer network data that may have acquired parameters near the time and location of the image (Bokoye et al. 2001).
3. Assume fixed standard values (Fedosejevs et al. 2000).
4. Use climatological values developed over time.
5. Estimate the required parameters from the image data themselves, using techniques such as the dark target approach (Teillet and Fedosejevs 1995).
6. Use data assimilation results based on dynamic models driven by analyzed meteorological data (O'Neill et al. 2002).

The challenge is to make optimum use of available ground-based and satellite-based atmospheric optical measurements and to ensure they are consistent and easily accessible. An atmospheric optical parameter

estimation system has been proposed (O'Neill et al. 2002; Freemantle et al. 2002) to provide optical parameters as on-line WWW maps for any time and place across extended regions such as Canada or North America based on available climate to meteorological scale data and models. Aside from making atmospheric corrections more operational, this concept of Networked On-line Mapping of Atmospheric Data (NOMAD) transfers the responsibility of quality atmospheric parameters from the user to the scientific and technical specialists maintaining the atmospheric parameter server.

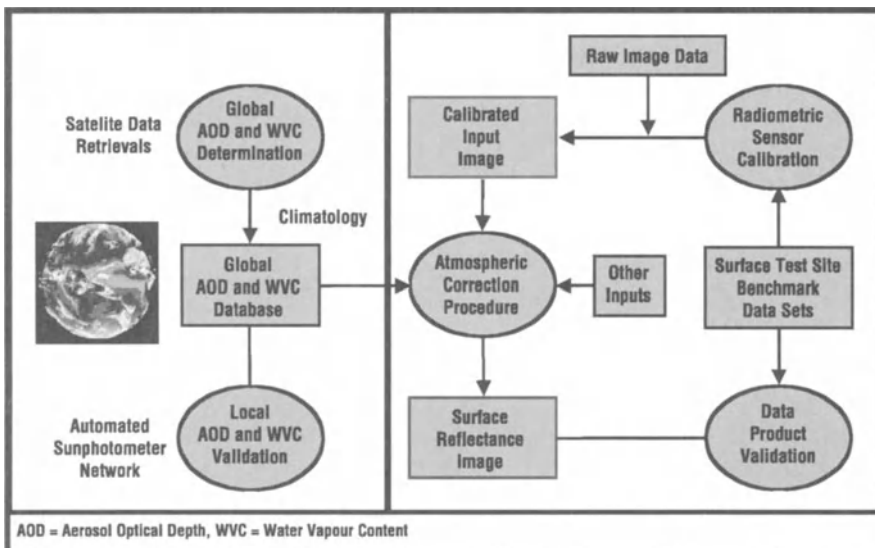


Figure 7-2. Elements of an operational surface reflectance retrieval scheme.

3.1.1 Spectral characterization

Although it receives relatively less attention than other aspects of image radiometry, spectral characterization is an important consideration for proper surface reflectance retrieval, regardless of how wide or narrow the spectral bands may be. Spectral bands are designed for specific applications and data products are susceptible to variations in spectral bandpasses that can occur after launch or spectral band differences between different sensors used in a given applications algorithm or model. Clearly, if the spectral bands have changed in position or width or there are uncertainties as to their characteristics, there is a direct impact on radiometric and atmospheric processing, as well as on derived information products (Flittner and Slater 1991; Teillet 1990; Suits et al. 1988). The issue arises in a significant way in the processing and analysis of high spectral resolution data, although relatively few studies have examined the impact of these effects (Goetz et al.

1995; Teillet et al. 1997a; Teillet and Irons 1990). In practice, there is little that users can do to take into account changes in spectral band performance. However, even when spectral bands perform as designed, users should be aware that similar information products derived from different sensors with dissimilar spectral bands may not be directly comparable.

3.2 Geometric effects on image radiometry

Reflectance anisotropy as a function of illumination and viewing geometry is a fundamental property of any terrestrial surface and is best described in terms of the bi-directional reflectance distribution function (BRDF). Forests are highly anisotropic in their reflectance properties and this has an important influence on image radiometric characteristics (Figure 7-3). Various approaches to modelling and dealing with BRDF effects are well documented in the literature (for example see Chen and Cihlar 1997). Nevertheless, it should be mentioned that, although anisotropic reflectance effects have been studied extensively, they remain challenging to deal with in an operational setting and there are many other geometric effects to consider apart from the BRDF.

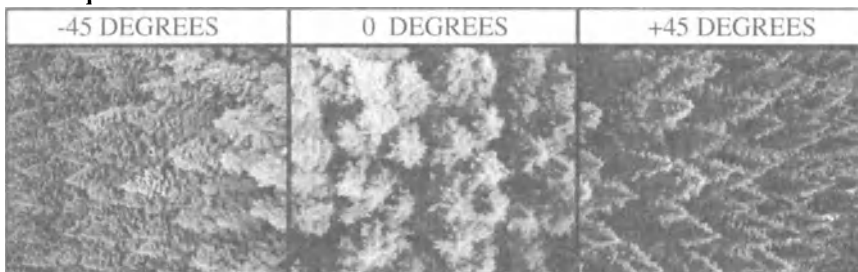


Figure 7-3. Three digital camera images of a black spruce (*Picea mariana*) canopy, Petawawa National Forestry Institute, illustrating anisotropic reflectance effects (solar illumination is from the right). (Photographed by Dr. Richard A. Fournier).

Except for large angles, the influence of varying illumination and viewing paths through the atmosphere is generally well handled by most atmospheric correction algorithms. However, image data acquired for high-latitude regions, where sun angles are typically far from the zenith, are more difficult to correct for atmospheric effects. Topographic effects are discussed in section 5 of this Chapter.

Increasingly, users are integrating data from different remote sensing systems (and from a variety of geospatial data sources), most if not all of which sample the Earth's surface in different ways. Even a given sensor acquires data in ways that can vary significantly spatially and temporally. It is critical to establish the validity of, and provide accuracy assessments for,

data fusion products and yet these considerations are not taken into account in current radiometric image processing systems.

The nature of the remote sensing image pixel (Townshend 1981) has been the subject of renewed attention in the literature in recent years (Townshend et al. 2000; Cracknell 1998; Fisher 1997). A pixel is not a true geographical object and, although some contemporary analyses attempt to allow for mixed pixels, it is easy to forget that a substantial proportion of the signal apparently coming from the land area represented by a given pixel comes from the surrounding areas. This has important ramifications on the per-pixel characterization of land cover and on the integration of remote sensing data into geographical information systems (GIS). It results from many factors, including the sensor's optical characteristics and image acquisition geometry as well as atmospheric effects.

3.3 Impacts of radiometry on higher level products: the NDVI example

Vegetation indices from remote sensing measurements are increasingly being used as an indirect means of studying a variety of Earth system properties (Bannari et al. 1995). Sensors with spectral bands in the red (RED) and near-infrared (NIR) lend themselves well to vegetation monitoring since the difference between these bands is a strong indicator of the amount of photosynthetically active green biomass (Tucker 1979). For example, the Normalized Difference Vegetation Index (NDVI = $[NIR - RED] / [NIR + RED]$) has been used in multi-temporal mapping of vegetation dynamics based on maximum-NDVI compositing, increasingly at continental to global scales (Townshend et al. 1994). While NDVI is mentioned as an example, the same principles potentially apply to many other high-level products.

Given that the spectral and spatial characteristics of imagery in the red and near infrared vary from sensor to sensor, NDVI values based on data from different instruments may not be directly comparable. Values of NDVI for a given vegetation target will also differ as a function of the radiometric processing applied to the image data (Price 1987; Goward et al. 1991; Guyot and Gu 1994; Roderick et al. 1996; Teillet et al. 1997a). The properties of NDVI space will vary considerably depending on whether NDVI is defined in terms of quantized levels, TOA radiances, TOA reflectances, or atmospherically corrected surface reflectances. Thus, it is essential to document the units of the quantities in the red and near-infrared spectral bands used to form the NDVI. The impact of changes in spectral bandwidth, spectral band location and spatial scale on NDVI has been examined in the

forestry context by Teillet et al. (1997a), but a review of those results is beyond the scope of this Chapter.

4. IMAGE NORMALIZATION

4.1 Introduction

Image normalization refers to the process of adjusting the radiometric properties of one image to match that of another. This is important in forest projects involving multiple images acquired over larger areas (e.g. forest inventory) or at different times (e.g. change detection and updates) that typically possess radiometric differences due to variations in solar illumination and atmospheric attenuation, resulting in different at-sensor radiance values unrelated to the actual reflectance of the land surface. Unfortunately, it may not be possible to compute surface reflectance directly for each image using the more detailed methods presented in section 3, since the required inputs are not always available or practical to obtain over larger areas or for historical image archives (Yuan and Elvidge 1996). Instead, a variety of image transformations can be applied to achieve a common level of image correction amongst a set of images, or to adjust all images to a common radiometric base.

This discussion is divided into two main categories: (1) scene specific normalization, in which a common adjustment or set of equations is applied individually to a series of images but without direct reference to other images, and (2) relative radiometric normalization, in which the radiometric properties of images are adjusted to match those of a pre-selected reference image. In both cases, the end product is intended to be a set of images that have a common radiometric base, or at least a common level of correction applied. More involved procedures, such as extensive spatial mosaicking, temporal compositing over lengthy time series and major radiometric image data production systems (e.g., Cihlar et al. 2002) are the focus of other Chapters in this book (Cihlar et al., Chapters 12 and 13; Huang et al., Chapter 14) and are therefore not treated here, however, these procedures utilise and extend many of the principles discussed here.

4.2 Scene specific normalization

4.2.1 Solar zenith angle corrections

One of the major factors influencing change in radiometric response at different times or at different places, in addition to actual surface variability, results from differences in solar position. Image data acquired under different SZA can be normalized to each other by calculating pixel brightness values with respect to a specified (common) solar position. Normalization procedures can be applied by dividing each pixel value by the cosine of the SZA for the particular time and location of imaging. However, these corrections do not account for atmospheric or topographic effects.

4.2.2 Uniform haze correction

The reduction or removal of atmospheric haze differences between sets of images can be approached by subtracting the digital counts (Q) associated with the darkest pixels present in a scene (Chavez 1988). This assumes that the contribution due to atmospheric haze will be equal to the Q values detected for a ground surface area having zero reflectance (Q_0). A similar approach was proposed by Tokola et al. (1999) which involved normalisation of image bands to a normal distribution by first subtracting an equivalent Q_0 value from each spectral band mean and then dividing the result by the standard deviation of the band. However, these methods can only provide an estimation of atmospheric haze at different wavelengths, with the further limitation that the zero reflectance assumption may not hold for a given area.

4.2.3 Surface spectral measurement

Image data sets can be radiometrically corrected with reference to surface spectral measurements. For example, the empirical line method (Marsh and Lyon 1981) requires relatively large, homogeneous bright and dark ground targets that are measured in the field using a spectroradiometer (Milton 1987), processed to reflectance (e.g., Peddle et al. 2001a), and used as the basis to adjust pixel Q values in one or more images to the corresponding measured surface reflectances that cover the dynamic range of data and compensate empirically for atmospheric effects. While sometimes feasible for a smaller number of images, these approaches are not widely applicable with larger numbers of scenes since appropriate targets may not always exist, and also because of the prohibitive amount of field measurement required. Field reference spectra may, however, be useful in smaller projects

or as a means of quality control and validation of selected individual scenes from a larger sample of images subjected to relative radiometric normalisation.

4.3 Relative radiometric normalisation

To address issues of obtaining suitable data for detailed atmospheric correction or ground spectral measurement over large areas, a variety of Relative Radiometric Normalisation (RRN) approaches have been developed based on empirical adjustments to provide radiometric consistency across multiple images (Hall et al. 1991; Crist and Cicone 1984; Schott et al. 1988). RRNs utilize one image as a reference data set and adjust the radiometric properties of other images to match that reference (Hall et al. 1991). The reference image is usually corrected to reflectance, however, this is not a requirement in which case the original radiometric condition of the reference image is retained. It is important to note that the radiometric normalisation techniques described here generally are only applicable to multiple data sets acquired by the same sensor system.

Empirical linear spectral normalisation is performed sequentially over large image sets in which each subject image (X) is radiometrically rectified (Hall et al. 1991) to a reference image (Y) based on a linear data transformation. The reference image is usually chosen as one with favourable atmospheric properties, known surface features, existing ground spectral and atmospheric data, and also with some consideration given to the location of other images and any major landform changes or known atmospheric changes, although none of these are requirements of RRN. The general form of the linear transformation function is derived using the data scattergram of image X and Y in each spectral band, with the line passing through the center of the scattergram defined as representing pixels that have not changed in terms of land cover type and radiometric properties. This defines the empirical relationship between radiometric values in different images, with the common form of radiometric rectification expressed as:

$$u_k = a_k x_k + b_k \quad (7)$$

where: x_k is the digital number (Q) of band k in subject image (X) on date 1, u_k is the normalized Q of band k on date 1, and a_k and b_k are normalisation constants for band k with respect to the reference image (Yuan and Elvidge 1996). A variety of methods, some with different purposes (e.g., different atmospheric conditions, or spatial normalisation versus single area multi-temporal images for change detection) and requirements (e.g., image thresholds and samples, pseudo-invariant features) have been developed

based on different approaches to deriving these normalisation constants (7), as discussed next.

Haze correction (HC) normalisation assumes that pixels with zero reflectance in image X and Y should have the same minimum Q values. HC normalisation sets the gain term to unity ($a_k=1$) and is therefore a simple offset correction with the normalisation coefficient:

$$b_k = y_k(\min) - x_k(\min) \quad (8)$$

where: $x_k(\min)$ and $y_k(\min)$ are the haze values in band k in images X and Y, respectively. Haze values are calculated as the Q threshold below which is the darkest 0.1 % of the image.

The Minimum-maximum (MM) method normalizes each given subject image (X) band to have the same minimum and maximum Q values as each corresponding band of the reference image (Y). Normalisation coefficients are computed as:

$$a_k = [y_k(\max) - y_k(\min)] / [x_k(\max) - x_k(\min)]$$

$$b_k = y_k(\min) - a_k x_k(\min) \quad (9)$$

where: $x_k(\min)$, $x_k(\max)$, $y_k(\min)$, $y_k(\max)$ are the minimum and maximum Q values of band k for the two images. The MM values for each image are derived as the Q thresholds required to isolate the upper and lower 0.1 % of the image data.

The Mean-standard deviation (MS) method normalizes image X to have the same mean and standard deviation as image Y (per band). The MS normalisation coefficients are computed as:

$$a_k = s_{yk} / s_{xk}$$

$$b_k = (\text{mean}) y_k - a_k (\text{mean}) x_k \quad (10)$$

where $(\text{mean}) x_k$ and $(\text{mean}) y_k$ are the mean values per band in image X and Y, and s_{xk} and s_{yk} are the standard deviations per band in image X and Y.

Simple regression (SR) normalisation uses a least-squares regression between image X and Y, with normalisation coefficients solved by minimising the least-squares regression equation over the entire scene:

$$[\text{scene sum}] (y_k - a_k x_k - b_k)^2 = \min \quad (11)$$

with normalisation coefficients:

$$a_k = s_{yk} / s_{xk}$$

$$b_k = (\text{mean}) y_k - a_k (\text{mean}) x_k \quad (12)$$

where:

$$s_{yk} = (1/n) (\text{[scene sum]} (x_k - \text{mean}x_k) (y_k - \text{mean}y_k)),$$

$$s_{xk} = (1/n) (\text{[scene sum]} (x_k - \text{mean}x_k)^2),$$

n = number of pixels in scene.

The Dark set-Bright set (DB) normalisation method uses the average of a set of dark pixels to replace the minimum value in the scene, and the average of a set of bright pixels to replace the maximum value, with normalization coefficients:

$$a_k = [(\text{mean}) y_k^b - (\text{mean}) y_k^d] / [(\text{mean}) x_k^b - (\text{mean}) x_k^d]$$

$$b_k = (\text{mean}) y_k^d - a_k (\text{mean}) x_k^d \quad (13)$$

where the dark (d) and bright (b) sets can be extracted from images X and Y using a Kauth-Thomas (KT) transformation (Kauth and Thomas 1976; Crist 1985; Hall et al. 1991) in cases where the image is predominantly vegetated, as is often the case in forest scenes. Other implementations of this approach have obtained dark sets from low reflectance areas such as deep, clear lakes or dense, dark vegetation, and bright sets from objects of high reflectivity such as rock outcrops, provided these cover sufficiently large areas and are not subject to illumination variations due to topographic effects.

Pseudoinvariant (PI) normalization (Schott et al. 1988) requires identification of objects or features that do not experience any significant reflectance change from two image dates, such as roads, urban features, or in some cases, large rock areas, playas or lake bed surfaces. These features can also be derived through analysis of the infrared to red ratio of image X and Y to identify pixels with minimal green vegetation, with a NIR threshold to exclude water pixels. Means and standard deviations (s) of the multi-date PI sets (X and Y) are incorporated in the normalization coefficients as:

$$a_k = s_{yk}^{(PI)} / s_{xk}^{(PI)}$$

$$b_k = (\text{mean})y_k^{(PI)} - a_k(\text{mean})x_k^{(PI)} \quad (14)$$

The No-Change (NC) regression normalization method (Yuan and Elvidge 1993; Elvidge et al. 1995) is a modification of the simple regression (SR) normalization approach in which, instead of using the entire scene, the normalization coefficients are derived using a subset of image data where there has been no significant reflectance change. This subset for analysis will typically comprise a narrow central belt in the scattergram of image X and Y whose width is primarily a function of phenological variation in vegetation. The equations for NC are identical to those for SR, except they are applied to the NC subset instead of the full scene. NC subsets are formally derived by first calculating the spectral midpoint of land and water pixels from distribution peaks in NIR band combination scattergrams, based on an assumption that >50 % of pixels did not experience any significant land cover change. After solving the least squares equation (11), the NC normalization coefficients are derived as:

$$a_k = S_{xkyk}^{(nc)} / S_{xkxk}^{(nc)}$$

$$b_k = (\text{mean})y_k^{(nc)} - a_k(\text{mean})x_k^{(nc)} \quad (15)$$

The derivation of NC subsets has been shown to be useful in excluding scene dependent elements such as clouds, shadow and snow from the normalization process. Also, since a relatively large percentage of the image pixels are used, any normalization errors are distributed amongst different land cover types, and the procedure does not require identification of bright and dark radiometric control pixels. However, the NC approach is designed for imagery acquired under similar illumination conditions and with little variation in forest phenology, and it also requires both water and land pixels to be present in each scene.

4.3.1 Ridge method

The Ridge method was developed by Cohen et al. (unpublished manuscript) primarily for normalization of multitemporal scenes in change detection, and it was subsequently evaluated and used by Song et al. (2001). This technique is based on the assumption that linear relationships can be established between images based on the presence of inherently stable features. However, unlike other methods that require pseudo-invariant features (PIFs), the Ridge Method uses density plots for all the pixels of a certain band in a given scene, with the separate dates of image acquisition

represented on each of two axes. Spectrally stable features within each scene are plotted in a linear fashion forming a 'ridge'. A straight (best fit) line passing through the centre of this ridge defines the relationship between the separate dates of imagery. This technique is then repeated for each pair of spectral bands.

By using a density plot of all image pixels within a scene, the ridge method circumvents the problem of identifying stable PIFs for each date of image acquisition. The ridge formed by plotting each date of imagery against the other does not change as a result of minor land cover changes between the two dates, as average values are computed for each scene. Song et al. (2001) found that, if large changes in land use / land cover exist between the two dates of imagery, the ridge method will not perform well. However, for basic change detection studies and relative atmospheric correction or normalization between two or more dates of imagery, the ridge method can be effective for defining the relationship between image pairs. The flexibility and robustness of this approach, coupled with the fact that it is not complex, results in it being an attractive option for consideration for large area, multi-scene radiometric processing applications.

5. IMPACTS OF TOPOGRAPHY

5.1 Introduction

Areas of higher relief such as mountainous environments as well as other areas of moderate relief comprise significant areas of forested terrain, and include different ecosystem properties and forest management practices. Terrain variations can significantly influence the radiometric properties of signals received by airborne and satellite sensors in these areas. As a result, a number of approaches have been developed to consider the topographic influence on radiometric signals. Some of these have used simple band-ratios (e.g., Holben and Justice 1981) or other multispectral transformations (Eliason et al. 1981; Pouch and Compagna 1990). However, these have been less successful (Richter 1997). Instead, most radiometric procedures use digital elevation models (DEMs) to provide terrain elevation, slope, aspect and other derivatives to explicitly describe the surface geomorphometry. These are reviewed, however, important issues such as DEM acquisition, processing and geometric correction are beyond the scope of this Chapter. Here, we focus on topographic normalization procedures that aim to minimise or eliminate the influence of terrain on image radiometry to facilitate consistent forest information extraction in these challenging areas. It should also be noted that some image analysis procedures deal with

topography by using DEMs and derivatives directly in the analysis (e.g., classification, see Franklin 1987; Carlotto 1998) and that topographic corrections have also been incorporated into detailed atmospheric radiative transfer codes (Richter 1997). However, these methods are outside the domain of radiometric image processing discussed in this Chapter.

Most approaches developed for forestry analysis have assumed a Lambertian surface, defined as being a perfectly diffuse reflector appearing equally bright from all viewing angles. This assumption neglects geometric influences and assumes an isotropic reflectance law (Richter 1997) and therefore in mountainous terrain this assumption can be problematic. Analyses using the Lambertian assumption are more likely to be valid when restricted to slopes $< 25^\circ$ and effective illumination angles $< 45^\circ$ (Teillet et al. 1982).

Two main categories of terrain normalization are presented here: (i) surface illumination based slope-aspect corrections that use the cosine of the incident solar angle (Smith et al. 1980; Teillet et al. 1982; Cavayas 1987), and (ii) model based corrections that deal with solar radiation interactions with forest canopies and stands.

5.2 Surface illumination corrections

5.2.1 Cosine correction

The amount of irradiance reaching an inclined pixel is proportional to the cosine of the incident angle, defined as the angle between the normal on the pixel in question and the zenith direction. However, the cosine law only takes into account terrain slope and the SZA, while assuming a Lambertian surface and that the distance between Sun and Earth is constant for all scenes. The cosine correction (Smith et al. 1980; Teillet et al. 1982; Cavayas 1987) is:

$$L^*_{\text{H}} = L^*_{\text{T}} (\cos(\theta_z) / \cos(i)) \quad (16)$$

where:

L^*_{H} = radiance observed for horizontal surface;

L^*_{T} = radiance observed over sloped terrain;

θ_z = solar zenith angle;

i = sun incidence angle in relation to the normal on a pixel.

However, this correction considers only the direct part of irradiance, even though weakly illuminated regions can receive substantial diffuse irradiance, in which cases the cosine correction has a disproportional brightening effect. As a result, Teillet et al. (1982) recommended the cosine correction be

applied only in cases where incident angles are $< 55^\circ$. As noted before, the cosine correction can also be applied in flat terrain to equalize illumination differences due to different sun positions in multitemporal datasets.

5.2.2 Minnaert correction

The Minnaert correction (Smith et al. 1980; Teillet et al. 1982; Cavayas 1987) is a modification of the cosine correction that incorporates a Minnaert constant (k) as a measure or estimate of the extent to which a surface is Lambertian:

$$L^*_{\text{H}} = L^*_{\text{T}} (\cos(\theta_z) / \cos(i))^k \quad (17)$$

The values of k vary between 0 and 1. The smaller the k value, the weaker the influence of the quotient (17), especially in areas with a $\cos(i)$ near zero, where k increases the denominator and prevents a division by small values, thereby reducing the overcorrection problem of the cosine correction. However, it is not always straightforward to specify the k parameter, and further, this will vary across the scene. Generally, a bulk estimate for k is used across a scene as a first-order correction. However, Meyer et al. (1993) suggest k can be determined empirically by linearizing (17) logarithmically and estimating the slope of a linear regression.

5.2.3 Statistical-empirical approach

The statistical-empirical approach (Teillet et al. 1982) correlates pixel Q values with the corresponding predicted illumination ($\cos i$) from a DEM. The slope of the regression line defines the statistical relationship between a given forest stand and how its radiometric response (Q) changes as a function of terrain slope, as:

$$L^*_{\text{H}} = L^*_{\text{T}} - \cos(i)m - b + (\text{mean})L^*_{\text{T}} \quad (18)$$

where terms in addition to those defined in (16) are:

- (mean) L^*_{T} = average of L^*_{T} for forested pixels (from ground data)
- m = slope of the regression line;
- b = y-intercept of the regression line.

This approach requires a prior specification of forested pixels, with the quality of the correction also partly dependent on the degree of explanation of the regression function.

5.2.4 C-correction

Teillet et al. (1982) described a modification to the cosine correction that utilises the slope (m) and intercept (b) of the regression line from the statistical-empirical approach. The parameter c is derived as the quotient of b and m and integrated as an additive term in (16) as:

$$c = b/m$$

$$L_H = L_T [(\cos(\theta_z) + c) / (\cos(i) + c)] \quad (19)$$

Teillet et al. (1982) describe how the parameter c might emulate the effect of path radiance on the slope-aspect correction, but the physical analogies are not exact (Meyer et al. 1993). Mathematically, the effect of c is similar to that of the Minnaert constant by increasing the denominator and reducing the overcorrection of faintly illuminated pixels (Meyer et al. 1993).

Any one of these four methods have been popular choices by investigators performing radiometric corrections for terrain. In general, results have varied, with more favourable outcomes found in non-complex forest canopies and also in areas where altitudinal zonation was low to moderate. However, results have been marginal in areas of more complex forested terrain (Allen 2000). There have been fewer direct comparisons of all four methods. For example, Meyer et al. (1993) performed a quantitative and visual assessment and comparison of the four methods described in this section for forest classifications in a mountainous environment in central Switzerland. They found similar levels of improvement using the Statistical-Empirical, Minnaert and C-correction methods (the so-called SMC methods, Meyer et al. 1993) in terms of classification accuracy and reduction of the visual topographic effect. However, in a different study, Franklin (1991) compared all four methods and found only small improvements in forest classification accuracy for several more complex, high-relief mountain environments.

5.3 Model based corrections

The SMC methods discussed above are based on Sun-surface-sensor geometry. However, in forested areas, the most significant topographic impacts are caused not by the underlying surface beneath trees but instead by changes in the proportions of sunlit canopy and shadow presented to a sensor in sloped terrain (Gu and Gillespie 1998). Ignoring this leads to error in topographic normalization, which is further exacerbated by

oversimplifications of canopy BRDF and improper treatments of diffuse radiation in forests. Accordingly, Gu and Gillespie (1998) proposed a Sun-*Canopy*-Sensor (SCS) approach in which the sub-pixel scale component of sunlit canopy is modeled with respect to surface terrain influences on stand structure illumination characteristics. They identified three scales of interaction between solar radiation and natural surfaces: (i) branches and needles, (ii) within-crown interactions, controlled by factors such as tree structure and leaf orientation, and (iii) canopies, which are affected by interactions of light amongst trees. Since trees are geotropic (vertical regardless of local slope angle) only the third (canopy) scale is affected by terrain and therefore considered in the SCS approach. The SCS model provides an estimate of the per-pixel sunlit canopy area with respect to sun-sensor geometry and local terrain position derived from a DEM. Gu and Gillespie (1998) note that more complex forest stand structures make exact characterisation difficult (e.g. variable density, age, height etc.) and addressed this using approximations based on simplified models of tree crown shape, height and density. It was also recognised that SCS only accounts for the sunlit portion of a canopy, and that shadows and background components further influence the overall pixel signal received. Nonetheless, the SCS model approach provided improved results compared to the SCM methods (Gu and Gillespie 1998).

Johnson et al. (2000) used a geometric optical reflectance model for terrain normalization as part of biophysical structural analyses of compact airborne spectrographic imager (casi) airborne imagery (Anger et al. 1994) of Canadian Rocky Mountain forests. In that application, the sub-pixel scale scene fractions of sunlit canopy (C), sunlit background (B) and shadow (S) were of interest following earlier work where these fractions provided improved predictions of LAI, biomass and NPP in boreal forest environments using spectral mixture analysis (Hall et al. 1995) and canopy reflectance models (Peddle et al. 1999) compared to vegetation indices (Peddle et al. 2001b). Johnson et al. (2000) adjusted the montane forest scene fractions to that of flat terrain using the Li and Stahler (1992) Geometric Optical Mutual Shadowing (GOMS) model, which includes slope and aspect in its formulation. The model was run in multiple-forward-mode (MFM) (Peddle et al. 2002), a new approach to obtaining model inversion results from non-invertible (and other) models. MFM works by matching modeled reflectance values with actual values acquired from a remote sensor, from which the physical canopy dimensions, terrain position and stand attributes that produced the modeled reflectance are output as the forest structural parameters of interest, together with the corresponding scene fractions (C, B, S) from the model. The only inputs to MFM that must be directly specified are the spectral values for each component

(endmember), since ranges are used for the structural inputs. The scene fractions, which were used as predictors of LAI in Johnson et al. (2000), were then normalized to flat terrain by running the GOMS model in forward mode using the forest structural parameters as determined by MFM for sloped terrain, but with the slope value instead set to zero (aspect undefined for flat terrain). The resulting model output was a new set of scene fractions (C, B, S) and pixel-level reflectance values that correspond to the mountain slope forest structure if placed on flat terrain. The MFM terrain normalized scene fractions were compared with scene fractions derived by separate spectral mixture analyses and NDVI of casi imagery that had been subjected to each of the statistical-empirical, Minnear, and C-correction (SMC) terrain normalization methods. Results from the original (uncorrected) imagery were also obtained. The basis for the comparison was the ability to predict LAI and effective LAI (eLAI) as determined on the ground using TRAC and LAI-2000 optical instruments, respectively, for both 1m and 2m spatial resolution 8-band casi imagery of a variety of coniferous and deciduous stands. Significant improvements were found using scene fractions compared to NDVI for each terrain normalization approach tested, with the best results obtained using the MFM modeling approach in all cases.

From these studies, it appears that these more specific, model based approaches warrant further attention and may be more appropriate for terrain normalization in forested areas.

6. CONCLUDING PERSPECTIVES

In forest applications, the level of information extraction has matured to the point where high quality digital image data are a necessary requirement. To achieve acceptable image products for analysis requires attention and, in some cases, expertise in a variety of radiometric image processing procedures to enable increasingly complex analyses to occur. It is essential to pay close attention to these issues since, if ignored, the raw or unprocessed imagery will not meet even the minimum expectations of any meaningful forest information requirement. As forest information needs accelerate in the face of pressing management and environmental concerns, and as image sensors and analysis procedures advance in quality and quantity, the danger of inappropriate radiometric image processing becomes even greater and could significantly impede progress and acceptance of the technology, despite the fact that the information content may indeed exist if appropriate radiometric procedures had been followed.

In the future, the process of radiometric calibration of Earth observation sensors and the computation of key surface parameters will have to become

increasingly transparent to the majority of users (Teillet et al. 1997b). Science users will want to know the details, but the vast majority of users will not, demanding instead product consistency accompanied by a seal of approval or some form of certification. Users will want a growing selection of higher-level and value-added products that are of consistent quality, easy to use, and reliably available. For this to be possible, data product validation and quality considerations will have to receive much more attention than in the past. The increased attention should be focused on making radiometric image processing part of the invisible quality infrastructure that characterizes any mainstream technology.

REFERENCES

- Allen, T. R. (2000). Topographic normalization of Landsat Thematic Mapper data in three mountain environments. *Geocarto International*, 15, 13-19.
- Anderson, G. P., Berk, A., Acharya, P. K., Matthew, M. W., Bernstein, L. S., Chetwynd, J. H., Dothe, H., Adler-Golden, S. M., Ratkowski, A. J., Felde, G. W., Gardner, J. A., Hoke, M. L., Richtsmeier, S. C., Pukall, B., Mello, J., & Jeong, L. S. (2000). MODTRAN4: Radiative transfer modeling for remote sensing, algorithms for multispectral, hyperspectral, and ultraspectral imagery VI. Shen, S. S., & Descour, M. R. (Eds.). *Proceedings of SPIE*, 4049, 176-183. Orlando, Florida, USA.
- Anger, C. D., Mah, S., & Babey, S. (1994). Technological enhancements to the compact airborne spectrographic imager (casi). *Proceedings, First International Conference on Airborne Remote Sensing*, 2, 205-213. Strasbourg, France.
- Bannari, A., Morin, D., Bonn, F., & Huete, A. R. (1995). A review of vegetation indices. *Remote Sensing Reviews*, 13, 95-120.
- Bokoye, A. I., Royer, A., O'Neill, N. T., Cliche, P., Fedosejevs, G., Teillet, P. M., & McArthur, L. J. B. (2001). Characterization of atmospheric aerosols across Canada from a ground-based sunphotometer network: AEROCAN. *Atmosphere-Ocean*, 39, 429-456.
- Carlotto, M. J. (1998). Spectral shape classification of Landsat Thematic Mapper imagery. *Photogrammetric Engineering and Remote Sensing*, 64, 905-913.
- Cavayas, F. (1987). Modelling and correction of topographic effect using multi-temporal satellite images. *Canadian Journal of Remote Sensing*, 13, 49-67.
- CEOS (1995). *Leadership to Ensure High-Quality Earth Observation Data: A Strategic Vision*. Committee on Earth Observation Satellites, Working Group on Calibration and Validation.
- Chavez, P. S. (1988). An improved dark-object subtraction technique for atmospheric scattering correction of multispectral data. *Remote Sensing of Environment*, 24, 459-479.
- Chen, J. M., & Cihlar, J. (1997). A hotspot function in a simple bidirectional reflectance model for satellite applications. *Journal of Geophysical Research - Atmospheres*, 102, 25907-25913.
- Cihlar, J., Chen, J., Li, Z., Latifovic, R., Fedosejevs, G., Adair, M., Park, W., Fraser, R., Trishchenko, A., Guidon, B., Stanley, D., & Morse, D. (2002). GeoComp-n, An advanced system for the processing of coarse and medium resolution satellite data - Part 2: Biophysical products for northern ecosystems. *Canadian Journal of Remote Sensing*, 28, 21-44.

- Cracknell, A. P. (1998). Synergy in remote sensing – What's in a pixel? *International Journal of Remote Sensing*, 19, 2025-2047.
- Crist, E. P. (1985). A TM Tasseled Cap equivalent transformation for reflectance factor data. *Remote Sensing of Environment*, 17, 301-306.
- Crist, E. P. & Cicone R. C. (1984). A physically-based transformation of Thematic Mapper data - the TM tasseled cap. *IEEE Transactions on Geoscience and Remote Sensing*, GE-22, 256-263.
- Dinguirard, M., & Slater, P. N. (1999). Calibration of space-multispectral imaging sensors: A review. *Remote Sensing of Environment*, 68, 194-205.
- Eliason, P., Soderblom, L. A., & Chavez, P. S. (1981). Extraction of topographic and spectral albedo function for multispectral images. *Photogrammetric Engineering and Remote Sensing*, 48, 1571-1579.
- Elvidge, C. D., Yuan, D., Weerackoon, R. D., & Lunneta, R. S. (1995). Relative radiometric normalization of Landsat Multispectral Scanner (MSS) data using an automatic scattergram controlled regression. *Photogrammetric Engineering and Remote Sensing*, 61, 1255-1260.
- Fedosejevs, G., O'Neill, N. T., Royer, A., Teillet, P. M., Bokoye, A. I., & McArthur, B. (2000). Aerosol optical depth for atmospheric correction of AVHRR composite data. *Canadian Journal of Remote Sensing*, 26, 273-284.
- Fisher, P. (1997). The pixel: a snare and a delusion. *International Journal of Remote Sensing*, 18, 679-685.
- Flittner, D. E., & Slater, P. N. (1991). Stability of narrow-band filter radiometers in the solar-reflective range. *Photogrammetric Engineering and Remote Sensing*, 57, 165-171.
- Franklin, S. E. (1987). Terrain analysis from digital patterns in geomorphometry and Landsat MSS spectral response. *Photogrammetric Engineering and Remote Sensing*, 53, 59-65.
- Franklin, S. E. (1991). Image transformations in mountainous terrain and the relationship to surface patterns. *Computers & Geosciences*, 17, 1137-1149.
- Freemantle, J., O'Neill, N. T., Teillet, P. M., Royer, A., Blanchet, J. -P., Aubé, M., Thulasiraman, S., Vachon, F., Gong, S., & Versi, M. (2002). Using Web services for atmospheric correction of remote sensing data. *Proceedings of the 2002 International Geoscience and Remote Sensing Symposium (IGARSS'02) and the Twenty-Fourth Canadian Symposium on Remote Sensing*, in press. Toronto, Ontario, Canada.
- Goetz, A. F. H., Heidebrecht, K. B., & Chrien, T. G. (1995). High accuracy in-flight wavelength calibration of imaging spectrometry data. *Summaries of the Fifth Annual JPL Airborne Earth Science Workshop*, 1, 67-69. AVIRIS Workshop, Pasadena, California.
- Goward, S. N., Markham, B. L., Dye, D. G., Dulaney, W., & Yang, J. (1991). Normalized Difference Vegetation Index measurements from the Advanced Very High Resolution Radiometer. *Remote Sensing of Environment*, 35, 257-277.
- Gu, D., & Gillespie, A. (1998). Topographic normalization of Landsat TM images of forest based on subpixel sun-canopy-sensor geometry. *Remote Sensing of Environment*, 64, 166-175.
- Guyot, G., & Gu, X. F. (1994). Effects of radiometric corrections on NDVI determined from SPOT-HRV and Landsat-TM data. *Remote Sensing of Environment*, 49, 169-180.
- Hall, F. G., Strelbel, D. E., Nickerson, J. E., & Goetz, S. J. (1991). Radiometric rectification: toward a common radiometric response among multiday, multisensor images. *Remote Sensing of Environment*, 35, 11-27.
- Hall, F. G., Shimabukuro, Y. E., & Huemmrich, K. F. (1995). Remote sensing of forest biophysical structure in boreal stands of *picea mariana* using mixture decomposition and geometric reflectance models. *Ecological Applications*, 5, 993-1013.

- Helder, D., Barker, J. Boncyk, W., & Markham, B. (1996). Short term calibration of Landsat TM: Recent findings and suggested techniques. *Proceedings of the 1996 International Geoscience and Remote Sensing Symposium (IGARSS'96)*, 1286-1289. Lincoln, Nebraska, USA.
- Holben, B. N., & Justice, C. O. (1981). An examination of spectral band ratioing to reduce the topographic effect on remotely sensed data. *International Journal of Remote Sensing*, 2, 115-133.
- Johnson, R. L., Peddle, D. R., & Hall, R. J. (2000). A modeled-based sub-pixel scale mountain terrain normalization algorithm for improved LAI estimation from airborne casi imagery. *Proceedings, 22nd Canadian Symposium on Remote Sensing*, 415-424. Victoria, BC. Canada. August 21-25, 2000. Canadian Aeronautics and Space Institute, Ottawa.
- Kauth, R. J., & Thomas, G. S. (1976). The tasseled cap - A graphic description of the spectral-temporal development of agricultural crops as seen by Landsat. *Proc., Machine Processing of Remotely Sensed Data*, 4B, 41-51.
- Li, X., & Strahler, A. H. (1992). Geometric-optical bidirectional reflectance modeling of the discrete crown vegetation canopy: effect of crown shape and mutual shadowing. *IEEE Transactions on Geoscience and Remote Sensing*, 30, 276-292.
- MacDonald, J. S. (1997). From space data to information. *Proceedings of ISPRS Joint Workshop on Sensors and Mapping From Space*, 233-240. Hannover, Germany.
- Markham, B. L., & Barker, J. L. (1987). Radiometric properties of U.S. processed Landsat MSS data. *Remote Sensing of Environment*, 22, 39-71.
- Marsh, S. E., & Lyon, R. J. P. (1981). Quantitative relationships of near-surface spectra to Landsat radiometric data. *Remote Sensing of Environment*, 10, 241-261.
- Meyer, P., Itten, K. L., Kellenberger, T., Sandmeier, S., & Sandmeier, R. (1993). Radiometric corrections of topographically induced effects on Landsat TM data in an alpine environment. *ISPRS Journal of Photogrammetry and Remote Sensing*, 48, 17-28.
- Milton, E. J. (1987). Principles of field spectroscopy. *International Journal of Remote Sensing*, 8, 1807-1827.
- O'Neill, N. T., Teillet, P. M., Royer, A., Blanchet, J. -P., Aubé, M., Freemantle, J., Gong, S., Stanley, D., Thulasiraman, S., & Vachon, F. (2002). Concept of a central optical parameter server for atmospheric corrections of remote sensing data. *Proceedings of the 2002 International Geoscience and Remote Sensing Symposium (IGARSS'02) and the Twenty-Fourth Canadian Symposium on Remote Sensing*, in press. Toronto, Ontario, Canada.
- Peddle, D. R., Hall, F. G., & LeDrew, E. F. (1999). Spectral mixture analysis and geometric optical reflectance modeling of boreal forest biophysical structure. *Remote Sensing of Environment*, 67, 288-297.
- Peddle, D. R., White, H. P., Soffer, R. J., Miller J. R., & LeDrew, E. F. (2001a). Reflectance processing of remote sensing spectroradiometer data. *Computers & Geosciences*, 27, 203-213.
- Peddle, D. R., Brunke, S. P., & Hall, F. G. (2001b). A comparison of spectral mixture analysis and ten vegetation indices for estimating boreal forest biophysical information from airborne data. *Canadian Journal of Remote Sensing*, 27, 627-635.
- Peddle, D. R., Franklin, S. E., Johnson, R. L., Lavigne, M. A., & Wulder, M. A. (2002). Structural change detection in a disturbed conifer forest using a geometric optical reflectance model in multiple-forward mode. *IEEE Transactions on Geoscience and Remote Sensing*, in press.
- Poros, D. J., & Peterson, C. J. (1985). Methods for destriping Landsat Thematic Mapper images – A feasibility study for an online destriping process in the Thematic Mapper

- Image Processing System (TIPS). *Photogrammetric Engineering and Remote Sensing*, 51, 1371-1378.
- Pouch, G., & Compagna, D. (1990). Hyperspherical directional cosines for separation of spectral and illumination information in digital scanner data. *Photogrammetric Engineering and Remote Sensing*, 56, 475-479.
- Price, J. C. (1987). Calibration of satellite radiometers and the comparison of vegetation indices. *Remote Sensing of Environment*, 21, 15-27.
- Richter, R. (1997). Correction of atmospheric and topographic effects for high spatial resolution satellite images. *International Journal of Remote Sensing*, 18, 1099-1111.
- Roderick, M., Smith, R., & Cridland, S. (1996). The precision of the NDVI derived from AVHRR Observations. *Remote Sensing of Environment*, 56, 57-65.
- Schott, J. R., Salvaggio, C., & Volchok, W. J. (1988). Radiometric scene normalization using pseudoinvariant features. *Remote Sensing of Environment*, 26, 1-16.
- Schott, J. R. (1997). *Remote Sensing, The Image Chain Approach*, ISBN 0-19-508726-7. Oxford University Press, Inc., 198 Madison Avenue, New York, New York 10016, USA.
- Singh, A. (1985). Thematic Mapper radiometric calibration research and development results and performance. *Photogrammetric Engineering and Remote Sensing*, 51, 1379-1383.
- Slater, P. N. (1980). *Remote Sensing, Optics and Optical Systems*, ISBN 0-201-07250-5. Addison-Wesley Publishing Company, Reading, Massachusetts, USA.
- Smith, J. A., Lin, T. L., & Ranson, K. J. (1980). The Lambertian assumption and Landsat data. *Photogrammetric Engineering and Remote Sensing*, 46, 1183-1189.
- Song, C., Woodcock, C. E., Seto, K. C., Lenney, M. P., & Macomber, S. A. (2001). Classification and change detection using Landsat TM data: when and how to correct atmospheric effects. *Remote Sensing of Environment*, 75, 230-244.
- Staenz, K., Williams, D. J., Fedosejevs, G., & Teillet, P. M. (1994). Surface reflectance retrieval from imaging spectrometer data using three atmospheric codes. *Proceedings of SPIE EUROPTO '94*, 2318, 17-28. Rome, Italy.
- Suits, G. H., Malila, W. A., & Weller, T. M. (1988). The prospects for detecting spectral shifts due to satellite sensor ageing. *Remote Sensing of Environment*, 26, 17-29.
- Teillet, P. M., Guindon, B., & Goodenough, D. G. (1982). On the slope aspect correction of multi spectral scanner data. *Canadian Journal of Remote Sensing*, 8, 84-106.
- Teillet, P. M. (1989). Surface reflectance retrieval using atmospheric correction algorithms. *Proceedings of the 1989 International Geoscience and Remote Sensing Symposium (IGARSS'89) and the Twelfth Canadian Symposium on Remote Sensing*, 864-867. Vancouver, B.C., Canada.
- Teillet, P. M., & Irons, J. R. (1990). Spectral variability effects on the atmospheric correction of imaging spectrometer data for surface reflectance retrieval. *Proceedings of the ISPRS Commission VII Symposium*, 579-583. Victoria, B.C., Canada.
- Teillet, P. M. (1990). Effects of spectral shifts on sensor response. *Proceedings of the ISPRS Commission VII Symposium*, 59-65. Victoria, B.C., Canada.
- Teillet, P. M., & Fedosejevs, G. (1995). On the dark target approach to atmospheric correction of remotely sensed data. *Canadian Journal of Remote Sensing*, 21, 374-387.
- Teillet, P. M. (1997). A status overview of earth observation calibration/validation for terrestrial applications. Teillet, P. M. (ed.). *Canadian Journal of Remote Sensing: Special Issue on Calibration/Validation*, 23, 291-298.
- Teillet, P. M., Staenz, K., & Williams, D. J. (1997a). Effects of spectral, spatial, and radiometric characteristics on remote sensing vegetation indices for forested regions. *Remote Sensing of Environment*, 61, 139-149.

- Teillet, P. M., Horler, D. N. H., & O'Neill, N. T. (1997b). Calibration / validation, stability monitoring, and quality assurance in remote sensing: A new paradigm. *Canadian Journal of Remote Sensing*, 23, 401-414.
- Teillet, P. M., Fedosejevs, G., Gauthier, R. P., O'Neill, N. T., Thome, K. J., Biggar, S. F., Ripley, H., & Meygret, A. (2001). A generalized approach to the vicarious calibration of multiple earth observation sensors using hyperspectral data. *Remote Sensing of Environment*, 77, 304-327.
- Teillet, P. M., Barker, J. L. Markham, B. L., Irish, R. R., Fedosejevs, G., & Storey, J. C. (2001b). Radiometric cross-calibration of the Landsat-7 ETM+ and Landsat-5 TM sensors based on tandem data sets. *Remote Sensing of Environment*, 78, 39-54.
- Thome, K. J. (2001). Absolute radiometric calibration of Landsat 7 ETM+ using the reflectance-based method. *Remote Sensing of Environment*, 78, 27-38.
- Tokola, T., Löfman, S., & Erkkilä A. (1999). Relative calibration of multitemporal Landsat data for forest cover change detection. *Remote Sensing of Environment*, 68, 1-11.
- Townshend, J. R. G. (1981). The spatial resolving power of earth resources satellites. *Progress in Physical Geography*, 5, 32-55.
- Townshend, J. R. G., Huang, C., Kalluri, S. N. V., Defries, R. S., & Liang, D. (2000). Beware of per-pixel characterization of land cover. *International Journal of Remote Sensing*, 21, 839-843.
- Townshend, J. R. G., Justice, C. O., Skole, D., Malingreau, J. -P., Cihlar, J., Teillet, P. M., Sadowski, F., Ruttenberg, S. (1994). The 1 km resolution global data set: Needs of the International Geosphere Biosphere Programme. *International Journal of Remote Sensing*, 15, 3417-3441.
- Tucker, C. J. (1979). Red and photographic infrared linear combinations for monitoring vegetation. *Remote Sensing of Environment*, 8, 127-150.
- Yuan, D., & Elvidge, C. D. (1993). Application of relative radiometric rectification procedure to Landsat data for use in change detection. *Proceedings of the Workshop on Atmospheric Correction of Landsat Imagery*, 162-166. Landsat Program Office, Torrance, CA, USA.
- Yuan, D., & Elvidge, C. D. (1996). Comparison of relative radiometric normalization techniques. *ISPRS Journal of Photogrammetry and Remote Sensing*, 51, 117-126.

Chapter 8

PER-PIXEL ANALYSIS OF FOREST STRUCTURE

Vegetation Indices, Spectral Mixture Analysis and Canopy Reflectance Modeling

Gregory P. Asner, Jeffrey A. Hicke, and David B. Lobell

Department of Global Ecology, Carnegie Institution of Washington, Stanford University, Stanford, California, 94305, USA

1. INTRODUCTION

For more than 30 years, analysis of image pixels has been central to the interpretation of multi-spectral remote sensing imagery of the Earth and celestial bodies. In the context of optical remote sensing of terrestrial ecosystems, “per-pixel analysis” focuses on the process of estimating biophysical and geophysical properties from the radiation reflected off materials found on the land surface. This reflected radiation occurs in five optical domains: spectral, angular, temporal, spatial and polarization. These optical domains are not independent, yet they are often considered individually during the development and use of per-pixel analytical techniques. The polarization domain is not covered in this Chapter. Some studies indicate the potential importance of polarization for estimating properties of plant foliage and canopies (e.g., Rondeaux and Herman 1991), and those were reviewed by Vanderbilt et al. (1991).

In per-pixel analyses of vegetation, a common dichotomy of thought and effort emerges by considering the observed radiation field as containing information about plant canopy structure or function. Here we define canopy function in the physiological and biochemical sense: fractional photosynthetically active radiation absorption (fPAR), leaf photochemical activity, stomatal conductance, water stress, and other process-oriented traits. In contrast, canopy structure describes the position, quantity, type,

extent and connectedness of plant parts in three-dimensional space and over time (Parker 1995). Canopy structural attributes include vegetation cover, canopy gap fraction, plant dimensions, leaf orientation, and leaf area index (LAI).

Structure and function are highly inter-dependent groups of canopy properties. Canopy structure partially determines functional properties, which in turn can affect canopy morphology and other structural variables over timescales of growth, development and evolution (Norman 1993; Larcher 1995). Nonetheless, viewing structure and function as distinct attributes of vegetation aids in narrowing our discussion. We are concerned with canopy structure in this Chapter, and we leave per-pixel remote sensing of plant functional properties to other authors.

Canopy structural properties are important throughout a range of ecological, biogeochemical and atmospheric science disciplines. Applications for canopy structural information range from faunal habitat studies to global climate modeling. The pronounced spatial and temporal variation of forest canopy structural attributes highlights the need for commensurate remotely sensed information.

In this Chapter we summarize several types of per-pixel analyses employed in studies of forest structure. These techniques include vegetation indices, spectral mixture analysis, and canopy reflectance modeling. We highlight how these approaches tap the four dominant optical remote sensing domains. We also indicate some of the challenges and caveats inherent to the application of these methods in studies of forest structure. The scope of this Chapter is limited to methods used for analyzing data acquired by passive optical systems; we do not treat active (e.g., radar, lidar) or thermal remote sensing techniques.

2. VEGETATION INDICES

A vegetation index (VI) is a dimensionless, radiation-based measurement computed from some spectral combination of remotely sensed data. It is used to infer vegetation properties by isolating the contribution of vegetation from other materials (e.g., soil or water). The appeal of an index is its simplicity and its relationship – either empirically or theoretically – to biophysical variables. Additionally, an index can be easily applied to different scenes from sensors on different satellites through careful processing (see section 2.3).

Vegetation indices have long been important in forest remote sensing. The earliest indices have been applied in remote sensing studies for over 20 years and remain the most widely used today. More vegetation indices have

been developed over time as the number of remote sensing studies has increased. A significant challenge for using vegetation indices is to separate the vegetation variable of interest (e.g., LAI) from the other vegetation properties that influence the index as well as from other environmental variables.

2.1 Types of indices

Figure 8-1 shows a normalized difference vegetation index (NDVI) image calculated from Earth Observing-1 (EO-1) Hyperion imaging spectroscopy data of tropical forest in the Eastern Amazon (G. P. Asner, *unpub. data*). Dark regions are clouds, water, or surface litter (non-photosynthetic vegetation or NPV) while light regions are forest, demonstrating the ability of a VI to distinguish different surface types. Examples of forest, litter, water, and clouds are indicated on the image, and corresponding reflectance spectra are provided (Figure 8-1). Vegetation indices take advantage of the large difference in vegetation reflectance between the visible (VIS) and near-infrared (NIR) parts of the spectrum. None of the other spectra exhibits these differences, and virtually no other materials on Earth do so. Plants absorb visible radiation and reflect strongly in the NIR, and typical indices use the ratio or difference of NIR and VIS

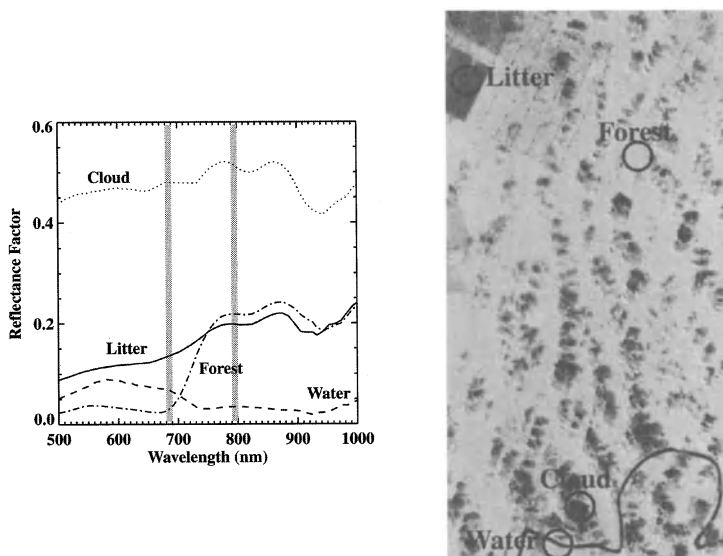


Figure 8-1. Normalized difference vegetation index of tropical forest and clearings in the Amazon basin from the NASA EO-1 Hyperion imaging spectrometer. Also shown are typical spectra corresponding to clouds, litter, forest, and water as well as the visible and near-IR bands (gray bars) used to create the NDVI image.

reflectance. Most commonly, indices are defined with VIS in the red (600-690 nm) region of the visible spectrum.

In this section, we define several common vegetation indices in use today. Our list of indices is not exhaustive, but it does cover the most common formulations and presents some of the newest indices as well. We discuss the specific relationships of these indices to forest structural parameters in the next section.

The simple ratio (SR) index (Jordan 1969) is one of the most commonly studied vegetation indices, and uses the NIR and VIS bands:

$$SR = NIR / VIS \quad (1)$$

The normalized difference vegetation index (NDVI) is the most widely used index, and was one of the first indices to be developed (Rouse et al. 1973; Tucker 1979):

$$NDVI = (NIR - VIS) / (NIR + VIS) \quad (2)$$

Kauth and Thomas (1976) determined that soil reflectance variation fell along a straight “soil line” when viewed with Landsat data. They showed that increasing vegetation extends perpendicularly from this line. Using Landsat Multispectral Scanner (MSS) data, Richardson and Wiegand (1977) utilized this result to develop the perpendicular vegetation index (PVI) to better account for soil background variations than the SR and NDVI:

$$PVI = (NIR - aVIS + b) / \sqrt{a^2 + 1} \quad (3)$$

where a and b are the slope and offset of the soil line. The normalization decreases the sensitivity to different solar zenith angles and partially accounts for variations in topography.

Aerosols, absorbing gases such as water vapor, and undetected clouds affect upwelling radiances measured by satellite instruments. Through its normalization of wavelength channels, the NDVI can partially overcome atmospheric effects that more strongly impact the individual channel radiances or reflectances. Despite its success, however, the NDVI is still sensitive to these atmospheric variables. The Global Environment Monitoring Index (GEMI) was designed to improve on the sensitivity of NDVI to undesirable atmospheric as well as soil brightness effects (Verstraete and Pinty 1996):

$$GEMI = \eta(1 - 0.25\eta) - \frac{VIS - 0.125}{1 - VIS} \quad (4)$$

where,

$$\eta = \frac{2(NIR^2 - VIS^2) - 1.5NIR + 0.5VIS}{NIR + VIS + 0.5}$$

The sensitivity of the NDVI to background soil brightness variation led Huete (1988) to develop the soil-adjusted vegetation index (SAVI). The SAVI minimizes soil brightness effects on a vegetation index while retaining the simplicity of other vegetation indices. Because the NDVI does not account for variations in soil brightness, a darkening of the soil following a rainfall, for instance, will cause a change in NDVI that will be interpreted as a change in vegetation. To account for changing soil brightness, SAVI utilizes an adjustment factor L that effectively shifts the origin of vegetation isolines in NIR/VIS reflectance space:

$$SAVI = [(NIR - VIS)/(NIR + VIS + L)] \times (1 + L) \quad (5)$$

Huete (1988) found that the optimal L depended on LAI, but suggested a value of 0.5 to reduce soil noise problems over a wide range of LAI values.

With the availability of additional wavelength bands on the NASA Terra Moderate Resolution Imaging Spectrometer (MODIS), Kaufman and Tanre (1992) developed the atmospherically resistant vegetation index (ARVI). ARVI takes advantage of an additional measurement in the blue region of the spectrum to correct the NDVI for atmospheric effects. Because MODIS reflectances are already corrected for molecular scattering and absorption, the ARVI was developed to reduce the sensitivity of a vegetation index to absorption and scattering by atmospheric aerosols:

$$ARVI = (r_{NIR}^* - r_{rb}^*) / (r_{NIR}^* + r_{rb}^*) \quad (6)$$

where,

$$r_{rb}^* = r_r^* - \gamma(r_b^* - r_r^*)$$

r^* is the red (subscript r), blue (b), or near infrared (NIR) reflectance, and γ is a parameter dependent upon aerosol type. Kaufman and Tanre (1992)

found that a single value of $\gamma = 1.0$ can be used and will substantially reduce the sensitivity of the index to aerosols.

The enhanced vegetation index (EVI) was also developed for use with MODIS satellite observations (Huete et al. 1994, 1999). The EVI combines the soil correction included in the SAVI with the atmospheric aerosol correction used by the ARVI:

$$EVI = 2 \frac{NIR - VIS}{L + NIR + C_1 \cdot VIS + C_2 \cdot BLUE} \quad (7)$$

where L is defined as for SAVI, and $BLUE$ is the reflectance in the blue channel. C_1 and C_2 are parameters that weight the blue channel in the aerosol correction (Liu and Huete 1995).

The Reduced Simple Ratio (RSR) index was proposed by Brown et al. (2000) to utilize measurements in the shortwave-infrared (SWIR) spectral region (1.55-1.75 μm) to minimize sensitivity to the background:

$$RSR = SR \cdot \left[1 - \frac{SWIR - SWIR_{min}}{SWIR_{max} - SWIR_{min}} \right] \quad (8)$$

$SWIR_{min}$ and $SWIR_{max}$ correspond to SWIR reflectances from completely closed and open canopies, respectively. Nemani et al. (1993) found that the addition of a SWIR reflectance to the NDVI improved its ability to estimate leaf area in open forest canopies. The SWIR observations improve the delineation of background materials (e.g., soil, litter), whose influence on a vegetation index increases with decreasing canopy closure. Using a geometric-optical model, Brown et al. (2000) found that simulated RSR had a reduced range of LAI compared to SR for a variety of realistic background reflectance conditions in the boreal forest. Their results suggest that improved LAI estimates can be obtained using the RSR in place of SR observations.

Several radiative transfer studies have compared vegetation indices to determine which are most sensitive to external factors such as atmospheric conditions or viewing geometry (Bannari et al. 1995; Curran 1980; North 2002; Rondeaux et al. 1996). In general, SR and NDVI are sensitive to both soil and atmospheric effects. The PVI and SAVI reduce the effects of soil brightness variation, while the ARVI and GEMI reduce the impacts of atmospheric constituents.

2.2 Forest structural applications

Vegetation indices can be used to study changes in canopy “greenness”. A relationship must be developed to link an index to a canopy structural variable such as LAI. However, many different vegetation and environmental (soil and atmosphere) characteristics influence VIs. The forest type of interest must be considered since, for example, the background reflectance and architecture of a boreal forest are distinct from an open forest in a semi-arid region. Relationships between canopy structure and VIs must also account for variations in atmospheric conditions and solar geometry (section 2.3).

Empirical relationships can be derived between VIs and canopy structural variables. This approach benefits from the use of actual measurements, and a robust relationship may be developed by constraining measurements to the geographic region of interest. However, empirical relationships do not readily allow exploration of the VI to internal (e.g., LAI) or external (e.g., atmosphere) factors. Empirical relationships also require intensive and often costly fieldwork.

Canopy photon transport models can be used to account for varying internal and external factors affecting observed reflectance signatures. These models range in complexity from one-dimensional light scattering simulations (e.g., Verhoef 1984) to sophisticated 3-D ray tracing models (McDonald et al. 1998). The difficulties in establishing a relationship between VIs and forest structural variables resulting from such processes as shadowing and multiple scattering imply that these characteristics must be taken into account. Thus, the more complex models such as hybrid geometric-optical/radiative transfer models (Li and Strahler 1992a) and ray-tracing models (McDonald et al. 1998) are now often used. The disadvantage of these more advanced models is their complexity and computational expense as well as the specification of many input variables. The two analytical approaches – empirical studies and modeling – therefore complement each other. The modeling studies are highlighted in section 4.

By far the most common forest structural variables estimated using VIs are LAI, forest canopy cover, and phenology. Phenology is defined here as the time-course of foliage development and loss from canopies. We summarize a variety of VI-related studies estimating these three structural variables from remote sensing observations.

2.2.1 Leaf area index

Because VIs are usually designed to be most sensitive to green foliage in canopies, they have been used extensively to map forest LAI at regional to

global scales (e.g., Myneni et al. 1997b; Spanner et al. 1994). Jordan (1969) demonstrated with field measurements that the SR could be related to forest LAI. Above- and below-canopy shortwave spectra revealed an increase in near-infrared radiation (800 nm) below the canopy relative to visible radiation (650 nm) resulting from greater absorption by chlorophyll at visible wavelengths. Jordan (1969) found an exponential relationship between the ratio of these wavelengths (simple ratio; SR) and field measurements of LAI.

The relationship between the SR and LAI for a temperate conifer forest in Oregon was explored by Spanner et al. (1994). They used remotely sensed SR observations from a variety of airborne sensors and compared them to field measurements of LAI, finding a strong log-linear correlation between SR and LAI up to values of 7-8 (Figure 8-2). Note that the VI-LAI relationships reported by Spanner et al. (1994) were different among the remote sensing instruments tested, particularly for the measurements collected by the Thematic Mapper Simulator (TMS). The large difference in the TMS results was primarily due to calibration issues associated with low visible (red) reflectances, to which the SR is sensitive.

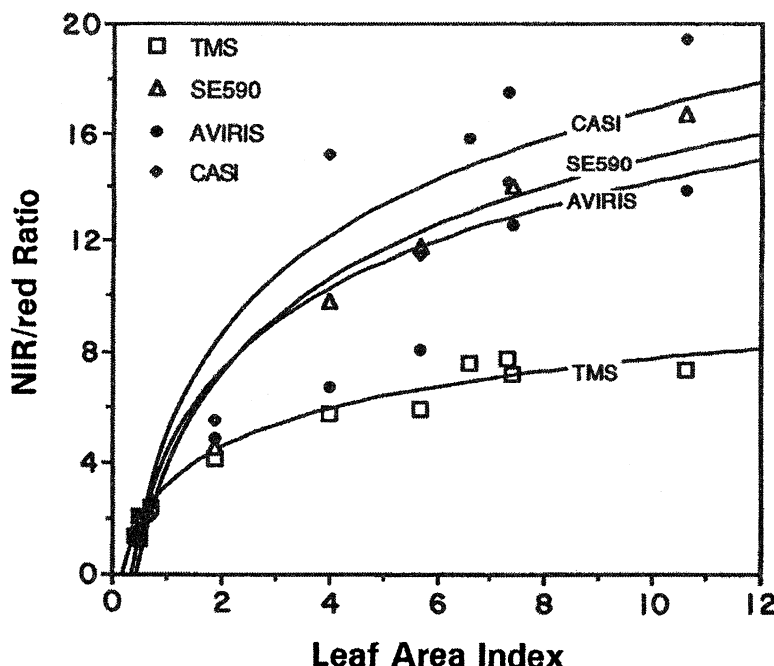


Figure 8-2. Leaf area index versus simple ratio (SR) computed using a variety of airborne instruments. From Spanner et al. (1994), with permission.

Chen and Cihlar (1996) compared LAI estimates from Landsat imagery of boreal forests to field measurements. The authors found that late spring comparisons were more favorable than in summer due to the lack of understory earlier in the growing season. The authors reported that the SR correlates better with LAI than does NDVI via a reduction in non-linear behavior of the index at high LAI values.

Coops et al. (1997) utilized ground-based measurements of LAI over 15 years at an Australian forest field site for comparison with LAI derived from 13 Landsat scenes collected over that time period. Measured LAI varied from 1 to 5. Linear relationships existed between field-measured LAI and both the NDVI and SR; the authors found good fits between measured and predicted LAI (r^2 of 0.84 and 0.73 for NDVI and SR, respectively). The authors then used these relationships to compare variations in Landsat-derived LAI with percentage crown closure observations from aerial photography. Despite the quality of the relationship at the single stand level, however, the spatial variation of predicted LAI did not reflect variations in the photography as well. Coops et al. (1997) attributed reduced correlations to regions having a different forest community as well as younger forests, highlighting the potential error when extrapolating relationships outside of the ecosystem in which the VI relationship was developed.

2.2.2 Forest cover and disturbance

Vegetation indices have long assisted forest cover studies. Lyon et al. (1998) analyzed Landsat scenes separated by 18 years to detect land-cover changes in the Mexican state of Chiapas, finding that 10 % of the land had changed in cover type. Of several vegetation indices tested, the NDVI demonstrated the best change detection capability when compared to laboratory and field measurements. Other VIs were more sensitive to topography.

Fung and Siu (2000) mapped land-cover change in Hong Kong using NDVI from the Systeme Pour l'observation de la Terre (SPOT) satellite. They found that NDVI was an effective tool for monitoring environmental quality influenced by socioeconomic changes. Young and Wang (2001) monitored land-use change using NDVI linked to field studies of vegetation productivity rather than to land-cover types. Masek (2001) compared NDVI calculated from Landsat scenes 25 years apart to investigate the structural stability of Canadian boreal forests. Despite being able to clearly identify the boreal forest-tundra boundary, he found no evidence of change between the 1970s and the 1990s.

An important way that remotely sensed forest structure could play a role in ecological studies and resource management efforts is through analyses of

vegetation disturbance. Many studies emphasize the frequency and intensity of disturbance, where intensity can usually be directly linked to changes in canopy structure (e.g., gap fraction, cover). Disturbances such as fire, insect outbreaks, selective logging, drought, and windstorms all impact the structure of vegetation.

Fire indices assist forest managers by estimating fire danger. Illera et al. (1996) developed a fire index from the slope of accumulated NDVI in order to estimate the potential of fire. This index is sensitive to canopy water stress and was applied in Mediterranean forest, where it was found to work well for the largest fires. Leblon et al. (2001) explored how fire weather index variables used by the Canadian Forest Fire Danger Rating System related to the NDVI for boreal forests. The authors reported only limited success since the NDVI is primarily sensitive to the photosynthetic capacity of forest canopies and not the drought condition.

Fire scar detection and the impact of fires on forest canopies have been studied using VIs. Kasischke et al. (1993) used the NDVI to map fire scars in Alaska; two NDVI images generated from 1 km AVHRR data and separated by 45 days were employed. A threshold was used for the difference in the NDVI between the two times to identify fire scars. The authors found good agreement with field-based maps of fire burn areas, particularly for the largest fires comprising most of the area burned. Kasischke and French (1995) demonstrated improvement on this technique by incorporating the seasonal dynamics of the NDVI during both the fire year and the year following fire. Figure 8-3 shows two years of NDVI for a burned and unburned pixel in Alaska. The fire can clearly be seen as the large decrease in July NDVI. In the year following the burn, the spring and fall NDVI of the burned area are reduced compared to the unburned area.

The NDVI has also been used to study hurricane damage in the southern United States. Ramsey et al. (1997) analyzed AVHRR observations at 1 km spatial resolution to investigate forested regions that had sustained damage in Hurricane Andrew in August 1992. The hurricane defoliated large regions along its track, resulting in increased foliar production between September and October. These increases were apparent in the satellite observations.

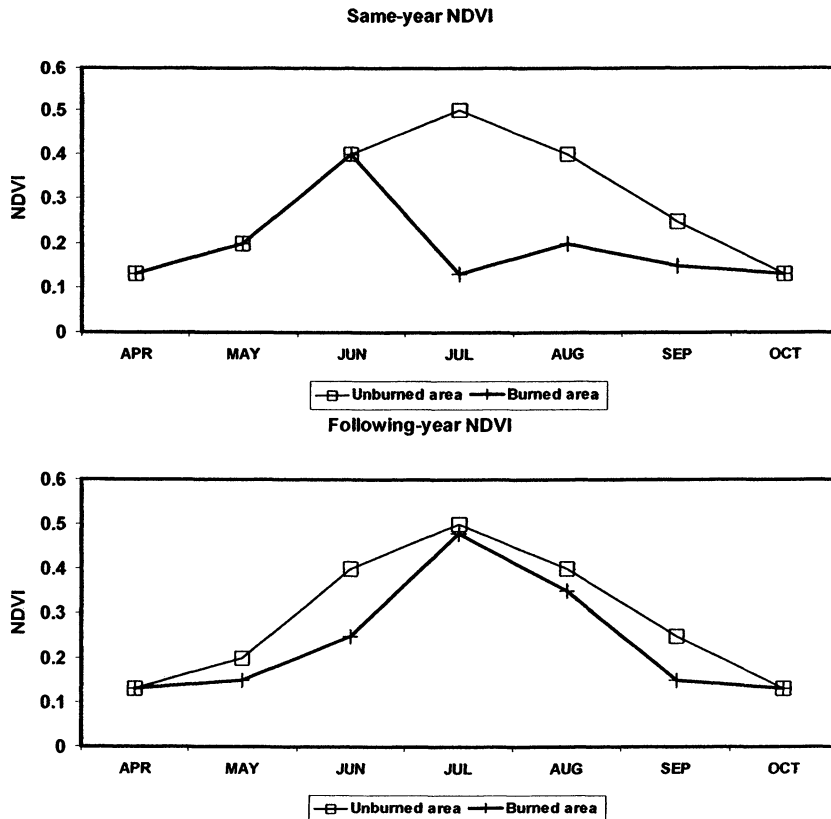


Figure 8-3. Annual cycles of NDVI from burned and unburned areas in Alaska. (Top) NDVI in year of fire. (Bottom) NDVI in year following fire. From Kasischke and French (1995), with permission.

2.2.3 Forest phenology

Vegetation indices have been used in numerous studies of forest canopy phenology, often for comparison with ecosystem models that predict phenology. Figure 8-4 shows a map of annual NDVI together with the annual cycle of four forests across North America, each displaying a different phenology. The mixed evergreen and deciduous forest in boreal Canada has a large NDVI amplitude. The deciduous forest in the northeast US shows a similar phenology, though with an extended growing season and greater amplitude. The evergreen forests on the west coast and in the southeastern US have almost no annual cycle due to the favorable growing conditions year-round.

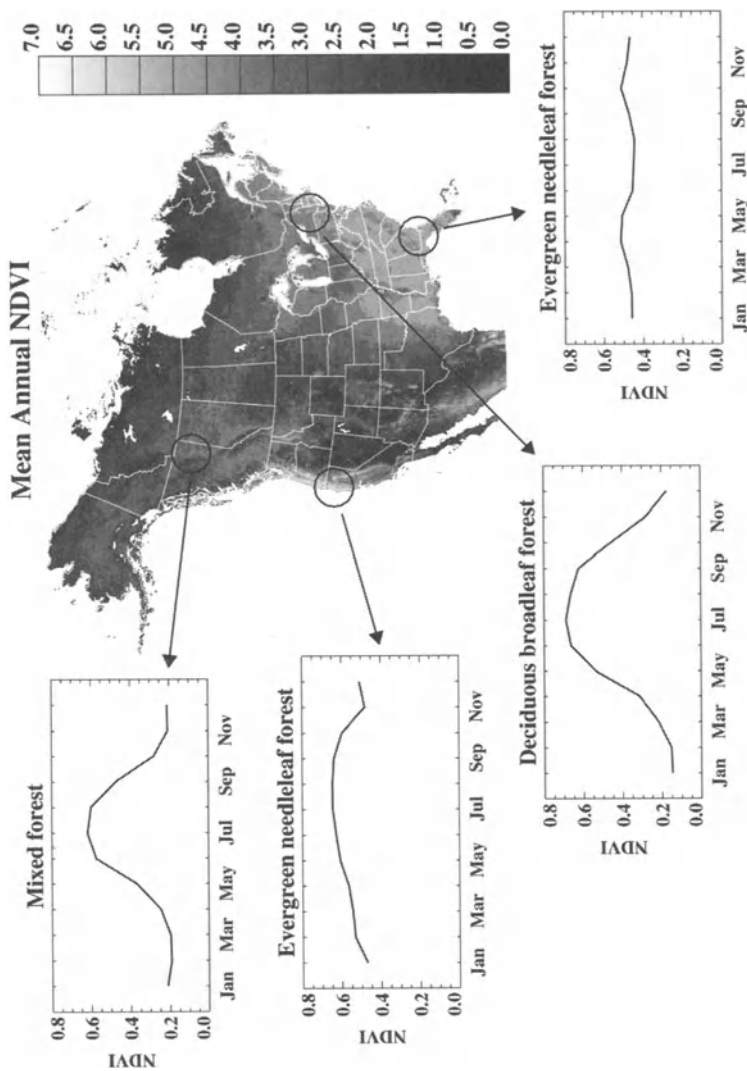


Figure 8-4. Map of annual NDVI averaged over 17 years. Time series show seasonal cycles of NDVI for four typical forested areas.

White et al. (1997) used the daily 1 km NDVI from AVHRR in combination with meteorological observations to estimate continental-scale phenology, fitting a temporal growth curve to the available data. They then defined onset and offset of canopy foliage using a ratio of the NDVI to its minimum and maximum values for a given site. The satellite-derived phenology was then used to evaluate a phenology model driven by meteorological data.

At a coarser spatial resolution, Botta et al. (2000) applied a phenology algorithm developed by Moulin et al. (1997) to compute leaf onset dates at 0.5° resolution. Moulin et al. (1997) used the NDVI to identify the beginning, end, and maximum of the vegetation seasonal cycle as represented in the NDVI time series. Ludeke et al. (1996) used the NDVI to estimate phenology at a global scale. They fit a three-spline function to the annual cycle of NDVI to identify leaf shooting and leaf abscission times. The NDVI-based results were then compared to the prognostic phenology generated by the Frankfurt Biosphere Model (Janecek et al. 1989).

Phenology is also useful for distinguishing land cover types, since the temporal dynamics of the NDVI aid in differentiating among vegetation types (e.g., DeFries et al. 1998; Hansen et al. 2000; Lloyd 1990). The mean, maximum and amplitude of the NDVI over the growing season are metrics used in these studies. Fourier transforms applied to monthly NDVI data have also been used to classify forest cover. For example, Moody and Johnson (2001) calculated the first and second harmonics, corresponding to the annual and biannual cycles, to characterize the phenology of vegetation in southern California. In contrast to metrics such as the maximum NDVI, however, the Fourier transform required multiple years of data, both increasing the processing complexity and decreasing sensitivity to the interannual variability of the NDVI.

Studies using NDVI have also investigated inter-annual behavior in phenology. Asner et al. (2000) found substantial variation in NDVI amplitudes in Amazonian tropical forests that was spatially correlated with inter-annual rainfall and the strength of the dry season. In turn, rainfall was coupled to the strength and duration of El Nino and La Nina events.

While VIs have been successfully used in phenological studies to differentiate land cover types, calculating the length of the growing season is more sensitive to the methodology used. White et al. (1997) found differences of up to nine days in the growing season when using different thresholds of a ratio using NDVI annual cycle amplitudes.

2.3 Importance of processing

Ideally, a vegetation index can be used to derive canopy properties spatially and temporally. Unfortunately, factors unrelated to biophysical properties, such as sensor calibration and atmospheric conditions, also change across time and space. These factors affect VIs, thus they must be accounted for in VI analyses of forest structure. A variety of techniques have been developed to limit the effects of sun and sensor angles, atmospheric composition including absorbing gases and aerosols, inter-calibration among

sensors, and clouds. In this section we summarize some of the studies that discuss this process, using the AVHRR-NDVI as an example.

Though not designed for vegetation studies, AVHRR observations were used in the first studies of global forest dynamics. The daily global coverage and spatial resolution of 1 km made the AVHRR-NDVI very attractive. Since the early 1980s, this data time series has been available continuously and thus has the potential to be used in long-term studies of forest structural properties. Figure 8-5 taken from Los et al. (2000) demonstrates the major problems that must be overcome to produce a quality interannual NDVI time series. Because the 20 years of AVHRR observations span three satellites, an inter-sensor calibration must be performed (Figure 8-5a). To account for these artifacts, studies typically take advantage of observations over deserts (e.g., Gutman 1999; Los 1998; Myneni et al. 1997a; Tucker et al., in press), where the reflectances are assumed to be stable. Clouds and other atmospheric constituents are minimized through the use of maximum-NDVI temporal compositing. Clouds and other atmospheric impacts reduce the NDVI, and therefore this step attempts to minimize these effects. Unfortunately, this method is not guaranteed to eliminate cloud or aerosol effects, and additional steps are often necessary. For instance, in humid tropical forests, the incidence of clouds may be very high (Figure 8-5c). Los et al. (2000) suppressed any intra-seasonal variation by assigning the known maximum NDVI throughout the year to all months; that is, they inserted surrogate data values where needed. Large volcanic eruptions also affected the NDVI; the most notable were the Mt. Pinatubo event in 1991 and the El Chichon blast in 1982 (Figure 8-5b). The resulting stratospheric aerosols spread globally and reduced the NDVI. Los et al. (2000) used prescribed aerosol optical depths to modify the NDVI time series. Atmospheric effects such as seasonal changes in water vapor also cause artifacts in the NDVI data set (Figure 8-5d), as do variations in viewing (Figure 8-5e) and solar (Figure 8-5f) geometry. Viewing geometry effects are minimized by eliminating pixels with extreme observational zenith angles.

With Terra-MODIS satellite observations beginning in 2000, it became possible to employ new VIs that greatly improved upon the NDVI. Additional corrections for atmospheric aerosols through the use of the blue spectral channel on MODIS are incorporated into the EVI (Huete et al. 1999). Gao and Li (2000) discuss an additional correction for thin cirrus clouds using the 1375 nm channel on MODIS.

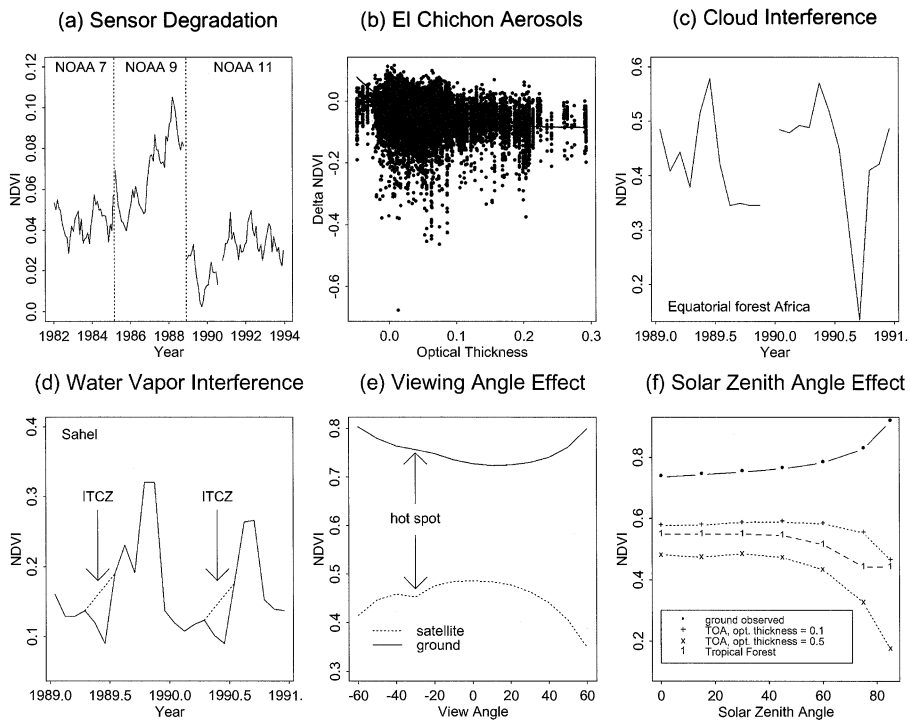


Figure 8-5. Sources of error and uncertainty in NDVI data due to: (a) variations in NDVI over the Saharan desert resulting from calibration differences and sensitivity changes in AVHRRs on board NOAA-7, -9, and -11 satellites; (b) effects of atmospheric optical thickness from El Chichón aerosols on average monthly NDVI; (c) temporal changes and missing data from clouds over a tropical forest; (d) decreased NDVI values at start of the rainy season, such as in the Sahel; (e) view angle-dependent variation in modeled NDVI at ground and satellite levels; and (f) effects of solar zenith angle on NDVI (DNDVI/Dq), here estimated for tropical forest (“1”), ground-based measured NDVI (filled circles), and simulated top-of-the-atmosphere NDVI. From Los et al. (2000), with permission.

3. SPECTRAL MIXTURE ANALYSIS

Forest ecosystems are characterized by spatially heterogeneous mixtures of vegetation and soil. For most satellite and airborne sensors, the instantaneous field of view (IFOV) is large enough that pixels comprise mixtures of land-cover types. For example, average widths of temperate coniferous tree crowns are less than 10 m while the resolution of the Landsat TM sensor is roughly 30 m. Mixing of cover types within pixels, termed sub-pixel mixing, is even more prominent for widely used global sensors with resolutions greater than 1 km, such as the AVHRR.

Sub-pixel mixing in remote sensing dictates that pixel reflectance cannot be simply interpreted in terms of properties of a single cover type. Instead, landscape reflectance (the scale resolved by most sensors) is primarily determined by variations in the proportions of each cover type (Asner 1998). Accounting for sub-pixel variations in cover types is therefore an essential step to analyzing pixel reflectance in heterogeneous forests.

The goal of linear mixture models is to estimate the fractional cover of each major landscape unit of interest (endmember) within image pixels. The inputs to mixture models are endmember reflectance and an image of observation vectors (pixel reflectance), and the output is a fraction image for each endmember along with an image containing an error of fit. These fraction images can then be used to constrain additional spectral analyses, as input to biophysical and biogeochemical models, or simply as a measure of land cover used to analyze spatial and temporal changes.

In contrast to vegetation indices, fractional cover estimates describe a physical property of the landscape and lend themselves to straightforward interpretation based on established ecological knowledge. For example, canopy cover is often closely related to important structural and functional landscape properties, such as leaf area index (LAI), biomass, and net primary production (NPP) (e.g., Hall et al. 1995). Another advantage of mixture models is that they can be applied to any combination of wavelengths. They have been applied to multispectral shortwave measurements, such as acquired by the Landsat sensors; hyperspectral data, such as from the Airborne Visible Near-Infrared Imaging Spectrometer (AVIRIS); and even multispectral thermal data (Gillespie 1992).

3.1 Mixture modeling theory

The problem of sub-pixel mixing in remote sensing has been recognized for decades (e.g., Horowitz et al. 1971; Graetz and Gentle 1982). Initial work on mixture modeling focused mainly on applications in geology (e.g., Adams et al. 1986; Settle and Drake 1993) and arid systems (e.g., Huete 1986; Smith et al. 1990), and has only more recently been extended to forests.

The assumption behind linear mixture modeling approaches is that pixel reflectance is the sum of reflectance for each cover type, weighted by their fractional presence within each pixel. This is represented schematically in Figure 8-6 for a simple case with two dimensions. Each point in this figure represents the position of a pixel in the space defined by two reflectance bands, x and y , and can be expressed as some linear combination of values at the vertices of a triangle enclosing all points. The weighting of each vertex, or endmember, to a pixel is between zero and one and is interpreted as its

fractional coverage within a pixel. For instance, the pixel at A is comprised mainly of EM3 with a small fraction of EM2, pixel B contains mainly EM2 with small fractions of EM1 and EM3, while pixel C has nearly equal proportions of all endmembers. In this example, bands x and y can be thought of as Landsat bands 3 and 4, in which case endmembers 1-3 could represent shade, soil, and green vegetation, respectively.

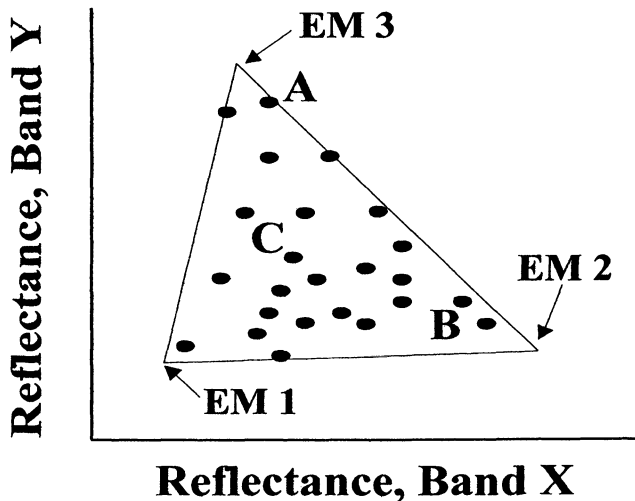


Figure 8-6. A schematic representation of linear mixing using two spectral bands. Each point in the scatter plot can be expressed as a linear combination of three endmembers. See text for details.

Mathematically, the mixture modeling framework can be expressed as:

$$\sum_{i=1}^m \rho_{i,b} C_i = \rho_b + \varepsilon_b \quad (9)$$

$$\sum_{i=1}^m C_i = 1.0$$

where $\rho_{i,b}$ is the endmember reflectance of cover type i in wavelength band b , C_i is the areal fraction of cover type i within the pixel, ρ_b is the pixel reflectance in b , ε_b is the error of fit in b , often termed the band residual, and the summation is over m endmembers. The second of these equations constrains the sum of fractions to unity, although individual fractions are generally allowed to be negative or greater than 1.

In spectral mixture modeling, the objective is to use prescribed values for each $\rho_{i,b}$, along with observations of ρ_b , to recover the fractions, C_1 , C_2 , ..., C_m . If only one observation is available, namely ρ_b , then there are two

equations (one measurement plus the unity constraint), and it is possible to solve for two unknowns. More generally, if reflectance is measured at n wavelengths, there are $n+1$ possible endmember fractions that can be estimated. The actual number of endmembers in practice depends not only on the number of bands, but on their uniqueness, as will be discussed below.

The system of $n+1$ equations can be written in the language of linear algebra as:

$$\begin{pmatrix} \rho_{1,1} & \dots & \rho_{1,n} \\ \vdots & & \vdots \\ \rho_{n,1} & \dots & \rho_{n,n} \\ 1 & \dots & 1 \end{pmatrix} \begin{pmatrix} C_1 \\ \vdots \\ C_n \\ 1 \end{pmatrix} = \begin{pmatrix} \rho_1 \\ \vdots \\ \rho_n \\ 1 \end{pmatrix} + \begin{pmatrix} \varepsilon_1 \\ \vdots \\ \varepsilon_n \\ 0 \end{pmatrix} \quad (10)$$

or

$$A \cdot C = R + \varepsilon$$

where A is a matrix containing the endmembers' reflectance and a row of ones, C is a vector of endmember fractions, R is the vector of observed reflectance, with a one added to constrain the fractions' sum to unity, and ε is a vector of band residuals. To solve for C , it is necessary to define some measure of ε to be minimized. A common approach is to minimize the sum of square residuals, which equates to solving the following equation.

$$C = (A'A)^{-1}(A'R) \quad (11)$$

Additional equations are occasionally used to constrain values of each fraction between zero and one. However, this “constrained solution” requires more sophisticated inversion techniques and is often unnecessary given that inspection of resulting images can easily reveal unrealistic fractions, in which case the endmembers probably need to be reselected.

Implicit in the above equations is the assumption that each cover type contributes linearly to pixel reflectance, and thus nonlinear interactions between endmembers are negligible. Nonlinear mixing results from multiple reflections of photons between endmembers, and as a result is highest at wavelengths of high endmember reflectivity such as the NIR for vegetated surfaces (Borel and Gerstl 1994). The validity of the linear mixing assumption is therefore wavelength dependent, and results of identical mixture models applied to different wavelength regions can vary significantly (Roberts et al. 1993).

3.2 Endmember selection

The selection of endmembers is a critical component to successful application of mixture modeling. Two general approaches exist for deriving endmembers, each with their own advantages and shortcomings. The first uses reflectance spectra measured in the field or laboratory. This method allows great control over the selection of endmember spectra, but requires that raw image data be correctly converted to reflectance, an often difficult task in remote sensing (Peddle et al., Chapter 7). It is also often difficult to obtain reference endmember spectra for all cover types, particularly in forest ecosystems where the size of tree canopies impedes field measurements of canopy reflectance. In addition, the use of reference endmembers can suffer from temporal variability in reflectance properties of cover types. For example, differences in soil moisture or canopy senescence between the times of field spectral measurements and image acquisition can hamper interpretation of cover fraction images.

The second approach derives endmember spectra directly from the image by extracting reflectance from relatively “pure” pixels (i.e., pixels at the vertices of the scatter plot in Figure 8-6). Using image endmembers bypasses the need for ground measurements of cover type reflectance, as well as the need to accurately atmospherically correct images. However, isolating a pure pixel is often impossible given the great surface heterogeneity at the scale of most remote sensors. For this reason, methods have been developed to derive endmembers from image data by constructing a simplex that includes all data points and extrapolating endmember reflectance at the vertices (e.g., Bateson and Curtiss 1996).

Another important consideration in mixture modeling is the spectral uniqueness of each endmember. In forest ecosystems, for example, it is often impossible to distinguish among soil types or vegetation species because the differences in reflectance are relatively small. This leads to high correlations between columns in the endmember matrix (linear dependence), which in turn leads to an unstable inverse matrix. The appropriate number of endmembers depends on the spectral information in a given scene, and can often be determined through a principal component analysis. Inspection of model results is another useful way to determine the correct number of endmembers, with confusion between endmembers revealed by a noisy, speckled pattern in fraction images (Mustard and Sunshine 1999).

3.3 Endmember variability

Despite their utility, mixture models require several simplifying assumptions that often limit their successful application. One issue is the

occurrence of nonlinear interactions between endmembers that violates the assumption of linear mixing (Roberts et al. 1993). While methods have been developed to relax the linear constraint, for instance through the use of artificial neural networks (Foody et al. 1997), nonlinear effects tend to be a secondary concern for model application.

In our opinion, the most serious shortcoming of traditional mixture model approaches is the failure to account for variability in endmember reflectance within and between images. As shown in eq. (9), a simple mixture model assumes that endmember reflectance is identical in each pixel. In reality, the reflectance properties of vegetation and soils can exhibit significant spatial and temporal variability. Sources of this variability for soils include changes in mineralogy, organic matter content, and moisture (Ben-Dor et al. 1999). Similarly, vegetation reflectance varies widely with changes in canopy structure and leaf chemistry (Jacquemoud et al. 1995; Myneni et al. 1989a; Ross 1981).

Where sharp contrasts exist between different vegetation or soil types within an image, it may be possible to include additional endmembers to resolve this variability. For example, two separate soil endmembers are often used where soils from different parent materials exist within an image. Some approaches even use different endmembers for each pixel by selecting endmembers from a database of vegetation and soil spectra until the best fit with the measured spectra is achieved (e.g., Roberts et al. 1998). However, often a continuum of variation both between and within pixels prevents separation of distinct classes of vegetation or soils, and the problem of endmember variability persists.

As an example, consider a pixel with 50 % soil and 50 % vegetation, where the LAI of the vegetation canopy increases from 3 to 4 over time between two images. While the fractional cover of vegetation remains unchanged, the pixel reflectance will be impacted by changes in LAI, so that a mixture model based on a single endmember reflectance applied to both images will produce different values for the hypothetical pixel. Similarly, variations in LAI across space would impede comparison of fractions between pixels.

A critically important (but often unasked) question when applying mixture models is therefore: What is the uncertainty in endmember fractions resulting from variability in canopy and/or soil reflectance? If the potential errors are large, then comparing fractions between pixels may not be justified. In practice, an accurate assessment of fractional cover uncertainty, in addition to the fraction itself, is needed to determine the utility within the context of the requirements of a given application.

One attempt to explicitly consider endmember variability was presented by Bateson et al. (2000), who constructed sets of endmembers, called

bundles, based on image data. A linear programming routine was then used to determine a minimum, mean, and maximum fraction of each endmember, with a difference between maximum and minimum values generally below 40 % in a simulated AVIRIS savanna image. This large range testifies to the importance of endmember variability, and the potential errors that can result from ignoring it. It also calls into question the utility of mixture modeling for detecting small changes in vegetation cover.

However, as noted by Asner and Lobell (2000), endmember variability can be significantly reduced if one focuses on a subset of wavelengths and spectral features. For example, a main difference between many soil spectra is overall brightness, which can be partially removed within the mixture-modeling framework by subtracting the reflectance at one band (ρ_0) from all other bands. The resulting spectra, which emphasize reflectance derivatives more than absolute values, are referred to as “tied” to a certain wavelength. As long as the transformation of the spectra is linear, it can be applied to both the measured and endmember spectra while preserving the linear relation in eq. (9):

$$\rho_b - \rho_0 = \sum_{i=1}^m \rho_{i,b} C_i - \sum_{i=1}^m \rho_{i,0} C_i = \sum_{i=1}^m (\rho_{i,b} - \rho_{i,0}) C_i \quad (12)$$

In contrast, a nonlinear spectral transformation, such as dividing by ρ_0 , would violate this equality:

$$\rho_b / \rho_0 = \sum_{i=1}^m \rho_{i,b} C_i / \sum_{i=1}^m \rho_{i,0} C_i \neq \sum_{i=1}^m (\rho_{i,b} / \rho_{i,0}) C_i \quad (13)$$

Asner and Lobell (2000) showed that employing tied spectra for vegetation, non-photosynthetic vegetation (NPV), and soil in the SWIR2 wavelength region (2080 – 2280 nm) greatly reduced endmember variability (Figure 8-7). The consistency of SWIR2 reflectance can be attributed to fundamental biophysical properties of each component. Green canopy reflectance is characteristically flat due to strong absorption by foliar water (Gates et al. 1965; Woolley 1971); NPV spectra exhibit an absorption near 2280 nm due to lignin and cellulose (Curran 1989); soil spectra possess a minimum near 2200 nm due to vibrational absorptions by clay lattice hydroxyls (Ben-Dor et al. 1999). The problem of endmember variability can be significantly reduced using spectral transformations that emphasize these unique and consistent spectral features.

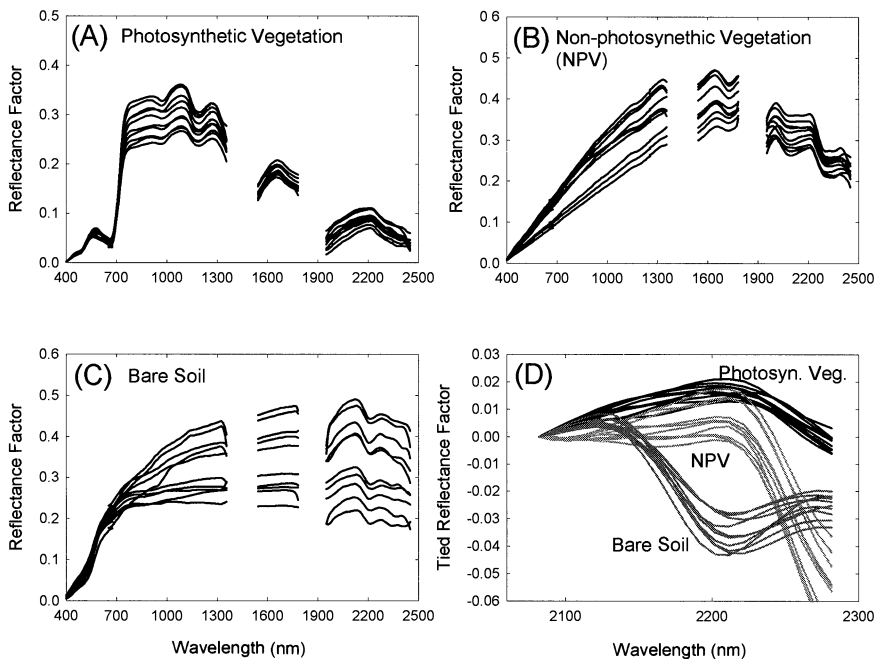


Figure 8-7. Representative reflectance spectra of (A) green vegetation; (B) non-photosynthetic vegetation, or litter; and (C) soils from field measurements, demonstrating the variability of full-range spectra. Significantly lower variability is observed when considering the tied SWIR2 spectra for each endmember class, as shown in (D). After Asner and Lobell (2000).

3.4 Forest applications

Linear mixture modeling has proven useful for a range of applications in tropical, temperate, and boreal forests. One of the most significant studies to date has involved the detection of land-use patterns and deforestation in the Amazon. Adams et al. (1995) unmixed four years of Landsat TM data using endmembers for green vegetation, non-photosynthetic vegetation (NPV; e.g., bark), soil, and shade. The authors found that temporal variations in endmembers revealed subtle changes in land-cover, and could be classified to identify pixels with common histories, such as forest converted to pasture or regrowing forest. A shade endmember is frequently employed to model topographic and canopy shading effects, and can often provide a simple diagnostic of canopy structure. For example, Shimabukuro et al. (1998) showed that shade fraction images easily distinguish between dense tropical forest and deforested areas, including bare soil, pasture, and regrowth.

Fraction images of other endmembers have also proved valuable for identifying land-use and land cover patterns. Cochrane and Souza (1998)

showed that the fraction of NPV within forested pixels successfully distinguished between unburned, recently burned, and older burned forests in the Brazilian Amazon. A recent study by Souza and Barreto (2000) investigated selective logging with soil fraction images, which highlighted cleared landings where logs are stored before being transported to mills. Asner et al. (2002) used an automated Monte Carlo spectral mixture model with Landsat Enhanced Thematic Mapper Plus (ETM+) imagery to detect landings, roads, skid trails and tree fall gaps associated with selective logging in the eastern Amazon (Colour Plate 5). These areas show up as blue tones in the image, indicating areas of exposed surface litter or forest slash. Forest canopy fractional cover is highest in areas shown in green.

Mixture models have also been extensively applied in temperate and boreal forests. In many cases, unmixing has been used to constrain the proportions of sunlit canopy, soil, and shade, which are then used with field-based regressions or more sophisticated reflectance models to estimate desired canopy structural characteristics (Rosema et al. 1992; Hall et al. 1996; Hall et al. 1995; Peddle et al. 1999). For example, Hall et al. (1995) derived the fraction of sunlit crowns, sunlit background, and shade from reflectance measurements collected from a helicopter over 31 black spruce stands. Comparison with field measurements revealed that the shade fraction predicted biomass, LAI, diameter at breast height (dbh), and NPP with standard errors of only 2 kg m^{-2} , 0.58, 2 cm and $0.07 \text{ kg m}^{-2} \text{ yr}^{-1}$, respectively. The authors showed that NDVI could not successfully retrieve these biophysical properties because it was responsive mainly to green canopy cover, whereas mixture models were able to capture more subtle differences between stands.

The utility of shade fraction images in forest ecosystems was also demonstrated in a recent study of Pacific-northwest U.S. coniferous forests by Sabol et al. (2002). The authors applied a four endmember mixture model consisting of green vegetation, NPV, soil, and shade to Landsat TM data. Combinations of vegetation and shade fractions were then used to trace the trajectory of canopy structural changes associated with regrowth, and thereby estimate stand ages (Figure 8-8). While considerable uncertainty in stand age remained due to endmember variability, mixture modeling was a major improvement over NDVI, which could not distinguish open canopies from large trees.

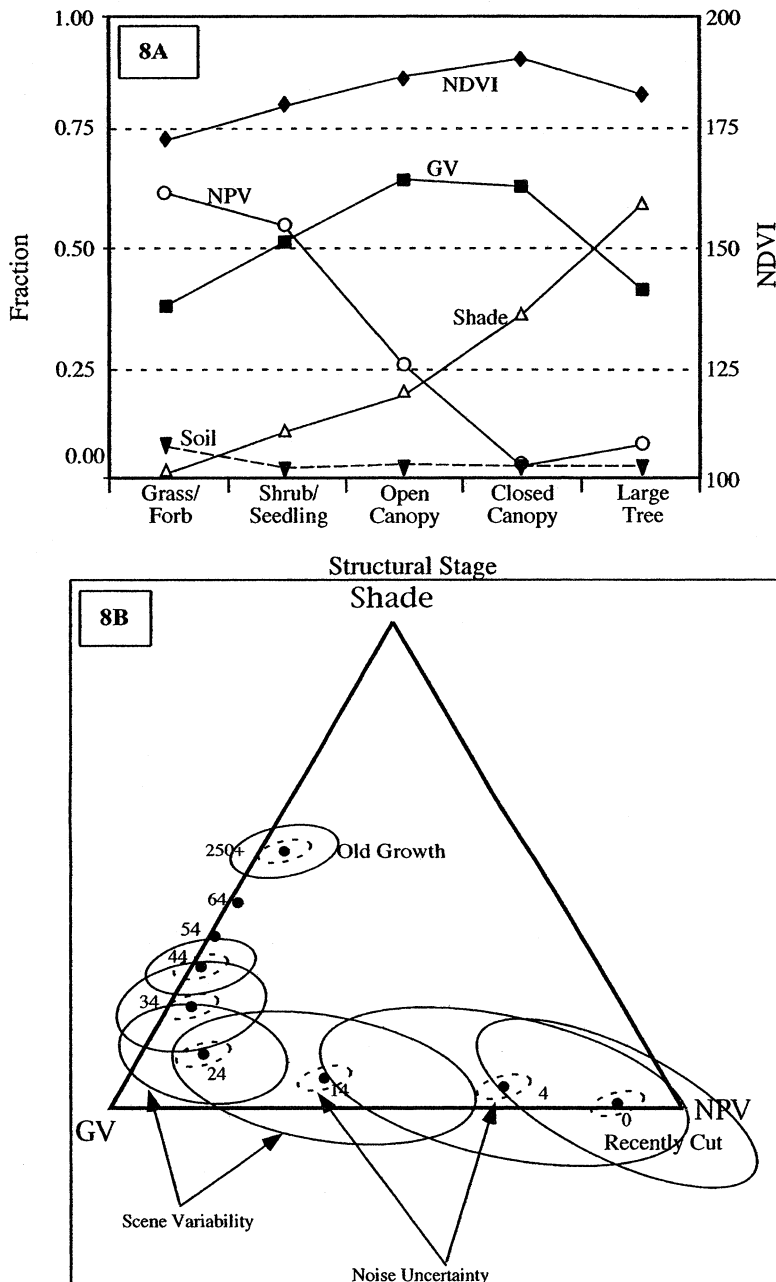


Figure 8-8. (A) Trajectories of NDVI and endmember fractions for aging forest stands. The shade fraction continues to increase after canopy closure while NDVI and green vegetation fraction (GV) eventually decrease. (B) A ternary diagram of the mean fractions in unmixed Landsat TM data for forest stands with different ages, based on 278 field samples. The outer ellipses contain 90 % of the data for each stand age, demonstrating the uncertainty in ages derived from the Landsat data. From Sabol et al. (2002), with permission.

In an effort to reduce the impacts of endmember variability on fraction uncertainties in forests, Lobell et al. (2001) applied the automated SWIR2 approach discussed in section 3.3 to AVIRIS data from a coniferous forest in Oregon. To highlight the importance of endmember variability in forest ecosystems, Figure 8-9 compares canopy cover derived from a traditional mixture model with four fixed endmembers (green vegetation, NPV, soil, and shade) with results from the SWIR analysis. Actual canopy cover was determined at 16 field plots with supervised classification of low-altitude aerial photos. Vegetation ground cover was estimated in the traditional model by dividing the vegetation fraction by $(1 - \text{shade})$, which is commonly done to normalize effects of sun-sensor geometry (Adams et al. 1995; Smith et al. 1990). The SWIR-based analysis did not include a shade endmember because tying largely removes the effect of shadows. While traditional mixture modeling results generally agreed with air photo values, the correlation suffered from endmember variability ($r^2 = 0.59$, rms = 11.4 %). The mean canopy fractions from SWIR analysis, which fundamentally accounted for natural variability, more accurately predicted vegetation cover at the plots ($r^2 = 0.85$, rms = 3.8 %).

4. CANOPY REFLECTANCE MODELING

Forests are complex three-dimensional structures containing large variations in the amount, orientation and architectural placement of vegetative tissues. These variations occur spatially and temporally, and can be only roughly known prior to remote sensing analysis. Generalized interpretation of vegetation indices (VI), such as in linking them to LAI or forest canopy cover, requires a range of assumptions regarding the canopy architecture (section 2). At continental to global scales, these assumptions are simplified and reduced through the use of prescribed maps of vegetation structural types (e.g., Myneni et al. 1997b). These maps are used to modify the empirical relationship between the VI and the desired structural variable. At landscape to regional scales, assumptions regarding canopy structure are much more challenging to accommodate in VI studies. Therefore, efforts at these finer spatial scales often rely upon field-based calibration studies to link VIs to the needed structural variable. Consequently, these "tuned" VI-parameter linkages are often difficult to apply in new biophysical settings.

A variety of assumptions are also inherent in per-pixel analyses that employ spectral mixture models. As discussed, the primary limitations in these studies arise from endmember variability and nonlinear mixing between endmembers. Errors due to these factors may be relatively small in certain situations, but may become intolerably problematic in others. These

conditions typically involve multiple scattering of photons by vegetation and other intra- and inter-pixel constituents such that the radiation received by the sensor has interacted with more than one scattering element. These elements may be multiple plant components such as foliage, wood and litter, or they may be volumetric quantities of a single type of tissue such as occurs when canopy LAI is greater than one (Asner 1998).

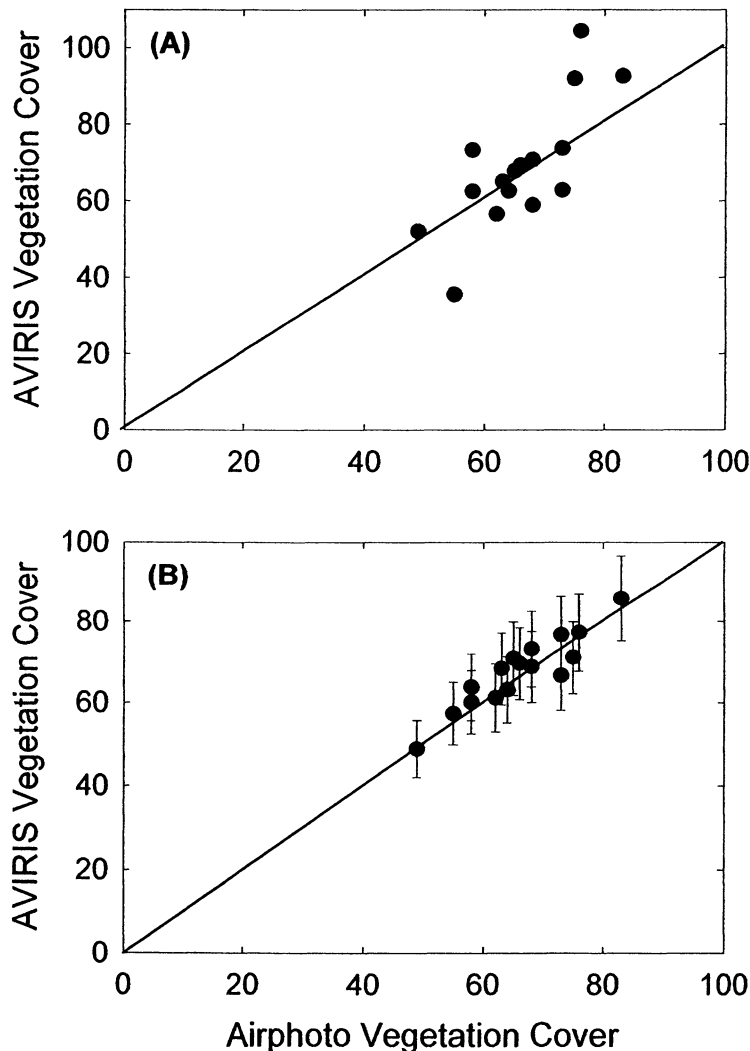


Figure 8-9. Vegetation canopy cover estimates for a coniferous forest in Oregon from (A) traditional full-range unmixing and (B) AutoSWIR applied to AVIRIS data, compared to low altitude air photo estimates at 16 field plots. Mean \pm one standard deviation is shown for AutoSWIR based on Monte Carlo simulations. After Lobell et al. (2002).

While canopy architecture and multiple scattering present major challenges to vegetation index and spectral mixture analyses, they are a core focus in canopy reflectance modeling studies. These models come in many forms, ranging from simple one-dimensional light extinction algorithms to sophisticated 3-D ray tracing simulators. The most common models fall into the categories of 1-D or 3-D turbid-medium, radiative transfer models. The 1-D models simulate the canopy as a plane-parallel, horizontally homogeneous cloud of scattering elements; no horizontal variation in structure or shadowing is represented. The 3-D turbid-medium models represent the pixel as populated with multiple ‘clouds’ of scatterers, each cloud confined to a geometric form or space. Geometric-optical models represent a pixel comprised of geometrical objects, with associated sunlit and shaded areas determined by the illumination and viewing geometry. Ray tracing models provide explicit simulation of photon trajectories into, within and out from a deterministic representation of the vegetation structure.

Excellent reviews of canopy photon transport theories and reflectance models are available (e.g., Chen et al. 2000; Disney et al. 2000; Goel 1988; Myneni et al. 1989b; Qin and Liang 2000) and thus will not be reiterated here. However, the use of these models for applications in per-pixel studies continues to grow and therefore warrants review. In this section, we summarize the use of these models in the “forward” simulation mode that is often employed to estimate canopy, pixel and top-of-atmosphere reflectance. We also highlight how these models can be inverted to estimate the structural attributes of forest landscapes. The discussion is cast in the context of spectral and angular optical data, as these two domains have been studied most rigorously by the modeling community.

4.1 Model inputs

Canopy reflectance models come in many forms and thus the principal equations describing them will not be presented here. However, nearly all of the physically-based models use a similar set of inputs to derive pixel reflectance as a function of wavelength ($R(\lambda)$):

$$R(\lambda) = f(GEOM, STR_{CANOPY}, STR_{LAND}, TISSUE OPT, \rho_{SOIL}) \quad (14)$$

Where,

$$GEOM = f(\theta_{SUN}, \theta_{VIEW}, \phi_{SUN}, \phi_{VIEW})$$

$$STR_{CANOPY} = f(LAI, NPVAI, LAD, NPVAD, TISSUE A:H, CLUMPING)$$

$$STR_{LANDSCAPE} = f(CRWN_{HGT}, CRWN_{SHP}, Stand density)$$

$$TISSUE OPT = \rho_{LEAF}, \tau_{LEAF}, \rho_{NPV}, \tau_{NPV} = f(Cw, Cm, Chl, \dots)$$

The *GEOM* parameters describe the sun and viewing zenith (θ) and azimuth (ϕ) angles, which are well known in an actual measurement made from aircraft or spacecraft vantage points.

The structure of individual canopies (e.g., trees), represented as STR_{CANOPY} , is comprised of leaf and non-photosynthetic vegetation area indices (*LAI*, *NPVAI*). These quantities can be dimensionless or they can be stratified into canopy layers as leaf or NPV area densities with units of m^2 tissue per m^3 of crown volume. The angular distribution of leaf and NPV tissues (*LAD*, *NPVAD*) indicate the orientation of the vegetative tissues in three-dimensional space. These distributions can be described statistically (Strebel et al. 1985) or explicitly (Chelle and Andrieu 1999). *LAD* and *NPVAD* can also be varied along the canopy vertical axis (z), although this is not common practice due to computational limitations. The canopy structural parameter, *TISSUE A:H*, describes the size of the photon scatterers (e.g., foliage) relative to their height distribution in the canopy. This parameter plays an important role in determining the reflectance behavior of a canopy at and near the retro-solar direction, or the direction aligning the sun and viewer (often called the 'hotspot'). The landscape structure ($STR_{LANDSCAPE}$) is defined explicitly or statistically with parameters describing the height (*CRWN_{HGT}*) and shape (*CRWN_{SHP}*) of individual tree crowns. Landscape structure is also a function of the number of individual plants per area, or stand density. Together the canopy and landscape structural parameters largely determine the absorption and scattering properties of simulated forests, particularly the angular distribution of reflected photons as described later.

The optical properties of plant tissues (*TISSUE OPT*) also play a central role in determining pixel-scale reflectance. Tissue optics, described by the reflectance (ρ) and transmittance (τ) characteristics of foliage and NPV, set up the wavelength-dependent radiation absorption features that are then modified by the vegetation structure (Asner 1998). For example, green foliage is an efficient absorber of incident radiation at 670-680 nm (red wavelengths) due to the activity of chlorophyll and other pigments (Gates 1970; Gausman 1983; Maas and Dunlap 1989). Adding more foliage to a pixel via increased *LAI* or stand density will lower pixel reflectance at red wavelengths (Figure 8-10). This occurs because the probability of absorption is increased with every scattering event within the canopy volume. Conversely, green foliage is a poor absorber of near-infrared energy (e.g., 700-1300 nm), and in such a case, structural parameters such as *LAI*, *LAD* and stand density exert even stronger control over the pixel reflectance. Increases in *LAI*, more horizontally oriented foliage, and increased stand density heighten the probability that the foliage will scatter photons back

toward the sensor since each leaf-photon interaction has a low absorption potential (high reflectance and transmittance) (Figure 8-10).

Although the tissue optics are key to determining pixel-scale reflectance, only a few studies have quantified tissue reflectance and transmittance properties for many samples (Jacquemoud and Baret 1990). This problem has impeded the application of canopy reflectance models to new ecological settings. Recently however, the optical properties of foliage and NPV have been modeled using as inputs the absorption spectra of tissue constituents such as water (C_w), chlorophyll (Chl), specific leaf area (C_m), and other factors (eq. 14; Dawson et al. 1998; Jacquemoud et al. 1995). These modeling developments have extended the value of photon transport simulations for forest ecosystem research.

4.2 Simulating spectral signatures

4.2.1 Forward modeling

To date, most canopy modeling studies have focused on the simulation of pixel reflectance using hypothetical or measured leaf, canopy and stand characteristics. The general practice of pixel reflectance modeling from a combination of parameters in eq. (14) is often referred to as 'forward modeling'. This approach has provided an economical way to investigate the effects of forest structural attributes on reflectance signatures, but most importantly, it has improved our understanding of the interactions and co-dependencies between structural parameters as they affect the radiation field. In turn, this knowledge has aided in the development of vegetation indices (section 2) and inverse modeling strategies (section 4.3) needed to study forest structure with actual remote sensing measurements.

Forward modeling studies of forest canopies have largely focused on the spectral dependence of reflectance and its relationship to forest structural and tissue optical variables. The first models were used to study how basic canopy attributes determine top-of-canopy reflectance at different wavelengths. In particular, radiative transfer models have been widely used to study the relationship between forest LAI and vegetation indices.

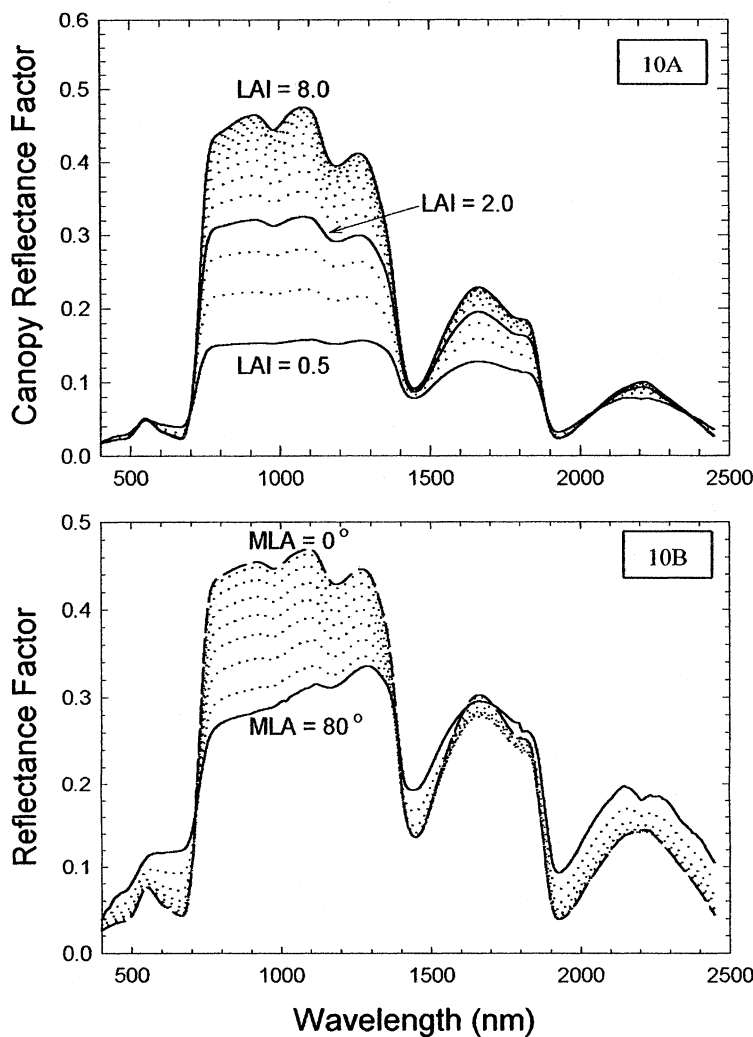


Figure 8-10. Top-of-canopy spectral reflectance simulations covering the 400-2500 nm wavelength region. (A) Effect of increasing leaf area index (LAI) on canopy reflectance; all other model parameters in eq. (14) held constant. (B) Effect of changing the mean leaf angle of a spherical distribution (Verhoef 1984) on canopy reflectance; LAI held constant at 4.0 and other model parameters held constant in eq. (14). After Asner (1998).

Sellers (1987) demonstrated with a 1-D radiative transfer model that the simple ratio index (SR) increases non-linearly with LAI. Huemmrich and Goward (1997) used a radiative transfer model to simulate the NDVI of ten tree species found in temperate and boreal forests. They showed that the NDVI was sensitive to background reflectance at low LAI values and to leaf optical properties at high LAI values. Baret et al. (1995) used the same

model to show that a number of vegetation indices, including the PVI, SAVI and GEMI, scaled linearly with canopy gap fraction. Asner (1998) demonstrated the theoretical sensitivity of vegetation reflectance to changing LAI and leaf angle distribution (LAD) across the exploitable shortwave range of 400-2500 nm (Figure 8-10). Both LAI and LAD were found to dominate reflectance variability in the NIR (700-1300 nm). However, LAD variation was more important than that of LAI at visible wavelengths (< 700 nm) and in the shortwave-IR region above 1900 nm (Figure 8-10B). These results imply that even the most basic, 1-D models are sensitivity to canopy structure and architecture, at least as seen via the LAD parameter.

More detailed 3-D geometric-optical, turbid medium, and ray-tracing models have been used to study the sensitivity of VIs to various vegetation and external properties in the context of forest structure. These more advanced models allow the effects of shadowing to be considered when comparing the indices, an improvement over earlier modeling studies that assumed a horizontally homogeneous canopy (e.g., Rondeaux et al. 1996). Using a hybrid radiative transfer/geometric-optical model, Eklundh et al. (2001) found that the SR and NDVI increased monotonically with increasing forest LAI, given a constant stand density (number of trees/area) and branch area index (BAI). However, the authors suggest that for boreal forests, varying the stand density, BAI and LAI is a more realistic test of the sensitivity of these indices. When the authors varied these parameters all together, both SR and NDVI increased at low LAI (to ~5) but decreased at higher values of LAI (Figure 8-11). This result cannot be readily achieved using a simple 1-D radiative transfer model. McDonald et al. (1998) used a hybrid geometric-optical/ray-tracing model to study the effects of canopy cover and height, solar angle and ground reflectance on a variety of vegetation indices in boreal forest ecosystems. Intra- and inter-crown shadowing was explicitly represented based on the physical attributes of the modeled forest canopy. Their results indicated a nearly linear NDVI increase with canopy cover but pronounced sensitivity to shadowing (Figure 8-12). Despite the fact that the PVI, SAVI, TSAVI, and GEMI were designed to reduce sensitivity to soil conditions, McDonald et al. (1998) discovered substantial variations in these indices when the background reflectance increased. The authors suggested that high background reflectance resulted from the nearly ubiquitous presence of moss on the forest floor.

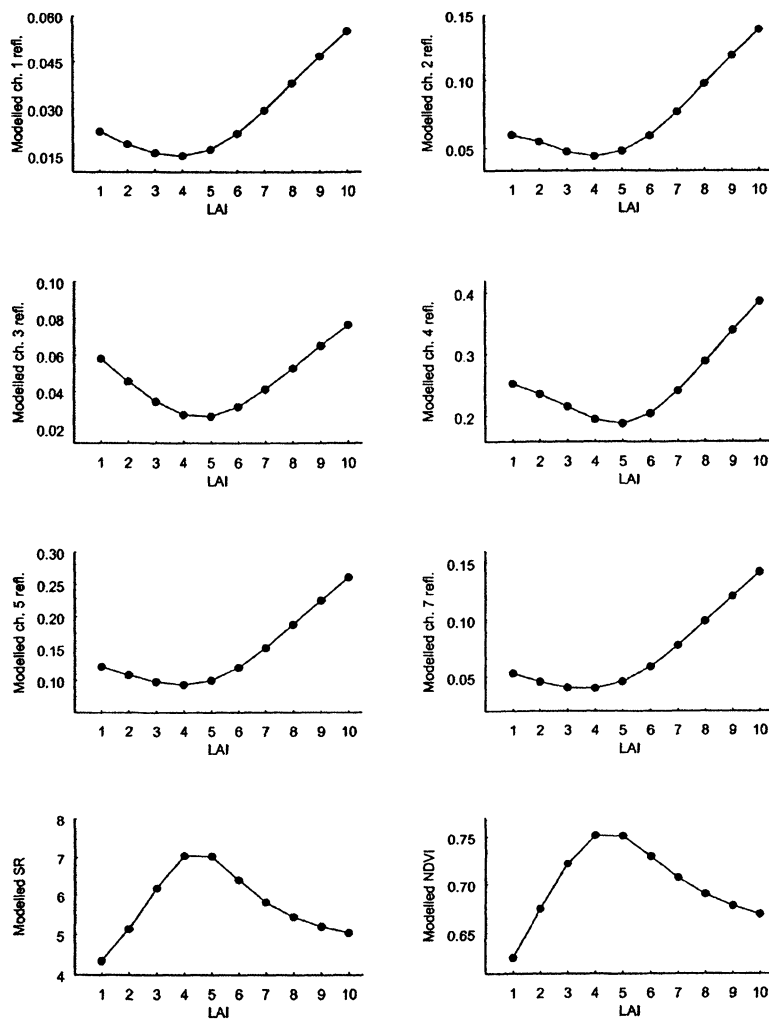


Figure 8-11. Model simulations of forest canopy reflectance response to changing LAI, branch area index, and tree density in Landsat ETM+ channels, the SR and the NDVI. From Eklundh et al. (2001), with permission.

Recently, Zarco-Tejada et al. (2001) confirmed the importance of 3-D shadowing in boreal forest reflectance spectroscopy collected with Compact Airborne Spectrographic Imager (casi) observations (Colour Plate 6). Hyperspectral reflectance data were collected at high spatial resolution from both sunlit and shaded areas within a forest stand. The spectra of sunlit crowns were significantly different from those of shadowed inter-spaces and crowns. As predicted by radiative transfer theory and analyses, the effects of shadowing were greatest in the near-IR and smallest in the visible part of the

spectrum (Colour Plate 6). Notably though, the shape of the pigment features in the 500–650 nm range were also highly sensitive to shadowing.

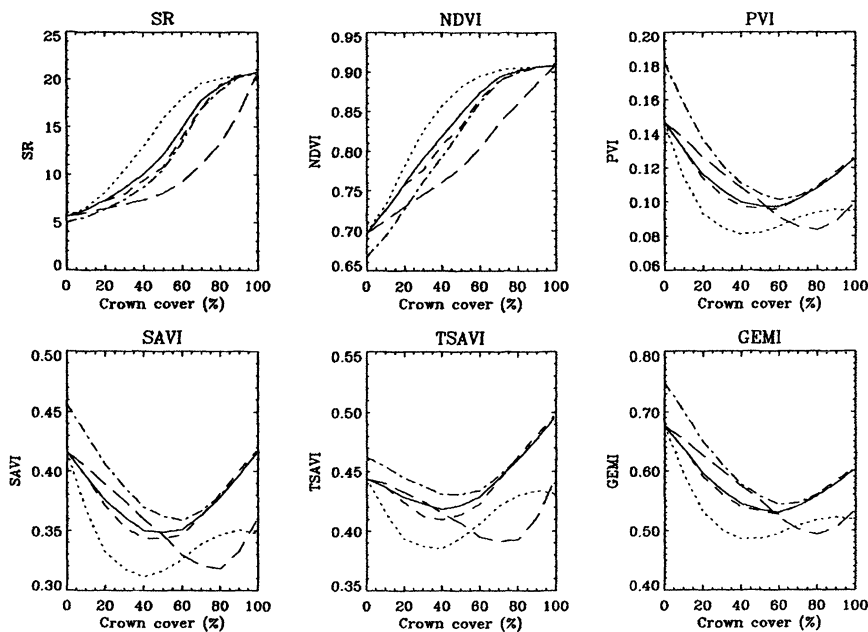


Figure 8-12. Six vegetation indices as a function of percentage tree crown cover calculated using a Monte Carlo ray-tracing model. Shown are a base case (solid curve), a solar zenith angle change from 30 to 60° (dotted curve), an increase in tree height variation (dashed curve), an increase in background reflectance (dotted-dashed curve). After McDonald et al. (1998).

4.2.2 Inverse modeling

Canopy reflectance models have also been used to estimate forest structural characteristics from remote sensing observations. Termed 'model inversions' or 'inverse modeling', these studies attempt to estimate canopy properties using numerical inversion approaches. The most common technique is summarized schematically in Figure 8-13. Spectral measurements are collected from field, airborne or spaceborne sensors, forming an observation vector to which modeled spectra are fit. The measured and modeled reflectances (R) are typically collected over the spectral (λ) and/or angular (i) domains (Figure 8-13). A model – turbid medium, geometric-optical or other – is used to simulate spectra iteratively. The goodness of fit between measured and modeled spectra is evaluated after each model run using a figure of merit function, such as the one shown in Figure 8-13. The modeled spectrum that most closely matches the

observation vector is found, and the model parameters leading to this best fit are then considered the estimated canopy attributes. While there are many issues and caveats to contend with when using inverse modeling techniques (recently reviewed by Kimes et al. (2000)), a few studies show the potential value of this approach for forest structural estimates.

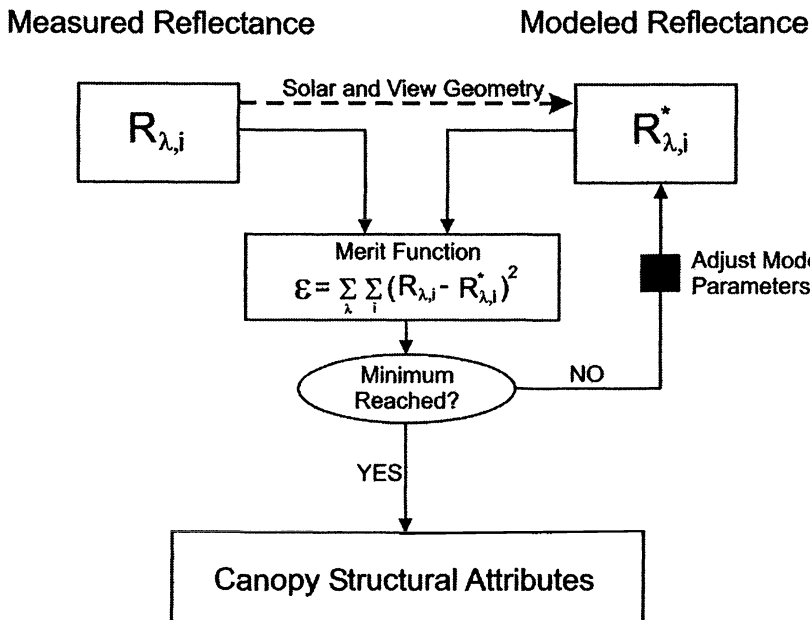


Figure 8-13. Schematic of a typical model inversion for canopy structural attribute estimation.

Woodcock et al. (1997) used a geometric-optical model to estimate tree crown density and dimensions from Landsat TM imagery. They focused on four national forests in the United States, and found that the model inversions provided verifiably accurate estimates of crown cover (M):

$$M = nR^2 \quad (15)$$

where n = stand density or number of individuals per area and R is the crown radius. The authors found that M could be estimated (inverted for) in conifer forests in the Sierra Nevada Mountains, but neither n nor R could be accurately determined. Woodcock et al. (1997) suggested that this was caused by a poor relationship between intra-pixel variance in stand density and crown size; that is, the nadir Landsat observations under-determined the model inversion. It was suggested that multi-view angle data would improve the ability to go beyond crown cover (M) in future studies.

Gemmell and Varjo (1999) used a 1-D canopy reflectance model with Landsat TM data to estimate forest canopy cover and LAI in boreal forests.

They found that the model was unable to provide accurate estimates due to highly varying forest floor reflectance. Later, Gemmell (1999) tried estimating crown cover in the same geographic areas using a geometric-optical model with the Landsat observations. He was able to achieve reasonable model inversion results ($r^2 = 0.76$) when background reflectance was permitted to vary in the analysis. Gemmell (2000) extended the model inversion study even further by using multi-angle ASAS data in replacement of the nadir-only Landsat imagery. The use of multi-angle observations greatly improved estimates of forest crown cover, but the accuracy remained sensitive to background reflectance variation.

4.3 Simulating angular signatures

4.3.1 Forward modeling

The bi-directional reflectance distribution function (BRDF) describes the angular reflectance properties of any medium. The shape of this angular distribution is a function of the orientation of photon scattering elements in 3-D space (Ross 1981). The BRDF of forests is thus highly affected by the orientation of foliage, litter and wood at canopy level (Myneni et al. 1989b; Qin 1993). However, at the landscape level, the spatial distribution and shape of individual tree crowns account for characteristic variation of the angular reflectance (Li and Strahler 1992b; Strahler and Jupp 1991). For example, the number and size of gaps between tree crowns significantly affect the BRDF (Wu and Strahler 1994).

Field-based, multi-angle remote sensing observations have provided insight into the angular reflectance distribution of plant canopies (e.g., Deering et al. 1999). These field studies demonstrate the universally anisotropic reflectance behavior of canopies. Airborne instrumentation, such as the Advanced Solid-state Array Spectroradiometer (ASAS; Irons et al. 1991) and the Multi-angle Imaging Spectroradiometer (AirMISR; Diner et al. 1998), has also highlighted the anisotropic reflectance properties of forest canopies (Colour Plate 7). Spaceborne observations, such as from the NOAA AVHRR, NASA MODIS and MISR instruments, are now capturing the complex variations in Earth's angular reflectance distribution as well. The spatial and temporal heterogeneity of forest canopy angular reflectances implies that biophysical properties are just as variable, so exploiting angular signatures may yield unique information pertaining to forest structure.

Several studies have shown that multi-view angle optical measurements provide information on forest structure distinct from what can be acquired through single-angle optical measurements. For example, Bicheron et al. (1997) showed that boreal forest mapping accuracies were substantially

improved when angular data were employed in addition to multi-spectral data. Using the airborne POLDER instrument during the NASA BOREAS campaign, they improved forest-mapping results from 79 % accuracy with single-angle data to 91 % accuracy using multi-angle measurements. The authors attributed the improvement to the sensitivity of multi-angle measurements to forest structural variation. Sandmeier and Deering (1999) used multi-angle data with hyperspectral sampling from ASAS to classify boreal forests. They showed that the additional information contained in the multi-angle observations allowed more detailed estimates of forest structural variables such as crown dimensions and height.

Canopy reflectance modelers have explored the interaction of structural characteristics as they affect angular reflectance signatures. For example, a geometric-optical model was used to study the contribution of varying sun angle to vegetation BRDF (Schaaf and Strahler 1993). They showed how increased solar zenith angle increased the apparent shadowing between tree crowns, leading to decreased pixel reflectance at all wavelengths. Abuelgasim and Strahler (1994) demonstrated that the same geometric-optical model could simulate the angular reflectance signatures contained in ASAS imagery of forest stands in Oregon. Their results suggested that forest stand density and crown variables could be estimated using these models with multi-angle observations.

Gerard and North (1997) used another geometric-optical model to quantify the effects of crown shape, canopy cover and gaps, and stand density on pixel reflectance of a tropical forest canopy. They found that the fraction of sunlit crown and understory dominate the dynamics of pixel reflectance. More importantly, they showed that the BRDF at red wavelengths was determined mainly by the understory illumination, which was most closely linked to canopy cover, tree pattern distribution and gaps. In contrast, the near-infrared BRDF was driven by variations in the illuminated crowns, which were determined by canopy cover, crown height distribution and crown shape (Gerard and North 1997).

Gastellu-Etchegorry et al. (1999) used a 3-D radiation transport model called DART to study the angular reflectance behavior of tropical broadleaf and boreal needleleaf forests. Their modeling studies were well grounded to field measurements, thereby increasing the realism and usefulness of their analyses. They focused on LAI and leaf optical property estimates across a range of changing spatial resolution, sun-view geometry and sky conditions. Most notably, all of their results suggested very strong anisotropic reflectance behavior of the simulated pixels; viewing geometry alone caused 25-50 % variation in the modeled spectral reflectance, depending upon the wavelength region.

Many other modeling studies have explored the BRDF of vegetation at canopy and pixel scales beyond those we present here. Although additional investigations could be covered in our review, the forward modeling effort as it applies to the angular reflectance domain has yielded a set of common results. First, all studies show a strong non-lambertian distribution of reflected photons from forest canopies. Second, the persistent but highly varying anisotropic behavior of the forest canopy BRDF among many studies implies that there is canopy structural information to be derived from multi-view angle measurements. It is here that per-pixel analyses have used canopy reflectance models to assist in the process of interpreting multi-angle observations.

4.3.2 Inverse modeling

At the present time, there are relatively few published papers on the application of canopy reflectance model inversions for forest structural studies. This is surprising given the availability of airborne multi-view angle data for some time now, and given the clearly defined need for structural information by the ecological, land-surface and biogeochemical research communities (Asner 2000; Asner et al. 1998).

There have been excellent studies on the validation of models with multi-angle observations, such as the ASAS study by Abuelgasim and Strahler (1994). Other studies have used ASAS and field-based angular measurements to estimate forest structural parameters without the use of models. Sandmeier and Deering (1999) used multi-angle ASAS data to classify boreal forest stands based on structural attributes such as crown closure and height. Recently, Lacaze and Roujean (2001) developed and validated a reflectance model using airborne multi-view angle POLDER data. They found an initial high sensitivity of the hotspot (retro-solar viewing direction) to foliage clumping in canopies. This work was extended to boreal forest sites using the spaceborne POLDER instrument, successfully demonstrating that foliage clumping could be quantified using a robust sampling of the forest BRDF (Lacaze et al. 2002). These few efforts highlight the unique potential for estimating forest structural properties using multi-angle observations with canopy reflectance models, though additional studies are currently emerging using POLDER and MISR observations.

5. CONCLUSIONS

In this Chapter, we summarized the major advances in per-pixel analyses of forest structure. The methods designed to estimate attributes of forest structure have evolved considerably in the past few decades. The use of vegetation indices is by far the most widespread in per-pixel studies of forest ecosystems. Vegetation indices are computationally efficient, but they can be difficult to interpret. Both field and modeling studies show that indices cannot be interpreted with respect to a single forest structural attribute. Vegetation indices will continue to serve much of the remote sensing and applications communities, and thus efforts to improve them over time is warranted. Indices such as the ARVI and EVI show promise in extending the capabilities of vegetation index approaches.

Linear mixture modeling has provided a very useful framework for evaluating land-use and land-cover changes in forest ecosystems. When compared to vegetation indices, endmember fractions are less susceptible to background effects and are easier to interpret and compare across images. However, few studies in forests have quantitatively compared image fractions derived from mixture modeling with field cover measurements. This is because, unlike in arid systems where field measurements are easier to carry out, many forest areas are either inaccessible or extremely difficult to characterize, even at the scale of Landsat pixels. Additional studies that provide direct validation are needed to fully assess the capabilities and potential errors of linear mixture models in forest ecosystems. Until these uncertainties are better understood, the ultimate utility of mixture models for various applications, and the relative capabilities of different algorithms and sensors, will remain unclear.

The use of canopy reflectance models for per-pixel analysis of forest structure is still in its infancy. Most studies have utilized field or airborne multi-view angle observations to evaluate model performance. Notably, many of the newest 3-D models – either turbid medium, geometric-optical or ray tracing simulations – appear to accurately represent the spectral and angular reflectance distribution of forests. As the models continue to develop their capabilities and improve their accuracy, the forward modeling problem will be exercised to a greater extent. Future studies will continue to clarify the relative importance of structural factors influencing actual remote sensing measurements collected over forested regions. In turn, forward modeling studies will continue to play a vital role in guiding field-based efforts and remote sensing applications.

REFERENCES

- Abuelgasim, A. A., & Strahler, A. H. (1994). Modeling bidirectional radiance measurements collected by the Advanced Solid-State Array Spectroradiometer (ASAS) Over Oregon Transect conifer forests. *Remote Sensing of Environment*, 47, 261-275.
- Adams, J. B., Sabol, D. E., Kapos, V., Almeida, R., Roberts, D. A., Smith, M. O., & Gillespie, A. R. (1995). Classification of multispectral images based on fractions of endmembers - Application to land-cover change in the Brazilian Amazon. *Remote Sensing of Environment*, 52, 137-154.
- Adams, J. B., Smith, M. O., & Johnson, P. E. (1986). Spectral mixture modeling: A new analysis of rock and soil types at the Viking Lander I Site. *Journal of Geophysical Research*, 91, 8098-8112.
- Asner, G. P. (1998). Biophysical and biochemical sources of variability in canopy reflectance. *Remote Sensing of Environment*, 64, 134-153.
- Asner, G. P. (2000). Contributions of multi-view angle remote sensing to land-surface and biogeochemical research. *Remote Sensing Reviews*, 18, 137-162.
- Asner, G. P., Braswell, B. H., Schimel, D. S., & Wessman, C. A. (1998). Ecological research needs from multiangle remote sensing data. *Remote Sensing of Environment*, 63, 155-165.
- Asner, G. P., Keller, M., Pereira, R., Zweede, J. C., & Silva, J. N. (2002). Forest canopy damage and closure following selective logging in Amazonia: Integrating satellite and field studies. *Ecological Applications*.
- Asner, G. P., & Lobell, D. B. (2000). A biogeophysical approach for automated SWIR unmixing of soils and vegetation. *Remote Sensing of Environment*, 74, 99-112.
- Asner, G. P., Townsend, A. R., & Braswell, B. H. (2000). Satellite observations of El Niño effects on Amazon forest phenology and productivity. *Geophysical Research Letters*.
- Asner, G. P., & Vitousek, P. M. Biochemical versus biophysical sources of variation in Hawaiian tropical forest reflectance spectroscopy. *Remote Sensing of Environment*, in review.
- Bannari, A., Morin, D., Bonn, F., & Huete, A. (1995). A review of vegetation indices. *Remote Sensing Reviews*, 13, 95-120.
- Baret, F., Clevers, J. G. P. W., & Steven, M. D. (1995). The robustness of canopy gap fraction estimates from red and near-infrared reflectances: a comparison of approaches. *Remote Sensing of Environment*, 54, 141-151.
- Bateson, A., & Curtiss, B. (1996). A method for manual endmember selection and spectral unmixing. *Remote Sensing of Environment*, 55, 229-243.
- Bateson, C. A., Asner, G. P., & Wessman, C. A. (2000). Endmember bundles: A new approach to incorporating endmember variability into spectral mixture analysis. *IEEE Transactions On Geoscience and Remote Sensing*, 38, 1083-1094.
- Ben-Dor, E., Irons, J. R., & Eperna, G. F. (1999). Soil reflectance, in *Remote Sensing for the Earth Sciences*. Rencz, A. N. (Ed.). *Manual of Remote Sensing*, 111-188. Wiley & Sons, New York, USA.
- Bicheron, P., Leroy, M., Hautecoeur, O., & Breon, F. M. (1997). Enhanced discrimination of boreal forest covers with directional reflectances from the airborne polarization and directionality of Earth reflectances (POLDER) instrument. *Journal of Geophysical Research*, 102, 29517-29528.
- Borel, C. C., & Gerstl, S. A. W. (1994). Nonlinear spectral mixing models for vegetative and soil surfaces. *Remote Sensing of Environment*, 47, 403-416.
- Botta, A., Viovy, N., Ciais, P., Friedlingstein, P., & Monfray, P. (2000). A global prognostic scheme of leaf onset using satellite data. *Global Change Biology*, 6, 709-725.

- Brown, L., Chen, J. M., Leblanc, S. G., & Cihlar, J. (2000). A shortwave infrared modification to the simple ratio for LAI retrieval in boreal forests: An image and model analysis. *Remote Sensing of Environment*, 71, 16-25.
- Chelle, M., & Andrieu, B. (1996). Radiative models for architectural modeling. *Agronomie*, 19, 225-240.
- Chen, J. M., & Cihlar, J. (1996). Retrieving leaf area index of boreal conifer forests using landsat TM images. *Remote Sensing of Environment*, 55, 153-162.
- Chen, J. M., Li, X., Nilson, T., & Strahler, A. (2000). Recent advances in geometrical optical modelling and its applications. *Remote Sensing Reviews*, 18, 227-262.
- Cochrane, M. A., & Souza, C. M. (1998). Linear mixture model classification of burned forests in the Eastern Amazon. *International Journal of Remote Sensing*, 19, 3433-3440.
- Coops, N., Delahaye, A., & Pook, E. (1997). Estimation of eucalypt forest leaf area index on the south coast of New South Wales using Landsat MSS data. *Australian Journal of Botany*, 45, 757-769.
- Curran, P. J. (1980). Multispectral remote sensing of vegetation amount. *Progress in Physical Geography*, 4, 315-341.
- Curran, P. J. (1989). Remote sensing of foliar chemistry. *Remote Sensing of Environment*, 30, 271-278.
- Dawson, T. P., Curran, P. J., & Plummer, S. E. (1998). LIBERTY : Modeling the effects of leaf biochemical concentration on reflectance spectra. *Remote Sensing of Environment*, 65, 50-60.
- Deering, D. W., Eck, T. F., & Banerjee, B. (1999). Characterization of the reflectance anisotropy of three boreal forest canopies in spring-summer. *Remote Sensing of Environment*, 67, 205-229.
- DeFries, R. S., Hansen, M., Townshend, J. R. G., & Sohlberg, R. (1998). Global land cover classifications at 8 km spatial resolution: The use of training data derived from Landsat imagery in decision tree classifiers. *International Journal of Remote Sensing*, 19, 3141-3168.
- Diner, D. J., Beckert, J. C., Reilly, T. H., Bruegge, C. J., Conel, J. E., Kahn, R. A., Martonchik, J. V., Ackerman, T. P., Davies, R., Gerstl, S. A. W., Gordon, H. R., Muller, J. P., Myneni, R. B., Sellers, P. J., Pinty, B., & Verstraete, M. M. (1998). Multi-angle Imaging SpectroRadiometer (MISR): Instrument description and experiment overview. *IEEE Transactions On Geoscience and Remote Sensing*, 36, 1072-1087.
- Disney, M. I., Lewis, P., & North, P. R. J. (2000). Monte Carlo ray tracing in optical canopy reflectance modelling. *Remote Sensing Reviews*, 18, 163-196.
- Eklundh, L., Harrie, L., & Kuusk, A. (2001). Investigating relationships between Landsat ETM plus sensor data and leaf area index in a boreal conifer forest. *Remote Sensing of Environment*, 78, 239-251.
- Foody, G. M., Lucas, R. M., Curran, P. J., & Honzak, M. (1997). Non-linear mixture modelling without end-members using an artificial neural network. *International Journal of Remote Sensing*, 18, 937-953.
- Fung, T., & Siu, W. (2000). Environmental quality and its changes, an analysis using NDVI. *International Journal of Remote Sensing*, 21, 1011-1024.
- Gao, B. C., & Li, R. R. (2000). Quantitative improvement in the estimates of NDVI values from remotely sensed data by correcting thin cirrus scattering effects. *Remote Sensing of Environment*, 74, 494-502.
- Gastellu-Etchegorry, J. P., Guillevic, P., Zagolski, F., Demarez, V., Trichon, V., Deering, D., & Leroy, M. (1999). Modeling BRF and radiation regime of boreal and tropical forests: I. BRF. *Remote Sensing of Environment*, 68, 281-316.

- Gates, D. M. (1970). Physical and physiological properties of plants. *Remote Sensing with Special Reference to Agriculture and Forestry*, 224-252. National Academy of Science, Washington, D.C., USA.
- Gates, D. M., Keegan, H. J., Schleter, J. C., & Wiedner, V. R. (1965). Spectral properties of plants, *Applied Optics*, 4, 11-20.
- Gausman, H. W. (1983). Visible-light reflectance, transmittance, and absorptance of differently pigmented cotton leaves. *Remote Sensing of Environment*, 13, 233-238.
- Gemmell, F. (1999). Estimating conifer forest cover with Thematic Mapper data using reflectance model inversion and two spectral indices in a site with variable background characteristics. *Remote Sensing of Environment*, 69, 105-121.
- Gemmell, F. (2000). Testing the utility of multi-angle spectral data for reducing the effects of background spectral variations in forest reflectance model inversion. *Remote Sensing of Environment*, 72, 46-63.
- Gemmell, F., & Varjo, J. (1999). Utility of reflectance model inversion versus two spectral indices for estimating biophysical characteristics in a boreal forest test site. *Remote Sensing of Environment*, 68, 95-111.
- Gerard, F. F., & North, P. R. (1997). Analyzing the effect of structural variability and canopy gaps on forest BRDF using a geometric-optical model. *Remote Sensing of Environment*, 62, 46-62.
- Gillespie, A. R. (1992). Spectral mixture analysis of multispectral thermal infrared images. *Remote Sensing of Environment*, 42, 137-145.
- Goel, N. S. (1998). Models of vegetation canopy reflectance and their use in estimation of biophysical parameters from reflectance data. *Remote Sensing Reviews*, 4, 1-222.
- Graetz, R. D., & Gentle, M. R. (1982). The relationship between reflectance in the Landsat wavebands and the composition of an Australian semi-arid shrub rangeland. *Photogrammetric Engineering and Remote Sensing*, 48, 1721-1730.
- Gutman, G. G. (1999). On the use of long-term global data of land reflectances and vegetation indices derived from the advanced very high resolution radiometer. *Journal of Geophysical Research-Atmospheres*, 104, 6241-6255.
- Hall, F. G., Peddle, D. R., & LeDrew, E. F. (1996). Remote sensing of biophysical variables in boreal forest stands of *Picea mariana*. *International Journal of Remote Sensing*, 17, 3077-3081.
- Hall, F. G., Shimabukuro, Y. E., & Huemmrich, K. F. (1995). Remote-sensing of forest biophysical structure using mixture decomposition and geometric reflectance models. *Ecological Applications*, 5, 993-1013.
- Hansen, M. C., DeFries, R. S., Townshend, J. R. G., & Sohlberg, R. (2000). Global land cover classification at 1 km spatial resolution using a classification tree approach. *International Journal of Remote Sensing*, 21, 1331-1364.
- Horowitz, H. M., Nalepka, R. F., Hyde, P. D., & Morgenstern, J. P. (1971). Estimating the proportions of unresolved objects within a single resolution element of a multispectral scanner. *Seventh International Symposium on Remote Sensing of Environment*, 1307-1320. University of Michigan, Ann Arbor, MI.
- Huemrich, K. F., & Goward, S. N. (1997). Vegetation canopy PAR absorptance and NDVI: An assessment for ten tree species with the SAIL model. *Remote Sensing of Environment*, 61, 254-269.
- Huete, A., Justice, C., & Leeuwen, W. V. (1999). *MODIS Vegetation Index (MOD 13): Algorithm Theoretical Basis Document*. NASA.
- Huete, A., Justice, C., & Liu, H. (1994). Development of vegetation and soil indexes for MODIS-EOS. *Remote Sensing of Environment*, 49, 224-234.

- Huete, A. R. (1986). Separation of soil-plant spectral mixtures by factor analysis. *Remote Sensing of Environment*, 19, 237-251.
- Huete, A. R. (1998). A soil-adjusted vegetation index (SAVI). *Remote Sensing of Environment*, 25, 295-309.
- Illera, P., Fernandez, A., & Delgado, J. A. (1996). Temporal evolution of the NDVI as an indicator of forest fire danger. *International Journal of Remote Sensing*, 17, 1093-1105.
- Irons, J. R., Ranson, K. J., Williams, D. L., Irish, R. R., & Huegel, F. G. (1991). An off-nadir-pointing imaging spectroradiometer for terrestrial ecosystem studies. *IEEE Transactions On Geoscience and Remote Sensing*, 29, 66-74.
- Jacquemoud, S., & Baret, F. (1990). Prospect: A model of leaf optical-properties spectra. *Remote Sensing of Environment*, 34, 75-91.
- Jacquemoud, S., Baret, F., Andrieu, B., Danson, F. M., & Jaggard, K. (1995). Extraction of vegetation biophysical parameters by inversion of the PROSPECT+SAIL models on sugar beet canopy reflectance data: Application to TM and AVIRIS sensors. *Remote Sensing of Environment*, 52, 163-172.
- Janecek, A., Benderoth, G., Ludeke, M. K. B., Kindermann, J., Kohlmaier, G. H. (1989). Model of the seasonal and perennial carbon dynamics in deciduous-type forests controlled by climatic variables. *Ecological Modelling*, 49, 101-124.
- Jordan, C. F. (1969). Derivation of Leaf-Area Index from quality of light on forest floor. *Ecology*, 50, 663-666.
- Kasischke, E. S., & French, N. H. F. (1995). Locating and estimating the areal extent of wildfires in Alaskan boreal forests using multiple-season AVHRR NDVI composite data. *Remote Sensing of Environment*, 51, 263-275.
- Kasischke, E. S., & French, N. H. F. (1997). Constraints on using AVHRR composite index imagery to study patterns of vegetation cover in boreal forests. *International Journal of Remote Sensing*, 18, 2403-2426.
- Kasischke, E. S., French, N. H. F., Harrell, P., Christensen, N. L., Ustin, S. L., & Barry, D. (1993). Monitoring of wildfires in boreal forests using large-area AVHRR NDVI composite image data. *Remote Sensing of Environment*, 45, 61-71.
- Kaufman, Y. J., & Tanre, D. (1992). Atmospherically resistant vegetation index (ARVI) for EOS-MODIS. *IEEE Transactions on Geoscience and Remote Sensing*, 30, 261-270.
- Kauth, R. J., & Thomas, G. S. (1976). The tasseled cap - A graphic description of the spectral-temporal development of agricultural crops as seen by Landsat. *Proceedings of the Symposium on Machine Processing of Remotely Sensed Data*, 4b, 41-51. Purdue University, Indiana.
- Lacaze, R., Chen, J. M., Roujean, J. -L., & Leblanc, S. G. (2002). Retrieval of vegetation clumping index using hot spot signatures measured by POLDER instrument. *Remote Sensing of Environment*, 79, 84-95.
- Lacaze, R., & Roujean, J. -L. (2001). G-function and hot spot (GHOST) reflectance model application to multi-scale airborne POLDER measurements. *Remote Sensing of Environment*, 76, 67-68.
- Larcher, W. (1995). *Physiological plant ecology*. Springer-Verlag, New York, USA.
- Leblon, B., Alexander, M., Chen, J., & White, S. (2001). Monitoring fire danger of northern boreal forests with NOAA-AVHRR NDVI images. *International Journal of Remote Sensing*, 22, 2839-2846.
- Li, X., & Strahler, A. H. (1992a). Geometric-optical bidirectional reflectance modeling of the discrete crown vegetation canopy: effect of crown shape and mutual shadowing. *IEEE Transactions on Geoscience and Remote Sensing*, 30, 276-292.

- Li, X. W., & Strahler, A. H. (1992b). Geometric-optical bidirectional reflectance modeling of the discrete crown vegetation canopy: Effect of crown shape and mutual shadowing. *IEEE Transactions On Geoscience and Remote Sensing*, 30, 276-292.
- Liu, H., & Huete, A. (1995). A feedback based modification of the NDVI to minimize canopy background and atmospheric noise. *IEEE Transactions On Geoscience and Remote Sensing*, 33, 457-465.
- Lloyd, D., (1990). A phenological classification of terrestrial vegetation cover using shortwave vegetation index imagery. *International Journal of Remote Sensing*, 11, 2269-2279.
- Lobell, D. B., Asner, G. P., Law, B. E., & Treuhaft, R. N. (2001). Subpixel canopy cover estimation of coniferous forests in Oregon using SWIR imaging spectrometry. *Journal of Geophysical Research-Atmospheres*, 106, 5151-5160.
- Los, S. O. (1998). Estimation of the ratio of sensor degradation between NOAA AVHRR channels 1 and 2 from monthly NDVI composites. *IEEE Transactions On Geoscience and Remote Sensing*, 36, 206-213.
- Los, S. O., Collatz, G. J., Sellers, P. J., Malmstrom, C. M., Pollack, N. H., DeFries, R. S., Bounoua, L., Parris, M. T., Tucker, C. J., & Dazlich, D.A (2000). A global 9-yr biophysical land surface dataset from NOAA AVHRR data. *Journal of Hydrometeorology*, 1, 183-199.
- Ludeke, M. K. B., Ramge, P. H., & Kohlmaier, G. H. (1996). The use of satellite NDVI data for the validation of global vegetation phenology models: Application to the Frankfurt Biosphere Model. *Ecological Modelling*, 91, 255-270.
- Lyon, J. G., Yuan, D., Lunetta, R. S., & Elvidge, C. D. (1998). A change detection experiment using vegetation indices. *Photogrammetric Engineering and Remote Sensing*, 64, 143-150.
- Maas, S. J., & Dunlap, J. R. (1989). Reflectance, transmittance, and absorptance of light by normal, etiolated, and albino corn leaves. *Agronomy Journal*, 81, 105-110.
- Masek, J. G. (2001). Stability of boreal forest stands during recent climate change: evidence from Landsat satellite imagery. *Journal of Biogeography*, 28, 967-976.
- McDonald, A. J., Gemmell, F. M., & Lewis, P. E. (1998). Investigation of the utility of spectral vegetation indices for determining information on coniferous forests. *Remote Sensing of Environment*, 66, 250-272.
- Moody, A., & Johnson, D. M. (2001). Land-surface phenologies from AVHRR using the discrete fourier transform. *Remote Sensing of Environment*, 75, 305-323.
- Moulin, S., Kergoat, L., Viovy, N., & Dedieu, G. (1997). Global-scale assessment of vegetation phenology using NOAA/AVHRR satellite measurements. *Journal of Climate*, 10, 1154-1170.
- Mustard, J. F., & Sunshine, J. M. (1999). Spectral analysis for earth science investigation. Rencz, A. N. (Ed.). *Remote Sensing for the Earth Sciences: Manual of Remote Sensing*, 251-306. Wiley & Sons, New York.
- Myinen, R. B., Keeling, C. D., Tucker, C. J., Asrar, G., & Nemani, R. (1997a). Increased plant growth in the northern high latitudes from 1981 to 1991. *Nature*, 386, 698-702.
- Myinen, R. B., Nemani, R. R., & Running, S. W. (1997b). Estimation of global leaf area index and absorbed par using radiative transfer models. *IEEE Transactions On Geoscience and Remote Sensing*, 35, 1380-1393.
- Myinen, R. B., Ross, J., & Asrar, G. (1989a). A review on the theory of photon transport in leaf canopies. *Agricultural and Forest Meteorology*, 45, 1-153.
- Myinen, R. B., Ross, J., & Asrar, G. (1989b). A review on the theory of photon transport in leaf canopies, *Agricultural and Forest Meteorology*, 45, 1-153.

- Nemani, R., Pierce, L., Running, S., & Band, L. (1993). Forest ecosystem processes at the watershed scale: sensitivity to remotely-sensed leaf area index estimates. *International Journal of Remote Sensing*, 14, 2519-2534.
- Norman, J. M., (1993). Scaling processes between leaf and canopy levels. Ehleringer, J. R., & Field, C.B. (Eds.). *Scaling physiological processes: Leaf to global*, 41-76. Academic Press, San Diego, CA.
- North, P. R. J. (2002). Estimation of fAPAR, LAI, and vegetation fractional cover from ATSR-2 imagery. *Remote Sensing of Environment*, 80, 114-121.
- Parker, G. G. (1995). Structure and microclimate of forest canopies, in *Forest Canopies*. Lowman, M., & N. Nadkarni N. (Eds.). *A review of research on a biological frontier*, 73-106. Academic Press, San Diego, CA.
- Peddle, D. R., Hall, F. G., & LeDrew, E. F. (1999). Spectral mixture analysis and geometric-optical reflectance modeling of boreal forest biophysical structure. *Remote Sensing of Environment*, 67, 288-297.
- Qin, W., & Liang, S. (2000). Plane-parallel canopy radiation transfer modeling: Recent advances and future directions. *Remote Sensing Reviews*, 18, 281-306.
- Qin, W. H. (1993). Modeling bidirectional reflectance of multicomponent vegetation canopies. *Remote Sensing of Environment*, 46, 235-245.
- Ramsey, E. W., Chappell, D. K., & Baldwin, D. G. (1997). AVHRR imagery used to identify hurricane damage in a forested wetland of Louisiana. *Photogrammetric Engineering and Remote Sensing*, 63, 293-297.
- Richardson, A. J., & Wiegand, C. L. (1977). Distinguishing vegetation from soil background information. *Photogrammetric Engineering and Remote Sensing*, 43, 1541-1552.
- Roberts, D. A., Gardner, M., Church, R., Ustin, S., Scheer, G., & Green, R. O. (1998). Mapping chaparral in the Santa Monica Mountains using multiple endmember spectral mixture models. *Remote Sensing of Environment*, 65, 267-279.
- Roberts, D. A., Smith, M. O., & Adams, J. B. (1993). Green vegetation, nonphotosynthetic vegetation, and soils in AVIRIS data. *Remote Sensing of Environment*, 44, 255-269.
- Rondeaux, G., & Herman, M. (1991). Polarization of light reflected by crop canopies. *Remote Sensing of Environment*, 38, 63-75.
- Rondeaux, G., Steven, M., & Baret, F. (1996). Optimization of soil-adjusted vegetation indices. *Remote Sensing of Environment*, 55, 95-107.
- Rosema, A., Verhoef, W., Noorbergen, H., & Borgesius, J. J. (1992). A new forest light interaction model in support of forest monitoring. *Remote Sensing of Environment*, 42, 23-41.
- Ross, J. (1981). *The radiation regime and architecture of plant stands*. W. Junk Publishers, The Hague, Netherlands.
- Rouse, J. W., Haas, R. H., Shell, J. A., & Deering, D. W. (1973). Monitoring vegetation systems in the Great Plains with ERTS-1. *Third Earth Resources Technology Satellite Symposium*, 309-317.
- Sabol, D. E., Gillespie, A. R., Adams, J. B., Smith, M. O., & Tucker, C. J. (2002). Structural stage in Pacific Northwest forests estimated using simple mixing models of multispectral images. *Remote Sensing of Environment*, 80, 1-16.
- Sandmeier, S., & Deering, D. W. (1999). Structure analysis and classification of boreal forests using airborne hyperspectral BRDF data from ASAS. *Remote Sensing of Environment*, 69, 281-295.
- Schaaf, C. B., & Strahler, A. H. (1993). Solar zenith angle effects on forest canopy hemispherical reflectances calculated with a geometric-optical bidirectional reflectance model. *IEEE Transactions On Geoscience and Remote Sensing*, 31, 921-927.

- Sellers, P. J. (1987). Canopy reflectance, photosynthesis, and transpiration. II. The role of biophysics in the linearity of their interdependence. *Remote Sensing of Environment*, 21, 143-183.
- Settle, J. J., & Drake, N. A. (1993). Linear mixing and the estimation of ground cover proportions. *International Journal of Remote Sensing*, 14, 1159-1177.
- Shimabukuro, Y. E., Batista, G. T., Mello, E. M. K., Moreira, J. C., & Duarte, V. (1998). Using shade fraction image segmentation to evaluate deforestation in Landsat Thematic Mapper images of the Amazon Region. *International Journal of Remote Sensing*, 19, 535-541.
- Smith, M. O., Ustin, S. L., Adams, J. B., & Gillespie, A. R. (1990). Vegetation in deserts: I. Regional measure of abundance from multispectral images. *Remote Sensing of Environment*, 31, 1-26.
- Souza, C., & Barreto, P. (2000). An alternative approach for detecting and monitoring selectively logged forests in the Amazon. *International Journal of Remote Sensing*, 21, 173-179.
- Spanner, M., Johnson, L., Miller, J., McCreight, R., Freemantle, J., Runyon, J., & Gong, P. (1994). Remote sensing of seasonal leaf area index across the Oregon transect. *Ecological Applications*, 4, 258-271.
- Strahler, A. H., & Jupp, D. L. (1991). Geometric-optical modeling of forests as remotely-sensed scenes composed of three-dimensional, discrete objects. Myneni, R. B., & Ross J. (Eds.). *Photon-Vegetation Interactions: Applications to Optical Remote Sensing and Plant Ecology*. Springer-Verlag, Berlin.
- Strebel, D. E., Goel, N. S., & Ranson, K. J. (1985). Two-dimensional leaf orientation distributions. *IEEE Transactions on Geoscience and Remote Sensing*, 23, 640-647.
- Tucker, C. J. (1979). Red and photographic infrared linear combinations for monitoring vegetation. *Remote Sensing of Environment*, 8, 127-150.
- Tucker, C. J., Slayback, D. A., Pinzon, J. E., Los, S. O., Myneni, R. B., & Taylor, M. G. (1999). Higher northern latitude NDVI and growing season trends from 1982 to 1999. *International Journal of Biometeorology*, in press.
- Vanderbilt, V. C., Grant, L., & Ustin, S. L. (1991). Polarization of light by vegetation. Myneni, R. B., & Ross J. (Eds.). *Photon-Vegetation Interactions: Applications to Optical Remote Sensing and Plant Ecology*, 190-228. Springer-Verlag, Berlin.
- Verhoef, W. (1984). Light-scattering by leaf layers with application to canopy reflectance modeling : the SAIL model. *Remote Sensing of Environment*, 16, 125-141.
- Verstraete, M. M., & Pinty, B. (1996). Designing optimal spectral indexes for remote sensing applications. *IEEE Transactions on Geoscience and Remote Sensing*, 34, 1254-1265.
- White, M. A., Thornton, P. E., & Running, S. W. (1997). A continental phenology model for monitoring vegetation responses to interannual climatic variability. *Global Biogeochemical Cycles*, 11, 217-235.
- Woodcock, C. E., Collins, J. B., Jakabhaazy, V. D., Li, X., Macomber, S. A., & Wu, Y. (1997). Inversion of the Li-Strahler canopy reflectance model for mapping forest structure. *IEEE Transactions on Geoscience and Remote Sensing*, 35, 405-414.
- Woolley, J. T. (1971). Reflectance and transmittance of light by leaves. *Plant Physiology*, 47, 656-662.
- Wu, Y. C., & Strahler, A. H. (1994). Remote estimation of crown size ; stand density ; and biomass on the Oregon Transect. *Ecological Applications*, 4, 299-312.
- Young, S. S., & Wang, C. Y. (2001). Land-cover change analysis of China using global-scale Pathfinder AVHRR Landcover (PAL) data, 1982-92. *International Journal of Remote Sensing*, 22, 1457-1477.

- Zarco-Tejada, P. J., Miller, J. R., Noland, T. L., Mohammed, G. H., & Sampson, P. H. (2001). Scaling-up and model inversion methods with narrowband optical indices for chlorophyll content estimation in closed forest canopies with hyperspectral data. *IEEE Transactions on Geoscience and Remote Sensing*, 39, 1491-1507.

Chapter 9

EXTRACTING INDIVIDUAL TREE INFORMATION

A Survey of Techniques for High Spatial Resolution Imagery

Darius S. Culvenor

CSIRO Forestry and Forest Products, Private Bag 10, Clayton South, Victoria, 3169, Australia

1. INTRODUCTION

Forest management is a dynamic science with evolving information requirements. Remote sensing, as an important means of acquiring forest information, must therefore adapt to meet changing management needs. In parallel with a need for adaptation are ongoing advancements in remote sensing technology and associated interpretation tools that provide new opportunities to meet the information demands of forest and resource managers.

In any remote sensing application the choice of spatial resolution of the sensing device is a fundamental factor (1990a), requiring consideration of the environment being studied and the type of information required (Woodcock and Strahler 1987). With growing demands for detailed forest information (Leckie et al. 1999), high spatial resolution remotely sensed data is becoming an increasingly valuable source of information for assisting forest management decisions.

Interpretation of the terms 'low spatial resolution' and 'high spatial resolution' is subjective and is largely dependent on the field of application (see Lefsky and Cohen, Chapter 2; Franklin et al., Chapter 10). In the context of satellite forest inventories, for example, (Päivinen 2001) refers to Landsat TM data (with a pixel size in the order of 30 m) as 'high resolution'. Conversely, for the aim of forest stand structure mapping, (St-Onge and Cavayas 1997) considered high resolution imagery to have pixel dimensions

≤ 1 m. For the purposes of this discussion, high spatial resolution imagery may be regarded as imagery that facilitates the direct recognition of features of interest, in this case, individual tree crowns.

2. HIGH SPATIAL RESOLUTION REMOTE SENSING

Aerial photography is a primary source of high resolution data that has been used extensively in forestry (Hall, Chapter 3). Aside from traditional manual interpretation, aerial photography has also been analysed quantitatively following conversion to digital format. Examples in forestry include species identification (Meyer et al. 1996; Key et al. 2001), forest type classification (Bliss et al. 1980), tree counting (Lowell 1998), estimation of tree spatial distribution (Uuttera et al. 1998) and canopy structure determination for damage assessment (Dralle and Rudemo 1996; Kasischke et al. 1997).

While aerial photography still sees wide application in many forestry applications, high spatial resolution airborne imagery is routinely acquired directly in digital format from video systems, digital cameras and scanning systems. Applications include the estimation of forest volume (Bolduc et al. 1999), prediction of forest structure (Wu 1988; Smith et al. 1991; Preston 1997), species and land cover classification (Gougeon 1995a), evaluation of forest canopy structure and damage (Hosking 1994), and the estimation of wildlife habitat quality (Coops and Catling 1997). The flexibility and near real-time data acquisition capabilities of airborne systems make them useful tools for rapid, quantitative mapping at the forest management scale.

An important recent development in high resolution remote sensing has been the commercial availability of high spatial resolution satellite data (Tahu et al. 1998). IKONOS and QuickBird satellites both offer panchromatic data with a spatial resolution of ≤ 1 m. As such data becomes more widely accessible and affordable, the potential exists for quantitative spatial forest assessment to be economically applied over broad areas at the individual tree scale.

2.1 Manual interpretation versus computer-assisted interpretation

In many countries, a decrease in the value of aerial photographs for forest inventory has been attributed to growing information requirements (Hyypä et al. 2000). As such, further development of modern remote sensing

systems and techniques as components of forest inventory is seen as a major task for the future (Preto 1992; Harries et al. 1993). The potential for major advancements in remote sensing has been largely brought about by digital technology. In particular, the integration of modern information techniques with powerful, low cost computers, can help foresters capture better information in a shorter time (Schieler 1992). Although still a maturing technology relative to film sensors, the trend towards digital acquisition of remotely sensed data (Light 1996) has also encouraged the development of computer-assisted interpretation techniques. Indeed, (Gougeon 1995b) states that the full potential of digital imagery in forestry will only be realised when most of the image analysis procedures are automated.

While computer-assisted image interpretation still lags behind most human interpretation capabilities in terms of feature recognition, computer-assisted approaches offer a number of benefits over manual interpretation, notably the potential for objective, repeatable analysis. Obvious processing efficiencies mean there is also an ability to process large areas of imagery at high resolution. A key outcome could be the production of both local and regional datasets from a common source of information, thereby reducing incompatibilities between datasets collected at different scales and employed at different management levels (Pelz 1993; O'Hara et al. 1995). Current and future-generation high resolution satellite imagery may provide a suitable source of remotely sensed data for both local and regional mapping requirements.

High spatial resolution remotely sensed data offers the potential to improve the accuracy of traditional forest inventory attributes while also retrieving important information relating to the structural diversity of forests (Häme et al. 1999). However, analysis of high resolution imagery poses a number of challenges (Quackenbush et al. 2000) that require specific image interpretation procedures. In particular, simple per-pixel spectral classifiers commonly applied to low spatial resolution data are not suitable due to the spectrally heterogeneous nature of the data (Townshend and Justice 1981; Woodcock and Strahler 1987; Dikshit 1996). The characteristics of high resolution data which limit traditional interpretation techniques can, however, be exploited as a source of information about the scene. Approaches include image texture classifiers (Wang and He 1990; Sali and Wolfson 1992; Hay et al. 1996; Ryherd and Woodcock 1996; Dikshit 1996), variance/resolution graphs (Woodcock and Strahler 1987; Coops and Catling 1997) and semivariograms (Curran 1988; Woodcock et al. 1988b; Cohen et al. 1990; Levesque and King 1996; St-Onge and Cavayas 1997).

While classification schemes that operate in the spatial domain may yield more reliable estimates of forest canopy structure (1987), it has been accepted that pattern recognition methods alone are inadequate in situations

which require an awareness of context or *a priori* knowledge (Estes and Sailer 1986). As such, in cases where scene objects exhibit commonly identifiable traits, the development of 'intelligent' algorithms advances the science of image interpretation to new levels. A relatively new approach to image interpretation, one which exploits both spatial and spectral information, involves the automated identification and delineation of tree crowns in high spatial resolution digital imagery.

3. AUTOMATED TREE CROWN DELINEATION

In the last decade, a shift in scientific focus has seen more emphasis placed on individual trees rather than whole stands as the primary spatial unit of interest (Dube et al. 1998). This trend is not driven by a desire to manage forests on an individual tree basis, rather it is a recognition of trees as the fundamental structural elements in forests, and questions the acquisition of forest data as a stand-scale average. The incentive behind individual tree based inventories is the potential for detailed descriptions of forest structure based on individual tree information. While individual tree information can be retrieved manually from large scale aerial photography, to do so across an entire photograph would be prohibitively time consuming (Hyyppä et al. 2000). Therefore, an automated approach to tree delineation may facilitate the implementation of efficient, consistent and reliable tree-scale inventories across the whole landscape.

3.1 Assumptions implicit in automated tree crown delineation

The most suitable scale for remote sensing observations is a function of the type of environment being studied and the nature of the information required (Woodcock and Strahler 1987). An obvious requirement for the automated identification and delineation of tree crowns is that the crowns be at least visually recognisable as discrete objects in the remotely sensed imagery. For our eye-brain vision, the spatial properties of context, pattern and texture are almost certainly more significant in the discrimination of objects than the spectral property of colour (Warner et al. 1998). Attributes such as context, shape, and texture can only be determined from relative observations (e.g. a neighbourhood or a line of pixels) rather than any one value. Consequently, the recognition of individual crowns requires the spatial resolution of the imagery to be considerably higher than the size of the crowns in the scene.

In addition to high spatial resolution, a fundamental assumption inherent in crown delineation algorithms is that the centre of a crown is brighter than the edge of the crown, or more particularly, the boundary between crowns. The assumption is somewhat intuitive, but can also be explained theoretically.

The influence of canopy structure on reflectance generally occurs at different scales within the canopy, ranging from individual leaves and stems, to internal crown structure and the interaction of light between neighbouring crowns (Gemmell 1998). At the whole-tree scale, the typically convex shape of a crown means that its peak is more likely to be directly illuminated (and therefore consistently brighter) at varying sun angles than the edge of a crown. Furthermore, in dense forest canopies, neighbouring trees will shade and obscure the edges of their co-neighbours (Li and Strahler 1992), resulting in characteristically darker image values at tree boundaries.

The combined effects of illumination angle, view angle, tree geometry and bidirectional reflectance cause large variation in pixel intensity at different positions within the crown (Leckie et al. 1992), resulting in a non-uniform crown reflectance profile. This profile can be expected to vary as a function of crown depth, which is lesser near the edge of a crown and greater towards the centre (Li and Strahler 1992). Accordingly, a radiometric crown profile derived from remotely sensed imagery may generally be considered similar in shape to the geometric profile of the tree crown, thereby providing a useful basis for performing automated image interpretation at the individual tree scale.

Given the assumed relationship between geometric and radiometric crown shape, the combined spatial and radiometric structure of high resolution imagery of forests may be likened to a mountainous landscape (Gougeon 1995b). This three-dimensional analogy is a useful way of describing the primary image attributes used in an automated tree delineation process. The spatial information in the image is represented in the x and y dimensions, while the brightness of the image is depicted in the vertical dimension, resulting in a radiometric 'topography'. Local radiometric maxima (peaks) and minima (valleys) are the fundamental image features used to locate and delineate crowns. Maxima are considered synonymous with radiometric crown centroids and are assumed to be indicative of, but not necessarily coincident with, geometric crown centroids. Local minima may be used to define likely crown boundaries. The concept of radiometric topography, local maxima and local minima is illustrated in Figure 9-1.

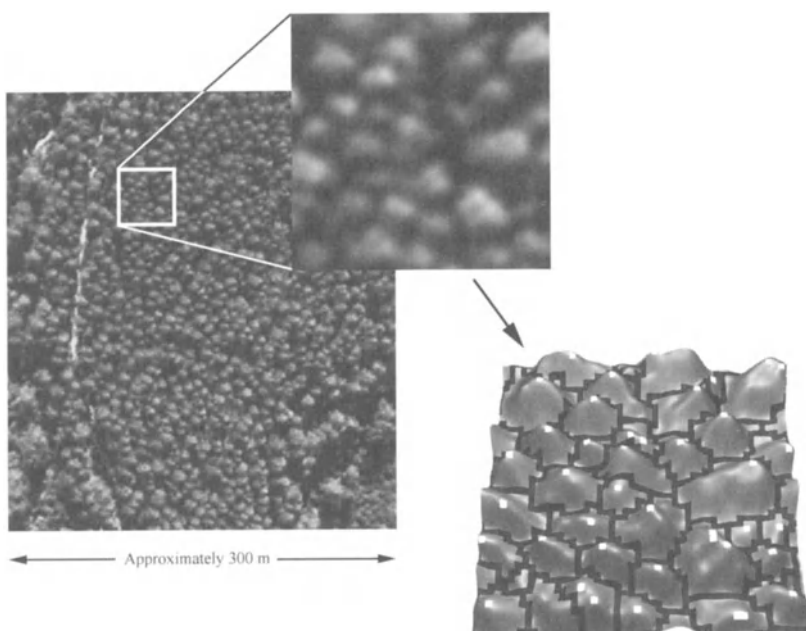


Figure 9-1. Radiometric 'topography' extracted from 1 m resolution digital airborne video image acquired over Australian native eucalypt forest. Spectral topography derived from near-infrared reflectance. Local minima (valleys) are displayed as black, local maxima are displayed as white.

A variety of algorithms exist for the purpose of automated tree crown identification and delineation. These may be broadly categorised as either 'bottom-up' algorithms, 'top-down' algorithms, or 'template matching' algorithms. The first group of algorithms focuses on the valleys of shadow between trees as a means of isolating crown boundaries. The second group involves initially estimating the location of tree crowns from radiometric maxima, and subsequently locating the boundary using the characteristic decrease in brightness from the centre of a crown to its edge. The final group of algorithms are based on the use of pre-defined templates describing the expected radiometric appearance of tree crowns in high resolution imagery. Although not exhaustive, a number of algorithms in each category are discussed below.

3.2 Tree isolation – ‘bottom-up’ algorithms

3.2.1 Valley-following

(Gougeon 1995b) developed the first and possibly best known method for automatically delineating tree crowns in high spatial resolution imagery. The algorithm exploits the bands of shadow that often occur between trees in moderately dense forest. These bands of shadow are termed ‘valleys’ by Gougeon, meaning ‘radiometric valleys’. Trees are delineated by traversing the valleys separating crowns. Prior to processing an image for valleys, a general mask is first applied to separate continuous forest cover from background vegetation, large areas of shadow and areas without significant numbers of trees. In dense forest stands, and when sun elevation is low, a simple threshold can be used to accomplish this. In more complex forests an unsupervised classification is used to achieve the same result (Gougeon 1995b).

After the mask has been applied, a 3 x 3 moving window is used to locate all local minima (all 8 values around the central pixel must be greater than the central value for it to be considered a minima). The image is then iteratively searched in four directions (top left – bottom right, bottom right – top left, top right – bottom left, bottom left – top right) for local minima, masked areas or ‘valley pixels’. If any such pixel is found, the immediate neighbours in the scan direction are examined to perpetuate the ‘valley’. A neighbouring pixel is considered a valley pixel if it is flanked by pixels with higher values. The iterations are continued until no further valley pixels are found. Many crowns are not completely isolated by the valley processing, and therefore the valleys are further refined using a rule-based program. The rule-based program works by finding partially-delineated crowns, and then traversing the boundary in a roughly clockwise direction to fully delineate likely crown objects. The application of the valley-following algorithm benefits from conical crown shape and high solar zenith angle at the time of image acquisition to accentuate the shadow between crowns. The main weakness of the valley-following algorithm lies in its prime assumption, i.e. that tree crowns are separated by bands of shade. As a result, applications may be limited to at least moderately dense stands where mutual shadowing of crowns can be expected (Gougeon 1998).

3.2.2 Directional texture

An algorithm developed for use in hardwood forest types is proposed by (Warner et al. 1998). This algorithm, based on directional interpretation of local texture, is developed specifically for use in the Eastern Deciduous

Forests of North America where the delineation of trees is a challenging task due to the variation in crown sizes, the relatively planophile nature of the canopy, and the complex mosaic of individual crowns (Warner et al. 1998). The canopy tends to be more structurally complex than coniferous forest, although trees are still inclined to be surrounded by narrow bands of shadow. Unfortunately however, the shadow also occurs between major branches within a crown, and these large branches can also occupy areas of the canopy greater than that of the small crowns (Warner et al. 1998).

A rank normalisation is required prior to tree delineation to reduce problems associated with variable illumination and vignetting. In this process, a moving window is used to rank the brightness of the central pixel relative to other pixels in the window. Because this is a fundamentally spatial operation, the size of the moving window will have a critical influence on the size of the image features accentuated. A window size of approximately three times greater than the average crown diameter was found to be the optimum size for enhancing the shadow between crowns (Warner et al. 1998).

The directional nature of the shadow between trees is ascertained using a minimum texture filter. This comprises a linear calculation of texture (e.g. 1 pixel wide by 11 pixels long) centred at a given pixel. This calculation is performed over numerous increments of direction at each pixel. The direction where minimum texture occurs is considered indicative of the direction of the shaded crown boundary. Unlike most texture-based analysis, the magnitude of the texture is not of interest. Instead only the directional information from the texture calculations are recorded (Warner et al. 1998). Clumps of pixels with similar directional properties can be grouped together and then linked with other, adjacent groups, or projected to nearby groups to achieve complete crown delineation.

This algorithm is distinctly unreliant on the local radiometric maxima which have proven useful for the initial location of tree crowns in other algorithms. This is due to the inherently planophile nature of the Eastern Deciduous Forest canopy, where local maxima do not necessarily coincide with the location of individual crowns. The approach used responds well to the bands of shadow between crowns, but is heavily dependent on the nature of image pre-processing, specifically, the size of the rank normalisation window. As such, in terms of delineation, it will likely be limited to a range of crown sizes compatible with the dimensions of the subjectively selected normalisation window. Application of the algorithm in sparse forest stands may be problematic due to the unpredictable nature of background brightness variation.

3.3 Tree identification and delineation – ‘top-down’ algorithms

3.3.1 Multiple scale edge segments

In image analysis, the recognition of individual crowns may only be possible over a certain interval of scale (Brandtberg and Walter 1998b). For example, at fine scales, only branches are evident and it may be difficult to amalgamate them into a single crown. Alternatively, at coarse scales, individual crowns may appear to have merged with their neighbours. To address this problem, (Brandtberg and Walter 1998b) developed an automated tree crown delineation algorithm which employs multiple-scale analysis for the identification of most-probable crown boundary features. The algorithm uses edge segments with convex grey level curvature derived from image brightness values at multiple scales for estimating the extent of tree crowns.

The algorithm has four key stages – image smoothing, edge detection, convex curvature filtering and generation of a primal sketch. The image smoothing process involves applying a discrete kernel with incrementally stronger intensity to produce multiple images with varying spatial scales. Crown edge detection is undertaken at the zero-crossing position of the first-order derivative of the curvature function in the smoothed images.

The edge pixels are initially filtered to remove all pixels that do not exhibit convex curvature. The remaining pixels are subsequently fitted with an elliptical crown shape model resulting in what is termed a ‘primal sketch’, taken to represent changes in boundary curvature (Asada and Brady 1986). This process is repeated for each image scale produced from the incremental smoothing process. After primal sketches have been derived from images at all scales, the values are scaled and summed for each pixel, giving a single ‘accumulated primal sketch’ image. Local maxima within the accumulated primal sketch are used to define the position of seed points for likely tree locations. Once all seeds have been defined, the crowns are ‘grown’ simultaneously. The crowns are only permitted to grow into areas of the image brighter than a global minimum threshold, and are not permitted to grow into other crown segments.

The technique developed by (Brandtberg and Walter 1998b) is aimed at addressing the common problem of non-optimum spatial resolution in forests with widely varying crown sizes. Optimising the spatial resolution for small trees results in segmentation of large trees, while optimisation for large trees typically results in the merging or omission of smaller trees. According to (Brandtberg and Walter 1998b), the algorithm compared very well with manual delineation results in a trial of natural mixed-species coniferous

forest using colour infrared aerial photography. Compared to ground truth however, the algorithm had difficulty identifying trees in close proximity, and numerous cases were noted where false identification occurred. Bright soil background was also identified as tree crowns in some cases. While the algorithm appears able to cope with widely varying crown sizes in an image, like other algorithms, it is still subject to errors of omission and commission in structurally complex forest canopies.

3.3.2 Threshold-based spatial clustering

The Tree Identification and Delineation Algorithm (TIDA) is a threshold-based spatial clustering algorithm designed to automatically delineate eucalypt tree crowns. The term 'clustering' is used to describe the spatial aggregation of contiguous pixels into spatially unique objects. The spectral maxima and minima are the primary image features used for the identification of crowns, being indicative of crown centroids and boundaries respectively (Culvenor et al. 1999; Culvenor 2000; Culvenor 2002).

TIDA uses a 'top-down' approach to tree delineation, which involves, at a broad level, three main steps: identification of local maxima, identification of local minima, and clustering of crown pixels. Local maxima are used to calculate the position of 'seeds' which define the image coordinates of likely crown peaks. Local maxima are identified from unconstrained linearly divergent searches in multiple search directions (horizontally, vertically, and in both 45 degree planes). In each search, the current pixel forms a central anchor and the pixel values in linearly opposing directions are systematically examined and compared with the immediately preceding pixel value.

A contextual analysis is subsequently applied to all local maxima to identify pixels most closely conforming to the assumption concerning the radiometric and geometric shape of illuminated tree crowns. A pixel that is repeatedly identified as a local maximum in multiple search directions is more likely to fit the analogy of a tree crown being brighter at its centre than its edges, with a maxima count of 4 (all four directions) being the highest probability.

The local minima are used to construct a continuous network of absolute crown boundaries, of one pixel width, between all likely tree crowns. Similar to the identification of local maxima, a four-way, centrally diverging linear search is used to locate local minima. However, unlike the maxima, a pixel identified as being a local minimum in any of the four directions is considered valid, regardless of the number of times it was identified. A number of filters are used to refine the identified minima pixels into a clear and continuous network of absolute boundaries.

The main steps in the minima refining process are: filling missing pixels in an otherwise continuous minima boundary, removing 'dead-end' or superfluous boundary pixels, and reducing the minima boundaries to a width of one pixel. The minima refining process removes many of the small radiometric valleys that occur due to internal crown structure, thereby minimising crown segmentation

Clustering of crown pixels is the third stage of the tree delineation process. The starting coordinates for the clustering of each crown is a pre-defined 'seed'. The clustering of pixels around a seed is a continuous procedure constrained by encountering a minima boundary, encountering pixels with a brightness below a specified threshold value, or encountering a previously delineated tree crown. The minimum brightness threshold is computed as the product of the seed brightness and a user defined value between 0 and 1, and is therefore specific to each crown being clustered.

Evaluation of TIDA has shown that it is most suited to forest canopies with dense crowns, as they are more likely to support the assumed relationship between geometric and radiometric crown shape. Dense canopies were also preferable due to prevalent shadow between adjacent crowns and minimal background brightness variation (Culvenor 2000).

3.3.3 Double-aspect method

During a study of forest canopy dynamics in an area of soil contamination, (Walsworth and King 1999) developed an algorithm for the delineation of tree crown apices of Aspen forest in Ontario, Canada. The objective was to monitor changes in the number, density and size of crowns over a 40 year period using archival black and white aerial photography. As a means of achieving this, a crown delineation methodology was developed based on the variation in aspect (double-aspect) of a radiometric surface.

The double-aspect method involved finding the radiometric surface aspect for each pixel in each of four directions (N-S, E-W, NE-SW, NW-SE). A change in radiometric aspect highlights either a ridge or gully surface feature. The intersection of ridge features indicates the position of tree apices, while the junction of gullies represents edges. Preliminary testing showed that the union of gullies provided only partial delineation of crown edges (Walsworth and King 1998), and therefore a supplementary crown delineation process was devised.

This consisted of first inverting the image brightness, and then employing a flooding model, based on region growing, in which the crown apices were treated as seeds. The regions were grown outwards in increasing order of brightness, and eventually, individual regions merged to produce a 'cost surface'. A 'cost function' was used to determine which pixels should be

allocated to which seeds by assigning each pixel the minimum cumulative cell traversal sum away from crown apex seeds (Walsworth and King 1998). The result is a weighted proximity surface around seeds which is then normalized based on the maximum value in each region. Crown edges are subsequently defined by selecting proximity thresholds for pixels associated with a given crown apex.

Evaluation of the double-aspect method showed suitability for dense, regularly spaced forest types with uniform height and illumination. It was proposed that a window-based high-pass filter technique for crown apex identification combined with the use of aspect calculations for estimating optimum window size could further improve tree crown identification.

3.3.4 Vision expert system

In the mid 1980's, a new forest inventory system was implemented in Austria with emphasis on monitoring forest health and vitality. A significant component of the system involved gathering data at the individual tree level by interpretation of high resolution aerial colour infrared imagery (Pinz 1998b). Currently this is performed manually using analytical plotters whereby 2-3 trees are interpreted in regularly spaced grids of 500 m² (Pinz 1998b). Given the process is repeated on a five-year cycle, the possibility of incorporating automated analysis (the Vision Expert System) was investigated (Pinz 1998b).

The goal of the Vision Expert System (VES) is to locate the centre of a tree crown, to estimate its radius, and be able to repeat this process for all the trees in the image (Pinz 1998a). Typically, only the central area of an image is used so that geometric distortions and difficult illumination effects near the periphery of the image can be ignored. Given the assumption that tree crowns in dense forests are brighter than the background, local maxima are used as the basis for finding tree crowns in the image. However, to avoid numerous maxima associated with internal crown structure, the input image is first smoothed using a low pass filter. As (Pinz 1998a) discusses, no single low pass filter will be optimum for all crown sizes in an image. Therefore a range of filter sizes are applied, each producing its own set of local maxima. The maxima from each scale are combined to produce a range of possible crown centroids.

Valid local maxima are chosen on the basis of 'radial brightness distributions'. This is computed by averaging the brightness of pixels occurring in successive concentric circles centred on a local maximum. The average brightness from each circle is then plotted as a function of circle radius (distance from maximum). The shape of the distribution is analysed in association with a user-defined threshold to determine, firstly, the likelihood

the maximum represents a crown peak, and if successful, an estimate of crown radius. Further validation processing occurs to check for violation of crown proximity to known objects (e.g. roads or other crowns).

The method involves relatively little user input and appears robust for the coniferous forest types evaluated. The main user interaction occurs through the choice of appropriate radial brightness distributions, and it is unclear how significantly this parameter affects the final results. (Pinz 1998a) argues that only tree location and an estimate of crown radius is required from the automated process. Indeed, he states that crown boundary delineation is difficult and unnecessary. This may be reasonable in young even-aged forests where crowns are often symmetrical. In structurally complex forests however, it has been suggested that attributes such as internal crown spectral reflectance and variance, the brightness of sunlit and shaded crown aspects and crown boundary shape can be useful attributes for modelling structural and physiological characteristics of the canopy (Preston 1997) and tree species (Fournier et al. 1995).

3.4 Template-matching algorithms

(Pollock 1996) developed an algorithm for use in Canadian forest types. Primary design criteria were that the algorithm be suitable for use in forest stands with variable spacing and crown size distribution, and able to process an entire image, not just the (undistorted) near-nadir section of the image. The algorithm involves matching a three-dimensional synthetic image model (or template) of tree crowns with radiometric values in the image. The template is defined by geometric and radiometric parameters. The shape of the template is derived from a synthetic crown envelope which is modified according to sensing geometry (i.e. the location in the image). An advantage of this procedure is the non-reliance on the detection of crown boundaries (e.g. local minima), making it suitable for application in sparse forest canopies where shading between crowns does not occur. This method also uses a novel way of accounting for the distortion of tree crowns as a function of view angle, and also modifies the crown template according to scene and sensor irradiance. Drawbacks are the initial *a priori* assumptions about crown size and shape, the relative inflexibility of the model to accommodate irregular crown form, and considerable computational expense.

In an extension of the work by Pollock, (Larsen and Rudemo 1997) developed an algorithm for detecting the peaks of Norway Spruce (*Picea abies*) trees in high resolution panchromatic imagery. This work was further extended in (Larsen 1997) and (Larsen and Rudemo 1998). Similar to Pollock, this algorithm uses an optical tree model and known remote sensing conditions to create a crown 'template', i.e. an estimate of what an average

tree might look like if placed at a given position in the image (Larsen 1999). The correlation between local brightness values in the image and the crown template is determined for each pixel, and a tree is 'located' if the correlation is high. This algorithm extends Pollock's previous work by adding a background to the modelled tree crowns. The elements that make up the optical tree model are a single crown, a background, light sources and a camera (Larsen and Rudemo 1998). The expected illumination of a crown is modelled assuming direct and diffuse skylight, but ignores the effects of multiple scattering from the background and neighbouring crowns. The shading effect of neighbouring crowns is also ignored, which may have a significant influence (Larsen 1999).

The initial crown shape is modelled as a hemispherical ellipsoid (i.e. the bottom half of the ellipsoid is truncated). The interior of the crown is assumed to contain randomly oriented scattering elements (needles and branches), and only first-order scattering is considered. The 'ground' plane is used to provide a contrasting background so that crowns may be silhouetted by a bright background, or conversely the crowns may cast shadows on the ground. Based on the coordinates of the pixel in the image, the synthetic crown model is illuminated and appropriately 'distorted' to replicate the expected appearance of a tree crown at that position. The local radiometric values in the image are subsequently tested for correlation with the locally-derived crown template. The template-matching algorithms use intelligent processing to estimate, *a priori*, the appearance of a tree crown based on known image attributes and a given crown shape. As a result, the algorithms actually benefit from the view of crowns in profile at off-nadir positions in the image, and similarly can account for illumination conditions at the time of image acquisition.

Larsen and Rudemo's approach provides very good results for the detection of tree peaks in even-aged Norway Spruce plantation (its intended application). The algorithm may be expected to work similarly well in other forest types where the size and shape of tree crowns is predictable and relatively constant within a given image. Although (Larsen and Rudemo 1998) describe a technique for optimising crown shape parameters, in highly variable natural forests, the template matching algorithm is unlikely to cope well with irregular crown form – a problem highlighted by (Pollock 1998) during trials in mixed species stands in Canada.

4. ALGORITHM PERFORMANCE CONSIDERATIONS

While a number of different algorithms exist for performing automated tree crown delineation, they typically exploit the same image features and exhibit similar limitations. Potential exists for further improvements in these algorithms, however, significant benefits in terms of accurate crown delineation can be achieved through careful image acquisition and image optimisation with respect to spatial and spectral characteristics. Therefore, in the short-term at least, intelligent application of existing algorithms may yield greater rewards than can be achieved through the development of new or more advanced algorithms.

4.1 Image spatial resolution

All tree delineation algorithms are developed for use with high spatial resolution imagery. While the optimum spatial resolution will vary between forest types and individual algorithms, they typically require that the resolution capability of the sensor be considerably higher than the size of the tree crown objects in the scene. The spatial resolution of imagery employed in existing algorithms ranged from 6 cm (Warner et al. 1998), 10 cm (Pinz 1998a), 36 cm (Pollock 1998), 47 cm (Walsworth and King 1999) to 80 cm (Culvenor 2002).

The range of resolutions used in these studies indicates there is a degree of tolerance surrounding the optimum spatial resolution for tree delineation in given structural forest types, however it is apparent that the choice of spatial resolution is both forest type and algorithm specific depending on the pre-processing undertaken prior to, or during, the delineation process. Algorithms that utilise window-based smoothing or normalisation filters as part of the delineation process tend to require higher spatial resolution imagery than those that undertake image interpretation directly.

(Culvenor 2000), using simulated forest imagery, showed that the internal structure of tree crowns is more significant than crown size in terms of influencing optimum spatial resolution. This arises from the effect of internal crown structure on within-crown shading and the subsequent relationship between geometric and radiometric crown shape. Large crowns with dense foliage, for example, may be accurately delineated alongside much smaller crowns because both present a smooth radiometric gradient from the tree peak to the edge, providing little within-crown variance to distract the algorithm. Trees with distinct internal structure are likely to be interpreted by tree delineation algorithms as a group of small trees rather than a single large tree without prior optimisation of spatial resolution or

image smoothing to remove local maxima and minima within the crown boundary. This requires a compromise, however, when attempting to delineate crowns in forests with widely varying crown size and structure, and remains one of the most difficult applications of automated tree crown identification and delineation. (Gougeon 1995b), for example, found some trees in a mixed-species coniferous plantation were delineated optimally at 31 cm spatial resolution, while other trees within the same image were best delineated at 70 cm resolution.

The most appropriate spatial resolution for automated tree crown delineation needs to be specified at the scene scale for structurally homogeneous forests (e.g. (Culvenor 2000), or, in forests with highly variable crown size and structure, at the individual tree scale. (Brandtberg and Walter 1998b) address this problem by using a master image to generate a series of bands with slightly varying spatial characteristics, all of which are supplied to the algorithm to facilitate multi-scale crown delineation. In terms of tree peak identification, this problem has been approached through the use of multiple-scale local maxima selection (e.g. (Pinz 1998a); Wulder et al. 2000).

Achieving individual whole-crown delineation in forests with widely varying crown size and structure may also be possible through a post-processing methodology to merge or further segment delineated objects. (Ticehurst et al. 2001) developed a series of spectral tools to split and combine crowns delineated using Gougeon's valley-following method. The tools have been used in association with hyperspectral remotely sensed imagery for improving tree crown delineation results in tropical forests suitable for species classification.

4.2 Spectral characteristics

In terms of spectral information for tree delineation, studies tend to use either the near-infrared region of the spectrum (Gougeon 1995b; Brandtberg and Walter 1998a; Pinz 1998a), or panchromatic imagery (representing the entire visible region of the spectrum and some near-infrared) (Niemann et al. 1998; Larsen 1999; Walsworth and King 1999). (Gougeon 1998) explains that the near-infrared band is usually chosen because of its sensitivity to illumination variation and good response to vegetation material. (Niemann et al. 1998) selected panchromatic orthoimagery for automated tree identification due to its low cost and accessibility, but noted its lack of spectral information as a disadvantage with respect to image enhancement and optimisation.

All algorithms currently described utilise a single spectral band for the tree delineation process. This enables the algorithms to be applied to a wide

range of remote sensing data sources, particularly the forthcoming high resolution satellites which will produce monochromatic images in their highest spatial resolution mode (Guindon 2000). It is likely however that there are benefits to be gained from multispectral image interpretation by virtue of the greater amount of information available. While it appears no algorithms are currently capable of exploiting multispectral information for crown delineation, some studies use band combinations for deriving a single optimum band. (Warner et al. 1998) derived a single band from the three visible bands of colour photography. This was called the illumination/albedo band and was computed as the square-root of the sum of the squares of the band. Preston (1999) combined the reflectance from three separate bands with different weightings to generate a single band more representative of the structural variation in the canopy. Coops et al. (2001) use a band computed from the slope of the red-edge (680 – 740 nm) to minimise background brightness effects when performing automated tree crown delineation in forests with sparse canopies.

4.3 View angle, sun angle and atmospheric effects

The non-uniform radiometric profile of a crown that is utilised for automated tree crown delineation is dependent on a number of factors. In addition to intrinsic crown spectral and structural properties, extrinsic factors in the remote sensing environment also determine the way in which the crown appears in an image. These include solar azimuth and zenith angle, viewing direction, atmospheric effects and sensor-specific characteristics.

Sun angle and view angle can be exploited to improve tree crown delineation, e.g. high solar zenith angles improve the separation of the canopy from the background and accentuate tree peaks (Gougeon 1995b), while matching crowns to templates can be easier with crowns viewed in profile than those viewed at nadir (Sheng et al. 2001). However, variation in view and illumination conditions within and between scenes can limit the usefulness of spatial and spectral information derived from a tree delineation process, and may be an impediment to monitoring and change detection at the individual tree scale.

In a trial of Gougeon's valley-following algorithm in New Zealand *Pinus radiata* D. Don (Radiata Pine) plantation, (Andrew et al. 1999) observed that the extent of internal crown segmentation varied as a function of sun angle. Specifically, remotely sensed imagery acquired at a high solar zenith angle produced less variable crown reflectance resulting in more cohesive crown delineation.

In an evaluation of the TIDA methodology using simulated forest imagery, (Culvenor 2000) found the algorithm to be highly influenced by

view and illumination conditions. Back-scattered radiation from the forest canopy was consistently more suited to automated tree crown delineation than forward-scattered radiation. Performance was notably poor at the hotspot position in images where the lack of scene shadow made it difficult to discern the three-dimensional shape of objects. View zenith angles greater than 15 degrees also caused a significant decline in algorithm performance. This resulted from a distortion of crown shape, bidirectional reflectance effects, and a reduction in scene information as crowns become less visible through mutual obstruction, particularly in structurally complex canopies.

Thorough algorithm evaluation under a range of conditions can be used to determine prescriptions for image acquisition to optimise tree delineation results. Alternatively, image pre-processing steps may be applied to reduce the effects of the remote sensing environment. (Quackenbush et al. 2000), for example, applied a chromacity filter to equalise the intensity of the input band as a means of minimising the variation in shading across the forest canopy.

Interestingly, atmospheric effects may be used to advantage to limit the influence of sun angle on tree delineation. Again, using simulated imagery, (Culvenor 2000) showed that imagery acquired under optically thick atmospheres (e.g. airborne imagery acquired under high cloud) results in improved tree delineation compared to scene illumination under strong direct light. The advantage stemmed from a strengthening of the relationship between geometric and radiometric crown shape. The directionless nature of scattered radiation provided uniform scene illumination that was only moderately sun angle dependent. This finding supports other studies where the effects of the atmosphere have been used to advantage (Myers 1982), and has particular implications with respect to multi-temporal image interpretation by both enhancing algorithm performance and limiting sun angle bias.

5. CONCLUSION

Accurate and consistent automated tree crown delineation has the potential to greatly improve the efficiency, detail and retrieval of information from forest inventories. Achieving this task, however, is extremely challenging given the variability in the remote sensing environment, the subjectiveness of image characteristics (including both spectral and spatial characteristics), and the inherently complex structure of natural forest canopies. Despite such difficulties, results from various practical trials of tree delineation technology have, in many cases, provided very encouraging results.

A variety of algorithms have been developed for the task of automated tree crown identification and/or delineation in a range of structural and floristic forest types. Most algorithms perform well in their intended application, but are highly sensitive to the quality and characteristics of the imagery provided to them. As in any image interpretation process, careful consideration needs to be given to image spatial resolution, selection or derivation of the spectral input layer and the influence of the remote sensing environment.

REFERENCES

- Andrew, R. M., Trotter, C. M., Höck, B. K., & Dunningham, A. (1999). Inventory of plantation forests using crown delineation techniques. *Fourth International Airborne Remote Sensing Conference and Exhibition / 21st Canadian Symposium on Remote Sensing*, 131-138. Ottawa, Ontario, Canada.
- Asada, H., & Brady, M. (1986). The curvature primal sketch. *IEEE Transactions on Pattern Analysis and Machine Intelligence*, 8, 3-14.
- Bliss, J. C., Bonnicksen, T. M., & Mace, T. H. (1980). Computer-aided classification of forest cover types from small scale aerial photography. *Environmental Management*, 4, 499-510.
- Bolduc, P., Lowell, K., & Edwards, G. (1999). Automated estimation of localised forest volume from large-scale aerial photographs and ancillary cartographic information in a boreal forest. *International Journal of Remote Sensing*, 20, 3166-3624.
- Brandtberg, T., & Walter, F. (1998). Automated delineation of individual tree crowns in high spatial resolution aerial images by multiple-scale analysis. *Machine Vision and Applications*, 11, 64-73.
- Brandtberg, T., & Walter, F. (1999). An algorithm for delineation of individual tree crowns in high spatial resolution aerial images using curved edge segments at multiple scales. *Proceedings Automated Interpretation of High Spatial Resolution Digital Imagery for Forestry*, 41-54. Victoria, British Columbia, Canada.
- Cohen, W. B., Spies, T. A., & Bradshaw, G. A. (1990). Semivariograms of digital imagery for analysis of conifer canopy structure. *Remote Sensing of Environment*, 34, 167-178.
- Coops, N. C. & Catling, P. C. (1997). Predicting the complexity of habitat in forests from airborne videography for wildlife management. *International Journal of Remote Sensing*, 18, 2677-2686.
- Coops, N. C., Stone, C. S., Culvenor, D. S., & Old, K. (2001). Forest vitality and health: Indicators of changes in fundamental ecological processes in forests based on eucalypt crown condition index (ECCI). *Report to Forestry and Wood Products Research and Development Corporation (FWRPDC) PN99.814*. CSIRO Forestry and Forest Products, Canberra, ACT, Australia.
- Culvenor, D. S. (2000). *Development of a Tree Delineation Algorithm for Application to High Spatial Resolution Digital Imagery of Australian Native Forest*. Ph.D. Thesis. The University of Melbourne, Australia.
- Culvenor, D. S. (2002). TIDA: An algorithm for the delineation of tree crowns in high spatial resolution remotely sensed imagery. *Computers & Geosciences*, 28, 33-44.

- Culvenor, D. S., Coops, N. C., Preston, R., & Tolhurst, K. G. (1999). A spatial clustering approach to automated tree crown delineation. *Proceedings Automated Interpretation of High Spatial Resolution Digital Imagery for Forestry*, 67-80. Victoria, British Columbia.
- Curran, P. J. (1988). The semivariogram in remote sensing: An introduction. *Remote Sensing of Environment*, 24, 493-507.
- Dikshit, O. (1996). Textural classification for ecological research using ATM images. *International Journal of Remote Sensing*, 17, 887-915.
- Dralle, K., & Rudemo, M. (1996). Stem number estimation by kernel smoothing of aerial photos. *Canadian Journal of Forest Research*, 26, 1228-1236.
- Dube, P., Hay, G., & Marceau, D. (1999). Voronoi diagrams, extended area stealing interpolation, and tree crown recognition: a fuzzy approach. *Proceedings Automated Interpretation of High Spatial Resolution Digital Imagery for Forestry*, 115-126. Victoria, British Columbia.
- Estes, J. E., & Sailer, C. (1986). Applications of artificial intelligence techniques to remote sensing. *The Professional Geographer*, 38, 133-141.
- Fournier, R. A., Edwards, G., & Eldridge, N. R. (1995). A catalogue of potential spatial discriminators for high spatial resolution digital images of individual crowns. *Canadian Journal of Remote Sensing*, 21, 285-298.
- Gemmell, F. (1998). An investigation of terrain effects on the inversion of a forest reflectance model. *Remote Sensing of Environment*, 65, 155-169.
- Gougeon, F. A. (1995a). Comparison of possible multispectral classification schemes for tree crowns individually delineated on high spatial resolution MEIS images. *Canadian Journal of Remote Sensing*, 21, 1-9.
- Gougeon, F. A. (1995b). A crown-following approach to the automatic delineation of individual tree crowns in high spatial resolution digital images. *Canadian Journal of Remote Sensing*, 21, 274-284.
- Gougeon, F. A. (1999). Automatic individual tree crown delineation using a valley-following algorithm and a rule-based system. *Proceedings Automated Interpretation of High Spatial Resolution Digital Imagery for Forestry*, 11-24. Victoria, British Columbia.
- Guindon, B. (2000). A framework for the development and assessment of object recognition modules from high-resolution satellite images. *Canadian Journal of Remote Sensing*, 26, 334-348.
- Häme, T., Holm, M., Rautakorpi, S., & Parmes, E. (1999). Forestry applications in high resolution imagery. Kanellopoulos, I., Wilkinson, G. G., & Moons, T. (Eds.). *Machine Vision and Advanced Image Processing in Remote Sensing*, 111-120. Springer-Verlag, Berlin, Germany.
- Harries, D., Curnow, W., & Davey, S. (Eds.). (1993). *Remote Sensing for Forest Management, Bureau of Resource Science Working Paper*. Bureau of Resource Sciences, Canberra.
- Harrison, B. A., & Jupp, D. L. B. (1990). *Introduction to Remotely Sensed Data*. CSIRO Australia, Canberra, Australia.
- Hay, G. J., Niemann, K. O., & McLean, G. F. (1996). An object-specific image-texture analysis of H-resolution forest imagery. *Remote Sensing of Environment*, 55, 108-122.
- Hosking, G. P. (1994). Evaluation of forest canopy damage using airborne video. *Resource Technology '94*, 286-293. Melbourne, Australia.
- Hyypä, J., Hyypä, H., Inkinen, M., Engdahl, M., Linko, S., & Zhu, Y. (2000). Accuracy comparison of various remote sensing data sources in the retrieval of forest stand attributes. *Forest Ecology and Management*, 128, 109-120.

- Kasischke, E. S., Melack, J. M., & Dobson, C. M. (1997). The use of imaging radars for ecological applications - a review. *Remote Sensing of Environment*, 59, 141-156.
- Key, T., Warner, T. A., McGraw, J. B., & Fajvan, M. (2001). A comparison of multispectral and multitemporal information in high spatial resolution imagery for classification of individual tree species in a temperate hardwood forest. *Remote Sensing of Environment*, 75, 100-112.
- Larsen, M. 1997. Crown modelling to find tree top positions in aerial photographs. *Proceedings of the Third International Airborne Remote Sensing Conference and Exhibition*, II, 428-435. Copenhagen, Denmark.
- Larsen, M. (1999). Finding an optimal match window for Spruce top detection based on an optical tree model. *Proceedings Automated Interpretation of High Spatial Resolution Digital Imagery for Forestry*, 55-66. Victoria, British Columbia.
- Larsen, M., & Rudemo, M. (1997). Using ray-traced templates to find individual trees in aerial photos. *Proceedings of the 10th Scandinavian Conference on Image Analysis*, 1007-1014. Lappeenranta, Finland.
- Larsen, M., & Rudemo, M. (1998). Optimising templates for finding trees in aerial photographs. *Pattern Recognition Letters*, 19, 1153-1162.
- Leckie, D., Burnett, C., Nelson, T., Jay, C., Walsworth, N., Gougeon, F., & Cloney, E. (1999). Forest parameter extraction through computer-based analysis of high resolution imagery. *Fourth International Airborne Remote Sensing Conference and Exhibition / 21st Canadian Symposium on Remote Sensing*. Ottawa, Ontario, Canada.
- Leckie, D. G., Yaun, X., Ostaff, D. P., Piene, H., & MacLean, D. A. (1992). Analysis of high spatial resolution multispectral MEIS imagery for Spruce Budworm damage assessment on a single tree basis. *Remote Sensing of Environment*, 40, 125-136.
- Levesque, J., & King, D. J. (1996). Semivariance analysis of tree crown structure in airborne digital camera imagery. *26th International Symposium on Remote Sensing of Environment: Information Tools for Sustainable Development*, 275-278 Vancouver, BC, Canada.
- Li, X., & Strahler, A. H. (1992). Geometric-optical bidirectional reflectance modelling of the discrete crown vegetation canopy: effect of crown shape on mutual shadowing. *IEEE Transactions on Geoscience and Remote Sensing*, 30, 276-291.
- Light, D. L. (1996). Film cameras or digital sensors? The challenge ahead for aerial imaging. *Photogrammetric Engineering & Remote Sensing*, 62, 285-291.
- Lillesand, T. M., & Kiefer, R. W. (1987). *Remote sensing and image interpretation* (2nd ed.). John Wiley & Sons, Singapore.
- Lowell, K. (1998). Evaluation of a moving-window algorithm for detecting individual tree stems from scanned aerial photographs in Victoria's eucalypt forests. *Australian Forestry*, 61, 226-234.
- Meyer, P., Staenz, K., & Itten, K. I. (1996). Semi-automated procedures for tree species identification in high spatial resolution data from digitized colour infrared-aerial photography. *ISPRS Journal of Photogrammetry & Remote Sensing*, 51, 5-16.
- Myers, B. J. (1982). Shadowless aerial photography for vegetation studies - a review of benefits and limitations. *Australian Forestry*, 45, 142-151.
- Niemann, O., Adams, S., & Hay, G. (1999). Automated tree crown identification using digital orthophoto mosaics. *Proceedings Automated Interpretation of High Spatial Resolution Digital Imagery for Forestry*, 105-114. Victoria, British Columbia.
- O'Hara, K. L., Latham, P. A., & Valappil, N. I. (1995). Parameters for describing stand structure. *S4.01 IUFRO 20th World Congress on Recent Advances in Forest Mensuration and Growth and Yield Research*, 134-145. Tampere, Finland.

- Pelz, D. R. (1993). National forest inventories: Past developments and future prospects. *Forest Resource Inventory and Monitoring and Remote Sensing Technology, Proceedings of the IUFRO Centennial Meeting*, 11-18. Berlin.
- Pinz, A. (1999a). Tree isolation and species classification. *Proceedings Automated Interpretation of High Spatial Resolution Digital Imagery for Forestry*, 127-140. Victoria, British Columbia.
- Pinz, A. (1999b). Austrian forest inventory system. *Proceedings Automated Interpretation of High Spatial Resolution Digital Imagery for Forestry*, 375-386. Victoria, British Columbia.
- Pollock, R. (1996). *The Automatic Recognition of Individual Trees in Aerial Images of Forests Based on a Synthetic Tree Crown Image Model*. Ph.D. Thesis, Department of Computer Science, University of British Columbia, Canada.
- Pollock, R. (1999). Individual tree recognition based on a synthetic tree crown image model. *Proceedings Automated Interpretation of High Spatial Resolution Digital Imagery for Forestry*, 25-34. Victoria, British Columbia.
- Preston, R. (1997). Monitoring of forest species and structure using Digital Multi-Spectral Video (DMSV) and expert spatial models *Sustainable Forest Management Technical Report: Assessing and monitoring condition of native forests in Queensland - some recent developments in airborne and satellite remote sensing*. Resource Sciences Centre, Brisbane, Australia.
- Preston, R. (1999). *Eastern Australia High Resolution Remote Sensing Baseline Mapping Project: Interim Report*, Image acquisition and exploratory modelling.
- Preto, G. (1992). Past and present of inventorying and monitoring systems. *Forest Resource Inventory and Monitoring and Remote Sensing Technology, Proceedings of the IUFRO Centennial Meeting*, 1-10. Berlin.
- Päivinen, R. (2001). How reliable is a satellite forest inventory. *Silva Fennica*, 35, 125-127.
- Quackenbush, L. J., Hopkins, P. F., & Kinn, G. J. (2000). Developing forestry products from high resolution digital aerial imagery. *Photogrammetric Engineering & Remote Sensing*, 66, 1337-1346.
- Ryherd, S., & Woodcock, C. (1996). Combining spectral and texture data in the segmentation of remotely sensed images. *Photogrammetric Engineering & Remote Sensing*, 62, 181-194.
- Sali, E., & Wolfson, H. (1992). Texture classification in aerial photographs and satellite data. *International Journal of Remote Sensing*, 13, 3395-3408.
- Schieler, K. (1992). Contribution of a permanent forest inventory to a national information system from the Austrian point of view. *Forest Resource Inventory and Monitoring and Remote Sensing Technology, Proceedings of the IUFRO Centennial Meeting*, 67-70. Berlin.
- Sheng, Y., Gong, P., & Biging, G. S. (2001). Model-based conifer-crown surface reconstruction from high resolution aerial images. *Photogrammetric Engineering & Remote Sensing*, 67, 957-965.
- Smith, N. J., Borstad, G. A., Hill, D. A., & Kerr, R. C. (1991). Using high-resolution airborne spectral data to estimate forest leaf area and stand structure. *Canadian Journal of Forest Research*, 21, 1127-1132.
- St-Onge, B. A., & Cavayas, F. (1997). Automated forest structure mapping from high resolution imagery based on directional semivariogram estimates. *Remote Sensing of Environment*, 61, 82-95.

- Tahu, G. J., Baker, J. C., & O'Connell, K. M. (1998). Expanding global access to civilian and commercial remote sensing data: implications and policy issues. *Space Policy*, 14, 179-188.
- Ticehurst, C., Lymburner, L., Held, A., Palylyk, C., Martindale, D., Sarosa, W., Phinn, S., & Stanford, M. (2001). Mapping tree crowns using hyperspectral and high spatial resolution imagery. *Proceedings of the Third International Conference on Geospatial Information in Agriculture and Forestry*. Denver, Colorado.
- Townshend, J., & Justice, C. (1981). Information extraction from remotely sensed data: a user view. *International Journal of Remote Sensing*, 2, 313-329.
- Uuttera, J., Haara, A., Tokola, T., & Maltama, M. (1998). Determination of the spatial distribution of trees from digital aerial photographs. *Forest Ecology and Management*, 110, 275-282.
- Walsworth, N. A., & King, D. J. (1999a). Comparison of two tree apex delineation techniques. *Proceedings Automated Interpretation of High Spatial Resolution Digital Imagery for Forestry*, 93-104. Victoria, British Columbia.
- Walsworth, N. A., & King, D. J. (1999b). Image modelling of forest changes associated with acid mine drainage. *Computers & Geosciences*, 25, 567-580.
- Wang, L., & He, D. C. (1990). A new statistical approach for texture analysis. *Photogrammetric Engineering & Remote Sensing*, 56, 61-66.
- Warner, T. A., Yeol Lee, J., & McGraw, J. B. (1999). Delineation and identification of individual trees in the eastern deciduous forest. *Proceedings Automated Interpretation of High Spatial Resolution Digital Imagery for Forestry*, 81-92. Victoria, British Columbia.
- Woodcock, C. E., & Strahler, A. H. (1987). The factor of scale in remote sensing. *Remote Sensing of Environment*, 21, 311-332.
- Woodcock, C. E., Strahler, A. H., & Jupp, D. L. B. (1988). The use of variograms in remote sensing: II. Real digital images. *Remote Sensing of Environment*, 25, 349-379.
- Wu, S. T. (1988). Utility of the C band RADAR scatterometer and video system for determination of key tree canopy parameters. *First Workshop on Videography*, 128-135. Falls Church, Virginia.
- Wulder, M., Niemann, K. O., & Goodenough, D. G. (2000). Local maximum filtering for the extraction of tree locations and basal area from high spatial resolution imagery. *Remote Sensing of Environment*, 73, 103-114.

Chapter 10

RATIONALE AND CONCEPTUAL FRAMEWORK FOR CLASSIFICATION APPROACHES TO ASSESS FOREST RESOURCES AND PROPERTIES

Janet Franklin¹, Stuart R. Phinn², Curtis E. Woodcock³, and John Rogan¹

¹ Department Geography, San Diego State University, San Diego, California, 92182-4493,
USA

² School of Geography, Planning & Architecture, University of Queensland, Brisbane,
Queensland, 4072, Australia

³ Department Geography, Boston University, Boston, Massachusetts, 02215, USA

1. CONCEPTS OF CLASSIFICATION

Classification has been an important tool in digital image analysis for land resources applications since early Landsat missions when it was recognized that multispectral digital images are composed of multivariate measurement vectors for each and every pixel. The hundreds of thousands of such vectors typically making up an image could be treated as class descriptors, and the spectral bands as explanatory variables related to categories of interest in the image. This is an application of the more general methodology of classification or pattern recognition (Ripley 1996). This Chapter provides a conceptual framework for selecting appropriate classification approaches to assess forest resources and forest (canopy, stand, and landscape) properties. It is beyond the scope of this Chapter to provide a comprehensive review of recent literature on image classification. S. E. Franklin (2001) provided an excellent overview of classification for the remote sensing of forests, and we use that work as a point of departure. Textbooks such as those by Jensen (1996) and Schowengerdt (1997) provide comprehensive explanations of the general problem of classification in remote sensing. Several recent reviews also outline advances in the use of

classification in forest remote sensing (Wulder 1998, Trietz and Howarth 1999, Lucas et al. in press, Woodcock in press).

Classification has been widely used in fields ranging from evolutionary biology to economics in cases where a large number of observations, belonging to categorical classes, need to be grouped on the basis of their associated traits. In remote sensing, multispectral imagery constitutes a set of spatially organized measurements, and so classification is applied when a map of a specific forest attribute is needed, for example forest type: *conifer*, *hardwood* and *mixed*. The underlying assumption is that each category of forest attributes exhibits a unique multispectral signature. Grouping image pixels with similar signatures results in a simplified image depicting variations in a forest attribute, rather than reflectance (Colour Plate 8). In other words, decision boundaries in measurement space are mapped back to geographical space at the scale of individual pixels.

Classification is, therefore, the most logical approach for predicting the categorical class membership (e.g. forest type) of an observation (pixel), based on its intrinsic traits (measurement vector or spectral band responses). However, it should be noted that classification can also be used to map continuous forest attributes, such as cover or biomass, when those variables are divided into ordinal categories. In some cases, this empirical approach is as effective as more physically based per-pixel modeling approaches or other empirical approaches designed for estimation of continuous variables, such as regression.

In remote sensing, the multiple spectral bands of an image form the core group of explanatory variables. Multitemporal, multisensor, and multiangle measurements, along with non-image data, can be used to add explanatory variables to an analysis that may help discriminate categories of interest. With hyperspectral data, reflected or emitted radiance is measured in so many narrow wavebands that it is often necessary to carefully select or preprocess the data (using compression or derivative analyses), to work with only those variables related to diagnostic (e.g., absorption) features, or that discriminate among classes of interest. However, despite this wealth of data, it has frequently been found that the forest categorical variables under consideration do not have unique spectral “signatures” that allow forest classes to be discriminated without confusion. For example, forest type is frequently an important variable to map (S. E. Franklin 2001), but forest types are usually defined on the basis of dominant and codominant tree species. Due to the scale of image data in relation to forest structure and composition, these forest types may not have unique spectral reflectance characteristics, or even temporal (phenological) patterns if they are evergreen, especially when viewed with the broad spectral bands and

moderate (> 20 m) spatial resolution of Landsat Enhanced Thematic Mapper and similar sensors. Variations in the structural attributes of the forest stand may have a greater effect on the reflectance characteristics than tree species composition. Therefore, other mapped environmental variables associated with, or controlling forest vegetation distributions, such as those related to terrain (digital elevation models), geology, soils, climate, or land use, can be combined with image data in the classification process in various ways to aid forest type discrimination (Skidmore 1989, Skidmore et al. 1996). This emphasizes the point that classification is simply a type of multivariate analysis and not unique to remotely sensed variables.

2. THE SCENE MODEL

Strahler et al. (1986) described information extraction from remotely sensed data in terms of models of the sensor, atmosphere, and the scene – the area of interest. In remote sensing of forests, the scene comprises some forested portion of the Earth surface viewed at a specific scale. These models explicitly consider the spatial, temporal, spectral and radiometric properties of each part of the sensor-atmosphere-surface system. Each type of image processing algorithm used is applied under the assumption that image pixels area either larger (low or L-resolution) or significantly smaller (high or H-resolution) than the target to be mapped. Strahler et al. (1986) defined classification as a H[igh] resolution method of information extraction because it is used when the attribute of interest (e.g. forest type) occurs over spatial extents (in forest stands) that are larger than the spatial resolution of the sensor (many pixels per stand). This assumes the image pixel is completely occupied by one forest type (Figure 10-1). Within a moderate resolution pixel, for example Landsat Enhanced Thematic Mapper (about 0.1 ha), there can be trees of varying species and sizes, as well as canopy and terrain shadow, understorey, soil, and other components affecting the measurements. However, a forest type is defined in terms of “average” species composition and structure, and so pixels that subsample a stand should have values typical of the category to which it belongs.

Strahler et al. (1986) also defined L[ow] resolution approaches to information extraction as those that estimate properties of the components within a pixel (many objects per pixel). They give the example of per-pixel empirical (regression) or physically based models (canopy reflectance models) relating biophysical subpixel properties of the forest stand (such as leaf area or canopy cover) to multispectral measurements (Jupp and Walker 1997, Scarth and Phinn 2000). L and H resolution approaches can be

combined in remote sensing of forests. For example, spectral unmixing can be used to estimate subpixel ground cover of tree canopy, soil, and other scene components, and those “fraction images” can be subjected to classification in order to identify forest classes based on their characteristic mixtures of those components (e.g., Adams et al. 1995).

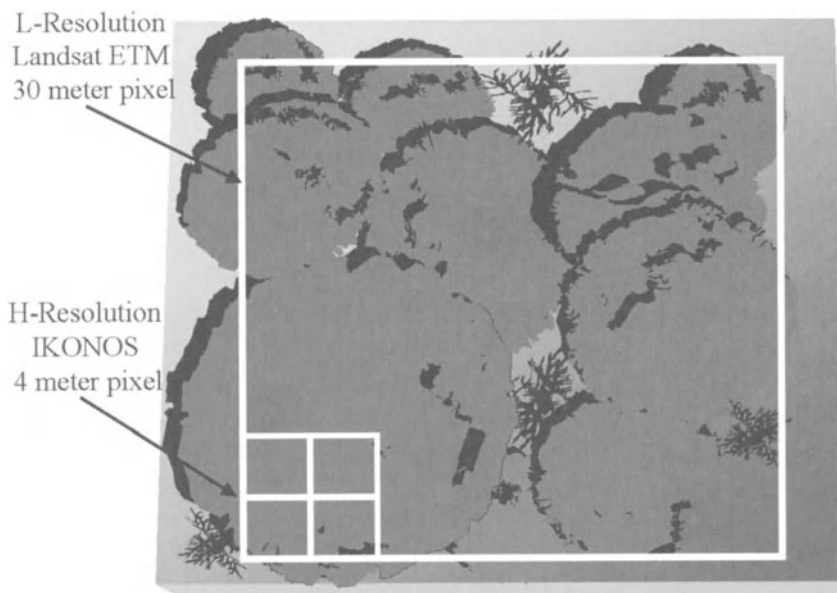


Figure 10-1. H- and L-resolution scene models for forested scene. At moderate resolution (ETM+: 30 m pixels) a forest attribute such as cover type is uniform across the pixel (H-resolution) while individual canopies are sub-pixel (L-resolution). At high resolution (IKONOS: 4 m pixel) individual canopies may be delineated (H-resolution) while subcanopy elements can not (leaf area; L-resolution).

The successful use of classification in remote sensing of forests relies on a number of assumptions. The first is that in order to discriminate among the categories of a forest attribute (e.g. forest type or structure class) they must have unique multivariate properties that are different (separable) from the other categories. This has been called the “spectral signature” concept in remote sensing because it is borrowed from the approach used in analytical chemistry of identifying compounds or materials based on absorption features measured using narrowband spectrometry. Identification of targets based on absorption signatures has been successfully applied in hyperspectral applications for mapping minerals and optical properties of water bodies. In forest applications this approach has been less successful because vegetation canopies tend to be made up of the same organic

compounds, and canopy architecture has been shown to have a greater effect on canopy and larger scale reflectance in many cases than its chemical composition (Gastellu-Etchegorry and Bruniquel-Pinel 2001). However, as long as classes are “separable” (e.g. occur in discrete, non-overlapping portions of multi-dimensional measurement space) then classification can be applied successfully. And, as noted previously, additional environmental data are often required in order to “add dimensionality” for discriminating among the classes of interest.

3. WHAT FOREST ATTRIBUTES CAN BE MAPPED?

The forest attributes most typically mapped using classification of remotely sensed (and other georeferenced) data are those described by nominal (unordered categorical) variables (Table 10-1). For dependent categorical variables the multivariate analyses options comprise various forms of classification or discriminant analysis (Franklin 1995). Important variables for forested landscapes include (a) land cover, general (physiognomic) vegetation types (e.g. *hardwood* versus *conifer*), or ecological land types (land systems); (b) forest types representing broad categories of species composition or structure (e.g. Ponderosa Pine versus Mixed Conifer; Simple Notophyll Vine Forest versus Complex Mesophyll Vine Forest); and (c) forest types defined by detailed species composition, canopy structure (e.g. the above categories with greater versus less than 60 % canopy closure), or both. S. E. Franklin (2001) described these variables as Level I, II and III classifications in a hierarchical framework (corresponding to the Anderson et al. (1976) land cover classification system) and discussed them in detail (see also Franklin and Woodcock 1997). Species can also be discriminated in some cases. For example, the use of multitemporal TM images helps discriminate many categories of forest type defined on the basis of the differing phenologies of their dominant species in deciduous forests (Wolter et al. 1995). Using airborne imagery with high spatial and moderate spectral resolution individual tree crowns have been delineated and species identified using classification (Yu et al. 1999, Cochrane 2000, Pu and Gong 2000, Wulder et al. 2000, Key et al. 2001, Held et al. 2001, Culvenor 2002). This is still an H-resolution approach, but in this case the object of interest is the individual tree canopy, rather than the stand, and the variable of interest is the species, rather than the forest type defined by dominant species.

Classification can also be used to map quantitative biophysical forest variables, at least as ordinal (ordered categorical, or ranges of numerical) variables. Examples of forest attributes that have been mapped using classification include canopy cover or crown closure, canopy height class, tree crown size class, biomass or timber volume classes, and successional or seral stages (see S. E. Franklin 2001, Chapter 7). It would seem preferable to directly estimate continuous variables using other empirical or physically based “per-pixel” models of biophysical variables. However, there are situations where classification may provide the only practical approach. This can occur when the training data are not adequate to calibrate a continuous model, or when the form of the relationship between the dependent and explanatory variables is complex (e.g. not linear). For example, monitoring tropical forest communities has focused on mapping successional stages or rainforest and wet sclerophyll communities using classification (Lucas et al. 2002).

Table 10-1. Forest attributes that can potentially be mapped at a given using classification based on an H-resolution scene model if applied to imagery of a specified dimension.

Attribute	Grain (MMU) ^a	Dimension ^b
Forest Class Level I: Land Cover	1 – 1000 ha	20 m – 1 km
Forest Class Level II: Forest Cover types	1 - 10 ha	10 – 100 m
Forest Class Level III: Species dominance	0.1 – 5.0 ha	1.0 – 30 m
Crown delineation and species identification	0.01 – 0.10 ha	0.1 – 2.0 m
Cover, Canopy size or Biomass class	1 - 10 ha	10 – 100 m
Seral stages	0.1 – 5.0 ha	1.0 – 30 m

^aMMU – minimum mapping unit or the area of the smallest polygon in the output map.

^bDimension of the sensor is expressed as the linear dimension of a square pixel.

4. CLASSIFICATION METHODS

The following section provides a road map of the choices a user makes when selecting a classification procedure to map forest attributes. Basic methodological choices are driven by the type and scale of forest information required (e.g. individual crowns, stands or community groups) and the form of available image and ancillary spatial data. Hence, the type of image data to select is the first critical choice and will largely determine the type of information that can be produced. Selection of supervised or unsupervised approaches along with hard or soft classification routines is the next choice. Assuming the optimal image data and general classification approaches are identified, the actual classification routine is selected from an array of techniques ranging from those with specific statistical requirements

for input data to those that are generally applicable. Our discussion of classification methods is not exhaustive, but focuses on those that have been widely used, or show great potential, for forest attribute mapping.

4.1 Selecting the best data for classification

Classification should be applied to remotely sensed and other data of the appropriate spatial, temporal and spectral resolution for the forest attribute information required. Until recently, the choice of remotely sensed data for forest mapping was limited by availability (sensors) and cost. However, in recent years the potential number of datasets from satellite and airborne platforms has exploded, and in some cases the cost has decreased. A systematic framework for selecting optimal remote sensing data, data transformations (e.g. preprocessing, band ratios), and analysis methods for a given environmental mapping problem was presented by Phinn (1997, 1998). The use of this type of logical and transparent method of selecting data and methods is likely to become increasingly necessary. Franklin (1995, 2001, *in press*) also reviewed the sources, selection and transformation of other types of mapped environmental data for mapping vegetation attributes and ecological land types (climate, geology, landform, soil, terrain). As with image data fusion, one of the greatest issues when introducing these non-remotely sensed variables to multivariate classification is their disparate spatial resolution.

Once the image-derived and ancillary variables are in hand, a best minimum subset of those variables has traditionally been selected for classification. Variable or “feature” selection has received considerable attention in the literature in both multivariate statistics and remote sensing. Almost all remote sensing students are required to carry out a separability analysis as an image processing lab exercise. They select the “best” combination of variables (minimal number, maximum variance among classes, and minimum variance within a class) for discriminating among the classes of interest based on some measure of multivariate distance among the descriptors of those classes. In an era of “data mining” and exponentially increasing computer speed, selecting a best minimum subset of the explanatory variables in a multivariate analysis is becoming less important. However, for some parametric methods, such as maximum likelihood classification, the assumption of independence recommends that highly redundant variables be deleted or that the data be transformed such as by principal components analysis. Also, if there are a very large number of potential variables (from hyperspectral data, image data fusion, digital terrain analysis and so forth), or if the classification method is

computationally intensive (artificial neural networks), it still may be necessary to select a subset of all potential variables – those that best discriminate between the classes and that are the least redundant (correlated). In fact, the effectiveness of some methods is undermined by including too many variables.

Multitemporal classification can also be mentioned here. It has been shown that for forests with seasonal patterns of leaf loss and leaf-out that vary by stratum or species, imagery from different times of year can be used to distinguish different structural classes or dominant species (Franklin 1991, Lambin and Strahler 1994, Wolter et al. 1995, Dustan et al. 2001). In effect, additional (image) variables are simply added to the analysis. Forest attributes are identified based on their typical reflectance variability over time and in some cases this may be used to assess forest processes such as disturbance recovery. In this case it is essential that the images are spatially coregistered with a high degree of accuracy. It may also be necessary that they be radiometrically normalized, although classification is somewhat forgiving in this respect, as long as separable multitemporal “signatures” can be developed for the classes.

4.2 Supervised versus unsupervised classification

A number of multivariate classification methods have been used successfully in remote sensing of forests. They differ in how they partition the multivariate measurement (hyper-)space (by developing discriminant functions or decision rules) in order to assign new observations to a category. Before describing the different classification algorithms, we review the distinction between “supervised” and “unsupervised” classification (as they are called in remote sensing). In supervised classification the (predefined) classes are characterized from observations of the dependent and explanatory variables, and then an algorithm is used to assign new observations to classes. This process is generally known as classification in statistics and other fields, or by other terms such as pattern recognition. For remote sensing this process assumes an *a priori* understanding of the distribution of forest parameters to be mapped, or access to ancillary data that can be used to help train or supervise the classification. In unsupervised classification the objective is to define classes from a set of measurements of the explanatory variables based on the similarity of those measurements. No *a priori* knowledge of scene characteristics or supporting ancillary data is used here; the approach is purely data driven. This is generally called clustering (or sometimes classification; Gordon 1999) in other fields.

In most forest applications, the categories of interest are already defined, although it certainly could be the case that a new classification is being developed at the same time, and in conjunction with, remote sensing based mapping (e.g. the USGS land cover classification, Anderson et al. 1976). However, unsupervised classification has often been useful in determining what "clusters" actually occur in the data as they are discriminated in multivariate space, and how well those clusters correspond to the information classes of interest (Strahler 1981). For case studies from our work see Franklin et al. (1986), and Woodcock et al. (1994), but there are many other examples. Non-hierarchical k-means clustering is commonly used both with multispectral image variables and other (mapped environmental) variables in forest applications (e.g., Host et al. 1995, Franklin in press).

There has been much debate about the relative merits of supervised vs. unsupervised classification. While no consensus exists regarding which approach is generally most suitable, it is possible to make some recommendations. When there is much training data available to support supervised classification, this approach is most appealing. Similarly, if a classification is to be repeated frequently in the same place or extended to surrounding areas, the investment required to develop training datasets is generally justified. However, for "once off" classifications in an area without extensive training data, unsupervised classification may be faster and easier. Unsupervised classification also tends to be most useful when the desired map classes are spectrally complex, that is, they are not well characterized by a single multivariate distribution function. This situation can result from a variety of factors that may influence the remotely sensed signature of a vegetation class including variability in: illumination and reflection geometry due to topography; forest structure, health or species composition between stands; or understorey and background reflectances. Unsupervised classification allows multiple spectral classes within individual map classes. The best approach when using supervised classification in this situation is to employ a nonparametric classifiers such as neural networks or decision trees (discussed later in the Chapter) or to develop multiple spectral classes for each map class through the training and classification steps.

4.3 Soft versus hard classification

We should also distinguish soft (or "fuzzy") versus hard classification. In hard classification an observation can belong to one and only one category. The classes are exhaustive and mutually exclusive. In fuzzy sets classification an observation can have degrees of membership in more than

one class. Many problems in classification lend themselves to this approach making fuzzy classification increasingly popular in remote sensing and other fields (Foody 1996a, 1999). For example, widely accepted and useful physiognomic forest classifications define forest versus woodland on the basis of tree cover (say, more than or less than 25 %). A stand with 26 % cover would be assigned to forest in a hard classification, but might have moderate degrees of membership in both classes in a fuzzy sets classification. Many classifiers estimate a probability or likelihood of class membership in all classes for each observation. In hard classification the observation would be assigned to the single class with the greatest likelihood. If the likelihood values are retained they can be used to produce a soft classification. It is important to note that these likelihood values, such as those derived from maximum likelihood classification or decision tree analysis, are not the same in the strict sense as the degree of class membership as defined in the theory of fuzzy sets (which are not constrained to sum to one). However, in practice, they offer alternative ways of producing soft classification (Foody 1996b). The concept of fuzzy sets has also been applied to forest map accuracy assessment (Linders 2000, Foody 2002). For example, a forest stand incorrectly mapped as woodland might constitute a less serious classification error to the map user than the same stand mapped as developed land (Gopal and Woodcock 1994). Tools for producing, viewing and analyzing fuzzy classifications have existed for a long time. However, most thematic maps derived from forest remote sensing are used as hard classifications in subsequent analyses. A challenge remains to develop methods for using fuzzy information in forest resource management and landscape planning.

4.4 Classification methods

Multivariate methods, including classification, can be grouped in a number of ways (for example, Franklin 1995), and we will discuss parametric, nonparametric, spatial-spectral and spectral-temporal classification (Table 10-2). These methods are thoroughly described elsewhere (see Schowengerdt 1997, Mather 1999), and we will emphasize their usefulness in remote sensing of forest attributes. Before selecting a classification approach it is useful to examine the characteristics of the classes to be mapped to determine the nature (normal, skewed, multi-modal) of their distributions and suitability for parametric or nonparametric algorithms. These methods are described in most remote sensing texts, and software for calculating descriptive statistics and visualizing data distributions is available in many image processing packages. Although

parametric methods are often robust to violations of the assumptions of normally distributed uncorrelated variables, they may not handle multimodal distributions well. This requires that the analyst explicitly characterize “subclasses” within an information class using additional training data.

Maximum likelihood classification is a parametric method that has been widely used in land cover mapping, forest [attribute] mapping, and other remote sensing applications. In this approach the forest attribute classes are characterized, from training data extracted manually or automatically, by their mean and covariance matrix. New observations (pixel measurement vectors) are assigned a probability of membership in each class using a maximum likelihood estimator, and in hard classification the pixel is assigned the label with the highest probability. It has long been noted that remotely sensed variables frequently do not meet the assumptions of being normally distributed and uncorrelated, and many of the non-parametric classifiers discussed below were implemented to overcome this problem. While nonparametric classifiers have been shown to outperform the MLC (i.e., by mapping the attribute of interest with higher accuracy), MLC is almost always used as the baseline to which other classifiers are compared. Often the increased accuracy achieved is in the range of only a few percent. While it would seem desirable to use an alternative nonparametric technique if it is better suited to the characteristics of the data describing the classes. MLC may hold one advantage. With many of the nonparametric approaches, the training sample needs to be very large. While the accuracy of MLC may improve with additional training sites, MLC may perform comparably to other methods when the available training data are limited. In MLC, when additional mapped environmental variables (e.g. elevation) are included to improve classification results, they are frequently used to geographically stratify the study area prior to MLC (reducing the number of categories in each subarea, and hopefully eliminating the occurrence of pairs that are very similar in their multispectral patterns), or used to post-stratify the “spectral” classes, separating them into the forest classes of interest – for example, based on soil type (Hutchinson 1982, Jensen 1996, Phinn et al. 2000). This approach has been used instead of incorporating the additional variables into the classification perhaps because of the underlying assumptions about variable distributions and covariance structure. Stratification has been used frequently to improve the map accuracy of forested lands resulting from classification. In many studies where Level II or III forest attributes were mapped with high accuracy, some combination of geographical or environmental stratification, iterative clustering, hybrid (supervised – unsupervised) and/or layered classification were used.

Assigning an observation to a class based on the minimum (Euclidean) distance (to class means) is another parametric technique, even though only the first order parameter (mean) is estimated from the data. This has the advantage of being computationally simple and fast compared to MLC. This approach has difficulty separating classes with high variability in reflectance, as may be found in relatively open forest areas.

Table 10-2. Summary of classification methods, and their advantages and availability for forest attribute mapping (IP = Image Processing; s/w = software).

Classifier	Comments	Availability
Parametric		
Maximum likelihood	Works for “well separated” classes (e.g. Land cover, forest classes with different physiognomy): Requires relatively few training sites but subclasses must be characterized; results improve using iterative “cluster busting”	Common in IP s/w
Minimum distance	Fast; Works for “well separated” classes with similar variability	Common in IP s/w
Box classifier or parallelepiped (mean and standard deviations)	Fast; Works for “well separated” classes	Common in IP s/w
Generalized Linear Model (GLM)	Useful if “response function” between dependent and independent variables well known, or of interest (e.g. tree species distributions)	Common in statistical s/w. Simple to apply binary models in GIS s/w.
Nonparametric		
Box or parallelepiped classifier (minimum, maximum)	Fast; Works for “well separated” classes; useful for “quick look” or to apply before MLC	Common in IP s/w
Artificial Neural Networks	Good results for forest classification; requires extensive training data	Requires specialized software and expertise; becoming more widely available for IP
Decision (Classification) Trees	Useful for combining remote sensing and other variables; decision rules are explicit; classification accuracies may not be much greater than MLC	Available in statistical s/w. Tools to apply models in GIS or IP s/w becoming more accessible.

Generalized linear models (GLMs) have been used to generate geographical predictions of the distributions of species and ecosystem properties (Franklin 1995). GLMs are a suite of parametric methods that allow more flexible response functions than traditional linear regression models, enabling them to cope with the natural variability associated with forest environments. Logistic regression, a type of GLM appropriate for categorical data, uses the cumulative logistic distribution to describe the relationship between dependent and explanatory variables. Logistic regression models are estimated using maximum likelihood rather than by ordinary least squares. Like MLC, logistic regression predicts a probability that an observation belongs to a class (binary) or classes (polytomous), and thus can generate a soft or hard classification. Although there is a long-standing precedent for using logit regression in image classification (Strahler et al. 1980), it has recently seen greater use in ecological modeling (Guisan and Zimmerman 2000). In part this may be because ecologists would expect the relationship between the distribution of ecosystem properties and environmental variables to take a particular form. For example, the relationship between a tree species distribution and average annual minimum temperature might be expected to be unimodal but perhaps skewed (Austin et al. 1990). Therefore, fitting a non-linear but parametric model has both empirical and theoretical value. Variables representing environmental gradients and multispectral response could be combined in a GLM. Related to GLMs are the nonparametric generalized additive models (GAM). To our knowledge GAMs have not been used with remotely sensed data as classifiers to map forest attributes. However, we mention them because they are being applied with increasing frequency to predictively map biotic distributions, and they can be used to complement GLMs as classifiers (Guisan and Zimmerman 2000).

Because remotely sensed measurements of forest classes frequently do not meet the assumptions of parametric classifiers such as MLC, a number of nonparametric classifiers have been developed and tested. A simple example is the parallelepiped or box classifier that assigns an observation to a class if its value falls within the range of the training data, in other words the k -dimensional “box” described by the minimum and maximum values, where k is the number of image bands used. A parametric version of this defines the boundaries of the box by the mean measurement vector plus and minus some number of standard deviations. The advantage of a box classifier is that it is very fast, and thus it is often used as an exploratory tool (for a “quick look”) in image classification. The disadvantage is that some other “decision rule” has to be invoked if the boxes describing the classes overlap in measurement space (which they often do) and the observed pixel falls within the overlap

area. In this case, the minimum distance to class mean rule could be used. Still, there are forest applications for which these simple classifiers could be useful. For example, if low altitude digital imagery or photographs were being used to derive forest canopy cover based on classification, the target classes, canopy and understorey, could be very well separated in their spectral response and a box classifier might be a rapid way of processing many images.

Another nonparametric classification algorithm is the nearest neighbour (NN), or k NN classifier in which the observation is assigned to the same class as the observation (pixel) in the training class (or majority of the k training classes) to which it is most similar (minimum Euclidean distance). This type of classifier is computationally intensive and therefore tends to be slow. However, it has been successfully used for forest attribute mapping in a number of recent studies (Mäkelä and Pekkarinen 2000, Franco-Lopez et al. 2001, Muinonen et al. 2001).

A group of classifiers sometimes called machine learning or artificial intelligence techniques use the training data in some way to “learn” a set of decision rules that assigns observations to the correct class. This is a similar approach to supervised classification in selecting training data, except that the classification rules generated are not based on unrealistic assumptions about the data distributions. These rules can then be applied to new observations (image pixels) to hopefully assign them the correct class label. This approach can be described as partitioning k -dimensional measurement space into regions associated with forest attribute classes (according to the decision rules) based on the empirical patterns in the training data, and not on any (parametric) rules concerning the dispersion of those training data.

Artificial neural network (ANN) algorithms (Ripley 1996) have been used with some success recently in remote sensing classification, including forest mapping (Carpenter et al. 1997, 1999, Kimes et al. 1999). There are many types of ANNs including the multilayer perceptron (which is generally trained with the back-propagation of error algorithm), learning vector quantization, Hopfield, Kohonen, and Fuzzy ARTMAP, to name a few. In simple terms, an ANN learns a pattern (the multivariate characteristics associated with a forest attribute class) by iteratively considering each observation in the training set whose class membership is known, then multiplying the explanatory variables by a set of weights, applying a transfer function to their weighted sum, and finally predicting membership in each class (Figure 10-2). The weights are adjusted in each iteration to improve the fit between actual and predicted class membership for the most observations. In some cases ANNs have outperformed other classifiers in terms of resulting forest map accuracy, sometimes substantially (Carpenter et al.

1997, 1999). In other cases they have been shown to perform about the same as MLC (German and Gahegan 1996, Skidmore et al. 1997). ANN is a useful approach to forest mapping in complex landscapes because it allows a “many-to-one” mapping of many (spectral) subclasses to one (forest attribute) class without explicit specification of the subclasses (Pax-Lenney et al. 2001), as would be necessary in MLC. Colour Plate 9 contrasts the decision boundaries partitioning measurement space and the resulting classifications of land cover in a forested Thematic Mapper scene (based on two bands) for three of the classifiers just described: box, MLC and ANN.

ARTMAP Neural Network

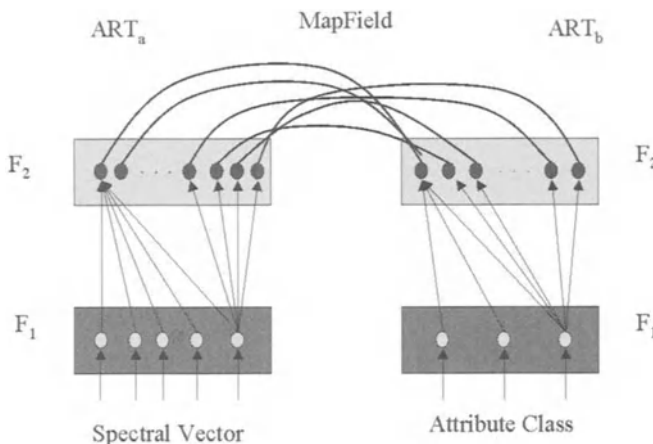


Figure 10-2. Schematic diagram of classification using an artificial neural network, ARTMAP.

Decision tree classification, sometimes called “classification trees” or “regression trees”, is another machine learning approach that has been used to classify and map forest attributes from remotely sensed and other variables at moderate and fine spatial resolutions (Moore et al. 1991, Michaelsen et al. 1994, Friedl and Brodley 1997, Preston et al. 1998, Franklin et al. 2000a). This approach also uses patterns in the training data to develop decision rules for class assignment. The dataset is iteratively divided according to the threshold value of one of the explanatory variables. The partitions are selected to increase the homogeneity of the resulting subsets. The decision rules can be used to classify new observations. DTs have been shown to have some advantages in classification of forests from remote

sensing. They are well suited to predict a categorical variable, and handle both categorical and continuous dependent variables (Franklin 1995, Preston et al. 1998). They can also automatically identify hierarchical relationships (interactions) among variables. They work well in situations where the boundaries between classes are well-characterized by thresholds or nested orthogonal “hyper-planes” in k -dimensional space. Several types of software for DT analysis are available. Given a set of training data, the models are relatively easy to develop and test, and the decision rules are explicit (the classification is less of a “black box” than those derived from ANN). However, DTs are not yet well integrated into commonly used remote sensing software, as opposed to most parametric and non-parametric classifiers (but see the Machine Learning Classifier implemented in Imagine by Huang and Jensen 1997). In comparisons DTs have been shown to outperform Maximum Likelihood Classification (e.g. Borak and Strahler 1999, Rogan et al. 2002), but do not necessarily achieve acceptable accuracy for level III forest classifications (Franklin et al. 2000b).

Multi-scale classification, that is spatial-spectral classification or image segmentation, is another approach that may see growing use. When mapping forest attributes we are frequently interested in mapping both the boundaries of, and assigning class membership to, multipixel objects, be they individual trees or forest stands. The spatial autocorrelation present in the contiguous pixels of a classified image can help to automatically identify those regions or segments in an image that may correspond to the objects of interest (Woodcock and Harward 1992). As Schowengerdt (1997) points out in his overview of spatial-spectral classifiers, the similar characteristics of observations within the region mean that it can be “averaged” and processed as a single observation using any classifier. This increases efficiency and hopefully accuracy, as subregional variability that may not be related to the attribute of interest would be smoothed. However, Woodcock and Harward (1992) found that forest attributes were mapped more accurately if the segmentation and classification steps were conducted separately and “layered.” In effect, the results of a per-pixel classification (resulting from a parametric or non-parametric classifier) are logically “smoothed” by assigning the majority class to the entire vegetation stand defined by segmentation. Classification and segmentation have been used together in a variety of forest mapping efforts from the local to regional scale and using both active and passive sensors (see Hill 1999; Raucooles and Thomson, 1999, Mäkelä and Pekkarinen, 2000, and Rodriguez-Yi et al. 2000).

5. SUMMARY

In any project where remotely sensed data will be used to map environmental characteristics, an explicit framework should be used to identify the optimal remotely sensed dataset (sensor, spatial resolution, acquisition date, bands or transformations) and processing methods for a particular set of objectives. An added benefit is that the map users must articulate their specific information requirements. Classification is and will remain a useful approach to information extraction for remote sensing of forests and is being used operationally to provide forest information from global to local scales. Thematic maps of categorical forest attributes such as ecological type, land cover type, or vegetation type, are basic datasets required for forest management (timber inventory), monitoring (land cover change), and research (e.g., modeling the carbon cycle, simulating harvest or disturbance regimes). Even for mapping continuous biophysical forest variables, classification offers an alternative when training data are inadequate for calibrating a statistical or physically based model.

A number of key issues, related to continued developments in operational mapping of forests using remote sensing, can be highlighted. One is the growing use of longer wavelength Synthetic Aperture Radar (SAR) image data and its combination with optical image datasets (e.g. Pohl and van Genderen 1998) to produce an increased number of explanatory variables that enable forest mapping, especially in the tropics and other cloudy areas (Lucas et al. in press). However, SAR data have some well known geometric and radiometric properties that can make classification problematic. The emergence of operational tree crown delineation programs (Culvenor, Chapter 9) for high spatial resolution data has seen image classification approaches being used increasingly to identify the tree species within the crown if possible. Another issue is the need to generate forest data for very large areas, both for global change studies and regional land management. In some cases general data (forest vs. non-forest) at moderate to fine spatial resolution are required. Although classification has often been applied on a scene by scene basis, calibrated by separate sets of training data, large area processing may require careful radiometric and geometric matching for “signature extension” across scenes (Woodcock et al. 2001). While classification has been successfully used in large area forest mapping by repeating the classification process in each remotely sensed scene (with very little radiometric calibration, e.g. Franklin et al. 2000b) preprocessing becomes increasingly important when training data need to be applied across space (multiple scenes) and time (mapping land cover change).

We predict that the standard classification techniques such as MLC and parallelepiped, the more computationally intensive machine learning and other non-parametric methods, spatial-spectral, and spectral-temporal classifiers will all have a place in operational forest mapping. ANN and related methods have not been widely adopted operationally because there is a steep learning curve, the software is only beginning to be integrated into standard image processing packages, and the outcome is to some extent dependent on the skill of the analyst (Carpenter 1999; but see German and Gahegan 1996). However, often in classification the main objective is developing a map of the highest possible accuracy, and it does not matter how you get there. While many observations are required for training data, in a number of cases ANN has produced significantly improved forest classification accuracy (but see Skidmore et al. 1997). The marginal costs may not be that great if these large datasets are being collected anyway, in the field or from air photos, for other forest monitoring purposes, and if they can be "recycled" (through signature extension) to different scenes or dates. More time can be spent collecting field data and less in fine tuning the layered, iterative and hybrid (unsupervised and supervised) classification approaches that have been used in the past to produce acceptable forest classification accuracy. Then foresters can spend more of their time in the field.

REFERENCES

- Adams, J. B., Sabol, D. E., Kapos, V., Filho, R. A., Roberts, D., Smith, M. O. & Gillespie, A. R. (1995). Classification of multispectral images based on fractions and endmembers: applications to land-cover change in the Brazilian Amazon. *Remote Sensing of Environment*, 52, 137-152.
- Anderson, J. R., Hardy, E. E., Roach, J. T. & Witmer, R. E. (1976). A land use and land cover classification system for use with remote sensor data. *U.S. Geological Survey Professional Paper 964*. U.S. Geologic Survey, Arlington, VA, USA.
- Austin, M. P., Nicholls, A. O. & Margules, C. R. (1990). Determining the realised qualitative niche: environmental niches of five Eucalyptus species. *Ecological Monographs*, 60, 161-177.
- Carpenter, G. A., Gjaja, M. N., Gopal, S. & Woodcock, C. E. (1997). ART neural networks for remote sensing: vegetation classification from Landsat TM and terrain data. *IEEE Transactions on Geoscience and Remote Sensing*, 35, 308-325.
- Carpenter, G. A., Gopal, S., Macomber, S., Martens, S., Woodcock, C. E. & Franklin, J. (1999). A neural network method for efficient vegetation mapping – an introduction. *Remote Sensing of Environment*, 70, 3276-338.
- Cochrane, M. A. (2000). Using vegetation reflectance variability for species level classification of hyperspectral data. *International Journal of Remote Sensing*, 22, 2075-2087.

- Culvenor, D. S. (2002). TIDA: an algorithm for the delineation of tree crowns in high spatial resolution remotely sensed imagery. *Computers and Geosciences*, 28, 33-44.
- Dustan, P., Dobson, E., & Nelson, G. (2001). Landsat Thematic Mapper: detection of shifts in community composition of coral reefs. *Conservation Biology*, 15, 892-902.
- Foody, G. M. (1996a). Approaches for the production and evaluation of fuzzy land cover classifications from remotely sensed data. *International Journal of Remote Sensing*, 17, 1317-1340.
- Foody, G. M. (1996b). Fuzzy modelling of vegetation from remotely sensed imagery. *Ecological Modelling*, 85, 3-12.
- Foody, G. M. (1999). The continuum of classification fuzziness in thematic mapping. *Photogrammetric Engineering and Remote Sensing*, 65, 443-451.
- Foody, G. M. (2002). Status of land cover classification accuracy assessment. *Remote Sensing of Environment*, 80, 185-201.
- Franco-Lopez, F., Ek, A. R., & Bauer, M. E. (2001). Estimation and mapping of forest stand density, volume, and cover type using the *k*-nearest neighbors method. *Remote Sensing of Environment*, 77, 251-274.
- Franklin, J. (1991). Land cover stratification using Landsat Thematic Mapper data in Sahelian and Sudanian woodlands and wooded grassland. *Journal of Arid Environments*, 20, 141-163.
- Franklin, J. (1995). Predictive vegetation mapping: geographic modeling of biospatial patterns in relation to environmental gradients. *Progress in Physical Geography*, 19, 474-499.
- Franklin, J. (2001). Geographic information science and ecological assessment. Bourgeron, P., Jensen M., & Lessard G. (Eds.) *An integrated ecological assessment protocols guidebook*. Springer-Verlag, New York.
- Franklin, J. (in press). Clustering versus regression trees for determining Ecological Land Units in the southern California mountains and foothills. *Forest Science*.
- Franklin, J., & Woodcock, C. E. (1997). Multiscale vegetation data for the mountains of Southern California: spatial and categorical resolution. Quattrochi, D. A. & Goodchild, M. F. (Eds.). *Scale in remote sensing and GIS*. CRC/Lewis Publishers Inc., Boca Raton, FL..
- Franklin, J., McCullough, P., & Gray, C. (2000a). Terrain variables used for predictive mapping of vegetation communities in Southern California. Gallant, J. P. & Wilson, J. C. (Eds.). *Terrain analysis: Principles and applications*. John Wiley & Sons, New York, NY.
- Franklin, J., Woodcock, C. E., & Warbington, R. (2000b). Multi-attribute vegetation maps of Forest Service lands in California supporting resource management decisions. *Photogrammetric Engineering and Remote Sensing*, 66, 1209-1217.
- Franklin, S. E. (2001). *Remote sensing for sustainable forest management*. Lewis Publishers, Boca Raton, FL.
- Friedl, M. A., & Brodley, C. E. (1997). Decision tree classification of land cover from remotely sensed data. *Remote Sensing of Environment*, 61, 399-409.
- Gastellu-Etchegorry, J. P., & Bruniquel-Pinel, V. (2001). A modeling approach to assess the robustness of spectrometric predictive equations for canopy chemistry. *Remote Sensing of Environment*, 76, 1-15.
- German, G. W. H., & Gahegan, M. N. (1996). Neural network architectures for the classification of temporal image sequences. *Computers and Geosciences*, 22, 969-979.
- Gopal, S., & Woodcock, C.E. (1994). Theory and methods for accuracy assessment of thematic maps using fuzzy sets. *Photogrammetric Engineering and Remote Sensing* , 60, 181-188.

- Gordon, A. D. (1999). *Classification*, (2nd ed.). Chapman & Hall/CRC, Boca Raton, FL.
- Guisan, A., & Zimmerman, N. E. (2000). Predictive habitat distribution models in ecology. *Ecological Modelling*, 135, 147-186.
- Held, A., Phinn, S., Scarth, P., Stanford, M., Ticehurst, C., Hartini, S., & Lymburnber, L. (2001). Hyperspectral mapping of rainforests and mangroves. *Proceedings of the International Geosciences and Remote Sensing Symposium*, July 9-13, Sydney. IEEE, Piscataway, NJ, USA, CD-ROM.
- Hill, R. A. (1999). Image segmentation for humid tropical forest classification in Landsat TM data. *International Journal of Remote Sensing*, 20, 1039-1044.
- Host, G. E., Polzer, P. L., Mladenoff, D. J., White, M. A., & Crow, T. R. (1996). A quantitative approach to developing regional ecosystem classifications. *Ecological Applications*, 6, 608-618.
- Huang, X., & Jensen, J. R. (1997). A machine learning approach to automated knowledge-base building for remote sensing image analysis with GIS data. *Photogrammetric Engineering and Remote Sensing*, 63, 1185-1194.
- Hutchinson, C. F. (1982). Techniques for combining Landsat and ancillary data for digital classification improvement. *Photogrammetric Engineering and Remote Sensing*, 48, 123-130.
- Jensen, J. R. (1996). *Introductory digital image processing: a remote sensing perspective*, Prentice-Hall, Upper Saddle River, NJ.
- Jupp, D. L. B., & Walker, J. (1997). Detecting structural and growth changes in woodlands and forests: The challenge for remote sensing and the role of geometric-optical modelling, Gholz, H. L., Nakane, K., & Shimoda, H. (Eds.). *The use of remote sensing in the modelling of forest productivity*, 75-108. Kluwer Academic Publishers, The Netherlands.
- Key, T., Warner, T. A., McGraw J. B., & Fajvan, M. A. (2001). A comparison of multispectral and multitemporal information in high spatial resolution imagery for classification of individual tree species in a temperate hardwood forest. *Remote Sensing of Environment*, 75, 100-112.
- Kimes, D. S., Nelson, R. F., Salas, W. A., & Skole, D. L. (1999). Mapping secondary tropical forest and forest age from SPOT HRV data. *International Journal of Remote Sensing*, 20, 3625-3640.
- Lambin, E., & Strahler, A. (1994). Change vector analysis in multi-temporal space: A tool to detect and categorise land cover change processes using high temporal resolution satellite data. *Remote Sensing of Environment*, 48, 231-244.
- Linders, J. (2000). Comparison of three different methods to select feature for discriminating forest cover types using SAR imagery. *International Journal of Remote Sensing*, 21, 2089-2099.
- Lucas, R., Held, A., & Phinn, S. (in press). Tropical forests. Ustin, S. (Ed.). *Manual of Remote Sensing, Volume 4, Remote Sensing for Natural Resource Assessment*. American Society for Photogrammetry and Remote Sensing, Bethesda, Maryland.
- Mäkelä, H., & Pekkarinen, A. (2000). Estimation of timber volume at the sample plot level by means of image segmentation and Landsat TM imagery. *Remote Sensing of Environment*, 77, 66-75.
- Mather, P. (1999). *Computer processing of remotely sensed images: An introduction*. (2nd ed.). John Wiley and Sons, Brisbane, Australia.
- Michaelsen, J., Schimel, D., Friedl, M., Davis, F. W., & Dubayah, R. C. (1994). Regression tree analysis of satellite and terrain data to guide vegetation sampling and surveys. *Journal of Vegetation Science*, 5, 673-686.

- Moore, D. M., Lees, B .G., & Davey, S. M. (1991). A new method for predicting vegetation distributions using decision tree analysis in a geographic information system. *Environmental Management*, 15, 59-71.
- Muinonen, E., Maltamo, M., Hyppänen H., & Vainikainen, V. (2001). Forest stand characteristics estimation using a most similar neighbor approach and image spatial structure information. *Remote Sensing of Environment*, 78, 223-228.
- Pax-Lenney, M., Woodcock, C. E., Macomber, S. A., Gopal, S., & Song, C. (2001). Forest mapping with a generalized classifier and Landsat TM data. *Remote Sensing of Environment*, 77, 241-250.
- Phinn, S. R. (1997). *Remote sensing and spatial analytic techniques for monitoring landscape structure in disturbed and restored coastal environments*. Ph.D. Dissertation. Departments of Geography, San Diego State University and University of California at Santa Barbara.
- Phinn, S. R., (1998). A framework for selecting appropriate remotely sensed data dimensions for environmental monitoring and management. *International Journal of Remote Sensing*, 19, 3457-3463.
- Phinn, S. R., Menges, C., Hill, G. J. E., & Stanford, M. (2000). Optimising remotely sensed solutions for monitoring, modelling and managing coastal environments. *Remote Sensing of Environment*, 73, 117-132.
- Pohl, C., & van Genderen, J. L. (1998). Multisensor image fusion in remote sensing: concepts, methods and applications. *International Journal of Remote Sensing*, 19, 823-254.
- Preston, R., Culvenor, D., & Coops, N. (1998). Modeling of tree species and structural attributes from high spatial resolution digital multi-spectral imagery using decision-tree analysis for east coast eucalypt forests of Australia. Hill, D. & Leckie, D. (Eds.). *International forum: automated interpretation of high spatial resolution digital imagery for forestry*, 225-242, February 10-12, 1998, Victoria, British Columbia. Natural Resources Canada, Canadian Forest Service, Pacific Forestry Centre, Victoria, B.C.
- Pu, R., & Gong, P. (2000). Band selection from hyperspectral data for conifer species identification. *Geographic Information Sciences*, 6, 137-142.
- Raucoules, D., & Thomson, K. P. B. (1999). Adaptation of the Hierarchical Stepwise Segmentation Algorithm for automatic segmentation of a SAR mosaic. *International Journal of Remote Sensing*, 20, 2111-2116.
- Ripley, B. D. (1996). Pattern recognition and neural networks. Cambridge University Press, Cambridge.
- Rodriguez-Yi, L., Shimabukuro, Y. E., & Rudorff, B. F. T. (2000). Image segmentation for classification of vegetation using NOAA-AVHRR data. *International Journal of Remote Sensing*, 22, 167-172.
- Rogan, J., Franklin, J., & Roberts, D. (2002). A comparison of methods for monitoring multitemporal vegetation change using Thematic Mapper imagery. *Remote Sensing of Environment*, 80, 143-156.
- Scarth, P., & Phinn, S. (2000). Determining forest structural attributes using an inverted geometric-optical model in mixed eucalypt forests, south-east Queensland, Australia, *Remote Sensing of Environment*, 71, 141-157.
- Schowengerdt, R. A. (1997). *Remote sensing: Models and methods for image processing*, (2nd ed.). Academic Press, San Diego.
- Skidmore, A. (1989). An expert system classifies eucalypt forest types using Thematic Mapper data and a digital terrain model. *Photogrammetric Engineering and Remote-Sensing*, 55, 1449-1464.

- Skidmore, A., Gauld, A., & Walker, P. (1996). Classification of kangaroo habitat distribution using three GIS models. *International Journal of Geographical Information Systems*, 10, 441-454.
- Skidmore A. R., Turner, B. J., Brinkhof, W., & Knowles, E. (1997). Performance of a neural network: mapping forests using GIS and remotely sensed data. *Photogrammetric Engineering and Remote Sensing*, 63, 501-514.
- Strahler, A. H. (1981). Stratification of natural vegetation for forest and rangeland inventory using Landsat digital imagery and collateral data. *International Journal of Remote Sensing*, 2, 15-41.
- Strahler, A. H., Estes, J. E., Maynard, P. F., Mertz, F. C., & Stow, D. A. (1980). Incorporation of collateral data in Landsat classification and modeling procedures. *Proceedings of the Fourteenth International Symposium on Remote Sensing of Environment*, 1009-1026, Ann Arbor: Environmental Research Institute of Michigan, USA.
- Strahler, A. H., Woodcock, C. E., & Smith, J. A. (1986). On the nature of models in remote sensing. *Remote Sensing of Environment*, 20, 121-139.
- Treitz, P. M., & Howarth, P. J. (1999). Hyperspectral remote sensing for estimating biophysical parameters of forest ecosystems. *Progress in Physical Geography*, 23, 359-390.
- Wolter, P. T., Mladenoff, D. J., Host, G. E., & Crow, T. R. (1995). Improved forest classification in the Northern Lake States using multi-temporal Landsat imagery. *Photogrammetric Engineering and Remote Sensing*, 61, 1129-1143.
- Woodcock, C. E. (in press). Temperate forests. Ustin, S. (Ed.) *Manual of Remote Sensing*, Volume 4, Remote Sensing for Natural Resource Assessment. American Society for Photogrammetry and Remote Sensing, Bethesda, Maryland.
- Woodcock, C. D., Collins, J., Gopal, S., Jakabhaazy, V. D., Li, X., Macomber, S., Ryherd, S., Harward, V. J., Levitan, J., Wu, Y., & Warbington, R. (1994). Mapping forest vegetation using Landsat TM imagery and a canopy reflectance model. *Remote Sensing of Environment*, 50, 240-254.
- Woodcock, C. E., & Harward, V. J. (1992). Nested-hierarchical scene models an image segmentation. *International Journal of Remote Sensing*, 13, 3167-3187.
- Woodcock, C. E., Macomber, S. A., Pax-Lenney, M., & Cohen, W. B. (2001). Monitoring large areas for forest change using Landsat: generalization across sensors, space and time. *Remote Sensing of Environment*, 78, 194-203.
- Wulder, M. (1998). Optical remote-sensing techniques for the assessment of forest inventory and biophysical parameters. *Progress in Physical Geography*, 22, 449-476.
- Wulder, M., Niemann, K. O., & Goodenough, D. (2000). Local maximum filtering for the extraction of tree locations and basal area from high spatial resolution imagery. *Remote Sensing of Environment*, 73, 103-114.
- Yu, B., Ostland, M., Gong, P., & Pu, R. (1999). Penalized linear discriminant analysis for conifer species recognition. *IEEE Transactions on Geoscience and Remote Sensing*, 37, 2569-2577.

Chapter 11

REMOTE SENSING OF FORESTS OVER TIME

Change Types, Methods, and Opportunities

Peng Gong and Bing Xu

Center for Assessment and Monitoring of Forest and Environmental Resources, University of California, Berkeley, California, 94720-3110, USA

1. TYPES OF FOREST CHANGE AND AN OVERVIEW OF REMOTE SENSING DETECTION

Forest change happens constantly at different spatial scales. At the individual tree level, the biochemical and biophysical properties may vary according to environmental conditions; physical appearance such as colour and size may change due to phenology or human disturbance. At the stand level, the structure of forest canopies may change in terms of horizontal measures of canopy closure and gap size and shape and vertical measures of number of layers of understorey, height of each storey, etc. At the watershed level, forest ecosystem change can be evaluated by different landscape measurements such as fragmentation indices, matrix and corridor structure and system complexity. Changes at even larger scales are usually caused by human-induced environmental changes and climate changes.

Forest changes can be classified in various ways. Possible divisions include gradual and abrupt, based on the rate of change; long term and short term, based on the duration of change; normal (e.g. growth and seasonal variation) and catastrophic (e.g. fires, wind throw and defoliation), based on the state of forest health; natural (e.g. growth and succession, disease and insect outbreaks) and anthropogenic (e.g. pollution, clearing, thinning and plantation), based on the cause of changes; and reversible and irreversible during a certain period of time, according to the possibility of recovery.

The magnitude of different types of change also differs, as do their importance and ease of detection. The importance of a particular type of change may be relative, depending on the interests of the observer. For example, forest managers have a strong interest in canopy structure disturbance caused by insects and disease, fires, bad weather conditions, resource exploitation, pollution and land clearing for development. Of lesser concern are changes related to interannual variability and growth variation caused by climate change. To global change modellers, however, this last type of change is of primary concern. Table 11-1 lists some of the major types of forest change, their temporal duration, spatial extents and rates and magnitudes of change on a daily basis. The effect of cumulative change may be derived by multiplying the duration and the rate. This determines the magnitude of change that may be observed visually or by remote sensing.

Table 11-1. Types of forest change and their temporal, spatial and rate of change on a daily basis.

Type of Change	Duration	Spatial Extent	Rate	Magnitude
Phenological	Days - months	All levels	Medium	Medium
Regeneration	Days-decades	Individual - stand	Slow	Small
Climatic adaptation	Years	All levels	Slow	Small
Wind throw/flooding	Minutes - hours	Individual - stand	Medium - fast	Large
Fire	Minutes - days	All levels	Fast	Large
Disease	Days - years	All levels	Slow - medium	Small-large
Insect attack	Days - years	All levels	Slow - fast	Small-large
Mortality	Days - years	All levels	Slow - fast	Large
Pollution	Years	Stand - watershed	Slow	Small-large
Thinning/pruning	Days	Stand - watershed	Fast	Large
Clear-cutting	Days	Stand - watershed	Fast	Large
Plantation	Days-decades	Stand - watershed	Fast	Small

Forest changes are caused by three types of force: internal growth and evolutionary development, natural forces such as climate variation, flooding, hurricanes, fire, insects and diseases, and human induced harvest and forest management such as clear cutting, thinning, trimming and burning. The types of forest change are organised according to these different causes (Table 11-1). With the exception of internal growth, most forest changes are caused by disturbances.

Remote sensing has been used in the detection, identification and quantification of forest change for a long time. For example, it has been applied to land cover classification to separate forest from non-forest lands; to tracking the temporal change of forested lands (Tokola et al. 1999; Cushman and Wallin 2000; Hessburg et al. 2000); to detecting thinning

(Olsson 1995), cutting (Varjo and Folving 1997; Zheng et al. 1997; Hame et al. 1998; Radeloff et al. 2000; Hayes and Sader 2001), defoliation (Franklin 1989; Muchoney and Haack 1994; Royle and Lathrop 1997; Chalifoux et al. 1998) and mortality (Collins and Woodcock 1996; Allen and Kupfer 2001); for fire mapping (Li et al. 2000; Remmel and Perera 2001), detection of forest pollution (Rigina et al. 1999; Diem 2002) and forest phenology (Pellikka 2001). Vegetation indices, particularly the normalized difference vegetation index, have been used to track seasonal and interannual vegetation dynamics (e.g., Qi and Gong 1996; Myneni et al. 1997).

The use of remotely sensed data to detect forest change is based on the premise that changes in land characteristics must result in changes in radiance values and the radiance changes due to land characteristics can be separated from those due to such factors as differences in satellite sensors, atmospheric conditions, solar angle, and soil moisture. There are situations, however, where other factors dominate and make change detection difficult without auxiliary data.

Prior to the advent of digital remote sensing, most forest mapping and monitoring was done by photographic interpretation. This method has some disadvantages. For instance, visual change detection is difficult to replicate; that is, different interpreters produce different results. Manual detection also incurs substantial data acquisition costs (Coppin and Bauer 1994). Compared with traditional photo-interpretation techniques, digital remote sensing provides a synoptic, timely, relatively objective and repeatable approach for change detection. Digital remote sensing enables one to examine the radiometric differences manifested by forest change in different spectral wavelength regions and changes in variables derived from remotely sensed data.

Remote sensing technology is characterised by five kinds of capabilities – the resolving power in the spatial, spectral and radiometric aspects, i.e., the spatial, spectral and radiometric resolution, and the spectral and temporal sampling frequency (see Lefsky and Cohen, Chapter 2).

Although it is usually better to have high resolution and more frequent sampling, the amount of computation and data processing may become prohibitively high. On the other hand, the capabilities of existing remote sensing systems may be insufficient to detect subtle changes or to capture the processes of abrupt changes. For example, it is simply impossible to monitor individual tree damage during a hurricane event because such a process requires highly frequent imaging over a large area with an imaging capability at the individual tree level. Similarly, there is no system that can monitor agricultural burning in a state as large as California because the time duration of an agricultural burning event is usually shorter than a couple of hours and the size of land to be burnt can be as small as one acre. Therefore,

it is necessary to choose an appropriate set of system configurations for a particular type of change detection task (Coppin and Bauer 1994; Coppin et al. 2001; Lefsky and Cohen, Chapter 2). This requires an analysis of system requirements for a given change detection task. Detecting and identifying forest change involves the use of a complicated set of remote sensing procedures including data acquisition, image calibration and enhancement, and a number of information extraction strategies.

Change detection using remote sensing can be done by either analysing a single-date image or comparing images taken at different times. One of the common single-date image analysis techniques is image classification, which has been widely used in forest defoliation mapping. For example, spruce budworm and hemlock looper damage causes conifer leaves to change colour to red/brown/grey. These colour differences can be differentiated into separate classifications from the normal colours of conifer leaves using both airborne and space borne sensors (Leckie 1987; Franklin 1989; Franklin and Raske 1994; Royle and Lathrop 1997).

This Chapter will focus on the methods developed for change detection by the comparison of temporally separated images. The following section provides a general overview of various techniques.

2. MULTI-TEMPORAL CHANGE DETECTION METHODS

Figure 11-1 shows the simplest multi-temporal (2 dates) change detection technique. It requires only one pre-processing procedure – geometric registration of image acquired on date T1 to a second image acquired on date T2 (see Toutin, Chapter 6). Change information is enhanced by taking the difference or ratio pixel by pixel across the common area between images T1 and T2. A set of thresholds is chosen to classify each pixel into the change or no-change category to produce a change mask (also called a change map). The simple procedure in Figure 11-1 uses raw data from the image, i.e., the digital numbers (DN) on each date. Other than DNs, pixels can take values in radiance, reflectance and/or albedo that are more physically meaningful in subsequent analyses. This would require an additional procedure to be included in digital change detection – radiometric calibration (see Peddle et al., Chapter 7). The complexity of digital change detection further increases as the images on T1 and T2 contain multiple bands. Either a band selection or a band combination procedure is required when multi-spectral images are used. Common band combination procedures include vegetation indexing (usually derived from the red and near infrared bands), Kauth-Thomas (KT) transform (Kauth and Thomas 1976), and principal component analysis

(PCA). The procedures in Figure 11-1 only allow change detection; the nature of the change cannot be determined. Figure 11-2 shows the simplest steps required for change identification. Each image is classified and then compared with each other to determine the “from to” type of changes pixel by pixel. Image registration can be done either before or after image classification. Image registration done before image classification may alter the radiometric values slightly due to image re-sampling. This is a typical type of post-classification comparison procedure in change detection. If the same set of training samples is used for classifying both images, image registration must be done before image classification. Radiometric calibration also needs to be carried out.

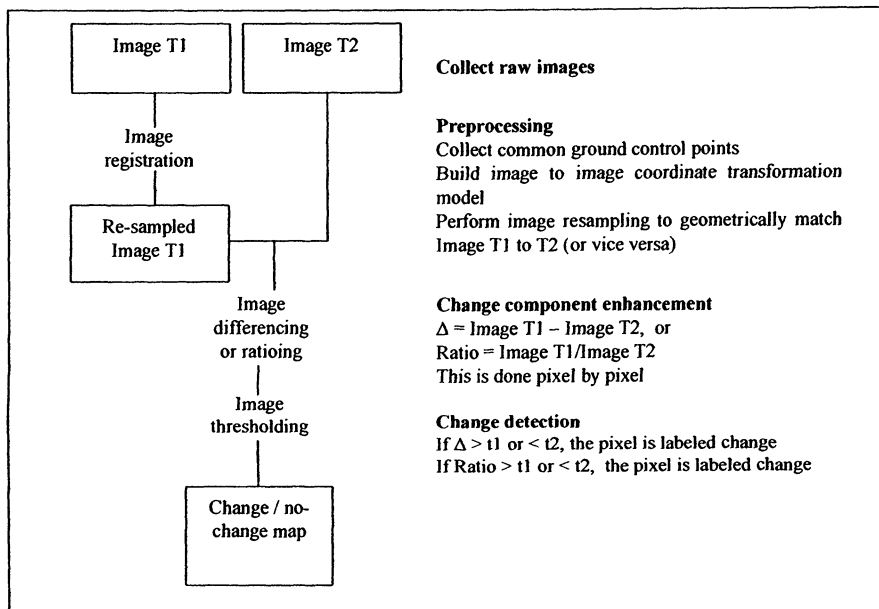


Figure 11-1. Procedures in a simple digital change detection task.

In order to compare the radiometric differences between images acquired at different times for the same location, precise image registration between different times is needed. Jensen (1996) suggests that a root mean square error (RMSE) of 0.5 pixels is the maximum tolerable error for image registration in change detection of urban areas. Townshend et al. (1992) found that a mis-registration of 1 pixel could cause normalized difference vegetation index (NDVI) difference errors of greater than 50 % and suggested that in order to maintain a less than 10 % error in NDVI differences a 0.2 pixel RMSE is required for image registration over densely vegetated areas. This is echoed by Dai and Khorram (1998), who also found that the near infrared channel of Landsat Thematic Mapper (TM) data was

most sensitive to registration errors. An over-estimation of change will occur due to mis-registration (Verbyla and Boles 2000). It should be noted that an RMSE of less than 1 pixel is hard to obtain. Most image registration procedures report an RMSE derived from co-ordinates of ground control points (GCP) that have been used in building the image-to-image co-ordinate transformation model. Therefore, RMSE calculated from GCPs would usually underestimate registration error. An unbiased estimate of RMSE can only be calculated from independent check points separately selected. Gong et al. (1992) proposed an adaptive filter technique to reduce the image differencing errors caused by mis-registration of greater than 1 pixel.

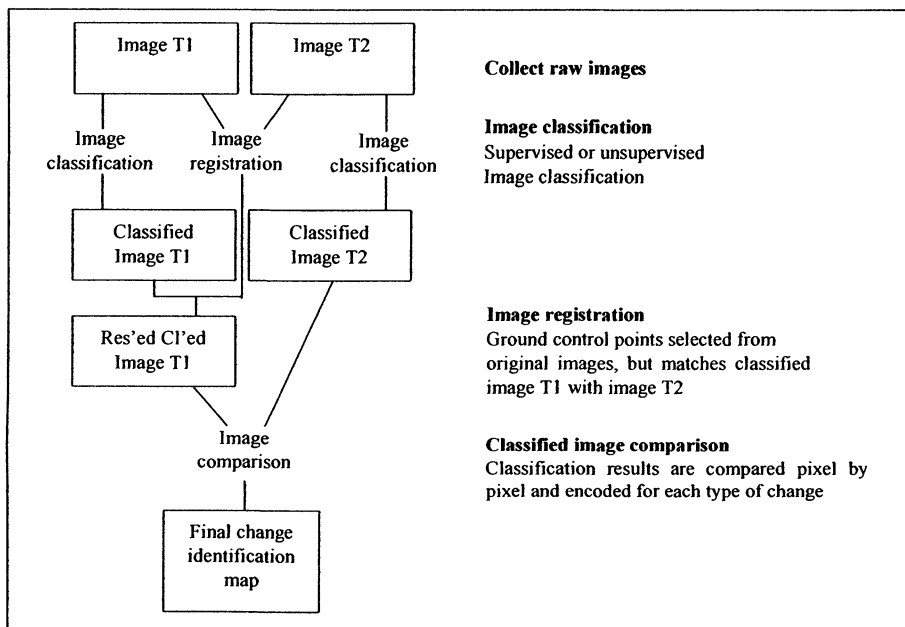


Figure 11-2. The simplest change identification procedure. "Res'ed Cl'ed Image T1" stands for "re-sampled classified image T1. Image registration can be done either before or after image classification. If image registration is done after image classification, then only nearest neighbour re-sampling can be applied to the classified image.

Radiometric calibration of data prior to change detection serves the purposes of establishing a more direct link between image and biophysical phenomena. It reduces illumination inconsistencies (caused by solar angle differences) and atmospheric interference during data acquisition and masks out unwanted data contamination (clouds). Radiometric calibration usually converts DN in the raw image into radiance or reflectance. This process includes sensor calibration, atmospheric correction and topographic correction (Gong 2002). It is not always necessary to do radiometric calibration. For example, atmospheric correction is unnecessary in single

image classification as long as the training data are specified for each single-date image. For Landsat TM data where the primary atmospheric distortion is due to scattering which is additive to the ground signal, atmospheric correction is essentially translating each image band without changing the internal data structure. Such operations are unnecessary for multi-date image classification, post-classification comparison, change detection based on image differencing, and linear transformations of multiple images such as KT transform and PCA (Song et al. 2001). It is necessary to perform atmospheric correction if multi-band ratioing (such as the NDVI) is used in change detection. Song et al. (2001) summarised two broad types of atmospheric technique – absolute correction using dark object subtraction (DOS) and dense dark vegetation (DDV) techniques, and relative correction using pseudo invariant features (PIF) to which a linear relationship is assumed to hold between image bands over time. A linear relationship can be built by selecting a certain number of PIFs that can be located on both images. It is desirable that the PIFs have a large radiometric range (Gong et al. 1994). A non-linear relative calibration can also be established through histogram matching (Gong 2002). The histograms must be generated from the same areas on both images where the same radiometric conditions on both dates are assumed. Olsson (1994, 1995) applied and compared a number of relative calibration techniques to Landsat TM data acquired over a boreal forest area in Sweden and found that thinning of the canopy at a magnitude of less than 20-25 % causes very small radiometric change (less than 0.01 in reflectance) in the visible and near infrared bands. Given the fact that image calibration could easily introduce an error greater than 0.01 in reflectance, this implies that for boreal forest it is difficult to detect canopy structure changes caused by thinning of low intensity.

Singh (1989) reviewed 11 general change enhancement / detection / identification techniques. They are:

1. Univariate image differencing (UID): subtraction of the same band of images acquired at different times.
2. Image regression (IRE): building a linear model that predicts digital values of day 1 compared to those of day 2 and then subtracts the predicted day 2 data from those actually acquired on day 2.
3. Vegetation index differencing (VID): taking the difference between vegetation indices derived from images of different dates.
4. Image ratioing (IRO): taking the ratio of the same band of images acquired at different times.
5. Principal component analysis (PCA): PCA has been applied in various ways. The two popular approaches are applying PCA to single date images or applying it to a combined 2-date or multi-date image. PCA serves as a regular image enhancement tool in the first approach while

- it directly transforms changes into specific components when the second approach is used.
6. Post-classification comparison (PCC): changes are derived by comparing image classification results separately derived from single date images.
 7. Direct multi-date classification (DMC): as in multi-date PCA, the combined multi-date image set is classified directly to identify changes.
 8. Change vector analysis (CVA): difference values obtained in each band are organised in a vector form so that each vector represents difference values from all bands at a particular pixel location. The vector magnitude reflects the intensity of change and the vector direction contains information about the type of change.
 9. Background subtraction (BST): slowly varying background radiance (low frequency components) are estimated and subtracted from the actual image to highlight spatial variation.
 10. Spectral correlation (SCO): computes a correlation coefficient between spectral data acquired from two different dates.
 11. Statistical test method (STM): tests two samples (each sample contains spectral values taken at the same location on different dates) to see if they are from the same population based on the Kalmogorov-Smirnov test.

UIF is a widely used technique (Coppin and Bauer 1994). The absolute value of the difference at a particular pixel exceeding a certain threshold will be considered as change.

IRE is an extension to UIF that normalises the atmospheric conditions. However, this becomes unnecessary if we apply UIF to images from different dates that have been radiometrically calibrated.

Use of vegetation indices in change detection is based on the premise that when foliage containing chlorophyll pigments is destroyed, the red and near-infrared reflectance ratio for green vegetation changes. This can be extended to any multi-spectral transformation of single date images. Image differencing can be subsequently applied. VID has been correlated with levels of defoliation to estimate level of forest damage (Royle and Lathrop 1997).

IRO has been widely applied for many years and obtained good results (Howarth and Wickware 1981; Singh 1989). The shortcoming of IRO is that the amount of radiometric change is not measured as a constant, making it hard to determine image thresholds.

PCA has been a popular technique especially when applied to a combined multi-date data set (e.g., Ingebritsen and Lyon 1985; Fung and LeDrew 1987). If the percentage of total changed area in the image is low,

change information is usually transformed into the 3rd or 4th principal component images (Richards and Jia 1999). However, this is not always true and it varies with the actual proportion of changed area in an image. To increase its general applicability, Gong (1993) suggests that PCA be applied to image difference data so that changes will be transformed into the first and second principal component image.

PCC has an advantage of not only detecting change but also directly revealing the types of change. However, it suffers from the compounding of misclassification on each individual date if image classification errors are randomly distributed. If each single classification has an accuracy of 80 %, the change information as derived from two classification maps would have an accuracy of 64 %. Change identification errors can be reduced if only detected changes are classified for comparison.

The number of categories in DMC could be exponentially greater than those in a single date classification. For example, if a single date classification has a classification scheme of 10 classes, a DMC for a two date image set could be as great as 100. This method is rarely used alone.

CVA, initially proposed by Malila (1980), is an exhaustive preservation of difference information among all spectral bands, as a result of which there is flexibility in subsequent analysis such as change magnitude calculation and trend of change evaluation. It does not, however, provide information about the initial state of surface type. It has been widely applied in change detection due to the relatively rich amount of change information contained in change vectors (Johnson and Kasischke 1998; Silapaswan et al. 2001). It is useful in discriminating between different types of phenological change and the relative components within and among changes. More details about CVA will be provided in the following section.

BST cannot be regarded as a regular change detection technique. It has the effect of a high pass filter.

SCO is another measure of similarity. Although promising, it is rarely used directly in change detection. Inner product analysis (IPA), a technique similar to SCO, can also be used (Yuan et al. 1998). Essentially all similarity measures are useful measures based on which change and non-change can be determined. STM is a method that is more suitable for comparing whether change has occurred among multiple pixels, perhaps at the forest stand level.

Since Singh (1989), a number of change detection techniques have been proposed and tested. For example, the above listed techniques (except STM) are pixel based operators. For boreal and temperate forests, it has been found that change detection at the stand level produces better accuracy than pixel based methods for detection and identification of clear cut and defoliation and low mortality (Coppin and Bauer 1994; Varjo and Folving 1997; Chalifoux et al. 1998). On the other hand, Foody and Boyd (1999) applied a

neural network algorithm to unmix NOAA Advanced Very High Resolution Radiometer (AVHRR) data in order to achieve sub-pixel levels of forest information for change detection. For the detection of forest mortality in northern California, Collins and Woodcock (1994) propose a Gram-Schmidt orthogonalisation technique (GST, the same technique used to derive Tasseled Cap (KT) transformation) to analyse multi-temporal Landsat TM imagery. When compared with the use of a neural network algorithm in detecting forest mortality using the same study site, Gopal and Woodcock (1996) found that the neural network algorithm was more accurate than GST. Hame et al. (1998) proposed an unsupervised automatic change detection based on clustering of single-date imagery for mapping clear cuts in boreal forest of southern Finland. Nielsen et al. (1998) proposed a multivariate alteration detection (MAD) transformation which is based on canonical correlation analysis.

While most of the previous studies use the optical remotely sensed data (primarily Landsat TM data), the suitability of ERS Synthetic Aperture Radar (SAR) data for detection of forest cover changes has also been studied. Grover et al. (1999) found that a ratio between two images acquired in two successive years by the short wavelength (C band) ERS SAR can detect approximately 50 % of forest cover changes detected by using Landsat TM data in a study site in the Amazon Basin. A similar finding was reported on the superiority of ratioing over differencing with SAR data in change detection (Rignot and Vanzy1 1993). They found that the longer wavelength (L band) JERS SAR imagery is more effective in forest cover change detection, but suffers from more distortion due to topographic effects. This is a result of the stronger penetration capability of the longer wavelength microwave energy.

Quegan et al. (2000) report an improvement of ERS SAR data application in forest cover mapping by including a time series of SAR imagery for analysis. They found that the C-band back-scattering coefficient of the forest was stable for stands above 30-40 tons/ha and exhibits higher variability for younger stands mainly due to changes in soil moisture. Without prior knowledge of an area, the temporal variation of C-band intensity data can be used to distinguish the stands and non-forest land by a threshold of biomass amount (30 tons/ha).

Gong et al. (2000) propose the use of digital photogrammetry to extract 3D morphological information from an oak woodland in California. Such 3D models are called digital surface models (DSM). Forest growth and decline in both the horizontal and vertical directions can then be determined by comparing DSMs derived from stereo aerial photos acquired at different times.

In practical change detection/identification, most procedures fall into one of two strategies: multi-date image comparison or combined analysis of multi-date images. Figure 11-3 combines two change detection procedures with the post-classification change identification procedure. It uses the change mask to filter out some of the false changes caused by classification comparison. In a particular application, one may choose to use only VIs as the variables for change detection. Similarly, KT indices may be used alone. "Unmix" stands for linear mixing analysis of a single date image to derive sub-pixel proportions of a selected group of surface cover types (Gong et al. 1994; Adams et al. 1995; Asner et al., Chapter 8). When the same set of cover types is selected for images of both dates, differences (DIF) can be derived to determine changes. There are many procedural variations for selecting the different variables for change detection, as well as for radiometric calibration between the two images. For example, if the change detection is for general surface cover, one may directly use the various spectral bands. However, for forest change detection, vegetation indices and KT transformed indices such as "greenness" and "brightness" are often used. Detailed calculation on how to obtain these indices will be discussed later. There are more than 50 VIs (Coppin and Bauer 1994). It is necessary to choose the most effective ones for a particular application. Although PCA can be applied separately to single date images, we do not recommend this type of use because physical interpretation of each resultant component varies from image to image and from time to time. The eigen structure of each individual image varies with the statistical properties of the image as reflected by the variance-covariance matrix. However, PCA has been widely adopted when a combined image set of multi-date images is analysed (Fung and LeDrew 1987).

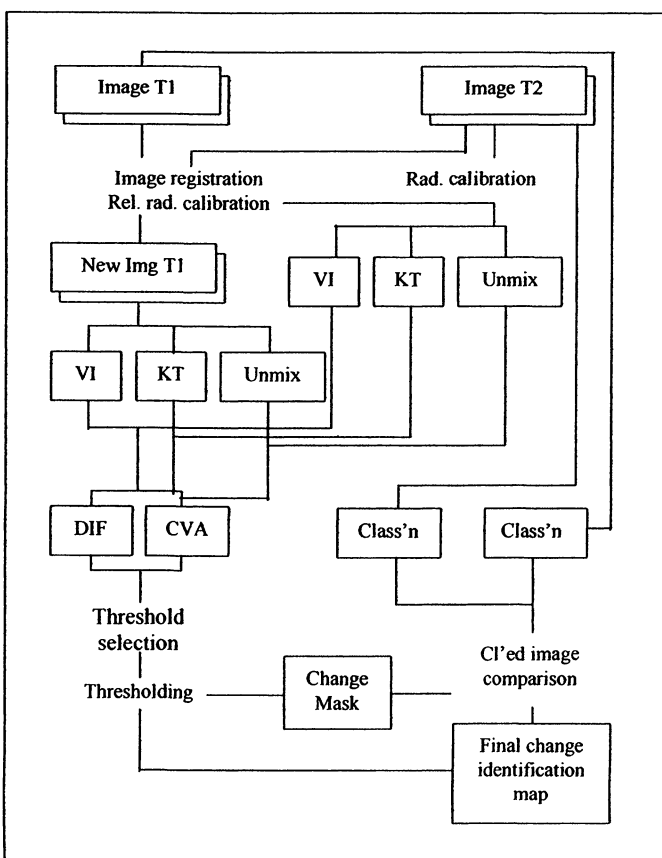


Figure 11-3. A typical image comparison procedure for change detection/identification.

Images are geometrically registered. Both images may be converted into radiance or reflectance through a radiometric calibration (Rad. Calibration) and then put through a relative radiometric calibration (Rel. rad. Calibration). "Class'n" stands for image classification. "Cl'ed" stands for classified. "New img T1" represents image T1 after geometric registration and radiometric calibration.

Some of the typical procedures used in change detection and identification with combined multi-date images are shown in Figure 11-4. Such procedures begin with image registration and radiometric calibration. The images from two different dates are then pooled together for subsequent analysis. The principle of applying PCA to a combined set of image bands has been discussed earlier. For more detail, please refer to Richards and Jia (1999, p.277) and Gong (1993). To overcome the lack of physical meaning of the PCA techniques, the idea of KT transform using Graham-Schmidt transformation (GST) has been expanded to multi-date images (Collins and Woodcock 1994). Like any other linear transformation techniques such as

KT transform and PCA, GST can be applied to the multi-date images to produce a set of new variables. Selected new variables can be regressed with field data or data from other independent sources to establish prediction models for change prediction or classification. Collins and Woodcock (1996) used such an approach to predict forest mortality from multi-date multispectral Landsat imagery. When GST was compared with a multi-date PCA and a multi-date KT transform (MKT) (Fung 1990) they found that the later two methods produced better results. Although DMC can be done, we do not recommend it for the reasons discussed earlier.

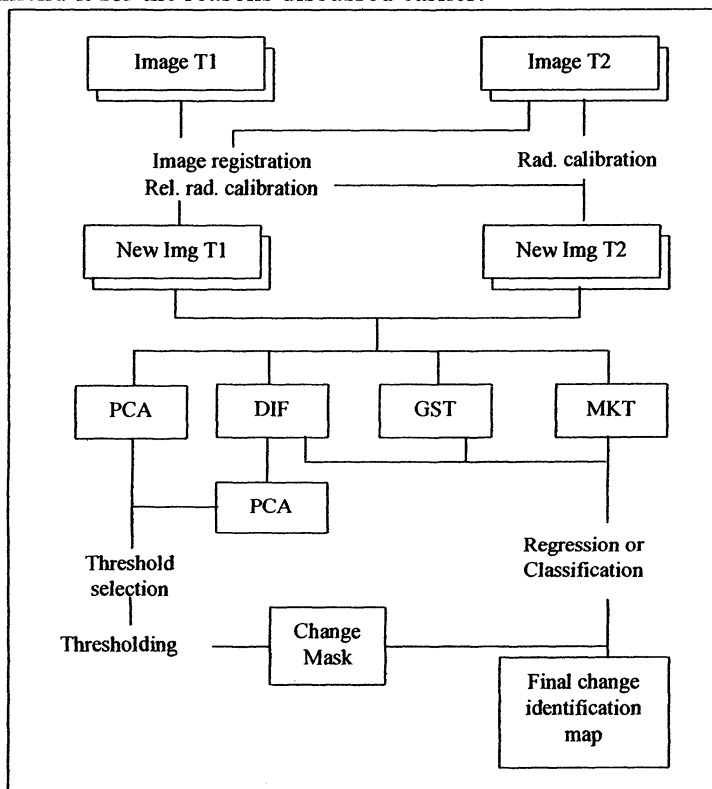


Figure 11-4. Some typical procedures for combined analysis of multi-date images for change detection and identification.

In summary, we reviewed many change detection algorithms. Selection of an appropriate one, in practice, often depends on requirements of information, data availability and quality, time and cost constraints, analysis skill and experience (Johnson and Kasischke 1998). Most change detection algorithms are relatively straightforward. To improve post-classification change detection/identification, a good classification algorithm must be used. In addition to some of the traditional supervised classification

algorithms, non-parametric classification algorithms are suitable candidates (Varjo and Folving 1997). Some of the classification algorithms are directly applicable to change detection. For example, artificial neural networks (Gopal and Woodcock 1996) and the unsupervised change detection mentioned earlier (Hame et al. 1998) have been successfully tested for forest mortality or clear-cut identification. While most of the change detection algorithms are based on general purpose image enhancement and classification algorithms that can be found elsewhere, CVA, MKT, and GST are primarily developed for change detection. The following two sections will introduce these methods in more detail.

3. AN IMPROVED CVA ALGORITHM

CVA can not only avoid the shortcomings of other post-classification techniques, such as cumulative error in single date classification, but also find changed pixels using all the bands and provide 'from-to' type of change category information. In the past few years, its advantages and potential have been demonstrated in some case studies (Michalek et al. 1993; Lambin and Strahler 1994a, 1994b; Sohl 1999; Allen and Kupfer 2001), and it has recently been employed as the basis for the initial 1-km Land-Cover Change Product using MODIS data (Zhan et al. 2000). However, CVA also has several drawbacks that limit its use. These include

1. A lack of automatic or semi-automatic methods to effectively determine the threshold of change magnitude between change and non-change pixels. As with other techniques that require a determination of optimal threshold between change and non-change pixels, selection of threshold is considered an important task and the greatest challenge of CVA (Yuan et al. 1998; Johnson and Kasischke 1998). The threshold in a specific CVA analysis is often determined empirically or with a manual trial-and-error procedure. Such threshold selection procedures usually depend on the experience of the image analyst and long trial times (Bruzzone et al. 2000).
2. Discrimination of different phenomenological types of change is problematic when the number of bands involved is large. Methods of discriminating change type in existing literature can be grouped into three classes: (a) trigonometric functions of vector angle in two spectral dimensions; (b) sector coding in more than two spectral dimensions; and (c) PCA in a multi-temporal space (Lambin and Strahler 1994a). In most CVA applications, the change category is distinguished and assigned by a combination of '+' or '-' symbols (increase in +, decrease in -) of each computational band and image

interpretation (Michalek et al. 1993; Johnson and Kasischke 1998; Sohl 1999). When CVA is applied in this manner (Sector Coding), two problems exist. (a) Sector coding can discriminate 2^n sectors when the number of bands is n . If there are 5 land cover types found at two different dates, respectively, and all possible types of change occur between those land covers during this period, the number of change types is $5 \times 4 = 20$. This implies that one sector code certainly represents more than one change type, which may lead to an assignment error of change category. (b) It is a strenuous and time-consuming job to discriminate and interpret change categories represented by sector codes with the increase of computational bands (n) because the number of sector codes increases geometrically.

In light of the above-mentioned drawbacks, Chen et al. (in press) propose an improved CVA for change detection which includes (a) a semi-automatic method, named Double-Window Flexible Pace Search (DFPS), aiming at determining the threshold of change magnitude efficiently; and (b) a new method of determining change direction (change category) which combines a single image classification and a minimum distance categorisation based upon direction cosines of a change vector.

A change vector can be described by an angle of change (vector direction) and a magnitude of change from date 1 to date 2 (Jensen 1996). If a pixel's grey level values in two images on dates T_1, T_2 are given in $G = (g_1, g_2, \dots, g_n)^T$ and $H = (h_1, h_2, \dots, h_n)^T$, respectively, n is the number of bands or variables derived from the original images, a change vector is defined as:

$$\Delta G = H - G = \begin{pmatrix} h_1 - g_1 \\ h_2 - g_2 \\ \dots \\ h_n - g_n \end{pmatrix} \quad (1)$$

where ΔG includes all the change information between the two dates for a given pixel, and the change magnitude $|\Delta G|$ is computed from:

$$|\Delta G| = \sqrt{(h_1 - g_1)^2 + (h_2 - g_2)^2 + \dots + (h_n - g_n)^2} \quad (2)$$

$|\Delta G|$ represents the total grey-level difference between two dates. The greater $|\Delta G|$ is, the higher is the possibility of a change. A decision that change has occurred is made based on whether the change magnitude exceeds a specified threshold. Once a pixel is identified as a change pixel,

the direction of ΔG should be examined further to determine the type of change for the pixel because the direction of the vector contains this information. The change type is often identified using the angle of the vector in two spectral dimensions, or sector codes if more than two spectral dimensions are involved. The geometric concept of CVA is applicable to any number of spectral bands, regardless of the measurement scale of radiance.

3.1 Selection of optimal threshold

Traditionally, the threshold of change magnitude is empirically determined based on the analyst's experience. This is subjective and varies from person to person. It is necessary to develop an automatic or semi-automatic method for this purpose. Chen et al. (in press) developed a DFPS algorithm. Threshold selection is based on sample areas containing all possible types of change. It is assumed that the sample area is representative to the entire study area. Thus, a threshold leading to the maximum accuracy of change detection within the sample area (as training data) is considered optimal for the entire study area. Based on this assumption, the flowchart of DFPS is shown in Figure 11-5 and its main steps are described in the following.

3.1.1 Selection of typical sample areas of land use / cover change

After $|\Delta G|$ is calculated from two images of different dates, some typical change areas are chosen as sample areas from the image of the later date in order to search for the optimal threshold to differentiate change and no-change pixels. This is carried out by comparing the two images with ancillary ground information. The images should be precisely registered and radiometrically calibrated in advance to allow for precise comparison and selection of sample areas.

The criteria for selecting sample areas are: (1) sample areas should cover as many change types as possible. Note that a change type is identified only by image colour and texture because the real change type has not been categorised at this stage; (2) sample areas should include only change pixels; and (3) sample areas should be encircled by no-change pixels as "islands". The threshold for identifying change and no-change pixels can be determined by searching for an optimal value of change magnitude to obtain the maximum accuracy of change detection within the sample areas. Obviously, as the threshold of change magnitude decreases, the number of change pixels inside a sample area will increase and the accuracy of change detection will be improved. However, it should be noted that the possibility of no-change pixels outside the sample area being identified as change pixels

would also increase leading to higher commission error. In consideration of this, an outside boundary is created by building a buffer (dashed boundary) for each sample area, forming a double area (called double-window). The outside boundary is used to assess the commission errors as the threshold changes (Figure 11-6).

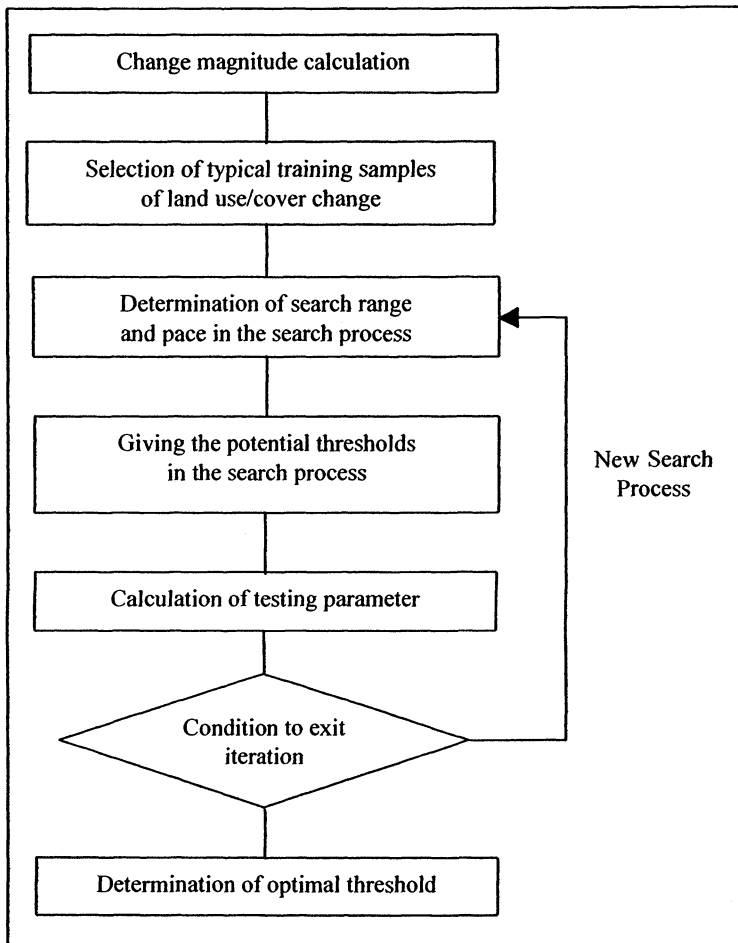


Figure 11-5. Flowchart of the Double-windows Flexible Pace Search (DFPS) method.

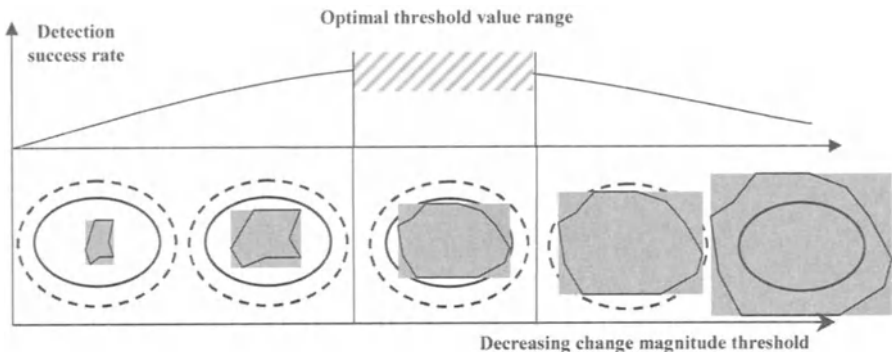


Figure 11-6. The relationship between the accuracy of change detection and threshold decrease in one training sample. The dashed area corresponds to an optimal threshold value.

3.1.2 Determination of the search range and pace

The threshold search range can be set as a difference between the minimum value (a) and the maximum value (b) of change magnitude, while the first search pace (increment) P_1 may be calculated according to the following:

$$P_1 = (b-a)/m \quad (3)$$

where m is a positive integer that can be set by examining the histogram of change magnitude. The potential thresholds to detect change pixels from the sample areas in one search process are given within the range of $[a, b]$ as $b - P_1$, $b - 2P_1$, and so on.

3.1.3 Definition and calculation of testing parameter

The success rate of change detection (L_k) for a threshold of k can be defined as following:

$$L_k = \frac{(A_{k1} - A_{k2}) \times 100}{A} \% \quad (4)$$

where A_{k1} is the number of change pixels detected inside sampling areas, A_{k2} is the number of change pixels which are detected incorrectly in the outside boundary of sampling areas and A is the total number of pixels within all the sample areas. In order to keep L_k from becoming negative, the outside border should be set to one or two pixels. From this definition of success rate, it is easy to see that the double-window concept is useful in controlling the commission error of change detection. Once the maximum

value of L_k is obtained at a particular threshold value k , the next search range is set in the range $[k-P_1, k+P_1]$ and a new smaller search pace is set based on the modified search range with formula (3).

3.1.4 Condition to exit the iteration

The steps described above are in an iterating process (Figure 11-5), which will terminate when the following formula is satisfied.

$$L_{\max} - L_{\min} \leq \delta \quad (5)$$

where L_{\max} and L_{\min} are the maximum and minimum values of the success rate in one search process, and δ is an acceptable error constant. The condition indicates that the change of search pace has little influence on the result of change detection. The threshold corresponding to L_{\max} is considered as an optimal threshold for change detection. The method of Double-Window Flexible Pace Search (DFPS) is a semi-automatic method for determining optimal threshold of change detection that only requires user involvement during the selection of typical sample areas of land use / cover change. The advantages of this method can be summarised as: (1) the optimal threshold can be obtained automatically after the selection of typical sample areas of land use / cover change; (2) the commission error caused by excessively decreasing the threshold can be controlled effectively through the double-window technique; (3) search efficiency is improved with the flexible and varied search pace. Although the new method may perform better compared with some previous empirical methods, it should be noted that it is dependent on sample area selection, which relies to a certain degree on the experience and skills of the image analyst.

3.2 Change identification method

Discrimination of change types plays an important role in change detection. Problems associated with existing change type discrimination by CVA were noted by Cohen and Fiorella (1998). They pointed out the possibility of other angle measurements for change vectors in three or more spectral dimensions, and noticed the importance of a 'reference image' in change type discrimination. Therefore it is necessary to combine single image classification (as a reference image) with minimum distance categorising based on direction cosines of a change vector. The direction of a vector can be described by a series of cosine functions in a multi-dimensional space. The direction of change vector containing change type information can also be defined by the cosine function of angles between the

vector and each axis. The change vector direction of one change pixel corresponds to one and only one point in a multi-dimensional space constituted by direction cosines. If some typical feature points (hereafter called seed points) and their corresponding change types in the space of direction cosines are known, the change type of a change pixel can be determined by a supervised classification on the basis of its proximity to those seed points. Obtaining seed points and their corresponding change types is the key to change type discrimination for all change pixels. For two images acquired on different dates T_1 and T_2 , after rigorous radiometric normalisation, we may assume that the spectral feature difference between any two kinds of cover types on either date are similar to their spectral change features from T_1 to T_2 . Using this assumption, we can firstly calculate the spectral difference vectors between any two kinds of cover types in a reference image and then transplant them into the direction cosine space. These points can be considered as the seed points (mean vectors) in a supervised classification for change type discrimination because their features are typical and their co-ordinates and change types are known.

3.2.1 Definition of direction cosines of change vector

Suppose $X(x_1, x_2, x_3, \dots, x_n)$ is an n dimensional vector, its magnitude can be calculated as:

$$|X| = \sqrt{x_1^2 + x_2^2 + x_3^2 + x_4^2 + \dots + x_n^2} \quad (6)$$

If the angles between X and each axis are $(\theta_1, \theta_2, \theta_3, \theta_4, \dots, \theta_n)$, respectively, and its direction can be described by cosine functions of these angles as

$$\cos\theta_1 = \frac{x_1}{|X|}, \quad \cos\theta_2 = \frac{x_2}{|X|}, \quad \dots, \quad \cos\theta_n = \frac{x_n}{|X|} \quad (7)$$

Through formula (7), the direction of a change vector can be represented as one and only one point, defined as a new vector $Z(\cos\theta_1, \cos\theta_2, \dots, \cos\theta_n)$, in the direction cosine space. All of the change pixels have their corresponding points in this space. According to this definition, the determination of change types is turned into a classification problem of points in the direction cosine space. Moreover, using the direction cosines instead of angle measurements can avoid the difficulty of 'baseline' establishment for angle measurement.

3.2.2 Extraction of all possible change types and their corresponding seed points

For two images acquired on different dates T_1 and T_2 , after rigorous radiometric normalisation, the spectral feature differences between any two kinds of cover types on either date are similar to their spectral change features from T_1 to T_2 . This assumption can be denoted as:

$$\Delta W_{ij} = P_j - Q_i \Leftrightarrow \Delta T_{ij} = H_j - G_i \quad (8)$$

where P_j , Q_i are grey value vectors of cover types j and i in either image of date T_1 or T_2 , ΔW_{ij} is their spectral difference vector; G_i and H_j are grey value vectors of cover types i and j at different dates T_1 and T_2 , ΔT_{ij} is spectral change vector from date T_1 to T_2 . Accordingly, surface cover classification is first carried out as accurately as possible on one of the images from either T_1 or T_2 . Then spectral difference vectors between any two kinds of cover types in the reference image are calculated. With formula (8), the spectral difference vectors can be thought of as equivalents of spectral change vectors of those cover changes. The mean of spectral difference vectors represents a typical feature of various changes between any two kinds of cover types, and direction cosine values of the mean of spectral difference vectors can be specified as seed points in the direction cosine space. Moreover, the standard deviation of spectral difference vectors that belong to the same change type can also be used to determine the threshold of unclassified class in a minimum distance classifier.

The mean of spectral difference vectors and their standard deviation can be calculated easily. It is assumed that grey values of pixels of various cover types in every band are normally distributed and independent of one another. We used EX_i , DX_i , EX_j , DX_j to denote the mean and standard deviation of the pixels classified to land use / cover types i and j , respectively.

$$EX_i = (EX_{i1}, EX_{i2}, EX_{i3}, EX_{i4}, \dots, EX_{in})^T \quad (9)$$

$$DX_i = (DX_{i1}, DX_{i2}, DX_{i3}, DX_{i4}, \dots, DX_{in})^T \quad (10)$$

$$EX_j = (EX_{j1}, EX_{j2}, EX_{j3}, EX_{j4}, \dots, EX_{jn})^T \quad (11)$$

$$DX_j = (DX_{j1}, DX_{j2}, DX_{j3}, DX_{j4}, \dots, DX_{jn})^T \quad (12)$$

Based on stochastic theory, if p, q are mutually independent and subject to normal distribution $p \sim N(u_1, \sigma_1^2)$, $q \sim N(u_2, \sigma_2^2)$, then $z = p - q$ (subject to normal distribution with $z \sim N(u_1 - u_2, \sigma_1^2 + \sigma_2^2)$). Thus the mean and the standard deviation of spectral difference vector of cover types j and i can be simply deduced from EX_i , DX_i , EX_j , DX_j as following:

$$EX_{ij} = (EX_{j1} - EX_{i1}, EX_{j2} - EX_{i2}, \dots, EX_{jn} - EX_{in})^T \quad (13)$$

$$DX_{ij} = (\sqrt{DX_{j1}^2 + DX_{i1}^2}, \sqrt{DX_{j2}^2 + DX_{i2}^2}, \dots, \sqrt{DX_{jn}^2 + DX_{in}^2})^T \quad (14)$$

3.2.3 Change type discrimination based on minimum distance classification

Due to their simplicity and effectiveness, minimum distance classifiers are commonly used in supervised classification of remotely sensed data. The classifier assigns an unknown pixel to a certain class or unclassified class based on a minimum distance to means of all candidate classes when the distance is within a certain threshold (Jensen 1996). It can be used to categorise change types in three steps: (1) calculating direction cosines of the spectral change vector for each change pixel according to formula (7); (2) calculating Euclidean distances of the changed pixels to seed points, obtained through classification in a reference image, corresponding to all possible change types in the direction cosine space; and (3) determining change types by applying the minimum distance rule. As with a conventional minimum distance classifier, the unclassified pixels are those falling outside the threshold range, based on the mean and standard deviation of every class. Those pixels may stand for new change types which are not already included in all possible change types obtained through land cover classification in the reference image.

As illustrated in Figure 11-3, this method is applicable, not only to multispectral data directly available from images of two different dates, but also to their derivatives such as vegetation indices and other physically meaningful features such as brightness and greenness as derived from KT transform which will be discussed in the next section. Allen and Kupfer (2001) analysed the changes of Fraser fir mortality using change vectors plotted in the 3D space of brightness, greenness and wetness. They converted two angles, the zenith (colatitude) and the azimuth (colongitude), and the change magnitude from the 3D space and plotted each angle with the magnitude to search for change patterns. Essentially, any intermediate product, such as texture features reflecting local spatial characteristics or

biophysical and biochemical parameters that can be derived from single-date imagery, can be subjected to CVA or DIF to detect change. Lambin and Strahler (1994a) applied CVA to detect interannual changes based on annual sequences of vegetation indices derived from NOAA AVHRR data. The 12 NDVI maximum composites in each vegetation growing cycle in western Africa were treated in the same manner as multi-spectral data in the same day. They further compared the annual surface temperature pattern and local variances calculated from AVHRR data to study interannual changes with CVA (Lambin and Strahler 1994b).

4. GRAMM-SCHMIDT TRANSFORMATION FOR CHANGE COMPONENT ENHANCEMENT

GST is a mathematical tool that operates rotational transformation in n-dimensional space, resulting in a series of orthogonal axes, each of which is a linear combination of the original axes. Applying GST to a single date multi-spectral image, Kauth and Thomas (1976) developed a set of new indices within the multi-spectral space constructed by the 4 bands of Landsat multi-spectral scanner (MSS). The new indices are brightness, greenness, yellowness and nonesuch. This transformation process is known as Tasseled Cap transform or KT transform. The brightness was developed based on a soil line linked between wet and dry soils in the multi-spectral space while the greenness was developed along a line drawn from a closed canopy vegetation point perpendicular to the soil line. These two indices can explain the majority of the image variation and are found to be related to surface cover conditions while the yellowness and nonesuch are sensitive to conditions of haze and water vapour in the atmosphere, respectively (Jackson 1983). Since the last two indices are related to exogenous factors that are considered as noise in terrestrial remote sensing, only brightness and greenness are widely used for Landsat MSS data. The coefficients for each of the indices are found in Kauth and Thomas (1976). For Landsat TM data the number of useful indices has been increased to 3 – brightness, greenness and wetness (Crist 1985).

The advantage of GST is that it enables one to create physically meaningful indices based on knowledge extracted from the images under investigation. Therefore, we can apply GST to images acquired by any type of sensor. For different applications, a different set of indices can be produced. In the following, we summarise the procedure of GST followed by an explanation of its application to multi-temporal images.

It requires $m+1$ pixel grey level vectors (X_1, X_2, \dots, X_{m+1}) to derive m indices. The first index is defined by a difference vector between two of the

grey level vectors, $X_2 - X_1$. Normalising this vector to unit length we have the coefficients for the first index,

$$V_1 = (X_2 - X_1) / |X_2 - X_1| \quad (15)$$

The coefficients for the second index are obtained by finding the unit vector along the perpendicular line of V_1 passing through X_3 . This can be obtained by first projecting vector $X_3 - X_1$ to the direction of V_1 , $(X_3 - X_1) \cdot V_1 V_1$, then subtracting the projected vector from vector $X_3 - X_1$ to obtain the perpendicular vector to V_1 ,

$$U_2 = (X_3 - X_1) - (X_3 - X_1) \cdot V_1 V_1 \quad (16)$$

Normalising U_2 we have the coefficients of the second index:

$$V_2 = U_2 / |U_2| \quad (17)$$

To derive the coefficients for the third index, we first find the line that is perpendicular to both V_1 and V_2 and passing through X_4 .

$$U_3 = (X_4 - X_1) - (X_4 - X_1) \cdot V_1 V_1 - (X_4 - X_1) \cdot V_2 V_2 \quad (18)$$

Similarly we get V_3 by normalising U_3 , $V_3 = U_3 / |U_3|$. This procedure guarantees that all indices derived in this manner are perpendicular to each other, implying the newly generated indices having no correlation among them. This procedure can be generalised to produce m indices and for the m^{th} index, $U_m = (X_{m+1} - X_1) - (X_{m+1} - X_1) \cdot V_1 V_1 - (X_{m+1} - X_1) \cdot V_2 V_2 - \dots - (X_{m+1} - X_1) \cdot V_{m-1} V_{m-1}$ followed by a normalisation of U_m .

Fung (1990) extended the KT-transform to two-date images by introducing three change vectors, brightness change ΔB , greenness change ΔG , wetness change ΔW , each of which is composed of two sets of coefficients with alternate signs and normalized to unity. By alternating the signs and applying the coefficients to a combined set of images, one achieves the same effect as applying the regular KT-transform to each single date image and subtracting the resultant values. Collins and Woodcock (1996) expanded this idea and suggested a multi-temporal KT transform (MKT):

$$M = 0.707 \begin{bmatrix} K & -K \\ K & K \end{bmatrix} \quad (19)$$

where M is the 12×12 multi-temporal KT matrix and K is the regular KT transform for TM imagery. The constant normalises row vectors to unity. Applying this matrix will result in 6 change vectors and 6 "stable" vectors. K can be constructed by following the method discussed above or using existing coefficients. Collins and Woodcock (1996) used the 6×6 KT coefficient matrix developed by Crist and Cicone (1984) for TM data. M is a transformation that not only preserves all the information from the original images but also compares the differences between the two TM images from two different dates. Although MKT is feasible, not all the indices are helpful to change detection. For certain applications one must evaluate the suitability of each change vector (index) in order to find the most effective one. This is more or less a data driven approach. If a particular type of change is to be derived and its spectral properties can be clearly identified, a goal (type of change) driven approach may be attempted. This would require one to construct a set of indices (i.e., change vectors) that are change specific and image specific. Collins and Woodcock (1994) constructed such indices for the detection of forest mortality in Lake Tahoe region of California. They used GST to determine change indices and applied them to a 10-band multi-temporal set of images (TM2-5 and TM7 from one 1988 and one 1991 scene). TM 1 was not used due to the high correlation among the visible bands. Both images were acquired in July. They constructed a four component GST by first selecting 5 vectors (Table 11-2).

The vectors in Table 11-2 are chosen by analysing both images. The first and second vectors were chosen from the 10-band image with a forest map (barren type) as a guide. A mean of six darkest soil samples was used as the "dark soil" vector. Similarly, a mean of six brightest soil samples was used as the "bright soil" vector. The two vectors constitute a soil line and the difference of the two vectors after normalisation becomes the brightness index (vector). Spectral vectors with low mortality and fairly distant from the soil line were chosen to construct the "healthy forest" vector. This leads to the construction of the greenness index. The "wetness-like" vector was chosen based on some empirical analysis of the data variation as explained by the two previously created indices, in comparison with the original data variability. The "mortality" vector was relatively easy to select. It was determined by taking the mean of high mortality stands. The resulting GST indices are listed in Table 11-3.

Multiplying each vector with the 10-band image, Collins and Woodcock (1994) obtained the four indices as listed in Table 11-3. The brightness, greenness, wetness, and change indices accounted for 78.3 %, 3.7 %, 13.6 % and 3 % of the total data variability, respectively. Of the four indices, the change in mortality index was found to have the highest correlation with field-surveyed mortality. Collins and Woodcock (1996) further compared the

GST change component approach with MKT and PCA over the Lake Tahoe area of California using all 12-band Landsat TM data acquired in 1991 and 1994. With radiometrically calibrated TM data, they found that the GST change index alone could predict mortality with an R^2 value of 0.60 to 0.70. Using PCA with multiple (3-5) components, a multivariate linear model can predict mortality with an R^2 value of 0.76 to 0.78. Using the three change indices from MKT (changes in brightness, greenness and wetness), a multivariate linear model can predict mortality with an R^2 value of 0.69 to 0.77. The index for change in wetness alone has a similar mortality predicting power to the GST change index.

Table 11-2. Spectral vectors used to build GST indices (Adapted from Collins and Woodcock 1994).

	Dark soil	Bright soil	Healthy forest	“Wetness-like”	Forest mortality
1988 TM 2	42	52	31	40	27
1988 TM 3	53	69	35	47	29
1988 TM 4	60	80	65	73	66
1988 TM 5	78	132	70	74	50
1988 TM 7	44	73	32	37	20
1991 TM 2	42	50	29	38	27
1991 TM 3	54	69	34	48	30
1991 TM 4	56	75	60	68	60
1991 TM 5	74	130	67	73	52
1991 TM 7	43	73	30	36	22

Table 11-3. GST vectors as derived from Table 11-5 (Adapted from Collins and Woodcock 1994).

	Brightness	Greenness	Wetness	Change in mortality
1988 TM 2	0.095	-0.312	0.153	-0.161
1988 TM 3	0.173	-0.445	0.193	-0.356
1988 TM 4	0.211	0.309	0.609	0.108
1988 TM 5	0.561	0.182	-0.271	-0.568
1988 TM 7	0.300	-0.181	-0.218	-0.148
1991 TM 2	0.088	-0.356	0.182	0.107
1991 TM 3	0.163	-0.529	0.250	0.172
1991 TM 4	0.198	0.278	0.558	-0.161
1991 TM 5	0.580	0.186	-0.140	0.451
1991 TM 7	0.319	-0.161	-0.143	0.471

5. CHALLENGES AND OPPORTUNITIES

In Table 11-1, we listed a number of different types of changes. There are more forest variables whose changes need to be monitored. These include species, coverage, height, volume, LAI, biomass, biochemical constituents, light condition, age, structure and forest environmental conditions such as soil temperature and moisture. No single source of remotely sensed data allows successful parameterisation of all these variables. Different sources of data, including photography, multi(hyper)spectral imaging, thermal imaging, field spectrometer, radar, lidar, and ultrasounding, on board a variety of platforms, should be considered for the extraction of forest change information. However, some of the remote sensing sources are more expensive than others, which is partly the reason why the more economical sources such as NOAA AVHRR and Landsat TM data have been widely applied to forest change detection efforts.

Some of the forest change types are categorical, while others require more quantitative analysis. When change and no-change must be distinguished, it is critical to determine the optimal threshold as discussed in some of the change detection algorithms based on image differencing, CVA and change indices. The DFPS algorithm could be applied to other difference-based change detection techniques. On the other hand, all change indices derived from multi-temporal images using techniques such as CVA, MKT and PCA contain quantitative information about change. For example, although not popularly used, magnitudes and angles in CVA analysis can be quantitatively correlated with other biophysical and biochemical factors to build prediction models, as was done by Collins and Woodcock (1996) with GST, MKT and PCA features.

In general, the more qualitative the change type, the easier it is to detect. Some change detection algorithms, such as those based on image classification, can only derive categorical change information. We believe that it is more important to develop capabilities for quantitative change detection so that subtle change in forest variables can be detected. This is clearly not an easy task and quantitative change detection is related to almost all information extraction strategies currently available. In an effort to develop the framework of photo-ecometrics, (Gong et al. 1999), Gong (forthcoming) has summarised six types of information extraction strategies for remotely sensed data. These include image classification, regression, shape extraction and analysis, morphological information extraction, inversion of radiative transfer models, and change detection. In fact, each of the first five strategies can be applied to single-date images acquired in a time sequence. The extracted information can then be compared to detect changes. For example, morphological information about such surface

features as tree crowns and topographic landforms can be derived from digital photogrammetry (Gong et al. 2000; Sheng et al. 2001), radar interferometry (e.g., Armour et al. 1998) and lidar techniques (e.g., Sun and Ranson 2000; Naesset 2002; Drake et al. 2002; St-Onge et al., Chapter 19). Canopy morphological information derived from any of these data acquired at different times can be compared to infer information about changes in canopy closure, height and biomass. Therefore, it is important to further evaluate the potential of different types of data source and different data analysis techniques in order to produce better change detection results. Additionally, different methods should be integrated for more effective use of different types of remotely sensed data in detection and identification of changes. An obvious area for further exploration is the integrated use of optical and microwave remote sensing in change detection.

We discussed earlier the minimum units of change detection. While most change detection methods have been proposed for change detection on a pixel basis, techniques have been developed for change detection at the stand level (e.g., Coppin and Bauer 1994). A stand is the smallest unit on which a forest resource is mapped when minimum mapping unit and resource management decisions are made. Naturally, it is helpful to combine stand information as an ancillary information source to remotely sensed data for change detection. At the stand level, spatial features such as texture and local variance can be used in change detection (Smits and Annoni 2000). However, it is necessary to go beyond the pixel and stand level or to use multiple spatial scales in change detection. At this point, spectral unmixing to obtain information at the sub-pixel levels and the calculation of landscape indices such as those used in landscape ecology are helpful (e.g., McGarigal and Marks 1995). Additionally, new methods such as echelon analysis, which operates at the watershed scale or larger for characterising spatial structural differences, should be evaluated (Smits and Myers 2000). Change detection methods that are object-oriented and allow for examination of spatial change processes such as forest fragmentation and succession should be further developed.

The multi-temporal analysis techniques examined in this Chapter are mostly “bi-temporal” although works using a real multi-temporal set of data have been mentioned (e.g., Lambin and Strahler 1994a, 1994b; Li et al. 2000). The only real multi-temporal data analysis methods are found in forest fire scar mapping and in global change studies of temperature and vegetation conditions. Techniques related to multi-temporal analysis of vegetation trends are usually done through statistical and time series analysis which is not emphasised here. Truly multi-temporal or hyper-temporal change analysis will become more and more important as the need for multi-temporal remotely sensed data in global change studies increases. When

multiple date images are used for trend analysis, stricter requirements should be placed on geometric correction and radiometric calibration. There are some results which show that the calibration of multi-temporal imagery slightly reduces the change detection accuracy (e.g., Collins and Woodcock 1996). Although we have reviewed some of the methods that simulate mis-registration errors and investigated their effects on the increase of false change detection, a full assessment of errors occurring in the image registration process among multiple date images should be further investigated. In particular, methods should be developed to detect and fix registration errors. A possible solution is to register images based on image matching of local neighbourhoods, rather than applying a general polynomial model to co-ordinate transformation.

Based on results obtained from the application of bi-temporal Landsat TM data, the most successful application of forest change detection has been in distinguishing clear-cuts from standing forest. Insect defoliation classifications have only been moderately successful. Reliable insect defoliation monitoring has often been limited to three classes (e.g., heavy, medium, and light) with accuracies around 70–80 %. Low defoliation levels remain difficult to detect (Radeloff et al. 1999). Low intensity thinning is also difficult to detect (Olsson 1995).

The final point we wish to make is the importance of assessing the accuracy of change detection and identification results. Biging et al. (1998) proposed a sampling and assessment scheme for assessing a change map with thematic information. The assessment of accuracy in predicting changes in biophysical and biochemical conditions of forests is equally important. Although correlation analysis is informative, more direct procedures should be adopted to evaluate change prediction results by assessing errors calculated from an independent source of measurements.

REFERENCES

- Adams, J. B., Sabol, D. E., Kapos, V., Almeida Filho, R., Roberts, D. A., Smith, M. O., & Gillespie, A. R. (1995). Classification of multispectral images based on fractions of endmembers: application to land-cover change in the Brizilian Amazon. *Remote Sensing of Environment*, 52, 137-154.
- Allen, T. R., & Kupfer, J. A. (2001). Spectral response and spatial pattern of Fraser fir mortality and regeneration, Great Smoky Mountains, USA. *Plant Ecology*, 156, 59-74.
- Armour, B., Tanaka, A., Ohkura, H., Saito, G. (1998). Radar interferometry for environmental change detection. Lunetta R. S. & Elvidge C. D. (Eds.). *Remote Sensing Change Detection, Environmental Monitoring Methods and Applications*, 245-279. Ann Arbor Press. Chelsea, Michigan, USA.
- Biging, G. S., Colby, D. R., & Congalton, R. G. (1998). Sampling systems for change detection accuracy assessment. Lunetta, R. S. & Elvidge C. D. (Eds.). *Remote Sensing*

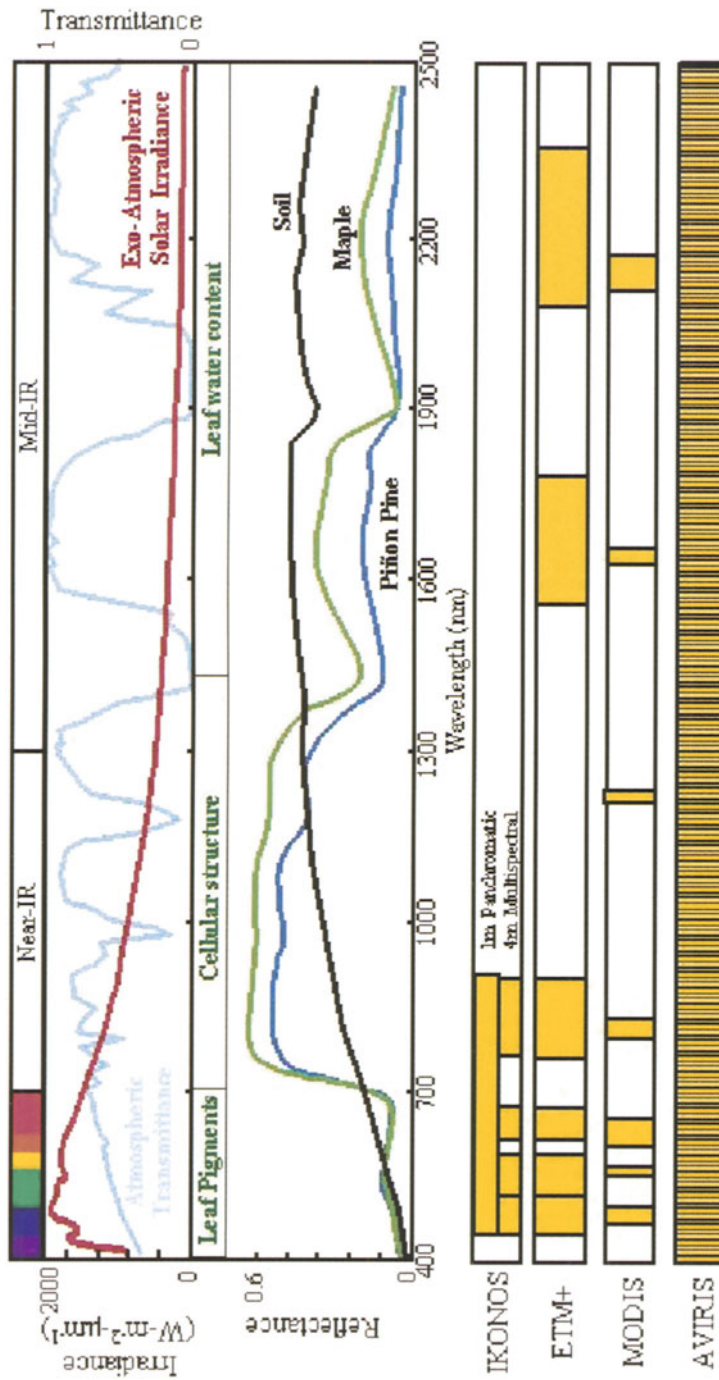
- Change Detection, Environmental Monitoring Methods and Applications*, 281-308. Ann Arbor Press. Chelsea, Michigan.
- Bruzzone, L., & Fernandez Prieto, D. (2000). Automatic analysis of the difference image for unsupervised change detection. *IEEE Transactions on Geoscience and Remote Sensing*, 38, 1171-1182.
- Chalifoux, S., Cavayas, F., & Gray, J. T. (1998). Map-guided approach for automatic detection of Landsat TM images of forest stands damaged by spruce budworm. *Photogrammetric Engineering and Remote Sensing*, 64, 629-635.
- Chen, J., Gong, P., He, C., Pu, R., & Shi, P. (in press). Land use / cover change detection using improved change vector analysis . *Photogrammetric Engineering and Remote Sensing*
- Cohen, W. B., & Fiorella, M. (1998). Comparison of Methods for Detecting Conifer Forest Change with Thematic Mapper Imagery. Lunetta R.S. & Elvidge C. D. (Eds.). *Remote Sensing Change Detection, Environmental Monitoring Methods and Applications*, 89-102. Ann Arbor Press. Chelsea, Michigan.
- Collins, J. B., & Woodcock, C. E. (1994). Change detection using the Gramm-Schmidt transformation applied to mapping forest mortality. *Remote Sensing of Environment*, 50, 267-279.
- Collins, J. B., & Woodcock, C. E. (1996). An assessment of several linear change detection techniques for mapping forest mortality using multitemporal Landsat TM data. *Remote Sensing of Environment*, 56, 66-77.
- Coppin, P. R., & Bauer, M. E. (1994). Processing of multitemporal Landsat TM imagery to optimize extraction of forest cover change detection. *IEEE Transactions on Geoscience and Remote Sensing*, 32, 918-927.
- Coppin, P., Nackaerts, K., Queen, L., & Brewer, K. (2001). Operational monitoring of green biomass change for forest management. *Photogrammetric Engineering and Remote Sensing*, 67, 603-611.
- Crist, E. P., (1985). A TM tasseled cap equivalent transformation for reflectance factor data. *Remote Sensing of Environment*, 17, 301-306.
- Crist, E. P., & Cicone, R. C. (1984). A physically-based transformation of thematic mapper data-the TM tasseled cap, *IEEE Transactions on Geoscience and Remote Sensing*, 22, 256-263.
- Cushman, S.A., & Wallin, D. O. (2000). Rates and patterns of landscape change in the Central Sikhote-alin Mountains, Russian Far East. *Landscape Ecology*, 15,643-659.
- Dai, X., & Khorram, S. (1998). The effects of image misregistration on the accuracy of remotely sensed change detection. *IEEE Transactions on Geoscience and Remote Sensing*, 36, 1566-1577.
- Diem, J. E. (2002). Remote sensing of forest health in southern Arizona, USA: evidence for ozone-induced foliar injury. *Environ Manage* 29, 373-384.
- Drake, J. B., Dubayah R. O., Clark, D. B., et al. (2002). Estimation of tropical forest structural characteristics using large-footprint lidar. *Remote Sensing of Environment*, 79, 305-319.
- Foody, G. M., & Boyd, D. S. (1999). Detection of partial land cover change associated with the migration of inner-class transitional zones. *International Journal of Remote Sensing*, 20, 2723-2740.
- Franklin S. E., (1989). Classification of hemlock looper defoliation using SPOT HRV imagery. *Canadian Journal of Remote Sensing*, 15, 178-182.
- Franklin S. E., & Raske, A. G. (1994). Satellite remote sensing of spruce budworm forest defoliation in western Newfoundland. *Canadian Journal of Remote Sensing*, 20, 37-48.

- Fung, T., & LeDrew, E. F. (1987). Application of principal component analysis to change detection. *Photogrammetric Engineering & Remote Sensing*, 53, 1649-1658.
- Fung, T. (1990). An assessment of TM imagery for land cover change detection. *IEEE Transactions on Geoscience and Remote Sensing*, 28, 681-684.
- Gong, P. (1993). Change detection using principal component analysis and fuzzy set theory. *Canadian Journal of Remote Sensing*, 19, 22-29.
- Gong, P. (forthcoming). Photo-ecometrics for natural resources monitoring. Andrea, G., Fabbri, G. G., & McCammon, R. B. (Eds.). *Deposit and Geoenvironmental Models for Resource Exploitation and Environmental Security*. Kluwer Academic Press, Dordrecht, The Netherlands.
- Gong, P. (2002). *Remote Sensing and Image Analysis Textbook* (web site: <http://camfer.cnr.berkeley.edu/~gong/textbook> (accessed August 14, 2002)
- Gong, P., Biging, G., & Standiford, R. (2000). The potential of digital surface model for hardwood rangeland monitoring, *Journal of Range Management*, 53, 622-626.
- Gong, P., Biging, G. S., Lee, S. M., Mei, X., Sheng, Y., Pu, R., Xu, B., & Schwarz, K.-P. (1999). Photo-ecometrics for forest inventory, *Geographic Information Sciences*, 5, 9-14.
- Gong, P., LeDrew, E. F., & Miller, J. R. (1992) Registration noise reduction in difference images for change detection. *International Journal of Remote Sensing*, 13, 773-779.
- Gong, P., Miller, J. R., & Spanner, M. (1994). Forest canopy closure from classification and spectral unmixing: a multi-sensor evaluation of application to an open canopy. *IEEE Transactions on Geoscience and Remote Sensing*, 32, 1067-1080.
- Gopal, S., & Woodcock, C. (1996). Remote sensing of forest change using artificial neural networks *IEEE Transactions on Geoscience and Remote Sensing*, 34, 398-404.
- Grover, K., Quegan, S., & Freitas, C. D. (1999). Quantitative estimation of tropical forest cover by SAR, *IEEE Transactions on Geoscience and Remote Sensing*, 37, 479-490.
- Hame, T., Heiler, I., & San Miguel-Ayanz, J. (1998). An unsupervised change detection and recognition system for forestry. *International Journal of Remote Sensing*, 19, 1079-1099.
- Hayes, D. J., & Sader, S. A. (2001). Comparison of change detection techniques for monitoring tropical forest clearing and vegetation regrowth in a time series. *Photogrammetric Engineering and Remote Sensing*, 67, 1067-1075.
- Hessburg, P. F., Smith, B. G., & Salter, R. B. (2000). Recent changes (1930s-1990s) in spatial patterns of interior northwest forests, USA. *Forest Ecology and Management*, 136, 53-83.
- Howarth, P. J., & Wickware, G. M. (1981). Procedure for change detection using Landsat digital data. *International Journal of Remote Sensing*, 2, 277-291.
- Ingebritsen, S., & Lyon, R. (1985). Principal component analysis of multitemporal image pairs, *International Journal of Remote Sensing*, 6, 687-696.
- Jackson, R. D. (1983). Spectral indices in n-space, *Remote Sensing of Environment*, 13, 400-421.
- Johnson, R. D., & Kasischke, E. S. (1998). Change vector analysis: a technique for the multispectral monitoring for land cover and condition. *International Journal of Remote Sensing*, 19, 411-426.
- Jensen, J. R. (1996). *Introductory Digital Image Processing, A Remote Sensing Perspective*. Prentice Hall, Upper Saddle River, New Jersey.
- Kauth, R. J., & Thomas, G. S. (1976). The tasseled cap – a graphic description of the spectral-temporal development of agricultural crops as seen by Landsat. *Proceedings of the Symposium on Machine Processing of Remotely Sensed Data*, 4b, 41-51. June 21-July 1, Purdue University, West Lafayette, Indiana.

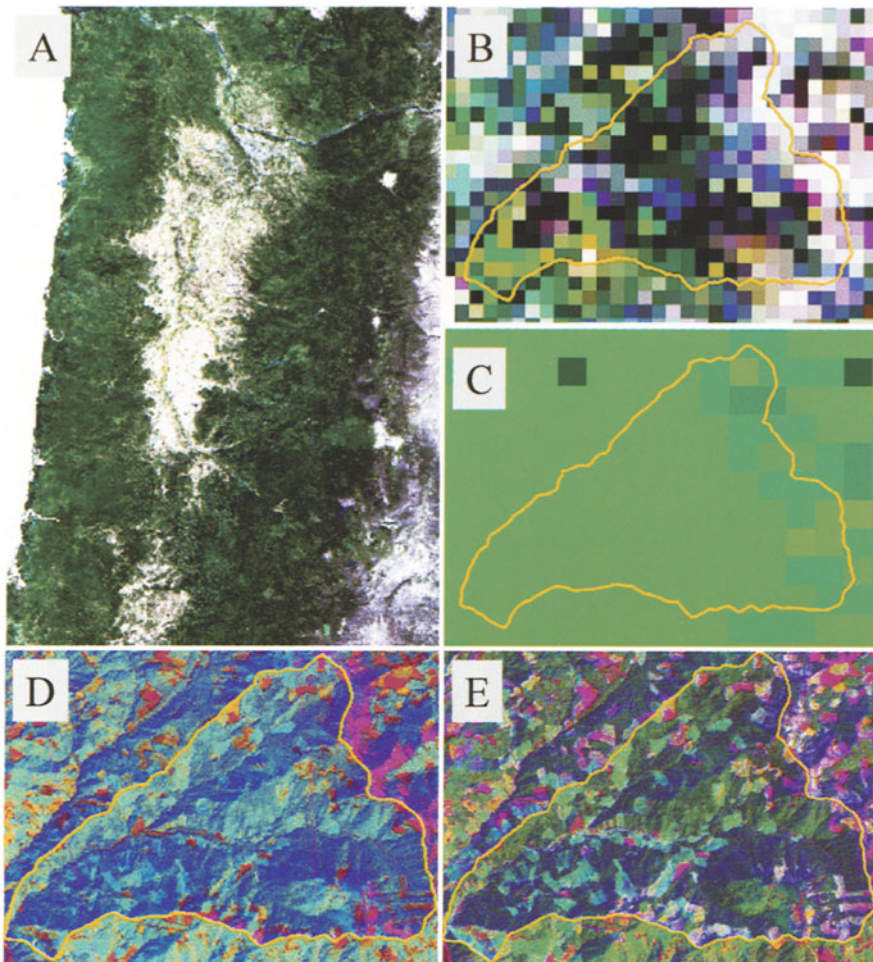
- Lambin, E. F., & Strahler, A. H. (1994a). Change vector analysis in multitemporal space: A tool to detect and categorize land-cover change processes using high temporal-resolution satellite data. *Remote Sensing of Environment*, 48, 231-244.
- Lambin, E. F., & Strahler, A. H. (1994b). Indicators of land-cover change for change vector analysis in multitemporal space at coarse spatial scales. *International Journal of Remote Sensing*, 15, 2099-2119.
- Leckie, D. G. (1987). Factors affecting defoliation assessment using Airborne Multispectral Scanner data. *Photogrammetric Engineering and Remote Sensing*, 53, 1665-1674.
- Li, Z., Nadon, S., & Cihlar, J. (2000). Satellite detection of Canadian boreal forest fires: Development and application of an algorithm, *International Journal of Remote Sensing*, 21, 3057-3069.
- Malila, W.A. (1980). Change vector analysis: an approach for detecting forest changes with Landsat. *Proc. Symposium Machine Processing of Remotely Sensed Data*, 326-336. Purdue University, West Lafayette, Indiana, USA, IEEE, Piscataway, New Jersey, USA.
- McGarigal, K., & Marks, B. J. (1995). *FRAGSTATS spatial pattern analysis program for quantifying landscape structure*. Report No PNW-GTR 351, USFS, Pacific Northwest Research Station, Portland.
- Michalek, J. L., Luczkovich, J. J., & Stoffle, R. W. (1993). Multispectral change vector analysis for monitoring coastal marine environments. *Photogrammetric Engineering and Remote Sensing*, 59, 381-384.
- Muchoney, D. M., & Haack, B. N. (1994). Change detection for monitoring forest defoliation. *Photogrammetric Engineering and Remote Sensing*, 60, 1243-1251.
- Myreni, R. B., Keeling, C. D., Tucker, C. J., Asrar, G., & Nemani, R. R. (1997). Increased plant growth in the northern high latitudes from 1981-1991. *Nature*, 386, 698-702.
- Naesset, E. (2002). Predicting forest stand characteristics with airborne scanning laser using a practical two-stage procedure and field data. *Remote Sensing of Environment*, 80, 88-99
- Nielsen A. A., Conradsen K., & Simpson, J. J. (1998). Multivariate alteration detection and MAF postprocessing in multispectral, bitemporal image data: new approaches to change detection studies. *Remote Sensing of Environment*, 64, 1-19.
- Olsson, H. (1994). Changes in satellite-measured reflectances caused by thinning cuttings in boreal forest, *Remote Sensing of Environment*, 50, 221-230.
- Olsson H. (1995). Reflectance calibration of thematic mapper data for forest change detection. *International Journal of Remote Sensing*, 16, 81-96.
- Pellikka, P. (2001). Application of vertical skyward wide-angle photography and airborne video data for phenological studies of beech forests in the German Alps. *International Journal of Remote Sensing*, 22, 2675-2700.
- Quegan S., Le Toan, T., & Yu, J. J. (2000). Multitemporal ERS SAR analysis applied to forest mapping. *IEEE Transactions on Geoscience and Remote Sensing*, 38, 741-753.
- Qi Y., & Gong, P. (1996). Metabolic and phenological response of vegetation to temperature gradient: evidence derived from AVHRR data. *Geographic Information Sciences*, 2, 64-72.
- Radeloff, V. C., Mladenoff, D. J., & Boyce, M. S. (2000). Effects of interacting disturbances on landscape patterns: budworm defoliation and salvage logging. *Ecological Applications*, 10, 233-247.
- Remmel, T. K., & Perera, A. H. (2001). Fire mapping in a northern boreal forest: assessing AVHRR/NDVI methods of change detection. *Forest Ecology and Management*, 152, 119-129.
- Richards, J. A., & Jia, X. (1999). *Remote Sensing Digital Image Analysis*. Springer, Berlin.

- Rigina O., Baklanov, A., & Hagner, O. (1999). Monitoring of forest damages in the Kola Peninsula, Northern Russia due to smelting industry. *Science of the Total Environment*, 229, 147-163.
- Rignot, E. J. M., & Vanzyl, J. J. (1993). Change detection techniques for ERS-1 SAR data. *IEEE Transactions on Geoscience and Remote Sensing*, 31, 1039-1046.
- Royle, D. D., & Lathrop, R. G., (1997). Monitoring hemlock forest health in New Jersey using Landsat TM data and change detection techniques. *Forest Science*, 42, 327-335.
- Sheng, Y., Gong, P., & Biging, G. S. (2001). Model-based conifer crown surface reconstruction from high-resolution aerial images. *Photogrammetric Engineering and Remote Sensing*, 67, 957-965.
- Silapaswan, C. S., Verbyla, D. L., & McGuire, A. D. (2001). Land cover change on the Seward Peninsula: The use of remote sensing to evaluate the potential influences of climate warming on historical vegetation dynamics *Canadian Journal of Remote Sensing*, 27, 542-554 .
- Singh, A. (1989). Digital change detection techniques using remotely-sensed data. *International Journal of Remote Sensing*, 10, 989-1003.
- Smits, P. C., & Annoni, A. (2000). Toward specification-driven change detection. *IEEE Transactions on Geoscience and Remote Sensing*, 38, 1484-1488.
- Smits, P. C., & Myers, W. L. (2000). Echelon approach to characterize and understand spatial structures of change in multitemporal remote sensing imagery. *IEEE Transactions on Geoscience and Remote Sensing*, 38, 2299-2309.
- Sohl, T. L. (1999). Change Analysis in the United Arab Emirates: An Investigation of techniques, *Photogrammetric Engineering and Remote Sensing*, 65, 475-484.
- Song, C., Woodcock, C. E., Seto, K., Lenney, M., & Macomber, S. (2001). Classification and change detection using landsat TM data: when and how to correct atmospheric effects? *Remote Sensing of Environment*, 75, 230-244.
- Sun, G. Q., & Ranson, K. J., (2000). Modeling lidar returns from forest canopies. *IEEE Transactions On Geoscience and Remote Sensing*, 38, 2617-2626
- Tokola, T., Lofman, S., & Erkkila, A. (1999). Relative calibration of multitemporal Landsat data for forest cover change detection. *Remote Sensing of Environment*, 68, 1-11.
- Townshend, J. R. G., Justice, C. O., Gurney, C., & McManus, J. (1992). The impact of misregistration on change detection. *IEEE Transactions on Geoscience and Remote Sensing*, 30, 1054-1060.
- Varjo, J., & Folving, S. (1997). Monitoring of forest changes using unsupervised methods: a case study from boreal forest on mineral soils. *Scandinavian Journal of Forest Research*, 12, 362-369.
- Verbyla, D. L., & Boles, S. H. (2000). Bias in land cover change estimates due to misregistration. *International Journal of Remote Sensing*, 3553-3560.
- Yuan, D., Elvidge C. D., & Lunetta, R. S. (1998). Survey of multispectral methods for land cover change analysis. Lunetta R. S. & Elvidge C. D. (Eds.). *Remote Sensing Change Detection, Environmental Monitoring Methods and Applications*, 21-39. Ann Arbor Press. Chelsea, Michigan.
- Zhan, X., Defries R., & Townshend, J. R. G., et al. (2000). The 250 m global land cover change product from the Moderate Resolution Imaging Spectroradiometer of NASA's Earth Observing System. *International Journal of Remote Sensing*, 21, 1433-1460.
- Zheng, D. L., Wallin, D. O., & Hao, Z. Q. (1997). Rates and patterns of landscape change between 1972 and 1988 in the Changbai Mountain area of China and North Korea. *Landscape Ecology*, 12, 241-254.

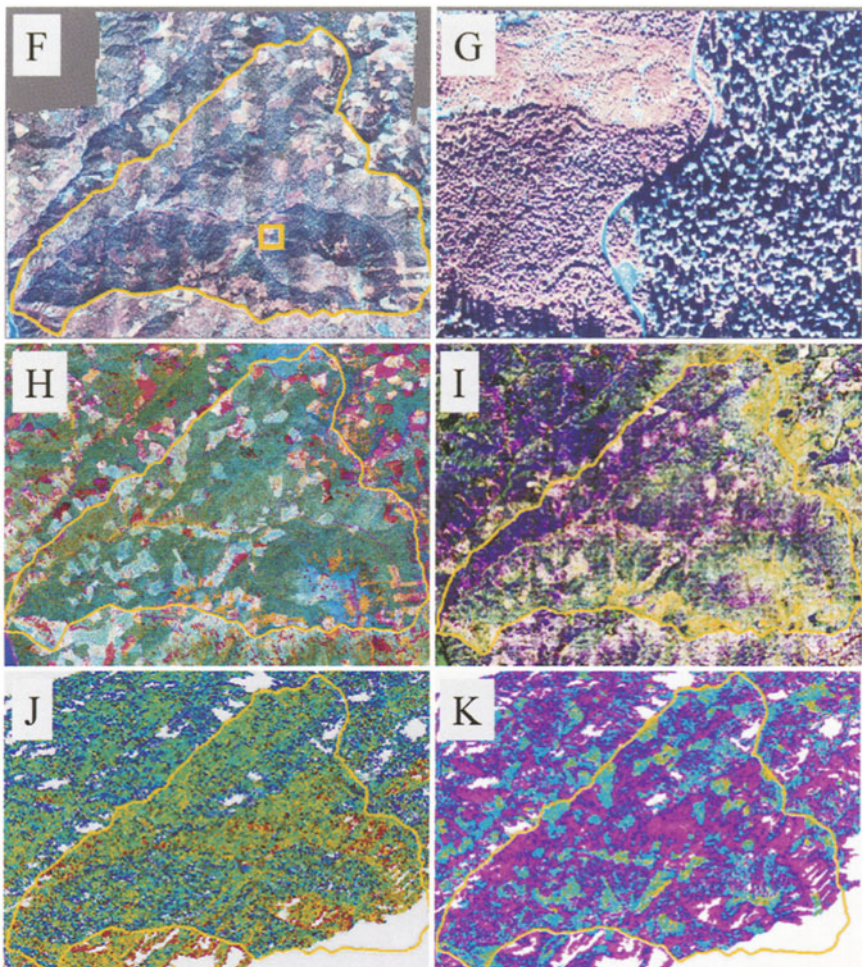
SECTION 3: CASE STUDIES ILLUSTRATING METHODS AND APPLICATIONS FOR REMOTE SENSING OF FORESTS



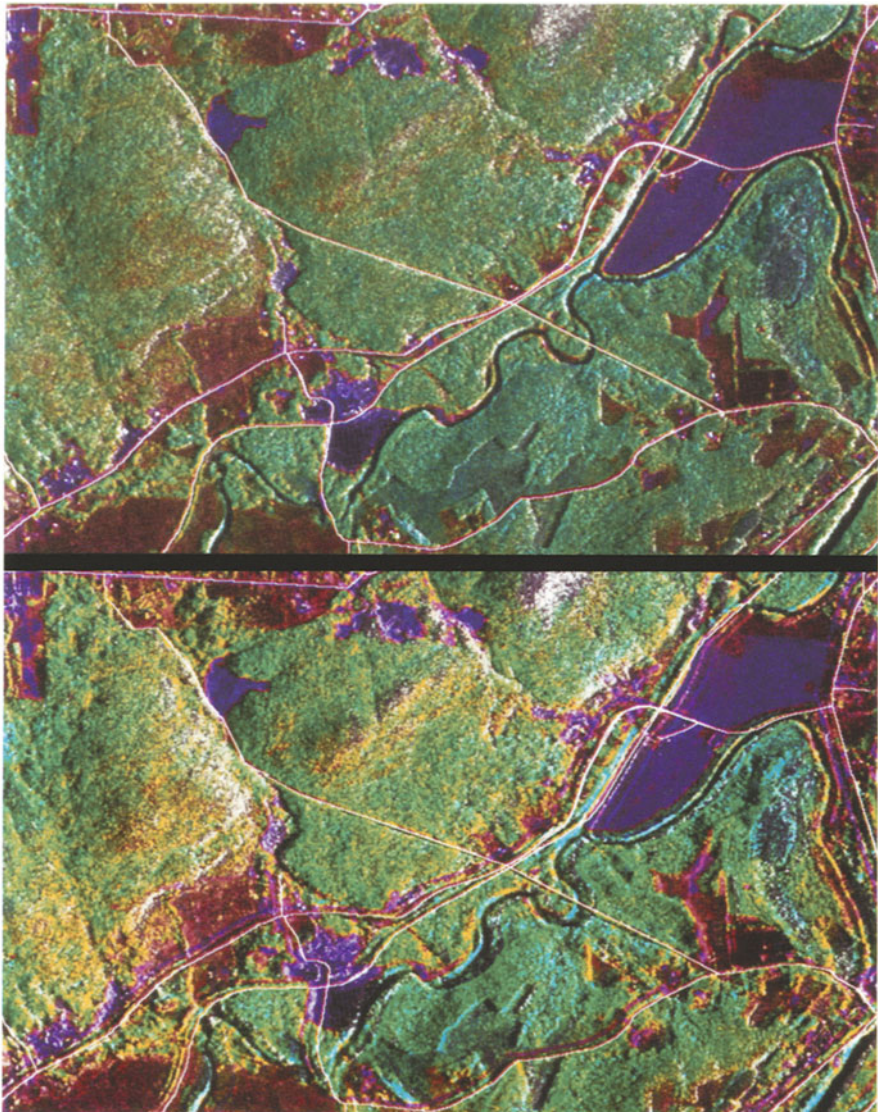
Colour Plate 1. Patterns of solar irradiance, atmospheric transmittance, and reflectance from 400 to 2500 nanometers. Uppermost insert displays the visible spectra and labels the near- and mid-infrared spectral regions. Top panel indicates the intensity of exo-atmospheric solar irradiance (red) and the degree of atmospheric transmittance (blue). Below this, an insert indicates what parts of foliage the wavelengths are most sensitive to. The middle panel indicates the reflectance of three materials, maple leaves (*Acer* sp.), pinyon pine needles (*Pinus edulis*),



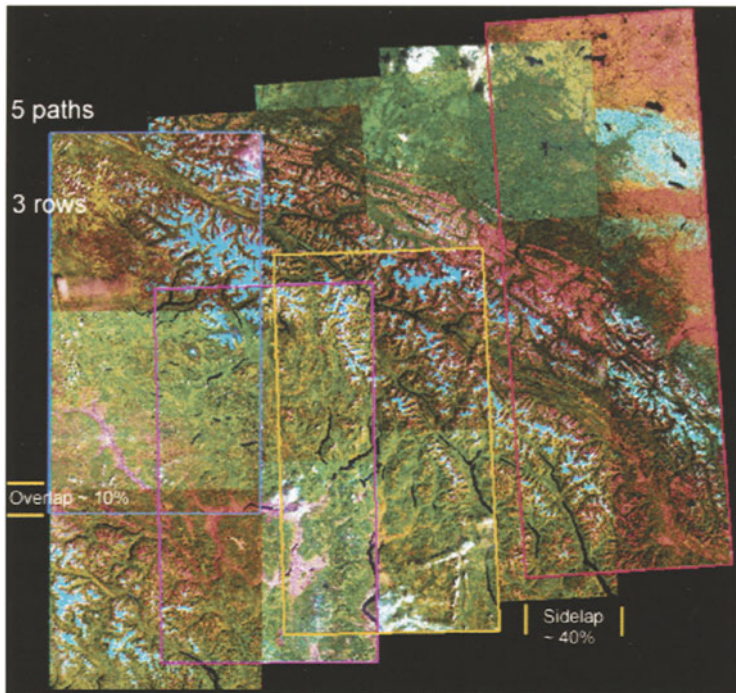
Colour Plate 2. Panel A displays a true-colour image created from the MODIS 500 m reflectance data product for the entire Willamette valley in western Oregon on the western slope of the Cascade range. A view of the area immediately around the H. J. Andrews Experimental Forest (HJA) is shown in Panel B, along with the 1 km Leaf Area Index product for the same area in Panel C. Panel D presents a single tasseled cap transformed TM image from the HJA, while Panel E shows the first three principal components from a 6 image stack of tasseled cap images for the same area, as described in Lefsky et al. (2001). (Continued on following Plate).



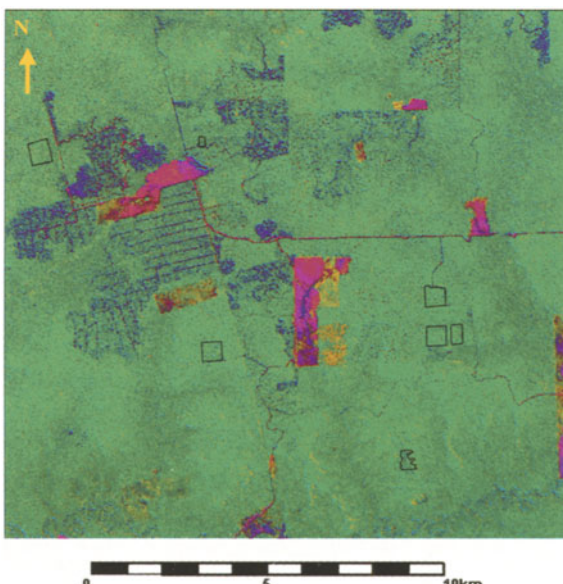
Colour Plate 2 (continued). Panel F shows high spatial resolution data from the ADAR 5500, and Panel G shows the area within the yellow box in Panel F. Panels H and I present the first (1-3) and second (4-6) set of three principal components of an AVIRIS image. Panel J shows C-band data collected by the AIRSAR instrument using a VV polarization, with the coherence, or phase correlation coefficient, measurement presented in Panel K. (See Lefsky and Cohen, Chapter 2).



Colour Plate 3. Composite sub-ortho-images (4 by 3 km; 5 m pixel spacing) of SPOT-PLA and two C-HH SAR airborne images using IHS transformation with the overlay of digital road network files: processed with 2D 2nd-order polynomial method (below), and 3D parametric method (above) (Toutin, 1995a). SPOT Image © CNES, 1996. (See Toutin, Chapter 6).

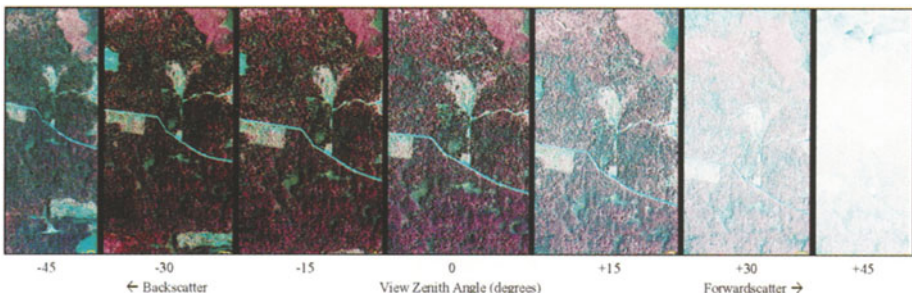
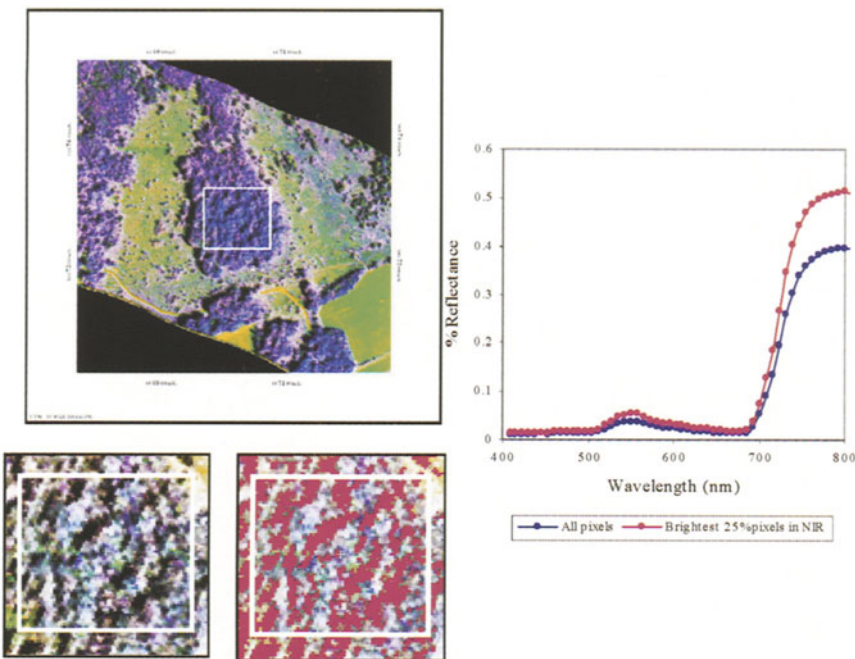


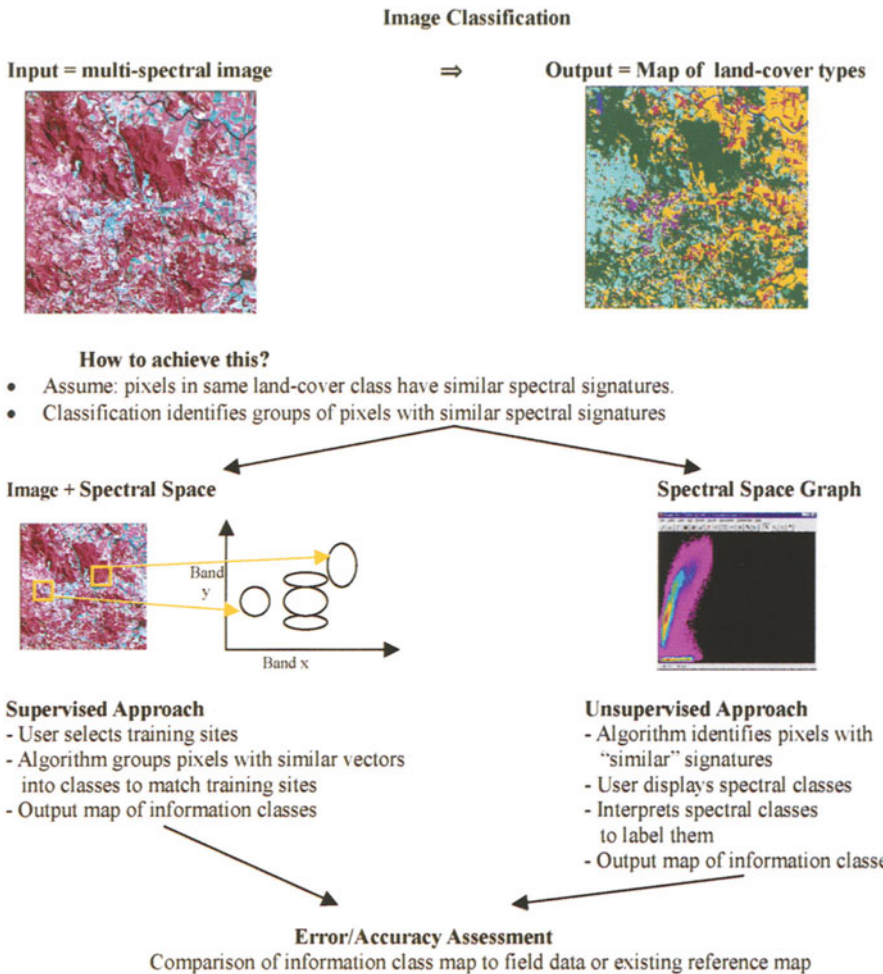
Colour Plate 4. Image block of 15 Landsat-7 ETM+ images, over the Canadian Rocky Mountains, generated from five strips and 3 rows. The outlined images are acquired from the same orbit and date and can be used as a single image with path / block bundle adjustment processing. Overlaps in the same strip are around 10% and side laps are around 40% (Toutin *et al.*, 2001b). (See Toutin, Chapter 6).



Colour Plate 5. Spectral mixture analysis of Landsat Enhanced Thematic Mapper Plus (ETM+) imagery collected over the eastern Amazon. Green tones indicate high forest canopy fractional cover, red tones indicate bare soil, and blue highlights areas with exposed surface litter. Field sites used in Figure 8-8b are shown in boxes. After Asner *et al.* (2002). (See Asner *et al.*, Chapter 8).

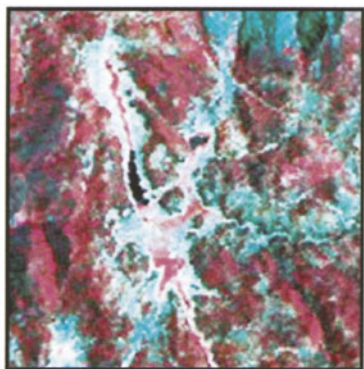
Remote Sensing of Forested Environments: Concepts and Case Studies



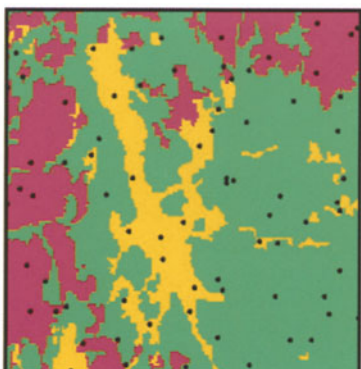


Colour Plate 8. Flow diagram presenting the general steps involved in classification: preparing a training set; statistical evaluation (separability); selecting input data; choice of classifier; evaluation. (See Franklin et al., Chapter 10).

(a) Landsat TM



(b) Forest Map

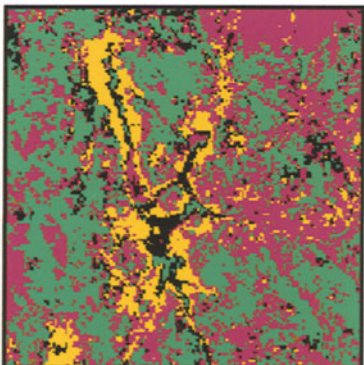


■ Shrub ■ Forest ■ Grass

● Training points

1 0 1 Kilometers

(c) Box



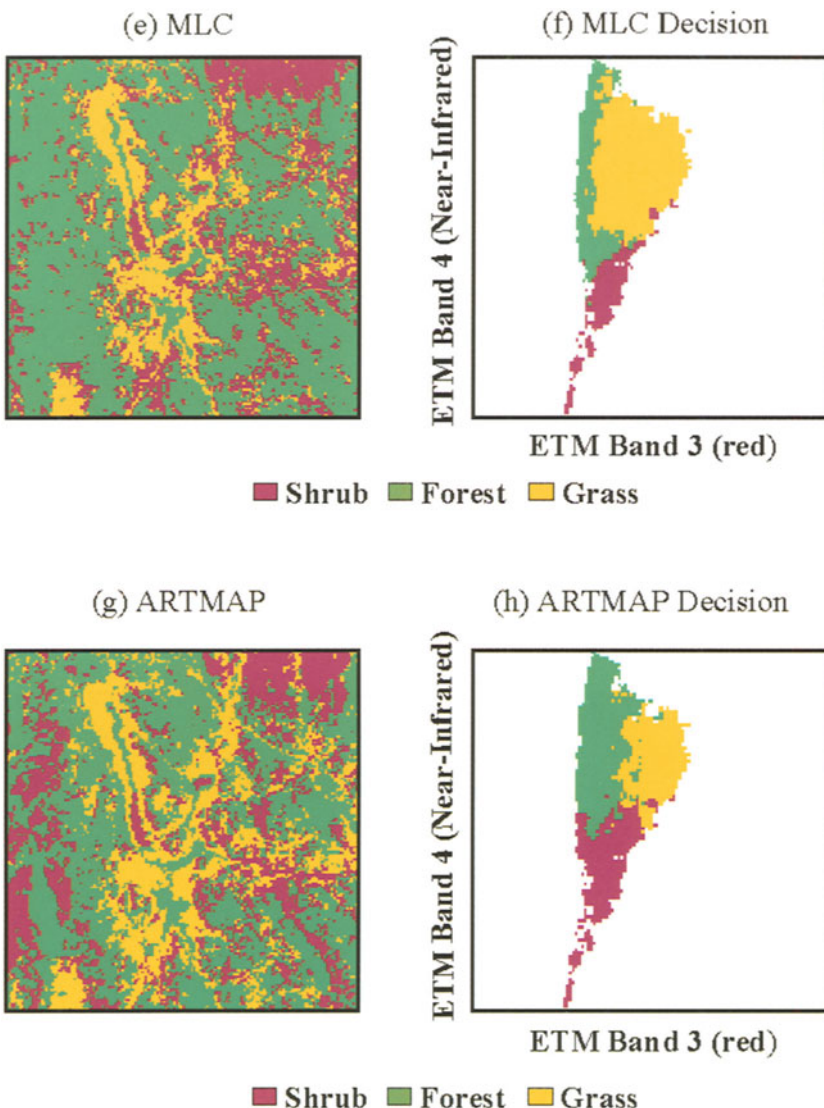
(d) Box Decision



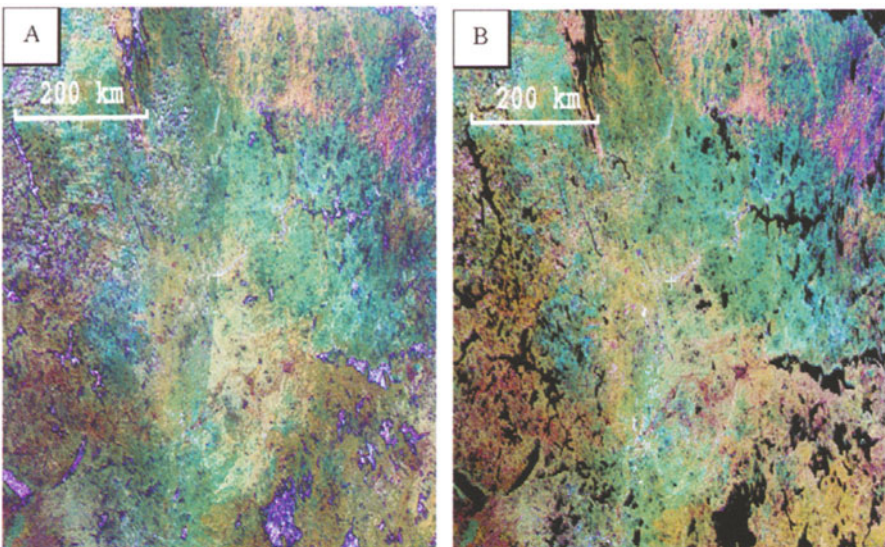
■ Shrub ■ Forest ■ Grass

■ Unclassified

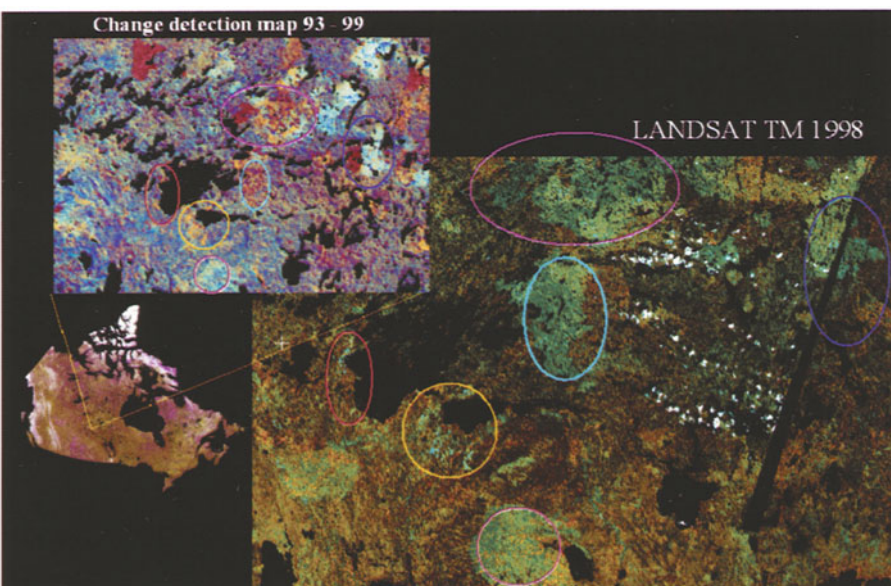
■ Shrub ■ Forest ■ Grass



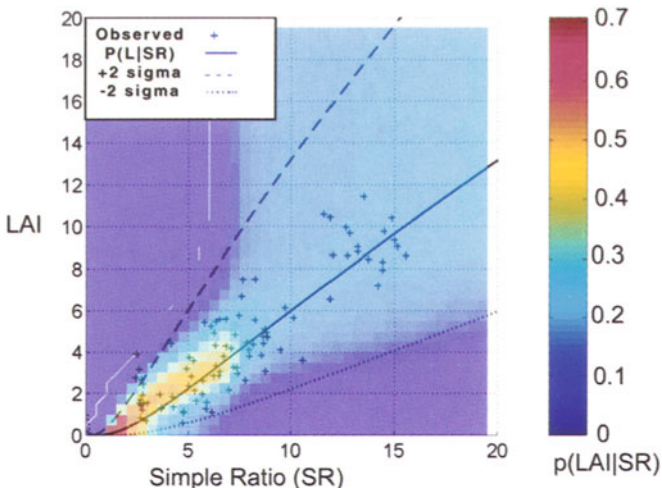
Colour Plate 9. a) A false colour-IR (bands 4, 3, 2) Landsat Thematic Mapper subimage of a 10 x 15 km area in the Laguna Mountains; b) a reference map showing three land cover classes: forest, shrub, and grassland; c) classified using a box classifier; d) decision boundaries in 2D space (band 3 versus 4) for the box classifier; e) classified using MLC; f) decision boundaries in 2D space for the MCL; g) classified using ANN (Fuzzy ARTMAP); h) decision boundaries in 2D space for the ANN classifier. (See Franklin et al., Chapter 10).



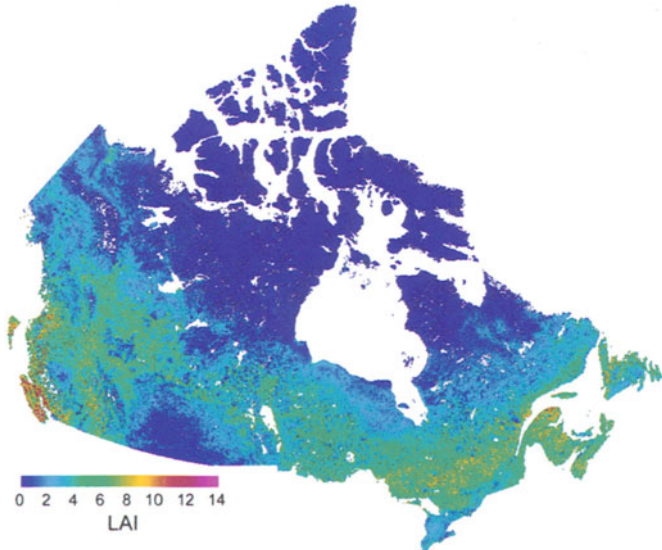
Colour Plate 10. Example of the effect of corrections on SPOT4/VGT 10-day composite images. The original images (before corrections, A) contain seams caused by different viewing geometries between adjacent orbits, and residual clouds. Both artifacts are removed using NTAM (Ch. 12, sec. 2.3) and CECANT (Ch. 12, sec. 2.4), respectively (B). Refer to Latifovic et al. (2002) and Cihlar et al. (2002c) for details. (See Cihlar et al., Chapter 12).



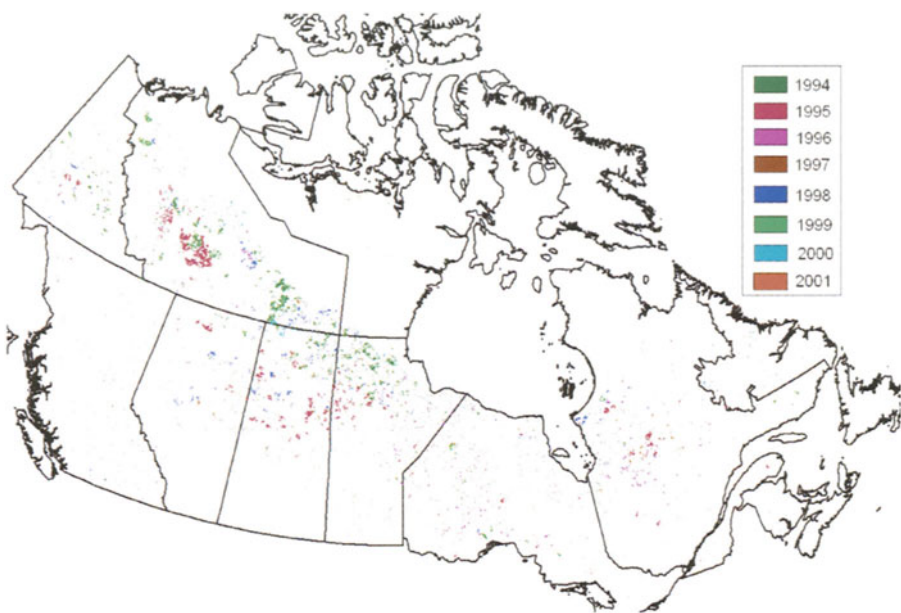
Colour Plate 11. Land cover change for area surrounding Lake La Ronge, Saskatchewan between 1993 and 1999, detected using the algorithm described in Chapter 13, section 2.2. A Landsat view of the same area is provided for a comparison. (See Cihlar et al., Chapter 13).



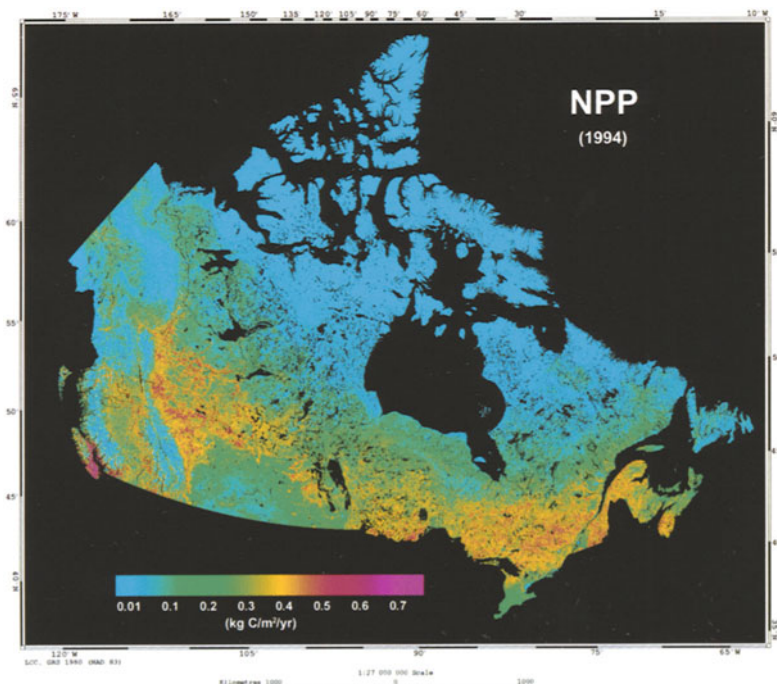
Colour Plate 12. Scatter plot of observations and structural regression of LAI versus Landsat Simple Ratio (TM band 4/TM band 3), superimposed on a density plot of reflectance model-based relationships between LAI and SR. Model simulations were based on uniform *a priori* input parameter distributions spanning the complete range of *in situ* observations. The general agreement between the maximum likelihood model outputs and the regressions implies that the field sample is likely unbiased. Note the critical point at a simple ratio above 10 where the reflectance model alone does not allow precise LAI estimation. (See Cihlar et al., Chapter 13).



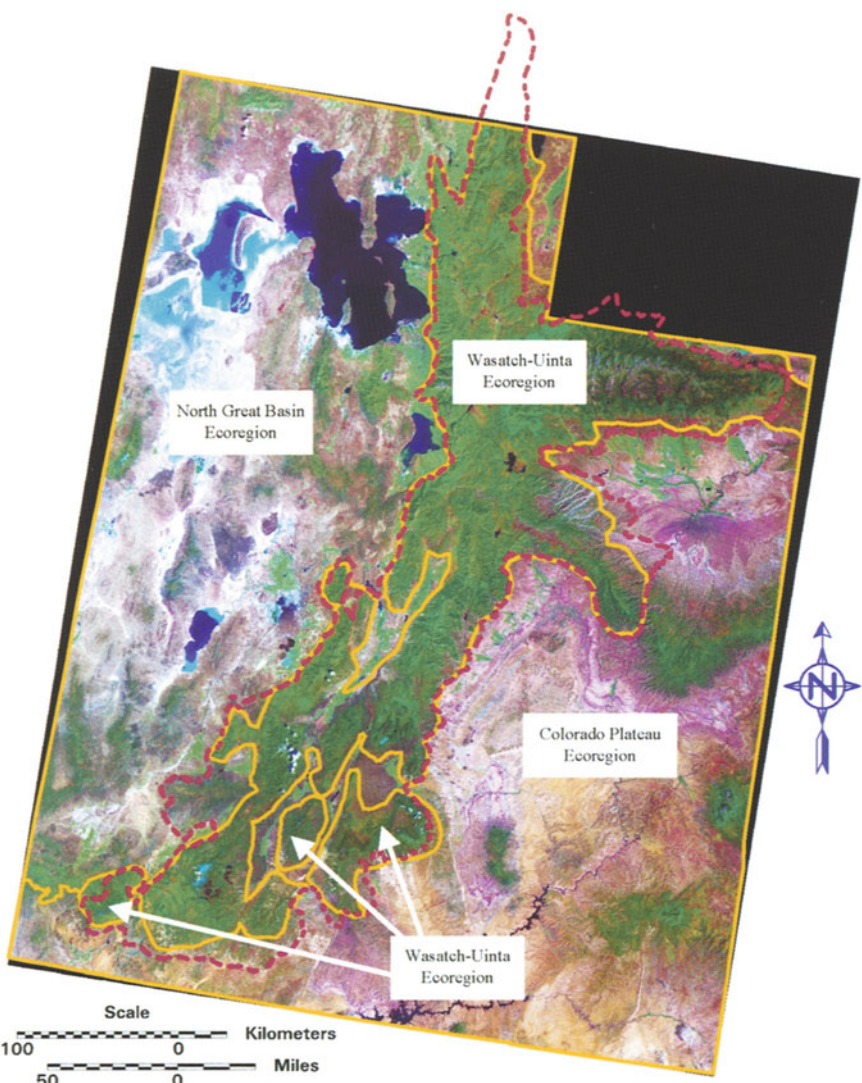
Colour Plate 13. Leaf area index (LAI) map of Canada at 1km resolution derived from SPOT4/VGT imagery (Fernandes et al., 2002b). (See Cihlar et al., Chapter 13).



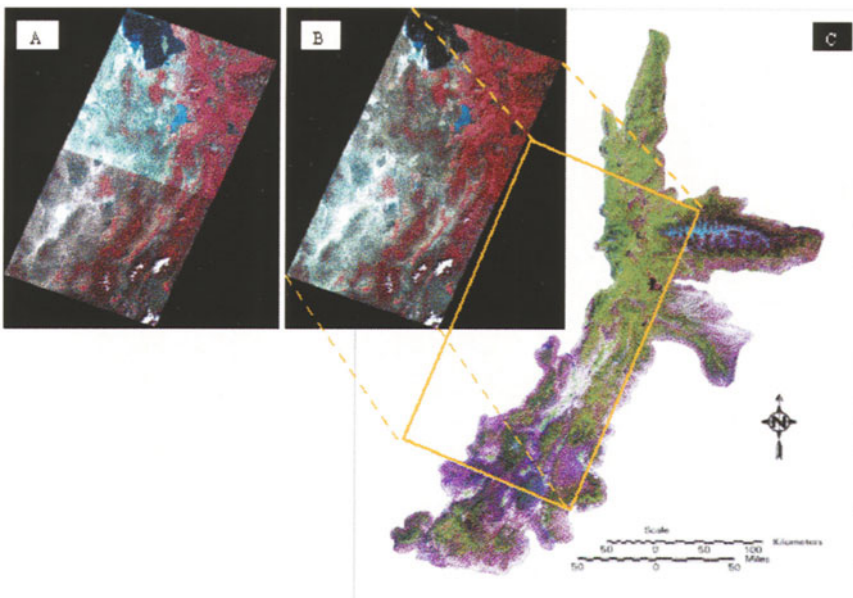
Colour Plate 14. Annual (1994 to 2001) composites of active forest fire locations across Canada derived by applying a fire detection algorithm to daily NOAA-AVHRR imagery. (See Cihlar et al., Chapter 13).



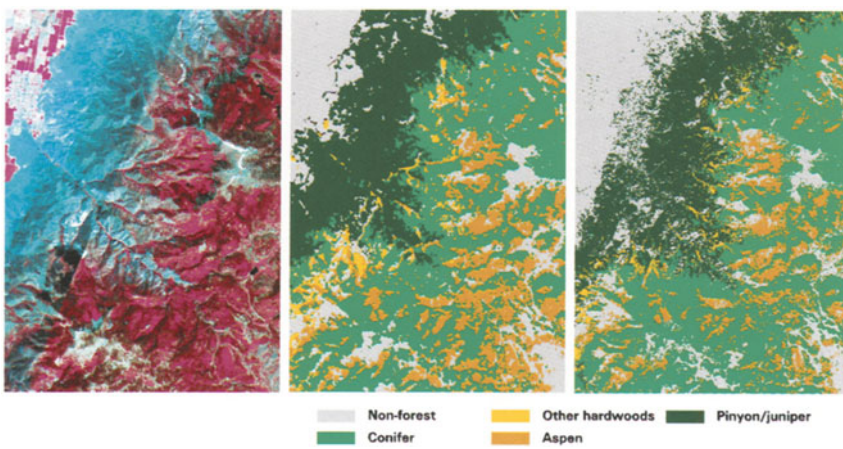
Colour Plate 15. Net primary productivity over Canadian landmass in 1994 computed using the Boreal Ecosystem Productivity Simulator (BEPS) (Chapter 13). (See Cihlar et al., Chapter 13).



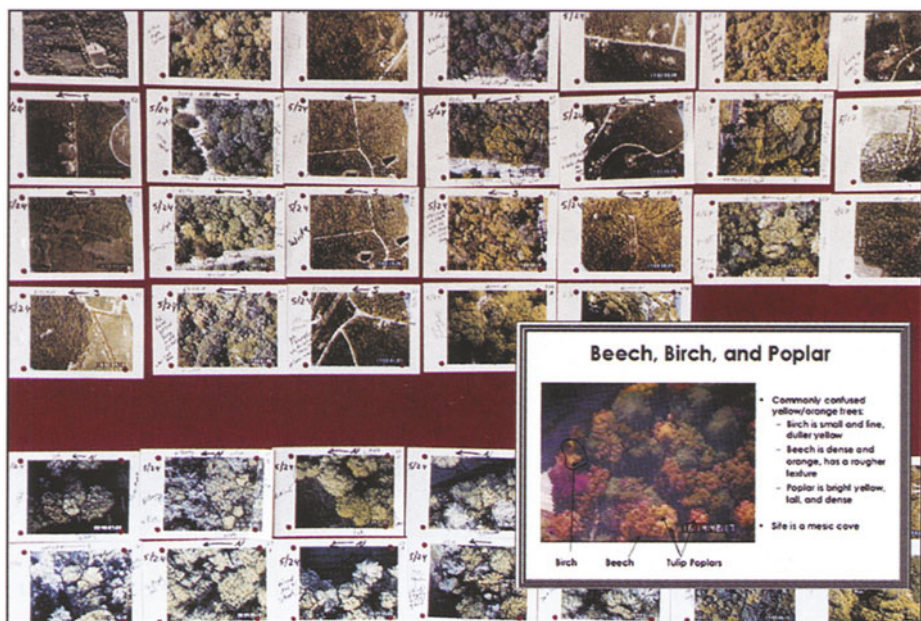
Colour Plate 16. TM image mosaic (bands 7, 4 and 2 for red, green and blue) for the Utah GAP land cover program, with boundaries of the three ecoregions in solid yellow lines and boundary of the MRLC 2000 pilot study in red dash lines. (See Huang et al., Chapter 14).



Colour Plate 17. Landsat standard false colour (bands 4, 3 and 2 for red, green and blue) image mosaics (path 38 row 32 and path 38 row 33) developed using digital number (A) and at-satellite reflectance images (B), and summer leaf on image mosaic (bands 5,4 and 3 for red, green and blue) for the entire study area of the MRLC 2000 pilot study (C), which included the two images shown in A and B (the yellow box in C shows their approximate location). (See Huang et al., Chapter 14).

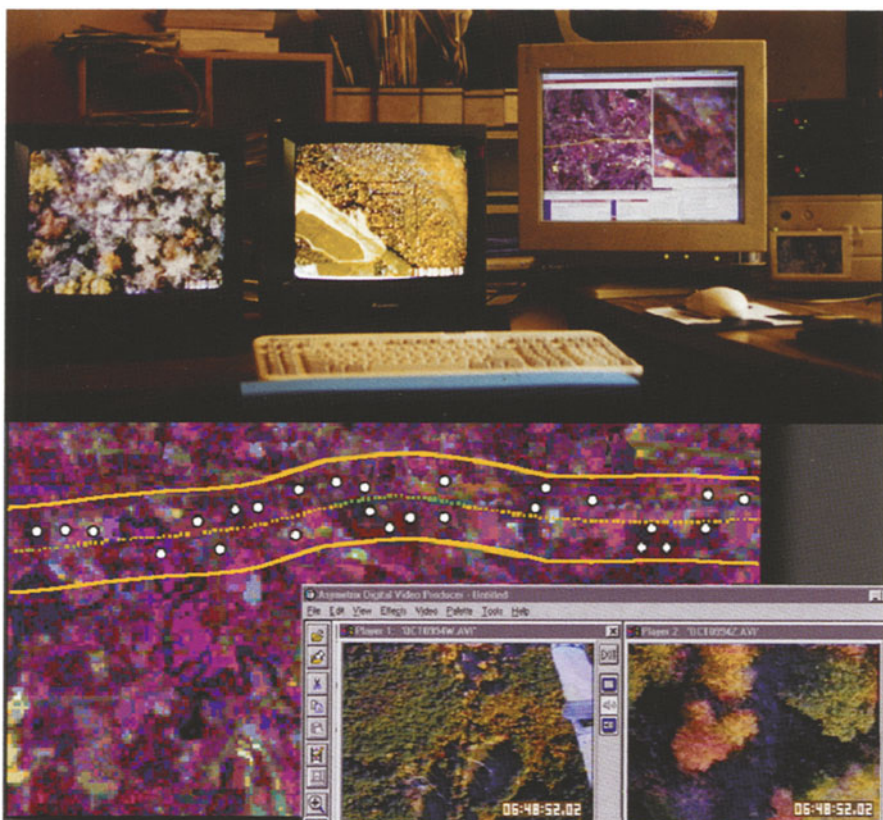


Colour Plate 18. Summer leaf-on Landsat 7 ETM+ standard false colour (e.g. bands 4, 3 and 2 for red, green and blue respectively) used in the MRLC 2000 pilot study (left), and land cover maps aggregated from classifications of the Utah GAP land cover program (middle) and MRLC 2000 pilot study (right). After converting DN to at-satellite reflectance, there were still some seamlines (as in the left image window) in the mosaic. The decision tree classifier handled the seamlines effectively and produced almost seamless classifications (right). (See Huang et al., Chapter 14).



Colour Plate 19. Example of a visual index board identifying tree species within the video data sets. These were referred to by the photographic interpreters to maintain a consistent and accurate identification between them. (See Slaymaker, Chapter 18).

Remote Sensing of Forested Environments: Concepts and Case Studies



Colour Plate 20. Ground reference points were first selected by comparing monitor displays of the video while following the GPS flight log across the Landsat image. Recent technological advances made it possible to digitize and import the video to display on-screen with the Landsat image, making comparison easier. (See Slaymaker, Chapter 18).

Chapter 12

NATIONAL SCALE FOREST INFORMATION EXTRACTION FROM COARSE RESOLUTION SATELLITE DATA, PART 1.

Data Processing and Mapping Land Cover Types

Josef Cihlar¹, Rasim Latifovic¹, Jean Beaubien², Alexander Trishchenko¹,
Jing Chen^{1,3}, Gunar Fedosejevs¹

¹ *Natural Resources Canada, Canada Centre for Remote Sensing, Ottawa, Ontario, K1A 0Y7,
Canada*

² *Natural Resources Canada, Canadian Forest Service, Laurentian Forestry Centre, Sainte-
Foy, Quebec, G1V 4C7, Canada*

³ *Department of Geography, University of Toronto, University of Toronto, Toronto, Ontario,
M5S 3G3, Canada*

1. INTRODUCTION

Forests provide essential economic and ecological services, and their essential role in the planetary system is being increasingly recognized. In parallel, the demand for timely and accurate information on the status and function of the forest biome, for a variety of purposes, is also increasing. While traditionally forest information was gathered *in situ* or through air photography, the role of satellite remote sensing is becoming central because of the need to match the spatial and temporal scales of observations to those of the key forest processes. In this Chapter, we briefly review (i) data processing issues underpinning the use of 'coarse resolution' optical satellite data for terrestrial studies, and (ii) an application to land cover mapping at the national level. An accompanying Chapter (13) describes the use of the processed data sets to derive information on biophysical parameters, land cover change, and carbon uptake. The discussion draws heavily on our work in Canada but the findings are applicable to similar geographic and ecoclimatic conditions elsewhere.

In recent years, information on land cover characteristics became a subject of intense interest for many applications. In forestry, aerial photography has been the traditional means for acquiring information on land cover (e.g., Colwell 1960). While this technique continues to be important for forest inventory in numerous countries, other remote sensing techniques have made significant inroads, fueled by the changing role of forests and the associated new information needs. In particular, the recognition of the importance of forests in the global carbon cycle, in the climate system, and for sustainable development planning and assessments have stimulated the need for information over large areas that is timely, albeit less detailed than that provided by aerial photographs.

Forest information needs encompassing large areas are not easily met. Traditionally, forest inventories have been repeated every 10 years or longer, while forest ecosystem processes respond on daily to interannual time scales. To record the effects of these processes, observation strategies providing compatible temporal resolution are required. For reasons of temporal frequency and data costs, substantial R&D has been carried out around the world with data from the National Oceanic and Atmospheric Administration's (NOAA) satellite series, particularly its Advanced Very High Resolution Radiometer (AVHRR). The AVHRR sensor was originally designed to provide data for weather prediction with accurate cloud and sea surface temperature data. The two optical channels served as a visual reference for ice, snow, clouds, water or land, and were not designed to provide accurate optical data for quantitative vegetation or other terrestrial studies.

For terrestrial applications, the AVHRR data have four main strengths: daily imaging of the global land surface, spectral measurements in the two most important spectral bands (responding to chlorophyll content and leaf structure), relatively long archive (since ~1983), and no cost beyond that of acquisition. These advantages are offset by the limited spectral content (only three bands have important uses for land cover analysis) and poor calibration of the principal bands. On balance, the advantages far outweighed the drawbacks during an important period in the development of earth observation for terrestrial ecosystems. AVHRR not only provided a unique data series documenting the changing status of forests and other biomes but also supported the development of methodologies for effective use of these data types, thus justifying the launch of better sensors of the same type. SPOT4/VGT (Saint 1992) and MODIS onboard EOS Terra (Salomonson et al. 1989) are examples of new sensors built on the experience gained with AVHRR.

In this Chapter we provide a brief overview of the issues involved in the use of coarse resolution data (pixel size ~ 250 m – 1000 m) for terrestrial applications. Although the discussion refers mostly to AVHRR, the methods have also been applied with equal success to VGT data sets. The developments have been aimed at obtaining consistent land cover information for the landmass of Canada which consists of forests ($\sim 45\%$) and other cover types such as agroecosystems, tundra and wetlands.

To make AVHRR and similar data useful for land cover analysis, numerous artifacts must be dealt with first, otherwise the extracted information will be corrupted to an unknown degree. The most important sources of error are sensor calibration, atmospheric contamination (including variable gaseous constituents, aerosol, haze and sub-pixel clouds), observational geometry, and snow at higher latitudes. These effects and the appropriate corrections are discussed below, followed by an overview of issues and techniques for land cover mapping.

2. PREPROCESSING

Although the various processing steps are discussed separately below, the algorithms may be combined for batch processing; both GeoComp-n (Adair et al. 2002) and the ABC3V2 (Atmospheric, Bidirectional and Cloud Contamination Corrections of CCRS; Cihlar et al. 2002c) are based on this property. Although the Chapter is based mostly on research carried out at CCRS it should be noted that other research groups have dealt extensively with these topics, with results published in various remote sensing journals. In addition, a comprehensive suite of algorithms has been developed for MODIS that take advantage of that sensor's capabilities (refer to <http://eospso.gsfc.nasa.gov/atbd/modistables.html>).

2.1 Radiometric calibration

To provide radiometric accuracy statements with data products or even to discuss data product errors or accuracies, one must convert (calibrate) the raw satellite data into geophysical quantities with specified units. Calibration is also critical when using multiple images mosaicked together spatially or overlaid temporally, images acquired from various sensors to be used in a consistent analysis, or images to generate calibrated products.

AVHRR data have a nominal ground pixel resolution of ~ 1.2 km 2 at nadir, with the spatial resolution decreasing at higher viewing angles to ~ 7 km 2 at 50° (Cihlar et al. 1996). The AVHRR/2 sensor onboard NOAA 14

and earlier NOAA satellites has five channels with approximate centre wavelengths for channel 1 (visible) at 0.63 micrometres (μm) and for channel 2 (near-infrared) at 0.87 μm . The approximate centre wavelengths of the thermal channels 3, 4 and 5 are 3.7 μm , 10.8 μm and 11.8 μm , respectively. For the more recent AVHRR/3 sensor onboard NOAA 15 and subsequent satellites, an additional 1.6 μm channel ('3A') has been added but its reception is traded off against that of the 3.7 μm (3B) band. NOAA made the operational decision to acquire all ascending (afternoon) orbits with the 1.6 μm band during the operational phase of NOAA satellites.

2.1.1 Optical data calibration

For remote sensing users, radiometric calibration of satellite sensor data entails the conversion of raw counts into at-sensor radiance, often referred to as top-of-atmosphere (TOA) radiance (see Peddle et al., Chapter 7). Raw AVHRR data can be calibrated to TOA radiance using onboard calibration data for the thermal channels or pre-launch calibration parameters as supplied by NOAA for the three optical channels (visible, near-infrared and SWIR) in the case of AVHRR/3 (refer to the NOAA Polar Orbiter Data User's Guide at URL <http://www2.ncdc.noaa.gov/docs/podug/> for NOAA 14 and earlier satellites, and to <http://www2.ncdc.noaa.gov/docs/klm/index.htm> for NOAA 15 and subsequent satellites). Because of post-launch sensor degradation and the absence of onboard calibration for the AVHRR optical channels, time-dependent calibration coefficients have been derived from vicarious data sets obtained over desert, ice and ocean surfaces. Numerous publications address the intricacies and relative merits of various calibration methods (e.g., Chen 1996; Dingirard and Slater 1999; Teillet 1997; Teillet et al. 2001). Post-launch calibration coefficients originally reported for NOAA 14 AVHRR optical channels by Rao and Chen (1996) were subsequently revised by Mitchell (1999) and Tahnk and Coakley (2001). Loeb (1997) provided post-launch calibration coefficients for the NOAA 12 AVHRR optical channels. While channel 3A may experience similar radiometric degradation no operational post-launch calibration information is available so far.

Traditionally, time-dependent calibration data must be applied retroactively to the entire temporal sequence of data. Radiometric calibration using piece-wise linear calibration (PWL) coefficients for annual segments (January 1 to December 31) was developed by Teillet and Holben (1994) and implemented in the AVHRR Geocoding and Compositing (GeoComp-n) system (Adair et al. 2002; Cihlar et al. 2002a). The GeoComp-n implementation is intended to provide an optimum estimation of the

calibration coefficients for the upcoming growing season (Cihlar and Teillet 1995). If the actual coefficients turn out to differ from the estimated ones, a recalibration of the TOA radiance data may be necessary. Accordingly, the ABC3V2 software system for post-season or historical data processing (Cihlar et al. 2002c) includes a recalibration option for the optical channels. The general relation for TOA radiance in the optical channels L_{TOA} is (e.g., Teillet and Holben 1994):

$$L_{TOA} = \frac{DN - O}{G} , \quad [1]$$

where:

$$G = A * \text{daysfromlaunch} + B ,$$

$$O = C * \text{daysfromlaunch} + D .$$

L_{TOA} is in $\text{Wm}^{-2}\text{sr}^{-1}\text{um}^{-1}$ and DN represents raw counts; G is calibration gain coefficient (counts/radiance); O is calibration offset coefficient (counts); and A , B , C and D are the time-dependent PWL calibration coefficients that are derived from post-launch calibration data provided by NOAA and other investigators (e.g., Cihlar and Teillet 1995). In the GeoComp-n system the radiometric calibration coefficient auxiliary file must be updated regularly as it contains both time- and satellite-dependent parameters.

Rigorous validation of the calibrated data requires coincident in-situ measurements over large uniform target areas or cross-comparisons with calibrated data from another sensor under similar viewing-illumination geometry. Rossow and Schiffer (1999) estimated that the relative uncertainties in the AVHRR radiance calibration are $\leq 5\%$ for channel 1 and $\leq 2\%$ for channel 2; the corresponding uncertainties in absolute calibration were found to be $<10\%$ and $<3\%$, respectively. Since the PWL method employs a second order polynomial and limited calibration data, uncertainties are associated with the source calibration data, methodology and the polynomial fit.

If TOA reflectance is required as input to an atmospheric correction module, the TOA radiance can be converted to TOA reflectance (Teillet and Holben 1994):

$$\rho_{TOA} = \frac{\pi d^2 L_{TOA}}{E_o \cos \theta_s}, \quad [2]$$

where d is the earth-sun distance in Astronomical units; E_o is the exo-atmospheric solar irradiance ($\text{Wm}^{-2}\text{um}^{-1}$); and θ_s is the solar zenith angle in degrees.

2.1.2 Thermal data calibration

The measurements in AVHRR channels 3B, 4 and 5 are converted to TOA radiance and/or brightness temperature (BT) using onboard calibration data. The telemetry (calibration sample) data include space counts, blackbody counts, and platinum resistance thermistors (PRT) values. These are used to compute gain and intercept calibration coefficients for converting raw counts to TOA radiance (Kidwell 1998). Note that the daytime radiance for AVHRR channel 3B includes reflected solar radiation in addition to the thermal emissive component.

While extensive pre-launch calibration tests have been carried out and NOAA quotes brightness temperature accuracies of ± 0.2 K (Kidwell 1998) the sensor performance of the detectors, mirror, blackbody and platinum resistance thermistors (PRTs) may change after launch. This possibility arises especially when the satellite drifts into a later orbit where solar contamination of the blackbody becomes an issue. Changyong et al. (2001) demonstrated that periodic solar contamination of the AVHRR sensor might impair the quality of the calibration data. Other deleterious effects such as degraded satellite reception quality as can occur at low antenna elevation angles may affect individual samples. Trishchenko and Li (2001) investigated the quality and long-term stability of the calibration data for the thermal channels, and Trishchenko (2002) presented statistical methods to model and correct for most of the anomalous calibration effects.

While absolute radiometric calibration of AVHRR data can provide accurate data products, attention must be given to the AVHRR spectral band differences between NOAA satellites when investigating long-term vegetation and climate trends, or applying models developed for a particular satellite to other satellites. Trishchenko et al. (2002a) investigated spectral differences and their impact on the Normalized Difference Vegetation Index (NDVI) from several NOAA satellites, and also provided empirical adjustment fits based on model calculations.

2.2 Atmospheric corrections

Atmospheric corrections of the satellite signal are made to compensate for the influence of the intervening atmosphere which may either enhance or attenuate the radiation emerging from the surface. These spectrally dependent effects are governed by absorbing and scattering properties of atmospheric gases and aerosols, as well as by thermodynamic properties of the atmosphere. As an example, Figure 12-1 shows spectral response functions of the latest AVHRR radiometer (onboard NOAA-16) together with total atmospheric transmission and transmission due to some specific atmospheric gases.

In AVHRR channels 1, 2 and 3A with wavelengths below 2 μm , the atmospheric thermal emission is negligible. Atmospheric correction for these channels deals only with the absorption and scattering of light. Channel 3 (3.7 μm ; 3B on NOAA- 15 and -16) is located in the spectral region where the thermal radiation emitted by surface and atmosphere has magnitude comparable to the reflected solar component. Therefore, atmospheric correction for this channel must take into account absorption, scattering, and thermal emission. The atmospheric correction in the AVHRR infrared (IR) channels 4 and 5 deals with thermal radiation only because the contribution of the solar component in this part of electromagnetic spectrum is negligible (Liou 1992). Because of the differences between spectral bands, atmospheric correction of channels 1, 2, 3A and 3B (daytime observations) aim at surface reflectance (Cihlar et al. 2002c), while channels 3B (night time observations), 4 and 5 are corrected to retrieve the surface skin temperature and/or surface emissivity (Qin and Karnieli 1999).

Major atmospheric absorbing gases within the AVHRR spectral bands are water vapour, ozone, carbon dioxide and oxygen; contributions of other gases are much smaller. Molecular (Rayleigh) scattering is important in channels 1 and 2 but is insignificant for the channels at longer wavelengths. In comparison, absorption and scattering by aerosol particles is more important for channels 1 and 2 but may also have some effect in other channels, depending on the total aerosol amount and its optical properties.

Tanré et al. (1992) summarized the major physical processes and formulae for the retrieval of AVHRR channel 1 and 2 reflectance from a plane surface. Significant advance in our knowledge of the absorbing properties of various atmospheric gases has been achieved since that time. In particular, Giver et al. (2000) reported important updates to the parameters of line and continuum absorption by water vapor. These and other updates have been incorporated into HIRTRAN spectroscopic database supported by Harvard-Smithsonian Center for Astrophysics (Rothman, et al. 1998) and

implemented in MODTRAN-4 radiative transfer model (Anderson, et al. 1999). The latest version of MODTRAN radiative transfer model (version 4.2 released in 2001; Berk et al. 2001) was used to estimate gaseous transmission shown in Figure 12-1. Generally, the resulting atmospheric absorption is higher than estimated with earlier models, such as 6S (Vermote et al. 1997a) or versions 2 and 3 of MODTRAN. This is especially evident for channel 2 where water vapour has several significant absorption bands. For example, the correction to gaseous transmission in AVHRR channel 2 may reach 5 - 15 % relative to that computed with 6S model version 4 (Vermote et al. 1997a). Depending on viewing geometry and atmospheric state, this may cause biases in the retrieved surface reflectance of up to 0.02-0.03 and lead to underestimation of NDVI by 10 % or more (Trishchenko et al. 2002a).

Atmospheric corrections are made using two main techniques, look-up-tables (LUT) and semi-analytical methods. In the LUT approach, a radiative transfer model is run for different combinations of atmospheric conditions and surface types to prepare a large multi-dimensional table. Atmospheric correction is then achieved through multi-dimensional interpolation among the LUT elements (Vermote et al. 1997b). This method provides fairly accurate results for a wide range of atmospheric and surface conditions. The disadvantage is a large number of combinations of the input parameters in the LUT - up to 10^9 or more elements depending on required accuracy of correction. The semi-analytical approach (Rahman and Dedieu 1994) is based on analytical formulae derived for simplified solution of radiative transfer equations, which are obtained by fitting to exact numerical radiative transfer modeling results. Rahman and Dedieu (1994) used 5S model for parameter fitting. MODTRAN 4.2 model was employed by Trishchenko et al. (2002b) for the same purpose.

The atmospheric correction in the AVHRR channel 3B spectral band requires combining solar and thermal measurements to remove the contribution due to surface and atmosphere thermal emission. A simple method for this correction is applied in the AVHRR data processing (Cihlar et al. (2002c) based on the following equation for computation of surface reflectance in channel 3B:

$$\rho_3 = \frac{L_3 - B(\lambda_3, T_s)}{\frac{S_{0,3}}{\pi} \mu_0 - B(\lambda_3, T_s)} \quad [3]$$

where ρ_3 is required surface reflectance, L_3 is satellite observed radiance, μ_0 is cosine of solar zenith angle, $S_{0,3}$ is the nominal solar constant for this channel, $B(\lambda_3, T_s)$ is black-body radiation corresponding to land surface temperature T_s and λ_3 is the central wavelength. Eq. (3) is derived assuming certain compensation between attenuation and emission terms, which was shown by Kaufman and Remer (1994) to hold with a good accuracy over the range of actual conditions. Thermal channels are used to estimate the land surface temperature T_s in Eq. (3). Roger and Vermote (1998) devised a more complex approach which employs an analytical expression for surface reflectance derived from the energy balance equation and analytical parameterization of a gaseous transmission computed with accurate radiative transfer scheme.

Although the major application of the AVHRR thermal channels is global mapping of the sea surface temperature (SST) (Reynolds and Smith 1993; Kidwell 1998) and estimation of cloud cover (Rossow 1989), the IR channels are also used for the retrievals of land surface temperature and emissivity (Qin and Karnieli 1999). Atmospheric correction of the AVHRR channels 4 and 5 and channel 3B (nighttime observation) is mostly concerned with accounting for water vapor absorption and non-blackness of surface. The absorption due to CO_2 and other gases as well as the vertical structure of the atmosphere may also play some role. Atmospheric correction of the AVHRR IR measurements employs the difference in water vapor absorbing properties within IR channels, by relating land surface temperature to one of the channels brightness temperatures BT and the BT difference between channels (Price 1984). The regression parameters depend on surface cover (water, vegetated surfaces, minerals, snow) because of spectral dependence of surface emissivity. For terrestrial applications, Cihlar et al. (1997d) employed the relationship between pixel NDVI and surface emissivity in channels 4 and 5.

Adjacency effects in atmospheric correction exist because of the scattering of radiation from neighbouring pixels (Lyapustin 2001; Reinersman and Carder 1995; Tanré et al. 1992). For coarse resolution satellite observations with pixel size ~ 1 km, the adjacency effect has generally been found insignificant. However, for higher resolution sensors like Landsat TM, it must be taken into account for accurate surface reflectance retrievals.

2.3 Bidirectional corrections and angular normalization

Coarse resolution images (250-1000 m), such as those from AVHRR, MODIS, and SPOT4/VGT, are usually acquired in large swaths (>2000 km).

Within a swath, the view zenith angle and the view azimuth angle relative to the sun vary over a large range, inducing considerable variability in the images. For regional applications, mosaics of several swaths acquired at different times of the day, or 10-day composites are often used. Seams between swaths in the mosaics and composites are often apparent (Colour Plate 10A). These measurement artifacts caused by the variable sun-target-sensor geometry within and among swaths must be removed before any quantitative applications of the images are possible.

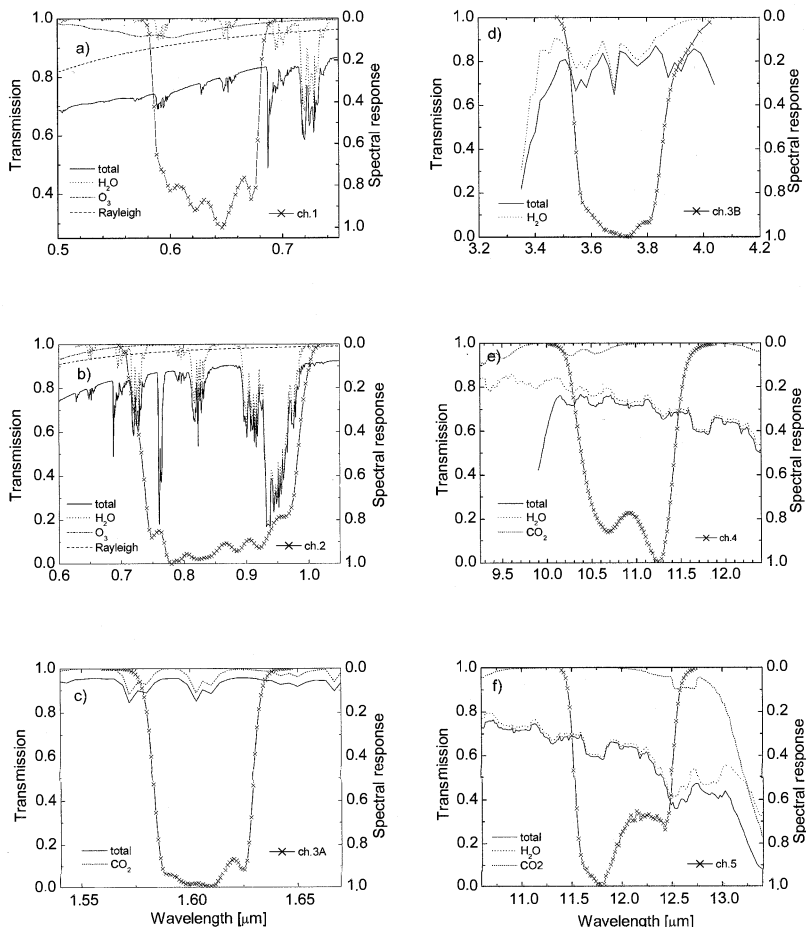


Figure 12-1. NOAA-16 AVHRR/3 spectral response functions. The left vertical axis corresponds to atmospheric transmission; the right vertical axis corresponds to spectral response (scale is inverted). Total transmissions along a 450 slant path, as well as contribution due to water vapour and other gases, are shown based on a subarctic summer (SAS) atmospheric profile. Radiative transfer computations were made with MODTRAN 4.2 and HITRAN 2001 spectroscopic database.

Models of bi-directional reflectance distribution function (BRDF) are often used for removing or reducing the artifacts through normalizing the image to a common sun-target-sensor geometry. In parallel with the development of simple BRDF models for this purpose (Walshall et al. 1985; Li and Strahler 1992; Roujean et al. 1992; Barnsley et al. 1994; Wanner et al. 1995), CCRS developed and refined a BRDF model with particular emphasis on the boreal landscapes (Wu et al. 1995; Li et al. 1996; Cihlar et al. 1997c; Chen and Cihlar 1997d; Latifovic et al. 2002). It is based on a semi-empirical kernel model originated by Roujean et al. (1992), which is similar to that of Li and Strahler (1992). The kernel approach assumes that the reflectance of a target consists of three additive kernels characterizing isotropic-scattering, geometric shadowing and volume scattering, respectively. The kernels, derived from simplified geometrical optics and radiative transfer theories, define the shape of the BRDF in terms of solar illumination and sensor viewing directions. The resulting operational BRDF model, named Nonlinear Temporal Angular Model (NTAM), consists of the original geometric and volume scattering functions of Roujean et al. (1992), a hot spot expression developed by Chen and Cihlar (1997), and a set of vegetation index - dependent coefficients (Latifovic et al. 2002):

$$\rho_i(\theta_s, \theta_v, \phi, \Delta_i) = \left[1 + (a_1 + a_2(1 - \Delta_i) + a_3(1 - \Delta_i)^2) f_1(\theta_s, \theta_v, \phi) + (a_4 + a_5\Delta_i + a_6\Delta_i^2) f_2(\theta_s, \theta_v, \phi) \right] \cdot [1 + a_7 e^{-\frac{\xi}{\pi}}],$$

$$\cos \xi = \cos \theta_s \cos \theta_v + \sin \theta_s \sin \theta_v \cos \phi,$$

$$f_1(\theta_s, \theta_v, \phi) = \frac{1}{2\pi} \left[(\pi - \phi) \cos \phi + \sin \phi \right] \tan \theta_s \tan \theta_v - \frac{1}{\pi} (\tan \theta_s + \tan \theta_v + \sqrt{\tan^2 \theta_s + \tan^2 \theta_v - 2 \tan \theta_s \tan \theta_v \cos \phi}),$$

$$f_2(\theta_s, \theta_v, \phi) = \frac{4}{3\pi} \cdot \frac{1}{\cos \theta_s + \cos \theta_v} \left[\left(\frac{\pi}{2} - \xi \right) \cos \xi + \sin \xi \right] - \frac{1}{3},$$

$$\Delta_1 = \frac{\rho_2 - \rho_1}{\rho_1 + \rho_2} \text{ for visible band}$$

$$\Delta_2 = \rho_2 - \rho_1 \text{ for near IR band}$$

[4]

where:

- θ_s, θ_v, ϕ are the solar zenith angle, view zenith angle, and difference in the azimuth angles between the Sun and the sensor;
- f_1 is the volume scattering function which describes the shape of the BRDF due to the scattering of radiation within the volume of the surface material and a weighting factor for this kernel that is expressed in terms of $(1-\Delta)$, the latter related to biophysical parameters;
- f_2 is the surface scattering function which accounts for the shadowing and occlusion effects based on geometric-optics. A weighting factor for this kernel is expressed in terms of Δ which is in turn related to biophysical parameters;
- a_i is a set of coefficients that depend of land cover type.

The inclusion of vegetation index Δ_i makes it possible to track seasonal variations of BRDF shapes with a set of time-invariant coefficients a_i . This makes one set of coefficients suitable for processing data from all seasons and latitudes. The last part of the Eq. (4) is the hotspot expression, derived by simplifying a theoretical hotspot function from the 4-Scale model (Chen and Leblanc 1997). It is necessary to include this expression as the original Roujean's model cannot characterize the pronounced BRDF shape near hotspot which often occurs in remote sensing images.

To apply the model to an image, coefficients a_i are determined for cover types of interest. The coefficients are obtained through multivariate regression analysis using cloud-free 10-day composites of AVHRR and VGT data. For the same cover types, the AVHRR coefficients were found to vary only in small ranges between different years (1993-1998). Colour Plate 10B shows the effects of the application of NTAM to the image in Colour Plate 10A.

2.4 Identification of contaminated pixels

The detection of pixels contaminated by small clouds, haze or similar effects is essential for quantitative applications of coarse resolution satellite data because any undetected features are by default interpreted as characteristics of the surface. Such detection is especially difficult over land because of the heterogeneity of land cover characteristics, and simple thresholds do not yield satisfactory results (e.g., Cihlar et al. 1999b). Based on the initial research by Los et al. (1994) and Sellers et al. (1994), Cihlar (1996) proposed a technique taking advantage of the high sensitivity of the NDVI to small atmospheric effects. With further refinements (Cihlar et al. 1999b, 2001), the CECANT algorithm (Cloud Elimination from Composites using Albedo and NDVI Trend) provides pixel- and period- specific

thresholds for detecting pixels contaminated by subpixel snow, clouds, haze, smoke and similar phenomena. It was developed for AVHRR data, thus requiring seasonal trajectories of AVHRR channels 1 and 2 only. The basic decision rule determines that a pixel is clear if

$$C1(i,j,t) \leq 0.3 \text{ and } R_{r,\min}(t) < R_r(i,j,t) \leq R_{r,\max}(t),$$

where $C1$ is surface reflectance in the visible channel, R_r is computed from R and Z values defined as (Cihlar et al. 2001):

$$R_r(i,j,t) = (R(i,j,t) - R_m(t)) \times \cos(\arctan(b(t))) + (Z(i,j,t) - Z_m(t)) \times \sin(\arctan(b(t))),$$

$$R(i,j,t) = \frac{NDVI(i,j,t) - NDVI_a(i,j,t)}{M(i,j)},$$

$$Z(i,j,t) = \frac{NDVI_{\max}(i,j,t) - NDVI(i,j,t)}{NDVI_{\max}(i,j,t)}, \quad [5]$$

where:

- $R_{\min}(t)$ = maximum acceptable deviation of the measured value $NDVI(i,j,t)$ below the estimated $NDVI_a(i,j,t)$. Lower $NDVI(i,j,t)$ values are considered contaminated;
- $R_{\max}(t)$ = maximum acceptable deviation of the measured value $NDVI(i,j,t)$ above the estimated $NDVI_a(i,j,t)$. Pixels with R values higher than R_{\max} represent anomalously high $NDVI$, e.g. due to local misregistration;
- $Z_{\max}(t)$ = maximum acceptable deviation of the measured value $NDVI(i,j,t)$ below the estimated $NDVI_{\max}(i,j,t)$. Pixels with lower $NDVI$ are considered unacceptable even if $NDVI > NDVI_a$.
- $NDVI$ = measured value;
- $NDVI_a$ = estimated average value obtained as a best fit to the $NDVI$ seasonal curve;
- $NDVI_{\max}$ = estimated maximum value obtained by fitting an upper envelope to the $NDVI$ seasonal curve;
- M = median value of the absolute difference between $NDVI$ and $NDVI_a$ for each pixel (i,j) and all periods t ;
- i,j = line and pixel coordinates, and t = compositing period.

3. VALIDATION AND QUALITY CONTROL

Validation is the process of assessing by independent means the accuracy of data products derived from the system outputs, in contrast to calibration which is the process of quantitatively defining the system response to controlled signal inputs (Justice et al. 2000). Quality control and accuracy assessment of satellite remote-sensed data and derived products are an essential component of remote sensing techniques. In a validation procedure the quantitative and qualitative performance of a product is defined, so that the product's usefulness for specific purposes may be established (Cihlar et al. 1997e). Validation also points out limitations in data and methods that may lead to further developments in data acquisition, processing and analysis.

Algorithm testing and validation is required at different steps of the data processing stream. In the case of AVHRR data processed through GeoComp, the geocoding and compositing algorithms were evaluated with respect to the ability to preserve spatial integrity of the original AVHRR measurements (Czajkowski et al. 1997). The CECANT algorithm was evaluated and compared to other cloud screening algorithms (Cihlar 1996; Cihlar et al. 1999b, 2001). Comparative studies of BRDF modeling approaches have also resulted in an improved procedure for normalizing seasonal data to common viewing geometry (Li et al. 1996; Cihlar et al. 1997b; Chen and Cihlar 1997; Latifovic et al. 2002).

Accuracy assessment and validation of higher-level seasonal products such as land cover and leaf area index are of concern to scientists who develop or use these products. Validation of products derived from coarse resolution data has been challenging due to problems related to scaling and the heterogeneous content of coarse resolution pixels. In validating remote sensing products over Canadian boreal forest both issues are of a high importance, and are usually manifested by difficulties in upscaling from plot measurements to 1 km pixels or finding a representative land cover label for heterogeneous pixel contents. Most frequently, the technique used is to upscale plot measurements to ~ 30 m pixels and then use these data to validate coarse resolution products (e.g., Chen et al. 2002; Cihlar et al. 2002b). It should also be noted that algorithms validated in one geographic setting may not perform well elsewhere, as their effectiveness depends on the assumptions made. Existing algorithms applied in new conditions should also be validated prior to their routine use.

4. LAND COVER PRODUCTS AND ACCURACY ASSESSMENT

The mapping of land cover distribution over large areas has been an early and important application of coarse resolution data, at both global (DeFries et al. 1998; Belward et al. 1999) and regional to national (Loveland et al. 2000) levels. These efforts were accompanied by research aimed at effective use of phenological information in the classification. Unsupervised classification exploiting seasonal trajectories of observations has been used frequently but not exclusively. For example, Hansen et al. (2000) employed decision trees to complete a global land cover map from AVHRR data.

In Canada, initial work has indicated that due to a combination of short growing season and strong cloudiness, the main value of multitemporal measurements is in reducing the measurement noise. Thus, so far we have based classification products on mean values computed from several composites in the peak green period. Since the classification is optimized for only a part of a continent, it is possible to obtain more detailed classification results than at the global scale.

Once the data are processed as described in section 2, the main challenges are spectral clustering, cluster labeling, and accuracy assessment. The Enhancement-Classification-Method (ECM; Beaubien et al. 1999) was employed in generating the two Canada-wide land cover products produced so far, one from AVHRR data for the 1995 growing season (Cihlar et al. 1999a) and one using 1998 SPOT4/VGT data (Cihlar et al. 2002d). The labeling was accomplished with the aid of Landsat TM/ETM+ images, field data, and general knowledge of land cover distribution.

Accuracy assessment is an important part of the mapping methodology. This may also be carried out by employing Landsat images, after they have been classified into land cover products. This permits a cost-effective inclusion of large areas in the accuracy assessment procedure. However, differences in spatial resolution between the two data types create additional complications (Cihlar et al. 1997a). Recently Cihlar et al. (2002b) completed the most extensive accuracy assessment of a coarse resolution land cover product to date, employing 27 entire Landsat TM scenes selected from across Canada using a selection algorithm (Cihlar et al. 2000b), and a consistent classification legend for VGT- and TM-derived maps based on the scheme of Grossman et al. (1998). The classified TM scenes (representing 8 % of the total area) were accurately registered to the VGT map, thus permitting a summation of land cover composition within individual VGT pixels. Accuracy was found to depend on several factors, particularly the homogeneity of land cover within the coarse pixels, the complexity of the

mapping legend, and acceptable combinations of land cover types within the 1 km² pixels. Over the range of these variables and also including labeling errors in both data types, the accuracy was found to vary between 20.4 % and 70.3 %. These results are consistent with assessments of other products for the boreal environment, and illustrate a fundamental limitation of the ability of coarse resolution products in providing land cover type information if each pixel has only one label. It is feasible to obtain more detailed information on the land cover composition within a pixel, but this requires different analytical approaches; this is considered in a companion Chapter (Cihlar et al., Chapter 13).

5. CONCLUSIONS

This Chapter provides an overview of the research carried out to extract sound information from satellite data at a national level. The research has focused on 'coarse' resolution satellite optical sensors (pixel size ~250 m – 1000 m) that in principle are capable of providing frequent and consistent information over large areas. The problem is then in developing methods that ensure high quality, high (and known) accuracy, and good reproducibility of the extracted information. This is a considerable challenge given that coarse optical data suffer from two major sources of noise, viewing geometry and atmospheric contamination, each requiring multiple strategies for a satisfactory solution. In this Chapter, we have shown that such solutions were found for significant geographic areas and under rather extreme conditions: low solar viewing angles, short growing season (down to few weeks), high cloudiness during the summer, and snow interference in late spring and early fall. These methods can be successfully used with different sensors and applications, such as mapping land cover types discussed here. However, ultimately the quality of the outputs is limited by the input data and in this respect, major improvements are underway.

Sound monitoring and assessment of forests demands that the temporal scales of the observations match those of the processes causing changes. 'Coarse' optical satellite data fill a unique niche in the range of observing methods, namely daily or more frequent observations over large areas. The astonishing success of AVHRR data through the efforts of many research groups worldwide has now resulted in several recent and planned satellite missions that will ensure the availability of high quality data for this niche over the next decade and beyond.

REFERENCES

- Adair, M., Cihlar, J., Park, B., Fedosejevs, G., Erickson, E., Keeping, R., Stanley, D., & Hurlburt, P. (2002). GeoComp - n, an advanced system for generating products from coarse and medium resolution optical satellite data. Part 1: System characterization. *Canadian Journal of Remote Sensing*, 28, 1-20.
- Anderson, G. P., et al. (1999). MODTRAN4: radiative transfer modeling for remote sensing. *Proceedings SPIE, Optics in Atmospheric Propagation and Adaptive Systems III*, 2-10.
- Barnsley, M., Morris, K., Strahler, A., & Muller, J. P. (1994). Sampling the surface bidirectional reflectance distribution function (BRDF): Evaluation of current and future satellite sensors. *Remote Sensing Reviews*, 8, 893-916.
- Beaubien, J., Cihlar, J., Simard, G., & Latifovic, R. (1999). Land cover from multiple Thematic Mapper scenes using a new enhancement - classification methodology. *Journal of Geophysical Research*, 104, 27909-27920.
- Belward, A. S., Estes, J. E., & Kline, K. D. (1999). The IGBP-DIS global 1-km land-cover datasets DISCover: a project overview. *Photogrammetric Engineering and Remote Sensing*, 65, 1013-1020.
- Berk, A., Anderson, G. P., Acharya, P. K., Chetwynd, J. H., Bernstein, L. S., Shettle, E. P., Matthew, M. W., & Adler-Golden, S. M. (2001). *MODTRAN4 Version 2 User's manual*. Air Force Research Laboratory, Air Force Materiel Command, Hanscom AFB, MA 01731-3010.
- Changyong, C., Weinreb, M., & Sullivan, J. (2001). Solar contamination effects on the infrared channels of the advanced very high resolution radiometer (AVHRR). *Journal of Geophysical Research*, 106, 33463-33469.
- Chen, H. S. (1996). *Remote Sensing Calibration Systems - An Introduction*, ISBN 0-937194-38-7. A. Deepak Publishing, Hampton, Virginia, USA.
- Chen, J. M., & Cihlar, J. (1997). A hotspot function in a simple bidirectional reflectance model for satellite applications. *Journal of Geophysical Research*, 102, 25907-25913.
- Chen, J., & Leblanc, S. (1997). A 4-scale bidirectional reflection model based on canopy architecture. *IEEE Transactions on Geoscience and Remote Sensing*, 35, 1316-1337.
- Chen, J., Pavlic, G., Brown, L., Cihlar, J., Leblanc, S. G., White, P., Hall, R. J., Peddle, D., King, D. J., Trofymow, J. A., Swift, E., van der Sanden, J., & Pellikka, P. (2002). Derivation and validation of Canada-wide coarse-resolution leaf area index maps using high-resolution satellite imagery and ground measurements. *Remote Sensing of Environment*, 80, 165-184.
- Cihlar, J. (1996). Identification of contaminated pixels in AVHRR composite images for studies of land biosphere. *Remote Sensing of Environment*, 56, 149-163.
- Cihlar, J., & Teillet, P. M. (1995). Forward piecewise linear calibration model for quasi-real time processing of AVHRR data. *Canadian Journal of Remote Sensing*, 21, 22-27.
- Cihlar, J., Ly, H., & Xiao, Q. (1996). Land cover classification with AVHRR multichannel composites in northern environments. *Remote Sensing of Environment*, 58, 36-51.
- Cihlar, J., Beaubien, J., Xiao, Q., Chen, J., & Li, Z. (1997a). Land cover of the BOREAS Region from AVHRR and Landsat data. *Canadian Journal for Remote Sensing*, 23, 163-175.
- Cihlar, J., Ly, H., Li, Z., Chen, J., Pokrant, H., & Huang, F. (1997b). Multitemporal, multichannel AVHRR data sets for land biosphere studies: artifacts and corrections. *Remote Sensing of Environment*, 60, 35-57.

- Cihlar, J., Chen, J., & Li, Z. (1997c). Seasonal AVHRR multichannel data sets and products for studies of surface-atmosphere interactions. *Journal of Geophysical Research – Atmospheres*, 102, 29625-29640.
- Cihlar, J., Ly, H., Li, Z., Chen, J., Pokrant, H., & Huang, F. (1997d). Multitemporal, multichannel AVHRR data sets for land biosphere studies: artifacts and corrections. *Remote Sensing of Environment*, 60, 35-57.
- Cihlar, J., Chen, J., & Li, Z. (1997e). On the validation of satellite-derived products for land applications. *Canadian Journal for Remote Sensing*, 23, 381-389.
- Cihlar, J., Beaubien, J., Latifovic, R., & Simard, G. (1999a). Land Cover of Canada 1995 Version 1.1, *Digital data set documentation*. Natural Resources Canada, Ottawa, Ontario.
- Cihlar, J., Latifovic, R., Chen, J., & Li, Z. (1999b). Testing near-real time detection of contaminated pixels in AVHRR composites. *Canadian Journal for Remote Sensing*, 25, 160-170.
- Cihlar, J., Tcherednichenko, I., Latifovic, R., Li, Z., & Chen, J. (2000a). Impact of variable atmospheric water vapour content on AVHRR data corrections over land. *IEEE Transactions for Geoscience and Remote Sensing*, 39, 173-180.
- Cihlar, J., Latifovic, R., Chen, J., Beaubien, J., & Li, Z. (2000b). Selecting representative high resolution sample images for land cover studies. Part 1. Methodology. *Remote Sensing of Environment*, 71, 26-42.
- Cihlar, J., Du, Y., & Latifovic, R. (2001). Land cover dependence in the detection of contaminated pixels in satellite optical data. *IEEE Transactions for Geoscience and Remote Sensing*, 39, 1084-1094.
- Cihlar, J., Chen, J., Li, Z., Fedosejevs, G., Adair, M., Park, W., Fraser, R., Trishchenko, A.P., Guindon, B., & Stanley, D. (2002a). GeoComp-n, an advanced system for the processing of coarse and medium resolution satellite data. Part 2: biophysical products for the northern ecosystem. *Canadian Journal of Remote Sensing*, 28, 21-44.
- Cihlar, J., Latifovic, R., Beaubien, J., Guindon, B., & Palmer, M. (2002b). TM-based accuracy assessment of a land cover product for Canada derived from SPOT VEGETATION data. *Canadian Journal of Remote Sensing*, In review.
- Cihlar, J., Latifovic, R., Chen, J., Trishchenko, A., Du, Y., Fedosejevs, G., & Guindon, B. (2002c). Systematic corrections of AVHRR image composites for temporal studies. *Remote Sensing of Environment*, in press.
- Cihlar, J., Beaubien, J., & Latifovic, R. (2002d). Land Cover of Canada 1998. *Digital data set documentation*. Natural Resources Canada, Ottawa, ON.
- Colwell, R. N. (Ed). (1960). *Manual for photographic interpretation*, The American Society of Photogrammetry, Washington, D.C.
- Czajkowski, K. P., Mulhern, T., Goward, S., & Cihlar, J. (1997). Validation of Geocoding and Compositing System (GEOCOMP) using contextual analysis for AVHRR images. *International Journal of Remote Sensing*, 18, 3055-3068.
- DeFries, R. S., Hansen, M., Townshend, J. R. G., & Sohlberg, R. (1998). Global land cover classification at 8 km spatial resolution: the use of training data derived from Landsat imagery in decision tree classifiers. *International Journal of Remote Sensing*, 19, 3141-3168.
- Dingirard, M., & Slater, P. N. (1999). Calibration of space-multispectral imaging sensors: A review. *Remote Sensing of Environment*, 68, 194-205.
- Giver, L. P. Jr., Chackerian, C., & Varanasi, P. (2000). Visible and near-infrared $H_2^{16}O$ line intensity corrections for HITRAN-96. *Journal of Quantitative Spectroscopy and Radiative Transfer*, 66, 101-105.

- Grossman, D. H., Faber-Langendoen, D., Weakley, A. S., Anderson, M., Bourgeron, P., Crawford, R., Goodin, K., Landaal, S., Metzler, K., Patterson, K. D., Pyne, M., Reid, M., & Sneddon, L. (1998). International classification of ecological communities: Terrestrial vegetation of the United States. Volume 1. *The National Vegetation Classification System: development status and applications*. The Nature Conservancy, Arlington VA, USA.
- Hansen, M. C., DeFries, R. S., Townshend, J. R. G., & Sohlberg, R. (2000). Global land cover classification at 1 km spatial resolution using a classification tree approach. *International Journal of Remote Sensing*, 21, 1331-1364.
- Justice, C., Belward, A., Morisette, J., et al. (2000). Developments in the 'validation' of satellite sensor products for the study of the land surface. *International Journal of Remote Sensing*, 21, 3383-3390.
- Kaufman, Y. J., & Remer, L. A. (1994). Detection of forests using mid-IR reflectance: an application for aerosol studies. *IEEE Transactions on Geoscience and Remote Sensing*, 32, 672-683.
- Kidwell, K. B. (Ed.). (1998). *NOAA Polar Orbiter Data User's Guide*. US Department of Commerce, NESDIS, NOAA, National Climatic Data Centre, Satellite Data Services Division, Washington, D. C., USA. <<http://www2.ncdc.noaa.gov/docs/podug/>>.
- Latifovic, R., Cihlar, J., & Chen, J. (2002). A comparison of BRDF models for the normalization of satellite optical data to a standard sun-target-sensor geometry. *IEEE Transactions on Geoscience and Remote Sensing*, (submitted).
- Li, Z., Cihlar, J., Zhang, X., Moreau, L., & Ly, H. (1996). The bidirectional effects of AVHRR measurements over boreal regions. *IEEE Transactions on Geoscience and Remote Sensing*, 34, 1308-1322.
- Li, X., & Strahler, A. H. (1992). Geometric-optical bidirectional reflectance modeling of the discrete crown vegetation canopy: effect of crown shape and mutual shadowing. *IEEE Transactions on Geoscience and Remote Sensing*, 30, 276-292.
- Liou, K. N., (1992). *Radiation and cloud processes in the atmosphere: theory, observation, and modeling*. Oxford University Press, Oxford, UK.
- Loeb, N. G., (1997). In-flight calibration of NOAA AVHRR visible and near-IR bands over Greenland and Antarctica. *International Journal of Remote Sensing*, 18, 477-490
- Los, S. O., Justice, C. O., & Tucker, C. J. (1994). A global 1° by 1° NDVI data set for climate studies derived from the GIMMS continental NDVI data. *International Journal of Remote Sensing*, 15, 3493-3518.
- Loveland, T. R., Reed, B. C., Brown, J. F., Ohlen, D. O., Zhu, Z., Yang, L., & Merchant, J. W. (2000). Development of a global characteristics land cover database and IGBP DISCover from 1-km AVHRR data. *International Journal of Remote Sensing*, 21, 1303-1330.
- Lyapustin, A. I. (2001). Three-dimensional effects in the remote sensing of surface albedo. *IEEE Transactions on Geoscience and Remote Sensing*, 28, 254-263.
- Mitchell, R. M. (1999). Calibration status of the NOAA AVHRR solar reflectance channels: CalWatch Revision 1, *CSIRO Atmospheric Research Technical Paper*, 42, 20.
- Price, J. C. (1984). Land surface temperature measurements from the split window channels of the NOAA 7 Advanced Very High Resolution Radiometer. *Journal of Geophysical Research*, 89, 7231-7237.
- Qin, Z., & Karnieli, A. (1999). Progress in the remote sensing of land surface temperature and ground emissivity using NOAA-AVHRR data. *International Journal of Remote Sensing*, 20, 2367-2393.

- Rahman, H., & Dedieu, G. (1994). SMAC: a simplified method for the atmospheric correction of satellite measurements in the solar spectrum. *International Journal of Remote Sensing*, 15, 123-143.
- Rao, C. R. N., & Chen, J. (1996). Post-launch calibration of the visible and near-infrared channels of the Advanced Very High Resolution Radiometer on NOAA-14 spacecraft. *International Journal of Remote Sensing*, 17, 2743-2747.
- Reinersman, P. N., & Carder, K. L. (1995). Monte Carlo simulation of the atmospheric point-spread function with an application to correction for the adjacency effect. *Applied Optics*, 34, 4453-4471.
- Reynolds, R. W., & Smith, T. M. (1993). Improved global sea surface temperature analysis using optimum interpolation. *Journal of Climate*, 7, 929-948.
- Roger, J. C., & Vermote, E. F. (1998). A method to retrieve the reflectivity signature at $3.75\mu\text{m}$ from AVHRR data. *Remote Sensing of Environment*, 64, 103-114.
- Rossow, W. B. (1989). Measuring cloud properties from space: a review. *Journal of Climate*, 2, 201-213.
- Rossow, W. B., & Schiffer, R. A. (1999). Advances in understanding clouds from ISCCP. *Bulletin of the American Meteorological Society*, 80, 2261-2287.
- Rothman, L. S., et al. (1998). The HITRAN molecular spectroscopic database and HAWKS (HITRAN Atmospheric Workstation): 1996 Edition. *Journal of Quantitative Spectroscopy and Radiative Transfer*, 60, 665-710.
- Roujean, J. L., Leroy, M. J., & Deschamps, P. Y. (1992.) A bidirectional reflectance model of the Earth's surface for the correction of remote sensing data. *Journal of Geophysical Research*, 97, 20455-20468.
- Saint, G. (1992). *VEGETATION onboard SPOT 4: mission specifications*, Report No. 92102. Laboratoire d'études et de recherches en télédétection spatiale, Toulouse, France.
- Salomonson, V. V., Barnes, W. L., Maymon, P. W., Montgomery, H. E., & Ostrow, H. (1989). MODIS: advanced facility instrument for studies of the Earth as a system. *IEEE Transactions on Geoscience and Remote Sensing*, 27, 145-153.
- Sellers, P. J., Los, S. O., Tucker, C. J., Justice C. O., Dazlich, D. A., Collatz, J. A., & Randall, D. A. (1994). A global 1° by 1° NDVI data set for climate studies. Part 2: The generation of global fields of terrestrial biophysical parameters from the NDVI. *International Journal of Remote Sensing*, 15, 3519-3545.
- Tahnk, W. R., & Coakley, J. A. Jr. (2001). Updated calibration coefficients for NOAA-14 AVHRR channels 1 and 2. *International Journal of Remote Sensing*, 22, 3053-3057.
- Tanré, D., Holben, B. N., & Kaufman, Y. J. (1992). Atmospheric correction algorithm for NOAA-AVHRR products: theory and application. *IEEE transactions on Geoscience and Remote Sensing*, 30, 231-248.
- Teillet, P. M., & Holben, B. N. (1994). Towards operational radiometric calibration of NOAA AVHRR imagery in the visible and infrared channels. *Canadian Journal of Remote Sensing*, 20, 1-10.
- Teillet, P. M., (Ed.). (1997). Special Issue on calibration/validation. *Canadian Journal of Remote Sensing*, 23, 289-423.
- Teillet, P. M., Fedosejevs, G., Gauthier, R. P., O'Neill, N. T., Thome, K. J., Biggar, S. F., Ripley, H., & Meygret, A. (2001). A generalized approach to the vicarious calibration of multiple earth observation sensors using hyperspectral data. *Remote Sensing of Environment*, 77, 304-327.

- Trishchenko, A. P. (2002). Removing unwanted fluctuations in the AVHRR thermal calibration data using robust techniques. *Journal of Atmospheric and Oceanic Technology*, submitted.
- Trishchenko, A. P., & Li, Z. (2001). A method for the correction of AVHRR onboard IR calibration in the event of short-term radiative contamination. *International Journal of Remote Sensing*, 22, 3619-3624.
- Trishchenko, A. P., Cihlar, J., & Li, Z. (2002a). Effects of spectral response function on the surface reflectance and NDVI measured with moderate resolution sensors. *Remote Sensing of Environment*, 80, 1-18.
- Trishchenko, A. P., Hwang, B., & Li, Z. (2002b). Atmospheric correction of satellite signal in solar domain: impact of improved molecular spectroscopy. *Proceedings of the 12th Atmospheric Radiation Measurement (ARM) Science Team Meeting*. St. Petersburg, FLA, USA.
- Vermote, E., Tanré, D., Deuzé, J. L., Herman, M., & Morcette, J. J. (1997a). Second simulation of the satellite signal in the solar spectrum: an overview. *IEEE Transactions on Geoscience and Remote Sensing*, 35, 675-686.
- Vermote, E. F., Saleous, N. E., Justice, C. O., Kaufman, Y. J., Privette, J. L., Remer, L., Roger, J. C., & Tanré, D. (1997b). Atmospheric correction of visible to middle-infrared EOS-MODIS data over land surfaces: background, operational algorithm and validation. *Journal of Geophysical Research*, 102, 17131-17141.
- Walther, C. L., Norman, J. M., Welles, J. M., Campbell, G., & Blad, B. L. (1985.) Simple equation to approximate the bidirectional reflectance from vegetation canopies and bare soil surface. *Applied Optics*, 24, 383-387.
- Wanner, W., Li, X., & Strahler, A. H. (1995.) On the derivation of kernels for kernel-driven models of bidirectional reflectance. *Journal of Geophysical Research*, 100, 21077-21089.
- Wu, A., Li, Z., & Cihlar, J. (1995). Effects of land cover type and greenness on AVHRR bidirectional reflectances: analysis and removal. *Journal of Geophysical Research*, 100, 9179-9192.

Chapter 13

NATIONAL SCALE FOREST INFORMATION EXTRACTION FROM COARSE RESOLUTION SATELLITE DATA, PART 2.

Forest Biophysical Parameters and Carbon

Josef Cihlar¹, Richard Fernandes¹, Robert Fraser¹, Jing Chen^{1,2}, Wenjun Chen¹, Rasim Latifovic¹, Jane Liu^{1,3}, and Zhanqing Li^{1,4}

¹ *Natural Resources Canada, Canada Centre for Remote Sensing, Ottawa, Ontario, K1A 0Y7, Canada*

² *Department of Geography, University of Toronto, University of Toronto, Toronto, Ontario, M5S 3G3, Canada*

³ *Department of Physics, University of Toronto, University of Toronto, Toronto, Ontario, M5S 3G3, Canada*

⁴ *Department of Meteorology, University of Maryland, College Park, Maryland, 20742-2425, USA*

1. INTRODUCTION

This is the second of two Chapters addressing the use of coarse resolution satellite data for large-scale applications in forestry. Here we review the use of AVHRR and VGT data for characterizing forest structure and carbon uptake. It is assumed that most of the observation artifacts were removed from the satellite data through prior processing, thus the corrected data represent intrinsic electromagnetic properties of the surface targets. Both forest structural properties (fractional composition and change in land cover, leaf area index, active fires and burns) and functional behaviour (net primary productivity, net ecosystem productivity, net biome productivity) are reviewed, based on research carried out for the forests of Canada.

From the perspective of environmental monitoring, the value of satellite observations may be realized only after the raw data are transformed into information describing some aspect of the Earth's environment. Depending

on the application, the transformation is a complex process that may involve numerous steps, including sensor calibration, removal of atmospheric effects, and compensation for the variations in viewing geometry. These corrections are critically important to a successful use of satellite data since any residual artifacts are implicitly regarded as the properties of the target. However, they are beyond the scope of this discussion and have been dealt with elsewhere (e.g., Cihlar et al., Chapter 12). Here we assume that artifacts or noise associated with satellite optical measurements have been removed using those or other procedures, the data represent mainly the properties of the target of interest, and the remaining errors are negligible or can be accommodated in the subsequent analysis.

Strictly speaking, satellite measurements represent electromagnetic properties of the targets, especially its reflectance or emission, in specific portions of the electromagnetic spectrum. The assumption in using these measurements is that a close relationship exists between the electromagnetic properties and biophysical, biochemical, or other environmental characteristics of the targets of interest. Thus successful use of satellite data depends on finding accurate and consistent ways of representing these relationships. They take the form of empirical functions or models whose usefulness depends primarily on the strength of the relationship between electromagnetic and other target properties.

Another important characteristic of satellite data is that the measurements are nearly instantaneous, while environmental processes vary strongly over time. Given this temporal variability and the fact that the electromagnetic signals represent the target properties of interest to various degrees, this leads to a very important role for models. Particularly significant are mechanistic process models that aim to describe the behaviour of the target of interest in relation to the changing environmental conditions, e.g. CO₂ uptake as affected by solar radiation and the availability of water. Since the processes of interest concern the exchanges of matter and energy in the environment, the mechanistic models are well suited to the use of satellite measurements.

In this Chapter, we briefly describe several applications of satellite data (corrected to remove measurement artifacts) to estimating biophysical variables and quantifying processes involved in the terrestrial component of the carbon cycle. Fractional land cover, land cover change, leaf area index, forest fires and burned areas are the primary biophysical parameters of interest in this context. Three measures of net productivity (primary, ecosystem, biome) are obtained by means of process models driven with satellite and meteorological measurements. The discussion is based on research carried out in boreal environment employing AVHRR and VGT

data, although the general (and in some cases specific) findings are applicable elsewhere as well.

2. BIOPHYSICAL VARIABLES

2.1 Fractional land cover

Traditionally, land cover maps have been labeled using a thematic scale corresponding to nominal categories specified in a legend (Robinson et al. 1995; Cihlar et al., Chapter 12). This approach poses some difficulties in the calibration, intercomparison and interpretation of land cover maps since legends may not be exhaustive of all possible land cover types, are spatial scale- and data source- dependent, and the boundaries between nominal land cover classes may be difficult to specify (Franklin et al., Chapter 10). Also, nominal land cover classes are intended to correspond to spatially discrete patches on the land surface while in reality land cover exists as mixtures, especially if pixels are much larger than patch sizes or if patches have complex edges. Both regional (Cihlar et al. 1997) and national (Cihlar et al. 2002) comparisons of nominal land cover maps based on fine (30m) versus coarse (1 km) resolution data indicate that the vast majority of 1 km pixels in forested regions of Canada are mixed. This is exacerbated by the sensor field of view increasing with viewing angle, resulting in areas exceeding 7 km² beyond 50° (Cihlar et al. 1996). Furthermore, the extent of mixing is substantial, with the most frequent land cover class for a simple 12- class legend occupying on average substantially below 50 % of a 1 km pixel (Cihlar et al. 2002). The ambiguity in sub-pixel mixing can be reduced by using finer spatial or thematic scales. Fine spatial scale remote sensing data are likely not feasible for most large area applications given the need for cost-effective and complete cloud free coverage. The alternative is to either grossly aggregate nominal land cover categories so they correspond to large patches or to adopt a measurement scale where the sub-pixel composition of land cover within each pixel is mapped.

Two different conceptual frameworks for sub-pixel land cover mapping are commonly employed, continuous fields and fraction of cover type. The continuous fields approach assumes that there is no spatial covariation among land cover attributes within the sensor footprint. The mapping task is then to identify the proportion of the pixel covered by each land cover attribute of interest (e.g., percentage of trees, herbs; needleleaf, broadleaf; uniform, clumped; etc.). Such parameters may be used directly in ecosystem process and climate models and hence remove the need for land cover labels.

However, there will still be a residual uncertainty in relating the retrieved continuous fields to land cover categories if spatial covariance of attributes occurs. For example, needleleaf trees are typically more clumped than broadleaf trees. Ignoring this covariation may lead to overestimates of understory light availability in broadleaf stands and underestimates in needleleaf stands.

The second approach, sub-pixel fractional land cover type mapping, assumes that continuous fields are spatially correlated so that they can be described by weighting of a finite number of co-occurring continuous fields. In the boreal forest for example, one category would correspond to 'evergreen needleleaf treed overstory with a deciduous broadleaf shrub understory layer' and another to 'deciduous broadleaf treed overstory with a deciduous broadleaf shrub understory layer'. The resulting map would then consist of separate layers identifying the proportional cover of each category within each pixel. The advantage of this approach over continuous fields is that it constrains the possible number of combinations of different continuous fields, such as leaf longevity or overstory coverage, prior to inversion of remote sensing measurements. However, fractional mapping may produce biases when the possible land cover categories are incorrectly specified.

Once the appropriate sub-pixel thematic scale is defined an estimation algorithm must be applied to generate the desired map product. We survey four common algorithms that have been applied for both continuous field and fractional cover estimation.

Cluster labeling. Spectral cluster labeling involves estimating the *a posteriori* probability of sub-pixel land cover categories from pixel reflectance. This is typically done by generating histograms using a representative training data set. Next, either the land cover mixture corresponding to the maximum *a posteriori* probability is selected; or, alternatively, a 'fuzzy label' is provided by weighting the vector of land cover mixtures by the associated *a posteriori* probabilities. The cluster labeling approach is equivalent to supervised classification where the legend has been extended to all unique combinations of land cover mixtures. There are three major issues involved in sub-pixel cluster labeling: quantization of mixtures and reflectance space, signature extension, and similarity between training data and target data (e.g., Duda and Hart 1973; Cihlar et al. 1998, 2000; Fernandes et al. 2002a).

Neural networks. In land cover classification, artificial neural networks (ANN) have been typically applied to produce discrete classifications by allocating each pixel to the class corresponding to the most activated unit (class) in the network output layer. However, the output activation levels are

usually continuous. By interpreting activation levels as a surrogate for the strength of membership in each class, ANNs have therefore been successfully used to derive fractional land cover categories (Foody 1996; Moody et al. 1996; Atkinson et al. 1997; Gopal et al. 1999). In these applications, a training set similar to the data used in cluster labeling is required although quantization is no longer a factor. Rather, the network is iteratively modified to provide the lowest prediction error over the training set. Cross-validation is typically done using a holdout sample to determine both the stopping point for network training and the expected prediction performance.

Regression. Multiple linear regression can be applied to estimate the composition of a pixel containing several sub-pixel land cover categories given reflectance measurements based on the availability of a calibration data set (Iverson et al. 1994; Settle and Campbell 1998; Maselli 2001). Regression has the advantage of being implemented in a variety of software tools with numerous diagnostics for feature selection and prediction performance.

Linear least squares inversion (LLSI). The LLSI method assumes a linear relationship between observed reflectance and sub-pixel cover types together with some noise source due to measurement or modeling uncertainties. A variety of continuous and discrete optimization algorithms are available to estimate sub-pixel land cover categories depending on the constraints specified and the assumptions regarding the noise models. Typical constraints include forcing the sub-pixel mixture proportions to sum-to-one and to individually lie between zero and one. A commonly applied algorithm is the constrained linear least squares inversion (Golub and van Loan 1989). The linear mixture model is defined by identifying reflectance-based attributes of endmembers corresponding to 'pure pixels', the latter containing extremes (100 % cover) of each fractional cover category (Hlavka and Spanner 1995) or continuous field (DeFries et al. 1995). Pure pixels may be sufficiently rare with coarse resolution data to prevent direct estimation from training samples. A practical solution is to perform linear regression on a training data set followed by extrapolating the regression results to the desired endmember level (DeFries et al. 2000). This solution has the added benefit of ensuring only endmembers that actually fit a linear model are selected.

2.1.1 Applications

A number of studies have evaluated the performance of the algorithms described above. However, the impact of spatial separation between

calibration and validation sites has only recently been given more attention (Maselli 2001). This is in spite of early validation of regression-based methods that indicated a substantial drop in performance for forest cover mapping as separation decreased (Iverson et al. 1994). This issue has been treated in more detail using a database of surface and high accuracy Landsat TM based land cover over the Boreal Ecosystem Atmosphere Study (BOREAS) area in the Canadian Boreal zone (Fernandes et al. 2002). The BOREAS region study applied all of the methods listed above to both continuous field and fractional cover mapping. Importantly, accuracy assessment was performed over both proximate (<150 km) and disparate (>300 km) training and validation Landsat scenes. As indicated in Figure 13-1, all of the algorithms except LLSI exhibited substantial bias with the disparate treatment. The bias is clearly in the direction of the mean sub-pixel proportions over the training data. There is also a theoretical basis (Settle and Campbell 1998; Fernandes et al. 2002a) that suggests that the observed bias is chiefly due to overfitting the algorithms over the training data. As such, careful spatial sampling of training data sets is required for all algorithms, although linear least squares inversion offers some robustness to bias errors. Ideally, cross-validation using disparate validation sites should be used when calibrating algorithms over large areas.

Only a few sub-pixel land cover maps of large areas have been completed to date. DeFries et al. (2000) produced a number of global continuous field products using linear mixture inversion based on a sample of Landsat Multi-Spectral Scanner (MSS) scenes. For an example of a global continuous field map of tree coverage derived from NOAA AVHRR data see DeFries et al. (2000).

A number of cluster labeling products have been generated over smaller regions such as the Pacific Northwest (Cohen et al. 2001) and Scandinavia (Fazakas et al. 1999). Recently, cluster labeling and neural networks have also been used to produce sub-pixel (<1 km) European forest cover maps (Kennedy and Bertolo 2002). Spectral signature overlap, signature drift, and the practical constraints on the number of calibration sites limit the performance of any algorithm for mapping sub-pixel land cover. Conversely, additional surface plot data sets and validated fine resolution land cover sources improve the derived maps. Perhaps the largest gains are to be made in the careful selection of data sources to constrain sub-pixel land cover estimates. Data fusion exercises based on existing topographic data bases (e.g., distribution of water bodies) and different sensors (such as using LIDAR or radars to distinguish between the extent of treed versus shrubby vegetation) may bear fruit. Research in these areas is continuing.

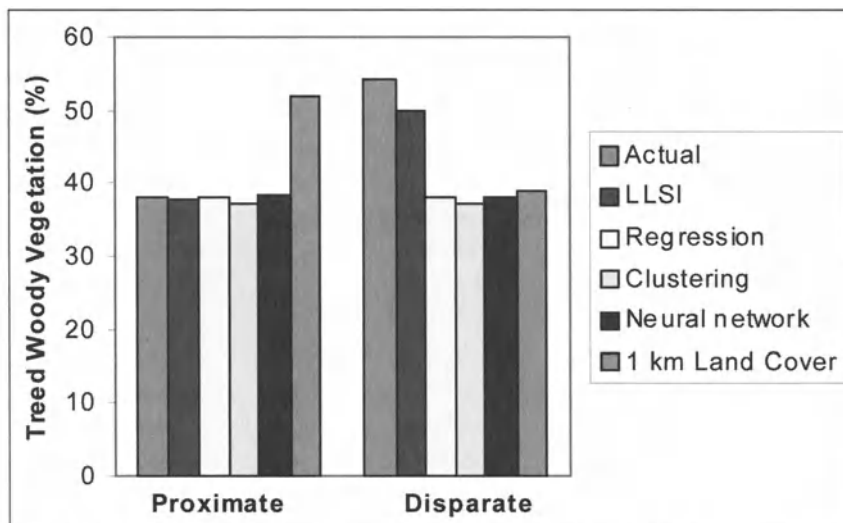


Figure 13-1. Comparison of sub-pixel land cover accuracy using both proximate (<100 km) and distant (>300 km) training and validation regions. The study region corresponded to an area covered by two, non-overlapping, Landsat TM scenes within the same ecozone and latitude in the central Canadian Boreal forest. LLSI is linear least square inversion. Adapted from Fernandes et al. (2002a).

2.2 Land cover change

Remote sensing offers timely, economical monitoring of land cover changes over large areas by generating environmental data on various temporal and spatial scales. In broad terms, digital change detection methods may be divided into post-classification methods and spectral change differencing methods (Gong and Xu, Chapter 11; Nelson 1983; Pilon et al. 1988; Singh 1989).

Post-classification change detection depends on comparing land cover labels in the classified images from different epochs. Land cover information may be obtained for each scene independently or by employing both images simultaneously, e.g. using the same training data set or a direct multidate classification method. The accuracy of change detection achieved by post-classification methods depends strongly on the classification accuracy of the component classifications.

Numerous spectral change differencing methods have been developed, particularly for monitoring changes in vegetation cover. Most of these are based on a comparison of multispectral vectors of a pixel at different dates. Multispectral vector differences as an indicator of change are quantified by band ratios, inner products or correlation coefficients. After computing the

change indicators, a threshold is defined that distinguishes 'real change' from measurement noise. Note, however, that changes may be gradual without obvious thresholds, such as forest thinning or selective harvesting (i.e., reduction in tree cover). In either case, an additional analysis is needed of the generated difference image to identify and characterize the detected change. Spectral differencing methods demand accurate co-registration of analyzed scenes and scene-to-scene radiometric normalization. While the differencing change detection methods perform fairly well when applied to fine resolution data (Coppin and Bauer 1996) they are less effective with coarse resolution data; some of the reasons are discussed below.

At regional scales, the most extensive source of satellite data is the archived record of AVHRR measurements with daily temporal coverage and a spatial resolution at nadir of 1.1 km in five spectral bands. At the local scale Landsat MSS, TM and ETM+ data with spatial resolutions of 80 m or 30 m span nearly 30 years. The spatial or temporal gaps of Landsat or SPOT (since 1986) archives implies that coarse resolution data will continue to be a useful source of land cover change information at regional scales. This indicates an important role for the recent (SPOT4/VGT, MODIS) and planned (MERIS, GLI) sensors, especially if the missions span a number of years. However, at this point, the AVHRR data are the primary data set for change detection studies.

Ideally, remotely sensed data used for change detection would be acquired by a sensor that collects data with the same field of view at approximately the same time of day with similar viewing geometry and constant radiometric resolution (Jensen 1996). Data provided by AVHRR and similar sensors are far from satisfying these requirements, therefore it is essential to understand the effects of the various sources of noise and the limitations on a change detection product derived from such data. The situation is complicated further by the compositing procedure conventionally applied to coarse resolution data (Cihlar et al., Chapter 12). While striving to obtain an image with minimum cloud contamination, the composite image contains observations from various dates, acquisition geometries and atmospheric conditions. These differences may result in (i) inaccurate co-registration (due to different instantaneous fields of view and registration errors); (ii) BRDF effects producing apparent differences in reflectance properties; and (iii) inadequate atmospheric corrections. The radiometric accuracy of a multiyear change detection analysis can be also affected by interannual differences in plant phenology (different timing of green up, seasonal peak or senescence). Individually and in combination, these effects cause difficulties in change detection analysis.

Presently, there are no land cover change products routinely generated from coarse resolution data. However, experimental products have been produced from AVHRR archived data, and a MODIS - based product is under development. The MODIS product employs a suite of change detection algorithms and majority voting to separate real changes from detection noise (Zhan et al. 1999). We have experimented with various algorithms using AVHRR data of Canada (1993-1999) in application to the boreal forest, and found that detection noise is a particular challenge because of the spectral heterogeneity of disturbed areas and other complexities of optical remote sensing at northern latitudes. We have developed a combined change detection algorithm that has the following features (Figure 13-2):

- Matching a reference template profile (derived for the reference year) to the pixel's profile in the target year. The template represents an average profile for pixels with the same land cover label as the pixel of interest, derived from the surrounding area. This approach is therefore sensitive to local land cover conditions. The selection of pixels for the above template profile combines two conditions: (i) a minimum number of pixels needed for a statistically representative template, and (ii) the maximum allowed distance of the sampled pixels from the pixel of interest. The overall standard deviation of the template profile is used to refine the sample of pixels selected for the template.
- A measure of matching (D) is computed as a difference between the template and target pixel (e.g., line D95, Figure 13-2):

$$D(m, n) = \sum_{i=1}^n \left| \frac{NDVI_{Ta-template}(i) - NDVI_{Tb-pixel}(i)}{\frac{\sigma_{Ta-template}(i)}{k}} \right|, \quad (1)$$

where:

- $NDVI_{Ta-template}$ = temporal profile derived from neighbourhood of pixel (m,n) in the reference year;
- $NDVI_{Tb-pixel}$ = temporal profile for the pixel (m,n) in the target year;
- $\sigma_{Ta-template}$ = standard deviation of $NDVI_{Ta-template}$;
- m,n = line and pixel number;
- i = compositing period;
- k = number of compositing periods.

- A seasonal average of D is computed for each pixel. A histogram of D values for all pixels (m,n) is then used to select the decision threshold for change/no change.
- The boundaries of the changed areas are refined by a texture change detection that assumes that most land-cover changes are accompanied by increasing spatial variability of surface reflectance, i.e. image texture (Zhan et al. 1999). We found that the coefficient of variation computed for a 7 by 7 pixel region produces less noise in the final change map.

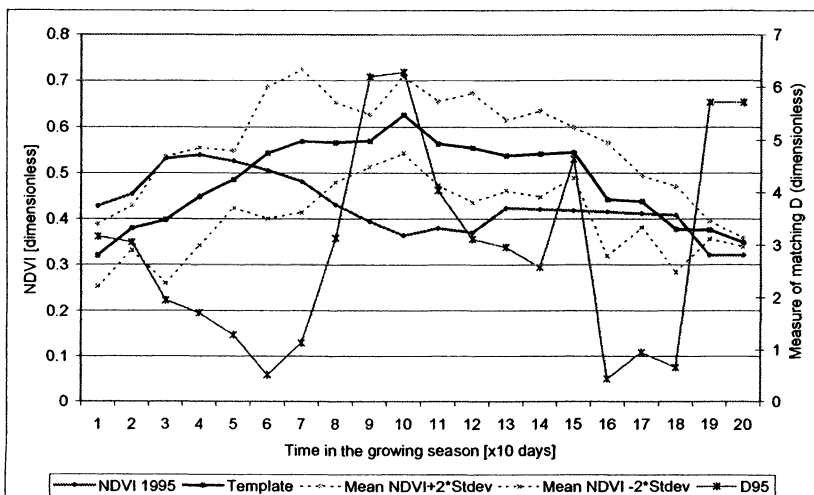


Figure 13-2. An example of the change detection elements for an AVHRR pixel in the 1995 growing season. Line 'NDVI 1995' represents the observed temporal profile for the selected pixel. Line 'Template' represents the expected profile for that pixel. Differences between the expected and the actual pixel profile are shown as line 'D95'.

Colour Plate 11 shows a resulting land cover change map for the Lake La Ronge, Saskatchewan area between 1993 and 1999; changes in various years are displayed in different colours. For visual interpretation and validation of the detected changes Colour Plate 11 also includes a Landsat TM image of the same area. Areas in red represent significant differences in multiyear seasonal profiles, most often due to forest fires or timber harvest. The change detection algorithm also identified spatial patterns within individual burns with intensive post- fire regeneration. Overall, the results show that AVHRR data enable the detection of changes in vegetation characteristics at regional scale, although identification or quantitative analysis must be performed using other data sources.

Anthropogenic activities generally cause land cover changes over areas smaller than 1 km², thus spatial and radiometric resolution of AVHRR is not adequate. To a lesser degree, such limitations are also present in SPOT/VGT

and Terra/MODIS data. Therefore, the MODIS 250 m global land cover change product (Zhan et al. 1999) is designed to serve as an alarm system rather than for change identification. However, such a product will also support the identification of disturbance effects or other natural changes taking place over larger areas.

2.3 Leaf area index

Leaf Area Index (LAI) is defined as one-half of the total surface area of all foliage per unit of ground surface area (Chen and Black 1992; http://www.fao.org/gtos/tems/variable_list.jsp). Here, the ground surface area corresponds to the horizontal projection of the ground surface onto the local horizontal datum. This definition strictly includes foliage attached to standing vegetation even if they have reduced vigour (e.g., undergoing chlorosis). LAI is a fundamental input parameter to a wide range of forest productivity and hydrology models (Band et al. 1991, Liu et al. 1997). There are three general approaches to LAI mapping: structural relationships using surface measurements, functional relationships using surface measurements, and functional relationships based on vegetation canopy reflectance models.

2.3.1 Structural relationships using surface measurements

In this approach statistical estimators are developed to predict LAI from observed reflectances. Vegetation indices (VIs) based on linear or non-linear combinations of reflectances are often used as regressor variables. The relationship between the VI and LAI often depends on increasing absorption at certain wavelengths with increasing LAI (Sellers 1985, 1987; Hunt and Rock 1989; Williams 1991). VIs are also designed to suppress one or more noise sources including viewing geometry, soil reflectance, atmospheric effects, variations in foliage and background reflectance, and canopy clumping (Horler and Ahern 1986; Chen 1996; Huete et al. 1997). Typically, co-located *in situ* LAI measurements and remote VI measurements are used to fit a regression relationship. There are three clear limitations to this approach that are violated to some degree in all implementations:

- a) The calibration sample must be representative of the area to be mapped;
- b) Classical regression assumes no measurement errors in the VI used and constant variance, with residuals in LAI estimates normally distributed around the regression line. Multiplicative measurement errors commonly found in both VIs and LAI violate both of these assumptions and can result in substantial biases in LAI estimates

(Fernandes and Leblanc 2002b). Structural regressions can be applied if a statistical measurement error distribution is known (Kendall and Stuart 1968). Alternatively, simple non-parameteric regression (Kendall and Stuart 1968) provides slightly lower precision with no need to model errors.

- c) Residuals in structural relationships may not be random in space or time but dependent on understory or surface characteristics, atmospheric properties, or viewing geometry.

In spite of the above constraints, effective predictive relationships can be developed between LAI and a simple vegetation index with only some sensitivity to leaf type or geographic location across a number of Landsat TM scenes spanning a large area (e.g., Figure 13-3 for Canadian forests).

2.3.2 Functional relationships using surface measurements

Functional relationships are similar to structural regressions except that the regression equation is assumed to correspond to a single physical relationship without natural variability due to factors other than LAI (Baret and Guyot 1991). This assumption may hold over small study areas (uniform in all respects except for LAI) but may be subject to bias over large areas due to variability in soil and vegetation characteristics. It is therefore not appropriate for large area mapping (Fernandes and Leblanc 2002b).

2.3.3 Functional relationships using canopy reflectance models

Functional relationships based on canopy reflectance models represent the extreme case where observations of LAI are only used to validate rather than calibrate parameters in a functional relationship. Canopy reflectance models use statistical or explicit mathematical descriptions of vegetation canopy structure and the physics of photon interactions within a canopy. Models range from rather simplified representations of a canopy as a stack of leaves (Sellers 1985), to radiative transfer approaches based on nuclear reactor theory (Knyazikhin et al. 1998), and statistical (Chen et al. 2000c) or explicit (Goel and Thompson 2000) geometrical representations of the interaction of light with tree crowns and understorey. The need for numerous ancillary parameters describing canopy and understorey characteristics is a major limitation to the use of reflectance models for remote sensing over large areas. There is increasing evidence that the *a priori* distribution of ancillary parameters can bias estimates in a manner similar to the bias observed with sub-pixel land cover algorithms (Fernandes et al. 2001; Combal et al. 2002). Even where geospatial databases of these ancillary

parameters exist, there has been no conclusive evidence that a reflectance model inversion will perform better than statistical methods based on these data (Eklundh et al. 2001).

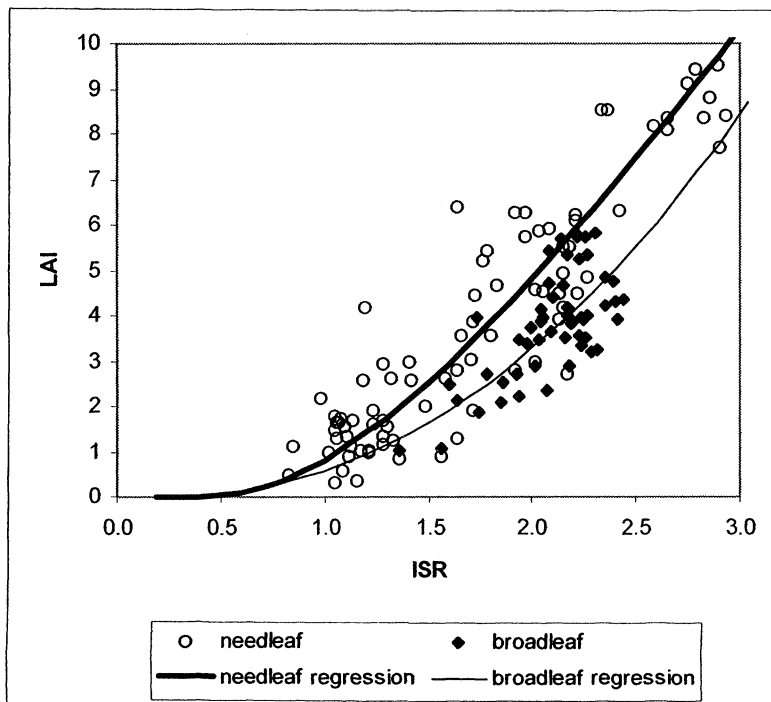


Figure 13-3. Structural regressions between the infrared simple ratio (ISR) of Thematic Mapper band 4 over band 5 from Landsat TM and ETM+ measurements and *in situ* LAI measurements over a range of forest stands across Canada (Fernandes et al. 2002c). Regressions are nonlinear due to transformations of axes to ensure homeoscedastic residuals. Substantial scatter is evident due to between- site differences and measurement uncertainties. The group of plots with LAI>7 correspond to old-growth stands on Vancouver Island, BC.

A limitation of all physically based methods for remote sensing LAI with passive optical sensors is the saturation in top-of-canopy broadband reflectance at LAI values of 3 to 4 (Knyazikhin et al. 1998). As such, calibration and inversion of functional models should be limited to sparse canopies. However, one useful application of reflectance models is to identify the maximum likely range of LAI values under a variety of structural parameters, thus helping to ascertain if structural regressions agree with the expected physics. For example, Colour Plate 12 compares structural regressions based on the same data set used in Figure 13-3 with model-based predictions assuming uniform ancillary parameters over the range of values typically encountered in Canada.

Both calibration and validation of LAI estimates require a means to relate *in situ* LAI estimates to satellite-based estimates. Various methods are available for estimating LAI *in situ* (Fournier et al., Chapter 4; Chen et al. 1997; Gower et al. 1999). However, it is difficult to measure the LAI within the footprint of a coarse resolution sensor using *in situ* techniques. A common solution is to first relate *in situ* LAI to reflectance fields from a fine resolution sensor such as Landsat ETM+ and then to scale these relationships to coarse resolution sensors by: a) generating fine resolution LAI fields that are then aggregated to coarse resolution and used as synthetic observations to develop coarse resolution relationships (e.g. Chen et al. 2002); or b) cross-calibrating the coarse and fine resolution vegetation indices and transforming the fine resolution algorithm using the cross-calibration function (Fernandes et al. 2002c). The second approach is preferred since it preserves traceability between *in situ*, fine resolution, and coarse resolution LAI values. For example, if at a later date one of the field measurements is found to be in error it can be removed from the regression without having to reprocess the fine resolution LAI fields. In any event, scaling up will reduce the precision of pixel LAI estimates by an additive factor equivalent to the cross-calibration error.

Colour Plate 13 provides a sample coarse resolution LAI image of Canada produced at 1 km from a 10-day composite SPOT4/VGT imagery. The structural regressions shown in Figure 13-3 were applied to forested regions, while regressions for non-forested areas were taken from other published data sets (Fernandes et al. 2002c). It is worth noting that the ratio of two infrared wavelength bands (near and shortwave) rather than an infrared and red wavelength band (e.g., the simple ratio or NDVI) was used to overcome the large uncertainty in red surface reflectance estimates for dark targets associated with typical levels of uncertainty in aerosol optical depths.

2.4 AVHRR for quantifying parameters related to forest fire

Wildfires are a significant disturbance in boreal forests where they exert a dominant control on stand age distribution and carbon storage. For example, during the 1989 to 1998 10-year period, forest fires burned an annual average of 3.4 million ha or 8 % of Canada's forested area. Most of the fires are caused by lightning which results in tree mortality over large tracts of forest (Stocks 1991). Between 1989 and 1998, fully 97 % of the area burned was due to fires larger than 10 km² (Canadian Council Of Forest Ministers 1999).

The AVHRR sensor onboard the NOAA satellites has been used for detecting actively burning wildfires for nearly twenty years (Li et al. 2001). By contrast, satellite-based techniques for large-area, post-fire mapping of burned vegetation are relatively less mature (Arino et al. 2001). Algorithms for both active fire (hotspot) detection and burned area mapping have been under development at the Canada Centre for Remote Sensing (CCRS) since 1997 and are now routinely applied over Canadian forests. The products generated (binary masks of daily active fire locations, daily smoke distribution maps, and annual burned area maps) are designed to serve two purposes. First, their uniform national coverage and GIS format make them suitable for global change studies dealing with carbon budget, fire emissions, and land cover change. Second, the products can complement the information produced by operational fire management agencies in Canada and the US. Although the spatial resolution and thematic accuracy of the AVHRR products are limited by comparison to *in situ* information from local fire monitoring, they have provided useful supplementary information in many cases, especially for non-active fire management zones in Canada.

An algorithm for identifying active forest fires using the NOAA-14 AVHRR sensor was developed by Li et al. (2000a,b). Before the hotspot algorithm is applied, raw radiance data are converted to TOA reflectance or brightness temperature, and precision geocoded using the GeoComp-n processing system (Cihlar et al., Chapter 12). The fire detection algorithm itself is based on a series of threshold tests. The first test ($T_3 > 315$ K) employs AVHRR mid-infrared channel (3.7 μm) to detect the thermal emissions produced by a fire. According to the Planck function, the mid-infrared range is highly sensitive to objects emitting radiation at the temperature of a wildfire (~1000 K), making this channel sensitive to flaming areas less than 1000 m^2 , or 0.1 % of the nominal AVHRR pixel size at nadir. The remaining tests use various combinations of the visible and thermal channels to eliminate false fire detections due to warm objects (such as recent burns) or highly reflective objects (e.g., clouds).

Colour Plate 14 shows annual composites of forest fire hotspots produced by applying the algorithm to daily AVHRR imagery from the 1994 to 2001 fire seasons. Most of the detected hotspots correspond to large fires occurring in remote spruce and jack pine forests within the Canadian Shield. Based on a validation of the algorithm conducted in the BOREAS study area in Central Canada (Li et al. 2000a), about 14 % of the hotspot pixels are likely false alarms. Considering the large number of satellite pixels examined (about 9.5 million/day), this represents a very low level of noise (~0.0001 %). Although the fire detection algorithm was found to reliably detect most fires that burn an area greater than 10 km^2 , it tends to

underestimate the actual area burned by about 35 % on average; this is due to the sensor providing only a once-per-day “snapshot” of fire activity, at which time a fire can be inactive or obscured by clouds or thick smoke.

For a more accurate estimate of the burned area, a separate algorithm was developed, dubbed Hotspot and NDVI Differencing Synergy (HANDS; Fraser et al. 2000a). As the name suggests, HANDS is designed to produce annual maps of burned forests by combining the active fire detection product with NDVI differencing, a common change detection technique. One challenge in applying conventional remote sensing change detection approaches (such as NDVI differencing) for mapping continental-scale burned area is to create a product with a commission error that is significantly smaller than the actual area burned (e.g., only about 0.5 % of Canada’s forests burns annually on average). The HANDS method substantially reduces noise levels by requiring that burned areas identified through NDVI differencing be co-located with the hotspots. The hotspot locations also serve as training pixels to derive spatially adaptive differencing thresholds that are sensitive to variation in forest type and burn severity.

The HANDS algorithm has been applied to Canadian forest for the 1995–2000 fire seasons using the annual hotspot masks (Colour Plate 14) and differencing of anniversary date September NDVI composites. Since 1998, AVHRR/NDVI composites have been replaced by a more sensitive SWIR-based vegetation index derived from the SPOT4/VGT instrument (Fraser et al. 2000b). The annual national burned areas were all within 15 % of estimates compiled by the Canadian Interagency Forest Fire Centre based on statistics from provincial and national fire management agencies. A comparison with burned area perimeters measured by fire agencies from aerial photo-interpretation (Fraser et al. 2000a) demonstrated that the 1 km product is best suited for mapping burns larger than about 10 km², which in most areas of Canada accounts for the vast majority of burned forests.

The AVHRR fire products have been made available through the Fire Monitoring, Mapping, and Modelling System (Fire M3; <http://fms.nofc.cfs.nrcan.gc.ca/FireM3/>). Fire M3 provides access to the daily hotspots and smoke products and to annual burned area products, using cartographic maps and an Internet Map Server. The system also uses the Canadian Forest Service (CFS) Canadian Forest Fire Danger Rating System to model fire danger and behaviour attributes, which can be interactively queried for each detected hotspot.

3. REGIONAL CARBON CYCLE ASSESSMENT

Carbon exchange between the forest ecosystem and the atmosphere is quantified by three related parameters: net primary productivity (NPP, total carbon uptake), net ecosystem productivity (NEP, NPP minus heterotrophic respiration), and net biome productivity (NEP minus disturbance losses). These quantities cannot be directly measured by satellite sensors because of the biochemical and temporal complexities of the carbon exchange processes and must therefore be estimated. However, in all cases satellite data provide critical information that may be used with advantage to constrain estimates obtained from the models. Since satellite data contain an up-to-date information on the ecosystem, the model estimates can be fine tuned to reflect the spatially and temporally highly variable exchanges of carbon.

3.1 Net primary productivity

Net primary productivity (NPP) is defined as the net carbon absorption rate by living plants. NPP is the rate difference between plant photosynthesis and autotrophic respiration and is usually expressed in grams of carbon per m^2 per year. It not only quantifies plant growth for practical usage but also is one of the important components in carbon cycle studies.

Two types of NPP models - process models and production efficiency (or 'epsilon') models - are mostly used for mapping NPP at regional or global scales (Cramer et al. 1999). In a process model, NPP is obtained through simulating a series of plant physiological processes such as photosynthesis, autotrophic respiration, and transpiration (Bonan 1995; Cramer et al. 1999; Foley 1994; Melillo et al. 1995b; Woodward et al. 1995). Production efficiency models are based on the concept of light use efficiency proposed by Monteith (1972), who suggested that NPP is linearly related to absorbed photosynthetically active radiation (APAR) under non-stressful conditions. The light use efficiency ϵ or LUE, is defined as a conversion factor from input energy (APAR) to output energy (NPP) and is regarded as a species-dependent quantity in the models.

Remotely sensed data can provide consistent large area coverage with frequent or regular updates, at nominal or no cost to users. In epsilon models, the vegetation indices (VIs) derived from remote sensing are used for the calculation of APAR (Field et al. 1995; Potter et al. 1993; Prince and Goward 1995; Ruijmy et al. 1996). VIs also serve as key driving variables in process models, such as those at regional scale (Band et al. 1991; Liu et al. 1997, Running et al. 1989) and those at the global scale (Hunt et al. 1996; Sellers et al. 1996). The information on vegetation type, resolved with

remote sensing techniques, is useful in parameterizing vegetation characteristics for process models (Liu et al. 1997). Some models also use remote sensing based meteorological variables (Prince and Goward 1995).

Process models take into account basic plant physiological processes, with the ability to explicitly describe these processes and their interactions (Coops and White, Chapter 15). The application of such models over large areas requires more spatially explicit data and larger computing resources; of these, the former is becoming a more serious impediment. Another challenge is to temporally and spatially scale up a process model that is initially developed at the leaf or stand level for a short period of time. Epsilon models have a high computing efficiency and low demand on input data.

With the same computing resources, higher spatial resolution can be achieved using an epsilon model than using a process-based model; even with current technological advancements, the computing capacity is still a major limiting factor for high-temporal and spatial resolution process modeling for large areas. More importantly however, an accurate estimation of ϵ under stressed conditions for different vegetation types remains a serious challenge. A recent study suggested that autotrophic respiration might be one of the reasons for NPP to deviate from its linear relationship with APAR (Ruijmy et al. 1996). In some studies, process models were used to provide independent estimate of ϵ for different vegetation types (Hunt and Running 1992; Liu et al. 1999).

An example of a process model using remote sensing and ancillary datasets is the Boreal Ecosystem Productivity Simulator (BEPS), which was developed to mimic plant growth and to provide estimates of NPP (Liu et al. 1997, 1999, 2002). Remote sensing inputs for BEPS are LAI (10-day intervals) and land cover (annual). Meteorological inputs include daily values of air temperature, relative humidity, total solar radiation, and total precipitation. Soil data used are the available soil water capacity or soil texture. Both meteorological and soil data are gridded with the same resolution and map projection as the remote sensing inputs. BEPS computes, at daily step, soil water balance, leaf stomatal conductance, sunlit and shaded leaf area index, sunlit and shaded leaf gross photosynthesis, total gross canopy photosynthesis, maintenance and growth respiration of leaves, stems and roots. BEPS outputs include NPP, evapotranspiration, and other parameters of interest.

Daily NPP values from BEPS were compared with those derived from simultaneous carbon dioxide flux measurements above and below the forest canopy at two sites in central Canada (Chen et al. 1999). It was possible to validate NPP calculations at hourly and daily time steps in this way for the first time. The NPP map validation was carried out using plot biomass data

in Quebec and ground NPP measurements in central Canada (Liu et al. 2002). The correlation coefficients between measured and modeled NPP are larger than 0.60 with statistical significance levels larger than 0.95 in all the comparisons. Estimated annual NPP values are comparable with other studies at several locations (Liu et al. 2002; Peng and Apps 1998). Colour Plate 15 shows BEPS-simulated NPP over Canadian landmass at 1 km resolution.

3.2 Net ecosystem productivity and net biome productivity

Net ecosystem productivity (NEP) quantifies the net exchanges of carbon between the land surface (vegetated or non-vegetated) and the atmosphere, without considering the direct carbon release due to disturbance. It is calculated as the difference between NPP and heterotrophic respiration (R_h):

$$NEP = NPP - R_h. \quad (2)$$

R_h results from the decomposition of dead organic material in soils and the litter layer above mineral soils. By this definition, when $NEP > 0$, the ecosystem acts as a carbon sink by absorbing more carbon than it releases.

Net biome productivity (NBP) is used to account for carbon losses due to disturbances at the biome level (Walker and Steffen 1997), and can be expressed as

$$NBP = NEP - D, \quad (3)$$

where D is direct carbon release at the time of disturbance and usually has three components:

$$D = D_{fire} + D_{insect} + D_{log}, \quad (4)$$

where D_{fire} , D_{insect} and D_{log} are the amounts of carbon release due to forest fire, insect-induced forest mortality and timber removal, respectively. The units of NEP and NBP are also grams of carbon per m^2 per year.

Numerous models have been developed for quantifying the terrestrial carbon cycle. They include CENTURY (Parton et al. 1987, 1993; Schimel et al. 1994, 2001), TEM (Raich et al. 1991; McGuire et al. 1992, 1995, 1997; Melillo et al. 1993, 1995a), BIOME-BGC (Hunt and Running 1992; Running and Hunt 1993), CASA (Potter et al. 1993), and CBM-CFS (Kurz

et al. 1992; Kurz and Apps 1995, 1999). These models employ different methods for estimating NPP, a critical component of the carbon cycle (Pan et al. 1998). CENTURY and TEM rely on empirical relationships between NPP and climatic, atmospheric and soil factors, while CASA estimates NPP as a function of absorbed photosynthetically active radiation (APAR). BIOME-BGC is one of many models that use a process-based leaf photosynthesis model (Farquhar et al. 1980) for canopy level estimation of gross carbon uptake. CENTURY, TEM, CASA and BIOME-BGC have been shown to be effective in estimating regional and global NEP when carbon release due to disturbance is not explicitly considered. Disturbance effects are especially important in boreal forest ecosystems because of the frequent occurrence of wildfires and insect-induced mortality (Kurz et al. 1992; Kurz and Apps 1995). The CBM-CFS model developed an empirical approach to estimating the disturbance effects from changes in forest stand age structure (Kurz et al. 1992; Kurz and Apps 1995, 1999). The impacts of climate and atmospheric changes on carbon cycle are not yet estimated in CBM-CFS.

Recently, an Integrated Terrestrial Ecosystem Carbon Cycle Model (InTEC) was developed to make use of satellite imagery for terrestrial carbon cycle estimation and to integrate the effects of both disturbance and non-disturbance factors (Chen et al. 2000a,b). This combined model mechanistically integrates the CENTURY model for carbon and nitrogen cycles in soils, and Farquhar's biochemical model of leaf photosynthesis. Empirical NPP-age relationships (Gower et al. 1996; Chen et al. 2002c) are used to estimate the stand dynamics. Processes considered in the model include nitrogen deposition and fixation, carbon release due to disturbances, forest regrowth, changes in growing season length, CO₂ fertilization, soil respiration, and changes in carbon/nitrogen ratios of different components in biomass and soil carbon pools. InTEC is capable of estimating the effects of both disturbance and non-disturbance factors on carbon cycle based on atmospheric (CO₂ concentration and nitrogen deposition), climatic (interannual variations in temperature and precipitation), and biotic changes (forest area and age- related structural changes due to disturbances) since the pre-industrial period.

In relation to balance mapping, satellite data provide three key inputs shown in Figure 13-4 (Chen et al. 2002b): (i) land cover type (important for characterizing the differences in photosynthesis capacity and in carbon allocation), (ii) leaf area index (to allow process-based modeling of photosynthesis and respiration of living organisms, and (iii) approximate date of recent forest burns (for the most updated information on disturbance). Evapotranspiration (ET) constrains the NPP estimate by controlling the stomatal conductance. The ancillary data required consist of

soil texture and daily meteorological data for ET and NPP mapping, long-term climate data for annual NEP estimation, and disturbance data (including fire, insect, and harvest) for NBP estimation.

Results from the spatially-aggregated modeling (Chen et al. 2000b) indicate that in the past 100 years, Canada's forests as a whole were a small carbon source of about 30 Mt C y^{-1} in the period 1895-1905 due to large disturbances near the end of the 19th century, estimated from age class data in 1920 (Kurz and Apps 1995); a large carbon sink of about 170 Mt C y^{-1} during the period of 1930-1970 due to forest regrowth in previously burned areas; and a moderate carbon sink of about 50 Mt C y^{-1} for the period 1980-1996 (Figure 13-5). The 1980-1996 sink is a net balance between the negative effects of increased disturbances and positive effects of other non-disturbance factors. The non-disturbance factors, in order of importance, were found to be (1) atmospheric nitrogen deposition measured by a national monitoring network, (2) net nitrogen mineralization and fixation estimated from temperature and precipitation records, (3) CO₂ fertilization estimated from CO₂ records using a leaf level photosynthesis model, and (4) growing season length increase estimated from spring air temperature records.

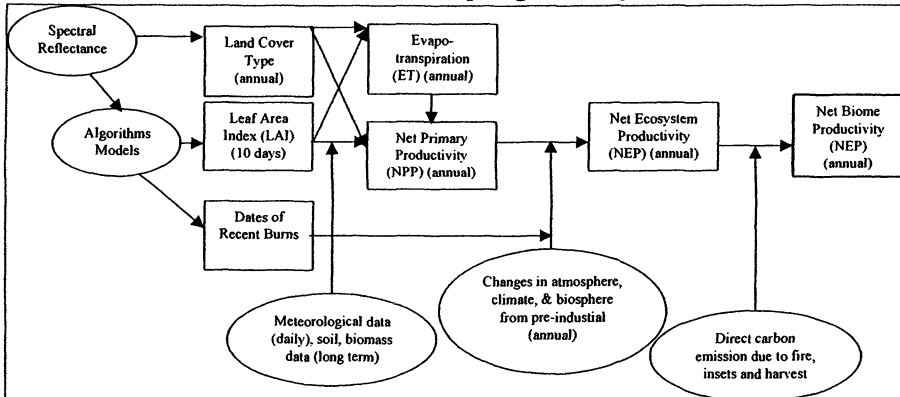


Figure 13-4. Main steps in estimating the full carbon cycle in terrestrial ecosystems. Remote sensing provides spectral reflectance data used to obtain the basic state variables (leaf area index, land cover, burn area and date), while the dynamic short-term and long-term processes of the carbon cycle within plants and soils are modeled using the additional inputs of climate, forest stand age from inventory and disturbance data. The end product is an estimate of net biome productivity.

Results from spatially explicit modeling (Chen et al. 2002b) show NBP variation patterns between 1901 and 1998 similar to those from spatially-aggregated modeling (Figure 13-5). The results strengthen the previous conclusions of Chen et al. (2000b) but add two new findings: (1) the interannual variability in NBP from spatially-explicit modeling is larger than

that from the spatially-aggregated modeling because of nonlinear effects of climate on the carbon cycle; and (2) averaged over the last century, the sink magnitude from the spatially-explicit modeling is 21 % smaller than that from spatially aggregated modeling. These differences are due to the interactions between temperature, latitude, soil respiration and forest regrowth (Chen et al. 2002b).

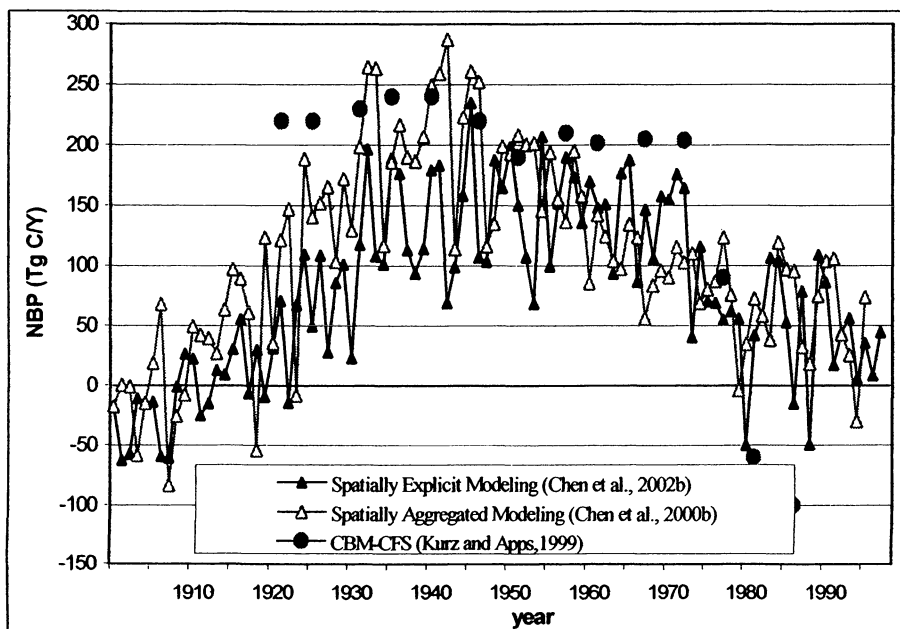


Figure 13-5. Comparison of three sets of NBP results, representing all Canada's forests from 1901 to 1998, illustrating the Carbon balance of Canada's forests over the last century from two studies: (1) spatially-aggregated modeling of annual NBP using InTEC (Chen et al. 2000b); and (2) spatially-explicit (approximately 1 km resolution) modeling using InTEC (Chen et al. 2002b).

4. CONCLUSIONS

Effective use of satellite data in environmental monitoring necessitates that quantitative information be extracted, accurately and reliably. This is a major challenge in case of optical data, primarily because effects of other parameters mask the information on a specific environmental parameter of interest. A combination of theoretical modeling, field data collection, and image data manipulation is often required to obtain satisfactory results. We have described successful techniques for obtaining information on land cover and cover change, forest structure (leaf area trend), and fires which

together are the main dynamic features of the boreal forest landscape. Our experience indicates that rigorous testing and validation of algorithms is both necessary and possible but it requires a systematic approach that takes into consideration the various possible sources of errors in the output products.

Following the development and use of satellite-derived products over several years, it has become clear that such products have a limited impact unless used as input into quantitative models. The basic reason is that the forest ecosystem is very complex, and only some of the factors governing its behaviour may be quantified through satellite observations; others must be determined from other environmental measurements or modeled. In this Chapter, models for estimating components of the forest carbon cycle are discussed that illustrate this point. Once the satellite-derived products are used in this way, they provide critical and unique information regarding the spatial distribution and temporal dynamics of key environmental factors and thus enhance the accuracy and representativeness of the final results over large areas. In general, methodologies for this combined approach are at relatively early stages of development. However, with rapid improvements in virtually all relevant observation and modeling areas, strong progress is being made towards satellite data assimilation in a comprehensive observation-modeling framework (Cihlar et al. 2002b). We expect that such a framework for terrestrial observation and assessment over large areas will become reality within the next 10 years.

REFERENCES

- Arino, O., Piccolini, I., Kasischke, E., Siegert, F., Chuvieco, E., Martin, P., Li, Z., Fraser, R. H., Eva, H., Stroppiana, D., Pereira, J. M. C., Silva, J. M. N., Roy, D., & Barbosa, P. (2001). Burn scars mapping methods. Ahern, F. J., Goldammer, J. G., & Justice, C. O. (Eds.). *Global and Regional Vegetation Fire Monitoring from Space: Planning a Coordinated International Effort*, 227-255. SPB Academic Publishing bv, The Hague, The Netherlands, 302 p.
- Atkinson, P. M., Cutler, M. E. J., & Lewis, H. (1997). Mapping sub-pixel proportional land cover with AVHRR imagery. *International Journal of Remote Sensing*, 4, 917-935.
- Band, L. E., Peterson, D. L., Running, S. W., Dungan, J., Lathrop, R., Coughlan, J., Lammers, L., & Pierce, L. L. (1991). Forest ecosystem processes at the watershed scale: Basis for distributed simulation. *Ecological Modeling*, 56, 171-196.
- Baret, F., & Guyot, G. (1991). Potentials and limits of vegetation indices for LAI and APAR assessment. *Remote Sensing of Environment*, 35, 161-173.
- Bonan, G. B. (1995). Land-atmosphere CO₂ exchange simulated by a land surface process model coupled to an atmospheric general circulation model. *Journal of Geophysical Research*, 100, 2817-2831.

- Canadian Council Of Forest Ministers, (1999). *National Forestry Database Program*. Canadian Forest Service, Natural Resources Canada, <http://nfdp.ccfm.org/>.
- Chen, J. M. (1996). Evaluation of vegetation indices and a modified simple ratio for boreal applications. *Canadian Journal of Remote Sensing*, 22, 229-242.
- Chen, J. M., & Black, T. A. (1992). Defining leaf area index for non-flat leaves. *Plant, Cell and Environment*, 15, 421-429.
- Chen, J. M., Rich, P. M., Gower, T. S., Norman, J. M., & Plummer, S. (1997). Leaf area index of boreal forests: theory, techniques and measurements. *Journal of Geophysical Research*, 102, 29429-29444.
- Chen, J. M., Liu, J., Cihlar, J., & Goulden, M. L. (1999). Daily canopy photosynthesis model through temporal and spatial scaling for remote sensing applications. *Ecological Modelling*, 124, 99-119.
- Chen, J. M., Li, X., Nilson, T., & Strahler, A. (2000). Recent advances in geometrical optical modelling and its applications. *Remote Sensing Reviews*, 18, 227-262.
- Chen, W. J., Chen, J. M., Liu, J., & Cihlar, J. (2000a). Approaches for reducing uncertainties in regional forest carbon balance. *Global Biogeochemical Cycles*, 14, 827-838.
- Chen, J. M., Chen, W., Liu, J., & Cihlar, J. (2000b). Annual carbon balance of Canada's forests during 1895-1996. *Global Biogeochemical Cycles*, 14, 839-850.
- Chen, J., Pavlic, G., Brown, L., Cihlar, J., Leblanc, S. G., White, P., Hall, R. J., Peddle, D., King, D. J., Trofymow, J. A., Swift, E., van der Sanden, J., & Pellikka, P. K. E. (2002a). Derivation and validation of Canada-wide coarse-resolution leaf area index maps using high-resolution satellite imagery and ground measurements. *Remote Sensing of Environment*, 80, 165-184.
- Chen, J. M., Ju, W., Cihlar, J., Price, D., Liu, J., Chen, W., Pan, J., Black, T. A., & Barr, A. (2002b). Spatial distribution of carbon sources and sinks in Canada's forests based on remote sensing. *Tellus*, submitted.
- Chen, W., Chen, J. M., Price, D. T., & Cihlar, J. (2002c). Effects of stand age on net primary productivity of boreal black spruce forests in Canada. *Canadian Journal for Forest Research*, in press.
- Cihlar, J., Ly, H., & Xiao, Q. (1996). Land cover classification with AVHRR multichannel composites in northern environments. *Remote Sensing of Environment*, 58, 36-51.
- Cihlar J., Beaubien J., Xiao Q., Chen J. M., & Li, Z. (1997). Land cover of the BOREAS Region from AVHRR and LANDSAT data. *Canadian Journal of Remote Sensing*, 23, 163-175.
- Cihlar, J., Latifovic, R., Beaubien, J., Palmer, M., & Fraser, R. (2002a). A TM-based accuracy assessment of land cover and leaf area index products for Canada derived from SPOT4/VGT data. *Canadian Journal of Remote Sensing*, accepted.
- Cihlar, J., Denning, S., Ahern, F., Arino, O., Belward, A., Bretherton, F., Cramer, W., Dedieu, G., Field, C., Francey, R., Gommes, R., Gosz, J., Hibbard, K., Igarashi, T., Kabat, P., Olson, R., Plummer, S., Rasool, I., Raupach, M., Scholes, R., Townshend, J., Valentini, R., & Wickland, D. (2002b). Initiative to quantify terrestrial carbon sources and sinks. *EOS Transactions, American Geophysical Union*, 83, 5-6.
- Cihlar, J., Xiao, Q., Beaubien, J., Fung, K., & Latifovic, R. (1998). Classification by Progressive Generalization: a new automated methodology for remote sensing multichannel data. *International Journal of Remote Sensing*, 19, 2685-2704.
- Cohen, W. B., Maiersperger, T. K., Spies, T. A., & Oetter, D. R. (2001). Modeling forest cover attributes as continuous variables in a regional context with Thematic Mapper data. *International Journal of Remote Sensing*, 22, 2279-2310.

- Combal, B., Baret, F., Weiss, M., Trubuil, A., Mace, D., Pragnere, A., Myneni, R., Knyazikhin, Y., & Wang, L. (2002). Retrieval of canopy biophysical variables from bi-directional reflectance: using prior information to solve the ill-posed problem. *Remote Sensing of Environment*, in press.
- Coppin, P. R., & Bauer, M. E. (1996). Digital change detection in forest ecosystems with remote sensing imagery. *Remote Sensing Reviews*, 13, 207-234.
- Cramer, W., Kicklighter, D. W., Bondeau, A., Moore B. III, et al. (1999). Comparing global models of terrestrial net primary productivity (NPP): overview and key results. *Global Change Biology*, 5, 1-15.
- DeFries, R. S., Field, C. B., Fung, I., Justice, C. O., Los, S., Matson, P. A., Matthews, E., Mooney, H., Potter, C. S., Prentice, K., Sellers, P. J., Townshend, J. R. G., Tucker, C. J., Ustin, S. L., & Vitousek, P. M. (1995). Mapping the land surface for global atmosphere-biosphere models: toward continuous distributions of vegetation's functional properties. *Journal of Geophysical Research*, 100, 20867-20882.
- DeFries, R. S., Hansen, M. C., & Townshend, J. R. (2000). Global continuous fields of vegetation characteristics: a linear mixture model applied to multi-year 8 km AVHRR data. *International Journal of Remote Sensing*, 21, 1389-1414.
- Duda, R. O., & Hart, P. E. (1973). *Pattern classification and scene analysis*. Wiley, New York.
- Eklundh, L., Harrie, L., & Kuusk, A. (2001). Investigating relationships between Landsat ETM+ sensor data and leaf area index in a boreal conifer forest. *Remote Sensing of Environment*, 78, 239-251.
- Farquhar, G.D., von Caemmerer, S., & Berry, J.A. (1980). A biochemical model of photosynthetic CO₂ assimilation in leaves of C₃ species. *Planta*, 149, 78-90.
- Fazakas, Z., Nilsson, M., & Olsson, H. (1999). Regional forest biomass estimation by use of satellite data and ancillary data. *Agricultural and Forest Meteorology*, 98-99, 417-425.
- Fernandes, R., White, H. P., Leblanc, S., Pavlic, G., McNairn, H., Chen, J. M., & Hall, R. J., (2001). Examination of error propagation in relationships between leaf area index and spectral vegetation indices from Landsat TM and ETM. *Proceedings of the 23rd Canadian Remote Sensing Symposium*, 41-51 Quebec City, Quebec, August 2001.
- Fernandes, R., Fraser, R., Latifovic, R., Cihlar, J., Beaubien, J., & Du, Y. (2002a). Approaches to fractional land cover and continuous field mapping: a comparative assessment. *Remote Sensing of Environment*, accepted.
- Fernandes, R. A., & Leblanc, S. G. (2002). Appropriate linear regression techniques for the calibration of remote sensing models: why classical linear regression should not be used. *Remote Sensing Reviews*, submitted.
- Fernandes, R. A., Butson, C. G., Leblanc, S. G., & Latifovic, R. (2002b). Calibration and validation of coarse scale LAI estimates across Canada. *Canadian Journal of Remote Sensing Special Issue on Landsat ETM+*, submitted.
- Field, B. C., Randerson, J. T., & Malmstrom, C. M. (1995). Global net primary production: combining ecology and remote sensing. *Remote Sensing of Environment*, 51, 74-88.
- Foley, J. A. (1994). Net primary productivity in the terrestrial biosphere: the application of a global model. *Journal of Geophysical Research*, 99, 20773-20783.
- Foody, G. M. (1996). Relating the land-cover composition of mixed pixels to artificial neural network classification output, Photogrammetric Engineering. *Remote Sensing*, 62, 491-499.

- Fraser, R. H., Li, Z., & Cihlar, J. (2000a). Hotspot and NDVI differencing synergy (HANDS): a new technique for burned area mapping over boreal forest. *Remote Sensing of Environment*, 74, 362-376.
- Fraser, R. H., Li, Z., & Landry, R. (2000b). SPOT VEGETATION for characterizing boreal forest fires. *International Journal of Remote Sensing*, 21, 3525-3532.
- Goel, N. S., & Thompson, R. L. (2000). A snapshot of canopy reflectance models and a universal model for the radiation regime. *Remote Sensing Review*, 18, 197-225.
- Golub, G. H., & van Loan, C. (1989). *Matrix computations*. The Johns Hopkins University Press, Baltimore, Maryland.
- Gopal, S., Woodcock, C. E., & Strahler, A.H. (1999). Fuzzy neural network classification of global land cover from a 1° AVHRR data set. *Remote Sensing of Environment*, 67, 230-243.
- Gower, S. T., Kucharik, C. J., & Norman, J. M. (1999). Direct and indirect estimate of leaf area index, fapar and net primary production of terrestrial ecosystems. *Remote Sensing of Environment*, 70, 29-51.
- Gower, S. T., McMurtrie, R. E., & Murty, D. (1996). Aboveground net primary production decline with stand age: potential causes. *Tree*, 11, 378-382.
- Hlavka, C. A., & Spanner, M. A. (1995). Unmixing AVHRR imagery to assess clearcuts and forest regrowth in Oregon. *IEEE Transactions on Geoscience Remote Sensing*, 31, 788-795.
- Horler D., & Ahern, F. (1986). Forestry information content of Thematic Mapper data. *International Journal of Remote Sensing*, 7, 405-428.
- Huete, A. R., Liu, H. Q., Batchily, K., & van Leeuwen, W. (1997). A comparison of vegetation indices over a global set of TM images. *Remote Sensing Environment*, 59, 440-451.
- Hunt, E. R., Jr., & Running, S. W. (1992). Simulated dry matter yields for aspen and spruce stand in the North American boreal forest. *Canadian Journal of Remote Sensing*, 18, 126-133.
- Hunt, E. R., Jr., Piper, S. C., Nemani, R., Keeling, C. D., Otto, R. D., & Running, S. W. (1996). Global net carbon exchange and intra-annual atmospheric CO₂ concentrations predicted by an ecosystem simulation model and three-dimensional atmospheric transport model. *Global Biogeochemical Cycles*, 10, 431-456.
- Hunt, E. R., Jr., & Rock, B. N. (1989). Detection of changes in leaf water content using near- and middle-infrared reflectances. *Remote Sensing of Environment*, 30, 43-54.
- Iverson, L. R., Cook, E. A., & Graham, R. L. (1994). Regional forest cover estimation via remote sensing: the calibration centre concept. *Landscape Ecology*, 9, 159-174.
- Jensen, R. J. (1996). *Introductory digital image processing: A remote sensing perspective*. Geographic Information Science Series, Prentice Hall, Upper Saddle River, NJ.
- Kendall, M. G., & Stuart, A. (1968). *The advanced theory of statistics*, Vol. 3. (2nd ed.). Charles Griffin & Company Ltd., London.
- Kennedy, P., & Bertolo, F. (2002). Mapping forests of Europe: combining satellite-derived spatial information with national and sub-national statistics. *Canadian Journal of Remote Sensing*, accepted.
- Knyazikhin, Y., Martonchik, J. V., Myneni, R. B., Diner, D. J., & Running, S.W. (1998). Synergistic algorithm for estimating vegetation canopy leaf area index and fraction of absorbed photosynthetically active radiation from MODIS and MISR data. *Journal of Geophysical Research*, 103, 32257-32276.

- Kurz, W. A., & Apps, M. J. (1999). A 70-year retrospective analysis of carbon fluxes in the Canadian forest sector. *Ecological Modelling*, 9, 526-547.
- Kurz, W. A., & Apps, M. J. (1995). An analysis of future C budgets of Canadian boreal forests. *Water, Air, and Soil*, 82, 321-331.
- Kurz, W. A., Apps, M. J., Webb, T. M., & McNamee, P. J. (1992). The C budget of the Canadian forest sector: Phase I, *Information Report NOR-X-326*. Forestry Canada, Northern Forestry Centre, Edmonton, Alberta.
- Li, Z., Kaufman, Y. J., Ichoku, C., Fraser, R., Trichtchenko, A., Giglio, L., Jin, J., & Yu, X. (2001). A review of AVHRR-based active fire detection algorithms: principles, limitations, and recommendations. Ahern, F., Goldammer, J. G., & Justice, C. O. (Eds.). *Global and regional vegetation fire monitoring from space: Planning a coordinated international effort*, 199-225. SPB Academic Publishing.
- Li, Z., Nadon, S., & Cihlar, J. (2000a). Satellite detection of Canadian boreal forest fires: development and application of an algorithm. *International Journal of Remote Sensing*, 21, 3057-3069.
- Li, Z., Nadon, S., Cihlar, J. & Stocks, B. J. (2000b). Satellite mapping of Canadian boreal forest fires: evaluation and comparisons. *International Journal of Remote Sensing*, 21, 3071-3082.
- Liu, J., Chen, J.M., Cihlar, J., & Park, B. (1997). A process-based boreal ecosystem productivity simulator using remote sensing inputs. *Remote Sensing of Environment*, 62, 158-175.
- Liu, J., Chen, J. M., Cihlar, J., & Chen, W. (1999). Net primary productivity distribution in the BOREAS study region from a process model using satellite and surface data. *Journal of Geophysical Research*, 104, 27735-27754.
- Liu, J., Chen, J. M., Cihlar, J., & Chen, W. (2002). Net primary productivity mapped for Canada at 1 km resolution. *Global Ecology and Biogeography*, in press.
- Maselli, F. (2001). Definition of spatially variable spectral endmembers by locally calibrated multivariate regression analyses. *Remote Sensing of Environment*, 75, 29-38.
- McGuire, A. D., Melillo, J. M., Kicklighter, D. W., Grace, A. L., Moore, B., III, & Vorosmarty, C. J. (1992). Interactions between carbon and nitrogen dynamics in estimating net primary productivity for potential vegetation in North America. *Global Biogeochemical Cycles*, 6, 101-124.
- McGuire, A. D., Melillo, J. M., Kicklighter, D. W., & Joyce, L. A. (1995). Equilibrium responses of soil carbon to climate change. *Journal of Biogeography*, 22, 785-796.
- McGuire, A. D., Melillo, J. M., Kicklighter, D. W., Pan, Y., Xiao, X., Helfrich, J., Moore, B. III, Vorosmarty, C. J., & Schloss, A. L. (1997). Equilibrium responses of global net primary production and carbon storage to doubled atmospheric carbon dioxide: sensitivity to changes in vegetation nitrogen concentration. *Global Biogeochemical Cycles*, 11, 173-189.
- Melillo, J. M., & VEMAP Members. (1995). Vegetation/Ecosystem Modeling and Analysis Project: comparing biogeography and biogeochemistry models in a continental-scale study of terrestrial ecosystem responses to climate changes and CO₂ doubling. *Global Biogeochemical Cycles*, 9, 407-437.
- Melillo, J. M., McGuire, A. D., Kicklighter, D. W., Moore, B. III, Vorosmarty, C. J., & Schloss, A. L. (1993). Global climate change and terrestrial net primary production. *Nature*, 363, 234-240.
- Melillo, J. M., Kicklighter, D. W., McGuire, A. D., Peterjohn, W. T., & Newkick, K. M. (1995). Global change and its effects on soil organic carbon stocks. Zepp, R. G. &

- Sonntag, C. (Eds.). *Role of nonliving organic matter on the Earth's carbon cycles*, 175-189. Wiley, New York.
- Monteith, J. L. (1972). Solar radiation and productivity in tropical ecosystem. *Journal Applied Ecology*, 9, 747-766.
- Moody, A., Gopal, S., & Strahler, A.H. (1996). Artificial neural network response to mixed pixels in coarse-resolution satellite data. *Remote Sensing of Environment*, 58, 329-343.
- Nelson, R. F. (1983). Detecting forest canopy change due to insect activity using Landsat MSS. *Photogrammetric Engineering and Remote Sensing*, 49, 1303-1314.
- Pan, Y., Melillo, J. M., McGuire, A. D., Kicklighter, D. W., Pitelka, L. F., Hibbard, K., Pierce, L. L., Running, S. W., Ojima, D. S., Parton, W. J., & Schimel, D. S. (1998). Modeled responses of terrestrial ecosystems to elevated atmospheric CO₂: a comparison of simulations by the biogeochemistry models of the Vegetation/Ecosystem Modeling and Analysis Project (VEMAP). *Oecologie*, 114, 389-404.
- Parton, W. J., Ojima, D. S., Cole, C. V., & Schimel, D. S. (1993). A general model for soil organic matter dynamics: sensitivity to litter chemistry, texture and management. *Soil Science Society of America Journal*, 147-167.
- Parton, W. J., Schimel, D. S., Cole, C. V., & Ojima, D. S. (1987). Analysis of factors controlling soil organic matter levels in Great Plains grasslands. *Soil Science Society of America Journal*, 51, 1173-1179.
- Peng, C., & Apps, M. (1999). Modelling the response of net primary productivity (NPP) of boreal forest ecosystems to changes in climate and fire disturbance regimes. *Ecological Modelling*, 122, 175-193.
- Pilon, P. G., Howarth, P. J., & Bullock, A. R. (1988). An enhanced classification approach to change detection in semi-arid environments. *Photogrammetric Engineering and Remote Sensing*, 54, 1709-1716.
- Potter, C. S., Randerson, J. T., Field, C. B., Matson, P. A., Vitousek, P. M., Mooney, H. A., & Klooster, S. A. (1993). Terrestrial ecosystem production: a process model based on global satellite and surface data. *Global Biogeochemical Cycles*, 7, 811-841.
- Prince, S. D., & Goward, S. N. (1995). Global primary production: a remote sensing approach, *Journal of Biogeography*, 22, 815-835.
- Raich, J. W., Rastetter, E. B., Melillo, J. M., Kicklighter, D. W., Grace, P., Moore, B. III, & Peterson, B. J. (1991). Potential net primary productivity in South America: application of a global model. *Ecological Applications*, 1, 399-429.
- Robinson, A. H., Morrisson, J. L., Muehrcke, P. C., Kimerling, A. J., & Guptill, S. C. (1995). *Elements of Cartography*, (6th ed.). John Wiley & Sons Inc., United States of America.
- Ruimy, A., Dedieu, G., & Saugier, B. (1996). TURC: A diagnostic model of continental gross primary productivity and net primary productivity. *Global Biogeochemical Cycles*, 10, 269-285.
- Running, S. W., Nemani, R. R., Peterson, D. L., Band, L. E., Potts, D. F., Pierce, L. L., & Spanner, M. A. (1989). Mapping regional forest evapotranspiration and photosynthesis by coupling satellite data with ecosystem simulation. *Ecology*, 70, 1090-1101.
- Running, S. W., & Hunt, E. R. (1993). Generalization of a forest ecosystem process model for other biomes, BIOME-BGC, and an application for global-scale model. Ehleringer, J. R., & Field, C. (Eds.). *Scaling processes between leaf and landscape*, 141-158. Academic Press, San Diego.
- Schimel, D. S., House, J. I., et al. (2001). Recent patterns and mechanisms of carbon exchange by terrestrial ecosystems. *Nature*, 414, 169-172.

- Schimel, D. S., Braswell, B. H., Holland, E. A., McKeown, R., Ojima, D. S., Painter, T. H., Parton, W. J., & Townsend, A. R. (1994). Climatic, edaphic, and biotic controls over carbon and turnover of carbon in soils. *Global Biogeochemical Cycles*, 8, 279-293.
- Sellers, P. J. (1985). Canopy reflectance, photosynthesis and transpiration. *International Journal of Remote Sensing*, 6, 1335-1372.
- Sellers, P. J. (1987). Canopy reflectance, photosynthesis, and transpiration. II: The role of biophysics in the linearity of their interdependence. *Remote Sensing Environment*, 21, 143-183.
- Sellers, P. J., Los, S. O., Tucker, C. J., Justice, C. O., Dazlich, D. A., Collatz, G. J., & Randall, D. A. (1996). A revised land surface parameterization (Sib2) for atmospheric GCMs. Part II: the generation of global fields of terrestrial biophysical parameters from satellite data. *Journal of Climate*, 9, 706-737.
- Settle, J., & Campbell, N. (1998). On the errors of two estimators of sub-pixel fractional cover when mixing is linear. *IEEE Transactions on Geoscience Remote Sensing*, 36, 163-169.
- Singh, A. (1989). Digital change detection techniques using remotely-sensed data. *International Journal of Remote Sensing*, 10, 989-1000.
- Stocks, B. J. (1991). The extent and impact of forest fires in northern circumpolar countries. Levine, J. S. (Ed.), *Global biomass burning: atmospheric, climatic, and biospheric implications*, 197-202. MIT Press, Cambridge.
- Zhan, X., DeFries, R., Hansen, M., Townshend, J., DiMiceli, C., Sohlberg, R., & Huang, C. (1999). *MODIS enhanced land cover and land cover change products algorithm theoretical basis documents (ATBD): MODIS enhanced land cover and land cover change*. University of Maryland, http://glcf.umiacs.umd.edu/MODIS/reports/atbd_mod29.pdf.
- Williams, D. L. (1991). A comparison of spectral reflectance properties at the needle, branch, and canopy level for selected conifer species. *Remote Sensing of Environment*, 35, 79-93.
- Woodward, F. I., Smith, T. M., & Emanuel, W. R. (1995). A global land primary productivity and phytogeography model. *Global Biogeochemical Cycles*, 9, 471-490.

Chapter 14

REGIONAL FOREST LAND COVER CHARACTERISATION USING MEDIUM SPATIAL RESOLUTION SATELLITE DATA

Chengquan Huang, Collin Homer, and Limin Yang

USGS EROS Data Center, Raytheon, Sioux Falls, South Dakota, 57198, USA

1. INTRODUCTION

Increasing demands on forest resources require comprehensive, consistent and up-to-date information on those resources at spatial scales appropriate for management decision-making and for scientific analysis. While such information can be derived using coarse spatial resolution satellite data (e.g. Tucker et al. 1984; Zhu and Evans 1994; Cihlar et al. 1996; Cihlar et al., Chapter 12), many regional applications require more spatial and thematic details than can be derived by using coarse resolution imagery. High spatial resolution satellite data such as IKONOS and Quick Bird images (Aplin et al. 1997), though usable for deriving detailed forest information (Culvenor, Chapter 9), are currently not feasible for wall-to-wall regional applications because of extremely high data cost, huge data volume, and lack of contiguous coverage over large areas. Forest studies over large areas have often been accomplished using data acquired by intermediate spatial resolution sensor systems, including the Multi-Spectral Scanner (MSS), Thematic Mapper (TM) and the Enhanced Thematic Mapper Plus (ETM+) of Landsat, the High Resolution Visible (HRV) of the Systeme Pour l'Observation de la Terre (SPOT), and the Linear Image Self-Scanner (LISS) of the Indian Remote Sensing satellite. These sensor systems are more appropriate for regional applications because they can routinely produce spatially contiguous data over large areas at relatively low cost, and can be used to derive a host of forest attributes (e.g. Cohen et al. 1995; Kimes et al.

1999; Cohen et al. 2001; Huang et al. 2001; Sugumaran 2001). Of the above intermediate spatial resolution satellites, Landsat is perhaps the most widely used in various types of land remote sensing applications, in part because it has provided more extensive spatial and temporal coverage of the globe than any other intermediate resolution satellite. Spatially contiguous Landsat data have been developed for many regions of the globe (e.g. Lunetta and Sturdevant 1993; Fuller et al. 1994b; Skole et al. 1997), and a circa 1990 Landsat image data set covering the entire land area of the globe has also been developed recently (Jones and Smith 2001). An acquisition strategy aimed at acquiring at least one cloud free image per year for the entire land area of the globe has been initiated for Landsat-7 (Arvidson et al. 2001). This will probably ensure the continued dominance of Landsat in the near future.

Extracting forest information from Landsat imagery has been a vigorous research activity over the past 30 years of Landsat history. Early forest applications used both digital and analogue methods to analyse satellite imagery. Images were often digitally enhanced for printing, with actual interpretation done on the hard-copy print. With the evolving need for more efficient and comprehensive analysis, a wide range of digital methods were developed (Townshend 1992; Hall et al. 1995), many of which were tested within local areas covered by single Landsat scenes. Rapid development in computer hardware and software over the last decade provided the computing capacity for deriving forest information from multiple satellite scenes. (Here, and throughout this Chapter, a scene refers to an area covered by a Landsat path/row, while an image refers to a specific image acquisition.) For example, Bauer (1994) mapped seven forest classes in five north-eastern Minnesota counties using six TM scenes. At national scales, over 20 land cover classes, including three forest classes, were mapped using TM images for Great Britain (Fuller et al. 1994a) and the conterminous U.S. (Vogelmann et al. 2001).

Use of a single TM image for forest studies can be a very complex process. Some of the challenges include radiometric and geometric correction, impact of topography and the atmosphere on image quality, and diversity and spatial heterogeneity of land cover, among others (Jensen 1986). Deriving forest information from multiple scenes further compounds these issues. For example, cloud cover often makes it difficult to obtain usable images for an entire study area within a specific time window. Another challenge is among-scene variability arising from differences in atmospheric condition, viewing and illumination geometry, vegetation phenology and soil moisture content. As a result, information extraction methods that work well in a single-scene application may fall apart in multi-

scene applications, or may be less effective when trained on one scene and applied to neighbouring scenes (Pax-Lenney et al. 2001). A third challenge is lack of reliable reference data sets. Such data sets are required for training many classification algorithms (see Franklin et al., Chapter 10) and for accuracy assessment (Czaplewski, Chapter 5). Because reference data are expensive to collect, at regional scales they are often compiled from different sources, provided such sources exist. Regardless, reference data sets from different sources are often collected by different parties at different times using different methods, and often have varying levels of reliability (DeFries and Townshend 1993). Use of such reference data sets may result in inconsistencies and varying reliability in derived data products.

In this Chapter, we will address these challenges through two case studies – the land cover mapping project of the Utah Gap Analysis Program (GAP) (Homer et al. 1997) and a pilot study of the Multi-Resolution Land Characteristics (MRLC) 2000 program, which for simplicity are referred to as Utah GAP land cover program and MRLC 2000 pilot study, respectively. While the unsupervised clustering approach employed in the Utah GAP land cover program has been used to develop many large area classifications (e.g. Cihlar et al. 1996; Cohen et al. 1998; Vogelmann et al. 1998), the supervised classification tree method used in the MRLC 2000 pilot study is gaining popularity due to its promising performance in regional and global applications (e.g. Friedl et al. 1999; Hansen et al. 2000). In the following sections, we first present the two case studies, with more emphasis on the MRLC 2000 pilot study. Results of the two case studies are then evaluated using an independent reference data set, following which some of the major issues on regional forest land cover characterisation using medium spatial resolution satellite data are discussed.

2. THE UTAH GAP LAND COVER PROGRAM

2.1 Background

In 1990, the U.S. Geological Survey (USGS) Gap Analysis Program (GAP) was established to map terrestrial vertebrate species and evaluate their protection status on the land where they occur throughout the United States (Edwards et al. 1993; Scott et al. 1993). Central to this analysis was a vegetation cover-type map which, when linked to wildlife habitat relation models, predicts the spatial distribution of animal species. Because no regional land cover information existed at the time when the program started, one of the requirements of this program was to develop a state-wide

vegetation cover-type map from Landsat data. This case study describes the development of this vegetation map for the state of Utah.

2.2 Image Standardisation and Mosaic Creation

Large study areas requiring the spatial resolution of Landsat TM data invariably cover multiple scenes. Analysis and classification of multiple scenes can be carried out either on individual scenes or multi-scene mosaics. Single-scene classification potentially offers better accuracy because of reduced pixel sample size and spectral variability. However, classifying single scenes independently within a multi-scene region can require a greater investment in time, training data collection, and subsequent edge-matching than the multi-scene mosaic approach. On the other hand, the mosaic approach has a possible disadvantage of increased within-class spectral variability and potentially higher confusion between spectrally similar cover types. For this application, the mosaic approach offered the best solution to our mapping objectives.

Spatially, 14 Landsat TM scenes cover Utah. Twenty-four images were required to provide a complete, cloud free mosaic for a single summer season, including 14 primary base scenes and ten secondary cloud patch scenes. The primary base scenes were acquired between June and August of 1988 and 1989. The dates for the additional ten images used for cloud patching varied from 1984 to 1993, but were all in the summer growing season.

A two-step approach of atmospheric standardisation and histogram adjustment was chosen to normalise image-to-image variations. First, the image acquired at path 37, row 33 was chosen as a "master" image because of its central location in the state (allowing maximum overlay with adjacent scenes) and because it covered a significant range of the ecological conditions likely to be encountered in the state. This image was adjusted for atmospheric haze by plotting each of the reflective spectral bands against the middle infrared band 7 (2.08 to 2.35 μm) as described in Jensen (1986). Then, a histogram adjustment method based on histogram bias (i.e., histogram shape is maintained but relative position is altered) was used to normalise among-scene variations due to the additive components of atmospheric effects. This method does not alter within-slave-scene unique radiometric characteristics, allowing for recognition of localised phenomena in digital classification. Selected areas of overlap between master and slave were compared band-by-band, and the average difference was calculated for each band. Band-by-band differences from the overlap sample areas were used as bias values to adjust radiometrically the slave to the master. Once a

slave image was radiometrically matched to the master, it became a master for its adjacent scenes. This method effectively reduced the among-scene variations in this study area, resulting in a near seamless mosaic (Colour Plate 16).

To reduce the spectral variability within individual classes and possible confusion between spectrally similar but ecologically different cover types, the image mosaic was segmented into three ecoregions, i.e., Wasatch-Uinta, Colorado Plateau, and Northern Great Basin. The Wasatch-Uinta ecoregion is characterised by high mountains and plateaux containing typical rocky mountain flora such as evergreen and deciduous forest. The Colorado plateau is characterised by lower elevation canyon lands, plateaux and buttes supporting arid and semi-arid shrub, grass, and woodlands. Typical landscapes in the Northern Great Basin ecoregion include mountain ranges and broad valleys trending north to south (Colour Plate 16, after Omernik (1987)).

2.3 Training Data

Though an unsupervised clustering approach was employed in this case study, training data were needed to link spectral clusters to vegetation cover types. The required training data were collected through interpreting low altitude aerial photos and conducting field work, with field location determined using Global Positioning System (GPS) units. A total of 657 field training sites were used in the Wasatch-Uinta ecoregion, of which 356 (53 percent) were collected using GPS units in the field, 221 (35 percent) using low-altitude aerial photographs, and 80 (12 percent) using both methods. Of the 518 training sites in the Colorado Plateau ecoregion, 422 (81 percent) were GPS located, 59 (12 percent) were photo-interpreted, and 37 (7 percent) were collected using both methods. In the Northern Basin and Range ecoregion, 490 training sites (86 percent) were GPS based, 26 (4 percent) were photo-interpreted, and 57 (10 percent) were collected using both methods, totalling 573 training sites.

2.4 Classification and Modelling

The three ecoregions were subset from the state image mosaic and processed using the ISODATA algorithm implemented in the ERDAS image processing package to generate unsupervised spectral clusters (Tou and Gonzalez 1974). Before clustering, agricultural and urban areas were masked from the image using an existing Geographic Information System database to further reduce spectral variability. A total of 125 clusters were initially

generated in the Wasatch-Uinta ecoregion, with 150 each in the Colorado Plateau and Northern Basin and Range. A minimum-distance-to-the-means classification algorithm was used to assign individual pixels to a spectral class.

Cover-type modelling consisted of two phases: statistical association of spectral classes with cover-types and post-classification ecological modelling based on ancillary information. The first phase of modelling included two sets of summary statistics generated from the weighted training polygon values: the proportion of each cover-type weighting ordered by spectral class and spectral class polygon weighting values ordered by cover type. These two sets of summary statistics were used in concert during ancillary modelling to provide balance between possible commission and omission errors.

The second phase of modelling incorporated ancillary data, including 3-arc-second resolution digital elevation, slope, aspect, and vegetation cover-type range polygons, to clarify cover-type associations by using post-classification stratification (Fleming and Hoffer 1979; Hutchinson 1982). Polygons delineating the general distribution of vegetation cover-type were developed from existing literature and maps, and were used to limit the geographic extent of some cover types. All localised ancillary parameters detailed in literature and field work were standardised to regional scales before being used in modelling. An intensive effort was made to ensure as much objectivity as possible in generating spectral class/ancillary data models. This second phase modelling was extensive for some spectral classes.

2.5 Results

A 38-class land cover map with sixteen forest classes was developed in this case study (Homer et al. 1997). An accuracy assessment based on a mixed sampling design that considered statistical validity, accessibility and efficacy yielded an overall map accuracy of 75.3 % for the entire state (Edwards et al. 1998). Further evaluation of this classification using an independent reference data set will be presented in a later section.

3. MRLC 2000 PILOT STUDY

3.1 Background

The MRLC consortium was initiated in early 1990s to address the need for consistent national and regional land cover data for the United States (Loveland and Shaw 1996). Through this consortium, a 1992-vintage National Land Cover Dataset (NLCD 1992) was developed for the conterminous United States (Vogelmann et al. 2001). MRLC is currently developing a second generation land cover product, NLCD 2000, using 2000-vintage Landsat-7 ETM+ images and relevant ancillary data. The guiding principles in designing NLCD 2000 included the need to: 1) develop methods that are as objective, consistent and repeatable as possible for generating standardised land cover products, 2) constrain methods to be simple, efficient and transferable to others, 3) develop land cover products flexible enough to meet the potentially diverse requirements of multiple users, 4) provide users with increased access to intermediate database products and derivatives enabling local application, and 5) maintain reasonable compatibility with NLCD 1992. The purpose of this MRLC 2000 pilot study is to develop a prototype procedure that follows the above guiding principles and is efficient and robust for use in all regions of the U.S. The MRLC 2000 classification scheme consists of over 20 land cover classes (Homer et al. 2002). We will examine only the forest classes in this Chapter.

3.2 Data and methods

The overall procedure of this pilot study consists of pre-processing of satellite imagery, ancillary data and reference data, classification using a decision tree method, and accuracy assessment using both cross-validation and independent test data sets (Figure 14-1). The study area primarily covered the Rocky Mountains of Utah, extending from the Cache National Forest, located north of Salt Lake City, to Zion National Park in the south. A large part of this study area overlapped with the Wasatch-Uinta ecoregion of the Utah GAP land cover mapping program (Colour Plate 16).

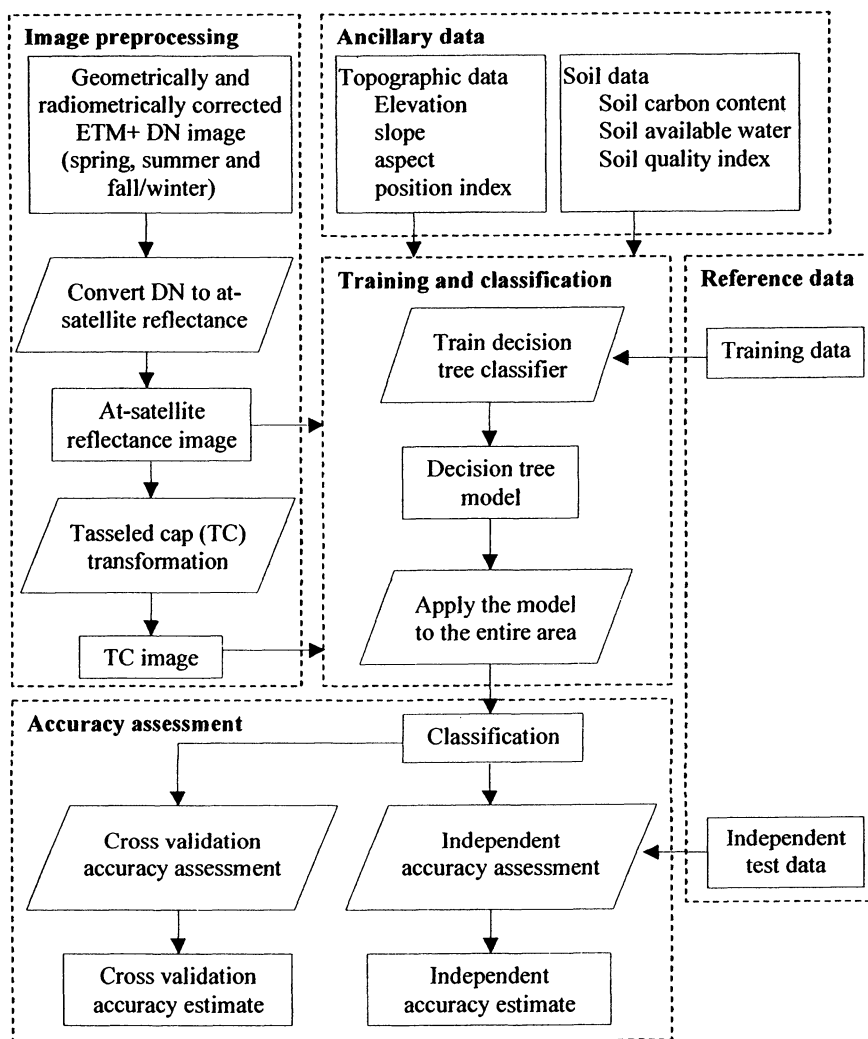


Figure 14-1. A flowchart of data and methods used in the MRLC 2000 pilot study.

3.2.1 Satellite imagery and ancillary data

Nine ETM+ scenes were required to cover the entire study area (Table 14-1). For each scene, near cloud free ETM+ images acquired on three dates between 1999 and 2001 were used to capture vegetation dynamics over a growing season and to maximise land cover type separability. Image selection was based on vegetation greenness profiles defined by a multi-year normalized difference vegetation index data set derived from the Advanced

Very High Resolution Radiometer (Yang et al. 2001). Two additional images acquired in the summer of 2000 were used to patch the clouds seen in two summer leaf-on images. All images were geometrically and radiometrically corrected using standard methods at the USGS EROS Data Center (Irish 2000). Terrain correction using the USGS 1-arc second National Elevation Dataset was performed to improve geolocation accuracy. To reduce among-scene variability due to different illumination geometry (Colour Plate 17A), raw digital numbers were converted to at-satellite reflectance for the 6 reflective bands, and to at-satellite temperature for the thermal band according to Markham and Barker (1986) and the Landsat-7 Science Data User's Handbook (Irish 2000). Colour Plate 17B shows that a large portion of the among-scene variations were removed using this method (also demonstrated in Huang et al. 2002b). All 7 bands of the images were resampled to a 30 m spatial resolution. Tasseled-cap brightness, greenness and wetness were calculated using at-satellite reflectance based coefficients (Huang et al. 2002b). Mosaics of the study area were developed using the at-satellite reflectance images and corresponding tasseled-cap images. Colour Plate 17C shows the summer leaf-on image mosaic.

Table 14-1. Landsat ETM+ images used in the MRLC 2000 pilot study. The unit for sun elevation is degree.

Landsat path/row	Spring		Summer		Fall/winter	
	Acquisition date	Sun elevation	Acquisition date	Sun elevation	Acquisition date	Sun elevation
36/32	04/28/2000	58	06/15/2000	65	10/19/1999	37
37/31	05/08/2001	60	06/06/2000	64	09/10/2000	49
37/32	05/08/2001	60	06/06/2000	65	10/10/1999	40
37/33	05/05/2000	61	06/06/2000	65	10/10/1999	41
37/34	05/05/2000	62	06/06/2000	66	10/10/1999	43
38/31	05/28/2000	63	06/29/2000	64	10/03/2000	41
38/32	05/28/2000	64	08/14/1999	57	10/17/1999	38
38/33	04/26/2000	59	07/31/2000	61	11/02/1999	34
38/34	04/26/2000	60	07/31/2000	61	11/02/1999	35

Ancillary data included the USGS 1-arc second National Elevation Dataset and three derivatives, i.e., slope, aspect and a topographic position index characterising a pixel's position relative to ridges and valleys. In addition, three soil attributes, i.e. available water capacity, soil carbon content and a soil quality index, were derived from the State Soil Geographic (STATSGO) Data Base (USDA 1991). All ancillary data layers were rasterized or resampled to have a spatial resolution of 30 m.

3.2.2 Reference Data Sets

Two reference data sets were available to this study. One was collected through the Forest Inventory and Analysis (FIA) program of the U.S. Forest Service in mid-1990. Through intensive field work, the FIA program provided detailed forest attributes at individual tree, sub-plot and plot levels. Covering an area of about 2×2 ETM+ pixels, an FIA plot consists of 4 to 5 sub-plots, each with a radius of about 7.3 meter. Considering the pixel size of ETM+ imagery and possible geolocation errors, only plot level data were deemed appropriate for use with the ETM+ imagery. There were 3037 FIA plot in this study area. Each FIA plot was classified using two classification schemes, forest/non-forest and a 4-class scheme. In addition, the 1852 forest plots were also classified using a forest type group scheme. Both the 4-class scheme and the forest type group scheme will be listed in the following section.

The other reference data set consisted of 1295 field points collected by the Fire Science Lab of the Rocky Mountain Research Station (RMRS) of the U.S. Forest Service in late 1990s. These points were distributed within the mid-southern portion of the study area. The collected information allowed the labelling of each point using the forest/non-forest and 4-class schemes. This data set was used to partially evaluate the classification results developed using FIA plot data.

3.2.3 Classification schemes

As mentioned in the previous section, three classification schemes were considered in this study: forest/non-forest, a 4-class scheme consisting of non-forest, deciduous, evergreen, and mixed, and a forest type group scheme. The FIA program requires a forest/non-forest map to implement a stratified sampling of forested land in order to produce accurate estimates of forest attributes (McRoberts et al. 2002). Deciduous, evergreen and mixed forest are the common forest categories in many regional land cover classification systems, including the MRLC 2000 classification scheme. Information on forest type group is required for species conservation planning, fire management and many other applications. Based on the FIA plot data, there were 9 major forest type groups in this area: pinyon/juniper, douglas-fir, ponderosa pine, fir/spruce/mountain hemlock, lodgepole pine, other western softwoods, aspen/birch, western oak and other western hardwoods.

3.2.4 Decision Tree Classifier

The ample reference data points available to this study made it possible to employ a supervised approach for deriving forest land cover classifications (Richards 1993). The popular supervised classification algorithms include the maximum likelihood classifier, neural networks and decision tree methods (Townshend 1992; Hall et al. 1995; Franklin et al., Chapter 10). The decision tree method was chosen for this study because it 1) is non-parametric and therefore independent of the distribution of class signature, 2) can handle both continuous and non-continuous variables, 3) generates interpretable classification rules, 4) is fast to train and is often as accurate as and sometimes more accurate than, many other classifiers (Hansen et al. 1996; Huang et al. 2002a). Tree classifiers have been used to develop land cover classifications at regional to global scales (e.g. Friedl and Brodley 1997; DeFries et al. 1998; Friedl et al. 1999; Hansen et al. 2000). The decision tree program used in this study, C5, employs an information gain ratio criterion in tree development and pruning. A general description of the functions of this program is given in a tutorial available at <http://www.rulequest.com/see5-unix.html>. A detailed description of an earlier version of this program, C4.5, was provided by Quinlan (1993).

One of the useful functions of C5 is boosting, a technique designed to improve classification accuracy (Bauer and Kohavi 1998). With this function, the program develops a sequence of decision trees, with each subsequent one trying to fix the misclassification errors in the previous tree. Each decision tree makes an independent prediction, and the final prediction is a weighted vote of the predictions of all trees. This function often improves classification accuracy by 5 % to 10 % (e.g. Friedl et al. 1999; Chan et al. 2001).

3.2.5 Accuracy assessment

Accuracy estimates of the classifications were derived in two ways. One was to use the independent test data set collected by the Fire Science Lab of the U. S. Forest Service RMRS. The other was to use a cross-validation function of C5. Cross-validation is designed to derive prompt accuracy estimates even when only a limited number of reference data samples are available for both training and accuracy assessment (Henery 1994). For an N-fold cross-validation, the training data set is divided into N equal-sized subsets. Accuracy estimates are derived by using each subset to evaluate the classification developed using the remaining training samples. The mean

accuracy and its standard error represent those of the classification developed using all reference samples.

3.3 Results

Two classifications, one with and the other without the use of boosting, were developed for each of the three classification schemes – forest/non-forest, 4-class and forest type group, using FIA plot data and Landsat-7 ETM+ images. Classification accuracies derived using cross-validation and the independent reference data set collected by the Fire Science Lab of RMRS are reported in Table 14-2. With the boosting function of the C5 program, overall accuracies of around 80 % were achieved for the forest/non-forest and the 4-class classifications and about 65 % for forest type group classification. The boosting function improved classification accuracy by about 2 to 9 percent in absolute values. Similar improvements using the boosting function have been reported in other studies (e.g. Chan et al. 2001). These classifications were visually evaluated by field crew members of RMRS and the Utah GAP Analysis program of Utah State University. Both parties agreed that these classifications were reasonably accurate.

Table 14-2. Classification accuracy estimates for the MRLC 2000 pilot study. The units for both accuracy and standard error are percent (%).

Classification level	Forest/non-forest		4-class		Forest type group	
	Accuracy	Std. Error	Accuracy	Std. Error	Accuracy	Std. Error
Cross-validation						
- Without boosting	80.4	0.4	78.0	0.4	56.6	0.9
- With boosting	82.7	0.4	81.2	0.6	65.8	1.2
Independent assessment						
- Without boosting	75.7	-	75.3	-	-	-
- With boosting	79.0	-	83.4	-	-	-

4. COMPARISON OF THE TWO CASE STUDIES

Using an independent reference data set provided by the FIA program of U.S. Forest Service RMRS, we were able to compare the classifications derived through the Utah GAP land cover program and the MRLC 2000 pilot study in the Wasatch-Uinta area, where the two study areas overlapped. This reference data set consisted of 68,358 points regularly spaced at a 1km interval in both the east-west and south-north directions. Based on aerial

photos acquired in the 1980s, each point was labelled with one of the following classes: non-forest, conifer, pinyon/juniper, aspen and other hardwoods. This reference data set allowed an independent assessment of the classifications developed in the two case studies by aggregating those classifications to this 5-class level as well as to the 4-class and forest/non-forest levels. The derived overall accuracies as well as both user's and producer's accuracies are reported in Table 14-3.

Table 14-3. Accuracies (%) estimated using 68,358 photo-interpreted points for classifications developed in the two case studies. Accuracies for the mixed class were unavailable because the reference data did not have a mixed class. MRLC 2000 classifications were developed using CS's boosting function.

	User's		Producer's		Overall	
	Utah GAP	MRLC 2000	Utah GAP	MRLC 2000	Utah GAP	MRLC 2000
forest/non-forest						
non-forest	62.3	69.7	68.7	75.9		
forest	77.3	86.2	72.0	82.1		
4-class						
non-forest	62.3	69.7	68.7	82.1		
deciduous	55.6	62.4	49.1	52.3		
evergreen	68.3	77.0	63.2	69.2		
mixed	-	-	-	-		
5-class						
non-forest	62.3	69.7	68.7	82.1	58.5	66.5
conifer	63.5	71.7	56.4	64.9		
other hardwoods	42.4	53.6	35.9	29.5		
aspen	44.0	48.7	46.2	56.7		
pinyon/juniper	58.2	66.3	56.2	59.2		

The overall accuracies of the classifications at the forest/non-forest, 4-class and 5-class levels were 70.7 %, 62.8 % and 58.5 % for the Utah GAP land cover program, and 78.4 %, 71.3 % and 66.5 % for the MRLC 2000 pilot study, respectively. The differences in overall accuracy between the two sets of classifications were about 8 % at all three levels. Classifications of the MRLC 2000 pilot study also had class specific user's accuracies of about 4 % - 11 %, and producer's accuracies of about 3 % - 13 % (except for the other hardwoods class) higher than the Utah GAP classifications. With the exception of the 4-class classification, the overall accuracies of the other two classifications of the MRLC 2000 pilot study were comparable to those estimated through cross-validation (Table 14-2, with boosting) or using the independent test data set collected by the Fire Science Lab, suggesting that these estimates were not significantly biased from each other. Colour Plate 18 shows a window of the two classifications at the 5-class level and the

summer leaf-on ETM+ image used in the MRLC 2000 pilot study. The overall accuracy of the 4-class map was about 10 % lower than the cross-validation estimate (Table 14-2, with boosting) and the one derived using the independent test data set collected by the Fire Science Lab. This might be partially due to the lack of a mixed class in the photo-interpreted reference data set.

The higher classification accuracies of the MRLC 2000 pilot study compared to the Utah GAP land cover program can be attributed to at least two factors. One is use of multi-temporal imagery, which often yields better classification accuracies than using single-date imagery (e.g. Coppin and Bauer 1994; Lunetta and Balogh 1999). Whereas only a single-date summer leaf-on image mosaic was used in the Utah GAP land cover program, image mosaics of three dates representing spring, summer and fall/winter were used in the MRLC 2000 pilot study. The other factor is use of a high quality training data set – FIA plot data. This data set consists of points collected following a probability-based sampling design. Each point was labelled according to intensive field work, and was revisited periodically. Collected nation-wide, this data set is highly valuable for use with intermediate spatial resolution satellite imagery in regional forest studies. To ensure the confidentiality, security and integrity of the data points, however, use of this data set should be arranged under security agreements.

5. DISCUSSION

The two case studies presented in this work demonstrate the feasibility of extracting forest information at regional scales using multiple Landsat scenes as a single mosaic. This information extraction process consists of a sequence of steps, including normalising among-scene variations independent of land surface conditions, selecting appropriate classification algorithms and validating classification results. As a result of the increased acquisition capacity of many local Landsat receiving stations, together with the high priority being given to the acquisition of global coverage by Landsat-7 (Arvidson et al. 2001), data availability has become less problematical in regional Landsat applications. The methods used in each step, however, can affect the reliability, efficiency and consistency of deriving forest information from Landsat data.

5.1 Normalisation of among-scene variability

Images of neighbouring scenes, especially of neighbouring Landsat paths, are often acquired on different dates. They can differ in atmospheric conditions, illumination geometry, and vegetation phenology, resulting in increased within-class signature variability and reduced among-class separability when these images are analysed as a mosaic. It is therefore desirable to normalise such among-scene variations before information extraction. Designed to retrieve surface reflectance from digital number, physically based atmospheric correction algorithms are, in theory, preferable for standardising the impact of the atmosphere and illumination geometry. However, use of available atmospheric correction algorithms on Landsat imagery over large areas has very limited success, partially because many required parameters concerning *in situ* atmospheric conditions are often not available or cannot be derived reliably (Cohen et al. 2001). Use of pseudo-invariant objects whose reflective properties remain relatively stable may provide a partial solution (Schott et al. 1988), provided enough pseudo-invariant objects can be identified in the overlap areas of neighbouring scenes. The histogram bias adjustment method introduced in the Utah GAP case study is similar to a dark object subtraction approach to atmospheric correction. One of the limitations of this approach is that it only normalises additive components of atmospheric effects (Teillet and Fedosejevs 1995). It can not handle non-additive components properly. The at-satellite reflectance method described in the MRLC 2000 pilot study effectively normalized the impact of illumination geometry, a non-additive component. For clear and near-cloud-free images, use of this method alone may generate satisfactory image mosaics. However, when varying hazy conditions exist among the images, applying the at-satellite reflectance method followed by the histogram bias adjustment method may substantially improve the quality of an image mosaic.

No efforts were made to normalise the among-scene variations arising from differences in vegetation phenology in the two case studies. Because such variations are functions of a number of factors, including vegetation type, agricultural activity, and perhaps topographically-induced soil moisture availability, there are currently no practical solutions to this problem. In the MRLC 2000 pilot study, we tried to address this problem by using scene identification number as an input to the decision tree program, and effectively removed some seamlines seen in the image mosaic from the derived classifications (Colour Plate 18).

5.2 Classification algorithm selection

The two case studies represent two different approaches to land cover classification, one supervised and the other unsupervised. While classifications developed in the MRLC 2000 pilot study had higher overall accuracies than those developed in the Utah GAP land cover program, it was not clear if the differences were partially due to selection of classification algorithms. As discussed in a previous section, two other factors, i.e., use of multi-temporal images and better reference data, may also have contributed to this. Whether to use a supervised or unsupervised method in a specific project depends on many factors. Supervised methods generally require substantial amounts of reliable reference data in order to be trained adequately. Because of this, Richards (1993) suggested that the supervised maximum likelihood classifier might be more time demanding than an unsupervised approach. However, results from the two case studies suggest that, with reliable and up-to-date reference data sets like the FIA plot data readily available, a supervised method is often more efficient and cost-effective than an unsupervised method. We estimated that, for land cover mapping with similar thematic content, the MRLC 2000 pilot study took less than one third of the effort the Utah GAP program took. Supervised methods will also probably be more efficient for remapping efforts, because for most areas the majority of the training points used in a previous mapping effort are not likely to change from one cover type to another during the mapping interval. The unchanged training points should be reusable after being identified through quality check. In addition to the advantages of the decision tree program discussed in the MRLC 2000 pilot study, this program can also produce instant accuracy estimates for the classification being developed, which may be relatively unbiased if the training data points are collected following a probability-based sampling design and are not spatially auto-correlated.

Unfortunately, for many large area forest land cover mapping activities, there are often insufficient reference data samples, and developing a large reference data set with adequate samples may not always be feasible for many practical reasons, including insufficient resources, time constraints and access problems. While it is often difficult to use supervised approaches in such cases, the Utah GAP land cover program and other studies (e.g. Vogelmann et al. 1998) have demonstrated that an unsupervised approach can yield satisfactory results.

5.3 Accuracy assessment

Validation of classification results at a regional scale is a considerable task. A statistically valid accuracy assessment can take tremendous amounts of resources and time. Even if the required resources are available, it often takes several months to several years to produce valid accuracy values after a classification is developed. To avoid this problem, it is highly recommended that the accuracy assessment be planned during the design phase of a mapping project. An accuracy assessment plan should include three components: a probability-based sampling design, a protocol for labelling reference data points, and an appropriate statistical procedure for deriving accuracy estimates (Czaplewski, Chapter 5; Stehman and Czaplewski 1998).

Alternatively, the cross-validation technique employed in the MRLC 2000 pilot study can be used to produce instant accuracy estimates. Whether these estimates are biased or not depends on the sampling design and spatial coverage of the training data points. Results from the MRLC 2000 pilot study suggest that such estimates might be unbiased if the training data set is collected following probability based sampling design and covers the entire study area. While inflated accuracies may result when significant spatial auto-correlations exist among the training samples (Campbell 1981), the cross-validation technique can, at the very least, provide users with preliminary information regarding the accuracy of the products they want to use.

The validity of classification accuracy estimates can be affected by two additional factors. One is possible labelling error of reference data points (Congalton and Green 1993), which may arise from errors of field crew members or photo interpreters, or from possible temporal discrepancies between reference data and satellite image. The other is location error that may exist between the reference data points and satellite image. Unfortunately, it is often difficult to quantitatively assess such errors and their impact on the validity of derived accuracy estimates.

5.4 Beyond classification

Landsat data can be used not only to develop forest land cover classifications, but also to estimate a suite of forest attributes, including tree canopy density, age, height, basal area, and tree bole diameter at breast height, among others (e.g. Cohen et al. 1995; Cohen et al. 2001). Information on such attributes at intermediate spatial resolutions is required for fire fuel modelling and many other forest management applications. In addition to the classifications developed in this Chapter, we have also

estimated sub-pixel tree canopy density at the 30m resolution for the entire MRLC pilot study area using a regression tree technique. Shown to be robust for approximating complex non-linear relationships (Huang and Townshend 2002), the regression tree method was also used to estimate tree canopy density from ETM+ imagery in three two-scene areas in Virginia, Utah/Idaho, and Oregon (Huang et al. 2001). In these studies, the mean absolute difference and correlation coefficient (r) between predicted and actual tree canopy density were about 9 to 12 percent tree cover and 0.8 to 0.9, respectively.

6. CONCLUSIONS

Through two case studies, we have presented two approaches to extracting forest information from Landsat imagery in multi-scene regions. In both case studies, classifications were performed on multi-scene mosaics, which was more efficient and helped to achieve a higher degree of class consistency across multiple scenes than classifying single scenes individually. The two image pre-processing procedures – histogram bias adjustment and at-satellite reflectance method, were found effective for normalising the among-scene variations of clear and near cloud-free images in a semi-arid environment. Both the supervised decision tree classifier and the unsupervised approach produced satisfactory classification results. With adequate, well-distributed training data points readily available, the decision tree method should be more efficient and consistent than an unsupervised approach, especially for an area that needs to be remapped periodically. With cross-validation, the decision tree program can also generate instant accuracy estimates, which may be reasonably unbiased if the training points follow a probability based sampling design. This can be highly valuable, because statistically valid accuracy assessment over large areas is often very expensive. When only limited or no reference data points are available, however, the unsupervised approach may be more appropriate for extracting forest information at regional scales.

ACKNOWLEDGEMENTS

This work is made possible in part by the Raytheon Corporation under U.S. Geological Survey (USGS) contract 1434-CR-97-CN-40274. The FIA plot data were made available through an inter-agency agreement between USGS EROS Data Center (EDC) and the Forest Inventory and Analysis

(FIA) program of U.S. Forest Service's Rocky Mountain Research Station (RMRS). The authors are especially grateful to Ronald Tymcio and Larry DeBlander of RMRS for processing the FIA field plot data and photo-interpreted data for use in this study. The Fire Science Lab of RMRS and the Utah State University Remote Sensing Lab provided independent test data sets. The MRLC 2000 pilot study was supported by the MRLC 2000 mapping strategy team at EDC.

REFERENCES

- Aplin, P., Atkinson, P. M., & Curran, P. J. (1997). Fine spatial resolution satellite sensors for the next decade. *International Journal of Remote Sensing*, 18, 3873-3881.
- Arvidson, T., Gasch, J., & Goward, S. N. (2001). Landsat 7's long-term acquisition plan - An innovative approach to building a global imagery archive. *Remote Sensing of Environment*, 78, 13-26.
- Bauer, E., & Kohavi, R. (1998). An empirical comparison of voting classification algorithms: bagging, boosting, and variants. *Machine Learning*, 5, 1-38.
- Bauer, M. E., Burk, T. E., Ek, A. R., Coppin, P. R., Lime, S. D., Walsh, T. A., Walters, D. K., Befort, W., & Heinzen, D. F. (1994). Satellite inventory of Minnesota forest resources. *Photogrammetric Engineering & Remote Sensing*, 60, 287-298.
- Campbell, J. B. (1981). Spatial correlation effects upon accuracy of supervised classification of land cover. *Photogrammetric Engineering & Remote Sensing*, 47, 355-363.
- Chan, J. C.-W., Huang, C., & DeFries, R. S. (2001). Enhanced algorithm performance for land cover classification using bagging and boosting. *IEEE Transactions on Geoscience and Remote Sensing*, 39, 693-695.
- Cihlar, J., Ly, H., & Xiao, Q. (1996). Land cover classification with AVHRR multichannel composites in northern environments. *Remote Sensing of Environment*, 58, 36-51.
- Cohen, W. B., Fiorella, M., Bray, J., Helmer, E., & Anderson, K. (1998). An efficient and accurate method for mapping forest clearcuts in the Pacific Northwest using Landsat imagery. *Photogrammetric Engineering & Remote Sensing*, 64, 293-300.
- Cohen, W. B., Maiersperger, T. K., Spies, T. A., & Oetter, D. R. (2001). Modelling forest cover attributes as continuous variables in a regional context with Thematic Mapper data. *International Journal of Remote Sensing*, 22, 2279-2310.
- Cohen, W. B., Spies, T. A., & Fiorella, M. (1995). Estimating the age and structure of forests in a multi-ownership landscape of western Oregon, U.S.A. *International Journal of Remote Sensing*, 16, 721-746.
- Congalton, R., & Green, K. (1993). A practical look at sources of confusion in error matrix generation. *Photogrammetric Engineering & Remote Sensing*, 59, 641-644.
- Coppin, P. R., & Bauer, M. E. (1994). Processing of multitemporal Landsat TM imagery to optimize extraction of forest cover change features. *IEEE Transactions on Geoscience and Remote Sensing*, 32, 918-927.
- DeFries, R. S., Hansen, M., Townshend, J. R. G., & Sohlberg, R. (1998). Global land cover classifications at 8km spatial resolution: the use of training data derived from Landsat imagery in decision tree classifiers. *International Journal of Remote Sensing*, 19, 3141-3168.

- DeFries, R. S., & Townshend, J. R. G. (1993). Global land cover assessments: comparisons of ground-based data sets to classifications with AVHRR data. Goody, G., & Curran, P. (Eds.). *Environmental remote sensing from regional to global scales*. John Wiley and Sons, Chichester.
- Edwards, T. C., Moisen, G. G., & Cutler, D. R. (1998). Assessing map accuracy in a remotely-sensed, ecoregion-scale cover-map. *Remote Sensing of Environment*, 63, 73-83.
- Edwards, T. C., Scott, J. M., Homer, C. G., & Ramsey, R. D. (1993). Gap analysis: A geographic approach for assessing national biological diversity. *Natural Resources and Environmental Issues*, 2, 65-72.
- Fleming, M. D., & Hoffer, R. M. (1979). Machine processing of Landsat MSS data and DMA topographic data for forest cover-type mapping. *Proceedings of the 1979 Machine Processing of Remotely Sensed Data Symposium*, 377-408. Purdue University/LARS, West Lafayette, Indiana.
- Friedl, M. A., & Brodley, C. E. (1997). Decision tree classification of land cover from remotely sensed data. *Remote Sensing of Environment*, 61, 399-409.
- Friedl, M. A., Brodley, C. E., & Strahler, A. H. (1999). Maximizing land cover classification accuracies produced by decision trees at continental to global scales. *IEEE Transactions on Geoscience and Remote Sensing*, 37, 969-977.
- Fuller, R. M., Groom, G. B., & Jones, A. R. (1994a). The land cover map of Great Britain: an automated classification of Landsat Thematic Mapper data. *Photogrammetric Engineering & Remote Sensing*, 60, 553-562.
- Fuller, R. M., Groom, G. B., & Wallis, S. M. (1994b). The availability of Landsat TM images of Great Britain. *International Journal of Remote Sensing*, 15, 1357-1362.
- Hall, F. G., Townshend, J. R., & Engman, E. T. (1995). Status of remote sensing algorithms for estimation of land surface state parameters. *Remote Sensing of Environment*, 51, 138-156.
- Hansen, M., DeFries, R. S., Townshend, J. R. G., & Sohlberg, R. (2000). Global land cover classification at 1 km spatial resolution using a classification tree approach. *International Journal of Remote Sensing*, 21, 1331-1364.
- Hansen, M., Dubayah, R., & DeFries, R. (1996). Classification trees: an alternative to traditional land cover classifiers. *International Journal of Remote Sensing*, 17, 1075-1081.
- Henery, R. J. (1994). Methods for comparison. Michie, D., Spiegelhalte, D. J., & Taylor, C. C. (Eds.). *Machine learning, neural and statistical classification*, 107-130. Ellis Horwood, New York.
- Homer, C., Huang, C., Yang, L., & Wylie, B. (2002). Development of a circa 2000 land cover database for the United States. *2002 ASPRS-ACSM Annual Conference and FIG XXII Congress*, Washington, D.C.
- Homer, C. G., Ramsey, R. D., Edwards, T. C., & Falconer, A. (1997). Landscape cover-type modeling using a multi-scene Thematic Mapper mosaic. *Photogrammetric Engineering & Remote Sensing*, 63, 59-67.
- Huang, C., Davis, L. S., & Townshend, J. R. G. (2002a). An assessment of support vector machines for land cover classification. *International Journal of Remote Sensing*, 23, 725-749.
- Huang, C., & Townshend, J. R. G. (2002). A stepwise regression tree for non-linear approximation: applications to estimating subpixel land cover. *International Journal of Remote Sensing*, in press.

- Huang, C., Wylie, B., Homer, C., Yang, L., & Zylstra, G. (2002b). Derivation of a Tasseled cap transformation based on Landsat 7 at-satellite reflectance. *International Journal of Remote Sensing*, 23, 1741-1748.
- Huang, C., Yang, L., Wylie, B., & Homer, C. (2001). A strategy for estimating tree canopy density using Landsat 7 ETM+ and high resolution images over large areas. *Third International Conference on Geospatial Information in Agriculture and Forestry*, Denver, Colorado, CD-ROM.
- Hutchinson, C. F. (1982). Techniques for combining Landsat and ancillary data for digital classification improvement. *Photogrammetric Engineering and Remote Sensing*, 48, 123-130.
- Irish, R. R. (2000). Landsat 7 science data user's handbook. *Report 430-15-01-003-0*, NASA, http://ltpwww.gsfc.nasa.gov/IAS/handbook/handbook_toc.html.
- Jensen, J. R. (1986). *Introductory digital image processing: a remote sensing perspective*. Prentice-Hall, Englewood Cliffs, New Jersey.
- Jones, B. T. & Smith, F. G. (2001). Mapping global land cover and changes economically and accurately: The GEOCOVER LC Approach. *Third International Conference on Geospatial Information in Agriculture and Forestry*. Denver, Colorado, CD-ROM.
- Kimes, D. S., Nelson, R. F., Salas, W. A., & Skole, D. L. (1999). Mapping secondary tropical forest and forest age from SPOT HRV data. *International Journal of Remote Sensing*, 20, 3625-3640.
- Loveland, T. R., & Shaw, D. M. (1996). Multiresolution land characterisation: building collaborative partnerships. *Proceedings of the ASPRS/GAP Symposium -- Gap analysis: a landscape approach to biodiversity planning*, 83-89. Charlotte, North Carolina.
- Lunetta, R. S., & Balogh, M. E. (1999). Application of multi-temporal Landsat 5 TM imagery for wetland identification. *Photogrammetric Engineering & Remote Sensing*, 65, 1303-1310.
- Lunetta, R. S., & Sturdevant, J. A. (1993). The North American landscape characterisation Landsat pathfinder project. *Pecora 12 Symposium: Land information from space-based systems*, 363-369. Sioux Falls, South Dakota.
- Markham, B. L., & Barker, J. L. (1986). Landsat MSS and TM post-calibration dynamic ranges, exoatmospheric reflectances and at-satellite temperatures. *EOSAT Landsat Technical Notes*, 1, 3-8.
- McRoberts, R. E., Wendt, D. G., Nelson, M. D., & Hansen, M. H. (2002). Using a land cover classification based on satellite imagery to improve the precision of forest inventory area estimates. *Remote Sensing of Environment*, 81, 36-44.
- Omernik, J. M. (1987). Ecoregions of the conterminous United States. *Annals of the Association of American Geographers*, 77, 118-125.
- Pax-Lenney, M., Woodcock, C. E., Macomber, S. A., Gopal, S., & Song, C. (2001). Forest mapping with a generalized classifier and Landsat TM data. *Remote Sensing of Environment*, 77, 241-250.
- Quinlan, J. R. (1993). *C4.5 programs for machine learning*. Morgan Kaufmann Publishers, San Mateo, California.
- Richards, J. A. (1993). *Remote sensing digital image analysis: an introduction*. Springer-Verlag, Berlin.
- Schott, J. R., Salvaggio, C., & Volghok, W. J. (1988). Radiometric scene normalization using pseudoinvariant features. *Remote Sensing of Environment*, 26, 1-16.

- Scott, J. M., Davis, F., Csuti, B., Noss, R., Butterfield, B., Groves, C., Anderson, H., Caicco, S., D'Erchia, F., Edwards, T. C., Ulliman, J., & Wright, R. G. (1993). Gap analysis: a geographic approach to protection of biological diversity. *Wildlife Monographs*, 123, 1-41.
- Skole, D. L., Justice, C. O., Townshend, J. R. G., & Janetos, A. C. (1997). A land cover change monitoring program: strategy for an international effort. *Mitigation and Adaptation Strategies for Global Change*, 2, 157-175.
- Stehman, S. V., & Czaplewski, R. L. (1998). Design and analysis for thematic map accuracy assessment: fundamental principles. *Remote Sensing of Environment*, 64, 331-344.
- Sugumaran, R. (2001). Forest land cover classification using statistical artificial neural network approaches applied to IRS LISS - III sensor. *Geocarto International*, 16, 37-42.
- Teillet, P. M., & Fedosejevs, G. (1995). On the dark target approach to atmospheric correction of remotely sensed data. *Canadian Journal of Remote Sensing*, 21, 374.
- Tou, J. T., & Gonzalez, R. C. (1974). *Pattern recognition principles*. Addison-Wesley Publishing Company, London.
- Townshend, J. R. G. (1992). Land cover. *International Journal of Remote Sensing*, 13, 1319-1328.
- Tucker, C. J., Catlin, J. A., & Schneider, S. R. (1984). Monitoring vegetation in the Nile Delta with NOAA-6 and NOAA-7 AVHRR imagery. *Photogrammetric Engineering and Remote Sensing*, 50, 53-61.
- USDA (1991). State Soil Geographic Data Base (STATSGO): Data users guide. *Report Miscellaneous Publication Number 1492*. U.S. Department of Agriculture, Soil Conservation Service, U.S. Government Printing Office.
- Vogelmann, J. E., Howard, S. M., Yang, L., Larson, C. R., Wylie, B. K., & Driel, N. V. (2001). Completion of the 1990s national land cover data set for the conterminous United States from Landsat Thematic Mapper data and ancillary data sources. *Photogrammetric Engineering & Remote Sensing*, 67, 650-662.
- Vogelmann, J. E., Sohl, T., & Howard, S. M. (1998). Regional characterisation of land cover using multiple sources of data. *Photogrammetric Engineering & Remote Sensing*, 64, 45-57.
- Yang, L., Homer, C., Hegge, K., Huang, C., & Wylie, B. (2001). A Landsat 7 Scene Selection Strategy for a National Land Cover Database. *IEEE International Geoscience and Remote Sensing Symposium*. Sydney, Australia, CD ROM, 1 disk.
- Zhu, Z., & Evans, D. L. (1994). US forest types and predicted percent forest cover from AVHRR data. *Photogrammetric Engineering & Remote Sensing*, 60, 525-531.

Chapter 15

MODELING FOREST PRODUCTIVITY USING DATA ACQUIRED THROUGH REMOTE SENSING

Nicholas C. Coops¹ and Joseph D. White²

¹ *CSIRO Forestry and Forest Products, Private Bag 10, Clayton South, Victoria, 3169, Australia*

² *Baylor University, Department of Biology, P.O. Box 97388, Waco, Texas, USA*

1. INTRODUCTION

The increased need for information on the growth of the worlds forests has led to a range of new approaches beyond traditional ground-based forest inventory surveys supplemented with aerial stereo-photography. The development of physiologically-based process models, which predict forest growth based on underlying physiological processes, and digital remote sensing in combination improve our ability to interpret and to predict forest growth patterns across landscapes. In this Chapter we review applications of these two rapidly maturing technologies. We cite selected examples of how data acquired through remote sensing have served to initialize, update, and validate models. From these studies we document improvements in our ability to assess, project, and track present and future forest growth patterns in changing environments across landscapes.

Demands on global forest resources including wood production, CO₂ uptake, and habitat have increased the need for repeatable and accurate information on the condition of forested areas. This has led to the development of new approaches to map and monitor patterns in growth, regeneration, health, and biological diversity of forested landscapes. Traditionally, forest growth has been assessed in two ways: (1) repeated plot measurements, and (2) aerial photo-interpretation. Field methods include establishment of permanent growth plots at which a series of individual tree

or stand based measurements are made at regular time intervals. These measurements provide data for documenting trends in stand growth, reforestation, and conversion of forest lands. Examples of large-scale permanent plot surveys are the US Forest Service Forest Information Analysis (FIA) (Gillespie 1999), and the Australian Permanent Growth Plot (PGP) (National Forest Inventory 1998) systems. Application of aerial photography for forest surveys was introduced in the 1940's which allowed foresters to stratify sampling to increase efficient selection of geographic distribution of forest types, their commercial value, and environmental sensitivity (Skidmore et al. 1987; Leckie et al. 1999). Today, aerial photography together with ground-based sampling remains the basis for most harvesting plans (Lawrence and Walker 1954; Preto 1992).

Since the 1960's digital imagery from satellites have provided expanded insights on forest structure, growth, condition, and spatial change over time (Gower et al. 1999). In addition, development computer technology has increased utilization of satellite data through increased computational speed, data storage capacity, and incorporation of geographic data such as of topography, climate, hydrology, and soils (Hutchinson 1989). The availability of these data have fostered integration with physiological process models thereby allowing spatially explicit information on forest canopy condition, growth and species composition to be developed.

Landsberg and Gower (1997) have compared a range of a process-based models and have identified a number of features which they share including: radiation absorption by the canopy, prediction of gross photosynthesis (or gross primary production, GPP), autotrophic (plant) respiration, net growth (net primary production, NPP), and photosynthate allocation to leaves, branches, stems, and roots. Accuracy in productivity modeling is influenced by characterization of long-term trends in climate, variation in pollution inputs, and soil fertility. With reliable estimates of these variables, process models of growth can reliably predict the extent that GPP is limited by such factors as variable climatic conditions and atmospheric gas composition (e.g. O₃, CO₂, etc.) to formulate forest management policies.

2. COUPLING REMOTE SENSING WITH FOREST PRODUCTIVITY MODELS

Remote sensing technology for forest resource management has the capacity to detect a wide range of the electromagnetic spectrum including short- and long-wave radiation (200 – 3000nm), thermal (3 – 10 μ m) and microwave (up to 1m) (Lillesand and Kiefer 1987). This spectral information

provides information on the instantaneous reflectance properties of the surface that can be interpreted either through physical radiative transfer modes or empirical relationships (Moulin et al. 1998). Information derived from these data can include photopigment and nutrient concentration, photosynthetic activity, foliar density, and stand structure. Spectral and thermal data also can provide biophysical information about the radiation, temperature, and moisture conditions necessary for driving certain models. Imaging spectroradiometers traditionally utilized with optical sensors provide complete coverage of forest areas. For modeling, this has the advantage of providing a complete census of observations and subsequent simulation in comparison to traditional survey methods that may be for a limited sub-sample of isolated points. Remote sensing data also provides accurate repeated observations therefore allowing a temporal sequence of reflectances to be calibrated to estimate particular forest components necessary for forest process modeling. Remote sensing in its broadest definition includes any type of detection or measurement of an object without direct physical contact. In this Chapter we limit discussion to digital imagery acquired from airborne or space-borne platforms and rely on Chapters by Hall (3), Fournier et al. (4), and Sanchez (16) for providing descriptions of analogue forest growth modeling.

Our examination of case studies reveals that coupling remote sensing with forest productivity models can be characterized by three basic approaches as proposed by Moulin et al. (1998):

- Initialization
- Incorporation
- Validation

Based on this structure, we will present examples and techniques of the integration of remote sensing data into models with emphasis on introducing methods and identifying types of data sets required for each of the three applications.

2.1 Model initialization

Process-based forest growth models simulate projected values at daily or monthly intervals over a range of spatial scales, from the leaf to the globe. All models require estimation of initial values for certain parameters. These parameters define the state conditions for the model for future simulations. As some parameters vary spatially, remote sensing data provides an excellent method for representing heterogeneity across landscapes. Image data from optical sensors are predominately collected in raster format, which provides a logical framework for grid-based modeling. For initialization,

remote sensing data can be analyzed to provide maps of areas with uniform ecological characteristics (e.g. vegetation type) or continuous values of biophysical or environmental variables (Figure 15-1).

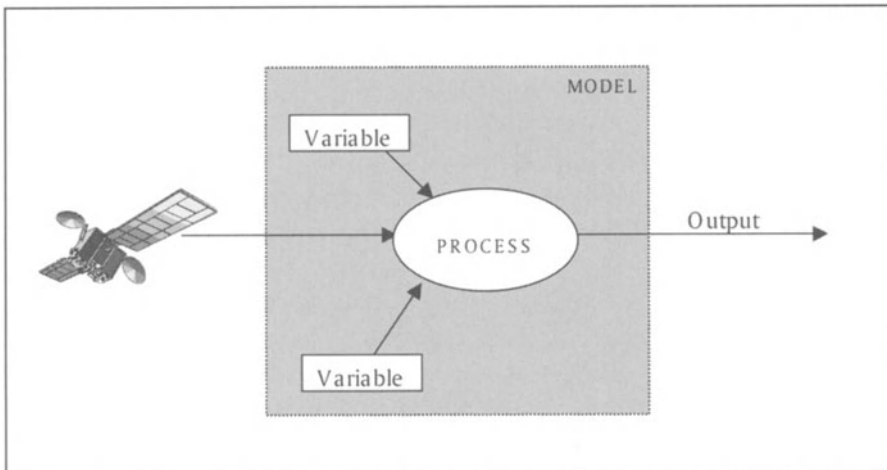


Figure 15-1. Schematic representation of coupling remote sensing with forest productivity models using imagery as a tool for model initialisation.

Vegetation maps are generally considered a fundamental product of remote sensing data analysis. For forest process modeling, vegetation maps can be utilized to spatially initialize a suite of ecological and physiological parameters given that variability of the parameters values is small within the vegetation mapping unit. For example, different types of North American montane forests have predictable fuel loads, flammability, susceptibility to injury levels, and regenerative capacity properties. Forest type maps are therefore the basis of spatially explicit fire-behavior and succession models such as FIRE-BGC (Keane et al. 1996a) in terms of defining state variables and parameter estimation. In Glacier National Park, USA, White et al. (2002) classified the landscape into units representing end states in vegetation succession (Pfister 1977) from Landsat-5 Thematic Mapper data with a 30 m spatial resolution. This information was utilized to initialize the FIRE-BGC model to simulate changes in vegetation as a response to climate variability and fire-suppression policies. The model predicted that in a future climate that was warmer and wetter, the occurrence of natural fires would result in a landscape with greater continuous patches of forests sharing similar composition and stages in development.

Large-scale remote-sensing derived maps are also useful for estimating initial conditions for regional carbon budgets. Cohen et al. (1996)

demonstrated that shifts in carbon balances associated with harvesting of U.S. Pacific Northwest old-growth forests could be estimated from Landsat-derived maps at selected intervals (1972, 1977, 1982, 1988, and 1991). An ecosystem model was utilized to estimate net losses in carbon for different cover classes regionally over the three decades. Integration of information about harvesting was required to estimate fluxes from living pools and soil as well as from forest products removed from the ecosystem. By keeping track of the life-span of various types of forest products both economic and ecological analyses could be performed simultaneously. This study highlights that multi-temporal satellite data can be used to re-initialize models at different points in time as changes in forest extent, species composition, and structure are observed.

Vegetation type is also associated with other physiological processes including trace gas emissions. Lindfors et al. (2000) demonstrated that accurate prediction of volatile organic compounds (VOC) emissions were estimated from boreal forests based on a model linking forest type, leaf area, nutrient status, and climate. VOC emissions, which can be converted into pollutants from reactions with sunlight, are known to vary with forest type (high for deciduous broadleaf trees, low for conifers) and projections of VOC emissions were made using species-specific equations which linked a spatial classification of forest species developed from Landsat TM imagery and meteorological data. Although model predictions of VOC production compared well with observed values for some regions, Lindfors et al. (2000) noted that further improvements could be made with more detailed vegetation maps at a finer spatial resolution. Improved capacity to accurately predict species composition is a continual need in forestry that may come from higher spectral resolution (e.g. Earth Observer-1 Hyperion sensor), higher spatial resolution (e.g. IKONOS, OrbView-3, and Quickbird) imagery, or a combination of both.

In addition to discrete mapping units, remotely sensed data can provide continuous variable coverages of important ecological variables such as leaf area index (LAI). This variable is utilized in most forest process models for estimating various elements of mass and energy budgets of the ecosystem including the fraction of absorbed solar radiation, interception of precipitation, and the initial foliage biomass (the latter derived from species-specific conversions from area to mass). The fraction of solar radiation absorbed is usually approximated as a simple exponential function of leaf area index using a simple model known as Beer's Law :

$$Q_a = 0.5Q_i(1 - e^{-kL}) \quad (1)$$

where Q_a is the photosynthetically active radiation absorbed by the forest canopy, Q_i is the incident incoming short-wave radiation, K is the light extinction coefficient and LAI is leaf area index (Landsberg et al. 1997). More precise formulations are also available that take into account self-shading of leaves, diffuse and direct radiation, and the transmissivity of different wavelengths through forest canopies (Leuning et al. 1995). Mapping LAI from satellite-derived reflectance in the near-infrared (NIR) and red (R) bands has a long history through correlations of LAI with simple vegetation such as the Normalized Difference Vegetation Index (NDVI) derived from satellite imagery (Tucker 1979; Peterson et al. 1987; Begue 1993; Spanner et al. 1994; Chen and Cihlar 1996; White et al. 1997; Nilson et al. 1999). Problems exist at low values of LAI, due to exposed ground (van Leeuwen and Huete 1996) and at high values of LAI, where spectral indices saturate (Fassnacht et al. 1997; Turner et al. 1999). Nevertheless, remote sensing using both simple empirical relationships and more complex algorithms that employ radiation transfer models has the ability to estimate LAI over large spatial domains. Because of the saturation problem, it is more logical to use a nearly linear relationship established between NDVI and the fraction of photosynthetically active radiation absorbed by the canopy. LAI can then be estimated by inverting Beer's law or using more sophisticated radiative transfer models (Gower et al. 1999). Adjustments of satellite-derived LAI values have been developed where LAI is constrained based on maximum potential LAI defined by climate-soil factors (Thornton 1998; Nemani and Running 1989).

In addition to LAI, ecosystem models can require additional information on a number of other canopy properties prior to simulation including leaf mass per unit area, nitrogen concentration, photosynthetic capacity, and maximum canopy stomatal conductance. In some cases these canopy properties can be inferred from association with satellite-derived classification of forest types (White et al. 1998; Running and Gower 1991; Kimball et al. 2000). However, vegetation type may be a poor predictor of these characteristics and direct measures may be attained with careful selection spectral bands from hyperspectral remote sensing imagery. Martin and Aber (1997) demonstrated that NASA's Airborne Visible/Infrared Imaging Spectroradiometer (AVIRIS), with 10 to 20 nm spectral resolution could accurately predict foliar canopy chemistry, in particular canopy nitrogen, at Harvard Forest in Petersham, Massachusetts. Regression equations using selected spectral bands also showed good correlations with canopy nitrogen and lignin concentrations. By applying the equations over the entire AVIRIS images, wall to wall spatial estimates of canopy nitrogen were derived to parameterize the ecosystem model PnET (Aber and Federer

1992) and predict spatial variation in net ecosystem carbon exchange (NEE) annually.

At the watershed scale, spatially-linked ecosystem models have been developed to predict changes in streamflow and forest production in response to large fires, such as one that burned significant portions of the North Fork of the Flathead River valley in Montana, USA in 1981 (White et al. 1994). Landsat TM data acquired before and after the fire provided a basis for updating vegetation conditions for modeling where vegetation type changed in response to fire extent and severity. These simulations predicted a marked increase in hydrologic discharge immediately following the fire that diminished the following year as herbaceous species invaded the burned area. This occurred in the model as the satellite estimates indicated increasing values of LAI as the vegetation regenerates post fire resulting in increased transpiration during periods of high water availability.

At the regional-scale, simulations also rely heavily on remote sensing data to provide a comprehensive definition of land cover and other forest attributes. Assessment of ecosystem management in the U.S. Interior Columbia River Basin was conducted by several U.S. state and federal agencies to determine the influence of land management on environmental issues including fire potential, disease susceptibility, erosion, and wildlife conservation. This effort was primarily based on sets of integrated geographic data including remote sensing data that was classified into land cover and stand structural classes (Hann 1997). These data were the basis for modeling succession of forests (Keane et al. 1996b) and forest productivity (Thornton and White 1996) through time based on current conditions.

Initial model conditions often dictate the accuracy of forest growth predictions especially when simulating growth of trees at different life stages. Remote sensing estimates of standing biomass coupled with cover type mapping greatly improves subsequent growth predictions. For example, Bergen and Dobson (1999) used synthetic aperture radar (SAR) to predict forest biomass and net primary production at sites in Michigan. Ground biomass can be accurately estimated for low biomass forests (100 Mg/ha) using regression relationships based on RADAR backscatter (Waring et al. 1995). In addition, SAR data can be used to provide a basis to classify the study area into the broad structural categories such as herbaceous, shrub, and tree cover. Once the vegetation classification of the site had been completed, and estimates of above ground biomass initialized with SAR-derived estimates of biomass to predict future growth. In addition, by constraining above ground NPP with the SAR data, the forest growth model provides better estimates of other ecosystem properties such as below ground biomass accumulation and leaf litter production, and fine root turnover (Bergen and

Dobson 1999). Similar approaches have also been developed using RADAR AIRSAR data and the ZELIG forest succession model (Ranson et al. 1997).

Lastly, remote sensing observations can be utilized to define background environmental conditions such as soil type and fertility. In Australia, eucalypt forests were extensively surveyed using quantitative soil surveys (Gessler et al. 1995). McKenzie and Ryan (2001) demonstrated that soil properties such as soil phosphorus content could be predicted from gamma radiometric counts combined with climatic data and Landsat TM imagery. These geographically registered soil properties were then incorporated by Tickle et al. (2001) in a forest growth model that was applied across the study area to predict forest growth and stocking.

2.2 Remote sensing incorporated into forest productivity models

Remote sensing observations can also be linked with forest production as driving variables of vegetation condition, function, or the biophysical environment (Figure 15-2). However, there is often a trade-off between spatial and temporal scales as fine spatial scaled remote sensing data tend to have low temporal frequency. Therefore, models that utilize inputs directly from remote sensing for assessing physiological processes will generally have a coarse spatial resolution as the imagery required is usually acquired from satellite platforms with frequent repeated orbits. These types of models are top down approaches, driven by contiguous satellite observations operating at either daily, weekly or monthly time steps, and use observations of canopy light absorption and utilization to estimate growth at regional, continental or global scales (Goetz et al. 1999).

The historical development of these types of process based forest physiological models have come via a simplification of models such as the relatively detailed stand/canopy model with hourly and daily time steps applied to a single plot location such as BIOMASS model (McMurtrie et al. 1990). In these models the carbon balance of the canopy is calculated from a radiation interception model that uses information about the canopy structure and foliage photosynthetic characteristics. The carbon balance of the stand is updated daily after calculation of the carbon lost by respiration. Water balance is calculated using the Penman-Monteith equation (Landsberg and Coops 1999). Models such as BIOMASS have proved very valuable as an experimental tool to understand forests; however, the large amount of information required to run the model effectively limits its use to single plot or stand locations making spatial extrapolation of the model over the landscape a difficult task.

Based on this history, a new series of models have been developed which attempt to simplify much of this detailed physiology and allow remotely sensed observations to effectively drive the model predictions at regular time intervals such as daily or monthly time-steps (Running and Coughlan 1988). Examples of these include the 3PGS (Coops et al. 1998), GLOPEM2 (Goetz et al. 1999), and NASA CASA (Carnegie – Ames – Stanford) Biosphere (Potter et al. 1993) models. The 3PGS model (the acronym stands for Physiological Processes Predicting Growth from Satellites) is a deliberate attempt to bridge the gap between growth and yield and carbon balance models (Landsberg and Waring 1997). The model is based on the 3PG model which uses a simple radiation absorption model to calculate the photosynthetically active radiation absorbed by a stand (Figure 15-3). This is modified to utilizable absorbed photosynthetically active radiation by accounting for the effects of soil drought, atmospheric vapour pressure deficits and stand age. GPP is obtained by applying a canopy quantum efficiency value to utilizable absorbed photosynthetically active radiation and NPP calculated from a simple ratio of NPP to GPP (see Waring et al. 1998) which, under certain assumptions and conditions, removes the need to calculate respiration.

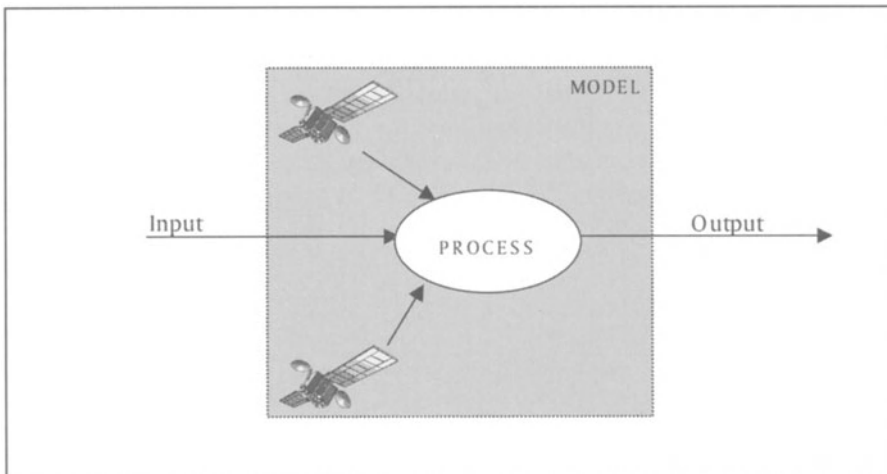


Figure 15-2. Schematic representation of coupling remote sensing with forest productivity models incorporating imagery within the model processes.

In 3PGS (Coops et al. 1998) the amount of incoming photosynthetically active radiation that is intercepted by the vegetation canopy is calculated by reducing photosynthetically active radiation by the fraction of photosynthetically active radiation absorbed by the forest canopies which is

estimated from a satellite-derived index. This spectral vegetation index has been shown, both empirically and theoretically, to be related to the fPAR (fraction of Photosynthetically Active Radiation) absorbed by vegetation canopies (Kumar and Monteith 1982; Sellers 1985, 1987; Goward et al. 1994). These satellite-based measures of canopy properties are highly desirable for NPP modelling because of their strong influence on canopy energy balances and rates of gas exchange. Observations typically have come from the Advanced Very High Resolution Radiometer (AVHRR) which has been launched on a number of NOAA satellites since the 1960's (Kidwell 1988). This sensor provides 1.1km spatial resolution imagery in 5 spectral channels including the visible and near infrared regions of the electromagnetic spectrum. Due to the large pixel size of the AVHRR sensor it can image the same location on the Earth's surface twice a day, producing a continuous broad scale dataset of changing atmospheric and vegetation conditions. In order to condense the large daily datasets, remove cloud contamination, and minimize errors due to poor viewing geometry monthly compositions of AVHRR data are produced and made available free of charge to of the general public.

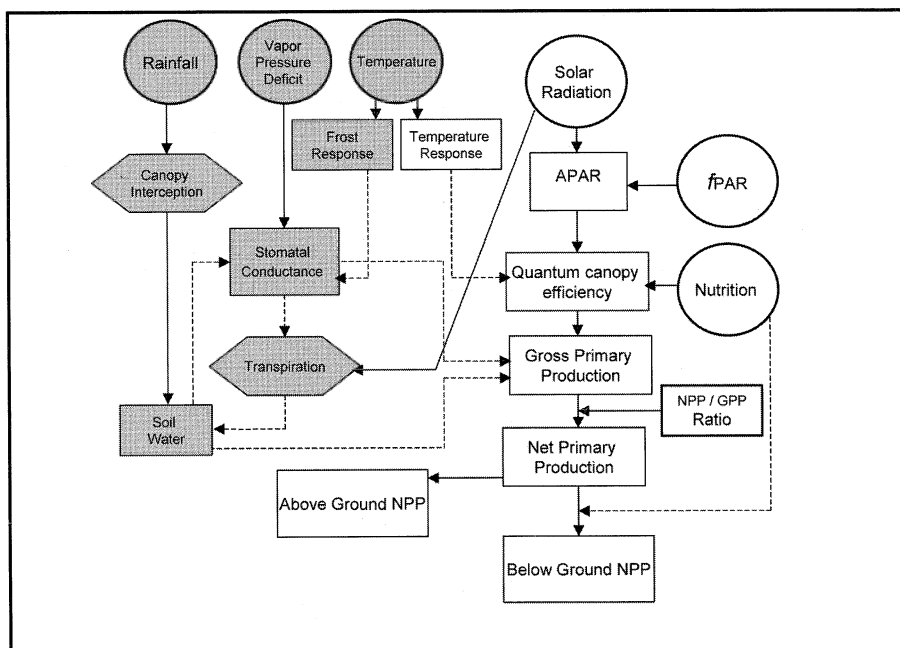


Figure 15-3. General Flow Diagram of 3PGS model.

Like many process based models 3PGS, requires meteorological data and information about soil depth and water-holding characteristics as inputs. Coops (1999) originally applied the 3PGS to predict above-ground NPP at contrasting forested sites in Australia and New Zealand and compared them with estimated NPP derived from field data using coarse-scale NOAA AVHRR imagery. In that study there was a linear relation between NPP predicted by the model and ground-based estimates of wood production for fully stocked, rapidly growing stands ($r^2 = 0.82$). Additional research has demonstrated that the model could be utilised in management applications by linking AVHRR data with Landsat Multi-Spectral Scanner (MSS) data to incorporate 'snapshots' of the forest using fine scale (80 m) spatial resolution data obtained at specific time intervals. These higher resolution remotely sensed data provided the possibility of including a number of additional key spatial variables not available at the 1 km scale, specifically, forest age classes, soil fertility and water holding capacity. NPP predicted by 3PGS in a *Pinus radiata* plantation in southern New South Wales, Australia was in excellent agreement ($r^2 = 0.84$) with measured actual forest productivity. The model has also been applied to forested environments in Oregon, USA where 3PGS was initialized with NDVI-derived estimates of fPAR to estimate at monthly time steps photosynthesis, respiration, and above-ground growth of forest vegetation within a 54,000 km² region in southwestern Oregon. Within this mountainous region considerable variation existed within each 1km pixel centered on each of the validation survey plots. Local variation in climate and soils played an equal if not greater role. When the sample plots were stratified into 14 broad forest types, within which growth potential varied similarly (coefficient of variation for each of the 14 types averaged 6 %), a good relation was found between predicted and measured forest growth capacity across all types ($r^2 = 0.82$) (Coops and Waring 2001).

The GLO-PEM2 and NASA CASA models follow similar approaches based on a radiation interception model using a light utilization factor (known as ϵ) which can be modified by a combination of environmental variables such as soil water, temperature, soil fertility, nutrient capacity, frost, vapor pressure deficit, soil texture and land use (Potter et al. 1999). Both GLO-PEM2 and NASA-CASA have been specifically designed to handle large datasets to facilitate prediction at global scales and both models have produced global estimates of NPP and growth for selected time periods (Goetz et al. 1999; Potter et al. 2001). To do this different parameter sets were derived for a range of vegetation types ranging from agriculture and pasture systems to both evergreen and deciduous forests. The NASA-CASA model is specifically designed to simulate seasonal patterns in net carbon

fixation and allocation, litterfall and soil nutrient mineralisation and soil CO₂ emissions over the globe. In a validation analysis using measured NPP estimates from thousands of sites around the globe covering a range of vegetation types the model was found to predict annual NPP with an overall error of less than 10 % (Potter et al. 2001).

The ongoing remote sensing observations driving these types of process-based models can extend beyond simply providing prediction on foliage radiation interception capacity. Earth observation and meteorological satellites can provide an alternative source to spatially sparse ground-based observations. For example, Goward et al. (1994) estimated the monthly integrated incident solar radiation across the Oregon transect using ultraviolet reflectance data from the Total Ozone Mapping Spectroradiometer (TOMS) (Goward et al. 1994). A similar approach has also been applied by Dye and Shibasaki (1995). The GOES satellite which is a geostationary meteorological observing satellite, with regular image acquisition (up to 1 full hemisphere every 30 minutes), has been shown to predict daily incident solar radiation well ($r^2 > 0.95$) compared to ground based measures. In Australia, where cloud cover is generally less, similarly good results have been found using the Japanese GMS satellite (Weymouth and Le Marshall 1994). Wang et al. (2000) combined Landsat TM imagery, a DEM, and an atmospheric model (LOWTRAN) to estimate surface net solar radiation over an agricultural site in the US with an average error of less than 1 % (Wang et al. 2000). The GLOPEM2 modeling framework is unique in that it attempts to provide global NPP measurements driven from datasets all obtained directly from remote sensing observations. For example rather than utilizing conventional meteorological observations to provide spatial estimates of surface temperature, AVHRR temperature channels provide an estimate of surface temperature and precipitable water allowing computation of vapor pressure deficit (Goetz et al. 1999).

In addition to driving the model using estimates of foliage cover and meteorological conditions from regular remote sensing images a number of other driving variables can be predicted. When NDVI and surface temperature, for example, are analyzed patterns emerge which can provide information on the surface resistance of the forest canopy. These types of measures provide information on the dissipation of the incident radiation on a forest canopy to sensible rather than latent heat as the surface temperatures increase and water availability (Nemani and Running 1989; Nemani et al. 1993). The slope of these types of relationships provide an estimate of surface resistance from which regional estimates of water vapor flux can be modeled over the landscape at regular time-steps. GLOPEM2 utilizes this

approach to provide estimates of root zone soil moisture using derived relationship (Goetz et al. 1999).

2.3 Remote sensing for model validation

To date, the least utilized application of remotely sensed imagery has been in validating model predictions of forest growth and succession (Figure 15-4). Potentially, laser-beam near-infrared sensors (LIDAR) have the ability to quantify standing biomass accurately up to values >500 Mg/ha, so with repeat sampling accurate estimates of net above-ground growth should be available for rigorous validation of model predictions (Lefsky et al. 2002). Voirin et al. (2001) utilized remote sensing observations when applying the ISBA (Interactions between Soil Biosphere and Atmosphere) SVAT model. In this research the SVAT model was used to predict vegetation transpiration, LAI, and soil water runoff in a series of regional catchments. The model used a growth model to predict LAI instead of utilizing remote sensing observations. The predictions of LAI were then compared to LAI as estimated from AVHRR remote sensing imagery.

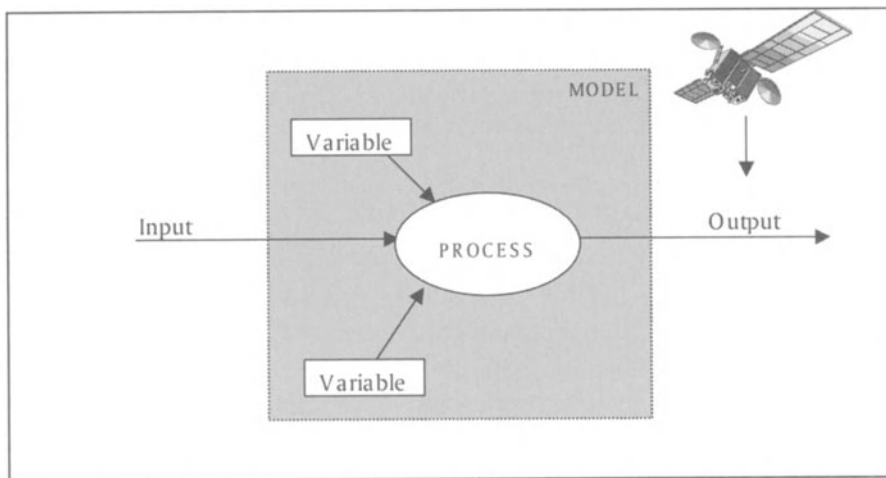


Figure 15-4. Schematic representation of coupling remote sensing with forest productivity models using imagery as a tool for model validation.

Water production is an indication of gas exchange capacity of forested systems. Silberstein et al. (1999) validated output from a coupled water and energy balance model (COUPLE) over small catchments in Western Australia using Landsat 5 thermal imagery. The COUPLE model operates at

a sub-daily time step to predict water movement through soil layers to provide short-term estimates of changes in water storage, runoff, and seepage. Linking the soil water balance model with an energy balance model, Silberstein et al. (1999) calculated atmosphere fluxes of water vapor and heat transport at 15 minute intervals. The COUPLE simulations were extended over a 4-year period and included predictions of surface temperature across entire catchments. Whilst standard hydrological measurements of surface runoff and water storage were validated using conventional methods (such as surface runoff data), predicted surface temperatures were verified using thermal remote sensing imagery extracted from selected scenes. Correlations between predicted surface temperatures across catchments and those inferred from thermal data were very good ($r^2 = 0.83$).

Landsat TM imagery provides an excellent basis for describing spatial changes in vegetation cover over time. The high quality of data has been recognized as suitable, in many cases, to validate a wide variety of models that predict spatial changes in vegetation cover. Mickler et al. (2002) adopted this approach in an analysis of current and future biomass under selected fire regimes across the southern United States using the PnET forest process model (Aber and Federer 1992). Both historical and current estimations of climate and subsequent variation in NPP across the region were predicted. Landsat TM imagery was then used to interpret current land use classes with a supervised classification to extract deciduous, evergreen and mixed forest types. With the Landsat imagery, PnET simulations could provide analysis by recognizing pure stands of individual species (Mickler et al. 2002).

With increasing confidence in the ability of ecosystem models to predict growth and other ecosystem properties across broad climatic regions, deviations from expected vegetation patterns can be interpreted as an expression of anthropogenic activity associated with land-use changes (Coops et al. 2001b). Remote sensing provides information on the state of present landscapes that may once have contained indigenous vegetation, grassland, or desert. Major increases or reductions in LAI from those expected have been interpreted as reductions in the distribution of natural vegetation attributed to man's exploitation and concentration of resources (energy, water, fertilizer, domestic animals (Waring and Running 1998, plate 13)).

3. DISCUSSION

Simulations of forest growth can be used to identify likely deficiencies in the spatial soil maps and climatic extrapolations assuming good agreement exists between the forest model predictions and reality. In such cases, adjustments in the original data layers may be justified (Veroustraete et al. 1996). With the MODIS sensor aboard the EOS Terra satellite, opportunities for the integration of remote sensing data as a driver of forest productivity modeling has reached a new level of accessibility. Calculation of vegetation production using data from the MODIS sensor is done in near real time and is publicly available over the Internet⁷. MODIS provides traditional raw spectral data along with various products derived from the remote sensing data after pre-processing (Running et al. 1994). One of these MODIS products (MOD17) is daily net photosynthesis and net primary production of the globe (Running et al. 1999a). The basis of this calculation is from a simple canopy radiation absorption efficiency model that reduces the maximum rate of production based on climatic limitations that can be themselves derived via remote sensing: solar radiation, humidity, surface temperature. The fraction of radiation absorbed by vegetation is predicted from satellite-derived estimates of LAI. From remote sensing derived land cover maps, vegetation-specific parameters are used to predict response to climatic variation in terms of biomass allocation. These coupled remote sensing and simple productivity models are potentially quite accurate. Their general validity is being evaluated through extensive field campaigns at the plot-level, from canopy and aerial flux measurements, and from collection of atmospheric gases using aircraft (Running, et al. 1999b).

4. CONCLUSION

Remote sensing plays an important role in *initializing* forest growth models. By incorporating remotely sensed data over time, the model predictions can be *verified* and *updated* if unpredicted changes in canopy properties are observed. With expansion beyond passive optical sensors, into active microwave and lasers, as well as thermal infrared sensors, much more information is available to parameterize and validate ecosystem flux estimates (CO₂, VOC emissions, water vapor and heat transfer) as well as the physical (biomass) and physiological state (N and lignin concentrations in foliage). Because remotely sensed data can be acquired at regular temporal

⁷ <http://modis.gsfc.nasa.gov/data/dataproducts/DescChart.html>

and spatial intervals and archived information is available, the data has a vital role to play as a basis for future analyses of local, regional, and global change.

It appears, from this review, that models for forest production that incorporate remote sensing are in a position to make much improved calculations of forest growth over large spatial areas. It is unlikely that these types of models, even with satellite-Lidar coverage, will eliminate the need for all ground-based measures of forest productivity. Coupled models, however, can play significant roles in predicting important trends that might not be discerned on a small sample of permanent plots. Different projections, based on a range of possible climatic changes and management, should also be valuable in evaluating various policies.

ACKNOWLEDGMENTS

We wish to thank Drs Richard Waring and Dr Lars Pierce and three anonymous reviewers for valuable comments on this manuscript.

REFERENCES

- Aber, J. D., & Federer, C. A. (1992). A generalized, lumped-parameter model for photosynthesis, evapotranspiration and net primary production in temperate and boreal forest ecosystems. *Oecologia*, 92, 463-474.
- Band, L. E. (1993). Effect of land surface representation on forest water and carbon budgets. *Journal of Hydrology*, 150, 749-772.
- Begue, M. E. (1993). Leaf Area Index, intercepted photosynthetically active radiation, and spectral vegetation indices. A sensitivity analysis for regular clumped canopies. *Remote Sensing of Environment*, 46, 45-59.
- Bergen, K. M., & Dobson, M. C. (1999). Integration of remotely sensed radar imagery in modeling and mapping of forest biomass and net primary production. *Ecological Modeling*, 122, 257-274.
- Chen, J. M., & Cihlar, J. (1996). Retrieving leaf area index of boreal conifer forests using Landsat TM images. *Remote Sensing of Environment*, 55, 153-162.
- Cohen, W. B., Harmon, M. E., Wallin, D. O., & Fiorella, M. (1996). Two decades of carbon flux from forests of the Pacific Northwest. *BioScience*, 46, 836-844.
- Coops, N. C. (1999). Linking multi-resolution satellite-derived estimates of canopy photosynthetic capacity and meteorological data to assess forest productivity in a *Pinus radiata* (D. Don) stand. *Photogrammetric Engineering and Remote Sensing*, 65, 1149-1156.
- Coops, N. C., & Waring, R. H. (2001a). The use of multi-scale remote sensing imagery to derive regional estimates of forest growth capacity using 3-PGS. *Remote Sensing of Environment*, 75, 324-334.

- Coops, N. C., & Waring, R. H. (2001b). Estimating forest productivity in the eastern Siskiyou Mountains of southwestern Oregon using a satellite driven process model, 3-PGS. *Canadian Journal of Forest Research*, 31, 143-154
- Coops, N. C., Waring, R. H., & Landsberg, J. J. (1998). Assessing forest productivity in Australia and New Zealand using a physiologically-based model driven with averaged monthly weather data and satellite derived estimates of canopy photosynthetic capacity. *Forest Ecology and Management*, 104, 113-127.
- Dye, D. G., & Shibasaki, R. (1995). Intercomparison of global PAR data sets. *Geophysical Research Letters*, 22, 2013-2016.
- Fassnacht, K. S., Gower, S. T., MacKenzie, M. D., Nordheim, E. V., & Lillesand, T. M. (1997). Estimating the leaf area index of north central Wisconsin forests using the Landsat Thematic Mapper. *Remote Sensing of Environment*, 61, 229-245.
- Gessler, P. E, Moore, J. D., McKenzie, N. J., & Ryan, P. J. (1995). Soil-landscape modelling and spatial prediction of soil attributes. *International Journal of Geographical Information Systems*, 4, 421-432.
- Goetz, S. J., Prince, S. D., Goward, S. N., Thawley, M. M., & Small, J. (1999). Satellite remote sensing of primary production: an improved production efficiency modeling approach. *Ecological Modeling*, 122, 239-255.
- Goward, S. N., Waring, R. H., Dye, D. G., & Yang, J. (1994). Ecological remote sensing at OTTER: Satellite macroscale observations. *Ecological Applications*, 4, 322-343.
- Gower, S. T., Kucharik, C. J. & Norman, J. (1999). Direct and indirect estimation of leaf area index, fAPAR and net primary production of terrestrial ecosystems. *Remote Sensing of Environment*, 70, 29-51.
- Hann, W. J., Jones, J. L., Karl, M. G., Hessburg, P. F., Keane, R. E., Long, D. G., Menakis, J. P., McNicoll, C. H., Leonard, S. G., Gravenmier, R. A., & Smith, B. G. (1997). Landscape Dynamics of the Basin. Quigley, T. M. & Arbelbide, S. (Eds.). *An Assessment of Ecosystem Components in the Interior Columbia Basin. Volume II*. General Technical Report PNW-GTR-405. USDA Forest Service, Pacific Northwest Research Station.
- Hutchinson, M. F. (1989). A new objective method for the spatial interpolation of meteorological variables from irregular networks applied to the estimation of monthly mean solar radiation, temperature, precipitation and windrun. Fitzpatrick, E. A. & Kalma, J. D. (Eds.). *Need for climatic and hydrological data in agriculture in Southeast Asia. Proceedings of United Nations University Workshop*, 95-104. CSIRO Water Resources Technical Memorandum 89/5.
- Keane, R. E., Menakis, J. P., Long, D., Hann, W. J., & Bevins, C. (1996a). Simulating coarse scale vegetation dynamics using the Columbia River Basin Succession Model – CRBSUM. *USDA Forest Service General Technical Report INT-GTR-340*.
- Keane, R. E., Ryan, K. C., & Running, S. W. (1996b). Simulating effects of fire on northern Rocky Mountain landscapes with the ecological process model FIRE-BGC. *Tree Physiology*, 16, 319-331.
- Keane, R. E., Morgan, P., & White, J. D. (1999). Temporal patterns of ecosystem processes on simulated landscapes in Glacier National Park, Montana, USA. *Landscape Ecology*, 14, 311-329.
- Kidwell, K. B. (1988). *NOAA polar orbiter data TIROS-N, NOAA-6, NOAA-7, NOAA-8, NOAA-9, NOAA-10, NOAA-11 users guide*. National Oceanic and Atmospheric Administration.

- Kimball, J. S., Keyser, A. R., Running, S. W., & Saatchi, S. S. (2000). Regional assessment of boreal forest productivity using an ecological process model and remote sensing parameter maps. *Tree Physiology*, 20, 761-775.
- Kumar, M., & Monteith, J. L. (1982). Remote sensing of plant growth. Smith, H. (Ed.). *Plants and the Daylight Spectrum*, 133-144. Academic Press. London.
- Landsberg, J. J., & Coops, N. C. (1999). Modelling forest productivity across large areas and long periods. *Natural Resource Modelling*, 12, 1-28.
- Landsberg, J. J., & Gower, S. T. (1997). *Applications of physiological ecology to forest management*. Acad. Press, San Diego.
- Landsberg, J. J., & Waring, R. H. (1997). A generalized model of forest productivity using simplified concepts of radiation-use efficiency, carbon balance, and partitioning. *Forest Ecology and Management*, 95, 209-22.
- Lawrence, P. R., & Walker, B. B. (1954). Methods and results of forest assessment using random sampling units in photo-interpreted strata. *Australian Forestry*, 18, 107-127.
- Leckie, D. G., Gillis, M. D., Gougeon, F., Lodin, M., Wakelin, J., & Yuan, X. (1999). Computer-assisted photointerpretation aids to forest inventory mapping: some possible approaches. Hill, D. A. & Leckie, D. G., (Eds.). *Proc. Int'l Forum on Automated Interpretation of High Spatial Resolution Digital Imagery for Forestry*, 335-343. February 10-12, 1998. Victoria, British Columbia, Canada. Natural Resources Canada, Canadian Forest Service, Victoria, B.C., Canada.
- Lefsky, M. A., Cohen, W. B., Parker, G. G., & Harding, D. J. (2002). Lidar remote sensing for ecosystem studies. *BioScience*, 52, 19-30.
- Landsberg, J. J., Prince, S. D., Jarvis, P. G., McMurtrie, R. E., Luxmoore, R., & Medlyn, B. E. (1997). Energy conversion and use in forests: the analysis of forest production in terms of utilisation efficiency (ϵ). Gholz, H. L., Nakane, K., & Shimoda, H. (Eds.). *The use of remote sensing in the modeling of forest productivity*, 273-298. Kluwer Academic Publishers, Inc, Dordrecht.
- Leuning, R., Kelliher, F. M., De Pury, D. G. G., & Schulze, E. D. (1995). Leaf nitrogen, photosynthesis, conductance, and transpiration: scaling leaves to canopies. *Plant, Cell, and Environment*, 18, 1183-1200.
- Lillesand, T. M., & Kiefer, R. W. (1987). *Remote Sensing and Image Interpretation*, (2nd ed.). New York, John Wiley and Sons.
- Lindfors, V., Laurila, T., Hakola, H., Steinbrecher, R., & Rinne, J. (2000). Modeling speciated terpenoid emissions from the European boreal forest. *Atmospheric Environment*, 34, 4983-4996.
- Martin, M. E., & Aber, J. D. (1997). High spectral resolution remote sensing of forest canopy lignin, nitrogen and ecosystem process. *Ecological Applications*, 7, 431-443.
- McKenzie, N. J., & Ryan, P. J. (1999). Spatial prediction of soil properties using environmental correlation. *Geoderma*, 89, 67-94.
- McMurtrie, R. E., Rook, D. A., & Kelliher, F. M. (1990). Modelling the yield of *Pinus radiata* on a site limited by water and nutrition. *Forest Ecology and Management*, 30, 381-413.
- Mickler, R. A., Earnhardt, T. S. & Moore, J. A. (2002). Regional Estimation of current and future forest biomass. *Environmental Pollution*, 116, S7-S16.
- Moulin, S., Bonneau, A., & Delécolle, R. (1998). Combining agricultural crop models and satellite observations: from field to regional scales. *International Journal Remote Sensing*, 19, 1021-1036.

- National Forestry Inventory 1998. *Australia's State of the Forests Report 1998*. Bureau of Rural Sciences, Canberra. Commonwealth of Australia.
- Nemani, R. R., & Running, S. W. (1989). Estimation of regional surface resistance to evapotranspiration from NDVI and thermal – IR AVHRR data. *Journal of Applied Meteorology*, 28, 276 – 284.
- Nemani, R., Pierce, L., Running, S., & Goward, S. (1993). Developing satellite-derived estimates of surface moisture status. *Journal of Applied Meteorology*, 32, 548-557.
- Nilson, T., Anniste, J., Lang, M., & Praks, J. (1999). Determination of needle area indices of coniferous forest canopies in the NOPEX region by ground-based optical measurements and satellite images. *Agricultural and Forest Meteorology*, 98-99, 449-462.
- Peterson, D. L., Spanner, M. A., Running, S. W., & Teuber, K. B. (1987). Relationship of thematic mapper simulator data to the leaf area index of temperate coniferous forests. *Remote Sensing of the Environment*, 22, 323-341.
- Pfister, R. D., Kovalchik, B. L., Arno, S. F., & Presby, R. C. (1977). Forest habitat types of Montana. *USDA Forest Service General Technical Report INT-34*.
- Potter, C. S., Randerson, J. T., Field, C. B., et al. (1993). Terrestrial ecosystem production: A process model based on global satellite and surface data. *Global Biogeochemical Cycles*, 7, 811-841.
- Potter, C. S., Coughlan, J. C., & Brooks, V. (1999). Investigations of BOREAS spatial data in support of regional ecosystem modeling. *Journal of Geophysical Research*, 104, 771-27,788.
- Potter, C. S., Alexander, S. E., Coughlan, J. C., & Klooster, S. A. (2001). Modeling biogenic emissions of isoprene: exploration of model drovers, climate control algorithms and use of global satellite observations. *Atmospheric Environment*, 35, 6151-6165.
- Preto, G. (1992). Past and present of inventorying and monitoring systems. *Forest Resource inventory and monitoring and remote sensing Technology*. Proc. IURFO Centennial meeting Berlin, 1-10.
- Ranson, K. J., Sun, G., Weishampel, J. F., & Knox, R. G. (1997). Forest biomass from combines ecosystem and radar backscatter modeling. *Remote Sensing of Environment*, 59, 118-113.
- Running, S. W., Baldocchi, D. D., Turner, D. P., Gower, S. T., Bakwin, P. K., & Hibbard, K. A. (1999b). A global terrestrial monitoring network integrating tower fluxes, flask sampling, ecosystem modeling, and EOS satellite data. *Remote Sensing of Environment*, 70, 108-127.
- Running, S. W., & Coughlan, J. C. (1988). A general model of forest ecosystem processes for regional applications. I. Hydrologic balance, canopy gas exchange, and primary production processes. *Ecological Modeling*, 42, 125-154.
- Running, S. W., & Gower, S. T. (1991). FOREST-BGC, a general model of forest ecosystem processes for regional applications. II. Dynamic carbon allocation and nitrogen budgets. *Tree Physiology*, 9, 147-160.
- Running, S. W., Justice, C. O., Salmonson. V., et al. (1994). Terrestrial remote sensing and algorithms planned for EOS/MODIS. *International Journal of Remote Sensing*, 15, 3587-3620.
- Running, S. W., Nemani, R., Glassy, J. M., & Thronthon, P. E. (1999a). MODIS daily photosynthesis (PSN) and annual net primary productivity production (NPP) product (MOD17). *Algorithm Theoretical Basis Document for NASA's MODIS Land Surface Team*. From http://modis.gsfc.nasa.gov/data/atbd/atbd_mod16.pdf.

- Running, S. W., Nemani, R. R., Peterson, D. L., Band, L. E., Potts, D. F., Pierce, L. L., & Spanner, M. A. (1989). Mapping regional forest evapotranspiration and photosynthesis by coupling satellite data with ecosystem simulation. *Ecology*, 70, 1090-1101.
- Sellers, P. J. (1985). Canopy Reflectance, Photosynthesis and Transpiration. *International Journal of Remote Sensing*, 68, 1335-1372.
- Sellers, P. J. (1987). Canopy Reflectance, Photosynthesis, and Transpiration 2. The role of biophysics in the linearity of their interdependence. *Remote Sensing the Environment*, 21, 143-183.
- Silberstein, R. P., Sivapalan, M., & Wyllie, A. (1999). On the validation of a coupled water and energy balance model at small catchment scales. *Journal of Hydrology*, 220, 149-168.
- Skidmore, A. K., Wood, G. B., & Shepherd, K. R. (1987). Remotely sensed digital data in forestry - a review. *Australian Forestry*, 50, 40-53.
- Spanner, M. A., Johnson, L., Miller, J., et al. (1994). Remote sensing of seasonal leaf area index across the Oregon transect. *Ecological Applications*, 4, 258-271.
- Tickle, P. K., Coops, N. C., & Hafner, S. D. (2001). Assessing forest productivity at local scales across a native eucalypt forest using a process model, 3PG-SPATIAL. *Forest Ecology and Management*, 152, 275-291.
- Thornton, P. E. (1998). *Regional ecosystem simulation: combining surface and satellite-based observations to study linkages between terrestrial energy and mass budgets*. Ph.D. Dissertation, University of Montana, School of Forestry.
- Thornton, P. E., & White, J. D. (1996). *Biogeochemical characterization of the Columbia River Basin using the BGC model: Model description, ecophysiological inputs and landscape description*. Final Report on file at USDA Forest Service Intermountain Fire Sciences Laboratory, Missoula, MT.
- Tucker, C. J. (1979). Red and photographic infrared linear combinations for monitoring vegetation. *Remote Sensing of Environment*, 8, 127-150.
- Turner, D. P., Cohen, W. B., Kennedy, R. E., Fassnacht, K. S., & Briggs, J. M. (1999). Relationship between leaf area index and Landsat TM spectral vegetation indices across three temperate zone sites. *Remote Sensing of Environment*, 70, 52-68.
- Van Leeuwen, W. J. D., & Huete, A. R. (1996). Effects of standing litter on the biophysical interpretation of plant canopies with spectral indices. *Remote Sensing of Environment*, 55, 123-138.
- Veroustraete, F., Patyn, J., & Myneni, R. B. (1996). Estimating net ecosystem exchange of carbon using the Normalized Difference Vegetation Index and an ecosystem model. *Remote Sensing of Environment*, 58, 115-130.
- Voirin, S., Calvet, J. S., Habets, F., & Nojlhan, A. (2001). Interactive vegetation modeling at a regional scale: Application to the Adour Basin. *Physical Chemical Earth*, 26, 479-484.
- Waring, R. H., Way, J., Hunt, E. R., Jr., Ranson, K. J., Weishampel, J. F., Oren, R., & Franklin, S. E. (1995). Imaging radar for ecosystem studies. *BioScience*, 45, 715-723.
- Waring, R. H., Landsberg, J. J., & Williams, M. (1998). Net primary production of forests: a constant fraction of gross primary production *Tree Physiology*, 18, 129-134.
- Waring, R. H., & Running, S. W. (1998). *Forest Ecosystems: Analysis at Multiple Scales*. Academic Press, San Diego, CA.
- Wang, J., White, K., & Robinson, G. J. (2000). Estimating surface net radiation by use of Landsat-5 TM and digital elevation models. *International Journal of Remote Sensing*, 21, 31-43.
- Weymouth, G., & Le Marshall, J. (1994). An operational system to estimate insolation over the Australian Region. *Proc. Pacific Ocean Remote Sensing Conference*, 443-449.

- White, J. D., Ryan, K. C., & Running, S. W. (1994). Remote sensing and ecological modeling of the 1988 Red Bench fire. *Proceedings of the 12th Conference on Fire and Forest Meteorology*, Oct. 26-28, 1993, Jekyll Island, GA. Society of American Foresters.
- White, J. D., Running, S. W., Thornton, P. E., Keane, R. E., Ryan, K. C., Fagre, D. B., & Key, C. H. (1998). Assessing ecosystem simulations for climate variability research at Glacier National Park, USA. *Ecological Applications*, 8, 805-823.
- White, J. D., Running, S. W., Nemani, R., Keane, R. E., & Ryan, K. C. (1997). Measurement and remote sensing of leaf area index in Rocky Mountain montane ecosystems. *Canadian Journal of Forest Research*, 27, 1714-1727.
- White, J. D., Running, S. W., Ryan, K. C., & Key, C. C. (2002). Fuzzy logic merger of spectral and ecological information for improved montane forest mapping. *Geocarto International*, 16, (in press).

Chapter 16

EXPERIENCES IN FIELD DATA COLLECTION

*In Support of Land Use and Land Cover Change Classification
in Boreal and Tropical Environments*

G. Arturo Sánchez-Azofeifa, Mark Kachmar, Margaret Kalácska, and Stephen Hamilton

*Earth Observation Systems Laboratory, Earth and Atmospheric Sciences Department,
University of Alberta, Edmonton, Alberta, T6G 2E3, Canada*

1. INTRODUCTION

Researchers and practitioners in the land use and land cover change (LUCC) community are often confronted with the need to prepare field expeditions to acquire data necessary to calibrate and validate processes associated with mapping areas / regions. As LUCC becomes more important for strategies aimed at planning for sustainable development, information related to the biophysical condition of the earth's surface (land cover) and the purpose for which the land is being used (land use) are critical for the correct interpretation of land surface observations obtained from airborne and space borne instruments. In the process of defining a monitoring system for LUCC to support the implementation of sustainable development policies, several questions, must be addressed, for example, what constitutes an appropriate data collection approach for the purposes of forest cover classification? What is the relative importance of canopy understorey information? How can direct ground observations be linked to observations from remote sensing platforms?

This Chapter is designed to provide reasonable and practical answers to these and related questions by demonstrating the procedures used in collecting ground data to support the mapping of land cover from Landsat Thematic Mapper (TM) data in two diverse environments: 1) the Alberta Ground Cover Characterisation (AGCC) project, a project aimed at

characterising land cover in the province of Alberta, Canada; and 2) the Tropical Dry Forest Monitoring program for Mesoamerica (TDFM), an initiative aimed at providing comprehensive information on the phenological stages and nature of the ecosystem composition along the Pacific Coast of Mesoamerica (Southern Pacific of Mexico to Panama). The information presented in this Chapter is not exhaustive; rather, collective field experiences are presented from these two long-term mapping projects. We explore issues ranging from the implementation of data fusion to the presentation of procedures developed to obtain biophysical information such as Leaf Area Index (LAI), using direct and indirect approaches.

2. INITIAL PLANNING

In any satellite imagery-based LUCC monitoring process designed to support sustainable forest management practices, an interdisciplinary field team is an essential component. The team should initially determine the size and spatial distribution of all land cover types as well as those of all geographic features including cities, towns, lakes and anthropogenic development within the study area. This preliminary visual analysis will help to identify problem areas that may be difficult to classify in the satellite image. Furthermore, these initial steps aid the image analysts in identifying some logistical issues; for example, whether certain areas are uncharacteristic of the landscape and need to be visited in the field, whether it will be possible / necessary to visit all parts of the study area and how much time must be spent in complex / heterogeneous areas.

The team must also understand the capabilities and limitations of the instruments that are currently available to support a suite of direct (in the field) and remote sensor observations. The initial planning process will provide a contextual background to the observations to be captured as well as to the capabilities of the instruments to be used in the field. In this way, the team can develop realistic expectations as to what can and cannot be mapped with the available tools. For example, the distribution of selected tree species in tropical rain forests cannot be mapped using sensors like Landsat TM, which provide little or no species-specific information (typically, as a result of band saturation in the red and near-infrared bands). The various limitations of the remote sensing instruments to be used must be taken into consideration, together with ways in which they can be combined to take advantage of their spatial and spectral resolutions; for example, the possibilities of performing data fusion (e.g. merging different spatial resolutions) may be offset by the increased cost of the higher spatial resolution information. Furthermore, some limitations are determined by the

geographic location where the fieldwork is implemented. For example, fieldwork activities in boreal regions will typically be more ancillary data-rich and comprehensive than in tropical regions, where level of economic development may affect the quality and amount of data sources available.

Ideally, satellite image classification should be supported by a well-planned field campaign aimed at acquiring critical land cover information. Occasionally, however, due to budgetary constraints, a ground campaign cannot be financed and field data cannot be collected. In this case, some form of ancillary data will need to be used as a surrogate for direct field observations. Hard-copy and / or digital maps can be useful alternatives to field data, as can aerial photography, but the amount, quality, and ease of acquiring these data sources can vary. Moreover, because ancillary data sources are often compiled with a specific interest / objective in mind, these data sets may not coincide with the satellite image classification data requirements. Furthermore, if ancillary data sources are used to substantiate map accuracy, but it is not known why or how the data was collected, these data sources can lead to discrepancies later. Often digital data can be separated into data that was gathered for inventory purposes and data that was captured for land-cover monitoring. The distinction between the two may not seem significant, but since each was collected for a specific purpose, it will be necessary to determine whether the data is suitable for supporting satellite image classification

3. FIELD DATA IN SUPPORT OF REMOTE SENSING

Site-specific field data is more beneficial than ancillary data, in that field data can be more strictly aligned with defined project objectives, facilitating greater control of the data set. A field campaign, however, is not independent of the image classification process, and therefore the goals of image classification and field data capture must be coincidental. Data collection is usually linked to end-user data requirements, however budgetary constraints can often dictate the level of information that can be taken in the field, ultimately influencing the field data capturing protocols. Before embarking on an image classification project, it may be necessary to first answer a number of questions concerning the field data collection.

3.1 Who will be collecting the data?

By actively engaging in a fieldwork campaign, image analysts can improve their general knowledge of dominant land cover types, and the natural patterns they tend to exhibit over the landscape. Through fieldwork, analysts may better appreciate the complexity of image classification, for example, and begin improving their understanding of what information the sensor collects with respect to the ground cover. Nevertheless, any individual evaluating / assessing a site will emphasise certain information types over others relative to their past-fieldwork experience. This observer bias should be considered and compensated for, but not necessarily discounted, as it is unavoidable and embedded in any field campaign. To minimise observer bias, however, it can be useful to delegate specific data capture tasks to key individuals, only allowing certain individuals to gather certain site information. This approach may standardise the field data collection process. In many cases when multiple partners are needed for data capture, it is not possible to determine who will be collecting the data. In these cases the data capture window may be limited, resulting from the number of sites to visit, their distance from one another, duration of the field season, phenological changes in land cover, etc. Multiple partners can aid a classification project in terms of both monetary and logistical support, particularly over large study areas. In such cases, data-gatherers need to be informed about the image classification process, including what field information is crucial and what is trivial.

3.2 What field data should be collected?

Multiple partners involved in a field campaign must understand their respective roles in capturing data with the overall project goal in mind. To facilitate increased efficiency and objective data capture, a project leader must inform all data gatherers as to what site-level information is critical for the research agenda, and also what information is irrelevant. By eliminating the capture of extraneous field data, time spent at each site can be minimised, increasing productivity. If site-level information is gathered with any ambiguity or misunderstanding of the classification process, the data collection process is compromised as those capturing data may feel that the information they are gathering is not relevant to the study objective.

3.3 Approaches to data sampling schemes

The choice of a proper sampling distribution is not a static one, but one that needs to be considered separately for individual study areas. Simple

area-based random sampling provides a statistically valid sampling procedure. However, random sampling approaches may not be able to account for land cover types that occur in small patches. Financial and temporal limitations (flight distance, time) combined with the inability to locate certain classes with simple random sampling, typically dictates that some variant of a stratified sampling method be adopted (Czaplewski, Chapter 5).

Data collection must be commensurate with the amount of detail the sensor is capable of detecting. Field data cannot be simply gathered; rather it is collected for a specific purpose / objective, thus information concerning canopy closure and / or understorey information should relate to the classes of interest. For many land cover types, particularly some shrub and deciduous canopies in northern Alberta, detailed information on understorey composition may not be relevant to the study objective, while this information could be of extreme importance in tropical dry forest environments, where subtle differences in understorey composition and / or surface moisture may significantly affect the information detected by the sensor. The data collection process must also be analysed for any logical errors in the classification scheme that would lead to ambiguous land definitions, and the classification scheme should be void of artificial classes (Congalton 1991).

In brief, the size and number of field sites that can be visited and documented for large area monitoring projects are usually governed by logistical and monetary constraints, precluding complex mathematical and statistical approaches that in some cases may create logistical problems. Therefore, by defining the degree of detail of ground cover to be collected, the classification process is parameterised and finite (i.e. there is an accepted level of detail that will be extracted from the image). A parameterised classification is necessary, for it not only controls the amount of data gathered, but also disregards extraneous ground features that will not be represented in the classification. An image classification project that is undefined in terms of data collection will be overwhelmed with unnecessary ground-level details.

3.4 Means of collecting field data

Visiting field sites by surface vehicle is often the most appropriate means of access to each field site, although in many cases field sites are difficult to locate. In general, the procedures determining which sites are to be visited should be planned out beforehand, but should also be flexible. It is recommended that the person who will classify the image also visit the sites of interest. In this manner, the image analyst has to play a more active role in

identifying the differences between what is on the ground and what is on the map. The analyst should also have a satellite image-derived field map (perhaps a colour composite) of the study area, and should document land cover types on the map that correspond to features on the image as they travel to and from the study sites. The analyst can be in full control of the information recorded directly onto the map and can focus on the landscape and vegetation.

3.5 Data collection sheet

A field data collection sheet is central to standardised site documentation. This sheet should include specific information concerning the geographic location and dominant physiognomic cover types. Room should be provided for field notes documenting any uncharacteristic features of the site (Figure 16-1). The field form should also include more general information such as time of visit, site number and number and direction of photographs. This information can then later be used to index the site by creating a point or polygon overlay onto the satellite image, provided it has been georeferenced. Direct field measurements may be combined to create indices related to a specific aspect of the forest. Complexity indices, such as the Holdridge Complexity Index (Holdridge 1988) are based on measures of tree height / diameter, stem density, and species richness to provide an objective measure of mature natural forest physiognomy. In other cases, remotely sensed data may be indirectly related to canopy properties such as biomass (Atkinson et al. 2000).

3.6 Helicopter data collection

A subset of field data collection may be accomplished using helicopters or fixed wing aircraft overflights designed to describe the essential land cover information. The flight path should be based on absolute travelling distance to make optimum use of helicopter time. Generally, three people are necessary in addition to the pilot. One person acts as flight-navigator and locator, linking ground observations to features on the field map. The second person calls the vegetation from the helicopter, while the third records the information of the vegetation caller. The flight path and number of sites to visit are based on the co-ordinates of the sites and the overall distribution of sites from previous flying days. The landscape provides key navigational information; in Alberta, for instance, seismic / cut lines and lakes are very helpful for navigating to a site, provided the helicopter is flying at an elevation at which they can be observed.

2001- Ft. Chip- Yr Project	Site Number	Obs. / / Crew N V. C. R	Obs. Level 1 2 3	AGCC CODE
1:50,000 Map Sheet		Obs. Date: / / Mo Day Year	Obs. Time: : Hr Min	
Digital Photo Session # Photo #		LAT (GPS) Decimal Degrees	LONG (GPS) Decimal Degrees	
		Drainage Class: Rapidly Well Imperfectly Poorly Innundated		
PHYSIOGNOMIC TYPE: (Circle Lichen where present)				
TREE	%Cov	Ht	HERBACEOUS	%Cov
Jack Pine			Forbs	
White Spruce			Horsetail	
Black Spruce			Fireweed	
Larch				
Balsam Fir				
Aspen				
Balsam Poplar				
Birch				
SHRUBS	%Cov	Ht	AQUATIC	%Cov
Rose			Emergent	
Raspberry			Cattail	
Chokecherry			Bulrush	
Hazelnut			Rush	
Dogwood			Arrowhead	
Saskatoon			Giant Bur-reed	
Blueberry			Reed Grass	
Kinnikinnick				
Silver Berry				
Willow				
Alder				
Bog Birch				
Labrador Tea				
Subtotal % Cover A			Subtotal % Cover B	Subtotal % Cover D
			Subtotal % Cover C	Grand Total % Cover A+B+C+D
			AGCC Polygon Code	FISH & WILDLIFE Polygon Code

Figure 16-1. Alberta Ground Cover Characterization field data collection sheet

3.7 Planning the flight path

There are numerous ways of organising the flight plan (Figure 16-2). The simplest method is to fly to the furthest point and then work back to the origin. However, it is recommended that the origin be near the airport, because in the event that the equipment does not work, or the site GPS locations are incorrect, or if some essential equipment has been forgotten, it is better to find this out as near to the airport as possible, while there is still time to turn back. By hiring a pilot who is familiar with the study and transit areas, one can learn a lot about the history of the area and any new developments that may have occurred after image acquisition. Sites and flight paths should be selected before going into the field; it is stressful as well as error-inducing to do this the night before, when the field team should be resting. The co-ordinates should be given to the pilot in advance, so they can be entered into the GPS without rushing the procedure. The pilots and field team members may make data entry mistakes so it is necessary to assure GPS data are properly input into the on-board GPS unit.

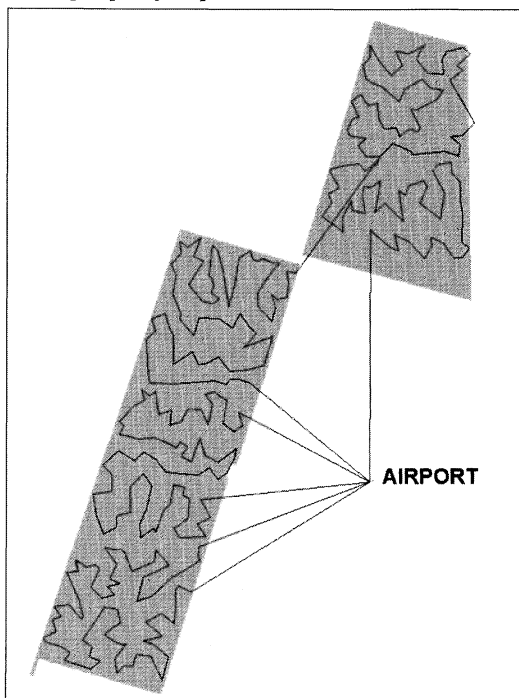


Figure 16-2. Example preliminary plan for a field work flight path, considering different options for route planning.

4. DATA FUSION

The success of any field campaign depends in great measure on the quality of the field maps. When locating and navigating to each site by either vehicle or helicopter, field maps and image composites may be crucial. These products can be printed at 1:50,000 and used to navigate to and from the field site. It is useful to print the satellite image, with accompanying vector data (i.e. roads, hydrological features) to increase the readability of the map. Unfortunately, multi-spectral imagery often lacks high spatial resolution. Even with the advent of high-resolution multi-spectral satellite sensors, the most cost-effective means of obtaining high detail using multi-spectral characteristics is data fusion. Data fusion usually integrates two data sources, a lower resolution multi-spectral and a higher resolution panchromatic image, to create an output image that combines multi-spectral information with high spatial detail. In most cases, a standard panchromatic band is of sufficiently high resolution to improve the level of detail visible in the multi-spectral image of interest. For example, Indian Remote Sensing (IRS-1C) panchromatic imagery (5.6m spatial resolution), or the 15m resolution panchromatic band of the Landsat Enhanced Thematic Mapper Plus imagery, can be merged with multi-spectral Landsat TM imagery, printed at 1:50,000 scale or better, and used for navigation. IRS-TM merged imagery can enhance linear features (i.e. roads and cutlines) that are not as easily visible on the Landsat TM imagery. Furthermore, variations in ground cover texture not apparent in the TM image, such as enhanced topographical information and smaller patches of forest can be observed in the IRS-TM merge. High resolution IKONOS (4m) imagery can also be fused with other data sources including Landsat TM to help identify changes in canopy texture. This technique can also be useful for finding individual trees in the field. Finally, if a thematic land cover map was available for the study area (a broad classification, life zone data, regional boundaries, etc.), data fusion techniques can merge these map themes with the intensities of the panchromatic image pixels. This product may help isolate areas of interest, much like using a GIS overlay but without using multiple files.

5. SITE CHARACTERISATION OF FOREST COVER

5.1 Leaf area index (LAI)

Fournier et al. (Chapter 4) provide an in-depth analysis of LAI and considerations that must be addressed when deciding how the measurements are to be taken. Depending on the scope and nature of the research question, as well as the geographic region where the research takes place, LAI can be an asset to the field data set, but the collection time, especially if different seasons are being studied, needs to be considered. It is also important to clarify whether a very detailed sampling strategy is desired, in which a particular forest class will be exhaustively covered (e.g. mature forest), or whether a broader regional estimation of many classes is desired. The expected variability of LAI within each measured forest / succession class should also be considered before determining how LAI is to be sampled. For example, a forest class exhibiting a high degree of spatial variability should be sampled more exhaustively than a uniform class. In addition, the nature of the successional stage of the forest ecosystem must be taken into consideration in the design of the sampling scheme. This is particularly important in tropical environments. Also, in seasonally changing ecosystems, the variability in LAI must be assessed for each season, in order to provide a proper measurement of the change in LAI. If all the research is to be conducted in only one season, this assessment is unnecessary. Table 16-1 present a series of practical field suggestions to take into consideration when LAI is measured.

For some tree species in the tropics, including Mahogany (*Swietenia macrophylla*), destructive sampling methods for calculating LAI or calibrating indirect measurement are not possible, as these trees are too valuable. Moreover, in areas of high species richness, the sheer number of trees per plot that need to be sampled creates logistical problems. For example, in some study areas in the tropics it is not uncommon to have upwards of 50-100 tree species in a single one-hectare plot. Another approach to direct sampling is to use one of a large variety of point contact methods. For instance, a pole can be raised through the canopy and the number of leaves it touches, through various intervals, are counted or a weight (plumb bob) is lowered through the canopy and each leaf it contacts is counted. While these procedures are useful sampling techniques in young plantations or for seedlings, they are less applicable in some tropical areas, particularly in multi-layer (multistratal) canopies and those extending twenty or thirty meters above ground.

Table 16-1. Practical Considerations for measuring LAI when using the LAI 2000 Plant Canopy Analyser.

Variable	Consideration
Direct sun	This should be avoided if possible. In cases where measurements must be made on a sunny day, both inside and outside (of canopy) measurements should be made with the sun behind the operator. Whenever possible try to keep the sensor in the shade.
Distance inside plot	In order for inside readings not to be influenced by the surrounding area, they should be at a minimum distance of three times the average canopy height inside the forest.
Slopes	The sensor should be parallel with the slope instead of being level. The outside measurements should be taken with the same inclination as the inside readings. Orient the sensor along the slope so it is facing neither up nor down the slope.
Gaps	In areas with significant gaps, measurements should be taken in such a way that the sensor "sees" only vegetation cover or only the gaps, but not with vegetation on one side of the sensor and a gap on the other.
Problems with the data	The outside measurements should be checked often for inconsistencies that will lead to problems when the data is being processed.

In every field campaign, the goal of the LAI sampling must be considered and in many cases, new methods that are specific to the current needs and limitations may be developed. The most important consideration, however, is to examine the environment and develop a sampling strategy that is appropriate for the environment. Not all methods perform equally well in all environments, and great care must be taken in selecting the approach that is most appropriate for both the goals of the project and the limitations posed by the environment. Therefore, many LAI sampling schemes developed for boreal and temperate environments may not work in tropical regions, where ecosystem complexity is higher at both the vertical and horizontal structure level.

5.2 Hemispherical photography

Each field plot can be sampled using hemispherical photography as a permanent record of canopy conditions (see Fournier et al., Chapter 4). It is well worth the time and effort to set up each shot carefully in the field. For print cameras, high-speed black and white film (e.g. Kodak Tri-X or Ilford HP5, both ASA 400) can provide the best contrast between foliage and non-foliage, although colour slides may also provide sufficient contrast (see Hall, Chapter 3). New digital cameras have provided promising results, and can be less expensive as there are no negatives to develop. Regardless of the camera

choice, the best photographs are obtained under even lighting conditions, with overcast skies or early in the morning or late afternoon. Other necessary equipment includes a compass, a tripod and a small level. All photographs must be taken at a predetermined height from the ground with the lens completely level. In addition, the photographs must be oriented in a certain cardinal direction so that when the images are processed, they can be properly registered. A common practice is to have the camera line up with true north so that the top of every photograph is facing that direction. If more than one camera is used each camera must be levelled separately for every photograph. It has been suggested that using a red filter will increase the contrast between the foliage and non-foliage elements, but our experience in tropical environments indicates that good results can be obtained without a filter. The participation of an experienced photographer is useful to determine the appropriate aperture, exposure, and shutter speed combinations. If possible, the camera should be placed on a self-timer or on a remote. This will decrease the chance of the lens being moved during the exposure or having the photographer appearing in the picture. However, with sufficient care it is possible to take the photographs manually.

If multiple transects or plots are to be sampled, it is recommended that a separate roll of film be used for each plot to avoid subsequent confusion since hemispherical photographs all look very similar. In addition, the first photograph on each role should be of an index card with the plot number, date, time and other useful information clearly marked. Even permanent markers can rub off of the film rolls and processing labs can make errors when they record the number after processing. The photo of the index card will ensure that plots are not mixed up, thus ensuring accurate cataloguing and sorting of the photos.

During the processing stage, if the photographs are in colour, most processing software products, such as Gap Light Analyzer (GLA) allow the photograph to be viewed in a single colour plane (red, green or blue) (Frazer et al. 1997). Under certain circumstances, the results when the photo is thresholded into foliage and non-foliage pixels will be different when the different colour planes are used, so the calculations of LAI will also be slightly different. Whether this difference is significant or not for the results should be considered when deciding between black and white or colour photographs. A final variable to consider is the projection of the lens that is used. Most lenses fall into four main categories of projections: polar or equiangular, equidistant, orthographic and equisolidangle, with the polar projection being the most common. Valuable results can be obtained with each type of projection, but the cost of the lenses will vary greatly. It is advisable to obtain the calibration data for the lens directly from the

manufacturer because in the processing stage there is usually the option to enter the exact calibration values for the lens.

5.3 Integrating GPS with site characterisation

GPS is used to record the co-ordinates for a given training / calibration area in the field and to support site documentation. If used in conjunction with field maps with a printed graticule, GPS units can aid in navigating to a site. GPS can also be used to determine elevation above sea level in topographically complex areas, however its precision in many situations may be questionable. To optimise the use of GPS when visiting a particular site, an area should be documented according to the physiognomic cover types and stand characteristics. At each site, it is beneficial to photograph and describe the land cover in four cardinal directions. If GPS points are taken but poorly described, these sites may prove difficult to locate post-field work, as in areas of heterogeneous land cover it may not be easy to determine to exactly what type of land cover a given point refers. GPS points are also useful for checking the rectification accuracy of a geo-referenced image. For example, if an IKONOS image has been rectified to a coarser resolution image, GPS points taken in the field can be used post-fieldwork to supplement and improve the georectification accuracy of the image.

Several new software systems have become available that integrate GPS and cartographic software into electronic notebooks and PDAs. Good cartographic and navigation software can improve field efficiency far more than a few extra meters of precision, especially when the precision of most GPS systems is sub-pixel in the majority of imagery used for land cover studies (e.g. Landsat TM). On the other hand, GPS units are built for fieldwork and continuous exposure to field conditions, whereas most notebooks and PDAs are not. Furthermore, from a logistical point of view it can be a nuisance to carry along several electronic devices to each study site and expensive to equip more than one field team.

6. DATA COMPILATION

Once collected, field data need to be quality controlled and assessed for ambiguities. At this stage, if multiple field teams are involved, documented feedback is invaluable. By receiving feedback from all the data gatherers regarding any problems or difficulties that arose during the fieldwork, one can pre-determine if certain areas will be more difficult to classify or where quality information is lacking beforehand. Once captured and compiled, this

field metadata can then be used to classify and validate the image classification process.

7. CONCLUSION

There are no substitutes for good quality field data. Based on experiences in two land use and land cover image classification projects in tropical forests in Costa Rica and boreal forests in Canada, suggestions for field and helicopter data protocols have emerged that can help to ensure successful remote sensing projects. These include issues associated with developing a field plan, characterising sites, collecting actual data (e.g. LAI), and using data fusion mapping / navigation aids. Image analysts should be involved in the field work and should take image products into the field according to a sampling design that will enable maximum efficiency to be achieved with the resources available.

REFERENCES

- Atkinson, P. M., Foody, G. M., Curran, P. J., & Boyd, D. S. (2000). Assessing the ground data requirements for regional scale remote sensing of tropical forest biophysical properties. *International Journal of Remote Sensing*, 21, 2571-2587.
- Congalton, R. G. (1991). A review of assessing the accuracy of classifications of remotely sensed data. *Remote Sensing of Environment*, 37, 35-46.
- Frazer, G., Trofymow, J., & Lertzman, K. (1997). A method of estimating canopy openness, effective leaf area index, and photosynthetically active photon flux density using hemispherical photography and computerized image analysis techniques. *Information report BC-X-373*. Pacific Forestry Centre, Canadian Forest Service, Natural Resources Canada.
- Holdridge, L. (1988). *Life Zone Ecology*. Tropical Science Center, San Jose.

Chapter 17

ESTIMATION OF FOLIAR CHEMISTRY OF WESTERN HEMLOCK USING HYPERSPECTRAL DATA

K. Olaf Niemann¹ and David. G. Goodenough²

¹ *Department of Geography, University of Victoria, Victoria, British Columbia, V8W 3P5, Canada*

² *Canadian Forest Service (Pacific Forestry Centre), Natural Resources Canada, Victoria, British Columbia, V8Z 1M5, Canada*

1. INTRODUCTION

The remote detection of environmentally induced stresses that manifest themselves in tree foliage is gaining in importance. These stresses can be the consequence of an invasion of insects or onset of disease, change in growth limiting factors such as temperature and/or moisture, or a decline in the availability of nutrients. These stresses may result in a full range of changes to the plant physiological processes from relatively subtle responses such as a decrease in the chlorophyll content and increasing chlorosis to very dramatic changes such as shedding of foliage (Dickson and Isebrands 1991).

The remote sensing of foliar stress is dependent on the detection of variations in the reflection of energy caused by changes in the biochemical composition of the foliage. While the physical manifestations of the state of the foliage may not be visible, other proxy indicators may be evident. One of the proxy indicators of environmental variability has been found to be the chemical composition of foliage. The more obvious chemical constituents are the pigments (chlorophyll a, chlorophyll b, and carotenoids) and nutrients (such as nitrogen), and carbon. The nutrients are controlled by plant physiological processes, some of which are susceptible to environmental stress such as those caused by moisture deficiencies, or excess salts. Nitrogen deficiencies can lead to chlorosis of older foliage, or in extreme

cases defoliation (Taiz and Zeiger 1991). In some cases the soil chemistry, with respect to heavy and trace metals, can also lead to stress in plants (Jackson et al. 1990). This relationship between soil chemistry and the status and health of trees is species dependent. For example, (Kayahara and Pearson 1996) suggested that although there is an inconsistent relationship between site index and soil chemistry there is a strong link between the nutrient levels found in soils and the composition of the foliage in Western Hemlock.

Previous work relating to the remote sensing of foliar biochemistry has fallen into two categories: the assessment of reflectance first at the leaf and second at canopy scales. The work carried out at the leaf scale involves the use of foliage harvested and assessed through the use of either laboratory or field spectrometers (Yoder and Pettigrew-Crosby 1995; Hurcom et al. 1996; Johnson and Billow 1996). Alternatively, spectrometer measurements taken from aircraft or satellites are used to assess the characteristics at the canopy scales (Aber et al. 1994; Bolster et al. 1996; Datt 1998; Johnson et al. 1994; Pinzon et al. 1998; Yoder and Pettigrew-Crosby 1995). While the field and laboratory based studies are valuable in assessing the theoretical relationships between reflectance and leaf biochemistry, they avoid the remote sensing problems associated with first the introduction of non canopy reflective elements such as understorey and soil, and second the effects of the atmospheric column.

A comprehensive summary of the theoretical chemical absorption regions of the electromagnetic spectrum was presented by Curran (1989). This summary is presented in Table 17-1. As is evident from this table a number of wavelengths are influenced by foliar chemicals. Studies following this publication have attempted to extract similar results at the leaf and canopy levels. These studies have yielded results that often are similar although not exactly as predicted by Curran (1989). These differences can often be attributed to the bonding of chemical elements within the leaf, or possibly to other confounding influences such as water content or scattering due to the cell wall (Grossman et al. 1996). It was noted by Blackburn (1998) that problems relating spectral reflectance of pigment concentrations are caused by the fact that different pigments absorb energy in the same spectral regions causing confusion. It was cautioned by Grossman et al. (1996) that the use of predicted ("standard") wavelengths in the assessment of foliar chemical analyses is not always possible. The strict reliance on published work for optimal spectral windows to assess the foliar constituents may therefore not be the best approach (Blackburn 1998).

Table 17-1. Relationship between foliar biochemistry and wavelength (Reprinted from Remote Sensing of Environment, Vol 30, P.J. Curran, "Remote sensing of foliar chemistry", pages 270-278, Copyright (1989), with permission from Elsevier Science)

Wavelength (μm)	Electron transition or bond vibration	Chemical(s)	Remote sensing considerations
0.43	Electron transition	Chlorophyll a*	
0.46	Electron transition	Chlorophyll b	
0.64	Electron transition	Chlorophyll b	
0.66	Electron transition	Chlorophyll a	
0.91	C-H stretch, 3 rd overtone	Protein	
0.93	C-H stretch, 3 rd overtone	Oil	
0.97	O-H bend, 1 st overtone	Water, Starch	
0.99	O-H stretch, 2 nd overtone	Starch	
1.02	N-H stretch	Protein	
1.04	C-H stretch, C-H deformation	Oil	
1.12	C-H stretch, 2 nd overtone	Lignin	
1.20	O-H bend, 1 st overtone	Water, Cellulose,	
	O-H bend, 1 st overtone	Starch, Lignin	
1.40	C-H stretch, C-H deformation	Water	
1.42	C-H stretch, C-H deformation	Lignin	
1.45	O-H stretch, 1 st overtone, C- H stretch, C-H deformation	Starch, Sugar, Lignin, Water	Atmospheric absorption
1.49	O-H stretch, 1 st overtone	Cellulose, Sugar	
1.51	N-H stretch, 1 st overtone	Protein, Nitrogen	
1.53	O-H stretch, 1 st overtone	Starch	
1.54	O-H stretch, 1 st overtone	Starch, Cellulose	
1.58	O-H stretch, 1 st overtone	Starch, Sugar	
1.69	C-H stretch, 1 st overtone	Lignin, Starch, Protein, Nitrogen	
1.78	C-H stretch, 1 st overtone, O- H stretch, H-O-H deformation	Cellulose, Sugar, Starch	
1.82	O-H stretch, C-O stretch, 2 nd overtone	Cellulose	
1.90	O-H stretch, C-O stretch	Starch	
1.94	O-H stretch, O-H deformation	Water, Lignin, Protein, Nitrogen, Starch, Cellulose	
1.96	O-H stretch, O-H bend	Sugar, Starch	Atmospheric absorption
1.98	N-H asymmetry	Protein	
2.00	O-H deformation, C-O deformation	Starch	
2.06	N-H bend, 2 nd overtone, N-H bend, N-H stretch	Protein, Nitrogen	

Wavelength (μm)	Electron transition or bond vibration	Chemical(s)	Remote sensing considerations
2.08	O-H stretch, O-H deformation	Sugar, Starch	
2.10	O-H bend, C-O stretch, C-O- C stretch, 3 rd overtone	Starch , Cellulose	
2.13	N-H stretch	Protein	
2.18	N-H bend, 2 nd overtone, C-H stretch, C-O stretch, C-N stretch	Protein, Nitrogen	
2.24	C-H stretch	Protein	
2.25	O-H stretch, O-H deformation	Starch	Rapid decrease in signal-to-noise ratio of sensors
2.27	C-H stretch, O-H stretch, CH ₂ bend, CH ₂ stretch	Cellulose, Sugar, Starch	
2.28	C-H stretch, CH ₂ deformation	Starch, Cellulose	
2.30	N-H stretch, C-O stretch, C- H bend, 2 nd overtone	Protein, Nitrogen	
2.31	C-H bend, 2 nd overtone	Oil	
2.32	C-H stretch, CH ₂ deformation	Starch	
2.34	C-H stretch, O-H deformation, C-H deformation, O-H stretch	Cellulose	
2.35	CH ₄ bend, 2 nd overtone, C-H deformation, 2 nd overtone	Cellulose, Protein, Nitrogen	

*chemicals in **bold type** have a wavelength of stronger absorption.

Given the obvious controversy associated with the remote sensing of canopy biochemical properties, a study was conceived using airborne hyperspectral imagery in a NASA supported project employing NASA's Jet Propulsion Laboratory's (JPL) Airborne Visible and Infrared Imaging Spectrometer (AVIRIS) sensor. The project goals were to assess whether there was sufficient signal in the remotely sensed data to detect site induced variations in the foliar biochemistry and secondly, if there was a biochemical signal, whether the theoretical absorption bands, were consistent with the results of the airborne – based study.

2. STUDY SITE AND DATA COLLECTION

The area chosen for this project encompassed a portion of Flores Island, off Vancouver Island's west coast (see Figure 17-1). The study area was chosen because it was undisturbed, and represented a wide range in

ecophysiological variables. The study area can be divided into three basic physiographic units. The first is an upland area with generally steep, well-drained slopes. These slopes are prone to fluvial incision and some naturally occurring slope instability. The dominant forest vegetation on these slopes is Western hemlock (*Tsuga heterophylla*) and Yellow cedar (*Chamaecyparis nootkatensis*). The second physiographic unit is composed of a poorly drained wetland, and located between the upland and the coastal zone. It has a number of small channels dissecting it that are confined within small levees. The predominant forest vegetation in this area includes Western red cedar (*Thuga plicata*) in the poorly drained areas and Western hemlock along the levees. The third physiographic unit is composed of well-drained coastal dunes. These dunes are covered with Western Hemlock.

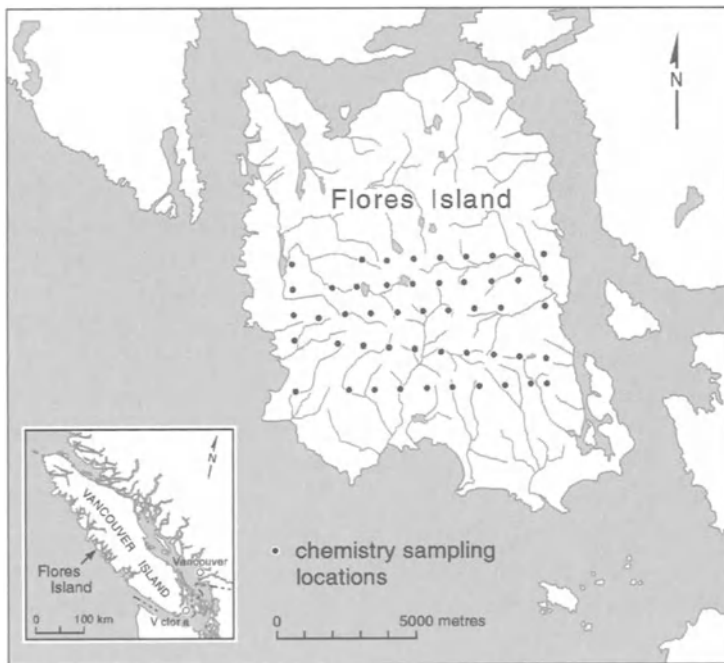


Figure 17-1. Location of study site and foliar sampling site distribution.

Samples of foliage were restricted to Western hemlock as cedar trees were inaccessible. Foliage samples were acquired through the use of a helicopter and removing a sample from the crown of trees at each site. A total of fifty (50) sites were sampled and analyzed (see Figure 17-1). These samples were placed on ice and immediately transported to the analytical facilities, where the needles were removed from the stems and both were analyzed for biochemical composition. The elements that were extracted

included chlorophyll a and b, carbon, nitrogen, and carotenoids as well a full suite of inorganic constituents. Only the results of the needle analysis will be discussed in this Chapter.

3. DATA PREPROCESSING

Imaging spectrometer data were acquired for the SEIDAM project (Goodenough et al. 1996) using AVIRIS mounted in an ER-2 aircraft. The data were acquired at an altitude of approximately 20 km and the processing of the AVIRIS data occurred in three phases. First the data were radiometrically, spectrally, and geometrically corrected for sensor effects (Chrien et al. 1990) at JPL. Second, AVIRIS radiance values were converted to reflectance by the removal of atmospheric effects using MODTRAN-II atmospheric correction software. MODTRAN-II accepts as inputs surface radiance measurements, atmospheric optical depth (radiosonde) data, and field calibration data in the form of measurements taken with a field spectrometer. For this study the MODTRAN-II model was calibrated to a single ground target measurement for which spectral measurements had been taken. The differences between the atmospherically corrected (post-MODTRAN) AVIRIS data and the ground measurements were used to create a forced-fit function which served to fine tune the imagery for residual atmospheric effects (Goodenough et al. 1996).

The third and final step in the AVIRIS processing was the linking of the imagery to absolute positional coordinates. This was accomplished through the use of a digital orthophoto mosaic with a pixel resolution of 1 metres. This orthophotomosaic was created from scanned 1:20,000 scale aerial photographs. Ground control points for geometric correction were collected from a geocoded digital orthophotomosaic. The AVIRIS image was tied to the orthophoto mosaic using a 2nd order polynomial and resampled using a nearest neighbour algorithm.

4. SPECTRAL MIXTURE ANALYSIS

The successful extraction of foliar chemistry from remotely sensed data assumes that we have the ability to assess crown reflectance without the influence of other reflective scene elements, including shadow, understorey and soils. As we are concerned with only the upper canopy chemistry, it is important that we separate the various reflective components. The process selected for this project known as spectral mixture analysis (SMA), has

received considerable attention in the literature (Adams and Smith 1986; Smith et al. 1990; Metternicht and Fermont 1998; Milton 1999; Asner and Lobell 2000; Gao et al. 1993; Peddle and Johnson 2000).

The technique of SMA as it is generally applied assumes a linear regression model to separate the reflective components, termed endmembers. The technique relies on the analyst to identify the spectra of "pure" reflectors. These spectra are subsequently used within a multiple linear regression analysis to estimate the contribution of each reflector for each pixel. The model is as follows:

$$DN_b = \sum_{i=1}^n F_i DN_{i,b} + E_b \text{ and } \sum_{i=1}^n F_i = 1 \quad (1)$$

where DN_b is the data number for a pixel; F_i is the fraction of the endmember i ; DN_b is the relative reflectance for each endmember of band b ; and E_b is the error associated with each endmember. If the above equation is constrained, the sum of the F_i will equal unity. The result of applying this analysis is a series of images, one for each endmember.

Much of the previous work in SMA has been carried out in regions where the reflective differences between the green vegetation, soil background, and shadow are unique and easily separable. In our situation, in the Pacific Northwest, we must employ a more complex strategy in that the background reflectance is commonly not soil, but rather other green vegetation, such as ferns or salal. This renders the process of separating out these various reflective components much more problematic.

Normally, to define each of the endmembers, reference spectra defining each of the reflective components are acquired. Where possible this involves the collection of spectra in the field from each of the identified reflective elements. In many cases, however, this may not be the best approach as it assumes that there is a linear relationship between a small sample collected in the field and that measured from an aircraft or satellite platform. The alternative is to find "pure" reflectors from the imagery from which representative spectra can be extracted for each of the endmembers. In situations where pixels cover moderate resolutions (for example 20 x 20 metres or greater), the opportunities to define pure reflectors are few. Rather, pixels tend to be composed of a number of reflectors (hence, the need for the spectral unmixing in the first place).

To address this problem we needed to develop a methodology to separate the crown from understorey reflectance. A method that identified areas that had complete crown coverage as well as those areas where no crown was evident was necessary. To attain this goal we needed to adopt a methodology

to identify these areas. The method that was chosen used the Local Maximum concept as outlined by a number of workers (see for example Larsen (1997), Niemann et al. (1998), Wulder et al. (2000)).

The main assumption adopted in the Local Maximum approach is that the reflectance off a tree crown (in this case the work is restricted to conifers) is greatest at its apex, also assuming that imagery is collected when the solar elevation is highest. The reflectance then decreases towards the sides of the crown. This is illustrated in Figure 17-2 where a 50 by 50 pixel window from an orthophoto (1 metre resolution) is plotted. The Z value in this case is not the height of the tree but rather the grey tone extracted from the orthophoto. It is clear from this that the individual trees can be identified from this plot.

To map the individual crowns a relatively simple search mechanism was developed (Niemann et al. 1998) to locate the highest reflectance value within a roving matrix. The search algorithm checks the central pixel value with respect to the enclosing pixel values. Once one such value has been located then its location is recorded. The individual points can then be exported as X-Y coordinates and imported into other applications.

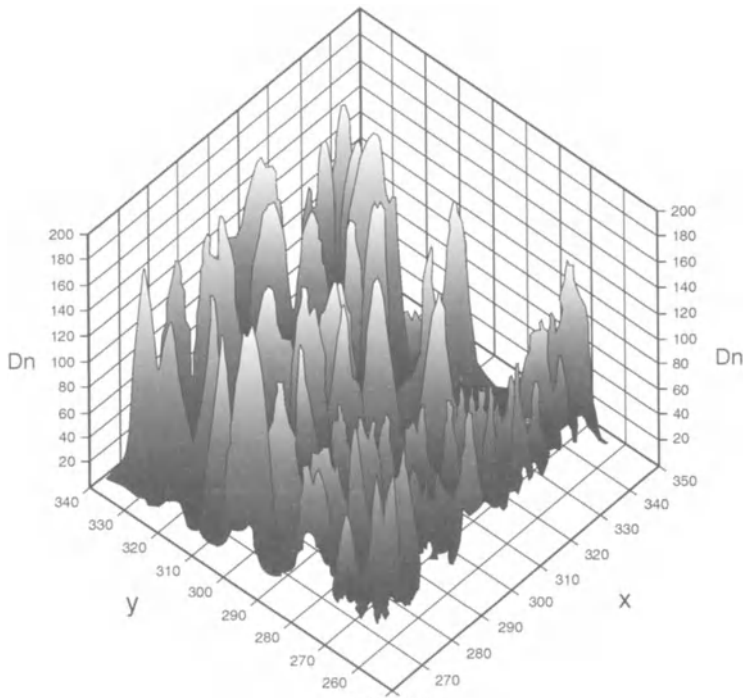


Figure 17-2. Forest stand representation from black and white aerial photograph.

In many instances it has been found that the logic used to detect the individual tree crowns occurs as a random distribution over ground cover that is not composed of tree crowns. These sites would normally be identified as being treetops using the local maximum rules. They can, for the most part, however, be eliminated due to the range in values surrounding the local maximum. In the case of tree crowns the range of values within the 3 by 3 window has been found to be considerably greater than that found in areas where the patterns occurs due to a random distribution. A user specified range of values has therefore been implemented which allows for the filtering of those sites where the range is less than that specified.

For the current project a 1-metre orthophotomosaic was used as the source image for the tree mapping exercise. The individual tree locations were extracted and subsequently summarized on a stems per hectare basis within a 20 metre pixel, corresponding to the AVIRIS pixel size, and coregistered with the AVIRIS imagery.

Spectra corresponding to a wide range of stand densities were extracted from the AVIRIS data. A plot of a few of these is presented in Figure 17-3. One point becomes strikingly clear when viewing Figure 17-3: there is a positive correlation between stem density and reflectance. This is especially noticeable in the near and mid infrared range (700 to 1400 nm). In the visible portion of the spectrum (400 to 700nm) this relationship is not as apparent.

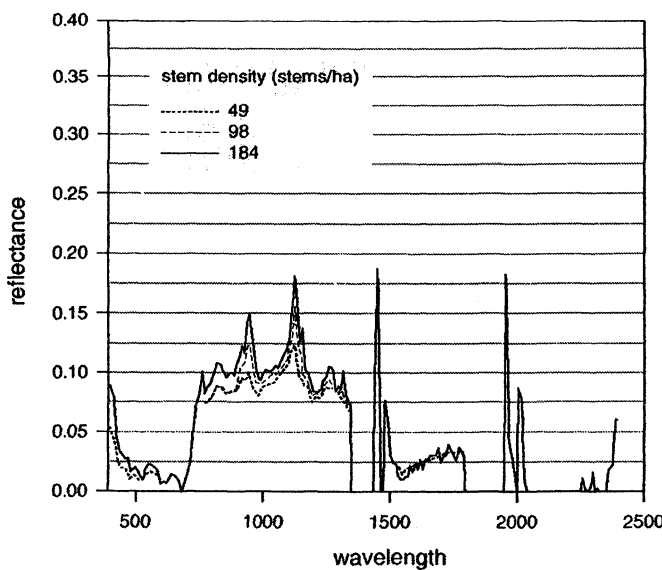


Figure 17-3. Stem density vs. reflectance for Western Hemlock.

Figure 17-4 illustrates the reflectance vs. stem densities for 900 nm. From this it is clear that there are two groupings of points: one representing samples from stem densities greater than 180 stems/ha, and a second for densities lower than 180 stems/ha. The grouping for the higher stem densities is characterized by a relatively small variance in reflectance and a flat slope. The other grouping has a greater variance and a steep slope. The first group of points is therefore interpreted as closed canopy where the reflectance is influenced by crown foliage and shadows. The second grouping is open canopy where differing degrees of canopy, understorey reflectance, as well as shadow contribute to the pixel reflectance.

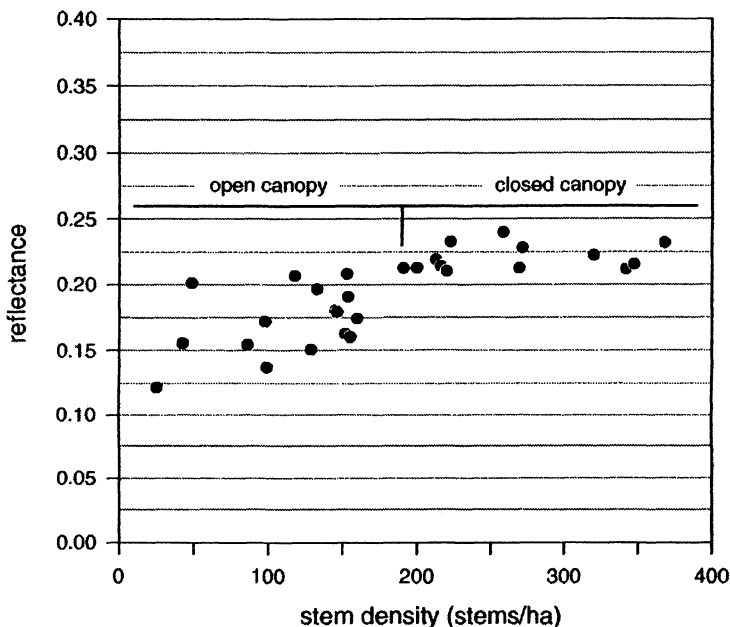


Figure 17-4. Stem density vs. reflectance at 900 nm.

The goal of defining these two groups was to develop a technique to extract an endmember representing the canopy contribution to the reflectance registered by each pixel. To achieve this two endmembers were required: the canopy and understorey. Reflectance values corresponding to closed canopy were defined by averaging the reflectance values for those points with stem densities greater than 180 stems/ha. For undergrowth reflectance a best-fit line was derived. The value for the y-intercept, that is 0 stems / ha, was determined. This analysis was performed on all of the 224 AVIRIS channels. The resultant spectral curves are presented in Figure 17-5. These two spectra were subsequently used to define the required

endmembers. The endmember corresponding to the overstorey was coregistered with the AVIRIS image and foliar sample site locations, and spectra and overstorey proportions were extracted for each of the canopy sample sites.

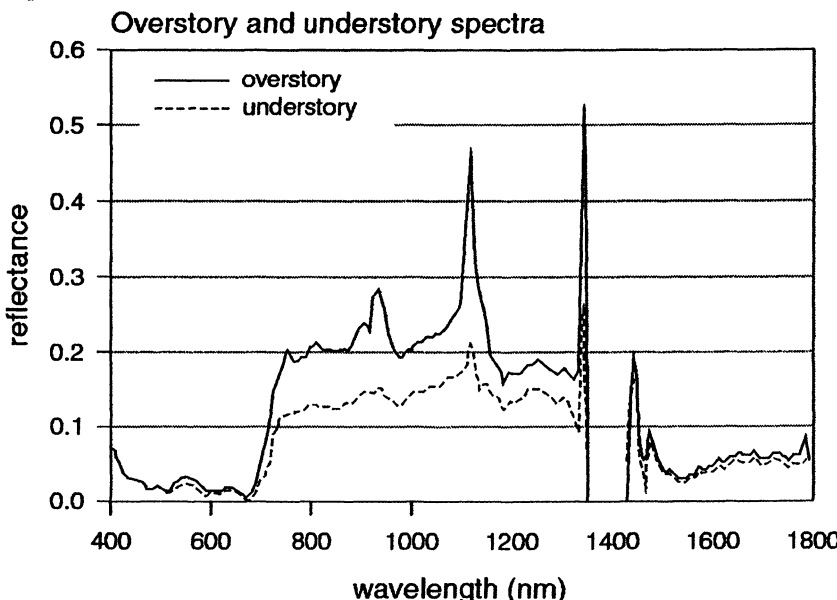


Figure 17-5. Derived overstorey and understory spectra for western hemlock.

5. RESULTS AND DISCUSSION

One of the objectives of the study was to assess whether it was possible to remotely detect variations in foliar nutrient levels directly or whether a proxy, such as through association with the pigments was necessary. It is commonly accepted that variations in levels of chlorophyll are most commonly detected through the use of remotely sensed imagery. This association between reflectance and quantities of chlorophyll is strong, especially in the visible portions of the spectrum. As a result it was necessary to first identify any associations existing between the nutrients and pigments. The result of these analyses is summarized in Table 17-2.

From Table 17-2 it is evident that there is a strong association between nitrogen and chlorophyll a ($R^2 = 0.71$). Only weak associations are evident between carbon and the pigments. It is clear that only nitrogen can be assessed through a proxy while carbon must be detected directly, if it is to be detected at all. The next assessment was to investigate the relationship between reflectance and the pigments (chlorophyll a and b and carotenoids).

The relationships between reflectance and the pigments were assessed through a correlation analyses. The results of this are presented in Figure 17-6 as a correlogram. The correlogram for carotenoids (Figure 17-6a) indicates a general inverse relationship with reflectance in the visible and near infrared peaking at $R = -0.40$ in the 750 to 875 nm window. At longer wavelengths there is very little relationship between reflectance and amount of canopy carotenoids. At wavelengths longer than 2200nm there appear to be larger correlations peaking at $R = 0.80$ at 2400nm. The pattern for chlorophyll a (Figure 17-6b) is also one of an inverse relationship in the visible and near infrared to 1400nm. The peak correlation coefficient is -0.55 at 700 nm. Again a positive correlation is observed at 2400 nm with $R = 0.74$. A similar pattern is observed for chlorophyll b (Figure 17-6c) although the correlation coefficients are somewhat larger in the visible and near infrared. Evident from these analyses is that a simple relationship between reflectance and pigment is not present in this data set for Flores Island.

Table 17-2. Summary of analyses investigating the relationship between the pigments.

	Ch A	Ch B	Carotenoids	% Carbon	% Nitrogen
Ch A	1.0	0.906**	0.3783**	0.3051*	0.7095**
Ch B		1.0	0.1797	0.3789**	0.5857**
Carotenoids			1.0	0.0192	0.3477*
% Carbon				1.0	0.3788*
% Nitrogen					1.0

**significant to 0.01, * significant to 0.05

A simple regression between reflectance and pigment and second a multiple regression incorporating the canopy endmember was performed. The results are illustrated in Figure 17-7. Figure 17-7a indicates the results of the analyses performed on carotenoids. What is immediately obvious is the increase in R^2 associated with the inclusion of the canopy endmember value representing crown closure. A well-defined peak in the near infrared at 0.7 is evident. Lower peaks in the visible (550 to 600nm) with R^2 values exceeding 0.50, 1100nm with R^2 of 0.50, and at 1450nm with R^2 of 0.60 are also evident. A final peak at 2500nm with R^2 of 0.70 is also evident, although there are little differences at this wavelength between the two regressions.

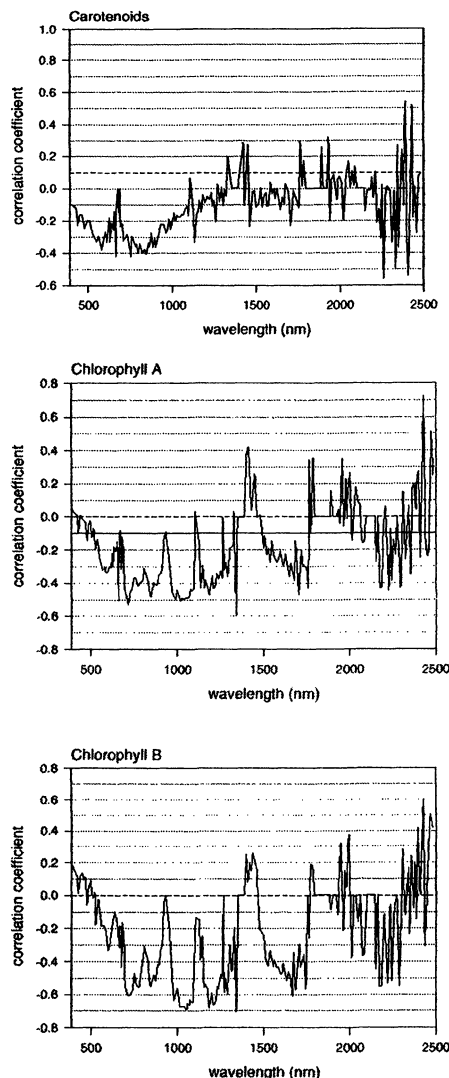


Figure 17-6. Correlograms for a) Carotenoids, b) Chlorophyll A and c) Chlorophyll B.

Figure 17-7b illustrates the results of the regression analyses with chlorophyll a. Again the inclusion of the crown endmember increases the R^2 substantially throughout the entire AVIRIS range. The peak in spectral reflectance is at approximately 1200 nm ($R^2=0.42$) and 1900 nm ($R^2= 0.50$). In both of these instances the inclusion of the crown endmember has lead to a substantial increase in descriptive potential. A high R^2 peak is located at

2450 nm ($R^2=0.55$) although the additional effect of including the crown endmember at this point is minimal.

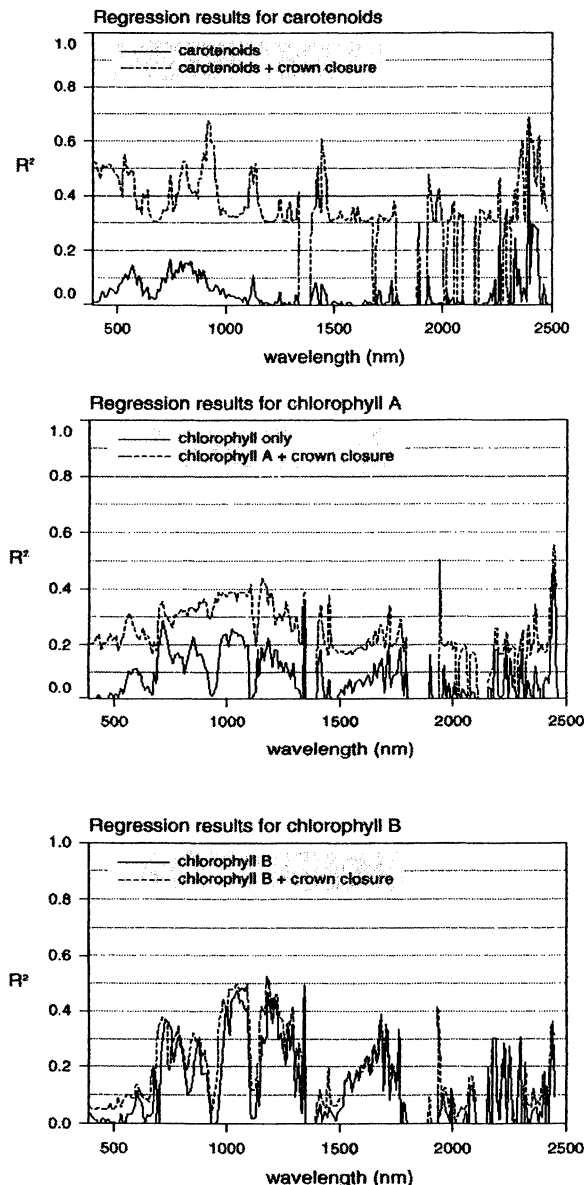


Figure 17-7. Regression results for a) Carotenoids, b) Chlorophyll A and c) Chlorophyll B.

The analyses of chlorophyll b indicate a different pattern than in the other analyses. In this case there is little improvement through the inclusion of the

crown endmember (Figure 17-7c). A maximum peak at 1200 nm ($R^2 = 0.52$) and a slightly smaller peak ($R^2 = 0.50$) occur between 1025 nm and 1100 nm.

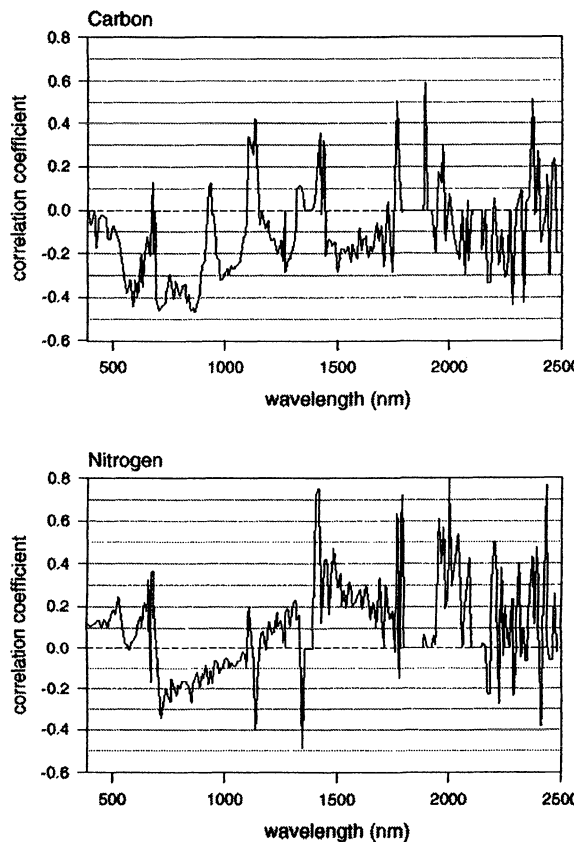


Figure 17-8. Correlogram for a) Carbon and b) Nitrogen.

It is clear from the plots presented above that the relationship between reflectance and chlorophyll a and b is weak for this data set. Any discussion of proxy measures is therefore limited. The alternative is to assess the relationship between nitrogen and carbon directly. The results of the correlation analyses for carbon are presented in Figure 17-8a. The patterns evident in this figure follow the patterns associated with chlorophyll a and b; the differences are mainly in the magnitude of the correlation coefficients. The correlogram for nitrogen and reflectance (Figure 17-8b) displays a somewhat different pattern with initial positive relationships in the visible portion of the spectrum to 700 nm. This is followed by a very marked change from positive to negative relationship at 700 nm. The R values are

quite low (maximum 0.40) indicating a relatively low correspondence between reflectance and nitrogen. At 1400 nm, however, there is a very strong positive spike ($r=0.75$). This spike is relatively narrow with a rapid decrease in subsequent wavelengths. Similar spikes were found between 1800 nm and 2450 nm.

Figures 17-9a and b illustrate the results of the simple and multiple regression analyses for carbon and nitrogen. The carbon plots indicate that a generally low degree of explanation of reflectance by either nutrient levels alone or in conjunction with the canopy endmember, with the maximum R^2 value is 0.40 at 1935 nm. The nitrogen plot however yields higher R^2 values especially in the mid infrared peaking at 0.70, with other minor peaks occurring at higher wavelengths.

Table 17-3 summarizes the results obtained by other studies of the remote sensing of canopy chemistry. The results of this study are also listed in Table 17-3. As can be seen the results of this study are not identical to other studies but the wavelengths of the peaks obtained in many cases are close. Those associations have been highlighted in Table 17-3 where the results of other studies match or are in close proximity to peaks obtained in this study. It is clear from the summary of the chlorophyll data that there is less correspondence between the results of this survey and the results of studies previously published. This can also be said of the individual studies previously published. Only at two wavelengths (707 nm for chlorophyll a and 1100 nm for chlorophyll b) are there any correspondences between the results obtained in this study and those obtained by others. There is no correspondence with the theoretical wavelengths as specified by Curran (1989).

Table 17-3, summarizing the nitrogen results, reveals a much closer correspondence with the results of the literature. Many of the wavelengths found by others to have high correlation with nitrogen were also found to have high R^2 values in this study. In addition, several of the wavelengths identified by Curran (1989) as being influenced by nitrogen, were also identified in this study.

Work reported in the literature on the remote sensing of carotenoids is sparse. Blackburn (1998) reported that 470 nm was the wavelength associated with carotenoids. Datt (1998) suggested that carotenoids could be retrieved through the following ratio:

$$R_{860} / (R_{550} * R_{708}) \quad (2)$$

where $R_{860, 550, 708}$ is the reflectance at 860, 550 and 708 nm respectively.

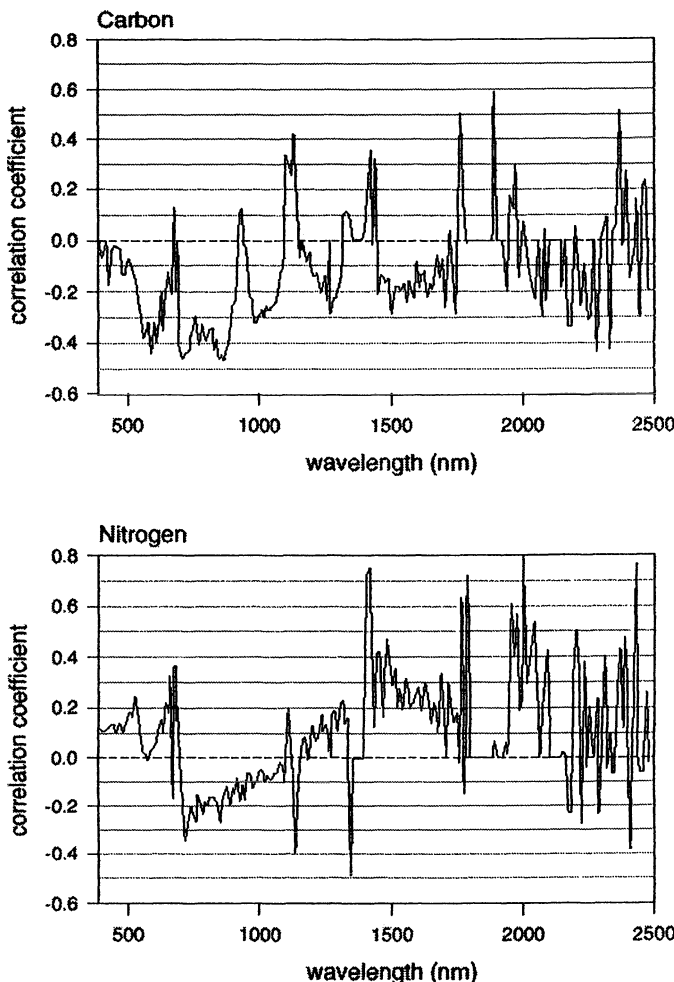


Figure 17-9. Regression results for a) Carbon and b) Nitrogen.

The results of this study (Table 17-3) indicate that correspondence between this study and previous studies for carotenoids is low. The high coefficients of determination (R^2) for at wavelengths centered at 925 nm and 1450 nm are encouraging, even though they do not correspond to results reported in the literature. These results suggest that further sampling and assessment is warranted. Signals from carbon resulted in a single correlation with work carried out by (Pinzon et al. 1998), who found that moderate correlation between reflectance and carbon at 700 ($R^2 = 0.48$ to 0.51) and 1920 nm. ($R^2 = 0.69$ to 0.71). In this study a peak in R^2 values (0.40) was

found at 1935 nm. This was not considered to be sufficient to warrant further investigation.

Table 17-3. Summary of the correspondence between foliar biochemistry and reflectance.

1*	2	3	4	5	6	7	8	This study
Carotenoids								
				470				
						550	541	
						708		
						860	814	
							925	
Chlorophyll								
						430(a)		
						460(b)		
						640(b)		
						660(a)		
	552	524					572(a)	
		620			652			
					665			
			690				707(a)	
	752	750					718(b)	
	935							
		1096					1010-1100(b)	
						1153(a)		
						1180(b)		
						1347(b)		
				1680				
				1834			1933(b)	
				2070				
Nitrogen								
				522	530			
					626		667	
					684			
	750	752	730	718				
	783							
	970						917	
	1200						1138	
	1400						1415	
							1450	
						1510		
						1690		
	1641			1670			1507	
							1758	
							1790	
	1900					1940		
						1980		
			2030			2060		
			2070	2068				

1*	2	3	4	5	6	7	8	This study
	2140	2164	2156					
				2206		2180		2198
		2290				2300		2301
								2434

*Sources: 1. Pinzon, et al. (1998); 2. Martin and Aber (1997); 3. Johnston, et al. (1994); 4. Yoder, et al. (1995); 5. Johnson and Billow (1996); 6. Blackburn (1998); 7. Curran (1989); 8. Datt (1998).

6. CONCLUSIONS

The results of the above analyses indicate that the detection and mapping of variations in foliar chemistry is possible through the use of AVIRIS data. This type of data, while experimental at present, will become available to the public through the launch of a number of future hyperspectral sensors. The following wavelengths had significant correlations between reflectance and chemical constituents and agreement with other investigations: 1) for chlorophyll a, 707 nm; 2) for chlorophyll b, 1010-1100 nm; 3) for nitrogen, 667, 1415, 1507, 2055, 2035, 2198, and 2301 nm; 4) for carotenoids, 541 nm; 5) and for carbon 1935 nm.

This study was conducted using 1994 AVIRIS data. The sensor has since been improved and this study will be repeated with 2001 AVIRIS data and other test sites. Methods to separate the chemistry of the overstorey from the understorey remain a challenge.

ACKNOWLEDGMENTS

The authors would like to thank the National Aeronautics and Space Administration (NASA) of the United States for supporting the SEIDAM (System of Experts for Intelligent Data Management) project, for providing AVIRIS data, and for valuable discussions. Foliar data were collected through a Forest Renewal British Columbia Grant held by Olaf Niemann. David Goodenough acknowledges the support of Natural Resources Canada and the Natural Sciences and Engineering Research Council. We are grateful to the SEIDAM participants and partners for their contributions to this research.

REFERENCES

- Aber, J. D., Bolster, K. L., Newman, S. D., Soulia, M., & Martin, M. E. (1994). Analysis of forest foliage II: Measurement of carbon fraction and nitrogen content by end-member analysis. *Journal of Near Infrared Spectroscopy*, 2, 15-23.
- Adams, J. B., & Smith, M. O. (1986). Spectral mixture modeling: a new analysis of rock and soil types at the Viking Lander 1 site. *Journal of Geophysical Research*, 91, 8098-8112.
- Asner, G. P., & Lobell, D. B. (2000). A biogeophysical approach for automated SWIR unmixing of soils and vegetation. *Remote Sensing of Environment*, 74, 99-112.
- Blackburn, G. A. (1998). Spectral indices for estimating photosynthetic pigment concentrations: A test using senescent leaves. *International Journal of Remote Sensing*, 19, 657-675.
- Bolster, K. L., Martin, M. E., & Alber, J. D. (1996). Determination of carbon fraction and nitrogen concentration in tree foliage by near infrared reflectance: a comparison of statistical methods. *Canadian Journal of Forest Research*, 26, 590-600.
- Chrien, J., Green, R. O., & Eastwood, M. L. (1990). Accuracy of spectral and radiometric laboratory calibration of the Airborne Visible / Infrared Imaging Spectrometer. *Proceedings Imaging Spectroscopy of the Terrestrial Environment*, 37-49. SPIE, Bellingham, WA.
- Curran, P. J. (1989). Remote sensing of foliar chemistry. *Remote Sensing of Environment*, 30, 270-278.
- Datt, B. (1998). Remote sensing of chlorophylla, chlorophyll b, chlorophyll a+b, and total carotenoid content in eucalyptus leaves. *Remote Sensing of Environment*, 66, 111-121.
- Dickson, R. E., & Isebrands, J. G. (1991). Leaves as regulators of stress response. Mooney, H. A., Winner, W. E., & Pell, E. J. (Eds.). *Response of Plants to Multiple Stresses. Physiological Ecology*, Academic Press, San Diego, USA, 4-34.
- Gao, B.-C., Heidebrecht, K. B., & Goetz, A. F. H. (1993). Detection of scaled surface reflectances from AVIRIS data. *Remote Sensing of Environment*, 44, 165-178.
- Goodenough, D.G., Charlebois, D., Matwin, S., & Robson, M. (1996). Automating reuse of software for expert system analysis of remote sensing data. *IEEE Transactions Geoscience and Remote Sensing*, 32, 525-533.
- Grossman, Y. L., Ustin, S., Jacquemond, S., Sanderson, E. W., Schmuck, G., & Verdebout, J. (1996). Critique of stepwise multiple linear regression for the extraction of leaf biochemistry information from leaf reflectance data. *Remote Sensing of Environment*, 56, 182-193.
- Hurcom, S. J., Harrison, A. R., & Taberner, M. (1996). Assessment of biophysical vegetation properties through spectral decomposition techniques. *Remote Sensing of Environment*, 56, 203-214.
- Jackson, P. J., Unkefer, C. J., Delhaize, E., & Robinson, N. J. (1990). Mechanisms of trace metal tolerance in plants. Kettelman, F. (Ed.), *Environmental Injury to Plants*, 231-257. Academic Press, San Diego.
- Johnson, L. E., Hlavka, C. A., & Peterson, D.L. (1994). Multivariate analysis of AVIRIS data for canopy biochemical estimation along the Oregon transect. *Remote Sensing of Environment*, 47, 216-230.
- Johnson, L. F., & Billow, C.R. (1996). Spectrometric determination of total nitrogen concentration in Douglas-fir foliage. *International Journal of Remote Sensing*, 17, 489-500.

- Kayahara, G. J., & Pearson, A. F. (1996). *Relationship between site index and soil moisture and nutrient regimes for western hemlock and Sitka spruce*. Research Branch, B.C. Ministry of Forests, Victoria.
- Larsen, M. (1997). Crown modelling to find tree top positions in aerial photographs, *Proceedings Third International Airborne Remote Sensing Conference and Exhibition*, 428-435, Copenhagen.
- Metternicht, G. I., & Fermont, A. (1998). Estimation of surface erosion features by linear mixture modeling. *Remote Sensing of Environment*, 64, 254-265.
- Milton, E. J. (1999). Image endmembers and the scene model. *Canadian Journal of Remote Sensing*, 25, 112-120.
- Niemann, K. O., Adams, S., & Hay, G. (1998). Automated tree crown identification using digital orthophotomosaics. Hill, D. & Leckie, D. (Ed.). *International Forum on Automated Interpretation of High Spatial Resolution Digital Imagery for Forestry*, 105-114. Natural Resources Canada, Victoria, B.C.
- Peddle, D. R., & Johnson, R. L. (2000). Spectral mixture analysis of airborne remote sensing imagery for improving prediction of leaf area index in mountainous terrain, Kananaskis, Alberta. *Canadian Journal of Remote Sensing*, 26, 177-188.
- Pinzon, J. E., Ustin, S., Casteneda, C. M., & Smith, M. O. (1998). Investigation of leaf biochemistry by hierarchical foreground/background analyses. *IEEE Transactions Geoscience and Remote Sensing*, 36, 1913-1926.
- Smith, M. O., Ustin, S., Adams, J. B., & Gillespie, A. R. (1990). Vegetation in deserts: I. A regional measure of abundance from multispectral images. *Remote Sensing of Environment*, 31, 1-26.
- Taiz, L., & Zeiger, E. (1991). *Plant Physiology*. Benjamin/Cummings.
- Wulder, M., Niemann, K. O., & Goodenough, D. (2000). Local maximum filtering for the extraction of tree locations and basal area from high spatial resolution imagery. *Remote Sensing of Environment*, 73, 103-114.
- Yoder, B. J., & Pettigrew-Crosby, R. E. (1995). Predicting nitrogen and chlorophyll content and concentration for reflectance spectra (400 - 2500 nm) at leaf and canopy scales. *Remote Sensing of Environment*, 53, 199-211.

Chapter 18

USING GEOREFERENCED LARGE-SCALE AERIAL VIDEOGRAPHY AS A SURROGATE FOR GROUND VALIDATION DATA

Dana Slaymaker*

University of Massachusetts, Department of Natural Resources Conservation, University of Massachusetts, Amherst, Massachusetts, 01003, USA

1. INTRODUCTION

When mapping forest regions and vegetation from satellite imagery or small-scale photography, it is essential to obtain an adequate sample of geographically distributed, unbiased verification and validation data to both drive the classification and assess the accuracy of the results. Traditionally, this has required on-site visits or “ground truthing” of a randomly selected set of locations distributed across the region to be mapped, an often expensive and time consuming process.

In 1989, the Gap Analysis Program (GAP) of the United States Geological Survey (USGS) began mapping biodiversity across the contiguous United States. The purpose of the program was to identify areas of unique species richness that were not presently covered by the existing network of protected lands controlled by state or federal agencies (Scott and Jennings 1998). This required an up-to-date, detailed vegetation map as a substrate for habitat analysis. For this purpose, the program made the largest single purchase of Landsat 5 satellite images at that time, a complete multi-temporal coverage of the United States (MLRC program). The classifying and mapping of this data involved government agencies and universities in every state and resulted in new methodologies for GIS (Geographic

* Current affiliation: Winrock International, Ecosystem Services Group, 22 Third Street, Turners Falls, Massachusetts, 01376, USA

Information Systems), GPS (Global Positioning Systems) and aerial imagery that have permanently changed the way these tools are used in resource inventory.

One product of that revolution was an alternative approach to ground truth verification which used the interpretation of very large-scale georeferenced aerial videography. The development of a time-coding device to automatically label video frames with Global Positioning System (GPS) co-ordinates in the 1980s (Graham 1993) made it practical to extend an aerial point sampling technique originally developed for 35 mm photography (Norton-Griffiths 1988) to extensive regional surveys, collecting large numbers of samples inexpensively. The original technique was based on the accepted premise that photographic interpreters can be trained to accurately identify trees and vegetation at a sufficiently large scale to detail individual crown structures (Sayn-Wittgenstein 1978; Drake 1996). By flying grid patterns of coverage across a region, thousands of georeferenced frame samples can be collected very quickly. Photographic interpreters are then trained on a small selected number of those sites within each forest stratum class. The sites are visited and trees in each video frame identified directly on a print of the image. Visual indexes are made of these prints, which identify each tree species or forest type within that specific set of coverage. Using those visual indexes to interpret the rest of the frame samples results in a much richer set of known ground reference points that can drive the classification of a satellite image or verify any interpretation made at a much smaller scale (Slaymaker et al. 1996).

Since the 1980s, aerial videography has seen increased use in applications where its advantages over traditional photography (lower cost and immediate availability of data) outweigh its disadvantages (poorer spatial resolution and difficulty of analysis due to lack of stereo imaging) (Mausel et al. 1992; Meisner 1986). King (1995) provides a comprehensive review of the evolution of video sensors and their applications, many of which focused on: 1. The measurement of transient phenomena such as wildlife populations (Sidle and Ziewits 1990; Strong and Cowardin 1995) and pest infestations (Everitt et al. 1994); 2. Mapping of dynamic land features such as wetland plant communities (Jennings et al. 1992) and coastal landforms (Eleveld et al. 2000); 3. Land cover mapping in remote areas with limited existing aerial photography and poor infrastructure (Marsh et al. 1994; Slaymaker and Hannah 1997).

2. METHODS

The basic technique of flying a grid of large-scale images to classify Landsat imagery was originally developed in 1980 by a team of researchers (Dunford et al. 1983) for several USAID projects in Africa. Using 35 mm film, vertical or oblique exposures were taken from 300 to 1000 feet above ground. Each exposure was fired by hand and manually georeferenced by reading co-ordinates off a Global-Nav system at the time of exposure.

Arizona was the first state Gap Project to try to use this modification of Norton-Griffiths's point sampling approach to classify the Landsat coverage. In spite of its lower resolution and poorer colour quality, video was chosen over 35 mm film because a GPS-based SMPTE (Society for Motion Picture and Television Engineers) time code generator had been developed by the Horita Corporation. Devices that wrote GPS co-ordinates directly onto video frames through a caption generator had been used before (Myhe et al. 1991), but these records were only accurate to the last one-second position. The Horita wrote the time code and frame number to every exposure, so that the geographic position of each frame could be calculated. Only one 35 mm camera, the Nikon F4 with a 250 exposure back, could label images to the nearest second provided its internal clock was manually matched to GPS time, and this was insufficient for the scale at which the coverage was to be flown. Cost and in-flight management of data were also major considerations as evident in the Tables 18-1 to 18-3.

Table 18-1. Cost of digital images for each system by data collection time

Time and media	Cost (US\$)
Two hours of aerial videotape	\$7.50
Two hours of 35 mm camera slides, 2 exposures every 10 seconds (stereo pairs) scanned to 2,000 by 3,000 pixels by Kodak and stored on CD.	\$2,085

Table 18-2. Cost of commonly used camera and video equipment in 1990.

Camera	Cost (in US\$)
Panasonic Super VHS camcorder	\$1,200
One Nikon F4 with 250 exposure back	\$8,000

Table 18-3. Intervals required to change film or tape

Camera	Time
Video camera	Every two hours
35 mm camera with 36 exposures.	Every 6 minutes
35 mm camera with a 250 exposure back	Every 50 minutes

Arizona is covered by 16 Landsat images in 5 tracking swaths. Video was flown over the state in a 30-kilometre grid using a Panasonic Super VHS camcorder and 12X zoom lens mounted vertically in an aerial photo aeroplane with a standard Fairchild camera mount. The camera was flown approximately 2,000 feet above ground, manually zooming to telephoto every 9 seconds, so as to provide both a wide-angle view of the terrain and a set of large-scale samples. Several thousand video points were collected over the state, but the total sample averaged about 600 ground reference points per Landsat image. This proved to be insufficient to successfully model the mixtures of vegetation and soil types within the range of slope/aspect variations that affected their spectral reflectance. The principal reason for the low number of sample points per image was the use of a single camera alternating between the wide angle and zoom settings, drastically reducing the number of large-scale images that could be used for sampling. In subsequent surveys, that system was replaced with two Hi8 video camcorders that were less expensive and could be mounted to the window of any Cessna aircraft. This arrangement allowed for much a denser sampling because the telephoto camera provided a continuous large scale swath within the wide-angle view, rather than an occasional zoom (Figure 18-1).

This technique was first used successfully to classify the forests of the North-eastern United States for the Gap projects of Maine, New Hampshire/Vermont and Southern New England (Massachusetts, Connecticut, and Rhode Island). Mapping vegetation in this part of the world represented some unique problems; the landscape is 50 % to 95 % forested with a wide variety of forest types occurring in relatively small stands interspersed in a pattern that does not follow any readily discernible rules. While most vegetation types in the United States have developed along natural limits and can often be modelled with respect to variations in elevation and terrain, the chief determiner of species distribution within the major forest regions of New England is historic human activity. Over 80 % of Massachusetts was agricultural land in the 1800's and has since been replanted or has re-grown to forest. The resulting landscape is an intricate mosaic of different forest communities arranged in a whimsical fashion. In addition, the initial examination of unsupervised classifications of the Landsat coverage available for the area showed a less than direct relationship between their classes of spectral reflectance and the SAF (Society of American Foresters) forest types that were to be classified. Most forest types were composed of mixtures of spectral classes. Few spectral classes represented more than 15 % to 35 % of any one forest type and most forest types contained most spectral classes to some degree. This spectral mixing is the essential problem of any image analyst trying to regroup spectral classes

into forest types. They are fundamentally different kinds of categories, one based on the reflectance of energy and the other on human perceptions of what constitutes a community of plants.

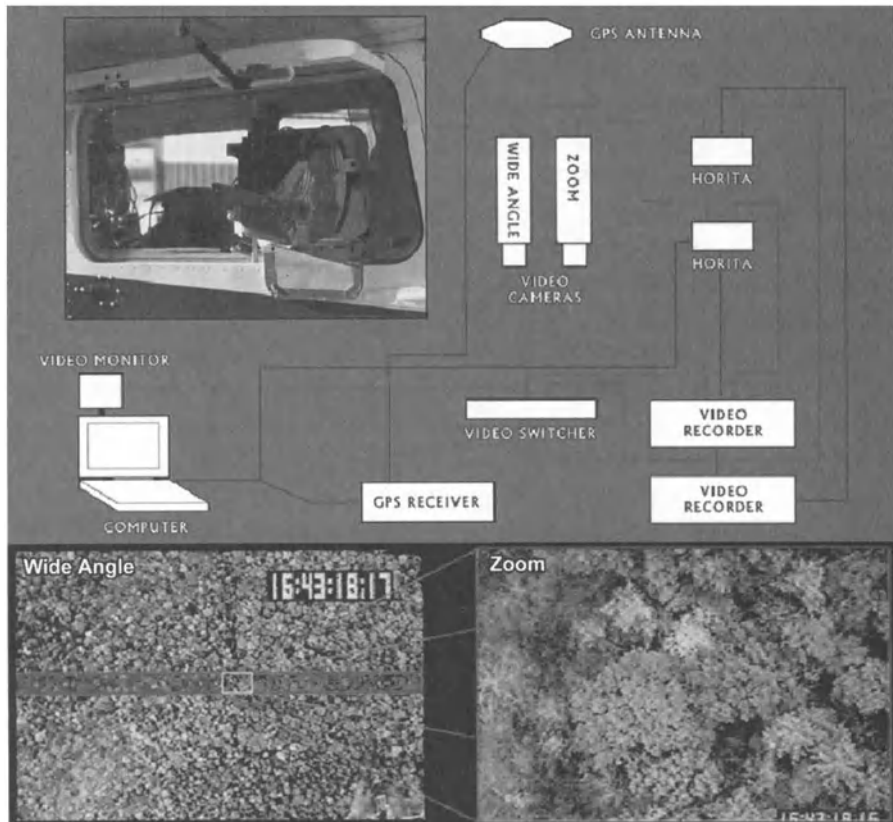


Figure 18-1. Dual camera Hi8 video system mounted in the window of a Cessna 172. A GPS receiver sends data to two Horita SMPTE time code generators, which write the time and frame number to every exposure. Flying at 2,000 ft. above ground, the wide-angle camera covered a 500-meter swath at one meter per pixel resolution. The zoom camera sub-sampled the centre portion of that swath at a resolution of 0.08 meters per pixel.

To deal with this complexity, these projects were much more densely sampled than the Arizona Gap Analysis coverage, flying grids lines 15 kilometres apart and collecting approximately 18,000 points per Landsat image in a stratified sampling to capture all vegetation types in all slope/aspect classes. Once the video was collected and reviewed, a sub-sample of sites that were representative of the different vegetation types and accessible by road was selected and visited by ground crews, who used prints from the video coverage of each site to label its dominant trees and

vegetation. These prints were collected into visual indexes used to train the photographic interpreters, using methods developed by Norton-Griffiths and used successfully in Arizona (Drake 1996) (Colour Plate 19).

Points were initially collected by superimposing the GPS flight log over each Landsat classification in an image processing program and viewing the video monitors beside the computer. Two video recorders were keyed to the same remote control, which kept them in relative sync during viewing. Advances in computer-based video eventually made it possible to display the video on-screen and rotate it to match the orientation of the satellite image (Colour Plate 20). Each point was collected by clicking on a pixel in the Landsat image that could be visually identified as belonging to a specific vegetation type on the corresponding video images. This brought up a point panel automatically labelled with X, Y (latitude, longitude) and a blank Z value. The interpreter filled in the Z value with a numerical code for the selected vegetation type and saved the point to a text file.

The advantage of this approach was that a visual comparison could be made between the wide-angle video images and a false colour-infrared colour composite of each Landsat image to correctly identify the location of individual trees in the corresponding zoom video. Because the GPS position of the aircraft could be anywhere within a nine pixel block of confusion when projected to the ground, having a visual image of the corresponding Landsat image made it possible to estimate the most probable location of a video frame within that context, which improved the accuracy of point identification. Slope/aspect classes from the topography of the region were also projected on screen to increase sampling in the less frequent terrain types. Sampling and labelling a point on screen took only a few seconds once the interpreter was familiar with the forest types; so collecting 18,000 points per Landsat image was not as onerous as it sounds.

The Landsat data used in Southern New England had been "hyperclustered" to 240 classes using a classification algorithm developed by the Los Alamos Laboratory in New Mexico (Kelly and White 1994). This type of clustering represented a considerable improvement in the discrimination of spectral classes, but increased the complexity of regrouping them into information classes. Therefore, the essential problem was how to use the thousands of collected ground reference points for each of these classifications to model a re-labelling procedure. It was necessary that this procedure considered both the spatial context of each pixel in the image and the mixture of spectral signatures associated with each forest type, then determined the most probable identity of that pixel. Richards et al. (1982) presented a methodology for regrouping a non-Gaussian unsupervised classification to information classes by incorporating

neighbourhood values into a probabilistic label relaxation procedure. There have been several variations on this method since (Stumpf and Koltun 1992). Southern New England Gap Analysis followed their basic concept, but implemented it through a set of hierarchical inference rules in GRASS (Geographic Resources Analysis Support System), an open source GIS program that is freely available on the web.

GRASS was used for this re-labelling because of two specific routines in the program: *s.menu* and *i.infer*. *S.menu* imported the list of ground reference points as a site file, then generated a list of values for each location from a stack of GIS layers. The layers included the Landsat classification, all ancillary layers (slope/aspect, ecological region, distance from water, etc.) and a number of neighbourhood matrix functions within a 25-pixel block (mode, max, min, diversity, etc.). In effect this procedure placed each point within the context of its surrounding spectral classes and geographic location. These lists of attributes for each reference point were then organised in contingency tables that identified several potential vegetation types for each spectral class. As stated, each vegetation type was seen as being made up of a mixture of spectral classes. Some spectral classes in that mixture would be significant indicators of a specific vegetation type in a particular set of slope/aspect and ancillary factors, and in association with other spectral classes within the immediate neighbourhood of each pixel. However, those same spectral classes could indicate a different vegetation type in a different set of associations or appear in vegetation clusters where their presence was not significant. Therefore, to label mapping units of information classes from the mixtures of spectral classes in the hyperclustered classification, it was necessary to identify each cluster of pixels that represented a specific vegetation type by its significant spectral class members, then absorb the non-significant pixels in those clusters into the same classifications.

Of the 240 spectral classes in the unsupervised hyperclustered classifications of multi-temporal Landsat images used in the Southern New England Gap Analysis, 180 were identified as relevant to vegetation. The net result of attributing these pixels with neighbourhood and slope values in GRASS was to increase the potential sets of spectral/ancillary signatures from 180 to over several thousand. This is why it was necessary to collect so many thousands of ground reference points from the video. They provided a sufficient population of samples to statistically model relationships between those spectral classes in the different contexts provided by the ancillary data layers. As these potential context classes were identified from the contingency tables, they were written into three successive sets of decision

rules in the GRASS program “i.infer”, which were run in a cascading fashion in a shell script as follows:

- Rule # 1 – Queried each pixel in the original classification and all underlying 5-pixel by 5-pixel neighbourhoods / ancillary data layers with a series of yes/no - if /and if questions. Pixels that could be assigned to a probable initial vegetation type were assigned; all others were labelled as zero. This rule set ran only once.
- Rule set # 2 – Queried each pixel in three layers, the original classification of spectral classes: the product of rule set # 1, and a 3-pixel by 3-pixel majority of that product (re-labelling each classified pixel as its most frequent neighbour). These rules only looked at those pixels in the Rule # 1 product whose majority vegetation type was different than the type they were assigned to. If that majority vegetation type was one to which the original spectral class of that pixel could belong to, according to the first rule set, then it was relabelled to that majority. Otherwise, it was labelled zero. The product of this rule set was then merged with the product of the first rules, re-labelling all non-zero results. This second rule set was repeated in a loop until the immediate product (those pixels that were reassigned) reached a minimum threshold of non-zero pixels, indicating that little further change would occur.
- Rule set # 3 – Queried each pixel in three layers: the original classification of spectral classes, the final product of Rule set # 2, and a 3-pixel by 3-pixel majority of that product. These rules only looked at those pixels in the final Rule set # 2 product whose value was still zero. If those pixels had a majority vegetation type and it was a type to which the original spectral class of that pixel could belong to, then it was relabelled to that majority. Otherwise, it was left as zero. The product of this rule set was then merged with the final product of the second rule set, re-labelling all non-zero results. This rule set was also repeated in a loop until the intermediate product of the rule reached a minimum threshold of non-zero pixels.

The final product of Rule set # 3 was then run through a series of calculations (“a” if “x” not zero, 0 otherwise) in the GRASS program “r.mapcalc”, in which “a” was the 3 by 3 majority of the product and “x” was a mask for all pixels in the original spectral classification associated with vegetation. This was also repeated until a threshold of no change occurred.

The purpose of this complicated cascade of decision rules was to correctly identify kernels of pixels within the natural clusters of vegetation types. It would then grow them towards each other to create the kind of

artificial boundaries that are not found in nature but are considered necessary for thematic classifications with minimum mapping units. This approach would be impossible without the large number of ground reference points that can be economically acquired with aerial videography.

Since only a small fraction of the video frames are actually used in driving the labelling process, the data source can also be used to verify the results. This was originally done in the Southern New England Gap project by setting aside a random subset of the interpreted points (stratified to cover all vegetation types) before generating the contingency tables to model the rules. Those points were then used in an error matrix between their interpretation and the labelled vegetation type. In later surveys, this procedure was changed to sort all the GPS positions in each flight line of the survey grid by their classification in the final map, then select a stratified random subset. These points in the video coverage would then be examined by a new set of photographic interpreters (other than those who had done the original classification) judging the associated vegetation type as: right, wrong or wrong but reasonable. When using this approach however, it was important to sort the original GPS points through an interspersion layer of the final vegetation map so that any points closer than two pixels from a boundary between classes was filtered out. This restricted the interpreters to judging the classification rather than the accuracy of an artificial boundary.

The initial vegetation maps for the Southern New England Gap Analysis program produced by this procedure had an overall accuracy for all classes of 89.7 % (83.6 % Kappa) for an Anderson level three classification (Anderson et al. 1976). Mis-classifying oak dominant communities as oak/maple/birch co-dominant communities caused the worst user's accuracy of 74 %. The worst producer's accuracy, 80 %, was from the same problem. These results were adequate for the Gap Analysis program's goal of 85 % accuracy and considerably better than the 70 % levels achieved in previous classifications of the same imagery without the sequential rules procedure. However, Maine, New Hampshire and Vermont had collected aerial video coverage for their state Gap Analysis projects at the same time as Southern New England. Those programs developed their own mechanisms for driving their classifications and verifying the results with similar success. Therefore, it would appear that it is the number of ground reference points available for modelling, rather than the specific expert system used to interpret them, that is important for the success of this approach in Landsat classification.

Having established that large-scale sampling with aerial videography was successful in classifying its Landsat data, the National Gap Analysis Program made the technique available to other state gap projects. The Southern New England Gap Analysis program worked in conjunction with

the Gap projects of West Virginia and Colorado to build eight additional Hi8 systems and distribute them as necessary to cover each state that requested one, holding workshops on their use through the National Gap Program and the U.S. Fish and Wildlife Service. Some states such as Maryland and Tennessee used the New England inference rules approach to re-label the unsupervised classifications of their Landsat data, but most developed their own mechanisms to fit the individual needs of their respective projects. In all, 35 states used some form of aerial videography in their projects, either to drive a classification or to verify the results.

A great deal was learned about the advantages and limitations of this system during the Gap Projects. The chief advantage was low cost of operation and ease of use. Because the system could be mounted to the window of any Cessna aircraft, it was easy for projects to find a pilot and aeroplane willing to fly their grids. A GPS tracking program, Geolink Powermap, was used to display both the flight lines and aircraft position in real time during the flight, making it easy for the pilot to follow predetermined tracks.

The biggest problem with the system was preserving the data. Viewing video images on a monitor with a freeze frame mechanism damages the tape, removing thin strips of image and eventually destroying the alignment of the images to the transfer head. Using copies of the tapes for interpretation and archiving the originals could avoid this, but only at a considerable loss of image quality and an understanding that the videotapes will eventually self-destruct even under archive conditions, slowly absorbing water until they become unplayable. Several projects eventually eliminated this problem by digitizing the video data for on-screen interpretation on the computer, but this was a difficult and expensive process with analogue video and most researchers did not have the available disk space to store all their video data as computer files.

Some interpreters also had difficulty visually matching the wide-angle video images and Landsat image to more accurately identify the location of zoomed frame samples. This step was necessary because the GPS in the original set-ups only gave the aircraft's geographic position and did not project the camera's orientation to the location of each frame on the ground. The wide-angle image was at a small enough scale that you could usually identify its surface pattern in the Landsat image, but this slowed down the process of interpretation in non-distinct areas.

The chief criticism of this approach from photographic interpreters and other critics of the Gap Analysis project however was the unavailability of stereo image pairs, which decreased interpretability of the crowns in a forest and limited information on its height and structure, important factors in

evaluating habitat. Stereo could be achieved by grabbing two video frames that overlapped by 60 % and printing them out to view in an optical stereoscope, but that was a time consuming process.

To resolve these limitations, efforts were undertaken to move the aerial videography system into a digital format and improve both its accuracy and interpretability (Slaymaker et al. 1999). The analogue camcorders were replaced with DV (Digital Video) cameras, recording to one-hour DAT tapes that could be reproduced without image quality loss (Figure 18-2). This imagery is also easily transferred to a hard disk in its original compressed format, wrapped in a Quicktime shell for computer access.

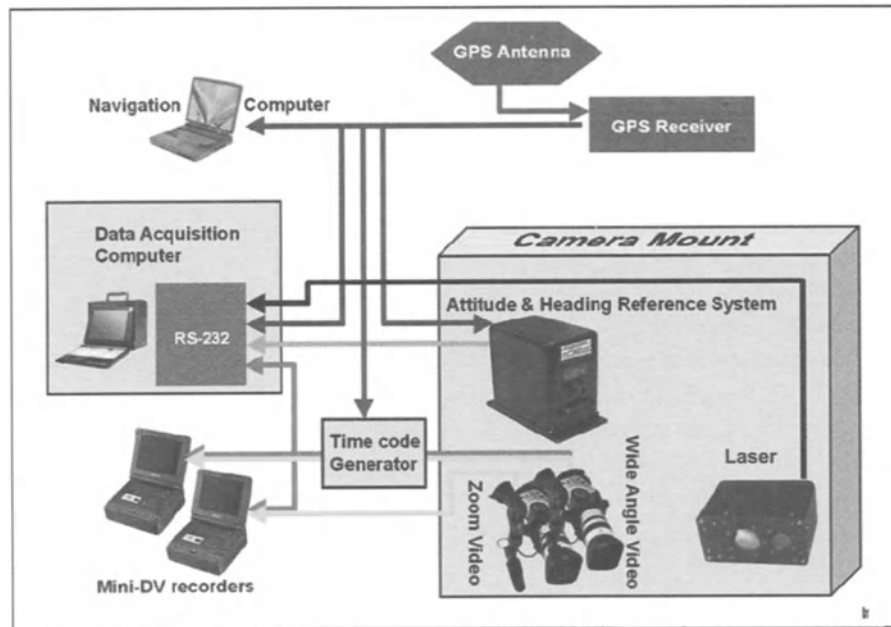


Figure 18-2. Layout of the digital video system.

A Watson attitude and heading reference system was added to the camera platform to determine orientation during flight, recording tip, roll and azimuth eleven times per second, and a pulse laser was added to record a profile of ground and canopy along each flight line. Firing 240 pulses per second, it was set to record the last return of each pulse so as to maximise penetration of the canopy. Horita SMPTE time code and GPS positions were still written to the audio track of the videotape, but the data were also recorded to a separate computer with the Watson and Laser data, using a National Instruments card to time-stamp each entry. The laser and Watson data were initially time-stamped to match the direct NMEA digital output from the GPS receiver. However, it was discovered that most GPS units

have a variable time lag between the receipt of a one-second signal set from satellites and the processing and delivery of the calculated position to a computer. This can introduce an error of up to a quarter of a second between the GPS position and the other data. The Trimble receiver used in this system could be programmed to send a single immediate pulse on receipt of a signal, but this pulse proved difficult to capture and program with the National Instruments card. A simpler solution was not to use the ASCII data output from the receiver directly, but to use the SMPTE data from the Horita GPS3 time code generator instead. The Horita GPS3 unit actually keeps time by counting video frames, labelling each and predicting the next zero frame GPS position. Data in the Trimble T-SIP format documents the time lag in each packet and the Horita uses this information to adjust its timing. The label for each video frame is recorded to the computer as it is written to tape, and the result is an excellent match between position, orientation and range on a frame-by-frame basis. Once the DV was recorded from tape to a Quicktime computer file, the individual frames and Horita code on the audio track could be parsed by software. Each frame was automatically extracted as a BMP image and labelled by its time code, which matched it to a corresponding position and camera orientation record in the combined flight data. The Vision Lab at the Computer Science Department developed a program to convert these frames into automatically geo-referenced mosaics of the video flight path, combining image matching techniques with the accurate geographic placement of the centre of each frame as calculated from the orientation and range data. Because of the extreme overlap of video frames, strips as thin as 4 pixels were extracted from each frame to construct the image swath, producing a mosaic from a very narrow field of view. When matching pairs of mosaics were constructed from the same swath of video images by extracting two sets of thin strips from points approximately two-thirds of the distance from the centre of each frame to its trailing and leading edges, they formed perfect stereo images in a stereoscope or 3D viewing program. These mosaics were actually consistent epipolar models from which a parallax image could be extracted and converted into a digital elevation model with vertical control points from the laser profile (Figure 18-3). This processing essentially mimics the products of more expensive commercial scanning laser and Lidar systems, which produce a direct elevation model of the ground of the ground by scanning across the swath. The difference is that the pulse laser provides a single meter-wide profile, which is then used as vertical control points to transform the parallax model generated from the video strips into a digital elevation model by calibrating it to the ground.

With this system, digital video could be transformed into automatically georeferenced strips of image and superimposed directly over the Landsat image for interpretation. Using the ERDAS program, Stereo Analyst, the epipolar strips could be viewed as stereo images in the same co-ordinate space, with vertical features measured in the image and recorded as text or a georeferenced 3D shape file (ESRI vector format). This approach allowed photographic interpreters to examine the terrain in stereo, outline polygons of vegetation, and then transfer them directly to the underlying Landsat image. They could also measure stand height, relative tree height, or slope and aspect within the images, viewing them directly on screen as optical stereo pairs with either anaglyph red/blue glasses or, more successfully, with Polaroid glasses. The latter block vision to each eye alternately in synchrony with the corresponding right or left image on screen. This takes place at the refresh rate of the monitor, so the viewer is only aware of seeing full colour 3D on screen.

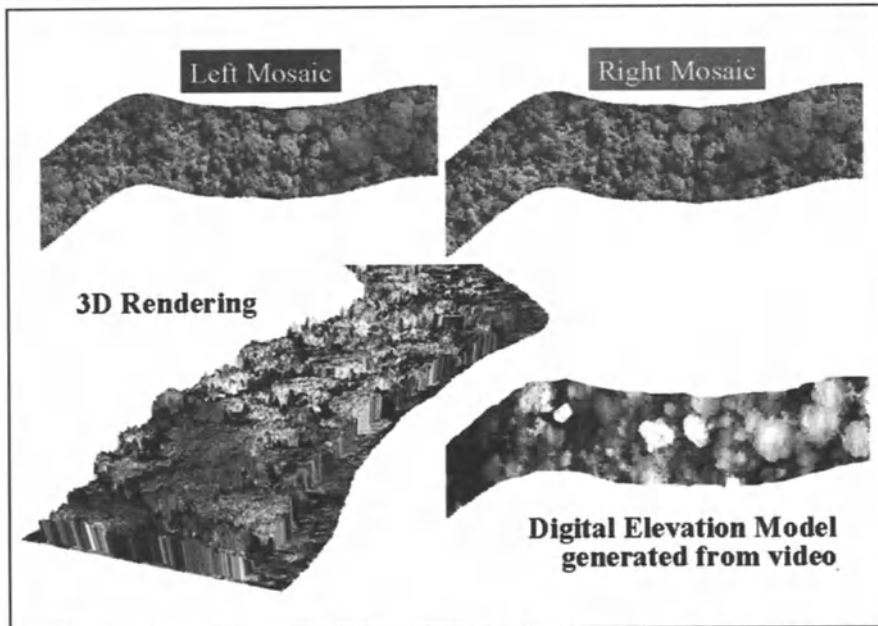


Figure 18-3. Image products from the dual mosaic strip construction of epipolar models.

By the time these improvements were available to the Gap Analysis programs, only Georgia, South Carolina and Alabama still needed coverage flown. They have used the new digital 3D system and it remains to be seen if the photographic interpreters for those states find the improvements sufficient to warrant the extra work and cost of obtaining them.

The DV camera set-up has also been used in other applications beyond Gap Analysis, flying approximately 170 hours of video across the Amazon Basin to provide ground verification for cover mapping with JERS-1 mosaics by the NASA LBA-Ecology Project's Global Rain Forest Mapping program (GRFM). It compared canopy height and forest structure to Synthetic radar (SAR) sensor response (Hess et al. 2002). In 2001, development of the system was taken over by Winrock International, a non-profit research foundation devoted to the development of new techniques for sustainable agriculture and forest management. Winrock is currently working with The Nature Conservancy on a joint grant from the Department of Energy (DOE) to develop new methods of estimating the carbon sequestered in tropical and temperate forests. The foundation is exploring the use of 3D videography to extrapolate ground site estimates of standing biomass across a forest region by developing positive correlations between crown diameter / height and dbh (diameter at breast height). Previous work with Winrock and NASA-LBA (Slaymaker et al. 1999; Hayward and Slaymaker 2001) indicates that this approach should work.

Winrock has also started working with some true digital cameras that record their data directly to a computer in an RGB or RGBIR format. Although a considerable improvement over analogue, DV still suffers from low resolution (480 by 720 pixels) and a poor quality colour-recording model (NTSC) that is composed of contrast and yaw, essentially a black and white image with colouring instructions. Recording the digital video signal to DAT tape format means that the tapes can be copied without any loss of image quality, but it also means that the original images have to be written in a lossy compression mode that has a definite effect in the image structure. By contrast, there are now relatively inexpensive high resolution RGB digital cameras available that produce a 2,000 by 3,000 pixel image of higher quality than a scanned 35 mm negative and reverse the economic limitations of the 35 mm format as compared to aerial video. Working with the Norwegian Space Centre, Winrock flew a Gap Analysis style survey of parts of that country in the summer of 2001, using a Kodak DSC 760 RGB digital camera, and exposing 3,000 to 5,000 frames per flight that were saved to a hard disk as 7 megabyte georeferenced tiff images. A firewire link between the camera and computer controlled all camera adjustments except focus and enabled the downloading of an image to disk at a maximum rate of one exposure every five seconds. An on-screen preview allowed the operator to compare each image to the previous exposure and determine if there was sufficient overlap. The camera software has a built-in intervalometer that can be set to fire the camera on the second at a specific interval. That timing is based on the computer's internal clock rather than GPS time, but one of the

Norwegian programmers was able to write a simple program that synced the computer's clock to incoming NMEA GPS data. The camera records the time of each exposure to 1/1000th of a second by computer clock time, so exposure positions between GPS records can be calculated. It can also input NMEA GPS data through its own serial port and write it directly to the header of each exposure if the last GPS record is sufficient. The Kodak DCS 760 costs around \$6,500 and can be operated at full speed by any recent laptop with built in firewire support and at least 520 megabytes of ram. This means that an effective high-resolution digital aerial system can be assembled for less than \$10,000. Kodak has also developed a 4,080 by 4,080 pixel camera back that attaches to the Mamiya AFD or Hasselblad medium format cameras and offers most of the same remote control capacities as the DCS 760 (although it cannot download GPS data directly). It costs around \$12,000 for the back alone, in addition to the cost of the front-end camera with a wide-angle lens. This back can be operated with the same type of laptop as the DCS 760, but with a significantly longer download time. The maximum firing rate of these digital cameras is a significant issue in determining their suitability for forest surveys and frame sampling applications. The minimum interval of 12 to 15 seconds between exposures required by the Kodak 4,080 by 4,080 pixel digital camera back limits its aerial exposures to scales of 0.7 meter per pixel or more for stereo coverage (60 % overlap), restricting its use to large area coverage at higher altitudes. The smaller image size and rectangular format of the Kodak DCS 760 allows it to fire stereo coverage at scales down to 0.5 meter per pixel with a 3,000-pixel swath, or 0.3 meter per pixel when turned sideways for a 2,000-pixel swath. This is the format that was used in the Norwegian Gap Survey.

The other major limitation of this camera and most high-resolution digital cameras on the commercial market is that they use a matrix filtering system to construct colour images from a single monochrome CCD sensor. Each pixel is coated with a different colour filter in a pattern of 25 % Red, 50 % Green, and 25 % Blue. The images are saved as a single layer image from which three layer RGB images are generated in software by the extrapolation of colour information to each pixel from its neighbours. The advantage of this approach is that the raw images are much smaller than the final product, making it easier to transfer and store very high-resolution files on a laptop with limited hard disk space. A 2,000 by 3,000 12-bit image can be captured and stored as a 7-megabyte file, then processed to a 35-megabyte 32-bit image after the flight. The disadvantage is a loss of some radiometric information and colour resolution as compared to a true RGB digital camera that uses 3 CCD monochrome chips behind colour filters.

High-resolution versions of 3 CCD cameras are still relatively rare and expensive, but Winrock is also working with a 3 CCD RGBIR multi-spectral digital camera, the Duncantech M4100, with a resolution of 1,024 by 1,920 pixels. The camera uses a 3-way prism behind the lens with two monochrome CCDs, recording red and near infrared images matched to Landsat bands 3 and 4, plus a colour matrix chip recording the green and blue bands. Since the colour chip is 50 % green, there is minimal resolution loss in the extrapolation of that band and while the blue colour layer is still generated from 25 % of the chip, but it is the lowest resolution band used in aerial imagery anyway. The output is processed to a four band RGBIR image in the camera, and the gain of individual bands can be adjusted in flight, allowing it to be calibrated to known spectral responses with a Barnes radiometer and ground panels. At \$17,000.00, the M4100 is a fraction of the cost of most multi-spectral digital systems, which start around \$125,000 as multi-camera arrays. It is connected to its host computer by a framegrabber or direct camera link, rather than firewire, allowing it to record images up to 10 frames a second at resolutions of less than 10 centimetres per pixel and overlaps of 80 % or more. This means that the Duncantech can replace digital video in large-scale applications that require high overlap if the operator has a computer that can handle that rate of data transfer. Even firing the Duncantech at a more modest rate of 5 frames a second (7.5 megabytes per image) accumulates data at a rate of 130 gigabytes an hour. Recent increases in computer speed and hard drive size make this rate of data acquisition feasible. Winrock's field computer (a lunchbox luggable) holds five 73-gigabyte 160 LVD SCSI drives, stripped to a single 266-gigabyte fault-tolerant array, which limits actual data collection in flight to about 2 hours. That data has to be copied to portable 160-gigabyte firewire drives after each flight, then written to Exabyte tapes over the next several days.

How this approach will work with large-scale sampling projects like the National Gap Program or the NASA-LBA coverage of the Amazon Basin remains to be seen. Most of the Gap Analysis states and the Amazon Basin were flown by starting in one corner of the grid and following the grid pattern until done, landing at local airports and staying at motels along the way. Organising the necessary data storage and transfer with that kind of schedule would be difficult now, but should become easier as larger IDE drives (200 to 500 GB) become available in firewire enclosures and their prices continue to drop. At this time, it costs about \$1.22 per gigabyte to store image data on Maxtor 5400 rpm 160 GB hard drives, which is less than the cost of storing the same data on Exabyte tape. This trend of faster computers with larger hard drives should continue in the future, making the handling of these large data files more practical.

The Computer Science Department at the University of Massachusetts is also working on a program that will write the stereo mosaics in real time during the flight, discarding the bulk of each image. This would solve the storage problem, but will also require faster computers than are available today, as well as a considerable leap of faith on the part of the camera operator.

3. CONCLUSION

Experienced aerial photographic interpreters have a heuristic ability to identify different tree species and plant communities at large scale under a range of slopes and lighting conditions. This is a uniquely human trait that has not been rivalled by the automated analysis of spectral signatures from satellite data. The Gap Analysis Program developed a practical frame sampling method that utilised this human capacity to improve the machine classification of Landsat data over large regional areas. The efficacy of this multi-scale approach to interpreting satellite imagery has proven itself over the life of the project.

During the 12 years of this effort, there was a general trend toward improving the quality and accuracy of the data with a corresponding increase in the cost and complexity of the equipment. The first dual camera Hi8 system cost approximately \$7,000. Switching to the DV system with an attitude indicator and laser increased its cost to \$32,000, while the complete Duncantech system runs over \$60,000 (including the on-board computing system and the several terabytes of data storage needed to manage the imagery post-flight). Analogue video systems are practically extinct and the cost of DV camcorders has dropped considerably, so it would still be possible to put together a simple video system for \$7,000 that had the advantage of digital data storage on DAT tape. The major expenses in building more complex systems lie in either capturing the orientation of the cameras at the moment of each exposure for automatic georeferencing / mosaicking programs, or moving into higher resolution, multi-spectral imagery. The researcher or forest manager who can meet his needs with natural colour imagery that has a more approximate geographic position attached to it can still put together an excellent imaging system, consisting of either DV or digital still cameras, that clamps to a Cessna and costs under \$10,000. When the Gap Analysis Program initiated its aerial frame sampling system, the driving factors to choose video over the higher resolution of scanned 35 mm film were the per frame costs, automatic operation of the camera outside the aircraft without having to change film and the ability to

tag each video image with a specific geographic position between the once per second GPS signals. With the evolution of inexpensive high-resolution digital cameras in 35 mm camera bodies, those advantages have been essentially eliminated. The digital frame cameras have better colour and resolution than digital video and bypass the compressed tape storage that limits the quality of DV images. The major limitation of these digital cameras is the long time interval between exposures, which is required to download each image through the relatively inexpensive firewire links. Cameras like the Duncantech or the Atmel (2,300 by 3,500 pixel) digital camera use more expensive framegrabbers or direct camera links and can download at much higher frame rates, but with a corresponding increase in cost and data management problems.

All of these systems are still very inexpensive, however, compared to commercial multi-spectral or hyper-spectral digital cameras, or scanning laser/video and Lidar systems, most of which will do a better job of aerial data collection, albeit for considerably more money. The history of video and digital aerial camera systems, like that of small format aerial photography in general, has been the development of "jury-rigged" systems to meet specific resource management objectives within severe budget limitations. What they lack in photogrammetric accuracy and spatial resolution is compensated for by their ease of mobilisation and subsequent temporal resolution: the ability to be available and affordable as needed for resource monitoring.

REFERENCES

- Anderson, J. R., Hardy, E. E., Roach, J. T., & Witmer, R. E. (1976). A land use and land cover classification system for use with remote sensor data. *U.S. Geological Survey, Professional Paper 964*. Washington, D.C.
- Drake, S. (1996). Visual Interpretation of Vegetation Classes from Airborne Videography: An Evaluation of Observer Proficiency with Minimal Training. *Photogrammetric Engineering & Remote Sensing*, 62, 969-978.
- Dunford, C., Mouat, D., Norton-Griffiths, M., & Slaymaker, D. M. (1983). Remote sensing for rural development planning in Africa. *The Journal for the International Institute for Aerial Survey and Earth Sciences*, 2, 99-108.
- Eleveld, M. A., Blok, S. T., & Bakx, J. P. G. (2000). Deriving relief of a coastal landscape with aerial video data. *International Journal of Remote Sensing*, 21, 189-195.
- Graham, L. A. (1993). Airborne Video for Near-Real-Time Vegetation Mapping. *Journal of Forestry*, 8, 28-32.
- Hayward, C. D., & Slaymaker, D. M. (2001). Estimating the significant above ground biomass of Amazonian rain forest using low altitude aerial videography. *18th Biennial*

- Workshop on Color Photography and Videography in Resource Assessment, in press. 16-18 May, ASPRS, Bethesda, Maryland.
- Hess, L. L., Novo, E. M. L. M., Slaymaker, D. M., Holt, J. Steffen, C., Valeriano, D. M., Mertes, L. A. K., Krug, T., Melack, J. M., Castil, M., Holmes, C., & Hayward, C. (2001). Geocoded Digital Videography for Validation of Land Cover in the Amazon Basin. *Journal of Remote Sensing*, in press.
- Jennings, C. A., Vohs, P. A., & Dewey, M. R. (1992). Classification of a wetland area along the upper Mississippi River with aerial videography. *Wetlands*, 12, 163-170.
- Kelly, P. M., & White, J. M. (1994). *Preprocessing remotely-sensed data for efficient analysis and classification*. Computer Research Group, MS B-265. Los Alamos National Laboratory.
- King, D. J. (1995). Airborne multispectral digital camera and video sensors: a critical review of system designs and applications. *Canadian Journal of Remote Sensing*, 21, 245-273.
- Marsh, S. E., Walsh, J. L., & Sobrevida, C. (1994). Evaluation of airborne video data for land-cover classification accuracy assessment in an isolated Brazilian forest. *Remote Sensing of Environment*, 48.
- Mausel, P. W., Everitt, J. H., Escobar, D. E., & King, D. J. (1992). Airborne videography: current status and future perspectives. *Photogrammetric Engineering and Remote Sensing*, 58, 1189-1195.
- Meisner, D. E. (1986). Fundamentals of airborne video remote sensing. *Remote Sensing of Environment*, 17, 63-79.
- Norton-Griffiths, M. (1988). Aerial point sampling for land use surveys. *Journal of Biogeography*, 15, 149-156.
- Richards, J. A., Landgrebe, D. A., & Swain, P. H. (1982). A means for utilizing ancillary information in multispectral classification. *Remote Sensing of Environment*, 12, 463-477.
- Sayn-Wittgenstein, L. (1978). Recognition of tree species on aerial photographs. *Information Report FMR-X-118*, Forest Management Institute, Canadian Forestry Service, Ottawa, Ontario.
- Scott, J. M., & Jennings, M. D. (1998). Large-Area Mapping of Biodiversity. *Annals of the Missouri Botanical Garden*, 85, 34-47.
- Sidle, J. G., & Ziewitz, J. W. (1990). Use of aerial videography in wildlife habitat studies. *Wildlife Society Bulletin*, 18, 56-62.
- Slaymaker, D. M., & Hannah, L. (1997). GPS-logged Aerial Video as a Georeferencing Tool For Digital Imagery in Remote Regions, a case study in Madagascar. *The Proceedings of the 16th Biennial workshop on Color Photography and Videography in Resource Assessment*. ASPRS, Bethesda, Maryland.
- Slaymaker, D. M., Jones, K. M. L., Griffin, C. R., & Finn, J. T. (1996). Mapping deciduous forests in southern New England using aerial videography and hyperclustered multi-temporal Landsat TM imagery. Scott, J. M., Tear, T. H., & Davis F. W. (Eds.). *Gap Analysis: A Landscape Approach to Biodiversity Planning*, 87-101. American Society of Photogrammetry and Remote Sensing, Bethesda, MD.
- Slaymaker, D. M., Schultz, H., Hanson, A., Riseman, E., Holmes, C., Powell, M., & Delaney, M. (1999). Calculating Forest Biomass with Small Format Aerial Photography, Videography, and a Profiling Laser. *The Proceedings of the 17th. Biennial workshop on Color Photography and Videography in Resource Assessment*, 241-260. April 1999, ASPRS, Bethesda, Maryland.
- Strong, L. L., & Cowardin, L. M. (1995). Improving prairie pond counts with aerial video and global positioning systems. *Journal of Wildlife Management*, 59, 708-719.

Stumpf, K. A., & Koltun, J. M. (1993). Rule based aggregation of raster image classifications into vector GIS databases with five and forty acre minimum size-mapping units. *ASPRS/ACSM Conference*, 261-278. Washington, D.C.

Chapter 19

TREE AND CANOPY HEIGHT ESTIMATION WITH SCANNING LIDAR

Benoît St-Onge¹, Paul Treitz², and Michael A. Wulder³

¹*Université du Québec à Montréal, Montréal, Quebec, H3C 3P8, Canada*

²*Queen's University, Kingston, Ontario, K7L 3N6, Canada*

³*Canadian Forest Service (Pacific Forestry Centre), Natural Resources Canada, Victoria, British Columbia, V8Z 1M5, Canada*

1. INTRODUCTION

A large part of the research efforts concerning the remote sensing of forests has been devoted to the development of repeatable methods for the extraction of information from monoscopic, two-dimensional images. Emphasis has been on spectral pattern recognition. Although appropriate for species or health characterisation, this approach comes with several limitations when detailed information on forest structure, e.g. three-dimensional aspects of forest canopies, is sought (Wulder 1998). Accurate measurements of height, density, volume, stratification, etc. at local scales, which are of prime interest for foresters and forest ecologists, and which have a geometric rather than radiometric nature, are still beyond the capabilities of two-dimensional remote sensing and image processing.

Three-dimensional remote sensing is a promising and fast growing field, and has already proven more accurate than spectral remote sensing for certain attributes (Hyyppä et al. 2000; Lefsky et al. 2001). Recent technological advances allow efficient soft copy photogrammetry, precise radar interferometry, and laser altimetry. Out of these three technologies, laser altimetry shows the best performance in producing three-dimensional data on both ground and canopy topography (Baltsavias 1999; Hyyppä et al.

2000; Hese and Lehman 2000). In particular, the ability of laser altimeters to penetrate forest canopies through to ground level presents new possibilities, such as mapping canopy height with high precision and accuracy.

Light Detection and Ranging (lidar) is a common research technique used in a variety of application areas including atmospheric research, chemical analysis and monitoring and distance measuring. When deployed as a remote sensing tool from airborne or spaceborne platforms it is referred to as laser altimetry. In common practise laser altimetry is performed using an active sensor that combines a high frequency pulsed laser (the transmitter) with a telescope and solid state photo-detector (the receiver). A portion of the incident laser pulse energy is reflected back to the sensor from each intercepted surface and the round trip travel time between the transmitted and reflected laser pulses between the airborne sensor and the target surface is converted to a range distance. In post-processing this range measurement is combined with synchronised platform position data from a precise differential GPS solution and platform orientation information from an on-board inertial navigation system (INS) to compute the position of the lidar echo, or "pulse return", from each terrestrial target.

Scanning the field of view of the sensor perpendicular to the flight path of the aircraft during flight provides greater swath coverage and more efficient data collection than a simple profiling system but introduces some complexities due to off-nadir look angles. The absolute elevation accuracy of the lidar data is typically 10-40 cm from a flying height of 1000 m for scanning lidar systems (Baltsavias 1999).

There are two distinct types of lidar systems in the commercial and research sectors: full waveform and discrete return. In the first case, the returned laser energy is densely sampled over a short time interval using an on-board high sampling rate signal digitizer to create a "full waveform" description, i.e. amplitude over time, of the return signal from a single pulse. This full waveform describes the energy intensity reflected back towards the sensor by the different strata of the vegetation column traversed by the pulse. It is a function of foliage density and structure (i.e. clumping, gaps) throughout the column (Ni-Meister 2001).

Discrete return lidar systems, on the other hand, typically record only the occurrence of first and last returns from a series of returns corresponding to discrete surfaces along the slant range. That is, they do not sample the full return signal waveform but rather record the time-of-flight (range) to the peak of any signal that exceeds the noise threshold. Sample and hold techniques are used to capture the last return of a series of returns when the vertical profile of the target is complex.

In a forest environment, the first return corresponds to the initial amplitude rise over the background noise level caused by the energy echoed

by the outer vegetation layer of a canopy. The last return corresponds to the last detectable signal above the noise threshold from a series of returns, at some time interval after the first return, when the pulse is intercepted by an opaque object, normally the ground. Last returns are (post-flight) classified such that "true" ground returns are separated from low vegetation returns. Some discrete-return lidar systems are now capable of recording up to five returns.

The majority of discrete return sensors in use today are built using solid-state, diode-pumped lasers that operate at near infrared wavelengths, $\sim 1 \mu\text{m}$, with pulse repetition rates from 5,000 to 35,000 Hz and pulse energies in the order of 100s of μJ .

Full waveform lidar systems, such as SLICER (e.g. Means et al. 1999) are generally profiling systems (with one to a few parallel profiles) and have only been used for research purposes. Discrete return scanning lidar systems are used commercially for topographic mapping, including wide area surveys (Hill et al. 2000). While the former have a large diameter footprint (several meters wide), discrete return lidar systems typically possess footprints of less than a metre in diameter. Even though only a fraction of all pulses reach ground level, the sampling of ground elevation remains sufficiently dense to allow for development of precise below-canopy digital elevation models (Kraus and Pfeifer 1998).

Due to their commercial availability (as opposed to full-waveform systems) and their mapping capabilities, the following discussion on lidar for forest attribute estimation will concentrate on the application of discrete return lidar systems. For detailed reviews of lidar technology and applications for forestry, the reader is referred to Wehr and Lohr, (1999), and Lim et al. (2002). The reader is also referred to Lefsky et al. (2001) and Harding et al. (2001) for examples of full waveform lidar applications for the study of forest canopies.

Here we discuss the methods used to produce, pre-process, and analyse discrete return scanning lidar data. We will review several methodological details that are critical to the success of a lidar mission for forestry and subsequent analyses. We begin, however, by presenting a brief review of forestry applications of lidar to give a general idea of the current status.

Subsequent sections include: methodological considerations pertaining to the acquisition of lidar data; pre-processing and analysis of lidar data for the extraction of forest information, specifically what we consider the most suitable methods for the estimation of stand height and individual tree height. For brevity, we have omitted detailed methodological considerations related to other forest attributes such as timber volume, biomass, density, etc. Our focus on height is motivated by the importance of this parameter for estimating other forest attributes, in particular volume and biomass. To

ensure completeness, the following overview section includes, where appropriate, attributes other than height.

2. THE STUDY OF FORESTS USING LIDAR

Lidar systems were first tested as remote sensing tools for topography and bathymetry in the 1960s (see Aldred and Bonnor 1985, for a review of early systems). The use of lidar for forest applications was first investigated in the 1970s (Soludukin 1977 cited in Nelson et al. 1997). Interest in the accurate estimation of stand height, volume, and biomass developed as early as the 1980s, when it was demonstrated that mean stand height estimates produced using lidar were as accurate as ground or standard photogrammetric measurements (Schreier et al. 1985; Aldred and Bonnor 1985).

Success in estimating timber volume and biomass was also achieved early. For example, MacLean and Krabill (1986) obtained high coefficients of determination ($0.72 \leq r^2 \leq 0.89$) for predictive models of volume.

Until 1993, the vast majority of forest studies using lidar were carried out with profiling systems, using either full waveform or discrete return approaches. Because the Global Positioning System (GPS) was not yet fully developed at the time, locating the lidar trace on the ground was problematic. Since the mid-nineties, several researchers have tested lidar scanners equipped with precision GPS and Inertial Navigation Systems (INS), also referred to as internal measurement units (IMUs). Estimates of stand height and volume comparable to those obtained using profilers have been achieved consistently (e.g. Nilsson 1996; Næsset 1997; St-Onge and Renaud 2000; Næsset 2002).

The return density of current scanning lidar systems enables the resolving of individual tree crowns, which allows for the estimation of individual tree heights (St-Onge et al. 1999; Lim et al. 2001; Persson et al. 2002). Methods for extracting tree and forest stand data will continue to improve through a better theoretical understanding of the lidar response of forest canopies.

As well as stand height and volume, other forest attributes are being studied, notably biomass and vertical foliage distribution. Most of these studies were performed using full waveform lidar systems (e.g. Lefsky et al. 1999).

3. LIDAR SURVEY SPECIFICATIONS

No systematic satellite lidar data acquisition programs comparable to Landsat in the field of multi-spectral imagery currently exist. Lidar space missions are planned, however, for instance the Geoscience Laser Altimeter System (GLAS) (Carabajal and Harding 2001), and the Vegetation Canopy Lidar (VCL) (Dubayah et al. 1997; Luthcke and Rowlands 2001).

The acquisition of lidar data from airborne platforms (light aeroplanes or helicopters) requires input parameter specifications for both the lidar instrument and the flight configuration, in order to achieve the desired sampling pattern. For this reason, users specify lidar survey acquisition parameters in consultation with the survey provider. It is therefore essential that the user understand the implications of flight and acquisition parameters for the quality and usefulness of the lidar data collected for their application.

In this section, we provide a summary of the key parameters to consider and present a few principles for adequately matching needs and specifications.

3.1 Platforms

Current lidar missions are performed using small aircraft operating at low altitudes. While small aeroplanes and helicopters are regularly used, the former tend to be used more frequently. Each platform possesses certain advantages and disadvantages. Aeroplanes tend to provide better pitch and yaw stability, which translates into more regular flight lines with fewer gaps between adjacent flight lines. Helicopters provide slower air speeds, a factor that is very useful in providing a high density of pulse returns. Some lidar systems can be quickly attached to standard helicopters, such as the ALMIS-350 operated by Mosaic Mapping Systems Inc. (Ottawa). The ALTM series of instruments from Optech can be mounted on an aeroplane or helicopter and offers roll compensation.

3.2 Flight altitude

The flight altitude interval of current lidar systems is quite narrow. The minimum altitude at which the sensor can be operated is governed by eye safety regulations; this varies from design to design but a good rule-of-thumb is approximately 500 m above ground level (AGL). At the higher end, the power of the laser and the peak pulse energy become the limiting factors, as sufficient energy must reach ground level for a clear return to be detected and recorded. In addition, intervening cloud cover becomes an issue at higher altitudes as, unlike radar sensors, lidar systems cannot penetrate

clouds, thus limiting the available data collection hours in areas where low-lying clouds are an issue.

For commercial sensors, the maximum operating altitude is 6000 m, but in practice most systems are limited to 2000 m AGL. Research systems such as NASA's LVIS sensor operate at higher altitudes, up to 8,000 m, although this is a waveform capture design (Blair et al. 1999). It is also important to note that with all other parameters held constant, the return density, i.e. the number of laser echoes recorded per unit area, decreases as altitude is increased. Technological developments will no doubt help raise this maximum altitude.

Meanwhile, low flight altitude and near vertical incidence angles make for narrow swath widths, numerous flight lines, and relatively high costs, but, when paired with a high repetition rate sensor, allow for extremely high-density data collection (multiple returns per sq. m).

3.3 Flying speed

While minimum and maximum flying speeds are normally limited by the aircraft's design specifications, other considerations such as the pattern of laser returns on the ground are equally important. The return density is typically much higher along the scan lines (cross-track) than along the flight path (along-track). Flying at too great a speed will increase the discrepancy between the along- and across-track target pulse return densities. The gap between two consecutive scan lines at nadir could reach such a size that many trees would be omitted from the along-track direction (Evans et al. 2001), even though individual trees could be resolved in the across-track direction. If the aim is an ideal isotropic return density, then altitude, speed, pulse frequency, scan width and scan frequency must be considered and adjusted as a set. In addition, the scan pattern produced by the sensor must be considered.

The majority of commercial sensors employ a single axis scanning mirror driven by a galvanometer that produces a saw-tooth pattern on the ground, but there are sensors that use rotating polygon mirrors to produce equidistant sampling in a well-defined grid. This type of scan pattern can be desirable if isotropic sampling is a primary requirement of the research. Survey providers normally use special software applications to plan missions according to target pulse return densities.

3.4 Divergence and footprint size

Divergence is the rate at which the collimated laser beam's diameter increases with range. It is measured in milliradians (mr) and can be readily

converted to footprint diameter using aircraft-to-ground distance. Some recent commercial lidar systems (e.g. Optech ALTM 1225 and 2033) offer two divergence settings.

Footprint size, not divergence *per se*, is the determining factor in forest studies. Two conflicting objectives generally arise when seeking an optimal footprint size. These are: 1) achieving a high penetration rate and a high spatial resolution; and 2) hitting tree apices as often as possible. The first goal demands a small footprint while the second imposes a larger footprint size. The decreased probability of hitting tree apices with a very small footprint size tends to be compensated for with very high pulse return densities.

While footprint size does affect data characteristics, it does not greatly influence the accuracy of canopy height measurement within the most commonly applied range of settings, at least when using nadir viewing profilers (Aldred and Bonnor 1985). Footprint size will impact the horizontal accuracy (XY position) of the data due to spatial ambiguity within the footprint; increasing footprint size will increase this ambiguity. However for most small footprint (< 1 m) sensors this is not a major error contributor. Moreover, the narrow flying altitude intervals and rigid system settings do not permit much flexibility in footprint size. However, next-generation sensors already under development should increase the options in this area.

3.5 Pulse frequency

Pulse frequency is a characteristic of the pulsed laser itself. Technological improvements have brought about a rapid increase in pulse frequency for commercial systems. For example, the ALTM series from Optech has evolved from a 5 kHz frequency for the 1020 model in 1993 to 33 kHz for the 2033 model in 2001. Development is continuing, with 50 kHz sensors being field tested and due to be online by mid 2002 while some studies have predicted 100 kHz sensors will be available by 2005 (Flood 2001). Surveys are generally conducted with the pulse frequency set to maximum. However, optimal lidar sampling theory for forest studies has yet to be fully developed.

Improvement in pulse frequency enables more cost effective data acquisition on a per unit basis since flying height, within a modest range, can be increased as pulse return density improves. It also allows denser sampling for a low flying aircraft, which means that commercial lidar systems can now achieve several pulse returns per square meter. This in turn opens up new research possibilities, as ever-smaller individual tree crowns can be sampled. Increased pulse density also allows for better fidelity of ground models as increased pulse rates will increase the number of pulses that pass

through the canopy to the ground. This can be of increasing importance when dealing with very closed canopy or where there is significant understorey or ground cover.

3.6 Scan frequency, swath width, and overlap

The typical single axis oscillating mirror design results in a saw-tooth scan pattern. In order to maximize lidar energy penetration through vegetation cover to the ground level, it is preferable to limit incidence angles to 15-20 degrees off nadir. Penetration improves as the scan approaches nadir. Due to low flying altitudes and near vertical viewing angles, swath width is generally quite low (e.g. 115 m), but can be as wide as 2,180 m (Optech 2001). Swath width and scan frequency can be adjusted concurrently with altitude, aircraft speed and pulse frequency to produce, on average, anisotropic return densities. Optech's ALTM 2033 (released in 2001) has a maximum scan frequency of 90 Hz. If the lidar systems and flying parameters are set to: (i) full pulse frequency (i.e. 33 kHz) (ii) typical flying speed of 64 m/s; (iii) flying altitude of 500 m, (iv) scan frequency of 66 Hz; and (v) swath width of 115 m, an average posting distance (i.e. the distance between two consecutive pulse returns) of 0.48 m will result (Optech 2001). Sensors based on rotating polygon mirrors provide a much more regular grid pattern but require a more complex receiver design and so are less common in commercial use.

Swath overlap, or inter-flight line distance, should be set in such a way that the probability of gaps appearing between swaths is minimized. Large variations in return density for overlapping and non-overlapping regions of the survey can result in inconsistencies in data processing. To alleviate this problem, it is often recommended to set a goal of 50 % overlap between flight lines. This will not only double the return density, but will provide for a more even distribution of returns. Sensors that include roll stabilisation or a fully stabilised mount can usually reduce this overlap to 25 % - 35 % while maintaining full coverage. Flying twice to increase the density can also be considered. When possible, it is preferable to lay out the second pass flight lines perpendicularly to that of the first one (e.g. Næsset 2002).

4. LIDAR DATA CHARACTERISTICS AND QUALITY

4.1 Composition of lidar datasets

A discrete scanning lidar dataset is minimally composed of X,Y,Z triplets representing the location of each recorded echo for at least the first or last return from the emitted pulse. These data are generally delivered in ASCII files; however a major industry initiative was started in 2002 to adopt a common binary format for the delivery and exchange of lidar data. When implemented, this initiative should improve the accessibility of lidar data by reducing file sizes and providing a common exchange format, while also promoting the development of third-party software tools for data analysis and manipulation.

Currently, lidar data sets require interpolation if a continuous grid representation is desired. Most current lidar systems capture a first and last return for each pulse. While these are often divorced in typical data products because the bulk of lidar users are solely interested in ground returns for topographical purposes, there are advantages to retaining the two triplets representing the first and last returns in the same ASCII record. Several uses can be made of this pairing. For example, the depth of the traversed vegetation column (i.e. $Z_{\text{first}}-Z_{\text{last}}$), and/or the occurrence of bare ground (i.e. $Z_{\text{first}} = Z_{\text{last}}$) can be determined. Moreover, as mentioned above, we see more lidar systems that record the intensity (I) of the return energy. These values are normally proportional to the reflectance of surfaces. However, incidence angle effects on the footprint size and on the specular reflection component can also affect the quantity of returned energy. Intensity measurements can help in discriminating between deciduous and coniferous trees, with the return intensity being a function of the nature of the reflecting surface and the wavelength and angle of incidence of the emitted lidar signal. However, the algorithms used to trigger first and last pulse recordings based on characteristics of the return signal may also affect the intensity value, as do variations in the transmitted pulse energy. It would be desirable that lidar manufacturers publish these algorithms and explicate how the radiance measured by the sensor is normalized (or not) and converted to digital numbers.

4.2 Spatial resolution and accuracy

Spatial resolution for typical remotely sensed data is dependent upon the size of the instantaneous field of view (IFOV). In the case of lidar, spatial resolution is determined by: (i) the footprint size; and (ii) the posting distance. This latter parameter is the primary factor defining spatial resolution for interpolated lidar elevation or intensity surfaces. Spatial resolution is used here to designate the extent to which details of canopy surface topography can be resolved. Footprint sizes from scanning lidar systems are typically just a few centimetres wide (15-50 cm). If such small footprint pulse returns were touching or overlapping, individual branches could easily be resolved. Normally, the average posting distance is of the order of one to a few meters.

A few important characteristics of the pulse return spatial distribution should be noted. First, laser returns are not evenly distributed over the area surveyed. The scan pattern, the attitude variation of the aircraft, the lost returns due to deflection, the topography of both the terrain and canopy surface, and the random manner in which incident pulses from two adjacent flight lines will criss-cross, all compound to distribute the pulse returns in unpredictable and uncontrollable semi-irregular patterns. Some patches might, for example, receive more than 10 pulse returns/m² while areas of several square meters might be devoid of any pulse returns. It is common to report resolution equivalents in the form of pulse return densities or average posting distance rather than in terms of IFOV or true spatial resolution. Rarely do authors state the variations around these average figures or report on the size of the largest lidar gaps. The irregular layout can seriously impact data quality, especially at low pulse return densities. Research on the effects that follow from this disorderliness are just beginning (e.g. Evans et al. 2001).

Lidar is, however, a very accurate instrument. Manufacturers and data providers report absolute elevation accuracies of 15 cm and even better relative accuracies. In the commercial sector, vertical accuracy is generally taken by system manufacturers to be a 1σ statistical measure of the sensor's accuracy against a known ground target, while data providers generally quote a 2σ or 95 % confidence level closer to 20 cm. Vertical accuracy of lidar data varies with vegetation cover and topography; in addition, the error budget for a lidar sensor is quite hard to establish (Shenk 2000).

Two sets of factors can affect elevation accuracy: system related and target related. Errors from the lidar system include ranging error, GPS error, timing errors and mounting error, which consists of errors in determining the offset between the onboard GPS antenna and the lidar system itself. By far the largest cause of "bad" lidar datasets is a poor GPS solution. A good GPS

solution is a necessary but not sufficient condition if any reasonable accuracy is to be expected from the lidar data; conversely, a poor GPS solution generally degrades the dataset quality, often significantly so. It is critical, when working with lidar data providers, to ensure they implement proper GPS planning (PDOP windows, baseline lengths etc).

Target related errors include slope-induced errors (i.e. error is known to increase with terrain slope), classification errors and uncertainty in precisely defining the first and last return ranges. Of these, classification errors produce the largest discrepancies between "true" and "observed" terrain elevations (see section 5.1). The impact of elevation errors on our capacity to accurately estimate stand height remains to be investigated.

Planimetric (i.e. X, Y) errors are known to be approximately five times greater than their elevation counterpart (Baltsavias 1999). As a rule of thumb, absolute planimetric errors are approximately 1/2000 of the above-ground altitude of the aircraft.

5. LIDAR DATA PRE-PROCESSING

Stages of pre-processing normally required to prepare lidar data for predicting stand parameters include: (i) calculation of a precise platform trajectory from the differential GPS solution; (ii) computation of the X,Y,Z values from in-flight ranging and combined GPS and INS data; (iii) classification of the pulse returns and (iv) interpolation of ground and vegetation returns. The survey provider will deliver X,Y,Z triplets and will very often carry out the classification. However, there are advantages to retaining control over the classification in order to test different classification parameter values.

Most data providers will deliver classified and unclassified datasets if requested. Unfortunately, classification software, such as Optech's REALM™ (Optech Inc., Toronto, Canada) or TerraScan™ (TerraSolid Inc., Helsinki, Finland) are proprietary to sensor owners (REALM) or still quite expensive to acquire (TerraScan). Lidar classification functions are not currently part of any common image processing software package, although this functionality will probably become standard over the next few years.

The user most often carries out interpolation of the lidar returns, using either their own code or routines available in the public domain. Here again, control over interpolation methods is preferable. Finally, lidar data volumes are considerable. Relatively modest datasets are composed of millions, or tens of millions of return triplets. A standard desktop computer is not designed to process lidar data in these quantities. Even for small study areas, a workstation with considerable disk capacity (60 GB); RAM (2 GB); and

CPU speed (1 GHz) is recommended for efficient processing of lidar data. These requirements will undoubtedly increase as study areas become larger (e.g. for operational surveys) and sample density increases.

5.1 Classification of lidar pulse returns

Classification, also referred to as “filtering”, essentially consists of assigning a particular return to ground level or to some other feature on the surface. Most often, it is carried out automatically using classification software, but manual interventions are still required for, among other things, building and vegetation removal. Classification techniques were initially developed in order to produce “bare-earth” digital elevation models (DEMs) and are still being perfected. For forest applications, classification relies on the following simple rationale: the lowest returns in a small neighbourhood will be ground, while the rest will correspond to vegetation, buildings or infrastructure. The approach consists of identifying which returns are most likely to correspond to ground level, and to assume that all other returns correspond to something else. In natural landscapes, these other returns are assumed to be vegetation.

Most classification algorithms use iterative statistical or morphological algorithms operating over window-based kernels. As an example, we describe here the algorithm used by the TerraScan™ software (TerraSolid Ltd., Helsinki, Finland). TerraScan™ is relatively affordable and widespread. The algorithm is published by Axelsson (2000).

After an initial coarse classification to remove gross errors (high and low points, or points outside the known range of expected returns), the algorithm builds a sparse TIN (Triangulated Irregular Network) from a subset of lidar pulse returns that are considered “sure pulse returns on the ground” (TerraSolid 2001). This initial subset is composed of the lowest points in each cell of a user defined virtual grid that is superimposed onto the dataset. Most triangular facets of this first TIN will be below the ground level. Returns are then added iteratively by selecting new points and rebuilding the TIN, with point selection based on angle and distance thresholds. The angle threshold consists, at the maximum, of the angle formed by a line joining a candidate point to the closest vertex of the facet on which it downwardly projects, and the line joining this vertex to the point projection location on the same facet. It is often suggested that different angle threshold values be used depending on the nature of the topography. The maximum distance threshold controls the single-iteration upward evolution of the TIN by limiting the vertical distance between a candidate point and the surface of the facet on which it vertically projects. The steepest allowable terrain slope also controls the algorithm. We have tested both TerraScan™ and

REALM™ on double return data acquired with Optech's ALTM1225. Both software packages classified dense bushes, which were virtually impenetrable by the lidar pulse, as ground. This finding is similar to that of Pfeifer et al. (1999). It led to the presence of conspicuous bumps on the otherwise smooth DEM. It supports our contention that automated classification for DEM generation requires further refinement.

5.2 Interpolating lidar pulse returns

Lidar data is typically composed of millions of X, Y, Z data points. While these can be visualised as point clouds, raster grid representations are usually more readily interpreted. Moreover, measuring tree or canopy heights requires that the elevation difference between the top of canopy and ground level be measured. Theoretically, it is close to impossible for a ground return to be recorded directly under a vegetation return located on a tree apex. For this reason, it is practical, and very common, to interpolate the ground returns to form a DEM. In most cases, TIN or spline interpolation (e.g. Magnussen et al. 1999) is used. Height is then obtained by computing the elevation difference between each vegetation pulse return and the underlying grid cell's elevation. Canopy pulse returns can also be interpolated, but more restrictive conditions apply.

Interpolation of vegetation returns is far more complicated than that of ground returns as the goal is to reconstruct the canopy surface to create a canopy surface model (CSM). Interpolation of the CSM to a raster grid greatly reduces the size of the lidar dataset and also allows for the application of standard raster GIS and remote sensing algorithms. It is our opinion that only very dense lidar vegetation pulse return datasets should be interpolated in this fashion. Once they are, the interpolated ground can be subtracted from the interpolated canopy to produce a canopy height model in which each pixel represents the height above ground of the canopy. Figure 19-1A gives an example of a canopy height model for a patch of forest also presented on an orthophoto (Figure 19-1B).

6. ESTIMATING CANOPY, STAND, AND INDIVIDUAL TREE HEIGHT

Tree height remains a primary attribute for forest inventory and timber volume estimation (Aldred and Bonner 1985; Schreier et al. 1985) and is one of the main factors determining light interception and inter-tree competition (Spurr and Barnes 1980). It is therefore not surprising that the estimation of

tree and canopy height using lidar data has received more attention than that of any other forest metric. Height estimation methods have been tested at different spatial scales (i.e. individual tree, plot, stand), with relatively positive results. Many authors have reported that lidar underestimates stand height (e.g. Nilsson 1996; Næsset 1997), which is in our opinion, and in light of the theoretical work done by Magnussen and Boudewyn (1998) and Magnussen et al. (1999), a statement which requires qualification.

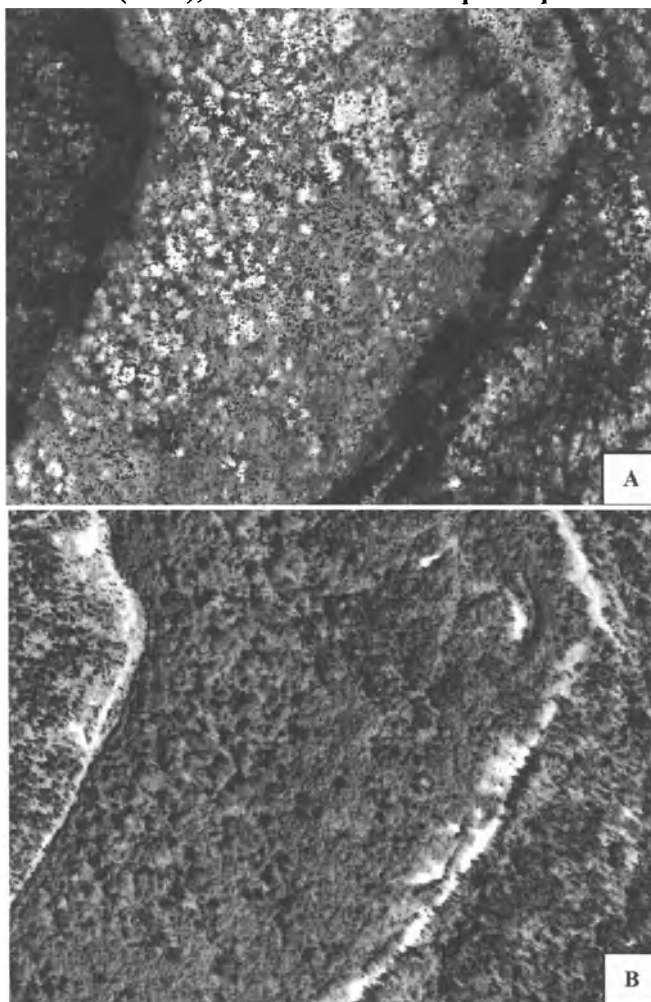


Figure 19-1. Lidar canopy height model of a forest patch located in Green River, New-Brunswick, Canada (with brightness proportional to canopy height) (A), and Orthophoto of the same patch (B).

6.1 Basic concepts and rationale

A tree is a discrete object for which boundaries can be established readily in the field. The height of an individual tree is simply the elevation difference between its ground level base and its apex. What constitutes canopy height or stand height is less straightforward. For clarity, we will use the following concepts: *canopy surface height*, *mean canopy height*, *mean tree height* and *Lorey's height*.

Canopy surface height refers to the “outer canopy envelope” containing the underlying vegetation volume. The height of a point on the canopy surface is the length of a vertical line that extends from the idealised canopy surface down to the ground level. We will call this point measure “canopy surface height” or, more simply, “canopy height” after Magnussen and Boudewyn (1998), and Magnussen et al. (1999). In this regard, lidar first returns (minus ground elevation) are considered a sample of the complete canopy height distribution (Magnussen et al. 1999).

Mean canopy height consists of the mean height of all canopy surface points. *Mean tree height* is simply the average height of all trees within a given area, while *Lorey's height* is defined as the basal area weighted average tree height within an area (Næsset 1997).

Having defined the key terms and concepts, we can now state the general problem. We have seen that the sampling pattern of a scanning lidar is semi-random and that only a small fraction of the canopy surface is intercepted by laser pulses. Most pulses miss tree apices. Hence, the average height of lidar (i.e. vegetation) first returns is primarily an estimator of mean canopy height, and can in no way be *directly* related to mean tree height nor Lorey's height. For this reason, it can be misleading to state that “lidar underestimates stand height”. This also means that we must find a way to predict, for example, Lorey's height by stand or forest polygon, or individual tree heights, using semi-random point samples of canopy surface height. It translates into a search for a method that can identify the most useful lidar returns and/or an unbiased statistical estimator of tree height, whether at the stand or tree level. These simple statements of complex problems have been rigorously formalised by Magnussen and Boudewyn (1998) and Magnussen et al. (1999).

6.2 Point estimates of canopy height

Before examining how stand or individual tree heights can be extracted from semi-random point patterns, we raise the issue of the accuracy of point estimates of canopy heights. In other words, what is the canopy height

accuracy of a single lidar pulse return? This matter has, to our knowledge, never been studied empirically in the case of forest canopies.

The uncertainty of the planimetric position of single pulse returns renders field validation extremely difficult (Filin 2001). The other problem relates to the definition of a canopy surface, which, as discussed above, is an abstraction. Stating the problem in more theoretical terms, we ask the question, “what is the minimum amount of tree material (cumulative, one side projected, leaf and twig/branch surface) required so that a single incident pulse will generate sufficient returned energy to trigger a first return recording?” The corollary question is “how deep must a single pulse travel below an idealised canopy surface before a first return is recorded?” A number of key parameters that affect the analysis of this problem include: (i) laser energy and its distribution; (ii) first-return detection algorithms and appropriate critical thresholds; (iii) foliage density or LAI; (iv) foliage reflectance; and (v) incidence angle.

Concerning tree material density, Magnussen and Boudewyn (1998) report an approximate measure of “1 m² of needle surface (one-side projected) per 1 m² of crown surface and per 1 m³ of crown volume” (p. 1018) for a 49 year old plantation of Douglas-fir (*Pseudotsuga menziesii* [Mirb.] Franco). This strongly suggests that first returns have a Z position that is at least a little below the elevation of the first needles in the case of conifers. It also indicates that a pulse intersecting a conifer apex directly would probably yield a Z value below the apex. The implication is that mean canopy height estimates, based on average lidar heights, are probably biased to provide a lower height estimate, a fact that is not often recognised. Therefore, when estimating stand-wise Lorey's height from lidar heights issues to consider include: 1) that pulse returns usually fall on tree sides (not apices); and 2) that they penetrate the canopy surface to a certain extent.

6.3 Stand height

Practical methods for estimating stand height from lidar data resemble other remote sensing methods in that they require field calibration. Obviously, a height recovery model that could work with lidar data input alone would be ideal. Two such models were proposed and tested by Magnussen et al. (1999). Although results were encouraging, these models “hinge on a series of simplifying assumptions that naturally limit their application domain” (p. 415), i.e. they are applicable to idealised monospecific stands of trees with solid conical crowns. Empirical approaches based on simple heuristics have also been quite successful.

Window-based quantile estimators are clearly the most common approach for measuring stand height (Aldred and Bonnor 1985; Nilsson

1996; Næsset 1997; Magnussen and Boudewyn 1998; Næsset 2002). Although influenced by crown shape (tree species), stand density and stand structure (Nelson 1997), window-based quantile estimators can be designed to generate unbiased estimates of Lorey's height (Magnussen and Boudewyn 1998).

The method consists of determining a quantile of the lidar canopy height distribution that will reliably reflect average stand height. For kernels of various sizes operating on a lidar canopy height dataset, the lidar canopy height observation corresponding to the n^{th} quantile is taken as the local value of stand height. The stand-wise average of all kernel-extracted n^{th} quantile lidar observations is then computed. Both the precise quantile and the optimal kernel generally have to be identified through trial and error (Næsset 1997). Most studies report optimal window sizes around 20 m x 20 m and quantiles from 85 % to 95 %.

Calibration for such studies usually consists of measuring a few dozen stands for which 10-20 plots are sampled in the field. The lidar predictor is established on a stand basis, and not by comparing lidar windows to field plots. This approach is influenced by species and canopy structure, so calibration should incorporate the majority of stand types to produce a general-purpose estimator. This methodology is also known to be fairly robust with respect to lidar pulse return density. Positive results have been obtained with older lidar systems such as the ALTM1020, with canopy pulse return densities of 6-14 returns per 100 m² (Magnussen and Boudewyn 1998). This would allow measuring stand heights from low density, large area lidar surveys. Higher densities should, however, yield greater spatial precision and higher accuracies.

6.4 Individual tree height

Attempts to estimate individual tree heights for large areas may seem overly ambitious. However, Magnussen and Boudewyn (1998) demonstrate that the optimal quantile estimator is dependent on forest structure, the vertical distribution of LAI, and other variables for which accurate values are not normally available. This puts an upper limit on the accuracy of the grid-based methods for evaluating stand height. If the height of all trees emerging from the canopy could be estimated, then stand height estimation would be less influenced by forest structure. Furthermore, if the height of trees could be measured over a given area, significant insight could be gained into the structure of forest canopies, since height distributions and accurate stem maps (of visible trees) could be easily generated. This would undoubtedly open up new research possibilities in forest ecology. It could

also replace, in some cases, field measurements of forest inventory plots or assist in calibration of lower density / wider coverage lidar surveys.

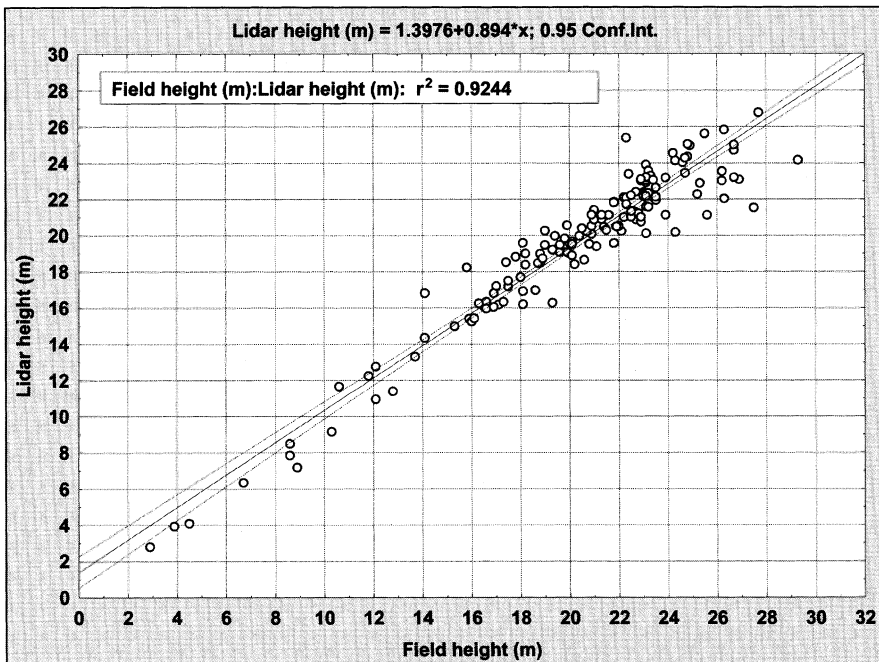


Figure 19-2. Scatter plot of field- and lidar-derived individual tree heights including regression line (reproduced with permission from Lim et al. 2001)

Individual tree height estimation is a relatively new area of research, as lidar systems that can provide sufficiently dense coverage have only recently entered the market. To our knowledge, only a few studies have addressed this issue (St-Onge 1999; Lim et al. 2001; Andersen et al. 2002; Persson et al. 2002). Results are encouraging, with typical field/lidar RMSE values approaching those of field-based measurements. In general, all attempts rely on identifying the highest lidar pulse in single crowns and comparing these values to the heights of the corresponding trees on the ground. As for stand height estimation, the fact that most pulse returns will be on the side of trees, and not on the apices, constitutes a problem. The probability of a pulse return falling close to a tree apex, however, increases at high pulse density. To alleviate this problem, field measurements are regressed against lidar estimations to produce a predictive equation (e.g. Figure 19-2). Coefficients of determination (r^2) for these are usually quite high (i.e. $r^2 \geq 0.90$).

7. SUMMARY AND CONCLUSIONS

Tree and canopy heights are an important attribute for studies of forest structure and function. Height information may be used as an attribute or as an input to allometric equations for estimates of volume and biomass. Advances in GPS and inertial navigation systems now allow for accurate positioning of each lidar pulse return. High frequency lidar pulse rates now enable high pulse return densities while maintaining a relatively wide data swath. Improvements in lidar technology and processing techniques have combined to position lidar as a valuable tool for the monitoring of forest structure and function.

As presented in this Chapter, there is currently a reliable suite of techniques available, based largely upon quantile estimators, for estimating tree and canopy height. Improvements in lidar data processing methods are additive in nature. Future improvements may be made to lidar sensors and the raw data generated, to processing of the point cloud to determine ground and canopy models, to the creation of interpolated surfaces from the point data, and finally to the conversion of surfaces to grids. Improvements in these aspects will ultimately improve the height estimation of forest stands and individual trees. Techniques for the improvement of estimates of tree and canopy height will no doubt be an ongoing research endeavour.

REFERENCES

- Aldred, A., & Bonner, M. (1985). Application of airborne lasers to forest surveys, *Information Report PI-X-51*, Canadian Forestry Service, Petawawa National Forestry Centre.
- Andersen, H. -E., Reutebuch, S. E., & Schreuder, G. F. (2001). Automated individual tree measurement through morphological analysis of a lidar-based canopy surface model. *Proceedings of the First International Precision Forestry Symposium*, 11-22. June 17-20, 2001, Seattle, WA.
- Axelsson, P. (2000). DEM generation from laser scanner data using TIN adaptive models. International Archives of Photogrammetry and Remote Sensing. *Proceedings of the International Society of Photogrammetry and Remote Sensing XIXth Congress*, B4, 110-117, Amsterdam, Netherlands.
- Baltsavias, E. P. (1999). A comparison of between photogrammetry and laser scanning. *ISPRS Journal of Photogrammetry and Remote Sensing*, 54, 83-94.
- Blair, J. B., Rabine, D., & Hofton, M. (1999). The Laser Vegetation Imaging Sensor (LVIS): a medium-altitude, digitization only, airborne laser altimeter for mapping vegetation and topography. *ISPRS Photogrammetry and Remote Sensing*, 54, 115-122.
- Carabajal, C. C., & Harding, D. J. (2001). Evaluation of Geoscience Laser Altimeter System (GLAS) waveforms for vegetated landscapes using airborne laser altimeter scanning data. *Proceedings of the Land Surface Mapping and Characterization using Laser Altimetry, Joint Workshop of ISPRS III/3 and III/6*, 125-128. October 22-24, Annapolis, MD.

- Dubayah, R., et al. (1997). The Vegetation Canopy Lidar Mission. *Land Satellite Information in the Next Decade II: Sources and Applications*, 100-112 American Society for Photogrammetry and Remote Sensing, Bethesda, MD.
- Evans, D., Roberts, S., McCombs, J., & Harrington, R. (2001). Detection of regularly spaced targets in small-footprint lidar data: Research issues for consideration. *Photogrammetric Engineering and Remote Sensing*, 67, 1133-1136.
- Filin, S. (2001). Recovery of systematic biases in laser altimeters using natural surfaces. *Proceedings of the Land Surface Mapping and Characterization using Laser Altimetry, Joint Workshop of ISPRS III/3 and III/6*, 85-91. October 22-24, Annapolis, MD.
- Flood, M. (2001). Lidar activities and research priorities in the commercial sector. *Proceedings of the Land Surface Mapping and Characterization using Laser Altimetry, Joint Workshop of ISPRS III/3 and III/6*, 3-7. October 22-24, Annapolis, MD.
- Harding, D. J., Lefsky, M. A., Parker, G. G., & Blair, J. B. (2001). Laser altimeter canopy height profiles: Methods and validation for closed-canopy, broadleaf forests. *Remote Sensing of Environment*, 76, 283-297.
- Hese, S., & Lehman, F. (2000). Comparison of digital surface models of HRSC-A and LASER scanner for forest stand characteristics. International Archives of Photogrammetry and Remote Sensing. *Proceedings of the International Society of Photogrammetry and Remote Sensing XLXth Congress*, 33-Part B7/2, 525-532. Amsterdam, Netherlands.
- Hill, J. M., Graham, L. A., & Henry, R. (2000). Wide-area topographic mapping and applications using airborne light detection and ranging (LIDAR) technology. *Photogrammetric Engineering and Remote Sensing*, 66, 908-914.
- Hyppä, J., Hyppä, H., Inkinen, M., Engdahl, M., Linko, S., & Yi-Hong, Z. (2000). Accuracy comparison of various remote sensing data sources in the retrieval of forest stand attributes. *Forest Ecology and Management*, 128, 109-120.
- Kraus, K., & Pfeifer, N. (1998). Determination of terrain models in wooded areas with airborne laser scanner data. *ISPRS Journal of Photogrammetry and Remote Sensing*, 53, 193-203.
- Lefsky, M. A., Cohen, W. B., Acker, S. A., Parker, G. G., Spies, T. A., & Harding, D. (1999). Lidar remote sensing of the canopy structure and biophysical properties of Douglas-fir western hemlock forests. *Remote Sensing of Environment*, 70, 339-361.
- Lefsky, M., Cohen, W., & Spies, T. (2001). An evaluation of alternate remote sensing products for forest inventory, monitoring, and mapping of Douglas-fir forests in western Oregon. *Canadian Journal of Forest Research*, 31, 78-117.
- Lim, K., Treitz, P., Groot, A., & St-Onge, B. (2001). Estimation of individual tree heights using LIDAR remote sensing. *Proceedings of the Twenty-Third Annual Canadian Symposium on Remote Sensing*, Quebec, QC, August 20-24, 2001 (CD-ROM).
- Lim, K., Treitz, P., Wulder, M., St-Onge, B., & Flood, M. (2002). LiDAR remote sensing of forest structure. *Progress in Physical Geography*, in press.
- Luthcke, S., & Rowlands, D. (2001). Spaceborne laser altimeter instrument parameter calibration from integrated residual analysis. *Proceedings of the Land Surface Mapping and Characterization using Laser Altimetry, Joint Workshop of ISPRS III/3 and III/6*, 81-83. October 22-24, Annapolis, MD.
- MacLean, G. A., & Krabill, W. B. (1986). Gross-merchantable timber volume estimation using an airborne LiDAR system. *Canadian Journal of Remote Sensing*, 12, 7-18.
- Magnussen, S., & Boudewyn, P. (1998). Derivations of stand heights from airborne laser scanner data with canopy-based quantile estimators. *Canadian Journal of Forest Research*, 28, 1016-1031.

- Magnussen, S., Eggermont, P., & LaRiccia, V. N. (1999). Recovering tree heights from airborne laser scanner data. *Forest Science*, 45, 407-422.
- Means, J. E., Acker, S. A., Harding, D. J., Blair, D. B., Lefsky, M. A., Cohen, W. B., Harmon, M. E., & McKee, W. A. (1999). Use of large-footprint scanning airborne LiDAR to estimate forest stand characteristics in the Western Cascade of Oregon. *Remote Sensing of Environment*, 67, 298-308.
- Næsset, E. (1997). Determination of mean tree height of forest stands using airborne laser scanner data. *ISPRS Journal of Photogrammetry and Remote Sensing*, 52, 49-56.
- Nelson, R., Krabill, W., & Maclean, G. (1984). Determining forest canopy characteristics using airborne laser data. *Remote Sensing of Environment*, 15, 201-212.
- Nilsson, M. (1996). Estimation of tree heights and stand volume using an airborne lidar system. *Remote Sensing of Environment*, 56, 1-7.
- Ni-Meister, W., Jupp, D. L. B., & Dubayah, R. (2001). Modeling lidar waveforms in heterogeneous and discrete canopies. *IEEE Transactions on Geoscience and Remote Sensing*, 39, 1943-1958.
- Nelson, R., Swift, R., & Krabill, W. (1988). Using airborne lasers to estimate forest canopy and stand characteristics. *Journal of Forestry*, 86, 31-38.
- Næsset, E. (1997). Determination of mean tree height of forest stands using airborne laser scanner data. *ISPRS Journal of Photogrammetry and Remote Sensing*, 52, 49-56.
- Næsset, E. (2002). Predicting forest stand characteristics with airborne scanning laser using a practical two-stage procedure and field data. *Remote Sensing of Environment*, 80, 88-99.
- Optech (2001). *ALTM 2033 Brochure*, Optech Inc., Ontario, Canada.
- Persson, Å., Holmgren, J., & Söderman, U. (2002). Detecting and measuring individual trees using an airborne laser scanner. *Photogrammetric Engineering and Remote Sensing*, in press.
- Pfeifer, N., Reiter, T., Briese, C., & Rieger, W. (1999). Interpolation of high quality ground models from laser scanner data in forested areas. *ISPRS Workshop on "Mapping surface structure and topography by airborne and spaceborne lasers"*, Commission III, Working Group 3, 31-36. La Jolla, Calif., 9-11 Nov. 1999.
- Schreier, H., Lougheed, J., Tucker, C., & Leckie, D. (1985). Automated measurements of terrain reflection and height variations using an airborne infrared laser system. *International Journal of Remote Sensing*, 6, 101-113.
- Solodukin, V. I., Kulyasov, A. G., Utenskov, B. I., et al. (1977). S"emka profilya krony dereva s pomoshch'yu laszer-nogo dal'nomera (Drawing the crown profile of a tree with the aid of a laser). *Lesn. Khoz*, 2, 71-73.
- Spurr, S. H., & Barnes, B. V. (1980). *Forest Ecology*, (3rd ed.). Krieger Publishing Company, Florida.
- St-Onge, B. (1999). Estimating individual tree heights of the boreal forest using airborne laser altimetry and digital videography. *ISPRS Workshop on "Mapping surface structure and topography by airborne and spaceborne lasers"*, Commission III, Working Group 3, 179-184. La Jolla, Calif. 9-11 Nov. 1999.
- St-Onge, B., & Renaud A. (2001). Estimating merchantable timber volume of aspen and spruce stands of the boreal forest using airborne laser altimetry. *Proceedings of the Twenty-Third Annual Canadian Symposium on Remote Sensing*, Quebec, QC, August 20-24, 2001 (CD-ROM).
- Wehr, A., & Lohr, U. (1999). Airborne laser scanning-an introduction and overview. *ISPRS Journal of Photogrammetry and Remote Sensing*, 54, 68-82.
- Wulder, M. (1998). Optical remote sensing techniques for the assessment of forest inventory and biophysical parameters. *Progress in Physical Geography*, 22, 449-476.

Chapter 20

REMOTE SENSING OF FOREST ENVIRONMENTS, CONCLUSIONS.

Challenges and Opportunities

Steven E. Franklin¹ and Michael A. Wulder²

¹Department of Geography, University of Calgary, Calgary, Alberta, T2N 1N4, Canada

²Canadian Forest Service (Pacific Forestry Centre), Natural Resources Canada, Victoria, British Columbia, V8Z 1M5, Canada

1. CONTEXT FOR DECISION-MAKING

Remote sensing has emerged, in only a few decades, as one of the premier observational and analytical tools for use in scientific understanding and managing of the world's forests. The widespread use of image data has been accompanied by the occasional request, by remote sensing scientists and forest practitioners alike, for solid evidence and examples to support the 'practical applications of remote sensing of forests'. To us, the practicality in remote sensing of forests is now virtually self-evident as the material in this book and other sources have become increasingly convincing. Never before have forest managers and scientists had more ready access to their forests through remotely sensed information acquired at multiple spatial and temporal scales, in analogue and digital forms, linked to ground observations, GIS data, and models, and tied to management or science objectives that range from the straightforward (where do we plan roads and harvest activities?) to the extraordinary (can we map nutrient status and photosynthetic capacity?). And not a moment too soon; the world's forests have never before faced such overwhelming challenges to their continued existence and healthy functioning. We need information, of a variety and richness never before contemplated, if we are to provide the scientific and technological answers required to preserve and maintain forest ecosystems for continued environmental and economic benefits. Only remotely sensed

data, handled by knowledgeable practitioners working in concert with field data and existing inventories, can feasibly provide the necessary information to ensure adequate context for continued management decisions at a variety of scales and in response to human values.

Remote sensing of forests begins with a well-designed data collection and data preparation activity; collecting the right data to answer well-defined questions. These questions are increasingly driven by those seeking insight into processes that operate in forests; photosynthesis, hydrology, nutrients, physical weathering, disturbances, and so on. Acquiring the right data for questions about these processes and others is an enormous task; understanding the appropriate role of remote sensing, and the types of remote sensing data, are absolutely essential before embarking on any data collection exercise. Uppermost are questions of data quality and resolution, repeatability, and validation. In many forest applications, there are few or no substitutes for ground data; there are few or no substitutes for aerial photographs; and there are few or no substitutes for remotely-sensed data. Each has a role to play; each can be designed optimally to satisfy different aspects of the information we seek to understand and manage forests. Fortunately, there are only better and better ways of integrating these different forms of data to create information products unavailable in any other way. Is it conceivable that national reporting of carbon budgets, for example, can be accomplished without inputs of both field and remotely-sensed data?

Such work requires minute attention to critical issues of data preparation and processing; geometric registration, calibration and atmospheric correction, choice and implementation of image analysis algorithm and approach. This book addresses the conceptual framework and specific case studies which represent successful remote sensing of forest environments at multiple scales. Our intention was to provide the reader with at least a taste of some of the myriad of issues that must be addressed – prior to embarking on the data analysis, and as part of the analysis protocol. Too often in the past, data analysis failed or provided only partial return on investment simply because the data were inadequately prepared or collected, with initial flaws that were simply too numerous or substantial to overcome later. In this book, the concepts and case studies merge into a well-documented resource to avoid this situation completely; here we discuss and highlight ‘best-practices’ as they have come to be understood and applied in a wide variety of the world’s forests, at several scales, and under different management regimes.

Remote sensing is not a static science, but instead is continually improving. The concepts and case studies presented here are thought to represent a reasonably complete summary of the existing and near-future

operational applications, and the supporting principles, of remote sensing in forest environments. Some of the gaps are obvious; radar remote sensing has improved and will continue to grow in importance as new sensors and methods of handling radar data are developed. Radar data have long been considered complementary to optical sensor data (Dobson 2000); there are early signs that such multiple sensing systems provide synergies far beyond what simple data redundancy algorithms have predicted. Unfortunately, because of space limitations, little has been said on the use of remote sensing for landscape structural analysis and quantification of forest fragmentation, wildlife habitat mapping, biomass, and biodiversity assessment (Dallmeier and Comiskey 1998). These applications are at the forefront of the research agenda as remote sensing information cuts across most disciplinary boundaries and finds value in supporting multidisciplinary perspectives on forests (Franklin 2001).

2. OPPORTUNITIES FOR IMPROVEMENT

Fifty years ago, forest managers were engaged in incorporating aerial photographs into their available tool-box; the result was the modern aerial-photo-based forest and vegetation inventories that have assumed such a prominent role in tactical, strategic, and day-to-day management decision making and information gathering. Twenty years ago there may have been a passing reference to available satellite imagery or a specialized aerial mission to acquire some crucial piece of information – typically at spatial or temporal scales not readily addressed by aerial photography. Today, it is not unrealistic to consider consulting assembled field data, aerial data, satellite data, model outputs, and GIS databases to answer questions about forests of far greater complexity and importance than could previously be considered. Issues of biodiversity and forest ecosystem health, embodied in the many criteria and indicators and forest certification initiatives (Vogt et al. 1999), for example, have all but guaranteed that the work is not yet complete.

What remains to be done? The promise of remote sensing has always been the routine collection of data, ready conversion of data to information, wise use of that information by knowledgeable decision-makers, and the distribution of the accumulated wisdom to improve the entire process and the well-being of humans and forests alike. Improvements are necessary in every aspect of the enterprise; presently, data collection cannot yet be called routine; conversion of data to information is anything but 'ready'; the acquired information sometimes does not even reach the decision-makers, let alone be used by them wisely; and the knowledge distribution process is not anywhere near optimal. The specialized remote sensing language alone,

surprisingly well-developed in only a short time of intense activity, can be considered an impediment to shared understanding. Remote sensing software systems are often byzantine; data linkages are typically empirical and local; models are black-boxes; image analysis methods are sometimes only poorly documented. But reasonably straightforward steps can be taken to bridge these gaps. For instance, those who do understand the science and application of remotely sensed imagery in the characterization of forests, can engage in non-traditional communication activities. The communication of the issues that outline the potential and limits of remotely sensed data on an application specific basis is useful for non-experts interested in using image data. Communication of applications success stories is also a means to illustrate what can be done in a particular situation, allowing new users to build applications around successful methodological examples. Understanding user needs is perhaps the best way to ensure that the applications developed continue to address issues of interest and importance, and contribute to successful forest science and management applications.

The broad range and significance of remote sensing to support science and management of the world's forest environments have increased almost exponentially in recent times. Our emphasis in this book has been on documenting these achievements in remote sensing and at the same time focusing on practical questions. Successful remote sensing applications are driven by understanding and balancing the myriad of issues associated with image radiometry, geometry, geospatial data characteristics, and analysis methods. While summarizing current understanding and highlighting the emerging research agenda, it is important to acknowledge the early efforts by the many developers and practitioners of remote sensing science and technology. Their work has provided the solid foundations upon which the present accomplishments have been made and which help ensure continued value in applying remote sensing to forest environments.

REFERENCES

- Dallmeier, F., & Comiskey, J. A. (1998). *Forest Biodiversity in North, Central, and South America and the Caribbean: Research and Monitoring*. Volume 21. UNESCO and the Parthenon Publ. Group. New York, USA.
- Dobson, M. C. (2000). Forest information from synthetic aperture radar. *Journal of Forestry*, 98, 41-43.
- Franklin, S. E. (2001). *Remote Sensing for Sustainable Forest Management*. Lewis Publishers/CRC Press. Boca Raton, FL, USA.
- Vogt, K. A., Larson, B. C., Gordon, J. C., Vogt, D. J., & Fanzeres, A. (1999). *Forest Certification: Roots, Issues, Challenges, Benefits*. CRC Press. Boca Raton, FL, USA.

Index

A	
Accuracy assessment	67, 115, 399
Confidence intervals	136
Cross-validation	399
Definition of types	118
Error matrix	118
Field data	435
Large area land cover	351, 405
Map classifier	117
Map object	117
Model predictions	423
Reference classifier	118
Sampling	115, 121
Steps to perform	120
With video data	477
Advanced Very High Resolution Radiometer (AVHRR)	27, 338, 366, 420
Burn mapping	372
Aerial photography	47
Change detection	310
Digital analyses	256
Film types	51
Interpretation	470, 478
Aerial videography	470
Airborne Visible Near-Infrared Imaging Spectrometer (AVIRIS)	224, 452
Atmospheric correction	343
Models	344
Attributes	
Biodiversity	469
Biomass	36, 417, 492
Canopy cover	34
Carbon	359, 375, 415
Chlorophyll	457
Cover-type	394, 417
Crown closure	48, 217, 284
Forest composition	37
Forest structure	359
Forest type	256, 283
Forest type by structure	283
Height	35, 492
Individual tree height	492, 505
Land cover	183, 256, 279, 283, 351, 390, 470
Mappable by spatial resolution	284
Species	256
Stand height	504
Stem density	456
Tree spatial distribution	256
Vertical foliage distribution	492
Volume	36, 256, 492
Wildlife habitat quality	256
B	
Bi-directional reflectance distribution function (BRDF)	15, 190, 243, 347
Boreal Ecosystem Productivity Simulator (BEPS)	376
Brightness	<i>See</i> Tasseled cap
C	
Canopy reflectance model	241
Carbon estimation models	378
Change detection	38, 301
Canopy morphology	327
Change vector analysis	314
Classes	301
Data characteristics	366
Identification of type	319
Land cover	365
Tasseled cap	323
Techniques	307
Threshold selection	316
Types of forest change	302
Classification	64, 279
Additive models	291
Algorithm selection	404
Cluster labeling	362

Decision tree classification	293, 399	Structure	78
Fuzzy	287	Structure measurement	80
Fuzzy ARTMAP	292	Fractional land cover	361
Linear least squares inversion	363	AVHRR	359
Linear models	291	Landsat	231
Maximum likelihood	289	SPOT VGT	359
Methods	288	G	
Minimum distance	290	Gap Analysis Program (GAP)	391, 469
Nearest neighbour	292	Gap-fraction	79, 82
Neural network	292, 362	Geographic information systems (GIS)	65
Parallelepiped	291	Geometric correction	148
Per-pixel	257	$\text{Sin}(x)/x$ function	173
Regression	363	Universal sensor model	159
Schemes	283, 398	Geometric distortion	143
Spatial-spectral	294	Types	147
Supervised	64, 286	Global Positioning System (GPS)	48, 470, 492
Texture	257	Gramm-Schmidt Transformation (GST)	<i>See</i> Tasseled cap
Training data	64, 393	Greenness	<i>See</i> Tasseled cap
Unsupervised	64, 286, 393, 475	Ground control point (GCP)	61, 163, 167
Cloud identification	348	H	
D		Histogram adjustment	392
Data fusion	441	Hyperspatial	31
Digital frame cameras	31	Hyperspectral	21, 25, 32
<i>Discrete-return</i>	<i>See</i> Lidar	I	
Disturbance	<i>See</i> Change detection	IKONOS	31, 62
E		Image rectification	61
Electromagnetic spectrum	14	Individual tree isolation	258
Endmember	227, 453	Algorithms	260
F		Inertial Navigation Systems (INS)	492
Forest		Instantaneous field of view (IFOV)	20, 30, 223
Biochemistry	448	Interferometric SAR (IFSAR)	18
Canopy architecture	235		
Canopy structure	80, 209		
Fragmentation	80, 301		
Growth	411		
Inventory	78, 101		
Phenology	219, 280		

Internal measurement unit (IMU)	492
K	
Kauth-Thomas transformation	<i>See</i> Tasseled cap
L	
Lambertian	15
Landsat	21, 30, 34, 117, 146, 281, 364, 366, 390
Attributes	405
Calibration	186
Estimation of LAI	217
Land cover	390, 433
Model input	414
Mosaicking	392
Laser altimetry	<i>See</i> Lidar
Leaf area index (LAI)	34, 81, 89, 369, 415
Allometric relationships	90
Foliage clumping	99
Foliage clumping	84
Leaf litter	90
Measurement limits	371
Validation	101
Vegetation index estimation	215
Lidar	18, 490
Height	36, 502
Systems	490
M	
Moderate Resolution Imaging Spectroradiometer (MODIS)	5, 29, 213, 314, 425
Mosaicking	392, 403
Multi-Resolution Land Characteristics (MRLC)	391
N	
Net primary productivity (NPP)	64, 375, 412
Normalization	
Relative radiometric normalization	192, 194
Scene specific	192
Normalized difference vegetation index (NDVI)	27, 191, 342. <i>See</i> Vegetation index (VI)
Model input	416
O	
Optical imagery	14
Orthoimage	143
Orthophotos	58
P	
Patch size	361
Per-pixel image processing	191, 209, 280, 284
Photogrammetry	59
Photograph scale	56
Photosynthetically active radiation (PAR)	33, 209
Physiological Processes	
Predicting Growth from Satellites (3PGS)	419
Pixel size	<i>See</i> Spatial resolution
Process model	375
Production efficiency model	375
Q	
Quantization	22
Photographs	53
Quickbird	31
R	
Radiance	25, 184
Radiometric calibration	186
AVHRR	339
Change detection	306
Radiometric cross-calibration	186
Radiometric resolution	22
Photographs	53

Reflectance	15	<i>W</i>
Reflectance signature	237	<i>Waveform-recording</i> <i>See</i> Lidar
<i>S</i>		Wetness <i>See</i> Tasseled cap
Solar radiation	14, 15	<i>Z</i>
Spatial resolution	20	Zenith angle 193, 244, 261, 346
H-resolution	25, 281	
Lidar	498	
L-resolution	25, 281	
Photographs	50	
Spectral mixture analysis (SMA)		
210, 223, 452		
Forest change	230	
Spectral reflectance	183	
Spectral resolution	21	
Photographs	51	
Sub-pixel land cover	361	
Synthetic aperture radar (SAR)	16, 417	
Polarization	17	
Systeme Pour d'Observation de la Terre (SPOT)	30, 34	
<i>T</i>		
Tasseled cap	37, 397	
Change detection	323	
Temporal resolution	22	
Texture	262	
Thermal remote sensing	14	
Top of atmosphere (TOA)	187, 341	
<i>V</i>		
Vegetation index (VI)	210, 369	
Burn mapping	218	
Forest change	217	
Forest cover	217	
Radiometric issues	191, 221	
Types	211. <i>Also see</i> NDVI	
View angle	259, 271	